R&D 7451-EN-02
N68171-94-M-6148

Austrian
Armed
Forces

Austrian Society
of Automotive
Engineers

6th EUROPEAN ISTVS CONFERENCE

4. ÖVK Symposium
"Off Road Vehicles in Theory and Practice"

Vienna, Austria
September 28-30, 1994

PROCEEDINGS
VOLUME I

DTIC
S ELECTE D
DEC 1 6 1994
F

This document has been approved for public release and sale; its distribution is unlimited.

ional
Society for
Terrain-
Vehicle
Systems

19941206 007

7451-EN-02

Austrian
Armed
Forces

Austrian Society
of Automotive
Engineers

6th EUROPEAN ISTVS CONFERENCE

4. ÖVK Symposium
"Off Road Vehicles in Theory and Practice"

Vienna, Austria
September 28-30, 1994

PROCEEDINGS
VOLUME I

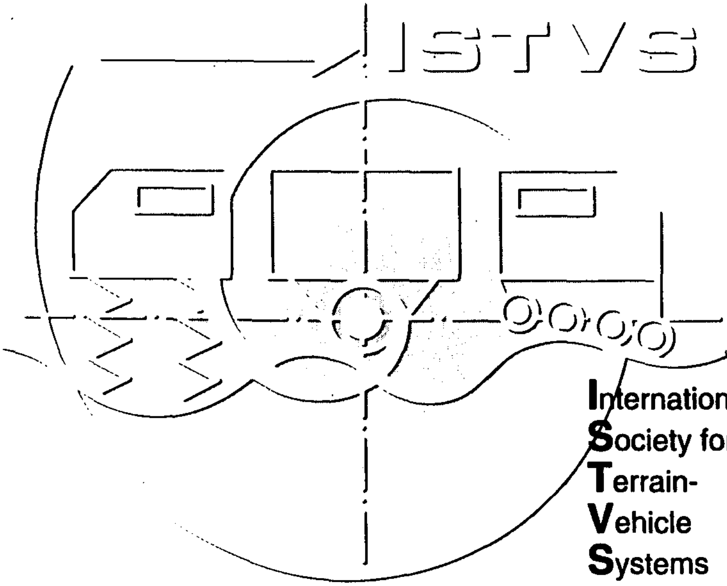

International
Society for
Terrain-
Vehicle
Systems

Table of Contents
Volume I
Plenary Lectures

Session I *General Views*
Sektion I *Grundlegender Überblick*

Terramechanics – Its Present and Future 1
Terramechanik – Gegenwart und Zukunft
J. Y. WONG
Carleton University, Ottawa, Canada

Interactions of Vehicle and Terrain
–Results from 10 Years Research of IKK 22
Wechselwirkungen zwischen Fahrzeug und Boden
– Ergebnisse aus 10 Jahren Forschung am IKK
I. C. SCHMID
IKK–University of German Armed Forces Hamburg, Germany

An Overview of Suspension Systems of Wheeled Off Road Vehicles 55
Ein Überblick über Fahrwerksysteme geländegängiger Radfahrzeuge
G.H. HOHL
Military Technology Agency, Vienna, Austria

Session II *Drive Line Systems*
Sektion II *Antriebssysteme*

Self Generated Torques in All Wheel Drive Power Trains 78
Blindmomente in Allrad–Antriebssträngen
J. STOCKMAR
Steyr–Daimler–Puch–Fahrzeugtechnik GmbH, Graz, Austria

The Effects of Limited Slip Differentials on the Handling
and Traction Properties of Off Road Vehicles 91
Die Auswirkungen schlupfbegrenzter Differentiale auf die
Fahreigenschaften und die Traktion von Geländefahrzeugen
E. B. MACLAURIN
Defence Research Agency, Chertsey, United Kingdom

ADM A New Drive Train Management 108
ADM Ein neues Antriebsstrangmanagement
F.X. STELZENEDER
Steyr–Daimler–Puch AG, Antriebstechnik, Steyr, Austria

DTIC QUALITY INSPECTED 6

Session III A Simulation 1
Sektion III A Simulation 1

Computer–aided Mobility Prognosis of Vehicles in the Field 135
EDV–unterstützte Bodenbefahrbarkeitsprognosen
A. HANDKE, M. BÜTIKOFER
Sieber Cassina + Handke AG, Chur, Switzerland

Theoretical Concepts in Soil–Wheel Interactions 151
Theoretische Konzepte für die Wechselwirkung zwischen Boden und Rad
D. R. P. HETTIARATCHI
The University of Newcastle upon Tyne, United Kingdom

The Interaction between the Rolling Tyre and the Soft Soil –FEM Simulation by VENUS and Validation 169
Die Wechselwirkung zwischen rollendem Reifen und weichem Boden –FEM–Simulation durch VENUS und Verifizierung
Th. AUBEL
IKK–University of German Armed Forces Hamburg, Germany

Session III B Simulation 2
Sektion III B Simulation 2

Ground Vehicle Performance Optimization Using the Genetic Algorithm 189
Leistungsoptimierung von Landfahrzeugen mit Hilfe genetischerAlgorithmen
J. L. OVERHOLT, A. A. ZEID, M. K.EILER
US Army TARDEC, Warren, Michigan, USA
This paper will be published in an appendix to the proceedings

The Simulation of the Phenomena between Tyre and Terrain with the Simulation System ORIS 190
Die Simulation der Phänomene zwischen Rad und Boden im Simulationsprogramm ORIS
K. J. RUFF
IKK–University of German Armed Forces Hamburg, Germany

Calculated and Experimental Simulation of Off Road Trucks 208
Rechnerische und experimentelle Simulation von geländegängigen Lastkraftwagen
W. EICHLSEDER, G. RAAB
Steyr–Daimler–Puch AG, Antriebstechnik, Steyr, Austria

Session IV *Off Road Tyres*
Sektion IV *Geländereifen*

Investigations on Tractor Tyres
Test Stands and Results 219
Untersuchungen an Ackerschlepperreifen
Versuchseinrichtungen und Ergebnisse
H. D. KUTZBACH
University of Hohenheim, Germany

Forces Acting on Driven Tractor Tyres with Stationary
and Instationary Slip Angles 238
Kräfte an angetriebenen stationär und instationär schräglaufenden
Ackerschlepperreifen
Th. BARRELMEYER
University of Hohenheim, Germany

Longitudinal Dynamics of Agricultural Tyres 263
Untersuchungen der Längsdynamik an Ackerschlepperreifen
J. PLESSER
University of Hohenheim, Germany

Session V *Tyre Inflation Pressure Systems*
Sektion V *Reifendruckregelanlagen*

Effect of Reduced Tyre Inflation Pressure on Agricultural Tyres 277
Auswirkung einer Luftdruckverminderung bei
landwirtschaftlichen Reifen
H. SCHWANGHART
Technical University Munich, Germany

Design and Performance of Central Tyre Inflation Systems 295
Ausführung und Leistung von Reifendruckregelanlagen
H.P. SCHLECHTER
Proving Ground of the German Armed Forces,
Trier–Grüneberg, Germany

Influence of Advanced Chassis Technology on Off–Road Mobility
Determined by Means of the "8x8 Experimental Vehicle" 321
Einfluß fortschrittlicher Fahrwerkstechnologie auf die Mobilität
im Gelände, ermittelt mit dem "Experimentalfahrzeug 8x8"
W. SÜNKEL
Mercedes–Benz AG, Stuttgart, Germany

☑
☐
☐
A-1

Session VI *Vehicle Dynamics*
Sektion VI *Fahrzeugdynamik*

Dynamic Simulation – Cost Benefits and Design Advantages 341
Dynamische Simulation – Kosteneinsparung und verbesserte Konstruktion
S. F. STOREY
Simatics Limited, Cambridge, United Kingdom

Ride Dynamics of Terrain Vehicles 346
Fahrdynamik geländegängiger Fahrzeuge
H. GÖHLICH
Technical University of Berlin, Germany

Controlled Suspension for Off Road Vehicles 358
Gesteuertes Fahrwerk für Geländefahrzeuge
D. A. CROLLA
The Univerity of Leeds, United Kingdom

Session VII *Vehicle Design*
Sektion VII *Fahrzeugkonstruktion*

Latest Developments in Superstructures for All–Terrain Logistic Support Trucks 370
Neue Aufbausysteme für geländegängige Versorgungs–LKW
E. PRANCKL, W. WIESER
Steyr Nutzfahrzeuge AG, Steyr, Austria

The New MAN Transfer Cases for Deployment in On Road and Off Road Vehicles 394
Die neuen MAN–Verteilergetriebe für den Einsatz in Straßen– und Geländefahrzeugen
K. V. SCHALLER
MAN Nutzfahrzeuge AG, Munich, Germany

Development and Experimental Evaluation of All Wheel Steer on a 6x6 Off Road Vehicle 413
Entwicklung und experimentelle Ergebnisse einer Allradlenkung bei einem 6x6 Geländefahrzeug
S. NELL
ERMETEK Ltd. Elandsfontein, South Africa

Session VIII *Soil Machinery*
Sektion VIII *Baumaschinen*

Optimization of Excavator Booms
Operating Loads, Structural Dynamics 431
Optimierung von Baggerauslegern
Betriebslasten, Strukturdynamik
E. GÜNER, W. POPPY, M. WEID
Berlin University of Technology, Germany

Ground Vibration by Motion of Construction Vehicles 454
Bodenschwingungen hervorgerufen durch Baufahrzeuge
K. KOGURE, M. AOYAMA, Y. MIYATA
The National Defense Academy, Yokosuka, Japan

Compaction Effect of Vibratory Soil Compactors
Modeling, Simulation, Operating Tests 466
Verdichtungswirkung von Vibrationswalzen
Modellbildung, Simulation, Betriebsmessungen
M. TETTKE, W. POPPY
Berlin University of Technology, Germany

Session IX *Special Topics*
Sektion IX *Sonderthemen*

The FEA Way to an Octagonal Ring
Transducer Design Optimization 482
Die Finite–Elemente–Methode zur Konstruktionsoptimierung
eines Octogonal Ring–Meßgerätes
G. FERRETTI, P. PAOLUZZI, G. RIGAMONTI
Italian National Research Council, Ferrara, Italy

Reliability and Maintainability Evaluation of Off Road Vehicles 492
Zuverläßigkeits– und Instandsetzungsbewertung von
Geländefahrzeugen
L. K. JOKUBAITIS, B. KAZMAREK
US Army TACOM, Warren, Michigan, USA

Off Road Vehicles Marketing 513
Geländefahrzeugmarketing
H. MOSER
4WD–Magazin, Wels, Austria

Session X *Tracked Vehicles*
Sektion X *Kettenfahrzeuge*

Stability of Tracked Vehicles on Inclined Ground 517
Stabilität von Kettenfahrzeugen auf geneigtem Gelände
M. KITANO, K. WATANABE, T. KAKINO
The National Defense Academy, Yokosuka, Japan

Transmission Systems for Tracked Vehicles
Yesterday – Today – Tomorrow 529
Getriebesysteme für Kettenfahrzeuge
Gestern – Heute – Morgen
St. BOLLMANN
ZF Friedrichshafen, Germany

On Constitutive Equations Used at Analysis of Steering of
Tracked Vehicles 560
Grundlegende Gleichungen für die Analyse der Lenkkräfte von
Kettenfahrzeugen
M. MÄGI
Chalmers University of Technology, Göteborg, Sweden

Table of Contents
Volume II
Postersession

The list of the paper is arranged in a alphabetical order according to the first named author of the paper.
Die Liste der Beiträge wurden in alphabetischer Reihenfolge nach dem erstgenannten Autor gereiht.

Robot–Motion in Unstructured Environment 570
Roboterbeweglichkeit im freien Gelände
M. B. BARTHA, M. EIBERT, P. LUX, C. H. SCHAEFER
DASA–Dornier, Verteidigung und Zivile Systeme
Friedrichshafen, Germany

Application of Intelligent Systems in Modern Bucket Loaders
Anwendung Intelligenter Systeme an modernen Radladern 584
P. DUDZINSKI, K. PIECZONKA, Z: WYSTOUCH
Technical University of Wroclaw, Poland

Parallel Tests with 6 and 7 Roadwheel Tracked Vehicles 603
Parallelversuche mit 6– bzw. 7–Laufrollen–Kettenfahrzeugen
A. ENGELER
Military Technology Agency, Vienna, Austria

FE–Simulation of Tyre–Profile–Effects on the Terrain Mobility of Vehicles 618
FE–Simulation des Reifenprofileinflusses für die Geländebeweglichkeit von Fahrzeugen
C. W. FERVERS
IKK–University of German Armed Forces Hamburg, Germany

Smart Electromechanical AWD x AWB x AWA Intelligent Main Battle Tank 634
Elegante elektromechanische AWD x AWB x AWA Lösungen für intelligente Kampfpanzer
B. T. FIJALKOWSKI
Cracow Univerity of Technology, Poland

Ceramic Components in Tracks for Construction Equipment 673
Keramikbauteile in Gleisketten für Baufahrzeuge
K. F. FISCHER, M. KETTING, M. WOYDT
Intertractor AG, Gevelsberg, Germany

Off–Road Tyres with Emergency Capabilities 696
Geländereifen mit Notlaufeigenschaften
H.HAAS
Hutchinson Industrie Produkte, Mannheim, Germany

The Prediction of Soil Strength on Basis of Climate Data
as Criterian of Off–Road Mobility 710
Die Vorhersage der Bodenfertigkeit als Kriterium der
Geländegängigkeit auf Basis von klimatischen Daten
D. HINTZE
IKK–University of German Armed Forces Hamburg, Germany

Experimental and Theoretical Analysis of a Cohesive Soil
Shoving Process (The Optimisation of the Process) 731
Experimentelle und theoretische Analyse kohäsiven Erdreichs
beim Verschiebevorgang (Optimierung des Vorganges)
A. JARZEBOWSKI, J. MACIEJEWSKI, D. SZYBA, W. TRAMPCZYNSKI
Polish Academy of Sciences, Warsaw, Poland

A New Type of Off Road Tyre, –Bionic Camel Foot Tyre
Ein neuer Geländereifen –Kamelfußreifen 741
X. JI, J. ZHUANG, X. QIU
Jilin University of Technology, Chang Chun, PR China

Numerical Simulation of the Dynamic Behaviour of
Agricultural Tractors 748
Numerische Simulation des dynamischen Verhaltens von
Traktoren
C. KAPLICK
Technical University Berlin, Germany

Environmental Friendly Fuel for Diesel Engines in Off Road
Vehicles 756
Umweltfreundliche Kraftstoffe für Dieselmotoren in
Geländefahrzeugen
W. E. KIEHTREIBER
Altfettmethylester Produktionsges. m. b. H,
Margarethen am Moos, Austria

State of the Art Report of the Mobility Research in Hungary 762
Bericht über die bisherigen "Mobilitätsforschungen"in Ungarn
L. LAIB
GATE University of Agriculture Sciences, Gödöllö, Hungary

Tractive Performance of a Four Wheel Drive Vehicle Moving up a Sloped Weak Terrain 806
Zugkrafteigenschaften eines Vierradfahrzeuges auf geneigtem schweren Gelände
T. MURO
Ehime University of Japan, Matsuyama, Japan

Terramechanical Experiments in Soil Bins
The ISTVS Publications' Review (1984–1993) 823
Terramechanische Versuche in Bodenrinnen
Übersicht der Veröffentlichungen von ISTVS (1984–1993)
M. M. PONCYLIUSZ, A. MASTALINSKI
Warsaw University of Technology, Poland

The Turning Resistance of Tracked Vehicles, Influenced by Lateral Elasticities of the Running Gear and the Tracks 833
Der Einfluß von Querelastizitäten in Laufwerk und Kette auf das Wendeverhalten von Gleiskettenfahrzeugen
St. POTT
IKK–University of German Armed Forces Hamburg, Germany

Mobility has Reached a New Dimension
The BV 206
Die Beweglichkeit hat eine neue Dimension hinzugewonnen
Der BV 206
W. RINKE
Hägglunds Vehicle Ges.m.b.H., Isernhagen, Germany
This paper will be published in an appendix to the proceedings

The Bucher -DURO- a Vehicle Concept for the Future 853
Der Bucher-DURO- ein Fahrzeugkonzept für die Zukunft
H. SASSE
Bucher- Guyer A.G., Zürich, Switzerland

The New Dornier Foldable Bridge DoFB 859
Die neue Dornier Faltbrücke DoFB
P. SCHMIDT, S. BÄUMEL
Eurobridge, Mobile Brücken GmbH, Friedrichshafen, Germany

Steyr 8090 and Seppi M. Miniforst Assembly in Sivicultural Work 887
Aggregat Steyr 8090 und Seppi M. Miniforst Einheit im Forstbereich
S. SEVER, D. HORVAT, K. JELCIC
University of Zagreb, Croatia

A Single Track Module in Multibody Systems Sense for Simulations of Steering of a Vehicle on Hard Ground 896
Ein Einkettenmodul im Mehrkörpersystem zur Simulation des Lenkens eines Fahrzeuges auf harter Fahrbahn
D. THUVESEN
Chalmers University of Technology, Göteborg, Sweden
This paper will be published in an appendix to the proceedings

Effect of the Way the Load Applies on the Bearing Capacity of Dry–Loose Sand 897
Einfluß der Art der Lastenaufbringung auf die Tragfähigkeit von trockenem lockeren Sand
J. ZHUANG, X. JI, X. QIU
Jilin University of Technology, Chang Chun, PR China

Session I
Sektion I

General Views
Grundlegender Überblick

TERRAMECHANICS - ITS PRESENT AND FUTURE

Professor J.Y. Wong[1]
Ph.D., D.Sc., F.I.Mech.E., F.A.S.M.E.

ABSTRACT

The current state-of-the-art of terramechanics, particularly as it relates to vehicle mobility over soft terrain, will be reviewed. Different methods of approach to the study of terramechanics, including empirical and computer-aided analytical methods, will be compared and critically examined. Empirical methods for predicting vehicle mobility have played a useful role in the past. However, with an improved understanding of the physical nature of vehicle-terrain interaction and of terrain response to vehicular loadings, a new generation of comprehensive and realistic computer simulation models has emerged over the past decade. In contrast to empirical models developed earlier, these models are based on detailed studies of the mechanics of vehicle-terrain interaction and take into account all major vehicle design features and terrain characteristics. They have played and will continue to play an increasingly important role in the future development of off-road vehicles.

1. INTRODUCTION

The term "terramechanics" was first coined by Dr. Bekker and appeared in his book "Off-the-Road Locomotion - Research and Development in Terramechanics," published in 1960 (1). Since then with the formation of the International Society for Terrain-Vehicle Systems and the publication of the

---

[1] Department of Mechanical and Aerospace Engineering,
Carleton University and Vehicle Systems Development Corporation
Ottawa, Canada

Journal of Terramechanics, terramechanics has become a recognized branch of applied mechanics, and has attracted the interest and enthusiasm of professionals in the field around the globe.

The aim of terramechanics is to provide the technological base upon which the design and performance of off-road vehicles and soil-engaging machinery may be improved. The basic issue in terramechanics is to integrate the knowledge of the behaviour of the terrain and the understanding of the characteristics of vehicle (machine)-terrain interaction into a framework with which the engineering practitioner can realistically predict the performance of the vehicle as functions of vehicle design features and terrain conditions. Thus, this framework could be a tool for the rational design, evaluation and selection of off-road vehicles for vehicle designers or procurement managers.

An understanding of terrain response to vehicular loading is of importance to the development of terramechanics, as quite often terrain properties impose severe limitations to vehicle mobility. A detailed knowledge of the characteristics of vehicle-terrain interaction is also essential to the development of a realistic and comprehensive framework for predicting off-road vehicle performance. Over the past few decades, a great deal of effort has been expended into the research of terrain behaviour and of the mechanics of vehicle-terrain interaction (2, 3). Based on the results of these investigations, two major types of framework (or simulation model) have emerged. One is based on empirical correlations, exemplified by the U.S. Army Engineer Waterways Experiment Station's Vehicle Cone Index (WES VCI) model, which forms the basis for the subsequent developments of the AMC'71 and AMM'75 mobility models and the NATO Reference Mobility Model (NRMM) (4). The other is based on the detailed analysis of the mechanics of vehicle-terrain interaction, exemplified by the computer simulation models NTVPM, RTVPM, and NWVPM, developed by Wong and his associates (3, 5, 6, 7, 8, 9, 10, 11, 12). In addition to these two types of simulation model, models based on the theory of plastic equilibrium and the finite element method have also been developed (3). However, little has so far been reported in the literature that these models have found any practical applications in the design evaluation off-road vehicles by either vehicle designers or procurement managers.

Owing to the limitation of space, this paper will concentrate on the discussion of terramechanics as it relates to vehicle mobility over soft terrain.

The current state-of-the-art in the measurement and characterization of terrain response to vehicular loading, in the modelling of vehicle-terrain interaction, and in the simulation models for performance and design evaluation of off-road vehicles will be reviewed. Future developments in terramechanics will be discussed.

2. CURRENT STATE-OF-THE-ART IN TERRAMECHANICS

2.1 Measurement and Characterization of Terrain Behaviour

In off-road operations, various types of terrain with differing behaviour, ranging from desert sand through soft mud to fresh snow, may be encountered. Consequently, the measurement and characterization of terrain response in relation to vehicle mobility are of importance. So far, however, there have been no universally accepted or standardized methods for measuring and characterizing terrain behaviour, although certain recommended practice was suggested by the Society of Automotive Engineers and others (13).

There are currently two principal techniques in use for measuring and characterizing terrain behaviour in relation to vehicle mobility.

2.1.1 Cone penetrometer technique. This technique was originally developed during the Second World War by the U.S. Army Engineer Waterways Experiment Station (WES) to provide military intelligence and reconnaissance personnel with a simple method for evaluating vehicle mobility on fine- and course-grained soils and on a "go/no go" basis. The original cone penetrometer developed by WES is a hand-held mechanical device with a cone base area of 0.5 in^2 (3.23 cm^2). Lately, a variety of cone penetrometers using electrical (or electronic) sensors for monitoring the force and penetration depth and computer technology for storing and processing data has been developed (3). For monitoring the firmness of snow, a Rammsonde cone penetrometer has also been developed (14). Dependent upon snow conditions, cones with a base diameter of 4 and 10 cm are available.

The cone penetrometer technique has been quite widely used in vehicle mobility studies, primarily due to its simplicity. In spite of its wide use and acknowledged role in providing a measure of terrain firmness, it is generally recognized that the cone index (CI), which is the penetration force per unit cone base area, is not sufficient for adequately defining the mechanical properties of the terrain that are pertinent to vehicle mobility. It has been shown that the cone index is a compound parameter reflecting the combined effects of shear, compressive and tensile strengths of the terrain and the cone-terrain interface frictional-adhesive properties. The cone index and its derivatives, such as the rating cone index (RCI), are used in the vehicle mobility simulation model NRMM and its predecessors.

2.1.2 Bevameter technique. This technique was originally developed by Bekker (2) and is based on the premise that terrain behaviour pertinent to vehicle mobility can best be measured under loading conditions similar to those exerted by an off-road vehicle. A vehicle exerts normal and shear loads on the terrain surface. To simulate these, the original bevameter technique comprises two separate sets of tests. One is a set of penetration tests and the other is a set of shear tests. To provide data for predicting the multipass performance of vehicle running gear and the additional sinkage due to slip, the measurements of the response to repetitive normal and shear loadings and the slip-sinkage characteristics of the terrain have recently been added. A computerized procedure based on the weighted least squares method for processing bevameter data obtained in the field has been successfully developed and gaining increasingly wide acceptance (15, 16). The terrain data obtained using the bevameter technique are used in the simulation models NTVPM (for vehicles with flexible tracks), RTVPM (for vehicles with rigid link tracks), and NWVPM (for off-road wheeled vehicles), developed by Wong et al.

Recently, a response surface methodology based on an orthogonal regression in the parameter space has been developed by Upadhyaya et al. to identify engineering properties of terrain based on in-situ tests (17). It has been reported that this methodology works very in a two-parameter hypo-elastic model for soil, as well as in a five-parameter model for soil having nonlinear elastic behaviour with Drucker-Prager yield criteria and associated plastic flow upon yield, under certain circumstances.

It should be noted that terrain data obtained by either the cone penetrometer or the bevameter described above are intended for the analysis of vehicle mobility and tractive performance under steady-state conditions. To evaluate the dynamic behaviour of off-road vehicles in the vertical or horizontal direction, additional terrain parameters, such as the equivalent dynamic stiffness and damping coefficient of the terrain, are required. As pointed out by Huck (18), the dynamic behaviour of the terrain is of importance to the assessment of the effects of track and undercarriage dynamics on the vibrations of the vehicle body, as well as to the prediction of its tractive performance under dynamic conditions. The dynamic behaviour of terrain pertinent to vehicle mobility is certainly an area open for further research and investigation.

2.2 Modelling of Vehicle Mobility and Vehicle-Terrain Interaction

There are currently two principal methods for the modelling of vehicle mobility. One is based on empirical correlations, and the other is based on the detailed analysis of the mechanics of vehicle-terrain interaction.

2.2.1 Empirical Models. These models are based on the empirical correlations between vehicle performance measured in the field and the corresponding field (terrain) conditions identified by simple measuring devices, such as the cone penetrometer. One of the best known empirical models currently in use is the NATO Reference Mobility Model (NRMM). NRMM has the capability, among others, to predict the tractive performance of both tracked and wheeled vehicles over two basic types of terrain, namely, fine- and coarse-grained soils. This model has been under continuous development. In 1992, WES released NRMM II, which incorporates a side slope mobility algorithm from the French Etablissement Technique d'Angers. As a separate part of NRMM, an updated, two-dimensional vehicle dynamics model for ride evaluation, referred to as VEHDYN-III, will soon be released. It includes additional suspension configurations and a new track profile interface model (17). A personal computer (PC) based version of NRRM, referred to as CAMMS, (Comprehensive Army Mobility Model System), was also recently made available.

It should be noted that since empirical models are based on empirical correlations, they are useful only in estimating the mobility of vehicles with design features similar to those that have been tested under similar terrain conditions. It is by no means certain that they are valid for evaluating new vehicle design concepts or for predicting vehicle performance in new operating environments.

2.2.2 Models Based on Detailed Analysis of the Mechanics of Vehicle Terrain Interaction. With growing competition in the global market, off-road vehicle manufacturers are driving for the reduction in product development time and cost. They are increasingly turning to computer simulations as a means of saving time and cost to supplement and ultimately reduce dependence on the more traditional and costly "cut and try" approach to product development and design. To be useful to vehicle development and design engineers, the simulation models must be comprehensive and realistic, and must take into account all major vehicle design features, as well as pertinent terrain characteristics. The models must also be user-friendly and efficient.

To meet all these requirements, a series of computer simulation models for tracked and wheeled off-road vehicles have been developed under the auspices of Vehicle Systems Development Corporation, Nepean, Ontario, Canada. They include NTVPM for vehicles with flexible tracks (3, 5, 6, 7, 8, 9), RTVPM for vehicles with rigid link tracks (10, 11), and NWVPM for off-road wheeled vehicles (3, 12). In contrast with empirical models, these models are based on detailed studies of the physical nature of vehicle-terrain interaction and the principles of applied mechanics. They take into account all major vehicle design parameters and basic terrain characteristics. As the performance of an off-road vehicle ultimately depends upon the interacting forces between the vehicle running gear and the terrain, these simulation models focus on the prediction of the normal and shear stress distributions on the vehicle-terrain interface, as functions of vehicle design parameters and terrain properties.

A. Computer Simulation Model NTVPM for Vehicles with Flexible Tracks

For high-speed tracked vehicles, such as military fighting and logistics vehicles and off-road transport vehicles, rubber tracks or link tracks with relatively short track pitch are commonly used. This kind of short-pitch track system typically has a ratio of roadwheel diameter to track pitch in the range from 4 to 6, a ratio of roadwheel spacing to track pitch in the range of 4 to 7, and a ratio of sprocket pitch diameter to track pitch usually of the order of 4. The rubber-belt track and the short-pitch link track will be referred to as "flexible tracks" in this paper and they may be idealized as a flexible belt in the analysis of track-terrain interaction (3, 5, 6, 7, 8, 9). A schematic of the flexible track system used in the model is shown in Fig. 1

The computer simulation model NTVPM has been developed for performance and design evaluation of tracked vehicles with flexible tracks. The latest version of the model, known as NTVPM-86, takes into account all major vehicle design parameters, including sprung weight, unsprung weight, location of the centre of gravity, number of roadwheels, location of roadwheels, roadwheel dimensions and spacing, locations of sprocket and idlers, supporting roller arrangements, track dimensions and geometry, initial track tension, belly (hull) shape, and angles of approach and departure of the track system. The longitudinal elasticity of rubber-belt tracks or of link tracks with rubber bushings are taken into consideration. The track longitudinal elasticity affects the tension distribution in the track and as a result influences the performance of the vehicle to a certain extent over marginal terrain. The characteristics of the independent suspension of the roadwheels are fully taken into account in the model. Torsion bar suspensions, hydro-pneumatic suspensions with non-linear load-deflection characteristics, and others can be accommodated in the model. Suspensions characteristics have a significant effect on vehicle mobility over soft ground. On highly compressible terrain, such as deep snow, track sinkage may be greater than the ground clearance of the vehicle. If this occurs, the belly (hull) of the vehicle will be in contact with the terrain surface and will support part of the vehicle weight. This will reduce the load carried by the tracks and will adversely affect the traction of the vehicle over terrain that exhibits frictional behaviour. Furthermore, belly contact will give rise to an additional drag component - the belly drag. The problem of belly contact is of importance to vehicle mobility over marginal terrain, and the characteristics of belly-terrain interaction have been taken into consideration in the model. Terrain characteristics, including the pressure-sinkage relation, shear strength, rubber-terrain shearing (for rubber tracks or tracks with rubber pads) and belly-terrain shearing characteristics, and responses to repetitive normal and shear loadings, are taken into account in the model.

The model can be used to predict the performance of single unit and two-unit articulated tracked vehicles over unprepared terrain. Its basic features have been validated with field test data obtaining using various test vehicles, including M113A1, BV202 and BV206, over a variety of unprepared terrains, including mineral terrain, organic terrain (muskeg) and snow-covered terrain. Figure 2 shows a comparison of the measured and predicted normal pressure distributions under the track pad of an armoured personnel carrier

M113A1 over a muskeg. A comparison of the measured and predicted drawbar performance of an M113A1 over the same type of terrain is shown in Fig. 3. Reasonably close agreements between the measured and predicted normal pressure distributions and drawbar performance obtained using NTVPM-86 confirm the validity of the basic features of the model.

NTVPM-86 can be employed to assess the effects of vehicle design parameters on vehicle mobility and the influence of terrain conditions on vehicle performance. The model can also be used in design optimization for a given mission and operating environment. As an example, Fig. 4 shows the effects of the number of roadwheels and the initial track tension on the drawbar pull to weight ratio (drawbar pull coefficient) of a reference vehicle with design parameters similar to that of the M113A1 over a deep snow, predicted using the simulation model (6). It can be seen that both the number of roadwheels and the initial track tension have significant effects on vehicle mobility over soft ground. For a given (or existing) vehicle, its mobility over marginal terrain can be greatly improved by increasing the initial track tension. This research finding obtained using NTVPM-86 has led to the development of a central initial track tension regulating system controlled by the driver. Over normal terrain, the driver can set the track tension at the regular level. However, when traversing marginal terrain is anticipated, the driver can readily increase the track tension to an appropriate level to improve vehicle mobility. It is installed on a new generation of high-mobility armoured vehicles (CV 90) currently in production in Sweden.

The model NTVPM-86 has been successfully used to assist manufacturers in the development of military vehicles and governmental agencies in the evaluation of vehicle candidates in Europe, North America and Asia. For instance, this model has been employed to assist Hagglunds Vehicle AB of Sweden in the development of a new generation of high-mobility fighting vehicles (CV 90), in the examination of the approach to the further improvement of the performance of the all-terrain carrier BV 206, and in the evaluation of competing designs for a proposed main battle tank. Recently, it has been used in the selection of an optimum configuration for a new, high-mobility version of an armoured vehicle (ASCOD) for a Spanish vehicle manufacturer (Empresa Nacional Santa Barbara) and in the assessment of the effects of design modifications on the mobility of a fighting vehicle over tropical terrain for an Asian firm. It has also been employed in the evaluation of the effects of design changes on the cross-country mobility of

Canada's main battle tank, Leopard C1, for the Canadian Department of National Defence and in the assessment of the mobility of a variety of container handling equipment used by the U.S. Marine Corps.

B. Computer Simulation Model RTVPM for Vehicles with Rigid Link Tracks

For low-speed tracked vehicles, such as those used in agriculture and construction industry, rigid link tracks with relatively long track pitch are commonly used. This type of track system has a ratio of roadwheel diameter to track pitch as low as 1.2 and a ratio of roadwheel spacing to track pitch typically 1.5.

The computer simulation model RTVPM has been developed for performance and design evaluation of tracked vehicles with rigid link tracks (10, 11). This model takes into account all major design parameters of the vehicle, including vehicle weight, location of the centre of gravity, number of roadwheels, location of roadwheels, roadwheel dimensions and spacing, locations of sprocket and idlers, supporting roller arrangements, track dimensions and geometry, initial track tension, and drawbar hitch location. As the track links are considered to be rigid, the track is assumed to be inextensible. For most low-speed tracked vehicles, the roadwheels are not sprung, and hence considered to be rigidly connected to the track frame. Terrain parameters used in this model are the same as those used in NTVPM.

The model RTVPM treats the track as a system of rigid links connected with frictionless pins, as shown in Fig. 5. As noted previously, the roadwheels, supporting rollers, and sprocket are assumed to be rigidly attached to the vehicle frame. The centre of the front idler is, however, assumed to be mounted on a pre-compressed spring.

The basic features of RTVPM have been validated with available field test data. Figures 6 and 7 show a comparison of the measured and predicted drawbar pull coefficient and tractive efficiency as functions of track slip, respectively, for a heavy tracked vehicle used in construction industry on a sandy loam (10). The measured data shown in figures are provided by Caterpillar Inc., Peoria, Illinois, U.S.A.

It can be seen that the tractive performance of the vehicle predicted using

RTVPM is very close to the measured one. This suggests that the model is capable of providing realistic predictions of vehicle performance in the field. It would be desirable, however, to further validate the model over a wider range of terrain conditions.

The applications of RTVPM to design evaluation and parametric study of vehicles with rigid link tracks will be demonstrated through examples. Figure 8 shows the effects of the track pitch on the drawbar performance on a clayey soil of a reference vehicle with a total weight of 372.4 kN, predicted using RTVPM (11). The vehicle has seven roadwheels on each track, a track pitch of 21.6 cm, an initial track tension of 22.30 kN, and a centre of gravity at the mid-point of the track contact length. It can be seen that within the range studied, the longer the track pitch, the higher the tractive performance will be. This is primarily due to the fact that with a longer track pitch, the normal pressure distribution under the track becomes more favourable. It should be noted, however, that with a longer track pitch, the fluctuation in speed and the vibrations of the track system may increase. Consequently, there is a practical limit to the track pitch for a given vehicle configuration.

Figure 9 shows the effects of the number of roadwheels on the drawbar performance of the reference vehicle on the clayey soil. It can be seen that increasing the number of roadwheels enhances the tractive performance of the vehicle. The improvement in tractive performance with a larger number of roadwheels is due to a more uniform normal pressure distribution.

C. Computer Simulation Model NWVPM for Off-Road Wheeled Vehicles

NWVPM has been developed for the evaluation of the overall performance and design of off-road wheeled vehicles over unprepared terrain, as well as for the selection of tires for cross-country operations. The model takes into account all major design parameters of the vehicle as well as the tire. The vehicle design parameters considered include: vehicle weight, axle load, axle spacing, location of the centre of gravity, axle suspension stiffness, function of the axle (driven or non-driven), axle clearance, track of the axle, belly (hull) shape, and drawbar hitch location. The tire parameters considered include: outside diameter, tread width, section height, lug area/carcass area, lug height, lug width, inflation pressure, average ground contact pressure, and tire construction (radial or bias). Terrain parameters used in the model are the same as those used in NTVPM and RTVPM.

The model NWVPM consists of two sub-models, one is the tire sub-model and the other is the vehicle sub-model.

The tire sub-model used is that developed by Wong (3, 5, 12). Based on the dimensions of the tire, the inflation pressure and carcass stiffness (or alternatively the average contact pressure on a hard surface), the normal load, and terrain characteristics, the operating mode of the tire ("rigid" or "elastic") is first predicted. Based on a detailed analysis of the mechanics of tire-terrain interaction, a set of equations for the equilibrium of the tire can then be established. The solutions to this set of equations determine the normal and shear stress distributions on the tire-terrain interface, the motion resistance (including the internal resistance of the tire), thrust, and sinkage of the tire. The tire sub-model is incorporated into the vehicle sub-model to provide a complete framework for performance and design evaluation of off-road wheeled vehicles (3, 12). The vehicle sub-model takes into account the dynamic inter-axle load transfer and the suspension stiffness of the axles. Any number of axles can be accommodated. When the track of the front (preceding) axle is the same as that of the rear (following) axle, the tires on the rear axle run in the ruts formed by the tires on the front axle. Terrain properties in the rut will be different from those in the virgin state. To take into account this "multipass" effect, the responses of the terrain to repetitive normal and shear loadings are taken into consideration in the model. In addition, both single and dual tires can be accommodated. The output of the model includes the load, sinkage, motion resistance and thrust of the axles, and the drawbar pull and tractive efficiency of the vehicle as functions of wheel slip.

The basic features of the model have been verified with available field test data. Figures 10 and 11 show a comparison of the measured and predicted drawbar performance of a tractor obtained using NWVPM on a plowed and stubble field, respectively.

NWVPM can be used for parametric analysis of the performance and design of off-road wheeled vehicles and for the selection of tires for a given operating environment. For instance, Fig. 12 shows the effects of design and inflation pressure of the front and rear tires on the tractive performance of a two-axle vehicle on a medium soil, predicted using NWVPM. The first and second numbers in the inflation pressure combinations shown in the figure represent the inflation pressure of the front tires and that of the rear tires, respectively.

The model NWVPM has been used in the assessment of the effects of different types of tire on the mobility of a 6 x 6 and an 8 x 8 armoured wheeled vehicle for the Canadian Department of National Defence and in the evaluation of the mobility of container handling wheeled vehicles used by the U.S. Marine Corps.

3. SOME THOUGHTS ON THE FURTHER DEVELOPMENTS OF TERRAMECHANICS

With the growing integration of the world economy, competition has become more fierce in today's global markets. To shorten product development and design cycle and to reduce the associated cost, vehicle manufacturers increasingly turn to computer simulations as a means of lessening the dependence on the lengthy and expensive "build and test" methodology. This trend is accelerating in recent years with rapid advances in computer technology. Simulations in the form of "virtual reality" is also gaining popularity.

To develop comprehensive and realistic computer simulation models for evaluating vehicle mobility requires an in depth understanding of terrain behaviour and of the physical nature of vehicle-terrain interaction. It also needs a skilful integration of these knowledge bases into a user-friendly analytical framework, with which engineers can optimize vehicle designs and procurement managers can evaluate vehicle candidates in an expeditious manner.

With this scenario in mind, the following suggestions concerning the further developments of terramechanics are offered:

A. At the present time, most of the research effort has been concentrated on the prediction and evaluation of vehicle mobility over soft terrain under steady-state conditions. In reality, various dynamic effects are present while an off-road vehicle traverses unprepared surfaces. This suggests that the response of terrain to dynamic loading should be considered.

The measurement and characterization of the dynamic properties of terrain, such as its equivalent dynamic stiffness and damping coefficient, are areas requiring further research. Furthermore, the characterization of the slip-sinkage phenomenon, the mechanics of vehicle-terrain interaction during turning manoeuvres, and the dynamic interaction between the vehicle and deformable terrain during vibrations are also some of the topics requiring further investigation and elucidation.

B. Simulation models based on empirical relations have played a useful role in the past. However, to be useful in guiding the future development and design of off-road vehicles, computer simulation models must be based on detailed analyses of the mechanics of vehicle-terrain interaction and take into account all major design features of the vehicle and its subsystems. In addition to the further refinement of the simulation models for evaluating vehicle mobility over soft terrain described above, comprehensive and realistic computer simulation models for evaluating the manoeuvrability and ride quality of off-road vehicles over deformable terrain are needed.

C. In these changing political and economic times, to effectively and efficiently use the limited resources available, future research in terramechanics should be carefully planned and much more focused to the needs of the manufacturers and users of off-road vehicles. It should be aimed at providing the technological basis upon which the overall performance and design of off-road vehicles may be enhanced and product innovations may result. It should also be emphasized that while research into individual facets of vehicle-terrain interaction can provide a better understanding of this complex phenomenon, it must be carried out with a clear and overall objective in mind. Furthermore, it is also of great importance to integrate new knowledge bases of terramechanics into a practical and user-friendly framework that will enable practising engineers to improve their products.

Acknowledgements

The provision of field test data by Caterpillar Inc., Peoria, U.S.A., for the validation of the computer simulation model RTVPM is appreciated. This does not imply, however, that the views expressed in this paper necessarily represent those of Caterpillar Inc.

This paper was prepared with the support of Vehicle Systems Development Corporation, Nepean, Ontario, Canada and of the Natural Sciences and Engineering Research Council of Canada.

References

1. Bekker, M.G. (1960), "*Off-the-Road Locomotion - Research and Development in Terramechanics*," University of Michigan Press.

2. Bekker, M.G. (1969), "*Introduction to Terrain-Vehicle Systems*," University of Michigan Press.

3. Wong, J.Y. (1989),"*Terramechanics and Off-Road Vehicles*", Elsevier Science Publishers, B.V., Amsterdam, the Netherlands.

4. Jurkat, M.P., Nuttall, C.J. and Haley, P.W. (1975), "The U.S. Army Mobility Model (AMM-75)," Proceedings of the 5th International Conference of the International Society for Terrain-Vehicle Systems, Vol. IV, pp. 1-48.

5. Wong, J.Y. (1993), *Theory of Ground Vehicles, 2nd Edition*, John Wiley, New York.

6. Wong, J.Y. and Preston-Thomas, J. (1986), "Parametric Analysis of Tracked Vehicle Performance Using an Advanced Computer Simulation Model," Proceedings of the Institution of Mechanical Engineers, Part D, Transport Engineering, Vol. 200, No. D2, pp. 101-114.

7. Wong, J.Y. and Preston-Thomas, J. (1988), "Investigation into the Effects of Suspension Characteristics and Design Parameters on the Performance of Tracked Vehicles Using an Advanced Computer Simulation Model," Proceedings of the Institution of Mechanical Engineers, Part D, Transport Engineering, Vol. 202, No. D3, pp. 143-161.

8. Wong, J.Y. (1992), "Optimization of the Tractive Performance of Articulated Vehicles Using an Advanced Computer Simulation Model," Proceedings of the Institution of Mechanical Engineers, Part D, Journal of Automobile Engineering, Vol. 206, No. D1, pp. 29-45.

9. Wong, J.Y. (1992), "Computer-Aided Methods for Optimization of the Mobility of Single-Unit and Two-Unit Articulated Tracked Vehicles," Journal of Terramechanics, Vol. 29, No. 4/5, pp. 395-421.

10. Gao, Y. and Wong, J.Y. (1994), "The Development and Validation of a Computer-Aided Method for Design Evaluation of Tracked Vehicles with Rigid Links," Proceedings of the Institution of Mechanical Engineers, Part D, Journal of Automobile Engineering, Vol. 208 (in press).

11. Wong, J.Y. and Gao, Y. (1994), "Applications of a Computer-Aided Method to Parametric Study of Tracked Vehicles with Rigid Links," Proceedings of the Institution of Mechanical Engineers, Part D, Journal of Automobile Engineering, Vol. 208 (in press).

12. Wong, J.Y. and Preston-Thomas, J. (1986), "Development of Vehicle Performance Prediction Software," Unpublished Report prepared for the Division of Energy, National Research Council of Canada.

13. Society of Automotive Engineers, Off-Road Vehicle Mobility Evaluation -SAE Recommended Practice J939, 1967.

14. Wong, J.Y. and Irwin, G.J. (1992), "Measurement and Characterization of the Pressure-Sinkage Data for Snow Obtained Using the Rammsonde," Journal of Terramechanics, Vol. 29, No. 2, pp. 265-280.

15. Wong, J.Y. (1980), "Data Processing Methodology in the Characterization of the Mechanical Properties of Terrain," Journal of Terramechanics, Vol. 17, No. 1, pp. 13-41.

16. Holmes, C., Hefer, G.J. and Hintze, D. (1987), "The Influence of Shape and Size of a Penetration Body on the Pressure-Sinkage Relationship," Proceedings of the 9th International Conference of the International Society for Terrain-Vehicle Systems, Vol. I, pp. 28-36.

17. Upadhyaya, S.K. (1994), "Determination of Engineering Properties of Soil In-Situ," Proceedings of the Workshop on Modelling the Mechanics of Off-Road Mobility, sponsored by U.S. Army Research Office, Vicksburg, Mississippi, April 5 - 6.

18. Huck, F.B. (1994), "A Case for Improved Soil Models in Tracked Machine Simulations," Proceedings of the Workshop on Modelling the Mechanics of Off-Road Mobility, sponsored by U.S. Army Research Office, Vicksburg, Mississippi, April 5 - 6.

19. Murphy, N.R. Jr., Randolph, D.D. and Ahlvin, R.B. (1993), "Mobility Modelling and Automated Analysis - New Development and Applications," Proceedings of the 11th International Conference of the International Society for Terrain-Vehicle Systems, Vol. I, pp. 44 - 53.

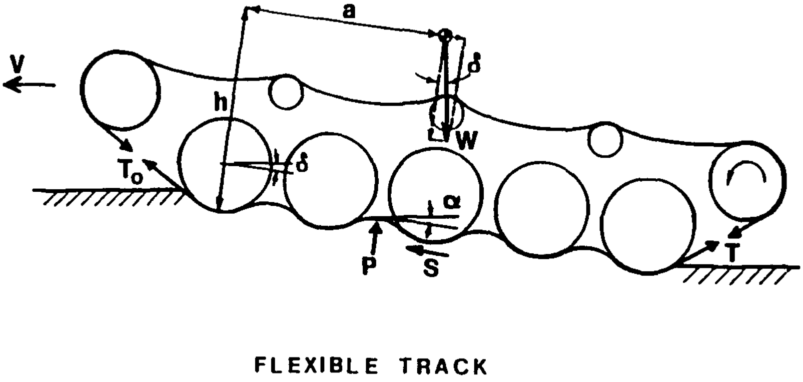
a
V
h
δ
W
δ
T_o
α
P
S
T
FLEXIBLE TRACK

Figure 1. A flexible track model

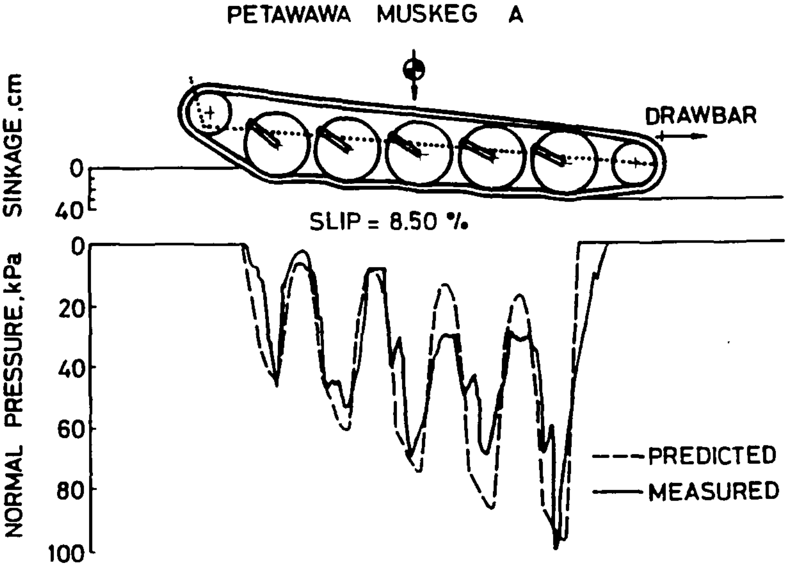

Figure 2. Comparison of the measured and predicted pressure distribution under an M113A1 on a muskeg

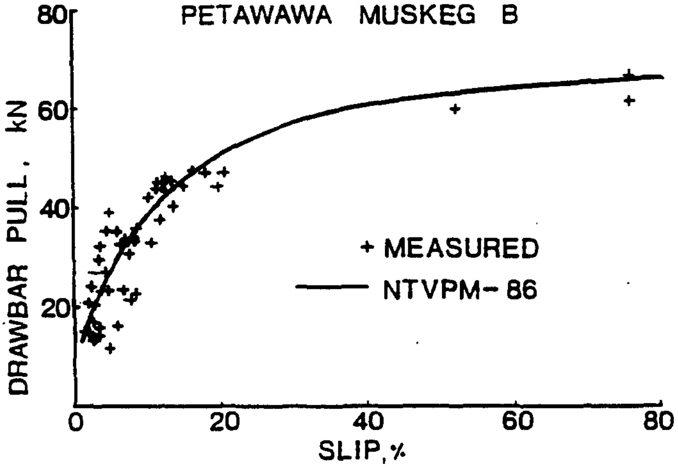

Figure 3. Comparison of the measured and predicted drawbar performance of an M113A1 on a muskeg

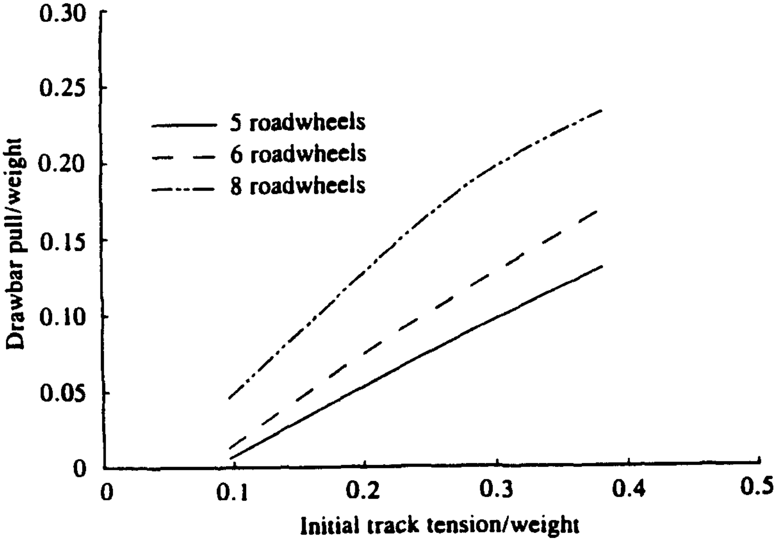

Figure 4. Effects of the number of roadwheels and initial track tension on vehicle performance on a snow

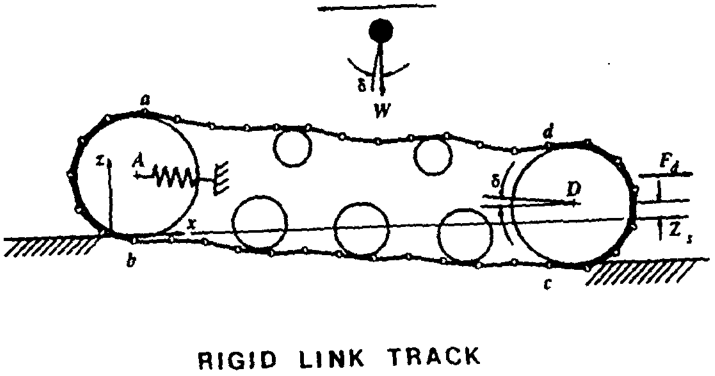
δ
W
a
d
z
A
F_d
δ
D
x
Z_s
b
c
RIGID LINK TRACK

Figure 5. A rigid link track model

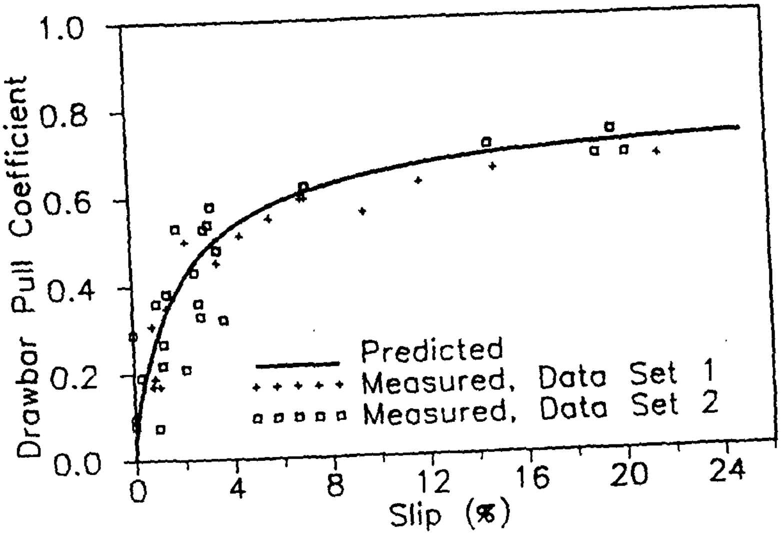

Figure 6. Comparison of the measured and predicted drawbar performance of a tractor on a sandy loam

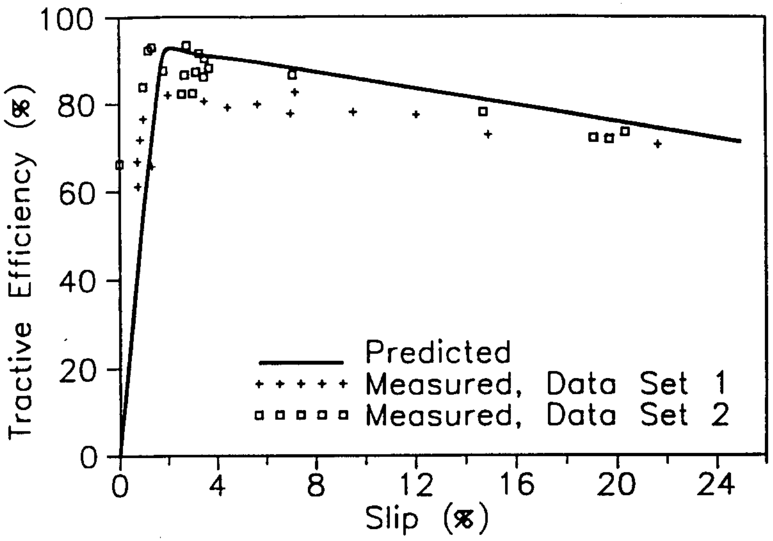

Figure 7. Comparison of the measured and predicted tractive efficiency of a tractor on a sandy loam

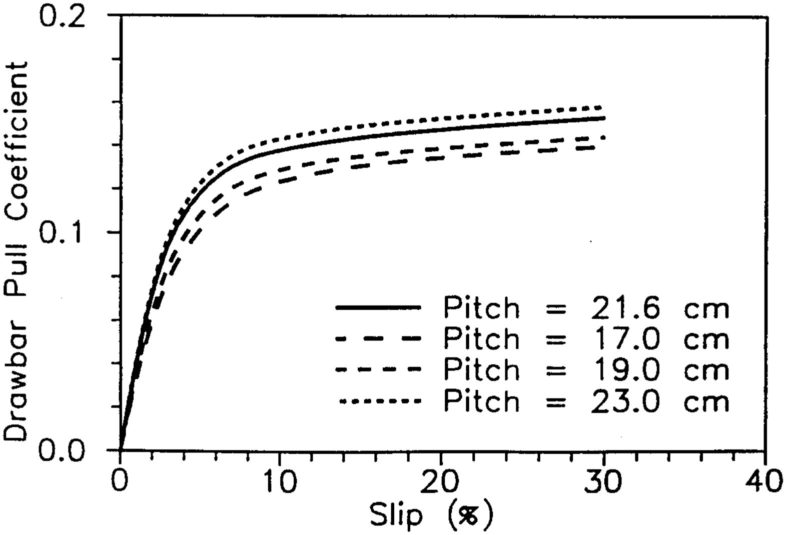

Figure 8. Effects of track pitch on the performance of a tractor on a clayey soil

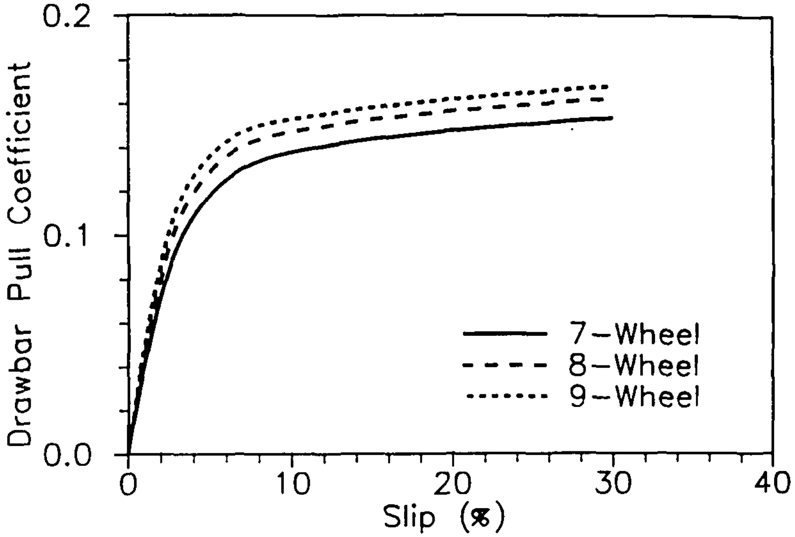

Figure 9. Effects of the number of roadwheels on the performance of a tractor on a clayey soil

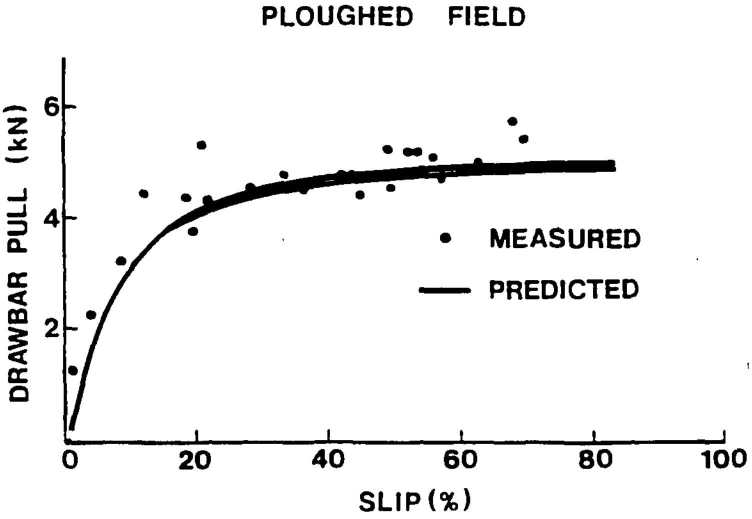

Figure 10. Comparison of the measured and predicted performance of a wheeled tractor on a plowed field

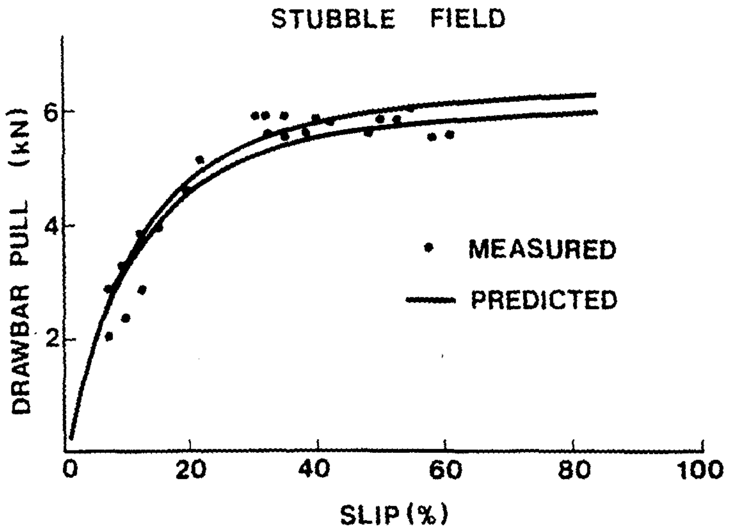

Figure 11. Comparison of the measured and predicted performance of a wheeled tractor on a stubble field

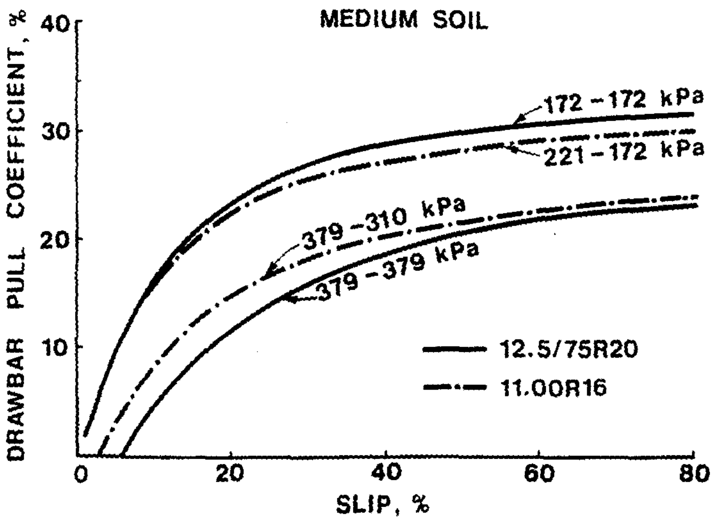

Figure 12. Effects of inflation pressure on the drawbar performance of a two-axle wheeled vehicle on a medium soil

INTERACTION OF VEHICLE AND TERRAIN RESULTS FROM 10 YEARS RESEARCH OF IKK

Ingobert C. Schmid
Institute of Automotive Engineering IKK
- Prof. Dr.-Ing. I.C. Schmid -
University of the Federal Armed Forces Hamburg, Germany

1 INTRODUCTION

The Institute of Automotive Engineering (Institut für Kraftfahrwesen und Kolbenmaschinen IKK) of the University of the Federal Armed Forces Hamburg, moved into newly built laboratories in autumn 1982. After installing and putting into service the test-facilities, IKK could start with research tasks in November 1983. The field of activities covers vehicle dynamics, human aspects of car-driver and passenger, traffic systems, structural mechanics, testing techniques and computer simulation. Terramechanics and terrain vehicles gradually cristallized to become the main field of activities. On the basis of contract research, a program could be developed, in which a spectrum of problems was investigated. Results from the program were presented in 34 papers [1] to [34] on occasion of ISTVS conferences inclusive Vienna 1994. Final results have been subject of a number of doctoral thesis [35] to [40]. In the actual paper a comprehensive survey is given, in order to join together the particular contributions.

2 STARTING POINTS FOR THE IKK-RESEARCH PROGRAM

The central problem of the interaction of wheel/track and soil is considered by one of the following three ways:

1) Analytical Method (M.G. BEKKER School)
   -- physical models for vehicle-soil interaction

- mathematical/physical models for soil properties based on experiments

2) Empirical Method (WES, NRMM)
   - measurement of soil strength CI or RCI
   - mathematical definition of vehicle terrain requirement VCI based on practical experience

3) FINITE ELEMENT Method
   - simulation of vehicle-soil interaction
   - basic soil parameters from experiments.

The first and the second method have been in use for many years and each provides specific advantages for certain applications. Both have proofed giving satisfying results, so that one may think, there is only to apply the methods but nothing more to develop. However, the problems are very complex, many-sided and diverse, and still a lot of unsolved questions exist in understanding and modelling the phenomena. Besides of that there is a gap in practical application of theory to vehicle development and vehicle operation.

The WES-method, based on empirical experience, is easy to handle also in the field, and therefore this method is very valuable for in-situ decisions during tactical missions. On a higher level of sophistication, the NRMM, including the WES-philosophy, is useful for mission planning, however it would be expected too much, to use this model as a tool for vehicle development: A model can satisfy the needs of vehicle development only, if the vehicle parameters, the design-engineer has to destine, are input-parameters for the model. This requirement can be fulfilled only by an analytical model, where the different phenomena are described in detail with equations. Here, in principle the BEKKER-philosophy is the way to go. Of cause, the basic BEKKER-model is not sufficient. Influences, such as elasticity of the tyre (inflation pressure), circumfirencial slip, sinkage due to slip, multipass of the following wheels in the track etc. are to be noticed. Thereon the actual load on each wheel must be considered. The terramechanical phenomena between the tyres and the soil must be integrated into the dynamics of the vehicle: The internal dynamics concern with the drive-line system providing the propulsion torques on the wheels. The external dynamics describe the vehicle motion as a result of the acting forces. All the influences and functions must be modelled, and by joining the detail-models, their interactions are to be simulated in the over-all model.

Such analytical over-all-model for closed loop system simulation with integration of vehicle, terrain and driver was not available so far. Therefore, it was one important goal of the research program, to complete or add the needed models and to integrate these in the new model for driver-vehicle-terrain-system-simulation, which was named the ORIS-Model (Off-Road-Interactive-Simulation).

The Finite Element Method (FEM) is comparatively new for application to the tyre-soil problem. This method is of special advantage, as hereby the deformations of the tyre and of the ground, and consequently the shape of the contact-contour, really are the result of the interaction, whereas in the BEKKER-philosophy the contact-contour is assumed to be section of a circle. Therefore the FEM is suitable especially for clearing up all the phenomena concerning deformations, such as the effect of inflation pressure reduction, or the bulldozing resistance. Additionally FEM provides new possibilities to investigate the pressure transfer onto the ground and into the depth, and therefore on soil compaction.

The Finite Element Method had been introduced early, however problems concerning the real tyre-soil pressure-interaction, the state of real rolling as well as the consideration of plastic soil properties still were unsolved, and therefore the method had been not yet satisfying. All these problems could be overcome by the so-called VENUS-program (VEhicle-NatUre-Simulation), developed in the IKK-research program.

For every model, the soil properties must be known. The input is the soil strength, which is given either by cone-values (CI, RCI) or by BEKKER-soil-coefficients (φ, c, k_c, k_φ, n). These values have to be evaluated by measurements, however they are true only at the time and at the site of their measurement. In nature, however, the soil strength values in a site are diverging stochastically. Furthermore they may be altered by soil cultivation and by vegetation, and additionally they are changing continually within short terms due to climatic influences. Such impacts of agriculture and of nature cause tremendous uncertainties on the actual soil strength.

To face these problems, basic investigations on soil properties seemed to be necessary. The scattering made need for introduction of statistic methods for soil-parameter evaluation. In order to consider the influences of cultivation and of climate-effects on soil strength, influences as that of density and of moisture-content had to be investigated systematically and possibly modelled. And furtheron a model to simulate the influence of climate was necessary, to make calculable the soil changes dependent on the course of the weather-history.

It is a final objective, to calculate trafficability on the basis of geological soil maps, which are stationary for ever, and to consider the actual soil condition due to climate and cultivation, based on model-simulation and statistics. Until this goal will be reached, the research on the taken ways must be continued.

As the soil strength depends on penetration speed, and this means on vehicle speed, the dynamic soil properties, which were not yet known sufficiently, had to be investigated, too.

All the investigations of soil-properties mentioned above were part of the IKK-research program for the benefit of the empirical method as well as of the analytical method.
Besides these points of interest, the turning resistance of tracked vehicles and of wheeled vehicles with skid steering was part of the research program [1, 6, 7, 14, 19, 23, 24, 35, 40]. Another part of the program concerns with the excitation of vehicle oscillations by the irregular surface of the soft soil. However these investigations will not be included in the following survey.

3 SOIL PROPERTY MODELS

3.1 Geological Factors

The strength-properties of a soil at first depend on the type of soil, which can be characterized by the grain size and grain size distribution. In so far the soil at a site in terrain is given in the nature and will not change over long times. Therefore the reality can be documented in soil-maps, fig. 1. However it is much more problematic to describe the soil strength (or the trafficability) in form of a map, because soil strength is influenced essentially by the density and by moisture content, and these can change within short periods.

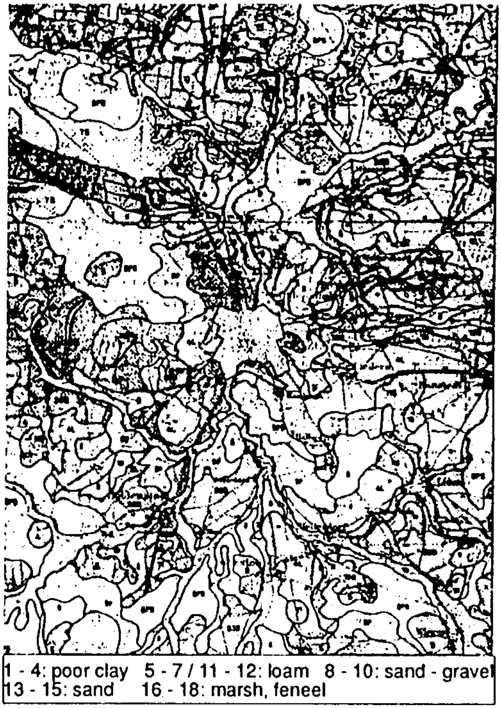
1 - 4: poor clay 5 - 7 / 11 - 12: loam 8 - 10: sand - gravel
13 - 15: sand 16 - 18: marsh, feneel

Fig. 1: Soil map (example)

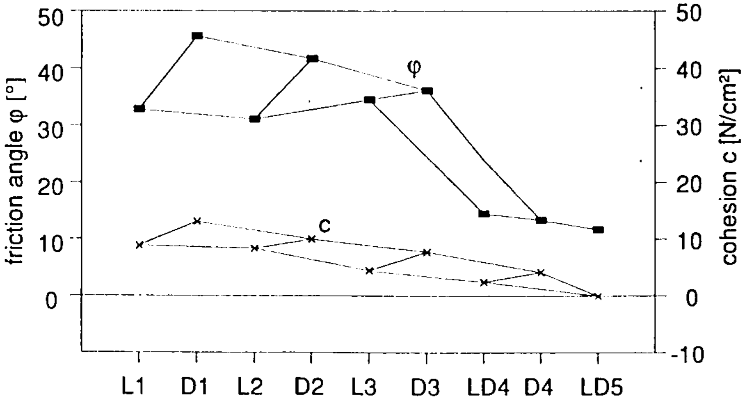

Fig. 2: Influence of density and of water content on angle of internal friction φ and cohesion c of loam

L = low density; D = high density
1, 2, 3, 4, 5 = moisture content level

In order to calculate the strength of the inalterable soil-consistence dependent on the actual physical state of the soil, especially dependent on moisture content and on density, a basic study on the physics of soils with systematic experiments was carried out by WAGNER [36]. The results - with regard to tendencies - were well-known before, however, the goal was to quantify the influences, and to describe them with mathematical models.

As is to be expected, for frictional soils (sand) only density is of considerable influence, whereas the influence of water content is low. However, for cohesive soils both influences are important, and they depend on each other, as is to be seen in fig. 2 by way of example of a certain loam: Higher moisture contents (content level 1 .... 5) result in a decrease of the angle of internal friction and in a decrease of the cohesion. Higher density (D) means higher cohesion as at lower density (L); however regarding the angle of internal friction, a higher density (D) means a higher strength value only for low water-content (content level 1 ...... 3), whereas for wet loam (content level 4 and 5) higher density results in a decrease of the frictional angle. Such sensibility of soils naturally is different for different types of soils. On the basis of the measurements, for the considered soils the influence of density and of water content could be described in mathematical models, so that changes of soil strength due so alternation of moisture content and of density can be calculated.

3.2 Climatic Factors on Soil Strength

The most important impact of nature on soil strength is the climate with rainy and dry, cold and warm periods. Thereon the amount, duration and frequency of precipitation and furthermore of humidity and temperature of the air are very important. Furthermore the ground itself is of influence on the actual moisture-content: the roughness and porosity of the surface, the up- and down-permeability of water, and the level of the ground water. All these factors could be considered by formulas, partly as physical models, partly as mathematical models based on systematic experiments.

By putting together these models, and balancing the **plus** due to daily rainfall and ascension of ground-water, and the **minus** because of evaporation (dependent on air humidity, temperature, wind speed, soil surface and vegetation) and seepage of water into the depth, HINTZE [10, 17, 32, 37] developed a model, with which the changes of moisture content and the changes of soil strength (CI-value) can be calculated.

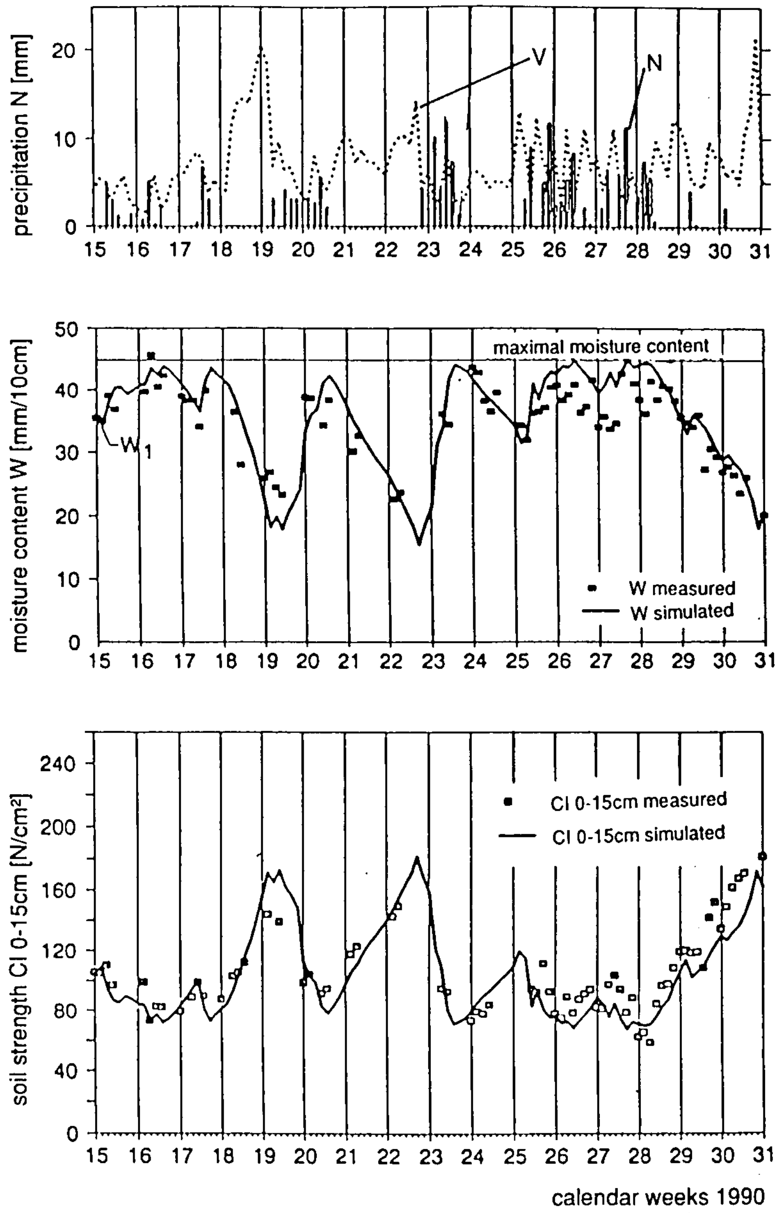

Fig. 3: Climatic influence on moisture content and soil strength - simulation results compared with measurements, loam

The input data for the simulation-model are the moisture content and the CI-value at the beginning, and the current climatic data provided from the regional meteorological office. The model was verified by comparison of simulated results and measurements in terrain over a period of 3 months on several sites. It is astonishing, how well the simulated moisture-content and CI-values correspond to the current measurement-values, which were found independently, fig. 3. The model is a very useful tool, to update measurements of yesterday or to precast the values on the basis of the weather forecast.

3.3 Stochastic Soil Strength

Another fact is, that in nature the soil strength is scattering on a site, as can be seen from the pressure-sinkage-curves measured on a terrain, which seemed to be of regular consistence, fig. 4. Therefore one measured value is not reliable at all, and also a mean-value of few measurements is not trustful. To face this problem, statistic methods have been introduced in the studies by HEIMING, where frequency distribution, mean value and standard deviation, and other characteristics were considered [3, 9, 32].

To manage the great number of measurements, needed for statistic consideration, a special cone-penetrometer was developed by IKK, fig. 5 [16]: A penetrometer as is usual in trade, was equipped with electronic measurement devices for force and sinkage, and with a computer to record and evaluate the measurement-results. The important advantage of the IKK penetrometer is, that the number of measurements, which are still to be carried out, in order to reach the needed width of confidence interval (accuracy) and the wanted confidence coefficient S (reliability), is permanently computed and displayed. The final output is the average value and the standard deviation, and these results - and this is important - are mathematically confident.

The stochastic soil characteristics combined with the application of a mobility model, e.g. NATO Reference Mobility Model, enable a statistic mobility analysis, which will provide higher safety of mobility forecast. fig. 6 shows the principle of the procedure: Based on the sum-frequency distribution of soil strength (result of stochastic soil strength evaluation) and the drawbar pull of a vehicle dependent on soil strength (result from mobility model), the cumulative-frequency distribution of the expected drawbar pull as the characteristic mobility parameter can be followed.

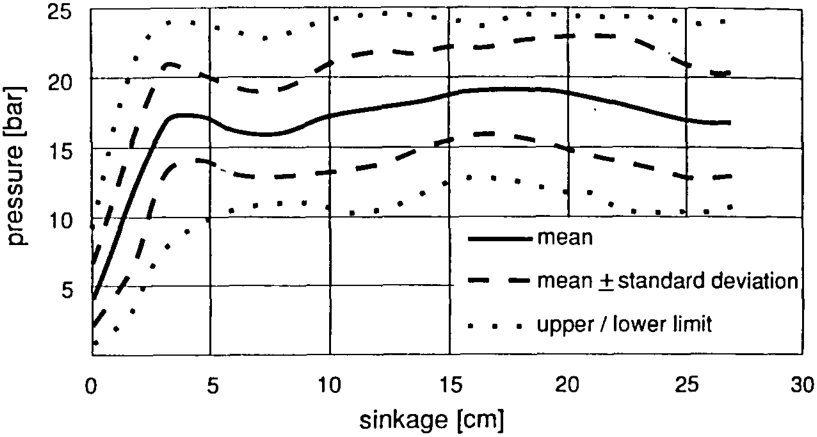

Fig. 4: Scattering of pressure-sinkage-curves on a certain site

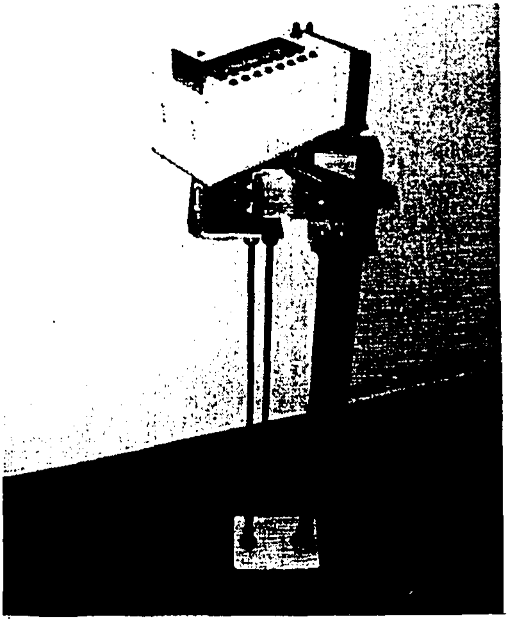

Fig. 5: Cone penetrometer with computer for statistic evaluation of CI-values

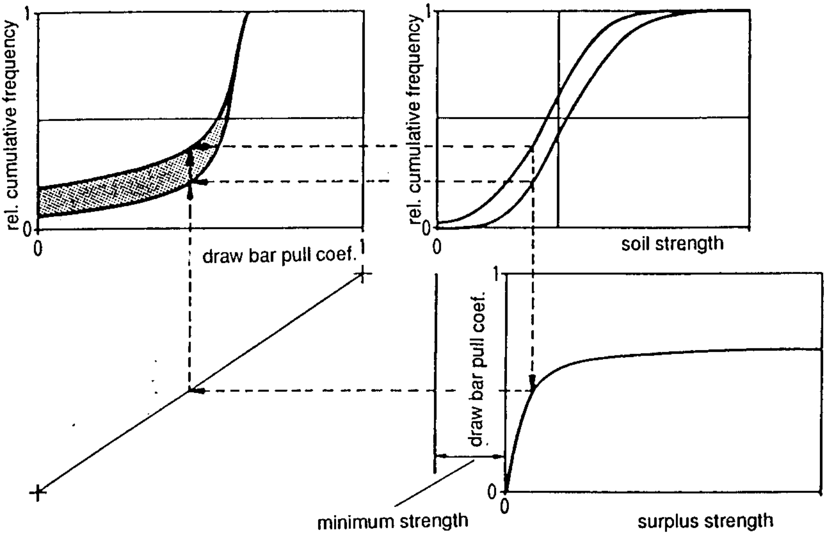
rel. cumulative frequency
1
0
0
draw bar pull coef.
1
rel. cumulative frequency
1
0
0
soil strength
draw bar pull coef.
1
0
0
minimum strength
surplus strength

Fig. 6: Statistic mobility analysis

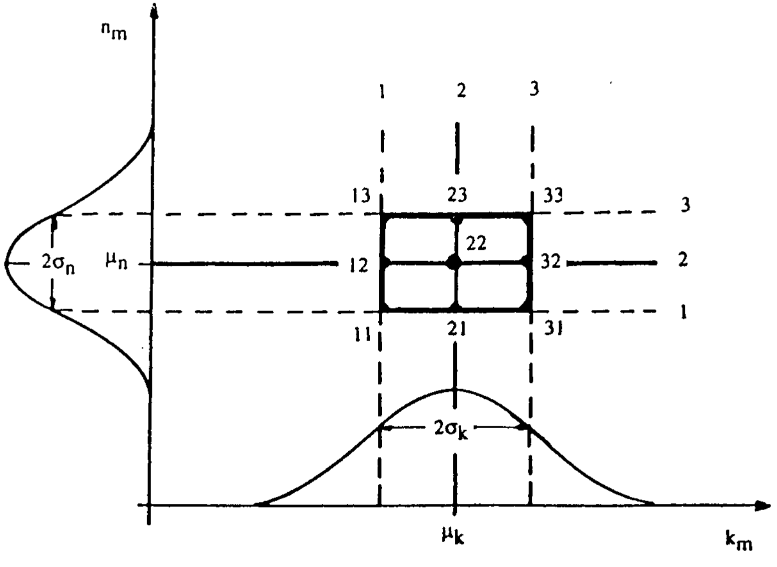
n_m
1
2
3
13
23
33
3
22
$2\sigma_n$
μ_n
12
32
2
11
21
31
1
$2\sigma_k$
μ_k
k_m

Fig. 7: Correlation of soil coefficients n and k

This means that the result of mobility prediction is not purely "GO" or "NO GO" or the "SPEED", but includes also the probability, to which the predicted mobility will be reached.

As experiments have shown, it is very difficult to find a correlation between the different soil parameters. With this regard it is interesting, that LUDEWIG has found, there seems to be a correlation on a stochastic base [41]. This assumption is supported with the results in fig. 7 for the example of n and k (in the equation $p = k \cdot z^n$). Similarly statistic correlations were found between the CI-value and the BEKKER coefficients. These findings, which are a side-product of the investigations, were not followed further on so far. However, in case of a general validation, such experiences could help to reduce the expenditure for experimental terrain evaluation.

3.4 Dynamic Soil Strength

Measurements carried out by GRAHN [4, 12, 39] have shown, that the pressure-sinkage-relationship depends on the penetration-speed: While in a loam, a higher penetration speed leads to higher pressure-values, in sand a higher penetration speed results in lower pressure-values, fig. 8. This dynamic behaviour could be described with mathematical equations. Considering, that the penetration speed of the tyre into the ground depends on driving speed, and furthermore that it is changing along the contact area, GRAHN developed a model to calculate pressure distribution in the tyre-soil contact area. An example of a result is given in fig. 9 for a rigid wheel at a pregiven sinkage on humid loam (16%): As can be seen, the vehicle speed essentially influences the pressure distribution. The maximum pressure, which is expected under the wheel, due to dynamic soil effects, here is shifted further in front when speed is increased. Because of these influences on the pressure and on its distribution, the sinkage z_0 of a freely rolling wheel is decreasing with higher vehicle speed; therefore the rolling resistance becomes smaller. This effect is stronger, if the moisture content is higher, and it is weaker, if the moisture content is lower. It should be noted, that on sand the effects are quite different from loam (see fig. 8).

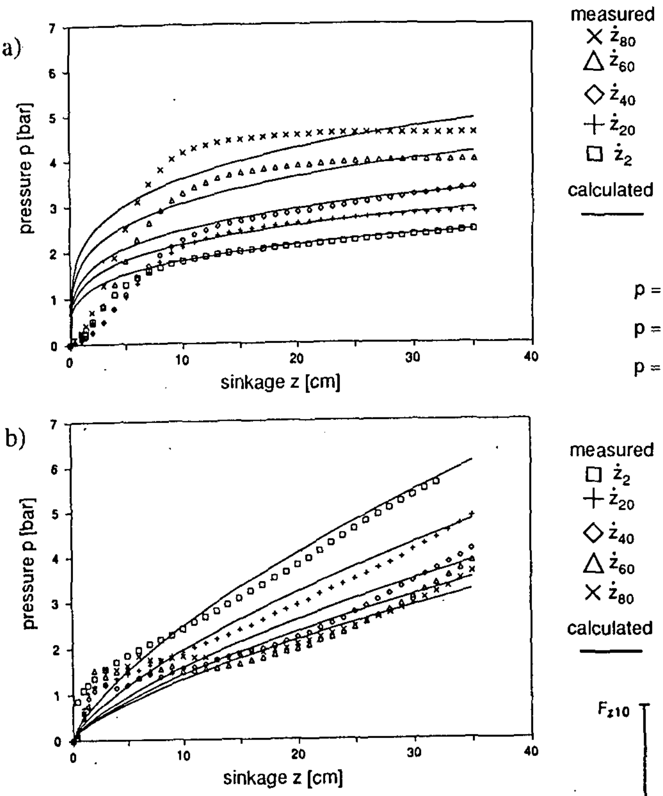

$$p = k \cdot z^n$$

$$p = p_{stat} + p_{dyn}$$

$$p = (k_{stat} + k_{dyn}) \cdot z^n$$

Fig. 8: Influence of penetration speed (of round plate 600 cm²) on pressure-sinkage-curves

a) loam with 16% moisture content
b) sand with 5% moisture content

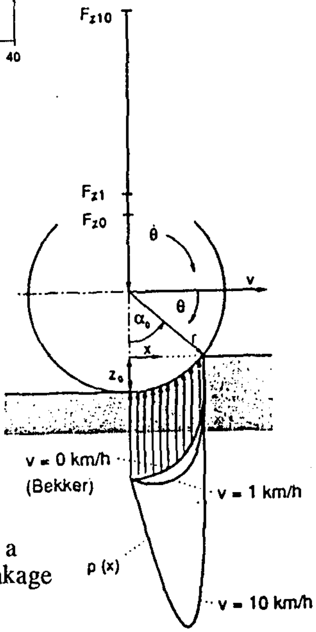
F_{z10}
F_{z1}
F_{z0}
$\dot{\theta}$
v
θ
α_0
r
x
z_0
v = 0 km/h
(Bekker)
v = 1 km/h
p (x)
v = 10 km/h

Fig. 9: Pressure distribution (calculated) under a wheel and wheel-load with pregiven sinkage dependent on rolling speed, loam with 16% moisture content

4 ANALYTICAL MODELS FOR TYRE-SOIL INTERACTION

4.1 Parabolic Tyre-Soil-Contact Contour

A central problem of tyre-soil interaction is the pressure distribution along the contact area. It depends on the local deformations of the ground, which are described by the tyre-soil-contact-contour. While the maximum sinkage z_0 results from the equilibrium condition of wheel load and pressures, the type of shape of the contact contour is an assumption in all the analytical models, fig. 10. In the most simple case (a), the contact contour consists of the section of a circle and a straight horizontal secant. A better approach (b) is to replace the elastic tyre (D) by a bigger rigid wheel (D *> D) within the area of ground-contact.

SCHMID recently proposed assumption of a parabolic shape of the contour (c) [21, 42]. The parabolic model approximates the circle-section (D*) very tightly, and allows a much more elegant mathematical treatment, because there is no necessity for cut-away terms in a mathematical row, as is in case of the circle-section (D*). The equations of the parabolic model are given in fig. 11.

4.2 Surrogate Wheel Diameter D*

The principle idea, to replace the elastic tyre (D) by a rigid wheel with a bigger diameter (D*) was originated by M.G. BEKKER, and SOEHNE at first gave an equation for D*. However, the exact geometry SOEHNE has considered, results in a complex formula, and the need of input data to be estimated.

Therefore SCHMID proposed a much easier equation [21, 42} neglecting the relaxation of the soil behind the wheel. This assumption is a reasonable simplification as can be seen from fig. 12.

4.3 Tyre Inflation Pressure

Tyre inflation pressure control is a very effective method to enlarge contact area and to improve mobility (It is an alternative to a big wheel-diameter). A decrease of the inflation pressure results in larger length L of the contact area and larger tyre deformation f_k, as can be seen from the tyre spring characteristics, fig. 13.

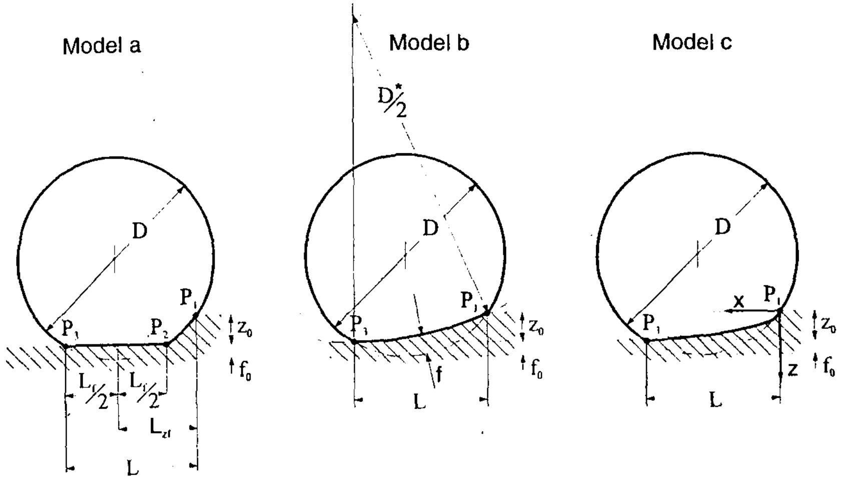
Model a
Model b
Model c
D
D
D
D*/2
P1
P2
P1
P1
P1
P1
x
z0
z0
z0
f0
f0
f0
Lf/2
Lf/2
Lzf
L
L
L
f
z

Fig. 10: Optional models for the contact geometry between elastic tyre and soft ground

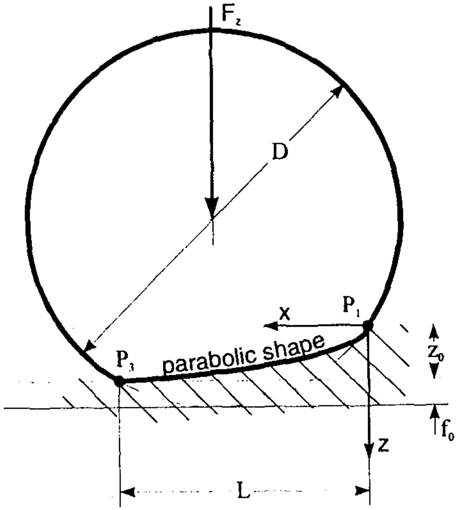
Fz
D
x
P1
P3
parabolic shape
z0
f0
z
L

$$z(x) = \frac{z_0}{\sqrt{L}} \cdot x^{\frac{1}{2}}$$

$$p(x) = k \cdot \left(\frac{z_0}{\sqrt{L}}\right)^n \cdot x^{\frac{n}{2}}$$

$$L \approx \sqrt{D^* \cdot z_0}$$

$$z_0 \approx \sqrt[2 \cdot n+1]{\left[\frac{F_z \cdot \left(\frac{n}{2}+1\right)}{B \cdot \sqrt{D^*} \cdot k}\right]^2}$$

Fig. 11: Parabolic model for the contact contour

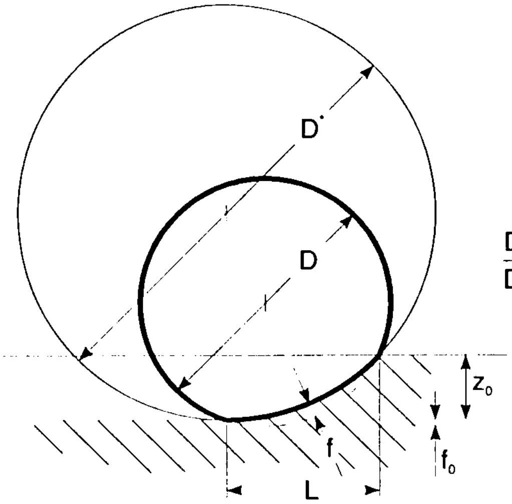

$$\frac{D^*}{D} \approx \left[\sqrt{1 + \frac{f_0}{z_0}} + \sqrt{\frac{f_0}{z_0}} \right]^2$$

Fig. 12: Surrogate-diameter-model for the elastic tyre

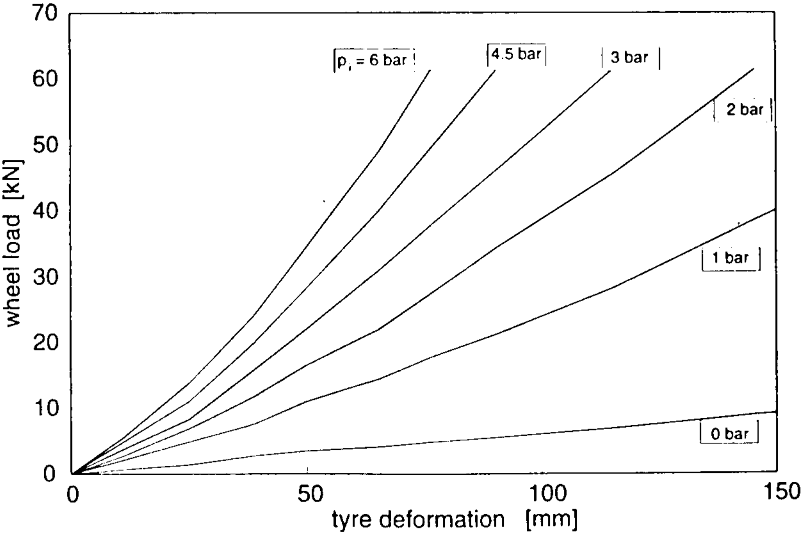

Fig. 13: Spring characteristics of the tyre 14-R-20 mil
for different inflation pressures

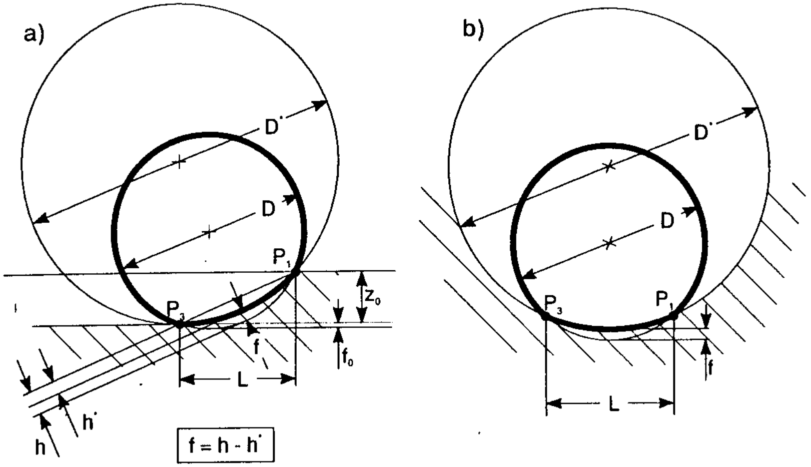
a)
D*
D
P1
P3
z0
f
f0
L
h
h*
f = h - h*
b)
D*
D
P3
P1
f
L

a) Elastic tyre on soft ground b) Elastic tyre in an inside-surface-drum

Fig. 14: Analogue geometry

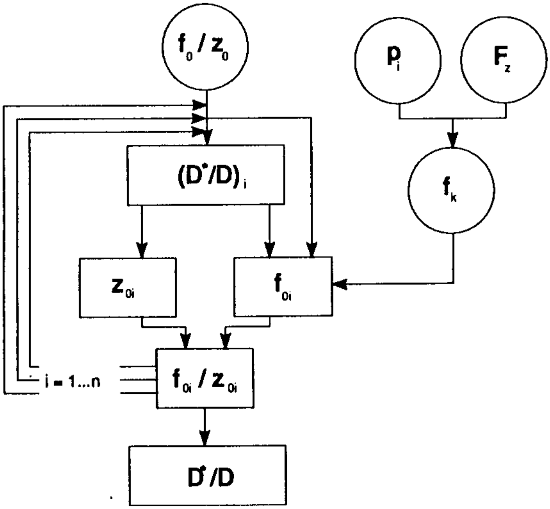
f0 / z0
pi
Fz
(D*/D)i
fk
z0i
f0i
i = 1...n
f0i / z0i
D*/D

Fig. 15: Programmed procedure to calculate D^*/D iteratively

The problem is, to transfer the tyre deformation f_k measured on a flat and rigid surface to the conditions on the soft soil. For this transfer, SCHMID developed a model [26], which makes use of the analogy, that the elastic wheel (D) in soft soil, replaced by a surrogate wheel (D* > D), shows the same geometry like an elastic wheel (D) in an inside test drum with diameter D*, fig. 14. For the latter case equations are known to transfer the tyre deformation f on the bended surface of the drum to the tyre deformation f_k on the flat road. These equations can help also to derive the tyre deformation f on soft ground from the tyre deformation f_k, given in the usual spring characteristics of the tyre. With the equations in fig. 14 and with the tyre spring characteristics, the diameter D* is calculated iteratively, fig. 15. Thereon the inflation pressure can be selected, and in such a way the effect of tyre inflation pressure control can be calculated.

4.4 Multipass

In the trace, produced by a wheel which had rolled over virginal ground, the soil properties were changed essentially, so that the wheel of the following vehicle-axle will find conditions quite different from those of the first wheel. HOLM [27, 43] had developed at first a model for the multipass, where new parameters of the compacted soil were used, which had to be generated by computation.

It is known, however, that the original pressure-sinkage-curve will be reached again after relaxation, when a repeated load with increased pressures is applied, fig. 16. Therefore, in principle, the original soil parameters k and n are still valid and there is no need to calculate new soil parameters. This was considered in a multipass model developed by SCHMID and LUDEWIG, which - using the parabolic formulation for the contact contour, allows to calculate the additional sinkage Δz of following wheels in a trace, fig. 17. This way of calculation always works well for the multipass of rigid wheels, and also for tyres on very soft soils. For elastic tyres on compacted hard ground in the trace, there may occur problems, because the calculation of the additional sinkage Δz requires an iterative process, which does not converge, if $\Delta z \rightarrow 0$, $D^* \rightarrow \infty$.

If the soil for the multipassing wheel is hard and the conditions are close to those of a tyre on a rigid road, where the pressure distribution in the contact area only depends on the tyre deformation but not on deformation of the ground, there are adequate phenomena to be considered and this requires an approach different from the way above:

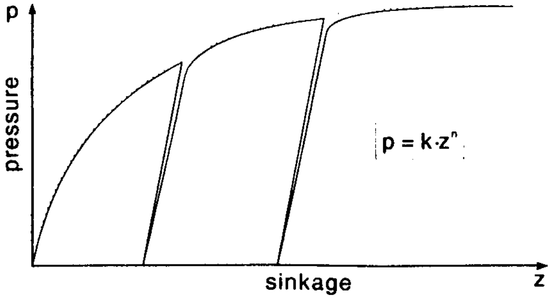

Fig. 16: Effect of multiload on pressure-sinkage relationship

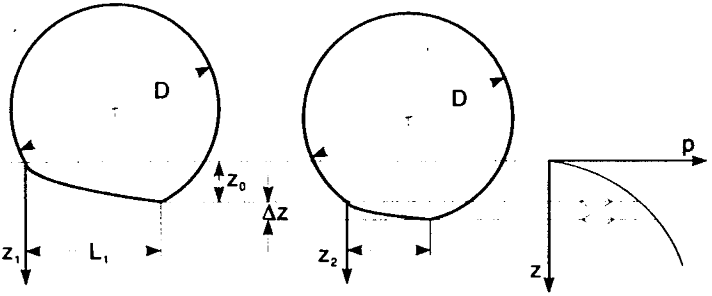

$$\Delta z \approx \frac{F_z^2}{\left(1+\frac{2}{3}\cdot n\cdot\frac{\Delta z}{z_0}\right)^2\cdot B^2\cdot k^2\cdot z_0^{2\cdot n}\cdot\frac{D^*}{D}\cdot D}$$

Fig. 17: Additional sinkage Δz due to multipass with wheel-load F_z

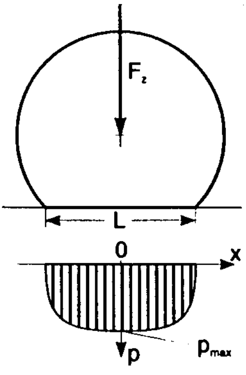

$$p(x) = p_{max}\cdot\left(1-\frac{16}{L^4}\cdot x^4\right)$$

$$p_{max} = 1{,}25\cdot\frac{F_z}{L\cdot B}$$

Fig. 18: Pressure distribution in the contact area of a tyre on rigid road surface

SCHMID and LUDEWIG therefore assumed for the multipassing elastic wheel at first similar pressure and equal contact area as on the rigid road surface. For this assumption according to experience the pressure distribution can be described by a parabolic curve, fig. 18. In such a case the maximum pressure is 25% higher than the average pressure. As is given in the figure, a simple equation for the additional sinkage Δz is obtained on this way. If necessary, the accuracy can be improved by iterative correction of the size of contact area due to sinkage and due to change of tyre deformation.

5 ORIS - OFF ROAD INTERACTIVE SIMULATION

5.1 Requirements

The final goal is, to develop a comprehensive simulation computer-program as a tool for terrain-vehicle-system-development. Thereby all the parameters, the designing engineer can dispose of, must be individually included, as far as they are of influence on vehicle-terrain interaction. Besides dimensions of the vehicle, and especially of the tyre, the effect of inflation pressure control, the influence of the suspension on the wheel-loads, furthermore the engine power-, the clutch- and the torque converter characteristics, the gear steps, the possibilities to optimize the algorithms for automatic gear-changing, the effect of lock up of the differentials or of slip control of the differentials, the effect of propulsion slip control, all these factors must be considered in the desired development tool. It is evident, that those sophisticated requirements cannot be fulfilled by an empirical approach, such as the NATO Reference Mobility Model NRMM. For the intended propose detailed models are needed. Therefore IKK extended the physical philosophy, and put together the individual models in the Off Road Interactive Simulation-program ORIS. This simulation system was worked out by RUFF and JACOBS [20, 25, 31].

5.2 Model Concept

The model simulates the interactions in the system "vehicle-terrain-driver" fig. 19. The concept of ORIS is modular; it consists of sub models, describing the functions and the phenomena.

The components of the model are shown in fig. 20.
The mechanical structure and function of the DRIVE-LINE, consisting of the engine, torque converter with a clutch, the gears, central differential and axle differentials with lock-up and wheel-drive-gears, is depicted accurately. Changing of the gears and dynamic effects due to the inertia of rotating masses are considered there on. The drive-line model is combined with the complex WHEEL-SOIL-INTERACTION model, which considers the elastic tyre, the inflation pressure, the multipass, slip-sinkage. The VEHICLE DYNAMICS model simulates the motion of the vehicle as well as the rotational motion of the wheels, and also the actual load on each wheel.

The TERRAIN is integrated in the simulation as a digital map of a section of nature. In the map the height-levels and the local soil parameters according to the type and state of the soil are registered. These data are available from geological authorities in Germany in digitalized form, so that the terrain-section can be selected and exchanged quickly. Lateron it will become possible, to simulate the alterations of the soil parameters due to the impact of the climate by coupling the model by HINTZE [31, 37], so that also the influence of the weather on mobility can be regarded.

5.3 ORIS - Utilization

The vehicle is operated interactively on a vehicle-driver-INTERFACE. The driver can see the motion of his vehicle in the map on a monitor, and he can handle the vehicle by steering, speeding up or braking, changing the gears and so on. All the important functions and phenomena are computed in the background (DRIVE LINE, WHEEL-SOIL INTERACTION, VEHICLE DYNAMICS).

The special advantage is, that it is possible to view into the system and observe the OPERATIONAL DATA, for instance the actual traction and the resistance of any wheel, the wheel loads, the slip on each of the wheels, the slip in the differentials and in the gear-changing clutches, or the rotational speeds of the pumps and the turbine of the torque-converter etc. Examples of results are to be seen in fig. 21. It is also possible to simulate the fuel consumption or exhaust emissions. Many of the processes in the vehicle-terrain system, which are measured today in expensive field-tests on a prototype, now can be studied by means of simulation.

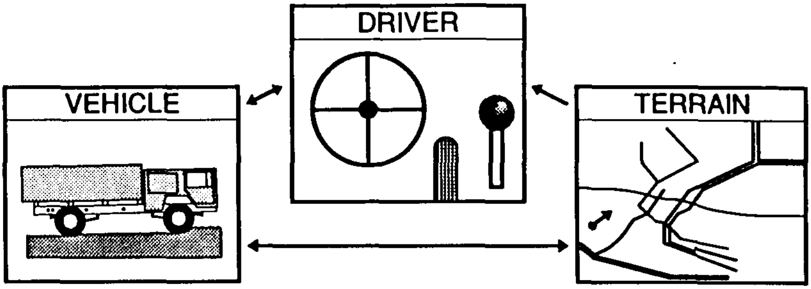
DRIVER
VEHICLE
TERRAIN

Fig. 19: Simulation System ORIS

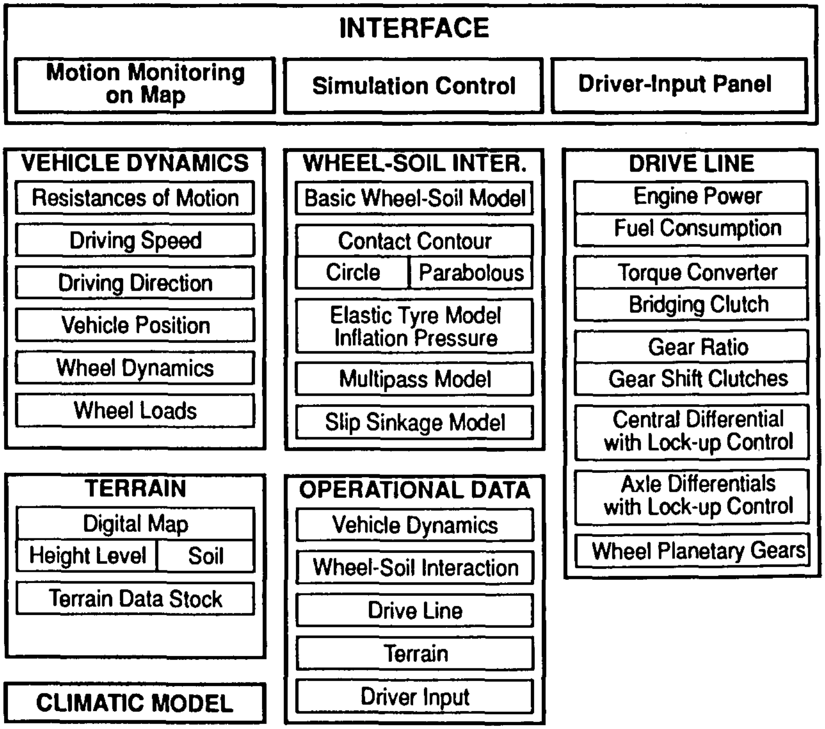
INTERFACE
Motion Monitoring on Map
Simulation Control
Driver-Input Panel
VEHICLE DYNAMICS
Resistances of Motion
Driving Speed
Driving Direction
Vehicle Position
Wheel Dynamics
Wheel Loads
WHEEL-SOIL INTER.
Basic Wheel-Soil Model
Contact Contour
Circle
Parabolous
Elastic Tyre Model Inflation Pressure
Multipass Model
Slip Sinkage Model
DRIVE LINE
Engine Power
Fuel Consumption
Torque Converter
Bridging Clutch
Gear Ratio
Gear Shift Clutches
Central Differential with Lock-up Control
Axle Differentials with Lock-up Control
Wheel Planetary Gears
TERRAIN
Digital Map
Height Level
Soil
Terrain Data Stock
OPERATIONAL DATA
Vehicle Dynamics
Wheel-Soil Interaction
Drive Line
Terrain
Driver Input
CLIMATIC MODEL

Fig. 20: Modules in the ORIS-program

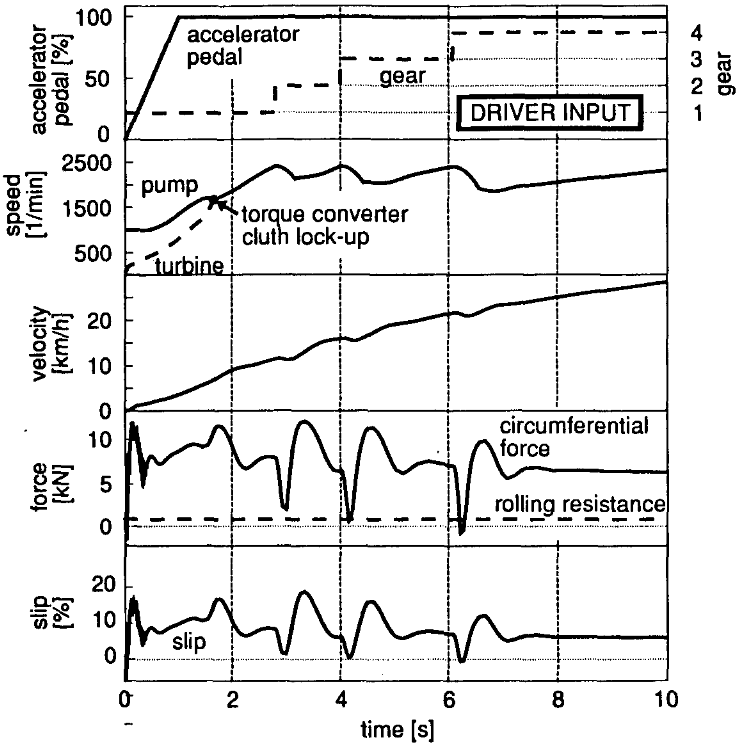

Fig. 21: Examples of operational data from ORIS-simulation (forces and slip on the rear wheels)

ORIS will enable to simulate real missions of military vehicles as well as real applications of constructional or agricultural vehicles and machinery, in order to find the best vehicle concept or to find the most economic route, and to optimize other mission parameters such as the needed time, fuel consumption, loads onto the drive-line-components, wear of the tyres, maintenance-and service-cost. Therefore ORIS is considered to be a most sophisticated tool for vehicle development, and for optimal mission planning.

6 FINITE ELEMENT METHOD IN TERRAMECHANICS

6.1 INTRODUCTION of the FE-Method

The **analytical** models known so far presume a certain geometry of the contact contour between tyre and soil, for instance "section of a circle" in case of the BEKKER-formulation. Such assumption is an estimation, but does not meet the fact, that the geometry of the contact area results from deformation of the tyre and deformation of soil due to the interaction of both. In order to consider the real phenomena by means of a physical model, the Finite Element Method (FEM) seemed to be useful. First steps to use FEM for the wheel-soil-problem were gone by PERUMBRAL et. al. as early as 1971 and by YONG et. al. in 1976, however the real interaction of an elastic tyre and the soil, and especially the rolling process, has been successfully developed by AUBEL [15, 28, 30] at the IKK during the last years:

6.2 The FEM-Simulation Program VENUS

The FE-model developed was called VENUS, as abbreviation for VEhicle NatUre Simulation. It consists of sub models for the soil, for the tyre and for the interaction of soil and the rolling tyre, fig. 22.

In the soil-model, the soil has elasto-plastic properties, and the strength-limits in the three-dimensional state of stress defined by DRUCKER-PRAGER, fig. 23, were considered (The MOHR-COULOMB-conditions are not convenient here). On this basis the FE-soil-model can be applied not only for frictional soils, but - with certain modification - also for cohesive soils. In the tyre-model, the tyre is considered to consist of three concentric rings (tread, carcass, wheel-rim), each of which is homogenous and possesses certain elastic properties.

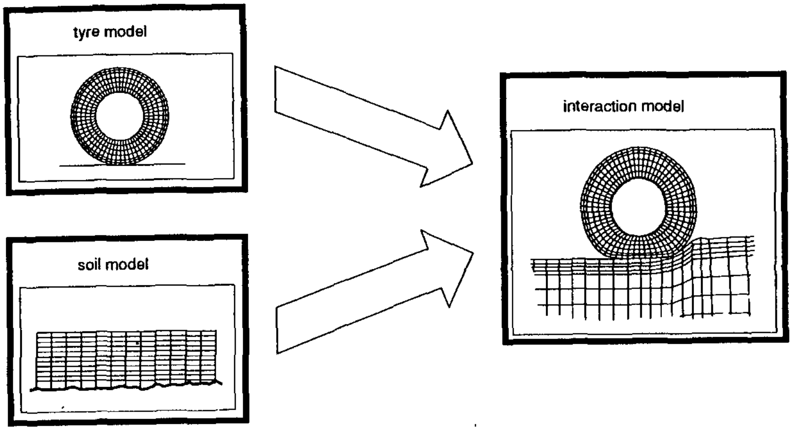
tyre model
soil model
interaction model

Fig. 22: FE-simulation system VENUS

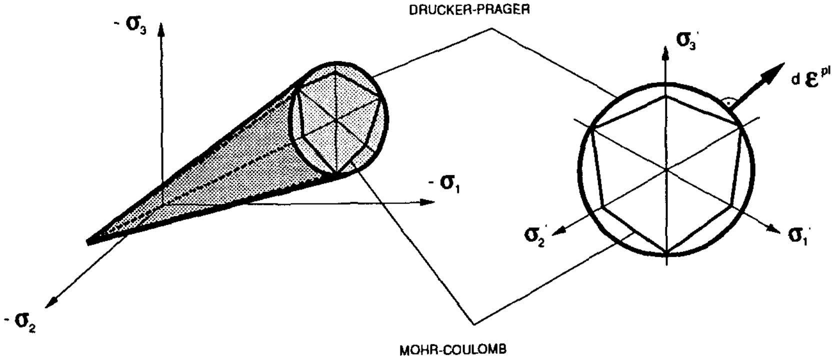
DRUCKER-PRAGER
$-\sigma_3$
$-\sigma_1$
$-\sigma_2$
σ_3'
$d\,\varepsilon^{pl}$
σ_2'
σ_1'
MOHR-COULOMB

Fig. 23: Yield surface by DRUCKER-PRAGER and by MOHR-COULOMB

This tyre-model represents the tyre in the actual problem sufficiently. The interaction-model considers the conditions of contact, especially during rolling without and with circumferential slip.

With this model the deformations of the soil and the deformations of the tyre, and therefore the shape and size of the contact area are a result of the simulated interaction, fig. 24. Sinkage, rolling resistance and circumferential force as well as circumferential slip can be computed. Influences like those of wheel-load, tyre dimensions, inflation pressure-propulsion torque on the wheels, furthermore the effects of soil-strength and of ground structure (layers with different soil properties) can be studied. It is possible, to calculate the deformations of the tyre and of the soil. Not only the vertical deformations, but also the horizontal deformations of the ground can be observed under the wheel as well as in front of the contact area and behind it. Of quite special interest is the bulldozing effect. Studies with the VENUS-program could give information on the formation of the bulldozing effect, clear up the bulldozing contribution to the rolling resistance, and demonstrate the possibilities to avoid the bulldozing resistance.

It is also very important, that VENUS allows the simulation of the effects of traffic on the ground, especially the ground-deformation of the surface and the ground-deformation and pressure-distribution in the depth of the ground, fig. 25. Therefore, the VENUS-program will be very useful for environmental investigations on soil compaction with regard to the growth of plants or with regard to the water-household. Another interesting possibility is to investigate the forces on roots of plants (forest-trees) and the damages as a consequence of traffic in terrain.

6.3 FEM-Simulation of Tyre-Profile-Effects

In the VENUS-program, at first, the tyre-profile was not regarded. As a step of further program-development, the tyre profile as an important factor is taken into account in the investigations by FERVERS [34]. One of the problems was a suitable discretisation especially of the ground, but also of the tyre, in order to depict the fineness of the object. So far, the model-development was of primary interest, and the simulations aimed at demonstration of the phenomena in principle. Systematic investigations to find out an optimal profile for different soils were not carried out yet.

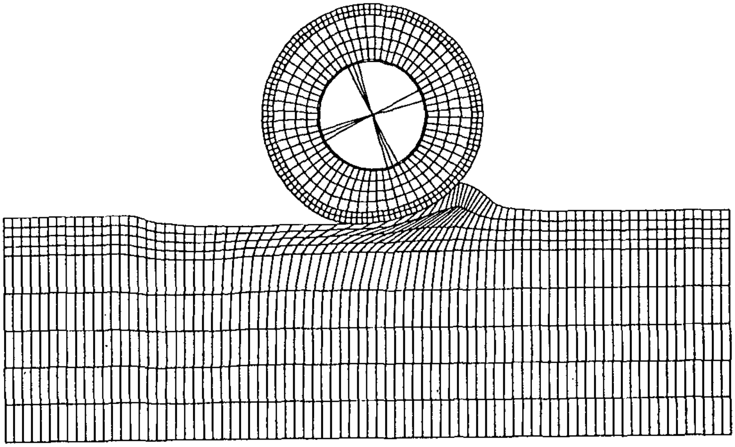

Fig. 24: FE-simulation of a rolling tyre on soft soil (VENUS)

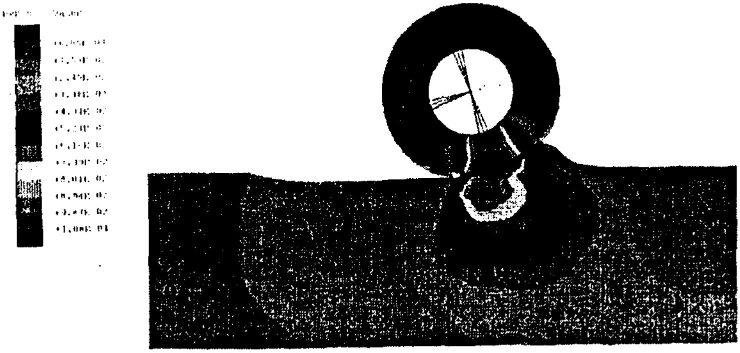

Fig. 25: Pressure distribution in the ground (and stress in the tyre) simulated with VENUS

As can be seen in fig. 26, the simulation works well and the tyre, rolling without circumferential slip, leaves clear profile traces in the track. When slip does occur, the impression is deformed and disturbed. The additional sinkage due to slip could already be simulated and the traction-slip characteristics could be evaluated. Different geometry of the profile were simulated in first attempts, and it could be shown by the FE-simulation, that the profile involves effects on circumferential force, on rolling resistance, on sinkage and even on the bulldozing wave.

6.4 FEM-Simulation of Slope-Stability

One domain, terramechanics for terrain vehicle systems was not yet concerned with so far, is the stability of steep slopes. The problem arises for instance, when a vehicle is approaching a deep excavation at a building site, or when a mobile military bridge is laid on an unstabilized steep embankment. In such a case, there is the danger, that the soil will break and the slope will slide down. At IKK FERVERS developed the Finite Element Method for use on this problem [44]. Examples of results from the FE-simulation are given in fig. 27:

The figure (A) shows a case, where the support of a military bridge causes an external load onto the slope. Here the maximum equivalent plastic strain occurs right up above at the edge of the support-contact-area. The region, in which the fracture will happen, is to be seen from the course of the equivalent plastic strain curves.

The figure (B) shows, what happens, when a steep and high slope does not have sufficient soil strength and the weight of the soil material causes the fracture. The equivalent plastic strain, indicated by the curves in the diagram, here show their maximum values at the bottom of the slope. This indicates, that in this case the fracture will start there.

In civil engineering, empirical methods based on experience are used so far, to calculate the stability of slopes. It is interesting, however, that the region of fracture assumed thereby, is very close to that, simulated with the Finite Element program.

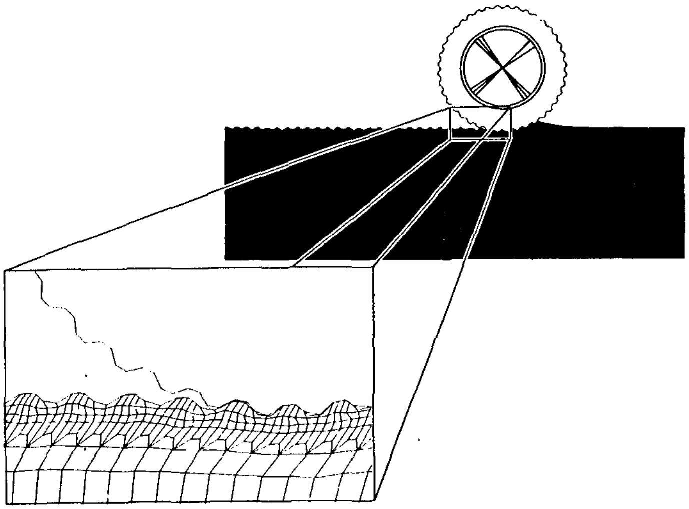

Fig. 26: FE-simulation of the profile-effect for a tyre on soft ground

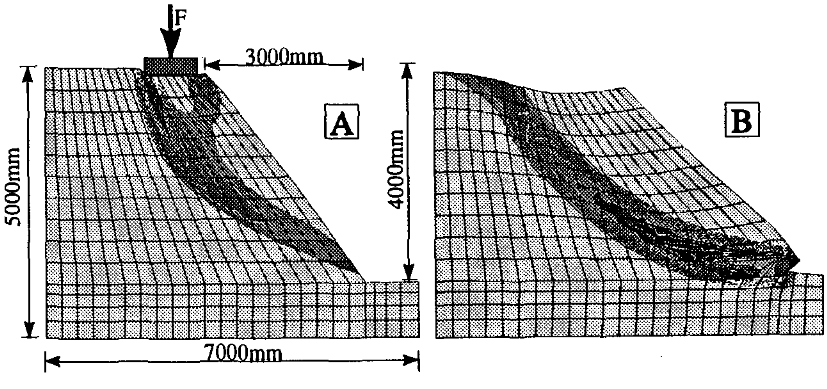
F
3000mm
A
4000mm
5000mm
B
7000mm

Fig. 27: FE-simulation of equivalent plastic strain on a steep slope

A: Reaction due to external load
B: Reaction due to own weight of ground at low soil strength

7. SUMMARY

The IKK Research Program comprises

- experimental evaluation of terrain data
  and formulation of analytical models for soil properties

- development of models for the different soil-wheel interactions

- development of a high sophisticated model ORIS
  for Off-Road-Interactive-Simulation of the driver-vehicle-terrain system
  and the utilization for vehicle development and mission optimization

- development of Finite Element Methods, e.g. VENUS,
  and their utilization for multiple terramechanical problems

With the achievements, the team of scientists of the Institute of Automotive Engineering of the University of the Federal Armed Forces Hamburg (IKK) could contribute essentially to the state of the art.

It is the nature of science-development, that problems are recognized to be important and treated by several institutions in the world often at the same time. Also in case of the IKK-research program, some problems may have been investigated in parallel by others. This indicates the actuality of the research program, and gives the chance of discussion and cooperation between the different scientist groups in the world, to ensure the new pieces of knowledge.

REFERENCES

[1] I.C. Schmid: Simulation of Tracked Vehicles' Field Operations on the PAISI Test Stand System, 8th International Conference ISTVS, Cambridge, 1984

[2] C. Holm, G.J. Hefer, D. Hintze: The influence of shape and size of a penetrometer body on the pressure-sinkage relationship, 9th International Conference ISTVS, Barcelona, Spain, 31st August - 4th September, 1987

[3] G.W. Heiming: Statistical procedures for evaluation of terrain measuring data, 9th International Conference ISTVS, Barcelona, Spain, 31st August - 4th September, 1987

[4] M. Grahn: Investigation of the influence of penetration velocity on the pressure/sinkage relationship, 9th International Conference ISTVS, Barcelona, Spain, 31st August - 4th September, 1987

[5] B. Hug: Grundsatzuntersuchungen für das Überwinden von Gewässern, 9th International Conference ISTVS, Barcelona, Spain, 31st August - 4th September, 1987

[6] I.C. Schmid: Some aspects on high mobility development of tracked vehicles, 9th International Conference ISTVS, Barcelona, Spain, 31st August - 4th September, 1987

[7] I.C. Schmid, W. Ehlert, St. Pott: Mobility of tracked Vehicles and Simulation of the dynamics of motion on the PAISI Test Plant, 22th FISITA-Congress, ISTVS-Session, SAE 885114, Detroit, USA, Sept. 25-30, 1988

[8] M. Grahn: The influence of penetration velocity on the pressure sinkage relationship, 4th European Conference ISTVS, Wageningen, The Netherlands, 21-23rd March, 1989

[9] G.W. Heiming: Statistical mobility analysis, 4th European Conference ISTVS, Wageningen, The Netherlands, 21-23rd March, 1989

[10] D. Hintze: The influence of seasonal moisture changes on soil strength, 10th International Conference ISTVS, Kobe, Japan, Aug. 20-24, 1990

[11] C. Holm, M. Grahn, G. Heiming: A comparison of experimental and theoretical investigations of motion resistance and drawbar pull for vehicles in soft soil, 10th International Conference ISTVS, Kobe, Japan, Aug. 20-24, 1990

[12] M. Grahn: Prediction of sinkage and rolling resistance for off-the-road vehicles considering penetration velocity, 10th International Conference ISTVS, Kobe, Japan, Aug. 20-24, 1990

[13] G.J. Hefer: The influence of vibratory compaction on soil strength and trafficability, 10th International Conference ISTVS, Kobe, Japan, Aug. 20-24, 1990

[14] W. Ehlert, B. Hug, I.C. Schmid: Field measurements and analytical models as basis of test stand simulation of the turning resistance of tracked vehicles, 10th International Conference ISTVS, Kobe, Japan, Aug. 20-24, 1990

[15] Th. Aubel: Application of the Finite-Element Method on soil mechanical processes, 5th European Conference ISTVS, Budapest, Ungarn, Sept. 4-6, 1991

[16] G.J. Hefer, G.W. Heiming: Automatic data recording and in situ statistical survey of cone penetrometer tests, 5th European Conference ISTVS, Budapest, Ungarn, Sept. 4-6, 1991

[17] D. Hintze: The prediction of soil strength with the aid of climatic data, 5th European Conference ISTVS, Budapest, Ungarn, Sept. 4-6, 1991

[18] I.C. Holm, I.C. Schmid: A modulated carrier-concept for army-engineer equipment, 5th European Conference ISTVS, Budapest, Ungarn, Sept. 4-6, 1991

[19] St. Pott: Friction between rubber track pads and ground surface with regard to the turning resistance of tracked vehicles, 5th European Conference ISTVS, Budapest, Ungarn, Sept. 4-6, 1991

[20] K. Ruff: Interactive simulation of the driver-vehicle-terrain-system, 5th European Conference ISTVS, Budapest, Ungarn, Sept. 4-6, 1991

[21] I.C. Schmid, J. Ludewig: Improved calculation of sinkage of a wheel on soft ground, 5th European Conference ISTVS, Budapest, Ungarn, Sept. 4-6, 1991

[22] P.J. Wagner: The calculation of pressure-sinkage curves based on shear strength measurements, 5th European Conference ISTVS, Budapest, Ungarn, Sept. 4-6, 1991

[23] I.C. Schmid, W. Tomaske: Power and torque requirements for skid steering vehicles, FISITA-Congress, ISTVS-Seminar Off-Road Vehicles, London, United Kingdom, June 10-11, 1992

[24] St. Pott: Improved calculation of the turning resistance of tracked vehicles, FISITA-Congress, ISTVS-Seminar Off-Road Vehicles, London, United Kingdom, June 10-11, 1992

[25] K. Ruff, R. Jakobs: Interactive Simulation of Vehicle Movement in Terrain, 11th International Conference ISTVS, Lake Tahoe, Nevada, USA, Sept. 27-30, 1993

[26] I.C. Schmid: Inflation Pressure Control to Improve Terrain-Trafficability: A Model for Simulation, 11th International Conference ISTVS, Lake Tahoe, Nevada, USA, Sept. 27-30, 1993

[27] I.C. Holm: Multi-Pass Behaviour of Wheels in Soft Soil, also in a Curve, 11th International Conference ISTVS, Lake Tahoe, Nevada, USA, Sept. 27-30, 1993

[28] Th. Aubel: FEM Simulation of the Interaction between an Elastic Tyre and Soft Soil, 11th International Conference ISTVS, Lake Tahoe, Nevada, USA, Sept. 27-30, 1993

[29] I.C. Schmid: Interaction of Vehicle and Terrain-Results from 10 Years Research of IKK, 6th European Conference ISTVS, Wien, Austria, Sept. 28-30, 1994

[30] Th. Aubel: The Interaction between the Rolling Tyres and the Soft Soil FEM Simulation by VENUS and Validation, 6th European Conference ISTVS, Wien, Austria, Sept. 28-30, 1994

[31] K. Ruff: The Simulation of the Phenomena between Tyre and Terrain with the Simulation System ORIS, 6th European Conference ISTVS, Wien, Austria, Sept. 28-30, 1994

[32] D. Hintze: Simulation of Climatic Influences on Ground Strength and Trafficability, 6th European Conference ISTVS, Wien, Austria, Sept. 28-30, 1994

[33] St. Pott: The Turning Resistance of Tracked Vehicles, influence by Lateral Elasticities of the Running Gears and the Tracks, 6th European Conference ISTVS, Wien, Austria, Sept. 28-30, 1994

[34] C.W. Fervers: FE-Simulations of Tyre-Profile Effects on Traction on Soft Soil, 6th European Conference ISTVS, Wien, Austria, Sept. 28-30, 1994

[35] W. Ehlert: Prüfstandssimulation der Fahrwiderstände von Gleiskettenfahrzeugen, insbesondere bei Kurvenfahrt, University of the Federal Armed Forces Hamburg, Germany, Diss. 1991

[36] P.J. Wagner: Beurteilung der Geländebefahrbarkeit auf der Basis bodenphysikalischer Kennwerte,
University of the Federal Armed Forces Hamburg, Germany, Diss. 1992

[37] D.G. Hintze: Einfluß der Witterung auf die Bodenfestigkeit als Kriterium der Geländebefahrbarkeit,
University of the Federal Armed Forces Hamburg, Germany, Diss. 1992

[38] Th. Aubel: Simulationsverfahren zur Untersuchung der Wechselwirkung zwischen Reifen und nachgiebiger Fahrbahn auf der Basis der Finite Element Methode,
University of the Federal Armed Forces Hamburg, Germany, Diss. 1994

[39] M. Grahn: Einfluß der Fahrgeschwindigkeit auf die Einsinkung und den Rollwiderstand von Radfahrzeugen auf Geländeböden,
University of the Federal Armed Forces Hamburg, Germany, Diss. 1994

[40] St. Pott: Analytische Methoden zur Bestimmung des Wendewiderstandes von Gleiskettenfahrzeugen unter Einbeziehung von Laufwerkselastizitäten,
University of the Federal Armed Forces Hamburg, Germany,
Diss. (in preparation)

[41] J. Ludewig: Erstellung eines verbesserten Befahrbarkeitsmodells unter Berücksichtigung statistischer Bodenstreuungen, University of the Federal Armed Forces Hamburg, Germany, IKK-Report Nr. 92-08, 1992

[42] I. Schmid: Grundlagen der Geländegängigkeit - Wechselwirkungen zwischen Rad und nachgiebigem Boden, 3. Auflage 1990. Printed manuscript of lectures, University of the Federal Armed Forces Hamburg, Germany

[43] I.C. Holm: Das Verhalten von Reifen beim mehrmaligen Überfahren einer Spur auf nachgiebigem Boden und Einfluß auf die Konzeption mehrachsiger Fahrzeuge, Universität München, Diss. 1971, Fortschrittsberichte der VDI-Zeitschriften Reihe 14, Nr. 17

[44] C.W. Fervers: FEM-Simulation der Böschungsbeanspruchungen durch Pionierbrückenauflager, University of the Federal Armed Forces Hamburg, Germany, IKK-Bericht Nr. 94-03

AN OVERVIEW OF SUSPENSION SYSTEMS OF WHEELED OFF–ROAD VEHICLES

Günter H. HOHL
Austrian Armed Forces
Austrian Society of Automotive Engineers

ABSTRACT

This paper provides an overview of and a comparsion between several suspension systems for wheeled off–road vehicles.

Suspension systems for wheeled off–road vehicles are classified into two major categories; namely, **non–independent** and **independent** types, according to the mechanical relationship to the wheels.

As both systems are successfully used, it is worth while to investigate their advantages and disadvantages. Suspension systems are examined with respect to

- their ability to twist,
- body roll in curves and on slopes,
- wheel and steering control,
- economic, practical and design considerations and
- overall height & configuration of vehicle bottom.

To maximize the **twisting ability**, rigid axles are superior in their off–road capabilities, as the difference in wheel loads of two axles twisting in opposite directions is smaller than that for independent suspension systems.

Contrary to the above, independent suspensions, are better with respect to **body roll** in **curves** and when crossing **slopes**.

A hump crossed by one wheel causes a vertical displacement, relative to the chassis. In case of a rigid axle not only the wheel which crosses the obstacle is influenced, but also the other wheel of that axle. This causes a gyroscopic moment which has a negative influence on the **steering ability** and on **wheel control**.

After the introduction of models and theory, some calculation results are presented.

From an **economical, practical** and **design standpoint**, rigid axles have the advantage that they can be adapted from standard commercial trucks and that they

can be connected to the spring system in a simple and inexpensive way. Maintenance, service, and inspection also benefit from the simplicity of the rigid axle design. This is one of the reasons why rigid axles have been used for off–road vehicles since a very early stage of development.

The **overall height** is lower for independent suspensions. Another advantage of independent suspensions for armored wheeled vehicles is that the driveline is located inside the hull and the **underside of the hull** is flat and has no axle beams or universal joints.

1. INTRODUCTION

The purpose of the suspension system of a wheeled vehicle is to support the weight of the vehicle, to separate the axles from the vehicle chassis, and thus to isolate the structure as far as possible from shock loading and vibrations caused by irregularities of the terrain.

Since wheeled off–road vehicles are often mobile gun platforms and have to carry sensitive loads, the suspension systems of such vehicles must provide stability and maintain a comfortable ride, even when moving over rough ground.

To examine cross–country capability, it is important to evaluate the twisting ability, steering ability, wheel control and slope stability while negotiating obstacles.

In the last years, there has been much research on the subject of interaction between the vehicle and unprepared terrain, with special attention to the immediate contact between running gear and terrain. But for the design or evaluation of off–road vehicles, all components of the terramechanic model presented by Wong in /1/ have to be taken into consideration. In the pertinent literature too little has been published about the influence of the suspension system on off–road mobility.

The author published the basic considerations and the mathematical models about independent and non–independent types of suspension systems at the 11th ISTVS Conference at Lake Tahoe in Sept. 1993.

In this paper, more details and the influence of suspension parameters are presented.

The mathematical model in this paper can be used to predict the twisting ability and wheel control while negotiating an obstacle and the body roll in curves and on slopes.

Frames of modern off–road vehicles have torsion–resistant chassis.
Following this trend, the theoretical considerations of this paper are based on a rigid frame for soft–skinned vehicles and a rigid hull for armoured vehicles.

To classify the several suspension systems and to evaluate the parameters, vehicles of the same overall dimensions, but with different suspension systems, are compared.

2. PRINCIPAL SUSPENSION SYSTEMS FOR WHEELED VEHICLES

According to the mechanical relationship among wheels, axles, springs and the frame (hull), the suspension systems for off–road vehicles can be classified in two major categories as in Fig 2. 1.

- non–independent types
- independent types

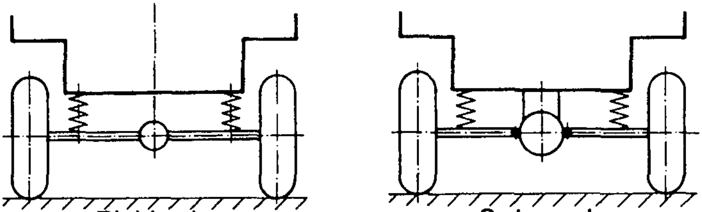

Rigid axle

Swing axle

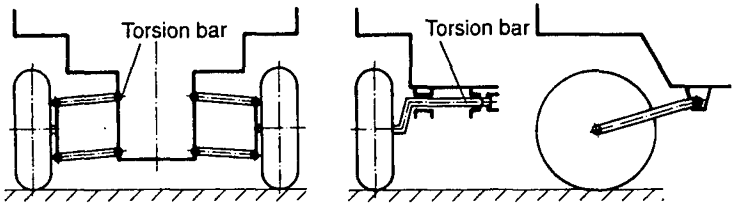

Double wishbone axle

Single trailing axle

Figure 2.1 Suspension systems for wheeled vehicles.

2.1 Non–Independent Suspensions

Non independend suspensions are characterized by rigid transverse structural members connecting the opposite wheels. With this arrangement, a vertical displacement of one wheel causes a displacement of the other wheel of the same axle.

The non–independent category consists only of one type, the **rigid axle** or also sometimes called **beam axle**, which is the oldest and most widely used system.

The rigid axle assembly consists of a rigid member connecting the opposite wheels. The housing contains the differential and the power transmitting shafts.

The rigid axle system with leaf springs (see Fig. 2.2) is one of the most commonly used suspension systems for heavy military and commercial road and off–road vehicles. The torque reactions, driving thrust and road–induced forces are transmitted to the springs which must be rigid enough to maintain reasonable wheel and axle alignment under these conditions.

For this reason, laminated leaf springs with a relatively short spring travel are mounted lengthwise to the frame.

Laminated springs consist of several layers, starting with the main leaf that is supported by shorter ones.

For road vehicles these semi–elliptic leaf springs are usually slung beneath the axles, but in off–road vehicles they rest on the axle to permit more ground clearance.

In the past years, a special development in the quality of leaf springs has taken place. New designs and new materials were introduced. A recent design is the socalled taper–leaf spring, also known as the parabolic leaf or minimum leaf spring. In this the number of leaves is reduced and the thickness of the single leaf is increased.

This reduction of the number of leaves and their overall thickness, as well as the fact that the leaves can be accurately tapered from the center to the ends for efficient material utilization, means that such a spring can be about 30% lighter than its conventional equivalent.

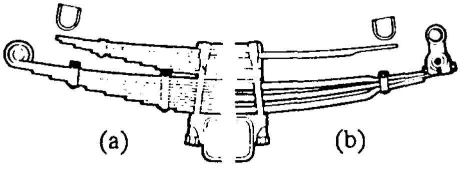

Figure 2.2
Conventional semi–elliptic leaf spring (a) and taper leaf spring (b) with helper springs.

In more recent designs, the materials used for the leaves are composites, such as Kevlar with longitudinal laminated fibres to reinforce the polyurethane resin of the leaf. With such a composite material the weight of the springs themselves can be reduced by 50% for multi–leaf, and by 30% for taper–leaf springs.

But for optimal spring travel, coil springs (see Fig. 2.3) have to be used. With coil springs, a progressive spring characteristic can be achieved. The disadvantage of this system is that the lateral and longitudinal forces cannot be transmitted. Therefore, transverse links are required.

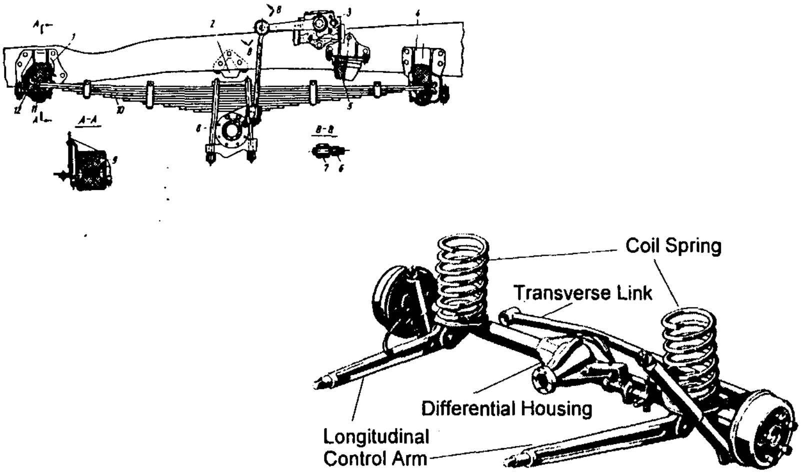

Figure 2.3 Classic design for a rigid axle with leaf springs (left) and coil springs (right).

2.2 Independent Suspension

Independent suspension is characterized by the lack of a rigid structural member to connect the individual wheels. With this arrangement, a vertical displacement of one wheel does not directly affect the other.

A rarely used, but very elegant design for independent suspensions is the **swing axle**, which is always used in combination with a central tube frame.

Currently only the two legendary military off–road vehicles Haflinger and Pinzgauer (see Fig. 2.4) and the Czech heavy truck made by Tatra are equipped with swing axles. This "Tatra solution" is also tested by the U.S. Marine Corps as we learned at Lake Tahoe.

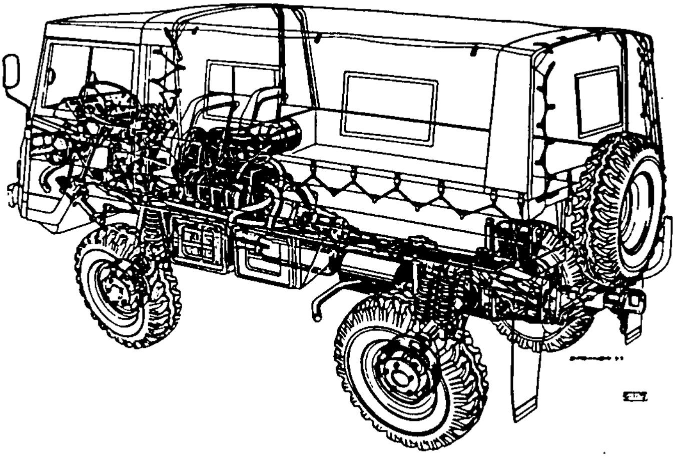

Figure 2.4 The Pinzgauer chassis.

The central tube reduces additional stresses and torsion of the body, caused by wheel travel when riding over rough ground.

In case of the Pinzgauer design (see Fig. 2.5), joints are located in the differential box. The wheel drive shafts are connected to the driving wheel of the differential. This design permits an axle movement of about ±15°

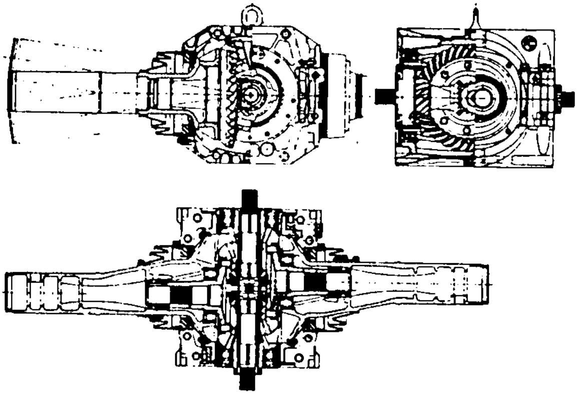

Figure 2.5 Differential of the 6x6 Pinzgauer version.

The advantages of a swing axle design are:

- small unsprung masses
- low weight of the frame (central tube)
- no universal joints
- elegant design

On the other hand, swing axles are a special design. Hardly any commercial components can be used. The connection between axles and differential is complicated and expensive. The ground clearance varies with loading. In the new Pinzgauer this problem is solved by using a pneumatic lifting system to maintain constant ground clearance.

The usual design for independent suspensions is the **double wishbone** axle with transverse links. If the two links are of the same length, we have an exact parallel guide of the wheel.

The springs can be coil springs or torsion bar springs which are mounted parallel to the longitudinal axis of the vehicle. An unusual design is the German off–road personnel carrier Iltis (see Fig. 2.6). The upper transverse link is a spring at the same time.

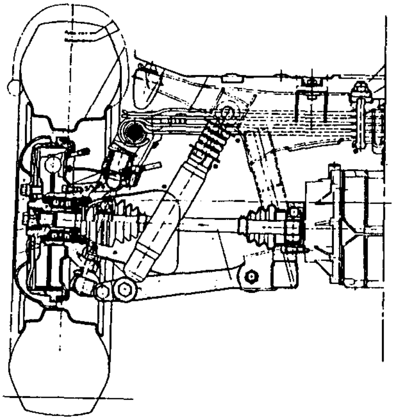

Figure 2.6
Double wishbone axle of the Iltis.

The **single leading** or **single trailing suspension** has its origin in the road wheel design of tracked vehicles. The spring is usually a torsion bar which is mounted crosswise to the longitudinal axis. With this design it is not possible to turn the wheel for steering. Therefore it can only be used for unsteered axles and skid steering vehicles.

An example for this principle is Fig. 2.7 which shows the Austrian wheeled armored combat vehicle Pandur, which has a combination of a modified double wishbone axle on the first two axles, and a single trailing axle in the rear.

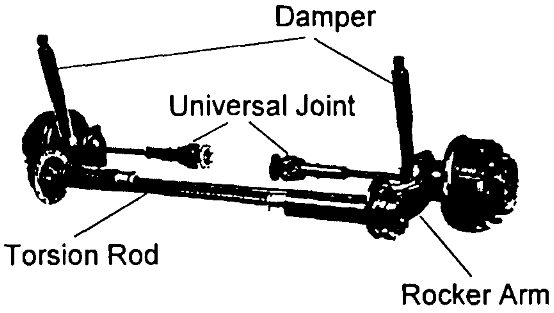

Figure 2.7
Rear unsteered suspension of a wheeled armoured 6x6 vehicle

3. TWISTING ABILITY

3.1 General

The differences between the wheel loads ΔW_i of diagonally opposed wheels while negotiating an obstacle can be regarded as one of the indicators of off–road mobility. Equal wheel loads result in more uniform tyre adhesion for the production of thrust. In case of unequal wheel loads, the wheels with the higher load cause increased rolling resistance. The other wheels with decreasing load cause a decrease of traction.

The model used for the mathematical equations is described in Fig. 3.1.

Obstacles are put in front of two diagonally opposed wheels – in this picture the left front wheel and the right rear wheel. Then the heights of the obstacles are increased until an opposite wheel loses ground contact. The purpose of the mathematical investigations is to find a correlation between obstacle heights ($h=h_1 + h_3$) and wheel load difference ΔW_i for several suspension systems.

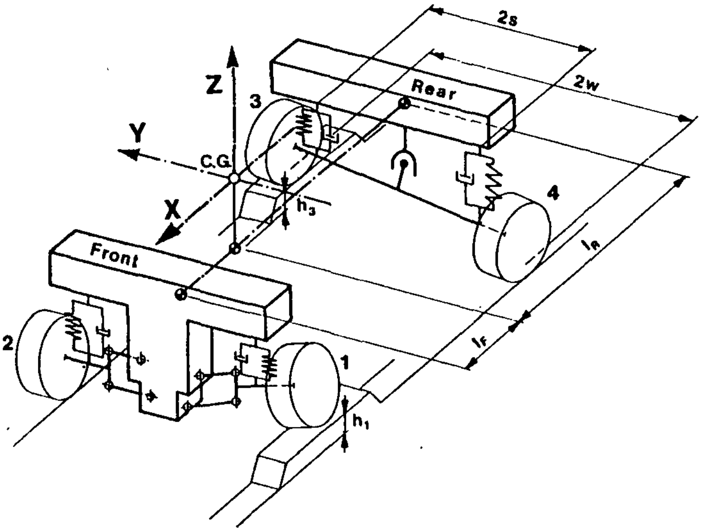

Figure 3.I. Basic model for twisting ability.

3.2 Wheel Load Difference

Twisting ability is characterised by the sum of the height (h_1 and h_3) of the obstacles.

$$h = h_1 + h_2 \tag{3.1}$$

Wheel load difference ΔW_i between before and after twisting is defined as follows:

$$\Delta W_i = W_i - W_{i0} \tag{3.2}$$

i .. Wheel index (1,2,3,4)
o .. Situation before twisting; that means the vehicle stands on a horizontal plane

The maximum twisting ability is reached when one wheel is lifted from the ground.

$$\Delta W_i = -W_{i0} \tag{3.3}$$

The following equations are valid for all types of axles:

- The sum of the wheel loads are equal to the total load W

$$\sum_{i=1}^{4} W_i = W \tag{3.4}$$

- The sum of the torques through the X– and the Y–axis is zero. Only the equation through the Y–axis can be expressed as one equation for all suspension systems.

$$(W_1 + W_2)l_F = (W_3 + W_4)l_R \tag{3.5}$$

- The equation for the Y–axis depends on the suspension types and can be derived from the geometrical relationships in fig. 3.2.

  A more detailed derivation of the equations can be found in Ref. /2/ and /3/.

To make the different axle designs comparable, the spring characteristic is expressed by spring travel under normal load (ϱ_i)

$$\varrho_i = \frac{W_{i0}}{c_i} \tag{3.6}$$

Wheel load differences in relation to total load W can be expressed as a function of the sum of both obstacle heights $h_1 + h_2$, the geometrical relationship, and the spring properties.

$$\frac{\Delta W_i}{W} = f(h), g\left(w_{F,R}, s_{F,R}, l_F, l_R\right) \tag{3.7}$$

Rigid axle:

$$\frac{\Delta W_i}{W} = h \frac{l_R \; l_F \; s_F^2 \; s_R^2}{4 w_F\left(l_F + l_R\right)\left(l_F \; s_R^2 \; w_F \; \varrho_F + 2 \; l_R \; s_F^2 \; w_R \; \varrho_R\right)} \tag{3.8}$$

Swing and wishbone axle:

$$\frac{\Delta W_i}{W} = h \frac{l_R l_F}{4\left(l_F + l_R\right)\left(l_F \varrho_F + l_R \varrho_R\right)} \tag{3.9}$$

The wheel load differences for this kind of suspension is independent of the wheel track – spring track relationship.

Usually spring track (s) and wheel track (w) are equal for both axles and the equation is easier to understand by looking at the s/w relationship.

Moreover, the influence of axle load distribution is more obvious when the IF/IR relationship is introduced into the equation.

Rigid axle:

$$\frac{\Delta W_i}{W} = h\left(\frac{s}{w}\right)^2 \frac{l_R/l_F}{4\,(l_F/l_R + 1)\left[(l_F/l_R)\,\varrho_F + \varrho_R\right]} \tag{3.10}$$

Swing axle and wishbone axle:

$$\frac{\Delta W_i}{W} = h\,\frac{l_R/l_F}{4\,(l_F/l_R + 1)\left[(l_F/l_R)\,\varrho_F + \varrho_R\right]} \tag{3.11}$$

3.3 Maximum Obstacle Height

The maximum height (h) of an obstacle is achieved when the wheel opposite to the wheel on the obstacle loses ground contact, which occurs when the wheel load is zero.

$$\frac{\Delta W_i}{W} = -\frac{W_{i0}}{W} \tag{3.12}$$

$$\frac{\Delta W_{i0}}{W} = \frac{1}{2(l_F/l_R + 1)} \tag{3.13}$$

Rigid axle:

$$h_{max} = \frac{2\left[(l_F/l_R)\,\varrho_F + \varrho_R\right]}{(s/w)^2} \tag{3.14}$$

Swing axle and wishbone axle:

$$h_{max} = 2\left[(l_F/l_R)\,\varrho_F + \varrho_R\right] \tag{3.15}$$

3.4 Discussion of the Results

The best way to demonstrate the twisting ability of several suspension systems is a diagram. The diagram in fig. 3.5 shows the relationship between wheel load difference and obstacle height.

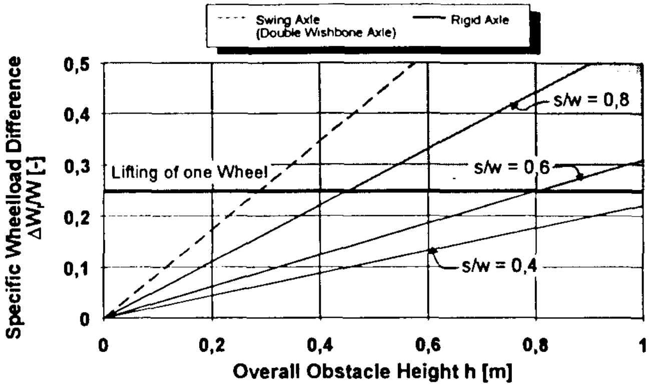

Figure.3.2. Specific wheel load difference vs. obstacle height

It is to be seen clearly that the specific wheel load difference ($\Delta W_i/W$) is less for the rigid axle than for independent suspension systems. The wheel load difference for the rigid axle depends on the relationship between wheel and spring track. In this diagram, the spring characteristic is equal for both front and rear axle and the C.G. is set halfway between the two axles ($I_F=I_R$).

Figure.3.3. shows the influence of axle load distribution and spring characteristics.

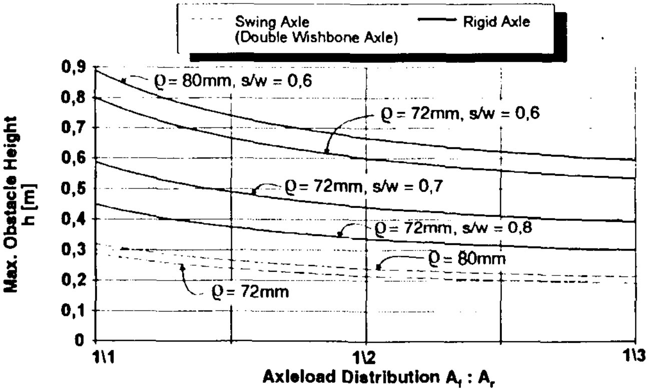

Figure 3.3 Max. obstacle height vs. axle load distribution

4. BODY ROLL

4.1 General

Off–road vehicle body roll in curves and on slopes is also an important indicator for cross–country ability. The roll angle should be small. A simple method to achieve this would be to use stiff springs. But for reasons of ride comfort and to protect both the vehicle itself and the cargo, the use of springs with stiff characteristics is not practical. Curve and slope stability are influenced by the height of the roll center. The roll center is the apparent stationary point around which the body rolls under the influence of centrifugal forces and slope components. The distance between the roll center and the C.G. is regarded as a lever for the torque exerted by roll forces and has a great influence on the roll angle.

The centrifugal force C is defined as follows (R is the radius of the curve, v is the vehicle speed, g is the gravitational acceleration)

$$C = \frac{W}{g}\frac{v^2}{R} \tag{4.1}$$

The effective lever is the vertical distance between the C.G. and the roll center.

4.2 Rigid axle

The roll center 0 of a rigid axle is easy to determine and is located at the point where the transverse forces are balanced by lateral forces in the springs.
For one axle the following conditions must be met to achieve equilibrium:

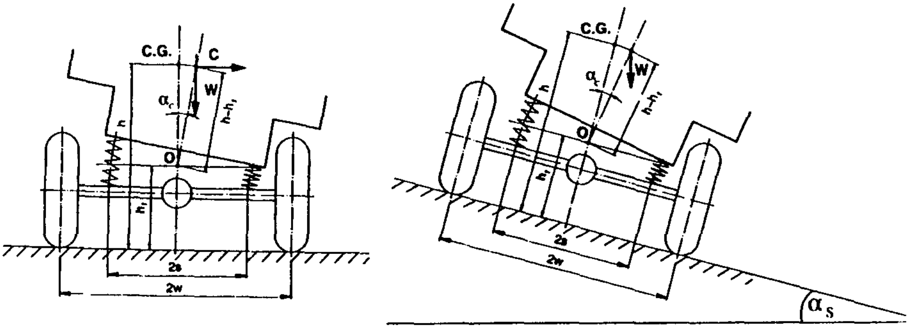

Figure 4.1 Centrifugal and slope forces acting on a rigid axle

$$C(h - h_f)\cos\alpha_c + W(h - h_f)\sin\alpha_c = 2\Delta Fs \tag{4.2}$$

ΔF . . . Difference between left and right spring loading at that instant
c . . . . . Spring constant

$$\alpha_c = \frac{(h - h_{fF})(h - h_{fR})}{(h - h_{fR})\frac{l_R}{l_F + l_R}\frac{s_F^2}{\varrho_F} + (h - h_{fF})\frac{l_F}{l_F + l_R}\frac{s_R^2}{\varrho_R} - (h - h_{fF})(h - h_{fR})}\frac{v^2}{gR} \tag{4.3}$$

For a vehicle on a slope according to fig. 4. 1, and the considerations from Ref. /2/ the relationship between the slope angle α_s and the roll angle α_c can be expressed as follows. Furthermore the C.G. is put halfway between the two axles and the spring capability is the same front and rear.

$$\alpha_c = \frac{(h - h_f)\sin\alpha_s}{\frac{s^2}{\varrho} - (h - h_f)\cos\alpha_s} \tag{4.4}$$

An analysis of the above equation shows that there is a square law relationship between α_c and the spring track s, but a linear relationship between the centrifugal force lever and α_c, which means that the wheel track w does not affect the situation.

4.3 Swing Axle

The roll centre of a swing axle is rather high. It is located at the point of intersection between the two straight lines of the left and the right wheel connecting the point of contact between tyre and surface and the centre of rotation of the axles.

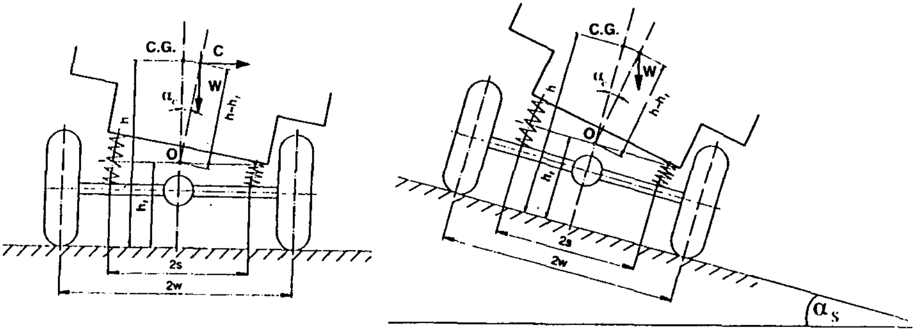

Fig. 4.2 Centrifugal and slope forces acting on a swing axle

As the full derivation of the relationship between the roll angle and the geometry of the suspension system goes beyond the scope of this paper, only the results are given.

With the simplifications pertaining to $\cos\alpha_c \sim 1$ and $\sin\alpha_c \sim \alpha_c$ and by transformation, which can be seen in detail in /2/, the result is as follows:

$$\alpha_c = \frac{\left(h - \frac{w_F}{z_F} r\right)\left(h - \frac{w_R}{z_R} r\right)}{\left[h - \frac{w_F}{z_F} r\right]\left[\frac{w_R^2}{\varrho_R} - \left(h - r + \frac{w_R}{r} k_R\right)\right]\frac{l_F}{l_F + l_R} + \left[h - \frac{w_R}{z_R} r\right]\left[\frac{w_F^2}{\varrho_F} - \left(h - r + \frac{w_F}{r} k_F\right)\right]\frac{l_R}{l_F + l_R}} \frac{v^2}{gR} \quad (4.5)$$

Examining the above equation, the following facts can be derived:

- Roll stiffness for swing axles is high and the roll centre is relatively high.
- There is no relationship between the roll angle and the location of the springs.
- The shorter the length of the semi–axle and the bigger the wheel diameter, the higher is the roll stiffness. This is exactly the opposite of what is required for good twisting ability.

For a vehicle on a slope according to fig 4.2 and the considerations of capter 4.2 the relationship between the slope angle α_s and the roll angle α_c can be expressed as follows:

$$\alpha_c = \frac{\left(h - \frac{w}{z} r\right) \sin \alpha_s}{\frac{w^2}{\varrho} - \left(h - r + \frac{w}{z} k\right) \cos \alpha_s} \qquad (4.6)$$

4.4 Double Wishbone Axle

As can be seen in Fig. 4.3, the roll centre of the double wishbone axle is close to the ground and moves almost vertically upwards when a wheel lifts.

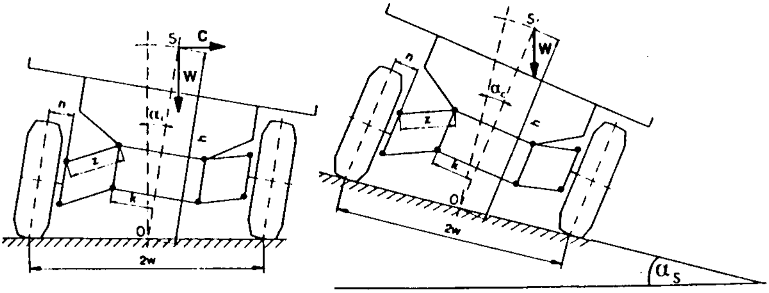

Figure 4.3 Centrifugal and slope forces acting on a double wishbone axle.

Following the general rule to substitute the spring constant with the spring travel at normal load, the following relationship can be deduced:

$$\alpha_c = \frac{h}{\frac{l_R}{l_F+l_R}\frac{w_F^2}{\varrho_F} + \frac{l_F}{l_F+l_R}\frac{w_R^2}{\varrho_R} - h}\,\frac{v^2}{gR} \tag{4.7}$$

For the relationship between slope and roll angle according the principles in capter 4.2 and 4.3 can be expressed as follows:

$$\alpha_c = \frac{h \sin \alpha_s}{\frac{w^2}{\varrho} - h \cos \alpha_s} \tag{4.8}$$

4.5 Discussion of the Results

Figure 4.4 shows the roll angle versus the several suspension systems. The best system is the one with the lowest roll angle. It is clear that the rigid axle has insufficient roll stability. The best situation can be seen in the swing axle.

The roll angle for the double wishbone axle is independent of the geometrical relationship.

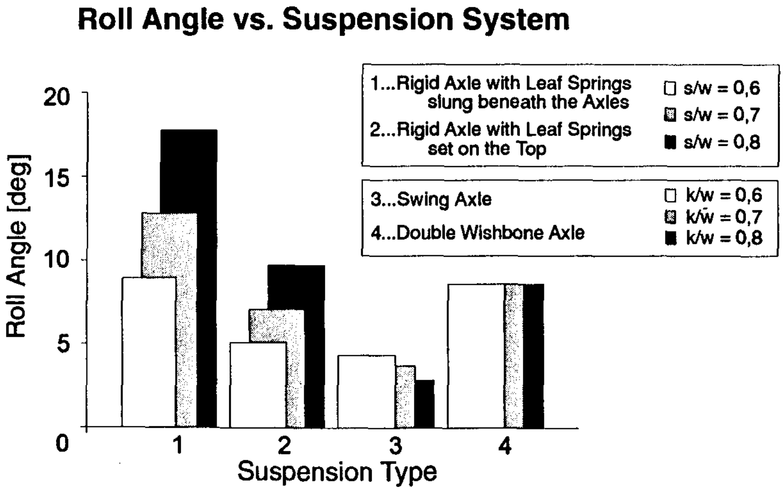

Figure 4.4 Roll angle vs. suspension system.

Fig. 4.5 shows the influence of the spring characteristic on the roll angle for several suspension systems:

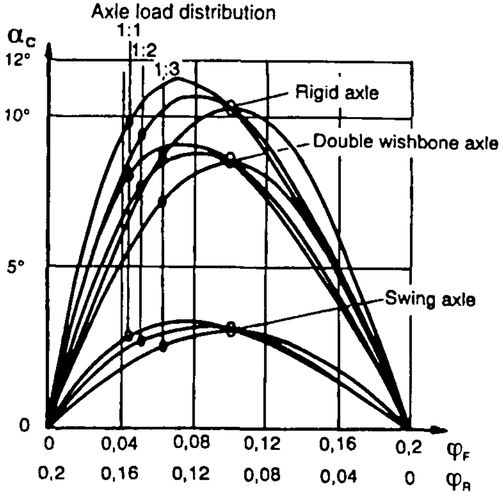

Figure 4.5 Roll angle vs. spring characteristic.

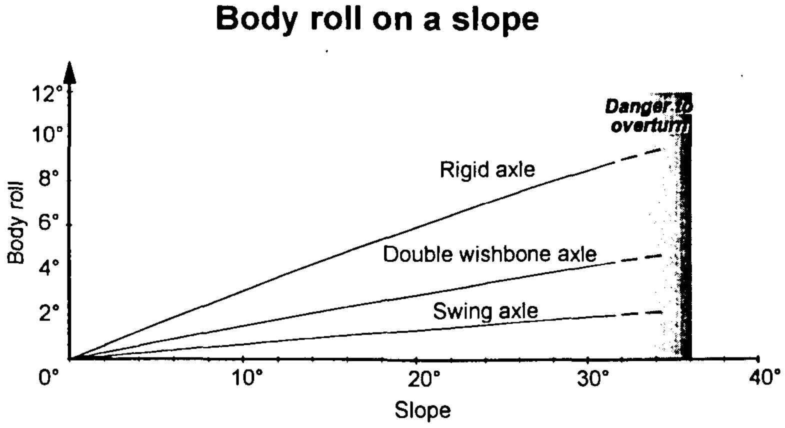

Figure 4.6 Roll angle vs. slope angle

5. STEERING ABILITY AND WHEEL CONTROL

Passing over terrain irregularities and negotiating obstacles is one major task for off–road vehicles. When one wheel of a rigid axle suspension passes over an obstacle, the axle executes angular movement in the vertical plane about an axis in the vehicle's longitudinal direction. The wheels are simultaneously displaced by approximately equal and opposite amounts relative to the chassis. Because the wheels in movement act as gyroscopes, a forced gyroscopic precession occurs which tends to make the steerable wheels swing about their kingpins.

When the axle returns to the horizontal plane the gyroscopic forces are reversed, thereby causing the wheels to oscillate about the king pins. This effect can be seen clearly in Fig. 5.1 without mathematical considerations.

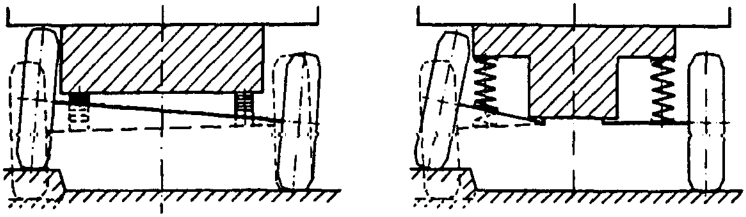

Rigid axle **Swing axle**

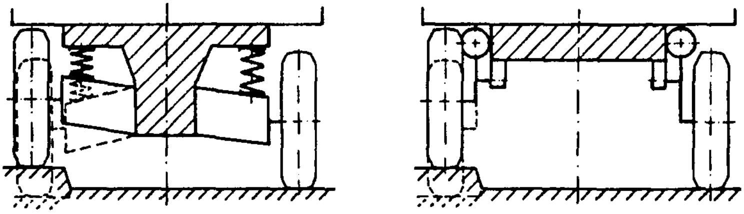

Double wishbone axle **Single wishbone axle**

Figure 5.1 Wheel control of the four main suspension types.

Another problem associated with rigid axle design is that the unsprung masses are higher than for any independent suspension system. This is undesirable when both wheels are crossing an obstacle at the same time, because the mass of the whole axle is involved.

In case of an independent suspension arrangement, a vertical displacement of one wheel does not affect the remaining wheels directly. When one wheel passes over an obstacle, both wheels will most, likely be deflected, but not simultaneously or to the same degree.

The kinetic behaviour of the wheels of a vehicle during vertical displacement relative to the body is influenced by the type of the suspension system. In case of a double wishbone axle it depends on the geometric arrangement of the control arms.

For parallel control arms of the same length or single trailing axles the plane of the wheel during vertical movement remains substantially unchanged, thereby eliminating the gyroscopic effect which produces wheel shimmy.

The camber angle of the wheel is not affected as in the rigid axle and a swing axle cases.

The swing axle has the best roll stiffness, followed by the double wishbone axle. The rigid axle has the worst α_c –values.

The following rules are valid for all three suspension systems:

1. Roll stiffness increases with spring stiffness.
2. Roll stiffness increases with decreasing height of the C.G.
3. Roll stiffness increases with the height of the roll center.

6. FURTHER CONSIDERATIONS

6.1 Dimensions

Ground clearance is a very important factor in off–road mobility. The rigid axle design has a constant ground clearance. The lowest point of the suspension system is the differential housing. In contrast to the independent suspension systems the ground clearance is constant and independent of loading.

On the other hand the differential housing is an obstacle when passing high terrain irregularities. In case of an independent suspension the vehicle's belly can be designed to be flat and the clearance is not obstructed by axle beams.

Another disadvantage of a rigid axle system is the overall height. This difference can be seen clearly in an example for a wheeled armoured vehicle. The rigid axle requires clearance between the axle and the hull to permit spring action.

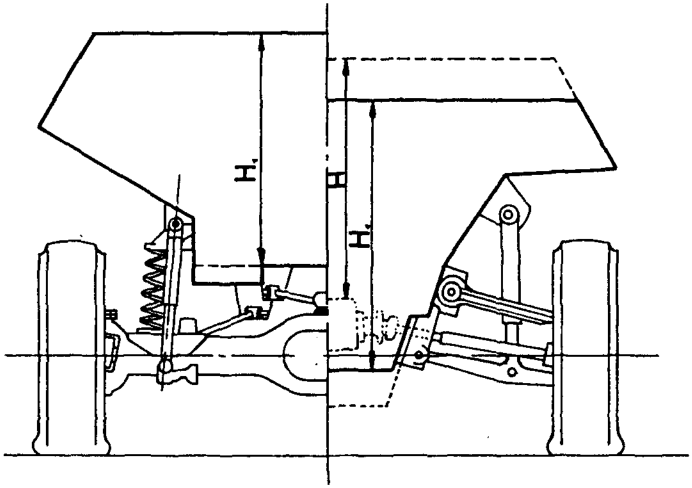

Figure 6.1 Wheeled armoured vehicle with non–independent and independent suspension design.

Independent suspension systems allow to put the entire driveline, such as gearbox, differentials, universal joints, etc., inside the hull. The difference in the overall height of the hull can be considerable. However, this space cannot be fully utilized for other purposes, because the driveline has to be accommodated inside the hull.

6.2 Cost and Maintenance

Because of the performance advantages of independent suspensions most wheeled armoured vehicles have them. If armoured vehicles and other military trucks belong to the same family, the rigid axle design is often preferred.

The disadvantages of independent suspension systems are primarily those of cost and maintenance. Rigid axle designs can be carried over from standard commercial trucks and therefore they are often simpler and cheaper.

References:

/1/ J.Y. WONG
"Theory of Ground Vehicles" John Wiley & Sons

/2/ R. KLANNER
"Die Radaufhängung des geländegängigen Kraftfahrzeuges"
Thesis Technical University Vienna

/3/ R. KLANNER
"Cross Country Trucks for Fast Off–Highway Negotiation"
8th ISTVS Conference, Vienna 1978

/4/ "Principles of Automotive Vehicles"
TM9–8000

/5/ "Engineering Design Handbook"
Automotive Series AMCP 706–356

/6/ M. MITSCHKE
"Dynamik der Kraftfahrzeuge"
Springer Verlag

/7/ K. NEWTON et al.
"The Motor Vehicle"
Butterworth

/8/ D.J. LEEMING and R. HARTLEY
"Heavy Vehicle Technology"
Stanley Thornes Ltd.

/9/ ANTONOW et al.
"Militärkraftfahrzeuge"
Militärverlag der DDR

/10/ G.HOHL
"The Influence of the Suspensions System
on the Mobility of Wheeled Off–Road Vehicles
11th ISTVS –Conference Lake Tahoe, 1993

Session II

Sektion II

Drive Line Systems

Antriebssysteme

SELF-GENERATED TORQUES IN ALL-WHEEL DRIVE POWER TRAINS

Jürgen Stockmar
Steyr-Daimier-Puch

Abstract

During many driving maneuvers, wind-up torques occur in power trains of all-wheel driven vehicles with rigid all-wheel drive, positive differential locks, or non-positive differential locks with high lock-up ratios. These self-generated torques are mainly caused by differing dynamic tire diameters, kinematic slip between front and rear axle during cornering, and kinematic slip between the wheels of one axle. However, different transmission ratios for front and rear axle of a rigid all-wheel drive power train, which also could cause high wind-up torques, are usually not selected.

The wind-up torques occuring in the power train can only be surmounted by power that linearly increases with the engine speed. This power loss, of course, cannot be used as tractive power for the vehicle. The generated power loss increases the fuel consumption, the wear and tear of all power train components, and the tire wear. Under extreme circumstances, over-heating and overload can considerably reduce the fatigue life and lead to an early failure of components.

1. Introduction

Although the need for speed-sensitive decoupling of the powered wheels of all-wheel drive vehicles by means of one or several differentials was realized and introduced already at an early stage of automotive engineering, many off-road vehicles still feature a manual actuation of the all-wheel drive, selflocking non-positive differentials, or manually actuated positive differential locks. Vehicles of the kind we deal with in detail at this conference are equipped with devices for partial or complete lock-up of the axle differentials. These devices, however, are no relic of the remote past of automotive industry, but a necessary means to improve off-road driving performance. On steep ascending gradients, during negotiating of obstacles, or during driving on ascending roads with different friction coefficiente (μ-split conditions), the friction loss of one single wheel or one axle - in the case of open differentials - can interrupt the torque transfer of the complete power train and stop the vehicle due to the extreme slip. Only when the spinning of one wheel or one axle is efficiently prevented by locked differentials, the engine torque can be converted into tractive force a all driven wheels.

2. Gradability limits with different 4 WD systems

Even in the case of less difficult off-road conditions the rigid all-wheel driv with locked differentials shows considerable advantages as compared to th differential brake or the open differentials, Fig. 1. The higher gradability lim that can be achieved by vehicles with locked center differentials and transvers differentials proves the need for differential lock controls or differential locks i off-road vehicles facing very exacting demands. The representation on han shows two friction coefficients typical for off-road application. The gradabilit limit in both cases can be improved if the complete drive train is rigid (A, Ā Considerably less steep gradients can be negotiated by the same vehicle wit the center differential being open (B, B̄). In the case of a viscous control parall to the differential, the achieveable gradability limit on low-friction surfaces i close to the one of a rigid all-wheel drive (C), on higher friction coefficient however, its performance lies between the one of a rigid all-wheel drive and a open center differential (C̄), [Lit. 1].

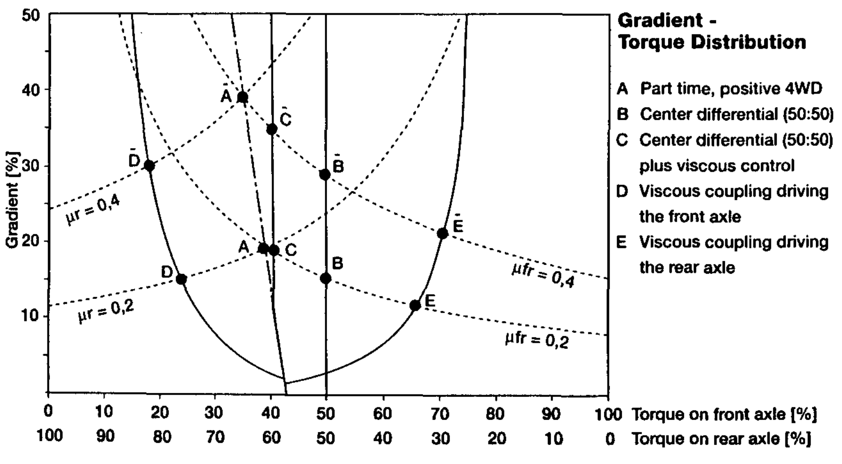

Fig. 1: Gradability limits with different 4WD systems

3. Effects on the steering behavior caused by differential locks

Probably all of us have at least once forgotten to deactivate the differential locks when we left a difficult terrain and continued to drive on an asphalt road. Thus we all are familiar with the effect resulting from this: above all with the front axle lock actuated the vehicle shows an extreme understeering tendency and can only be forced into a curve by means of an increased steering torque and a steering angle that is considerably more acute. Depending on the wheelbase and the track width, the curve radius at a given steering angle increases by more than 40%, Fig. 2, [Lit. 2].

In order to reduce this potential of danger caused by a drastically changed self-steering behavior, as well as to relieve the driver from operating the locks on difficult terrain, Steyr-Daimler-Puch Antriebstechnik developed the Automatic Drive Train Management (ADM). A center control unit automatically activates or deactivates the differential locks in dependence of the wheel speeds [Lit. 3].

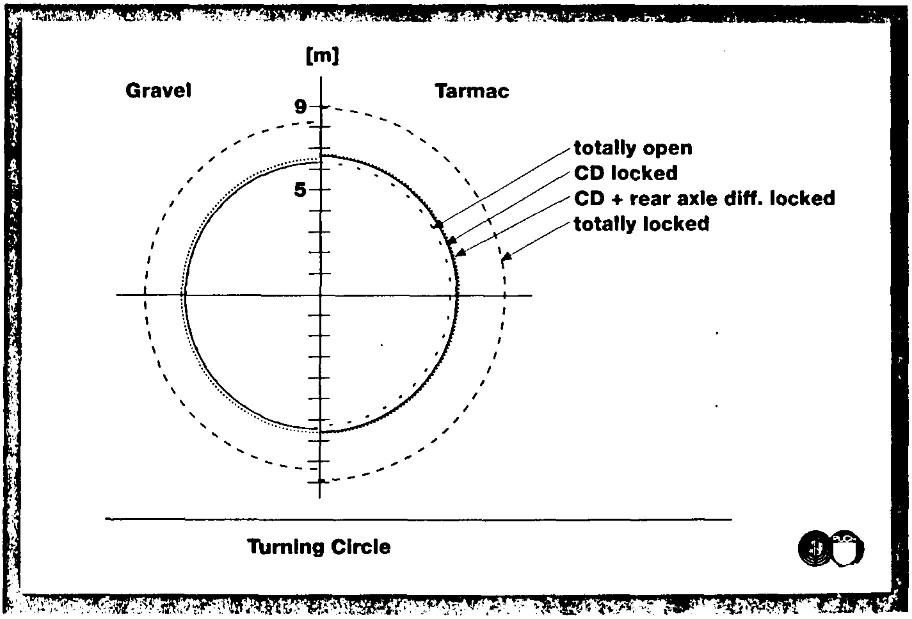

Fig. 2: Turning circle radius with different drive train configurations

4. Causes of the non-effictive torques in a drive train

During cornering with a rigid all-wheel drive train the wind-up of all involve transfer elements is considerably noticeable, the tire slip noises are very ofte even audible. In all transfer elements of the drive train, this wind-up in th described operation mode causes self-generated torques that cannot be utilize as tractive power for the vehicle. Apart from this operation mode, there a several other factors causing self-generated torques in locked all-wheel driv trains:

Kinematic slip between front and rear axle during cornering
Kinematic slip between the wheels of one axle during cornering
Different dynamic wheel diameters
Different transmission ratios for front and rear axle

The described vehicle-dynamic experiment shows that the highest sel generated torques in a locked drive train occur during driving through shar corners. The speed differences occuring in the case of the front and rear ax being decoupled, and the self-generated torques occuring with the axles beir coupled, depend on the following determinants (in order of their influence):

Steering angle
Wheelbase
Steering geometry, i.e. percentage in the Ackermann angle.

The track width is another influential factor for the magnitude of the sel generated torques. The formula, Fig. 3, shows the mathematical interrelationsh between the characteristic quantities.

In the case of vehicles with single universal joints at the steering axle, additio nal, periodically varying self-generated torques occur. The calculated speeds Fig. 4, of a high-volume production vehicle show the periodically varying spee of the front axle during driving at the smallest turning circle diameter. With th drive train open and at a speed of 5 km/h, the maximum momentary value o the speed difference Δn is 60 revolutions per minute, i.e. approximately 50% o the rear axle propshaft speed. With the drive train locked, this speed differenc must be absorbed by the tire slip of the wheels, which causes the self-generate torques [Lit. 4].

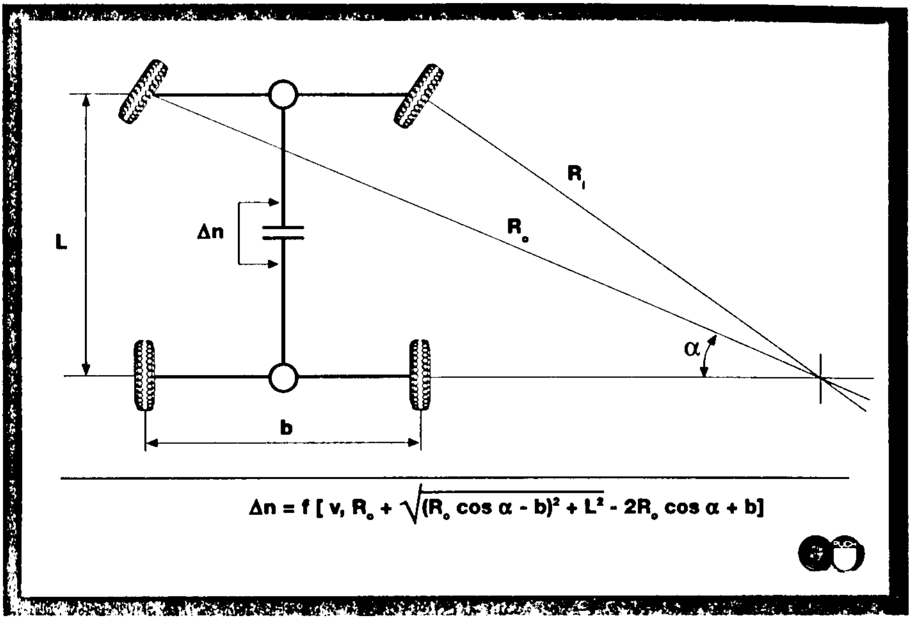
L
Δn
R_i
R_o
α
b
$\Delta n = f\,[\,v,\ R_o + \sqrt{(R_o \cos\alpha - b)^2 + L^2} - 2R_o \cos\alpha + b]$

Fig. 3: Speed difference due to steering kinematics

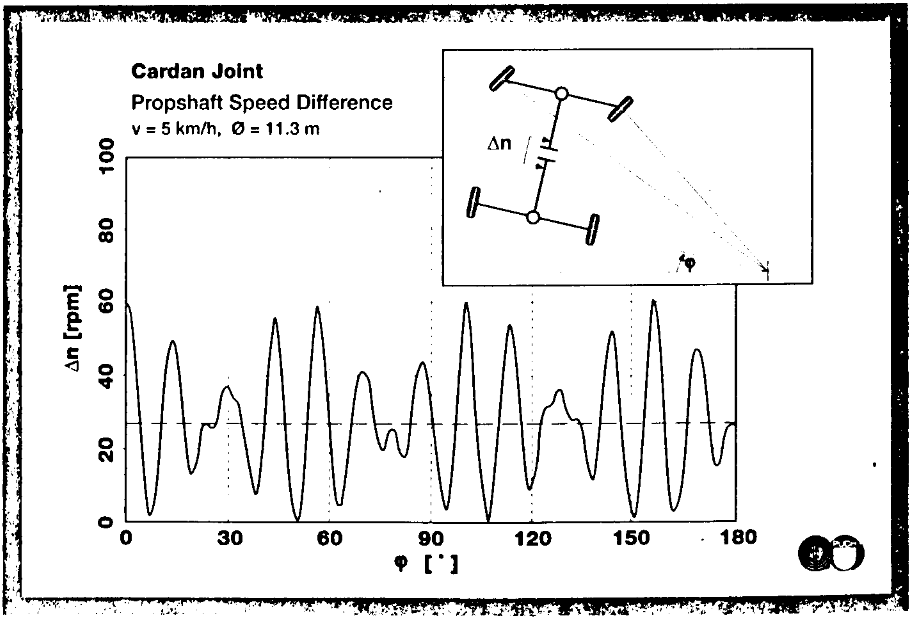

Fig. 4: Speed difference due to cardan joint kinematics

5. Influence of the dynamic tire radii

The change of dynamic tire radii in dependence of the parameters

- tires - vertical load
- tires - inflation pressure
- tread depth

is frequently underestimated. The changes in the dynamic tire radius measure at the widely-used off-road tire 205 R16 show the tire growth along with the tir pressure and the compression due to higher normal loads, Fig. 5. The chang of the tread depth directly enters into the length of the dynamic tire radius. Th axle loads alone, which usually differ from each other, and the dynamic tir radii that vary due to the different axle loads, can cause a theoretical spee difference between front and rear axle of more than one percent. Due to th positive coupling between front and rear axle by means of the mechanic drive train, the theoretical speed difference is suppressed, but the tire sli produces the self-generated torque in all transfer elements of the locked driv train [Lit. 2].

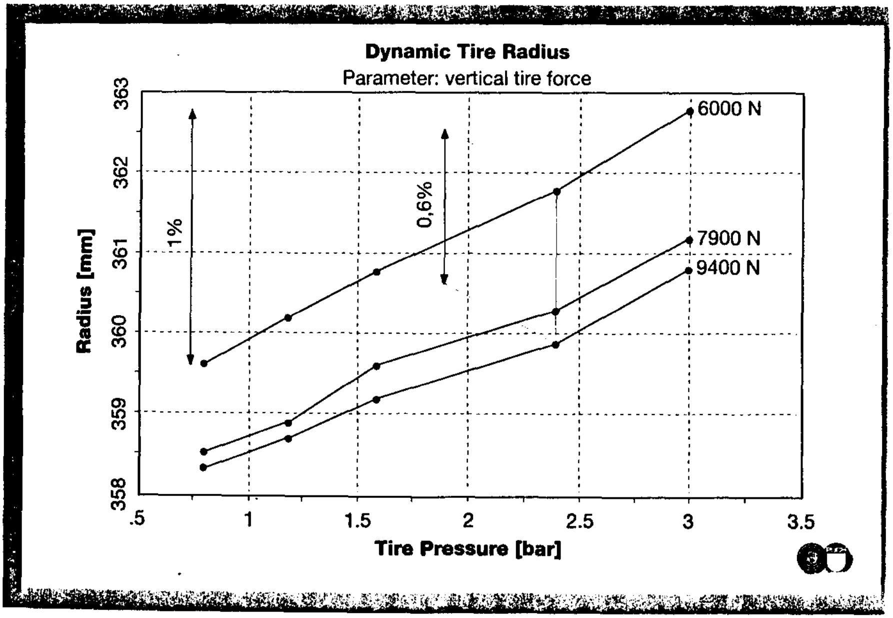

Fig. 5: Dynamic tire Radii depending on tire pressure and vertical load

6. Magnitudes of self-generated torques and self-generated power

The magnitudes of the self-generated torques, and the self-generated power resulting from them, were calculated at Steyr-Daimler-Puch Fahrzeugtechnik in the course of specific development activities for off-road vehicles under various driving conditions and with different vehicles. The self-generated power can be calculated from the product of the self-generated torques and the speed of the respective component.

With only the rear axle being driven, a Puch G requires an engine output of 1.3 kW for a speed of 10 km/h at a front wheel steering angle of 12°. The output distribution onto the rear axle, rear tires, and front tires is shown by the output flow chart, Fig. 6. If the rigid front axle drive is also actuated, the engine must generate 2.7 kW for the same operating conditions. The load on rear axle, front axle, and tires is significantly higher than in the rear-wheel drive mode. The magnitude of the self-generated power occuring in the drive train, however, is surprisingly high: between 13.2 kW and 10.5 kW self-generated power occur in the drive train, although the engine generates only 2.7 kW input power.

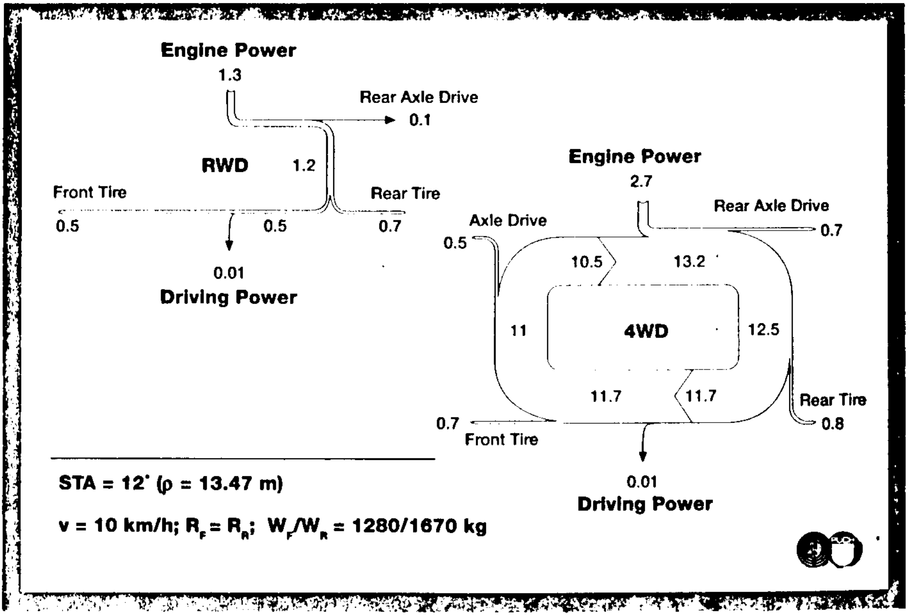
Engine Power
1.3
Rear Axle Drive
0.1
RWD
1.2
Front Tire
0.5
0.5
Rear Tire
0.7
0.01
Driving Power
Engine Power
2.7
Rear Axle Drive
0.7
Axle Drive
0.5
10.5
13.2
11
4WD
12.5
11.7
11.7
Rear Tire
0.8
0.7
Front Tire
0.01
Driving Power
STA = 12° (ρ = 13.47 m)
v = 10 km/h; R_F = R_R; W_F/W_R = 1280/1670 kg

Fig. 6: Power flow during cornering

For a high-speed test, the same vehicle was equipped with tires on the rea axle, the dynamic rolling circumference of which was smaller by 1 % than tha of the tires on the front axle, Fig. 7. A tractive power of 12.8 kW was required t reach the target speed of 100 km/h. When only the rear wheels were driven the engine had to generate 26.2 kW, the difference between engine power an tractive power was lost in the drive train and the tires.

When the front axle and rear axle are positively coupled to a rigid all-whee drive, an engine power of 31.1 kW must be generated to reach the targe speed of 100 km/h. Due to the difference of the overall ratios for front and rea axle, i.e. the difference of the dynamic tire radii, the tractive force is reduce because of the increased slip, and the loss in the axle drives is increased. Th self-generated torques, as one factor of the self-generated power in the driv train, affect all elements involved in the transfer of power, and due to th increased friction generate a power loss that cannot be utilized as tractiv force.

7. Power distribution in the case of non-positive axle coupling

Unexpected torque distributions can occur in vehicles with a non-positive powe

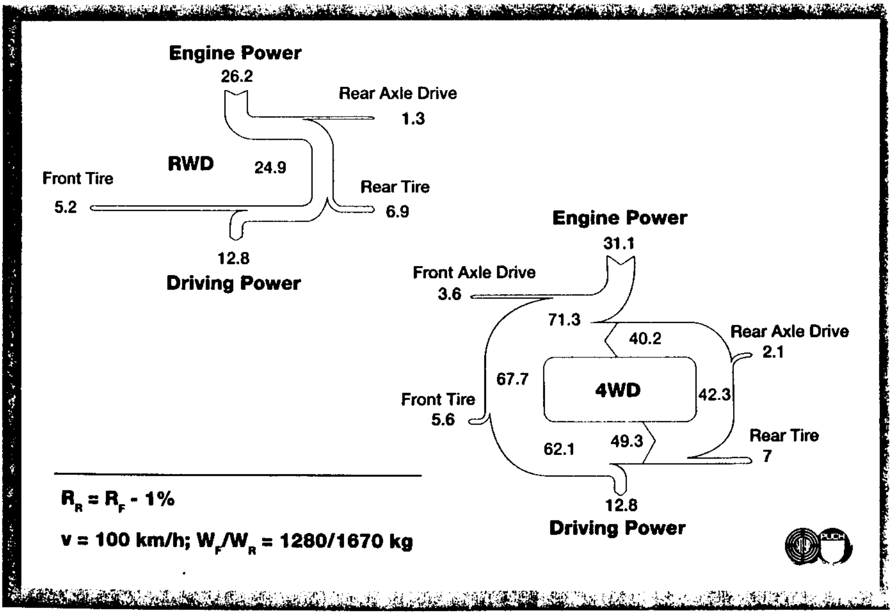
Engine Power
26.2
Rear Axle Drive
1.3
RWD
24.9
Front Tire
5.2
Rear Tire
6.9
12.8
Driving Power
Engine Power
31.1
Front Axle Drive
3.6
71.3
40.2
Rear Axle Drive
2.1
67.7
4WD
42.3
Front Tire
5.6
62.1
49.3
Rear Tire
7
12.8
Driving Power
$R_R = R_F - 1\%$
v = 100 km/h; W_F/W_R = 1280/1670 kg

Fig. 7: Power flow with different Tire radii

distribution system - such as, for example, a viscous coupling. In order to acquire data in connection with this phenomenon, a passenger vehicle was equipped with tires of different rolling circumferences. When the smaller tires, their circumference having been smaller by only 0.8%, were mounted on the front axle, approximately two thirds of the engine output were transferred to the rear axle via the viscous coupling, Fig. 8.

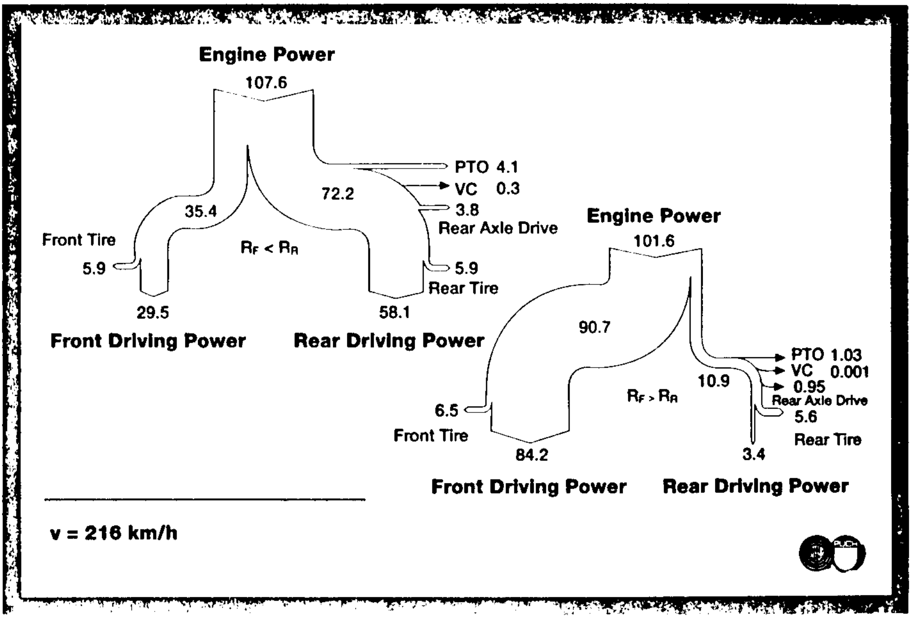
Engine Power
107.6
PTO 4.1
VC 0.3
72.2
35.4
3.8
Rear Axle Drive
Front Tire
5.9
RF < RR
5.9
Rear Tire
29.5
58.1
Front Driving Power
Rear Driving Power
Engine Power
101.6
90.7
PTO 1.03
VC 0.001
0.95
Rear Axle Drive
10.9
RF > RR
5.6
Rear Tire
6.5
Front Tire
84.2
3.4
Front Driving Power
Rear Driving Power
v = 216 km/h

Fig. 8: Power flow during high-speed test with a VC-equipped vehicle andtires with small radius difference

When the smaller tires were mounted on the rear axle, 90% of the total output were transferred to the front axle, but only 10% to the rear wheels. The higher degree of the total efficiency of the direct, mechanical power transfer from engine to front wheels allows of the same vehicle speed (216 km/h in this case) with this vehicle configuration and required only 101.6 kW engine output. The configuration described at first required 107.6 kW. Thus we are confronted with a power loss of approximately 6 kW or 5% in the case of the first configuration. This power loss is converted into heat and causes a considerable increase in temperature of the involved drive components. With the smaller tires mounted on the front axle, the manual transmission was heated up to above 150°C by the power loss, without reaching its steady-state temperature. The rear axle temperature rose to above 120°C until termination of the test. In the case of the second configuration with the considerably reduced powe loss, the steady-state temperatures of the manual transmission and the rea axle rose to approximately 150°C and 70°C, respectively, during the high-spee test, Fig. 9.

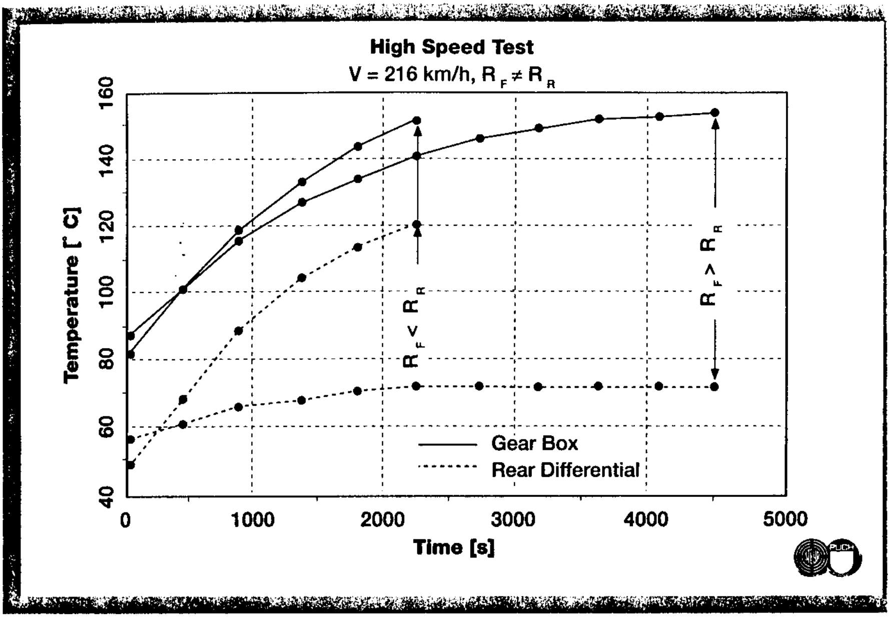

Fig. 9: Temperature measurements during high-speed test, different tire radii

In order to avoid unintended power distributions and the accompanying highe losses, different transmission ratios for front and rear axle can be use intentionally with vehicles featuring a non-positively coupled axle.

Steyr-Daimler-Puch applied this technology for developing the all-wheel driv of the Chrysler Voyager. The all-wheel version of the Voyager features a rea axle coupled via a viscous coupling. The intentional difference between th transmission ratio of the front axle and the one of the rear axle is.1,1% [Lit. 5] It guarantees that no superproportional change in the power distribution of th drive axles can occur, even with small rolling circumference differences betwee front and rear axle. In the case of different tire dimensions, the resultin component temperatures and loads are also reduced. Furthermore, a overrunning clutch integrated in the drive train allows of the rear wheels to tur faster than the front wheels without causing self-generated power. This case for example, occurs during abrupt braking with locked front wheels.

7. Reduced fatigue life due to self-generated torques

Not only can the self-generated torques and the resulting self-generated power lead to the destruction of lubricants and to damaging component temperatures, but also to considerable mechanical component wear due to the high reaction forces. Torque spectra determined during load spectrum measurements in various drive modes proved that the rear axle torque spectra, which were used as reference variable, remain lowest, if the center differential is open. As expected, the spectra increased by almost 100% in the case of only the rear axle being driven, Fig. 10.

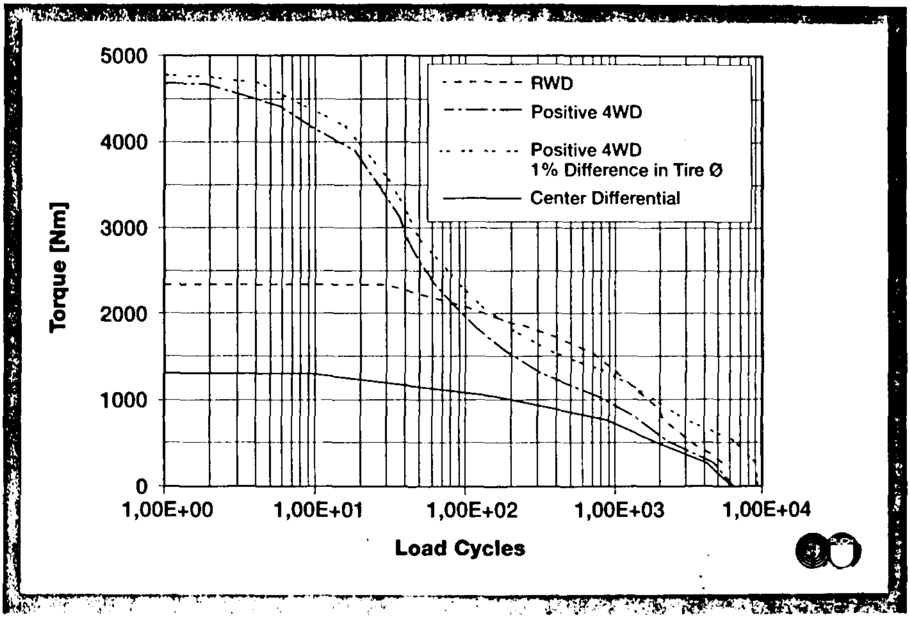

Fig. 10: Frequency distribution of rear axle torque with different drive train configurations (city cycle)

However, the torques sum up to four times their values as a result of the occuring self-generated torques with the all-wheel drive being locked, and the difference of the tire circumferences on the coupled axles being 1 %. These high non-effective torques cause such excessive material loads that those components of the drive train that are exposed to the highest loads, no longer are in the fatigue limit range, but only in the finite life fatigue strength range. The fatigue life analysis of the ring gear in the rear axle of an off-road vehicle driven according to a specified city cycle showed an unlimited fatigue life with the center differential being open. With only the rear axle being driven, the fatigue life during this specific cycle test came close to 26.000 km. This value will be considered 100% for further considerations.

If the same cycle run is carried out with a rigid all-wheel drive and on normal roads, the fatigue life of the rear axle ring gear is reduced to 20% due to the excessive load caused by the self-generated torques. If the tires on front and rear axle differ by 1%, the fatigue life is even reduced to 15% of the reference value, Fig. 11. If the vehicle weight is reduced, the ratios are the same, although the mileage covered is considerably higher.

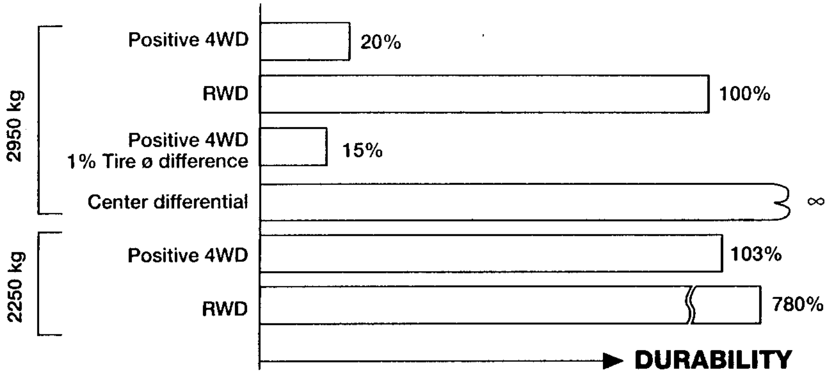

Fig. 11: Relative durability of 4 WD power train configurations

8. Summary

The magnitude of the self-generated torques and their resulting self-generated power in all-wheel drive power trains is frequently underestimated. The increased thermal load caused by these phenomena, and the considerably reduced fatigue life of components are also underestimated. The most important measures for avoiding such self-generated torques and their negative consequences is the proper operation of the differential locks. Transverse and center locks, if there is no automatic control, may only be actuated on off-road terrain. As soon as the vehicle is driven on surfaces with a high friction coefficient, the differential locks must be deactivated immediately in order to avoid high maintenance and repair costs as well as periods during which the vehicle is immobile.

References:

[1] Lanzer H.:
Allradsysteme in theoretischer Betrachtung, Symposium "Geländefahrzeuge in Theorie und Praxis", September 1989

[2] SFT Vorentwicklungsbericht 7/94:
Messung dynamischer Reifenhalbmesser, Wendekreis mit Sperren

[3] Dr. Reif, H.P.; Stelzeneder, F.X.:
A new automatic drive-train management system, Truck and Commercial Vehicle international 1993, Sterling Publications Ltd.

[4] SFT Vorentwicklungsbericht 13/93:
Verspannung bei Kurvenfahrt

[5] SFT Versuchsbericht U3738/1988
Aggregattemperaturmessungen T 115

THE EFFECTS OF LIMITED SLIP DIFFERENTIALS ON THE HANDLING AND TRACTION PROPERTIES OF OFF ROAD VEHICLES

Bruce Maclaurin
Defence Research Agency, Chertsey, UK

ABSTRACT

The paper describes the effects of limited slip and controllable differentials on the handling and traction properties of off road vehicles. A 4 x 4 test vehicle has been constructed which incorporates a controllable double differential in the side-to-side transmission of the vehicle. This enables various differential torque transfer characterstics to be employed. Results from handling and traction trials are described. Computer models have also been developed to predict the effects of differential torque transfer on vehicle handling behaviour both off and on the road. Various results from the models are described.

1. INTRODUCTION

The characteristics of limited slip and controllable differentials affect vehicle handling and traction properties both off and on the road. The paper describes a project being undertaken at DRA Chertsey to investigate these effects. Use is made of a test vehicle and various computer models.

2. THE TEST VEHICLE

The test vehicle is based on a 4 x 4 Fox armoured reconnaissance vehicle. Fox has an H-type transmission with a single centre differential which splits the drive side-to-side. The wheels on each side are constrained to rotate at the same speed (see fig 1a).

2.1 Double Differential

In the test vehicle the centre differential has been modified to behave as a double differential (1). The essential features are a main input drive shaft and two output shafts (as in a conventional single differential) plus a fourth control shaft. The control shaft can be used to either:

(a) control the speed difference between the output shafts - this is the method used to steer most modern high speed track laying vehicles, or

(b) control the torque difference between the output shafts. In this mode the double differential can be used to simulate the characteristics of various forms of limited slip differential as well as to provide a number of further control possibilities.

In the arrangement used in the test vehicle the standard differential is retained and a second differential is mounted parallel to it. This is arranged so that its output shafts rotate in equal and opposite directions and its input or control shaft is stationary for straight ahead running of the vehicle (fig 1b).

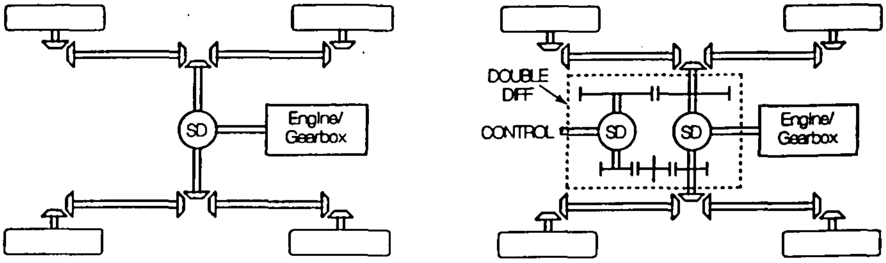

a. Standard Transmission

b. Modified Transmission

Fig.1 Modifications to the transmission of the Fox test vehicle to convert the single differential (SD) to a double differential

2.2 Differential Control

The control shaft is fitted with (a) a disc brake, and (b) a hydraulic power unit which can operate in pump or motor modes. These devices allow various methods of control to be used. Applied torques can be either a braking action (fig 2a) with torque transferred from faster to slower running output shaft, as in limited slip differentials, or a driving action with torque transferred from slower to faster running output shaft (fig 2b) as when steering high speed tracked vehicles.

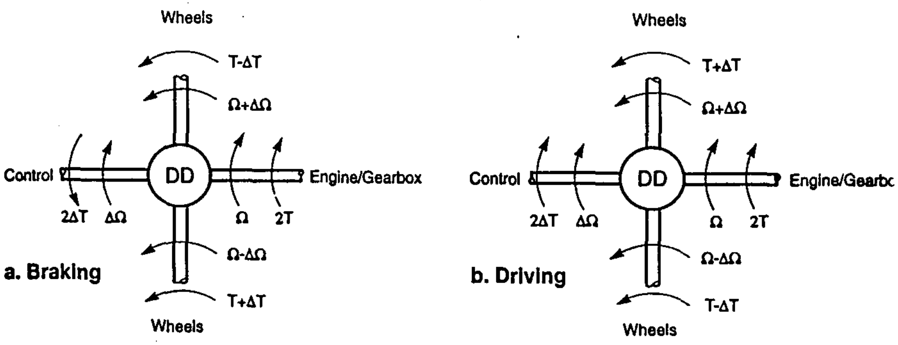
Wheels
T-ΔT
Ω+ΔΩ
Control
DD
Engine/Gearbox
2ΔT
ΔΩ
Ω
2T
Ω-ΔΩ
a. Braking
T+ΔT
Wheels
Wheels
T+ΔT
Ω+ΔΩ
Control
DD
Engine/Gearbc
2ΔT
ΔΩ
Ω
2T
Ω-ΔΩ
b. Driving
T-ΔT
Wheels

Fig. 2 Double differential (DD) showing torque transfers with braking and driving control torques

(a) Disc brake

The disc brake is hydraulically operated and initially braking torque was controlled manually by means of an adjustable spring acting on the disc brake master cylinder. Force on the master cylinder is now applied by a small hydraulic ram with pressure modulated by an electrohydraulic proportional valve (fig 3). The torque reaction on the disc brake is measured and this allows torque transfer to be continuously modulated via closed loop control independently of any changes in pad friction characteristics.

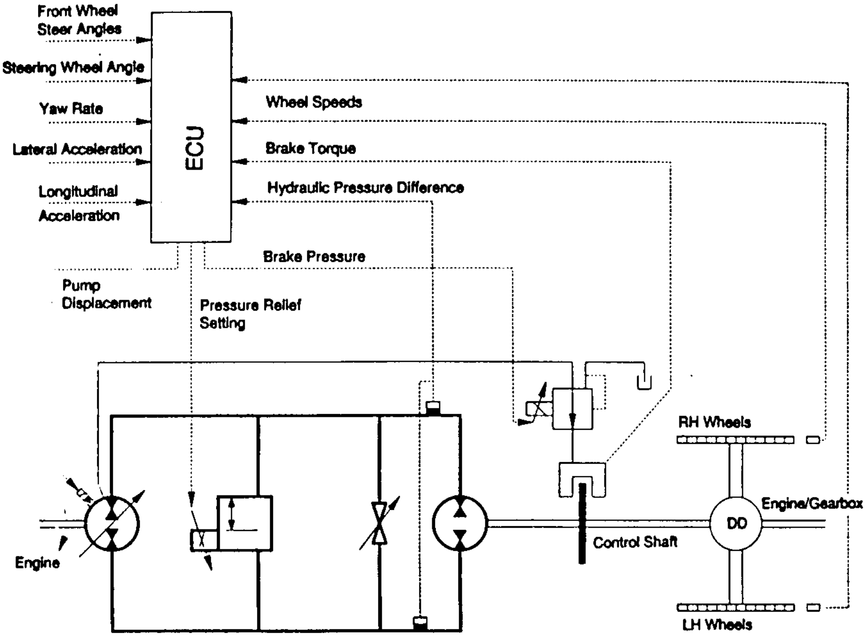
Front Wheel Steer Angles
Steering Wheel Angle
Yaw Rate
Lateral Acceleration
Longitudinal Acceleration
ECU
Wheel Speeds
Brake Torque
Hydraulic Pressure Difference
Brake Pressure
Pump Displacement
Pressure Relief Setting
RH Wheels
Engine/Gearbox
DD
Control Shaft
Engine
LH Wheels

Fig. 3 The control system for the double differential

(b) Hydraulic power unit

Pump mode: the unit can be used on its own as a pump with the output flow fed in closed circuit through a hydraulic restriction. In this mode a braking torque is applied to the shaft. The output flow can either be fed through a simple manually adjustable throttle valve or through an electrically adjustable pressure relief valve (fig 3). As with the disc brake this latter arrangement allows torque transfer to be controlled in closed loop using the pressure difference measured across the hydraulic unit.

Pump/motor mode: the differential hydraulic unit can also be fed in closed circuit from an engine driven variable displacement hydraulic pump (fig 3). By this means power can be fed into the control shaft allowing torque transfer from the slower to the faster running shaft.

Pump displacement, and hence differential control torque (driving or braking), or output shaft speed difference, is electrically controlled. In this mode power can be recovered from the control shaft when it is braked and fed back to the engine via the hydraulic circuit. Recovery will depend on mechanical and hydraulic efficiencies.

2.3 Electronic Control System

Electrical control signals for the disc brake, the pressure relief valve and the pump displacement are supplied by an on-board computer and sensor set (fig 3). Additional sensors and a data acquisition unit are used for measuring vehicle handling properties.

2.4 Test Vehicle Data

The test vehicle (fig 4) has double wishbone and coil spring suspension and is fitted with power steering. The driver sits at the front of the vehicle with the engine at the rear. The vehicle weighs 45 kN in its present form with a 45/55 front to rear weight distribution. Fig 5 shows the inside of the vehicle with the differential control motor and some of the associated hydraulic and electronic control systems.

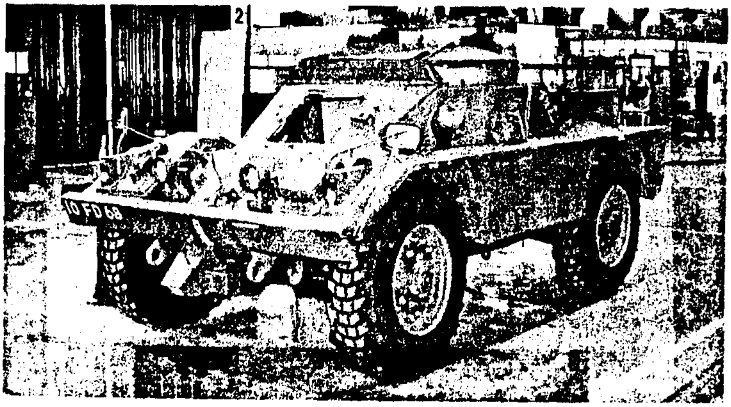

Fig. 4 The 4 x 4 test vehicle

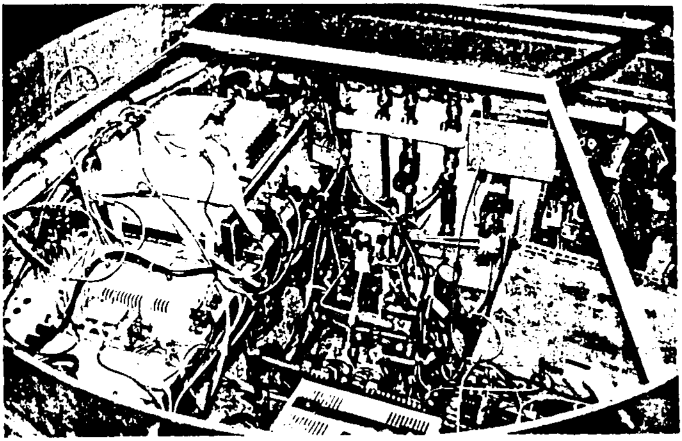

Fig. 5 Inside view of the test vehicle showing the differential control motor and some of the associated hydraulic and electronic control systems

3. COMPUTER MODELS OF STEERING AND HANDLING BEHAVIOUR

Two models have been developed to predict the effects of various types of differential on vehicle handling properties. One is mainly intended to predict on-road behaviour and the other behaviour on off-road surfaces.

3.1 On-Road Model

The model, called ACDIFF, was developed to predict the steady state handling behaviour of H-drive vehicles with various differential torque transfer characteristics. The model caters for the effects of detailed suspension and steering geometries, measured tyre characteristics, steering compliance and drive shaft angularity. It was developed and validated with the aid of handling trials with the Fox test vehicle. Two methods were used to produce differential torque transfer, a) disc brake with steady state torque settings and, b) pump and throttle valve ('viscous') control. The measured characteristics of the 'viscous' control for different settings of the control valve are shown in fig 6. Measured and predicted steady state handling behaviour for the different valve settings on the 45m radius steering pad test are shown in fig 7, which shows steering wheel angle against lateral accelation ('latac'). Comparison is seen to be good.

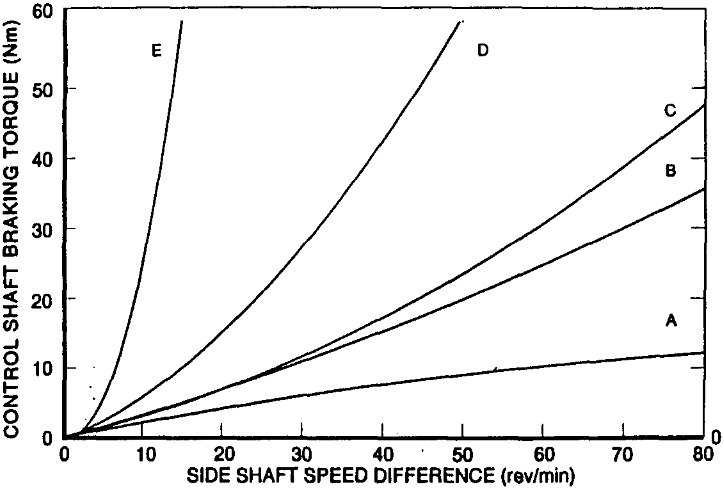

Fig. 6 Characteristics of hydraulic pump and adjustable throttle valve control at different settings

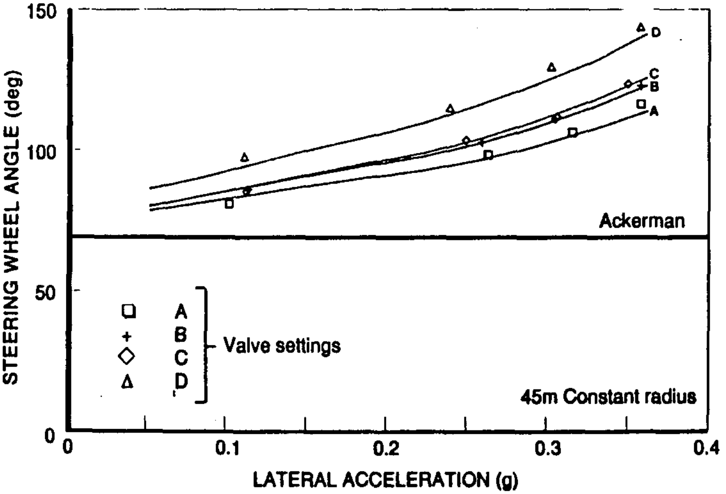

Fig. 7 Comparison of predicted and measured steering wheel angles for pump and throttle valve control

Predicted steady state behaviour of the vehicle at a constant speed of 60 km/hr and with varying radius is shown in fig 8. Response is shown for a disc brake limiting torque of 100 Nm and for 'viscous' control setting C. This type of display is more representative of normal driving conditions. At low latacs, large radii, the disc brake is locked and comparatively large increases of steering wheel angle are required to counter the yawing moments induced on the vehicle. Above about 0.04g the brake slips and the increase of steering wheel angle with latac is more gradual. The 'viscous' control shows a more progressive understeer characteristic leading to similar steering wheel angles to those for the disc brake control at higher latacs. Drivers do express a preference for the more progressive characteristic of the 'viscous' control.

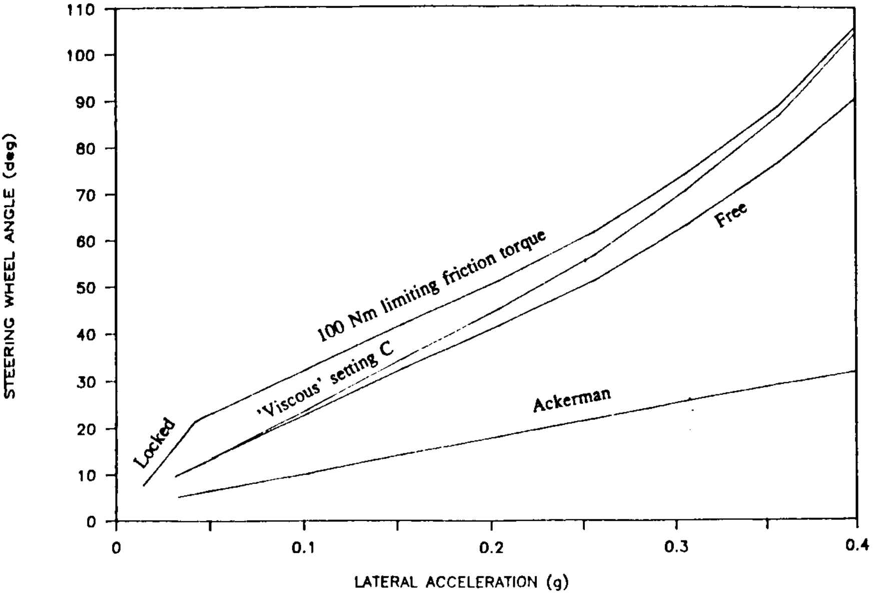

Fig. 8 Predicted handling behaviour of test vehicle comparing 100 Nm limiting friction and 'viscous' control at setting C for a constant speed of 60 km/hr

3.2 Off-Road Model

The other model, called STEERDIFF, is more specifically designed to predict behaviour in soft soils. Three types of tyre model are available one of which is also suitable for describing on-road behaviour. Two of the off-road tyre models make use of non-dimensional Mobility Numbers (1). Two types of wheel drive layout are available, a) the more conventional layout with differentials distributing drive between axles which in turn are fitted with differentials between the wheels, and b) the H-type layout, as used on Fox, with a single differential splitting the drive to wheels on each side of the vehicle which are usually constrained to rotate at the same speed. This layout is more commonly used on military armoured vehicles to reduce drive line intrusion into the hull space..

Axles can be driven or undriven and steered or unsteered. Suspension effects are limited to bounce and roll stiffnesses for the axles and a constant height roll centre is assumed. Various types of differential control can be specified:

- free
- locked
- constant setting friction torque transfer
- friction torque transfer proportional to input torque
- over-run, all torque to slower running shaft
- velocity proportional ('viscous'), $\Delta T = K \Delta\omega^n$

where ΔT = torque transfer
$\Delta\omega$ = speed difference between output shafts
K and n are constants.

In addition, for the H-type drive layout the differential can be 'actively' controlled with an output shaft speed difference specified as a function of steering wheel angle and forward speed. This is extended to include 'skid' steering with no Ackerman effect and steering controlled by adjusting the speed difference across the differential.

3.3 Results from the Off-Road Model

Fox Test Vehicle: Fig 9 shows results for the Fox test vehicle performing a 10m radius turn in soft soil with tyre/soil interface conditions equivalent to a Mobility Number N = 5 (giving a limiting coefficient of traction of 0.3). The figure plots mean front wheel steer angle against lateral acceleration. With the free differential the vehicle has a gently increasing understeering characteristic with a limiting lateral acceleration of 2.35 m/s^2. Generally speed is limited by the available lock angle. With the locked differential considerable increases in lock angle are necessary to counter the yawing moment caused by the increased traction from the inside wheels and reduced traction from the outside wheels. Limiting latac is 1.9 m/s^2. With the over-run type differential there is little effect at low latacs because drive tends to alternate between inside and outside wheels. At higher latacs drive increases on the inner, less highly loaded, wheels again requiring increases in lock angle.

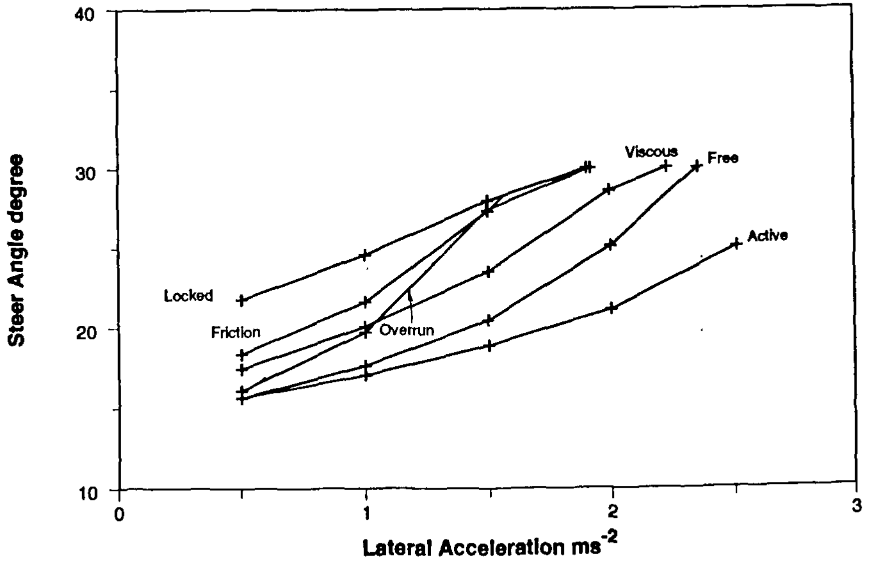

Fig. 9 Predicted steering behaviour of the Fox test vehicle performing a 10m radius turn in soft soil with various methods of differential control

The constant friction differential is shown with a low setting of 500 Nm limiting torque transfer giving ± 5% difference in tractive coefficient between the sides of the vehicle. The differential slips up to an acceleration of 1.6 m/s^2 and then locks. If the torque bias is increased to 1000 Nm then the differential locks at a latac of 0.5 m/s^2. The viscous coupling causes a more progressive characteristic.

The on-road behaviour of the Fox vehicle predicted by STEERDIFF for a 10m radius turn is shown in fig 10. Relative behaviour of the differentials is generally similar to that on soft soil although limiting latacs are of course higher. In this case the friction bias differential slips throughout the speed range. The active control permits a significant increase in limiting acceleration over the free differential, 4.5 m/s^2 compared to 3.5 m/s^2.

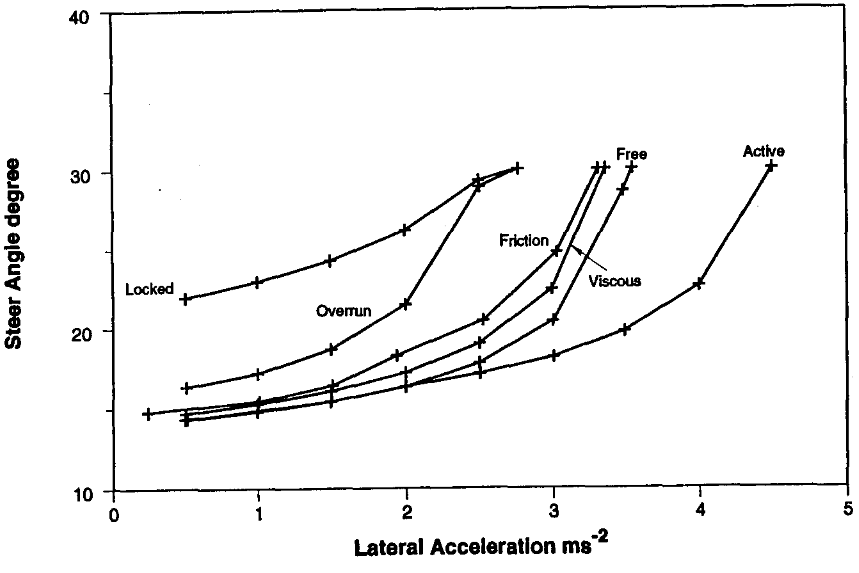

Fig. 10 Predicted on-road steering behvaiour of the Fox test vehicle performing a 10m radius turn with various types of differential control

6 x 6 Concept Vehicle: Similar results for a 6 x 6 concept vehicle are shown in fig 11. The vehicle weighs 160 kN with a wheelbase of 3.1 m (1.55 + 1.55) and a track of 2.4 m. Again a tyre/soil mobility number of N = 5 is used. Results are broadly similar to those shown for the Fox vehicle although in this case a much 'softer' viscous coupling was used. The predicted behaviour of the vehicle with skid steering was also investigated. Fig 12 shows wheel speed difference between the sides of the vehicle plotted against latac and indicates a steady increase of wheel speed difference with latac. Maximum latac is 0.195g with the skid steering compared to 0.215g with the free differential.

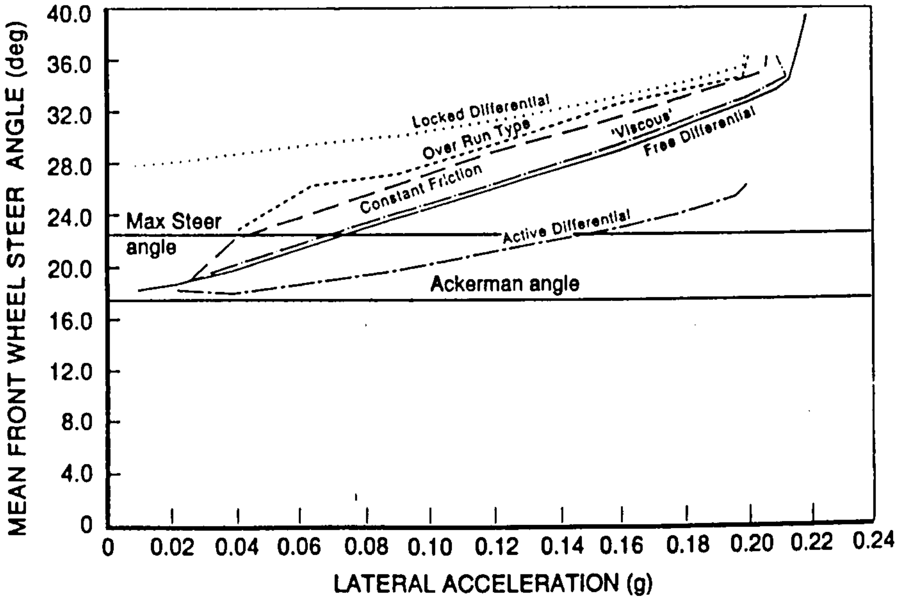

Fig. 11 Predicted steering behaviour of 6 x 6 concept vehicle performing 10m radius turn in soft soil (N = 5)

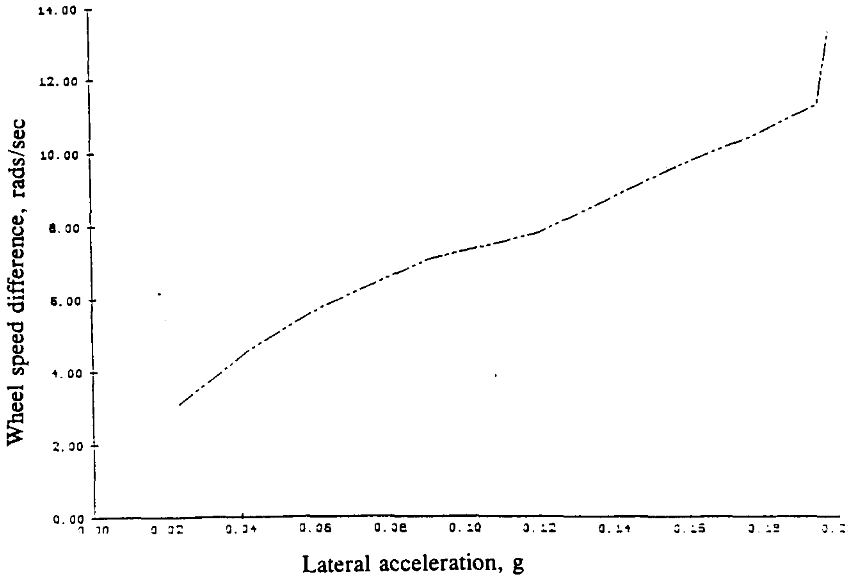

Fig. 12 Predicted behaviour of 6 x 6 concept vehicle with skid steering performing 10m radius turn in soft soil (N = 5)

Figs 13a to 13d compare the wheel drive torques with free, locked, 'active' and skid steer differentials. With the free differential the drive torques for the six wheels are similar, any difference reflecting 'wind-up' torques between the wheels on each side of the vehicle. With the locked differential drive torques are greater on the inside at low latacs because of the greater wheel slips. As latac and weight transfer increase the torques tend to equalise to values similar to those for the free differential. With the active differential the reverse situation applies with similar wheel drive torques on all wheels at low latacs but with greater torques on the outer wheels as the effect of the active differential becomes more apparent.

The wheel drive torques for skid steer are shown in fig 13d with the outer torques more than double the inner over most of the speed range. The torques required to overcome rolling resistance are about 4.5 kNm so the inner wheels are not producing net traction over most of the speed range.

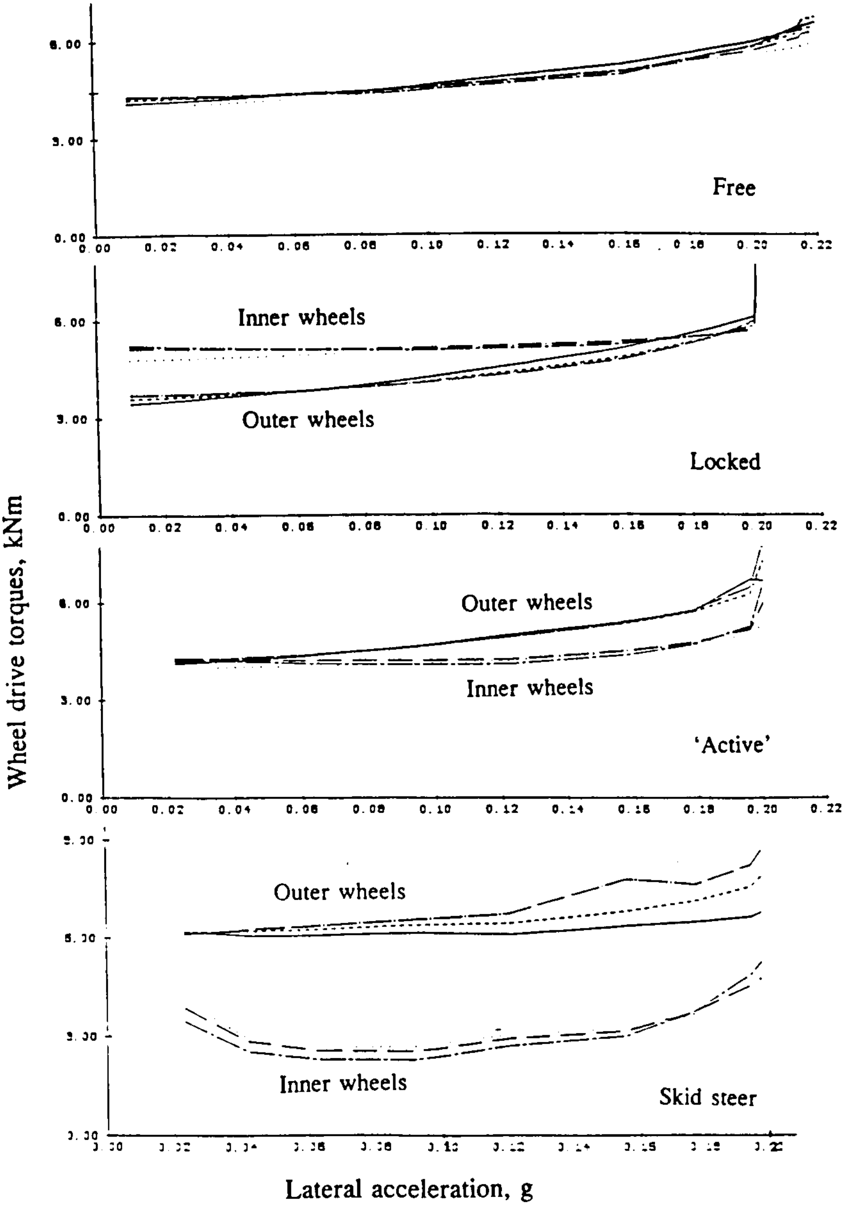

Fig. 13a,b,c and d. Predicted wheel drive torques for 6 x 6 concept vehicle performing 10m radius turn in soft soil (N = 5)

Power inputs to drive and steer the vehicle at a latac of 0.18g are shown in the following table.

Differential type	Power kW		
	Drive	Steer	Total
Free	213.4	-	213.4
Locked	237.8	-	237.8
Active	228.5	2.0	230.5
Skid steer	217.5	26.7	244.2

Largest power input is for the skid steer, as would be expected. The steer power input for the active control is comparatively small considering the effect produced and could be supplied by a modestly sized electric motor.

5. VEHICLE TRACTIVE PERFORMANCE

Traction trials were carried out with the Fox test vehicle in an indoor sandpit of loose dry sand. Average soil strength as measured by a cone penetrometer was 4000 kPa/m. The vehicle was driven in bottom gear with load reacted against a dynamometer vehicle. Trials were performed in two conditions:

a) with all wheels in the sand;

b) 'split-μ', with the wheels on one side running on sand boards.

The coefficient of net traction for various settings of the differential 'viscous' control are shown in fig 14. With all the wheels in the sand traction increases from 0.12 with free differential to 0.17 with setting E. This increase is probably due to small differences in soil strength between the sides of the vehicle as it progresses forward. With the free differential traction is limited by the side of the vehicle with the slightly lower soil strength. Differential restriction allows torque transfer to the side of the vehicle with stronger soil and overall traction increases.

In the 'split-μ' condition traction coefficient increases from 0.16 with the free differential to 0.25 with differential setting E. The increase in traction with the free differential compared to the all wheels in sand condition is caused by the reduced rolling resistance of the wheels on the sand boards.

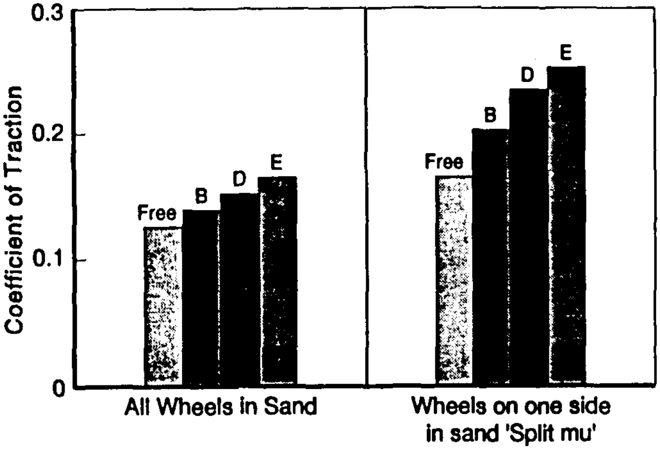

Fig. 14 Measured traction of test vehicle in sand showing effects of various settings of differential 'viscous' control

6. CONCLUDING REMARKS

The double differential and its associated control system have successfully demonstrated their ability to simulate various types of limited slip differential and their effects on vehicle handling and traction. Experience with computer control of the differential is also being accumulated, a) with the proportional throttle valve, and b) with full 'active' control of the differential motor. Drivers express a marked preference for the handling behaviour of the vehicle with 'active' control compared to the free differential - particularly when cornering under limiting conditions. The most marked improvement occurs during braking in a turn tests. With the free differential the vehicle slews round at 90° to the direction of travel. In contrast, with 'active' differential control the vehicle maintains its line.

The on-road computer model has successfully demonstrated its ability to predict the effects of differential torque transer on vehicle handling behaviour. The off-road model indicates that different types of differential control can have a marked effect on steering and manoeuvring performance in soft soils. Progress with the model depends on obtaining further tyre-in-soil performance data from the DRA Mobile Tester.

7. REFERENCES

1. Maclaurin, E B and Crolla, D A, "Wheel Spin Control for On/Off Road Vehicles", Proc I Mech E, Conference on Traction Control and Anti-Wheel Systems for Road Vehicles, London, 1988, Paper C363/88.

2. Maclaurin, E B and Hall, L C, "The Effects of a Controllable Double Differential on the Handling and Traction Properties of a 4 x 4 Vehicle", Proc I Mech E, Conference of Vehicle Ride and Handling, Birmingham, 1993, Paper C466/010/93.

ADM
A NEW DRIVE-TRAIN MANAGEMENT

Franz X. Stelzeneder
Steyr-Daimler-Puch AG
Antriebstechnik

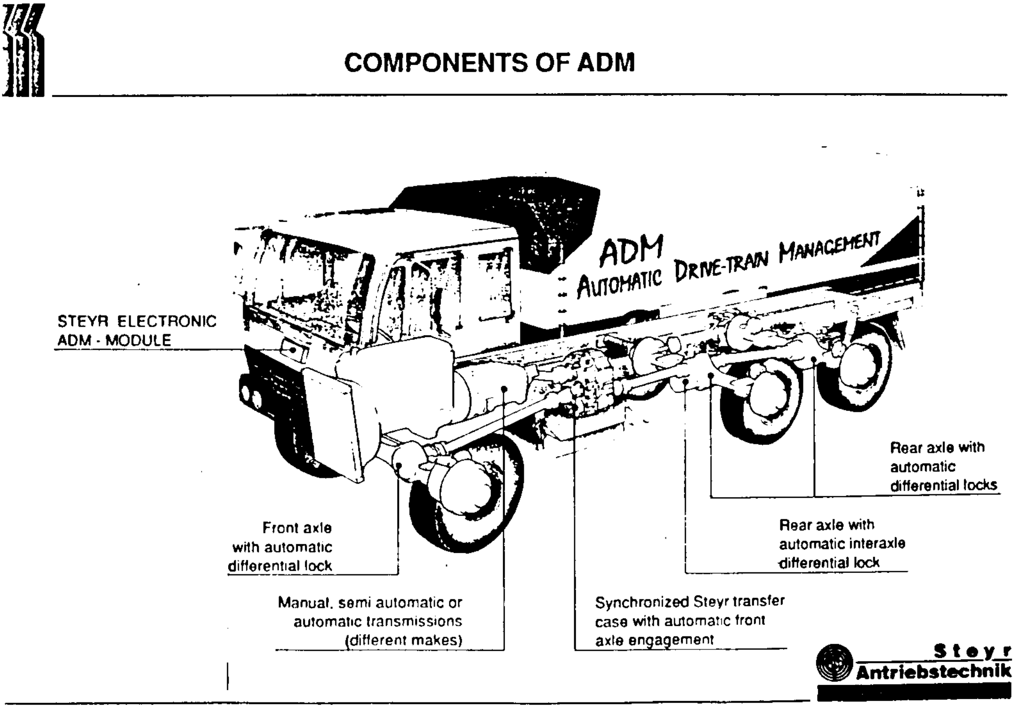
COMPONENTS OF ADM
ADM
AUTOMATIC DRIVE-TRAIN MANAGEMENT
STEYR ELECTRONIC ADM - MODULE
Rear axle with automatic differential locks
Front axle with automatic differential lock
Rear axle with automatic interaxle differential lock
Manual, semi automatic or automatic transmissions (different makes)
Synchronized Steyr transfer case with automatic front axle engagement
Steyr Antriebstechnik

Fig. 1 ADM Drive-Train

1. Introduction

The demand for safe and economical operation is in the performance specifications of virtually all vehicles. The fulfilment of this demand always depends on the state of the art at the time and on the budget available for the purchase of the vehicles.

- Simpler controls and
- greater comfort

are important measures for increasing safety because both of them allow the driver to devote his full concentration to steering the vehicle, advantageous both for the untrained and for the trained driver.

There has for some time been a call for automatic systems fulfilling these demands and that more precisely in the case of all-wheel-drive cross-country vehicles, for these have a lot of systems which in general can only really be properly used by well trained drivers.

Fire engines and other vehicles of the emergency services and of the armed forces as well as local authority vehicles such as snow-clearing vehicles, but also vehicles for the construction industry, have reached a very high technical level with respect to their equipment because of the high demands made of them, but are not quite at the state of the art so far as traction systems are concerned.

The main reason for this is that for the extreme demands made of the drive-train of cross-country trucks there have until now been no satisfactory solutions combining the desired increased safety with greater economy.

The new ADM drive-train management offers a new solution in this direction based on well proven material and utilising the very latest technology.

The application of this automatic system is in principle conceivable with suitable adaption for all multi-track vehicles.

It has, however, been developed on trucks for the class over 7.5 tonnes maximum permissible gross vehicle weight to which the following detailed explanations refer.

2. Automated Shifting of the Speeds in the Transfer box

2.1 The State of the Art

The shifting of the speeds in the transfer box is performed in a conventional all-wheel-drive truck either mechanically or pneumatically with the aid of dog clutches. On account of the normally large ratio it is necessary to stop the vehicle before changing from the high to the low gear, which means a loss of mobility that is just not acceptable in emergency vehicles.

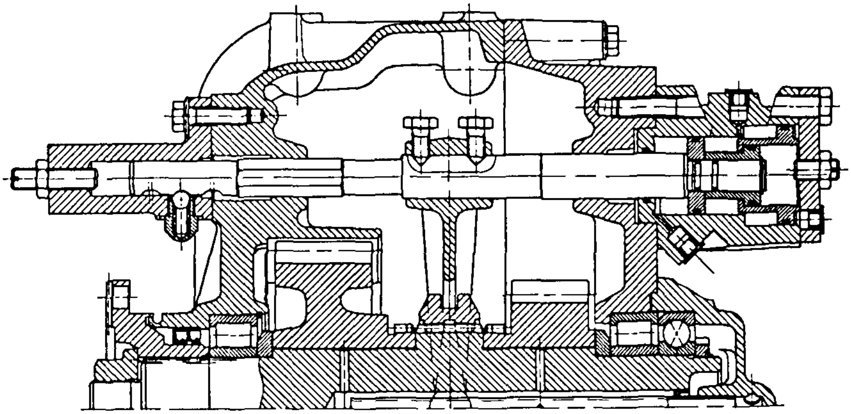

Fig. 2 High/Low Shifting on the VG750, existing Solution with a Dog Clutch

2.2 Aims

To remove this disadvantage we set ourselves the following targets:

- The possibility of shifting in the complete speed range
- Security against incorrect operation
- Partial automation of the shifting-action

- Short shifting-time
- Use of a series synchromesh unit
- Possibility of mounting in transfer boxes currently available
- Retention of all previous functions and versions of the transfer box

2.3 Solution

With the aid of a synchromesh unit and an electronic control unit the driver is enabled to shift from the high to the low gear with the vehicle in full motion. Compressed air, which is available in heavy trucks, is used for the operation.

To date our VG1200 and VG750 transfer boxes have been equipped with such a shifting-unit and are already available (see Fig. 3).

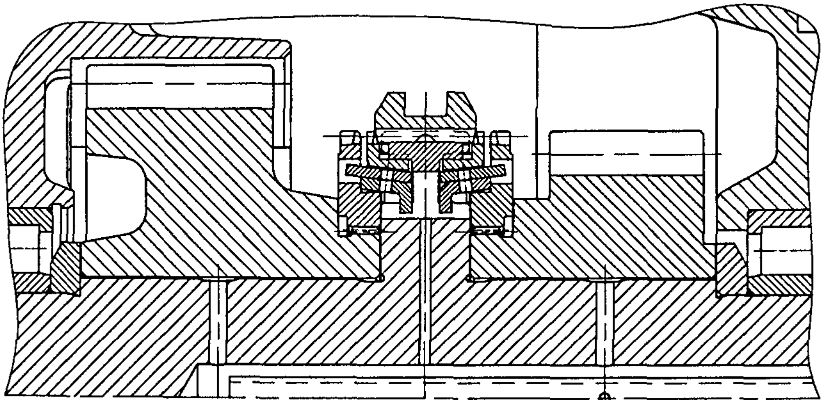

Fig. 3 Synchronised Shifting in the VG 750

The shifting-process is as follows:

The driver communicates to the electronics his wish to shift by preselection on a key and depresses the clutch pedal. The electronic control unit checks the engine rpm and the air pressure and if these are in order, the shifting is performed. When it is completed, there is an acoustic signal indicating to the driver that he can release the clutch pedal.

The electronic system performs a protecting function, on the one hand preventing overloading of the mechanical system and guaranteeing a long lifetime and on the other hand keeping the driver out of dangerous situations which could arise if the engine is overrevved or when there is a fault in the compressed air system through a sticking of the transfer box in neutral.

The shifting-time is the same as in manual shifting and amounts to about 0.7 seconds.

2.4 Testing

The fine tuning and testing of the functioning were mainly carried out on the vehicle.

The durability tests covered 10,000 shiftings to each gear. Two complete durability tests were performed on the test-bench and one in practical vehicle operation.

2.5 Prospects

The flexibility of the electronic control unit should permit complete automation of gear-changing when an automatic gearbox is used at the same time, which would be a further step in the direction of increased safety. The first studies have already been undertaken.

3. Automatic Management of All-Wheel Drive and Locks

3.1 The State of the Art

3.1.1 Manually shifted Traction Systems

Systems such as engaging axles and differential locks on the basis of dog clutches are widespread in commercial vehicles.

The advantage of such systems is above all the possibility of transmitting 100% of the available drive torque with small construction size because of the interlocking connection. This solution is also the lowest-priced possibility for an effective traction system.

The greatest disadvantage of these interlocking clutches operated by the driver is that he must know exactly in what situations the engaging of all-wheel drive or the locking of a differential helps the vehicle forward and in what situations the engaging of one or more of these systems presents possible danger.

The ability to assess the quality of the ground exactly in advance and to engage all-wheel drive or differential locks at the front or at the rear at the right time or more than one of these simultaneously and all that usually in difficult or critical driving-situations is possessed by hardly any drivers.

Incorrect operation can end in a broken clutch and create dangerous driving-situations for the driver.

3.1.2 Automatic Traction Systems

Automatic systems on the basis of friction clutches are often used in private cars but cannot give satisfaction in trucks. Multi-disc clutches with the high transmission of torque required in a truck cannot be fitted into the mounting space available in conventional axles. In addition to that such a solution costs many times the price of a dog clutch.

3.2 Development Aims

In the new ADM drive concept the advantages of a dog clutch are combined with those of automation.

The development aims pursued can be summarised as follows:

- Automatic operation on the basis of slippage control
- Transmission of torque 100%
- A low-priced solution taking into account the possibility of mounting in existing aggregates
- Engaging of the traction systems when required
- Engaging of the traction systems also when a stabilising effect is sought
- Automatic disengagement of the systems when their effect is no longer required
- Compatibility with ABS
- Intervention in the engine for the purpose of stabilising when the axles are locked (4x2, 6x2, 6x4)

To realise these aims an electronic control unit is used which activates every traction system available in a vehicle on an individual basis at the right moment.

3.3 Functioning

The automatic engaging of axles and locking of differentials as a function of ADM is based on the use of the dog clutches which are activated by an electronic control unit according to the slippage.

The sliding-sleeve is held by the operating-device for a short time in the engaged position and then left on its own. As long as a drive torque is transmitted on the clutch, i.e. its effect is needed, friction keeps the clutch meshed.

As soon as the torque transmitted becomes zero, a release device pretensioned in the moment of engaging pushes the sliding-sleeve back into its initial position.

3.4 Development

Practical tests formed the basis of the development of ADM.

The first functional tests, designed to establish the shiftability of dog clutches, were performed on the test-bench with the engagement of all-wheel drive in the VG1200 transfer box.

Interlocks and differential locks were not included until the functioning of the transfer box was assured.

Durability tests on the mechanical parts of the engagement of the all-wheel drive and of the differential locks were also carried out on the test-bench for reasons of cost. For this a variety of test-bench constructions were necessary.

The complete development of the electronic software was done in the vehicle.

The strength of the ADM clutches was calculated with the aid of finite element models.

Torque-measurements were performed to assess the loadings arising.

A drive-train simulation model permits the conversion of the measurements to all conventional drive-trains so that the effects of the use of ADM can be worked out for any truck within a short time.

3.4.1 Test-Bench Tests

3.4.1.1 Measurements of Shifting-Limits

One of the most important preconditions for the functioning of ADM is the shiftability of the dog clutch when there are different rpm's between the two clutch parts to be connected.

To test this part the drive-train was erected on the test-bench.

3.4.1.2 Durability Testing

To test the durability of all the shifting parts in a sensible manner it is necessary to make a model of the drive-train as close as possible to the real thing.

This problem was solved by putting a complete vehicle on a roller test-bench and performing the acceleration process and shifting process at certain settable rpm differences fully automatically. With safety measures it was possible to run 24 hours a day and so reach an acceptable test period at low cost.

3.4.2 Testing by Drivers

To assess the functioning of ADM it was important to test the system in as many different vehicles as possible with different drive-trains and different operating characteristics.

A total of six different vehicles with different drive-trains and designed for different operational demands were used. A description of these vehicles will be found in Appendix.

The most varied tests were performed with these vehicles in order to suit the system to as many applications as possible.

3.4.2.1 Desert Testing

The testing parameters in the desert were extreme climatic conditions and great variations in the ground quality, such as loose sand, compressed sand and rocks. The vehicles used here were:

- Steyr 12M18/4x4
- Hino Ranger/4x4
- Steyr 1491.330/6x6

About 6,000 km were covered by each vehicle in the Egyptian part of the Sahara.

3.4.2.2 Winter Testing

The opposite conditions to those of the desert testing were encountered in the Mühlviertel about 100 km North-East of Steyr in mid-winter conditions such as deep snow, ice and μ-split roads.

The vehicles used were:

- Steyr 19S37/4x2
- Steyr 12M18/4x4
- Hino Ranger/4x4
- Steyr 1491.330/6x6

The vastly different road conditions between asphalt and ice provided the most severe criterion for the functioning of ADM.

3.4.2.3 Road Testing

The road testing ranged from motorways to mountain passes with sharp gradients in different weather conditions.

The vehicles used were:

- Steyr 19S37/4x2
- Steyr 1291/280/4x4
- Steyr 12M18/4x4
- Steyr 1491.330/6x6

On these test runs the main criterion was the avoidance of unwanted engagements on roads with a good grip. Situations were also discovered, in particular when operating with a trailer on steep gradients, in which the engaging of certain traction systems has a stabilising effect and is therefore desirable.

3.4.2.4 Cross-Country Testing

A large part of the tests were carried out on the company's own testing-ground at St.Valentin, where an asphalt road, a rough track, mud, a gravel pit and gradients up to 50% provided ideal conditions for the necessary tests.

The results of all these tests will be dealt with in more detail in the next chapter.

3.5 Construction of the ADM System

The basic construction of the system can be seen in Fig. 4.

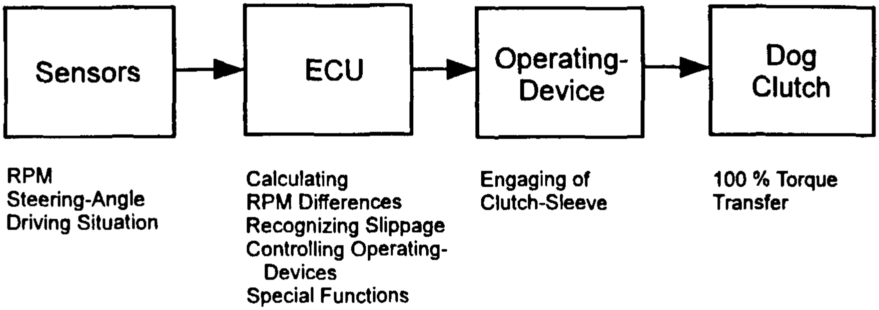
Sensors
ECU
Operating-Device
Dog Clutch
RPM
Steering-Angle
Driving Situation
Calculating
RPM Differences
Recognizing Slippage
Controlling Operating-Devices
Special Functions
Engaging of Clutch-Sleeve
100 % Torque Transfer

Fig. 4 ADM System Diagram

3.5.1 Sensors

3.5.1.1 Tasks of the Sensors

- To establish the driving-conditions
- To transmit an appropriate electric signal to the electronic control unit

The main input values are the wheel rpm's, from which the slippage is calculated.

The steering-angle is used in order to be able to take the effects of cornering into account in the calculation of slippage.

Further driving-values determined are the position of the accelerator pedal, the braking-situation and the position of the clutch. These enable the control unit to recognize the driving-situation and react to it.

In selecting the sensors we made use of units already well proven such as the ABS wheel rpm sensor.

3.5.2 Electronic Control Unit

3.5.2.1 Tasks of the Electronic Control Unit

- To process the signals from the sensors
- To recognize rapidly and surely the conditions under which each individual traction system has to be engaged
- To recognize conditions harmful to the mechanical system
- To control the operating-devices
- To act as an interface to other electronic control units in the vehicle
- To recognize and display faults

In the control unit the signals are filtered, the rpm differences are calculated and the individual traction systems such as all-wheel drive and differential locks are engaged individually depending on the requirements taking the driving-situation into account and following a fixed shifting-logic.

The ADM switching-logic contained in the software is the sum of the know-how gained during all the driving -tests and the subsequent discussions between all the members of the project and various specialists engaged.

The instrument FMEA (Failure Mode and Effects Analysis) was used amongst other things to analyse the effects of ADM on possible critical driving-situations and to react to them.This also greatly influenced the shifting-logic.

The ADM shifting-logic was compiled from the safety, optimum functioning and durability angles and consists of criteria for engaging and the interlinking of shiftings.

3.5.2.2 Criteria for Engaging

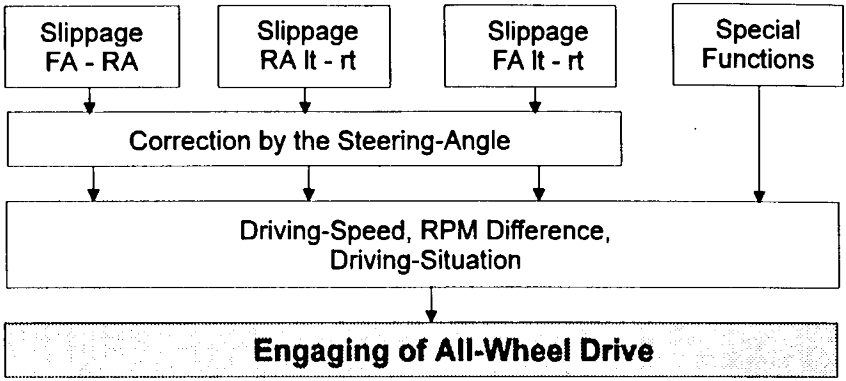
Slippage FA - RA
Slippage RA lt - rt
Slippage FA lt - rt
Special Functions
Correction by the Steering-Angle
Driving-Speed, RPM Difference, Driving-Situation
Engaging of All-Wheel Drive

Fig. 5 Criteria for Engaging All-wheel Drive

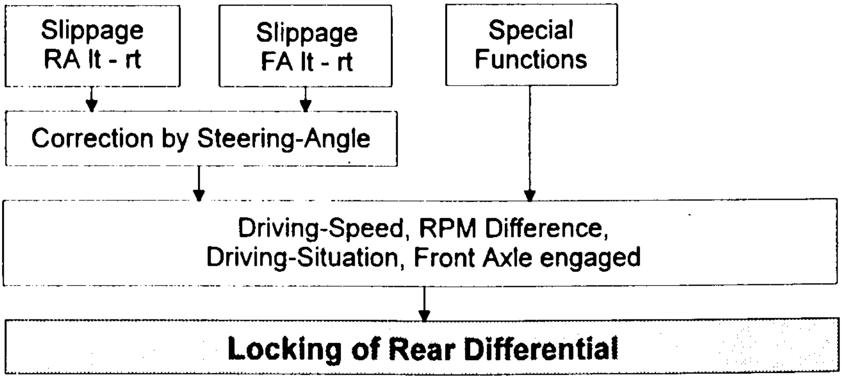
Slippage RA lt - rt
Slippage FA lt - rt
Special Functions
Correction by Steering-Angle
Driving-Speed, RPM Difference, Driving-Situation, Front Axle engaged
Locking of Rear Differential

Fig. 6 Criteria for Locking Differential on Rear Axle

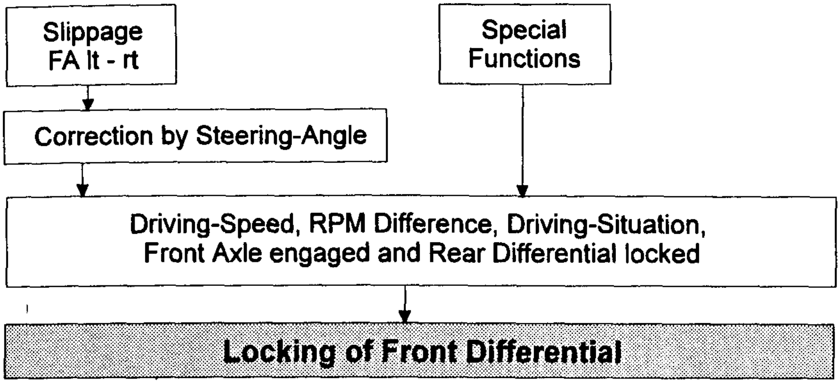
Slippage
FA lt - rt
Special
Functions
Correction by Steering-Angle
Driving-Speed, RPM Difference, Driving-Situation,
Front Axle engaged and Rear Differential locked
Locking of Front Differential

Fig. 7 Criterion for Locking Differential on Front Axle

The main factor determining the engaging of all-wheel drive or locking of differentials is the wheel slippage, which is corrected by the steering-angle so that the apparent slippage produced by the different bend radii of the individual wheels when cornering can be taken into account in the calculation.

The engaging of the individual ADM functions can be limited through the driving-speed. Our experience shows that all-wheel drive can be useful in all speed ranges because it often has the effect of stabilising the vehicle so that this limit can be raised to the maximum speed of the vehicle as long as no reasons specific to the vehicle or to the operation require a decision to the contrary.

The locking of the rear differential makes sense only up to a speed of about 40 km/h because this action only increases traction and has no stabilising function. When the engine is braking the vehicle travelling downhill on a very slippery road the lateral guidance of the wheels is needed on bends. For this reason the differential on the rear axle is not locked in this situation.

The use of the differential lock on the front axle brings with it a marked reduction in steerability. If the driver is not aware of this, critical driving-situations can result. For this reason and because of its relatively low effect, a differential lock is found on the front axle only of vehicles for extreme cross-country conditions where the traction reserves have to be used to the last dot.

In order to rule out such critical driving-situations with ADM, the differential on the front axle is locked only up to a speed of 15 km/h and never when the engine and rear axle are working against each other when travelling downhill and never when braking.

The limitation in the activation of the dog clutches through the rpm difference serves to protect the clutches from mechanical destruction. The limits are, however, so high that the functioning is not impaired and only misuse can find out the limits of the system.

In the braking-situation a distinction is made between vehicles with ABS and vehicles without ABS.

Whereas in vehicles with ABS all engagings are prevented in the ABS control range but all-wheel drive is permitted in the lowest speed range where the ABS does not function, the engaging of all-wheel drive is possible in the whole speed range in vehicles without ABS when the calculation of the slippage indicates the conditions for engaging.

Axle differentials are never allowed to be locked during braking.

3.5.2.3 Interlinking of Shiftings

The recognition that misuse of axle differential locks, in particular of that on the front axle, can cause critical driving-situations under certain conditions led to an interlinking of the systems, according to which the individual traction systems are always engaged in the order of their effect so that the activation of a lower-order system is then often no longer necessary.

This order is:

1. Engaging of all-wheel drive
2. Locking of the differential on the rear axle
3. Locking of the differential on the front axle.

The effect is thus achieved that the most critical system, locking of the differential on the front axle, has to be activated only in the rarest of cases.

The demand that all-wheel drive must be engaged before the differential on the front axle is locked (see Fig. 7) does not seem to be sensible because slippage cannot occur on the front axle until the all-wheel drive is engaged. This function is intended, however, above all to keep the front-wheel drive engaged as long as the differential on the front axle is locked.

Fig. 8-10 show the process from the measurement of the rpm to the activating of the dog clutches and how they are interlinked.

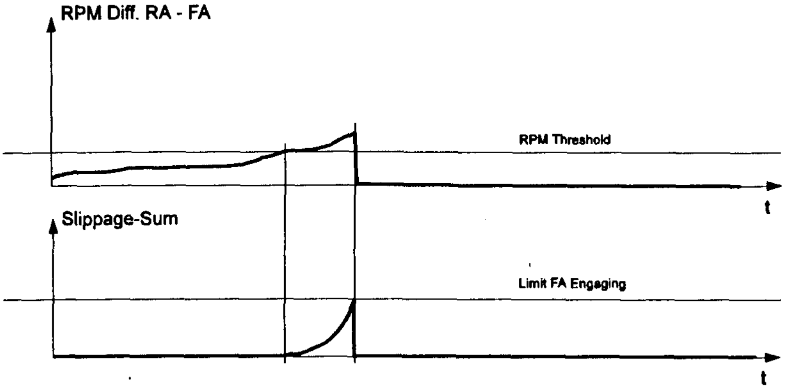

Fig. 8 Engaging of the Front Axle

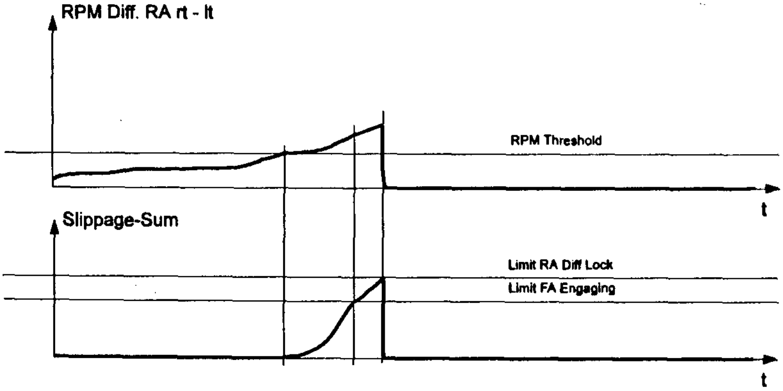

Fig. 9 Locking of the Rear Differential

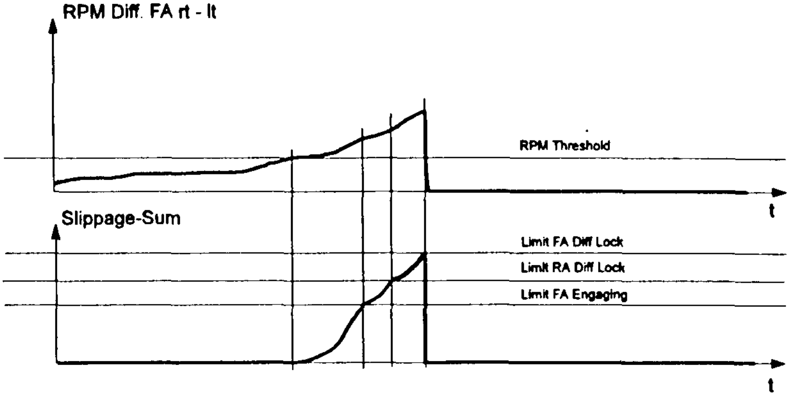

Fig. 10 Locking of the Front Differential

The figures show the course of an rpm difference pattern as it is calculated by the electronic system from the rpm's measured. When the response threshold is passed, what we call a slippage-sum counter is set in motion which in every run of the program, lasting 10 msecs, calculates the current slippage from the rpm difference present and totals it. As soon as this total exceeds the prescribed limit, the appropriate traction system is activated.

In this way the slippage arising is evaluated and the clutch is not activated immediately every time a prescribed slippage threshold is passed, which would lead to frequent unnecessary engagings. There are many disturbing factors which arise for a short time and are filtered out by this system.

As a matter of principle an rpm difference between the front and rear axles activates all-wheel drive and slippage between the left and right wheels of an axle causes the locking of the differential on that axle.

The interlinking arises because when there is slippage between the left and right wheels of an axle all-wheel drive is also activated and that earlier because of the lower threshold so that in most cases the all-wheel drive increases the traction sufficiently without any need to lock a differential.

When there is slippage on the front axle, the differential on the rear axle is locked before that on the front axle.

3.5.2.4 Data Bus

An important function of the electronic control unit for the future is the exchange of data with other electronic systems of the vehicle in order to gain more and more precise information about the driving-situation.

This function is realised through a CAN bus and an ISO interface.

These interfaces will have their first application in the communication with ABS, from which the wheel rpm's are taken, so that it is not necessary to fit double wheel rpm sensors.

3.5.2.5 Fault-Recognition and -Output

The fault-recognition installed is intended above all to enhance safety since it permits the evaluation of faults arising according to their effects and the disengaging or partial disengaging of the system depending on the gravity of the fault.

A fault-output by means of a diagnosis connection serves above all to find faults in the workshop, but also gives the driver the possibility by means of a flashing code on the ADM fault lamp of receiving information about the nature of the fault.

3.5.3 Operating-Device

By operating-device those components are meant which are involved in the engaging and releasing of the clutch sleeve (see Fig. 11)

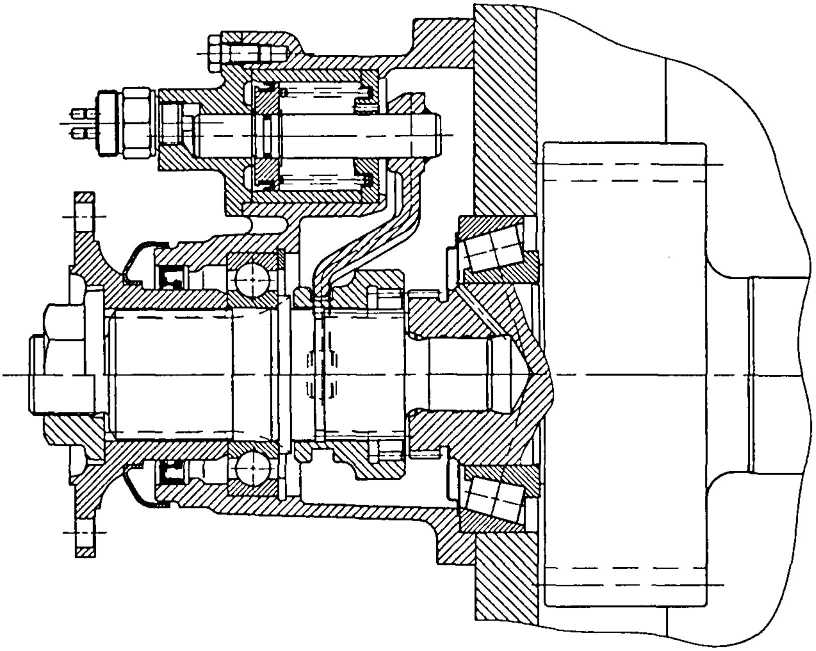

Fig. 11 Operating-Device VG 1200, existing Solution

3.5.3.1 Tasks of the Operating-Device

- A quick reaction to signals
- Sufficient operating-force
- Low masses moved
- Sufficiently high return force
- Possibility of high shifting-frequency

ADM was developed on heavy trucks with a permissible gross vehicle weight of over 7.5 tonnes. For this reason the operating-device was designed on the basis of the compressed air available in such vehicles.

ADM is not, however, tied to this medium. As long as the necessary criteria are fulfilled, any medium can be used.

3.5.3.2 Compressed Air System

Measurements of shifting-limits together with measurements of shifting-time provided the basis for optimising the compressed air system.

The result of these investigations is clear and can be formulated as follows:

- The air lines to the solenoid valves should be as short as possible and should have the largest possible cross-section.
- The air lines to the operating-cylinders should be as short as possible
- The optimum cross-section of these lines depends on their length
- The chamber in the cylinder into which the air flows should be as small as possible
- The optimum diameter of the cylinder depends on the masses to be moved

3.5.3.3 Shifting-Frequency

One of the results from the desert testing is the reason for the requirement of a high shifting-frequency. There the result shown in Fig. 12 was registered over a distance of 200 km in a period of 11 hours. In this test there was not yet any interlinking of the shifting and the individual systems were engaged independently of each other.

TEST VEHICLE "HINO RANGER (200kW)" EQUIPPED WITH

- AUTOMATIC ENGAGING OF FRONT WHEEL DRIVE
- AUTOMATIC ENGAGING OF REAR AXLE DIFFERENTIAL LOCK
- AUTOMATIC ENGAGING OF FRONT AXLE DIFFERENTIAL LOCK

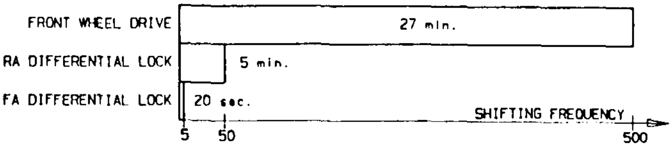

RESULTING DURABILITY REQUIREMENTS

FRONT WHEEL DRIVE	250 000 ACTUATIONS
RA DIFFERENTIAL LOCK	25 000 ACTUATIONS
FA DIFFERENTIAL LOCK	5 000 ACTUATIONS

Fig. 12 Result of Measurements of Engagings

There is a factor of 10 between the number of engagings of all-wheel drive and lockings of the rear differential and between the number of lockings of the rear and of the front differentials. This means that the major part of the additional traction required can be covered by the all-wheel drive and the locking of the front differential is required extremely seldom.

This result confirms the shifting-logic developed, in which all-wheel drive now has to be engaged before a differential is locked.

The high shifting-frequency in the transfer box also caused damage to the mechanical parts of the series operating-device used during the desert testing, as could be observed when the transfer box was dismantled for checking after the testing.

The sliding selector shaft was scraped at the bearing points and the shifting-fork was bent and severely worn on the sliding-surfaces for the sliding-sleeve.

Fig. 13 illustrates the solution improved on the basis of these results. There are better holding of the moved parts, a reinforced shifting-fork with sliding-surfaces coated with synthetic material.

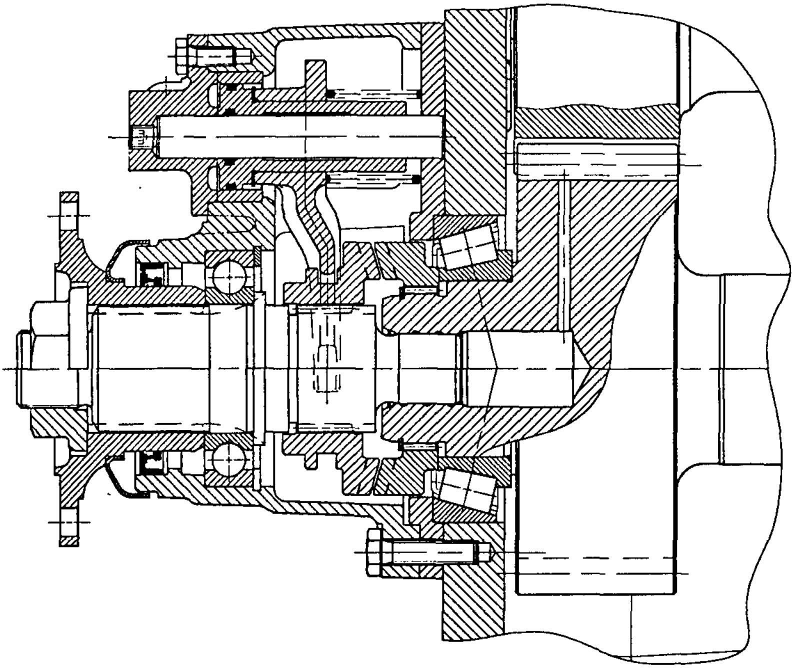

Fig. 13 Operating-Device VG 1200, Improved Solution

The solution illustrated has already withstood durability testing of 250,000 operations without any damage.

3.5.4 Dog Clutch

3.5.4.1 Tasks of the Dog Clutch

- To transmit the maximum drive torque arising
- To be shiftable when there is an rpm difference between the clutch parts
- To remain in position by itself under load
- To be easily releasable when there is no torque

One of the basic criteria for ADM was to find a dog clutch which allows the sliding-sleeve to be moved in at high rpm differences. This depends very much on the form of the toothing of the clutch.

The functions of remaining in position under load and releasability also depend on the form of the teeth.

The criterion of strength depends very much on the operating-conditions of the vehicle and can be influenced by the electronic system by the varying of different parameters to the extent that misuse of the system can be prevented

3.5.4.2 Functioning of the Shifting

The initial position was the series solution in the VG1200 transfer box which was selected as the one to bear the testing. In this transfer box the torque is transmitted through circumferential toothing with involute form, see Fig.11.

When the measurements were made it was found that this circumferential toothing is not suitable for ADM. We achieved higher shifting-limits with spur gears, which have the additional advantage of being particularly easily adaptable in respect of the functions of remaining in place, releasing and strength.

Fig. 14 shows this form, in the designing of which attention was also paid to low-priced production.

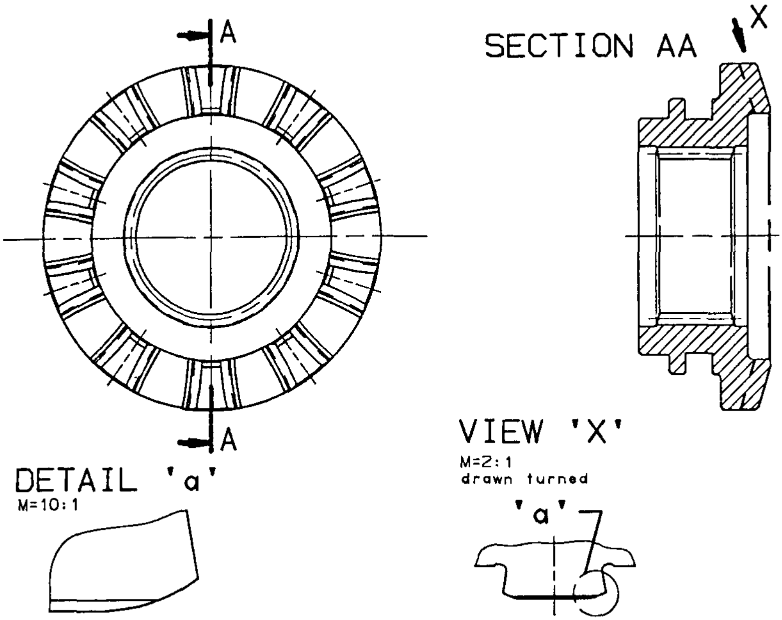
A
SECTION AA
X
A
DETAIL 'a'
M=10:1
VIEW 'X'
M=2:1
drawn turned
'a'

Fig. 14 ADM Sliding Sleeve

3.5.4.3 Strength

A finite element calculation was also made to optimise the strength.

The result of this calculation was above all the optimisation of the diversion of the force from the shifting toothing to the engaging toothing for the sleeve on the shaft, allowing a significant increase in strength

4. Development Potential

This new drive-train management opens up the possibility of our participation in and utilisation of all new developments in commercial vehicles.

The electronic control unit is capable of communicating with all other electronic control units of a vehicle by means of a data bus connection.

In the future electronic systems, such as an electronic accelerator pedal, electronic clutch systems, electronically controlled automatic gearboxes and electronic engine control, will relieve the driver of a lot of work and also considerably increase safety.

By the utilisation of these systems ADM can be still further improved and so increase safety even more. The interplay of all the systems mentioned is necessary to bring the maximum benefit for driving-safety.

ADM is, however, not limited to trucks. It can be used in all kinds of vehicles from cars to construction machinery. This is made possible by the universal design of the software.

It is necessary only to make the components specific to the vehicle, such as the operating-device, compatible with ADM.

In ADM we have developed a product that has already aroused interest amongst all well-known vehicle-manufacturers. We are in discussion with them.

A large number of projects concerning the mounting of ADM in the most varied types and brands of vehicles are already running. A number of test vehicles of renowned truck-manufacturers are already undergoing tests with ADM.

Appendix

ADM Test Trucks

Steyr 19S37/4x2 Truck-Tractor

ADM-equipment:
⇒ Automatic locking of rear differential

Vehicle data:

- Engine output: 270KW (370HP)
- Axle ratio: 4,42
- Tire equipment: 12 R 22,5 Semperit Athlet Steel
- Gross vehicle weight with semitrailer: 40,000kg

Steyr 1291.280/4x4 Tip Truck

ADM-equipment:
⇒ Automatic locking of differential in the transfer case
⇒ Automatic locking of rear differential

Vehicle data:

- Engine output: 205KW (280HP)
- Axle ratio: 5,73
- Tire equipment: 13 R 22,5 Semperit Athlet Steel
- Gross vehicle weight: 16,000kg

Steyr 12M18/4x4 Medium Size Military Truck

ADM-equipment:
⇒ Automatic engaging of all-wheel drive
⇒ Automatic locking of rear differential
⇒ Automatic locking of front differential

Vehicle data:

- Engine output: 132KW (180HP)
- Axle ratio: 6,12
- Tire equipment: 15,5-80 R 20 Michelin XL
- Gross vehicle weight: 9,400kg

Hino Ranger/4x4 Race Truck (Rallye Paris-Dakar)

ADM-equipment:
⇒ Automatic engaging of all-wheel drive
⇒ Automatic locking of rear differential
⇒ Automatic locking of front differential

Vehicle data:

- Engine output: 200KW (272HP)
- Axle ratio: 4,33
- Tire equipment: 14,5 R 20 Michelin XSP
- Gross vehicle weight: 9,100kg

Steyr 1491.330/6x6 Heavy Duty Military Truck

ADM-equipment:
⇒ Automatic engaging of all-wheel drive
⇒ Automatic locking of interaxle differential
⇒ Automatic locking of rear differential
⇒ Automatic locking of front differential

Vehicle data:

- Engine output: 240KW (330HP)
- Axle ratio: 5,73
- Tire equipment: 14,5 R 20 Michelin XS
- Gross vehicle weight: 17,600kg

Session III A
Sektion III A

Simulation 1

Simulation 1

Computer-aided Mobility Prognosis of Vehicles in the Field [1]

A. Handke, M. Bütikofer
Sieber Cassina + Handke AG
Engineers - Geologists - Planners CH-7000 Chur

SUMMARY

An EDP system ist presented enabling speedy, accurate and flexible prediction of terrain trafficability. The appraisal of a particular plot of terrain differs with the vehicle type and weather conditions.

The basis is provided on the one hand by simulation models describing the interaction between different vehicle types and the soil, as well as the state of the soil resulting from different weather conditions.

On the other hand a databank is used having the essential terrain features such as soil type, terrain slope and obstacles (settlement, woods etc.).

Finally the simulation models and the databank are integrated into a geographical information system (ARC-INFO). Presentation as maps is then possible of the trafficability information together with the geographic elements serving orientation.

The system finds application where the quantitative assessment of a vehicle's mobility or a comparison between military or civilian vehicles is involved. As the structural elements are strongly weighted, the system can be used also as an aid in the development of vehicles and tyres.

---

[1] The works were carried out on the behalf of the Equipment Services Group ot the Swiss Army under the direction of Dr. G. Regli.

1. INTRODUCTION

Quantitative assessment of the mobility of vehicles is of great practical importance, but at the same time it is also an extremely complex task on account of the large number of variables. Among the most important of these are the kind of vehicle, its structural elements and tyres, the nature of the terrain and the weahter.

Since a determination and prediction of the mobility of a vehicle are often related very much to the terrain and hence to a location, a cartographic processing and presentation are necessary as a rule.

A link-up between the extremely variable mobility information and the (for a given terrain) constant geographic elements can hardly succeed with traditional means, because these are slow and little flexible. On the other hand a synthesis of practical interest is possible by drawing upon geographic information systems as EDP data carriers of the geographic orientation elements and the mobility information.

2. CONCEPT

The link-up between the mobility information with the geographic orientation elements and the cartographic presentation is effected with the geographical information system ARC-INFO.

As purely geographic orientation elements, contours, populated areas, transport and waterway networks are set down in digital form.

The mobility information for a given terrain is determined ad hoc with the aid of suitable simulation models for the vehicle in question and for any weather conditions, and likewise made available location-related in digital form. The mobility of a vehicle on a given terrain is printed out in tree stages:

*	High mobility	Great mobility reserves available, i.e. the ground-related tractive force of a vehicle is much greater than is needed to overcome the ground slope
*	Poor mobility	Low mobility reserves available, in broken terrain vehicles may get stuck dependig on the local route chosen

* Immobility	The ground-related tractive force is no longer sufficient to overcome the ground slope, or obstacles like open water areas, forest areas and possible populated areas may render free mobility impossible

Determination of the mobility information is based on tree foundations, namely a vehicle/ground simulation model, a weather/soil humidity simulation model, and a databank with mobility-relevant terrain data.

3. APPLICATION AND PRESENTATION

The actual performance of a mobility prediction is screen-guided.

After starting the program environment, first comes the possibility of selecting the desired terrain (1:25 000 map of the Swiss national topography).

Next the main menu is entered. At this point a new prediction may be performed ad hoc, or an already existing prediction may be displayed. The procedure for a new prediction will now be shown.

For this purpose one is guided into the appropriate submenu, where the vehicle type is selected and then the weather conditions are simulated. With the simulation of the weahter conditions the state of soil, which influences the vehicle mobility to a large extent, can be determined. Here one starts by putting in an estimated value for the initial state of the soil. Any estimation of the initial state is relatively inaccurate, but this is unimportant if the weather data for the last 3-5 days are available. The initial state is then estimated for a point in time 3-5 days previous, and the development of the soil state is simulated with the help of the weather data. As result the present soil state is obtained, varying accorcding to the slope angle and the soil type. If a prediction of the trafficability at a point in time x days from today is now required, the soil state can be determined taking the national weather forecasts into account.

After this the driving performance of the vehicle in question can be calculated and finally linked to the geographic orientation elements.

Now in order to present the calculated mobility information we return to the main menu, where we select the desired orientation information, which is then overlaid as necessary.

Presentation is made in 1:25 000 map form. The maps may be put out in the screen or on paper. The quality of the screen display depends very much on the screen resolution and does not yet match the standard of a paper printout at the present time.

For a particular map presentation corresponding background information may be called up, i.e. statistical data on the trafficability information, terrain information for a point selected, weather events taken as basis etc. If necessary any parts of terrain may be enlarged also.

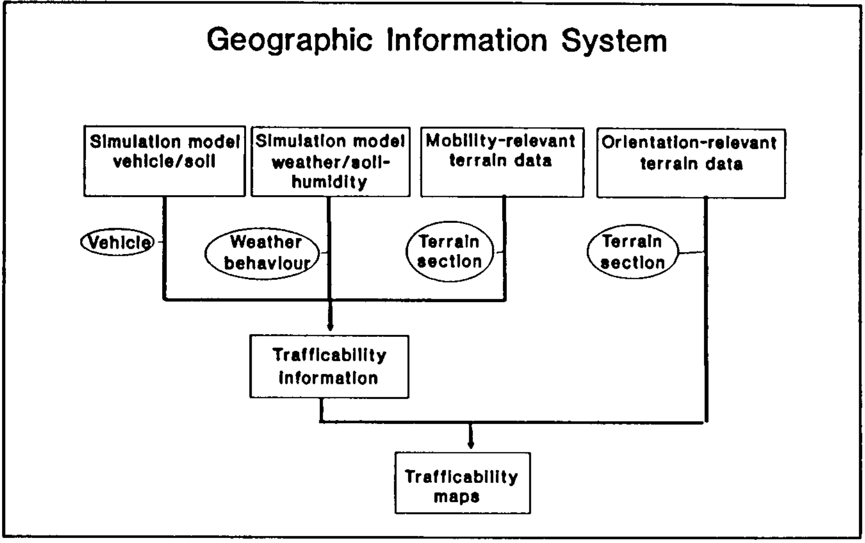
Geographic Information System
Simulation model vehicle/soil
Simulation model weather/soil-humidity
Mobility-relevant terrain data
Orientation-relevant terrain data
Vehicle
Weather behaviour
Terrain section
Terrain section
Trafficability information
Trafficability maps

Fig.1 Organization of calculation sequenzes in the geographic information system

4. BASIS

4.1. Vehicle/ground simulation model

In the present article new mobility models for predicting the driving behaviour of wheeled and tracked vehicles in the field are applied.

Using this model, the maximum ground slope tan α_{max} mastered by the vehicle, varying with the conditions of the soil, is determined.

Here the influence of the substrate has been given much weight, while the vehicles are considered as standardized.

During the development activities we came to the conclusion that the extremely complex interaction between vehicle and substrate calls for a thoroug analysis of both substrate and motion processes of the organs of motion.

We therefore tried to characterize the substrate with special regard to its mechanical properties. In nature it appears with a multilayer structure acc. to Fig.2. The relevant soil model should make it possible to sufficiently consider this natural arrangement of layers.

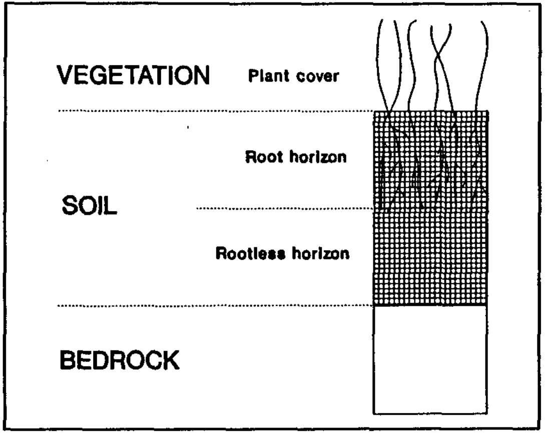

Fig.2 Multitayer substrate structure

In order to arrive at an adequate understanding of the complex processes and interrelations of traction, various analyses and studies were conducted, some of them using the finite element method [11], others with field mobility trials.

We finally tried to relate the main vehicle parameters to the parameters of the substrate, in order to obtain a statement on the trafficability of the terrain (tractive effort, rolling friction). The aim was to state these relations as simply as possible on an analytic basis, resulting in a useful instrument for practical prognoses.

In the following paragraphs the results are summarised.

Experience shows that most substrates in very dry condition lead to practically no vehicle tracks and thus to no sinkage of the organs of motion. In such cases the substrate is considered undeformable and the friction theory is consulted. The tractive forces are calculated as frictional forces in the contact area between the organ of motion and the substrate. (Fig.3).

The tangential limiting tension τ between organ of motion and substrate is determinde by the product of the friction coefficient μ and the normal contact pressure σ.

$$\tau = \sigma * \mu \qquad (1)$$

This relation is applied to each wheel j and from the resulting friction stress the frictional force is calculated as product of friction stress and contact area.

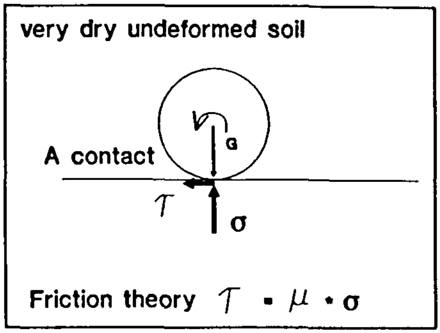

Fig.3 Application of friction theory for very dry soil

Therefore, the maximum ground slope mastered by the vehicle is:

$$\tan \alpha_{max} = \frac{Z_{max}}{G} = \sum_{j=1}^{m} \sigma_j * \mu * A_{contact\,j} * \frac{1}{G} \qquad (2)$$

The friction coefficient μ between the turf and the organ of motion is definded as quotient of tractive force Z_{max} above vehicle weight G, and is measured with a special tribometer in the field.

In the case, however, where the substrate is dry, humid or wet, the vehicles, depending on the conditions, sink in more or less and leave corresponding tracks. Here the surface phenomena no longer take effekt, but the mechanical properties of the deformable soil are decisive. The organs of motion penetrate into the ground when moving and lead to reactive stresses depending on the deformation, which are eventually responsible for the tractive forces (Fig.4).

Since in nature the soil structure is definitely in two layers, which also becomes apparent in its mechanical properties, we consider both layers of the soil. The stress-strain behaviour of the soil is determined by means of triaxial tests.

Measured curves in the upper soil horizon with many roots show that in dry and humid condition a typical friction behaviour (inner friction) with cohesion occurs, with varying densities of the different soil types. In wet condition all soil materials show practically no friction.

The curves for the lower soil horizon with fewer roots show a considerably stiffer and sturdier behaviour.

For the calculations with the simulation models an elastoplastic soil model is derived from the triaxial tests. For this purpose the entire field of curves is determined from the selected curves resulting from the triaxial tests, and expressed by the elastic material parameter $E_{1\text{-}5}$ by the plastic parameters or the inner friction $\phi_{1\text{-}4}$, and by the cohesion $c_{1\text{-}4}$ acc. to Fig.5 [11].

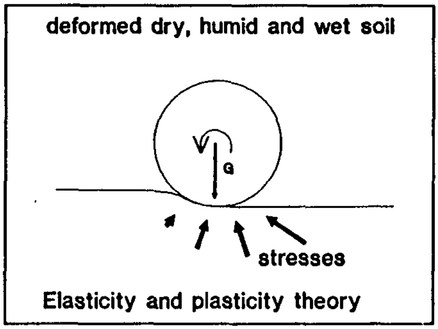
deformed dry, humid and wet soil
V
Q
stresses
Elasticity and plasticity theory

Fig.4 Application of elasticity and plasticity theory for dry, humid and wet soil

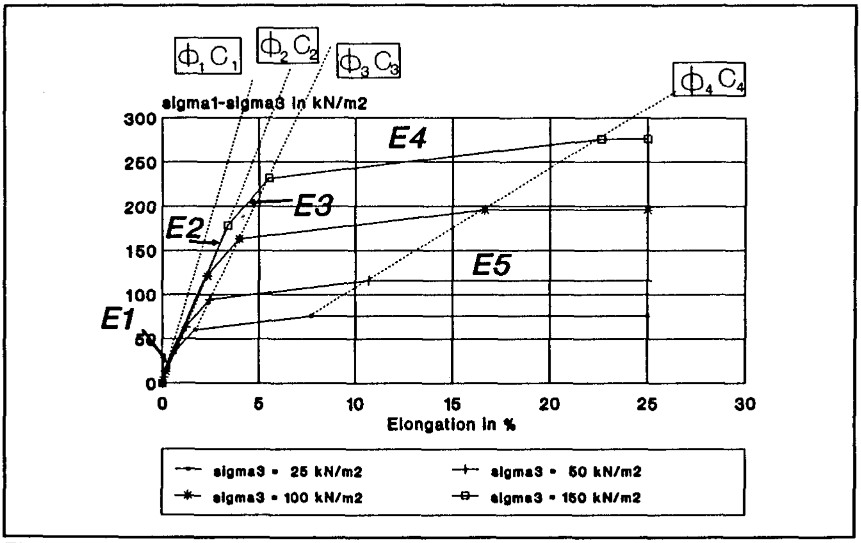

Fig.5 Elastoplastic soil model with model parameters E, ϕ and c

The priciple of simulation models for dry, humid and wet substrate is based on the following train of thought: first certain meaningful values of slip, trim angle and sinkage of the vehicle are assumed (Fig.6). These assumptions correspond to certain movements of the organs of motion, which are determined by means of kinematic considerations.

For this movement of the organs of motion the reactive stresses and the

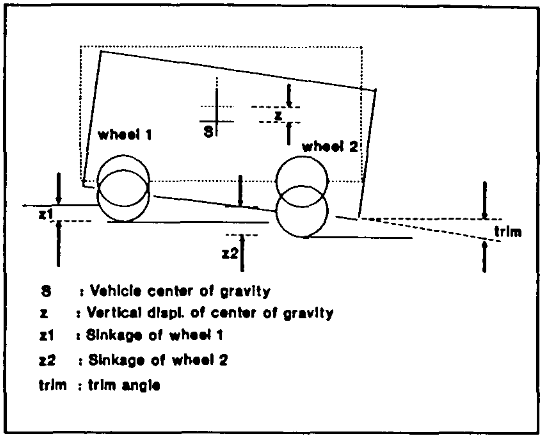
wheel 1
S
z
wheel 2
z1
z2
trim
S : Vehicle center of gravity
z : Vertical displ. of center of gravity
z1 : Sinkage of wheel 1
z2 : Sinkage of wheel 2
trim : trim angle

Fig.6 Definitions on the vehicle

resulting axle loads, motive powers, and rolling resistance forces are now determinded. The entire calculation system is iteratively adjusted until the calculated and the actual axle loads as well as the vehicle center of gravity are in agreement (Fig.7).

At first we will consider the kinematics of the organs of motion. For each vehicle it is definded by three factors, namely by slip, by sinkage at the vehicle center of gravity and by the trim angle, if the suspensions of the wheel axles or bogie wheels are considered to be rigid.

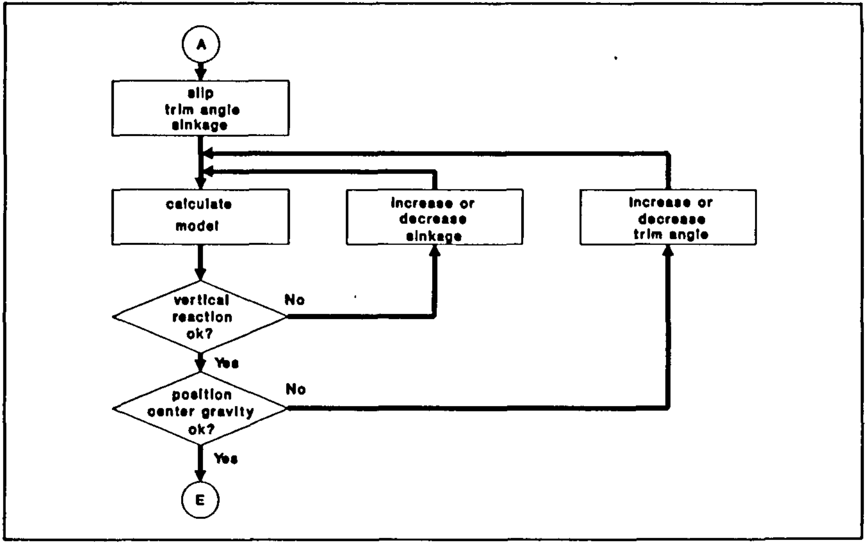
A
slip
trim angle
sinkage
calculate
model
increase or
decrease
sinkage
increase or
decrease
trim angle
vertical
reaction
ok?
No
Yes
position
center gravity
ok?
No
Yes
E

Fig.7 Iterative calculation procedure for determining the soil reaction stresses

For the determination of kinematics the organs of motion are divided into a series of members with equal dimensions (Fig.8). For instance, such a member is a track shoe with grouser or rubber pad or an idealized tyre member with cleat and space between the cleats. These members are further divided into so-called "elements", that is into plane partial surfaces.

In case of the wheel these four elements are the front of the cleat, surface of the cleat, back of the cleat and space between the cleats.

In case of the metal track with rubber pads they are, within one track shoe, the front, the surface and the back of the rubber pad, as well as the space between the rubber pads.

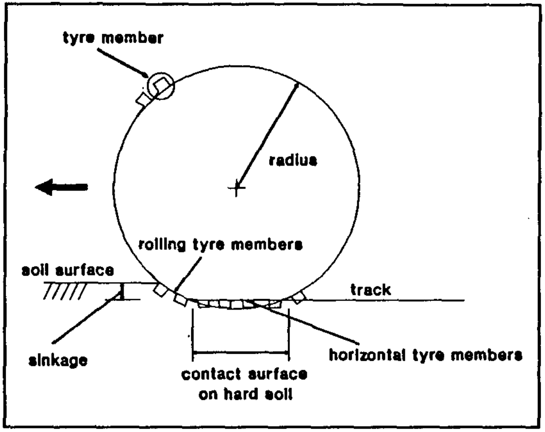

Fig.8 Subdivision of a radius into tyre members

In the case of the metal track with grousers they are, within one track shoe, the front, the surface, and the back of the grouser, as well as the space between the rubber pads.

The members are connected to form a compound, with the individual members being held by joints.

Kinematics define the successive positions of the members and their elements during the motion process, from the rolling motion to the penetration into the ground and reemerging from the ground. The individual components of motion result for each element from the superposition of the vertical movement of sinkage, the rotation of rolling and the horizontal movement relative to the ground due to the slip acc. to formulas 3-5 and Fig.9.

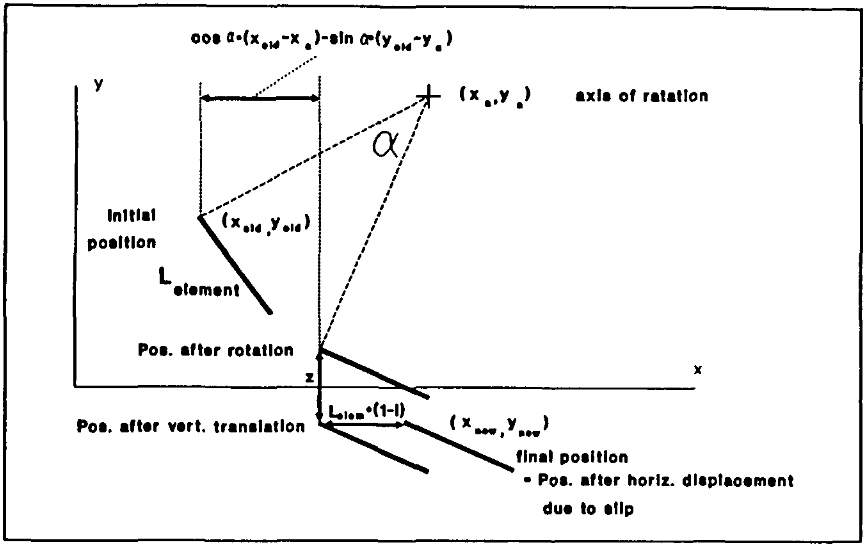
cos α•(x_old-x_a)-sin α•(y_old-y_a)
y
(x_a,y_a)
axis of ratation
α
Initial position
(x_old,y_old)
L_element
Pos. after rotation
x
z
L_elem•(1-i)
Pos. after vert. translation
(x_new,y_new)
final position
= Pos. after horiz. displacement due to slip

Fig.9 Kinematics of an element

$$x_{new} = \left[\cos\alpha * (x_{old}-x_a) - \sin\alpha * (y_{old}-y_a)\right] + x_a + L_{elem} * (1-i) \tag{3}$$

and

$$y_{new} = \left[\sin\alpha * (x_{old}-x_a) + \cos\alpha * (y_{old}-y_a)\right] + y_a - z \tag{4}$$

with slip being definded as follows

$$i = 1 - \frac{v_{effektive}}{v_{theoretical}} \tag{5}$$

For a tyre element of the wheel the calculated motion process is as shown in Fig.10.

Starting from the path of individual elements of the organs of motion defined by kinematics, the compressions created in the soil are calculated for each element. A reference length corresponding to the conditions is taken as standard value. The reference length characterizes the expansion o the soil sector, in which the organ of motion takes effect.

The soil compressed in this way leads to corresponding reactive stresses (expressed by the main stress field σ_1 and σ_3), which are given by the stress-strain behaviour determined by triaxial tests in the laboratory and can be calculated in a relatively easy manner.

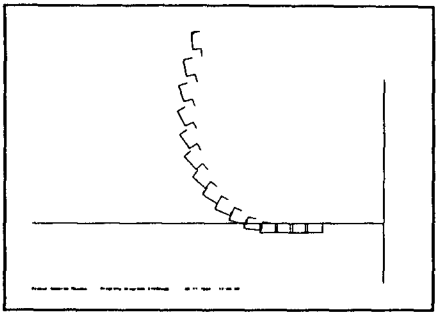

Fig.10 Calculated motion sequence of a tyre member

From this stress field we now calculate, on one hand, the stress normally acting on the element, by means of Mohr's stress nalysis acc. to formula 6.

$$\sigma_n = \frac{(\sigma_1 + \sigma_3)}{2} + \frac{(\sigma_1 - \sigma_3)}{2} * \cos 2\beta \qquad (6)$$

The angle β is enclosed by the direction of the normal stress on element σ_n and by the direction of the main stress σ_1.

The tangential stress τ acting opon the element is calculated using normal stress σ_n and compression ϵ_γ, in tangential direction acc. to the fractional law or Mohr-Coulomb (formula 7).

$$\tau = \left[1 - e^{-2.3 * \epsilon_\tau}\right] * (c + \sigma_n * \tan \phi) \qquad (7)$$

We introduce a dependence on compression ϵ_γ in such a way that the shear stress increases with shear deformation, up to a final value of c + σ_n* tan ϕ for very big deformation. The factor -2.3 means that for a deformation of 100%, 90% of the final value of τ is attained.

Finally the effective forces are determined from the stresses σ_n and τ and aded up for all elements of the organs of motion.

They are divided into:

- Horizontal forces:
  These are the shares of the forces from normal and shear stress projected onto the horizontal line:

$$H_\sigma = \sigma_n * B * L * \sin \gamma \qquad (8)$$

$$H_\tau = \tau * B * L * \cos \gamma \qquad (9)$$

  Where B is the width of the element surface
  L is the length of the element surface
  γ is the angle between element surface and horizontal line

- Vertical forces:
  These are the shares of the forces from normal and shear stress projected onto the vertical line:

$$V_\sigma = \sigma_n * B * L * \cos \gamma \qquad (10)$$

$$V_\tau = \tau * B * L * \sin \gamma \qquad (11)$$

The horizontal and vertical forces for each element result in the vertical reaction, the motive power and the rolling resistance acc. to the following formulas:

The vertical reaction of the wheel j by adding over all elements i:

$$V_j = \sum_{i=1}^{n} V_{\sigma,i} + \sum_{i=1}^{n} V_{\tau,i} \qquad (12)$$

The motive power of the wheel j by adding over all elements i:

$$T_j = \sum_{i=1}^{n} H_{\sigma-,i} + \sum_{i=1}^{n} H_{\tau-,i} \qquad (13)$$

and the rolling resistance of the wheel j by adding over all elements i:

$$R_j = \sum_{i=1}^{n} H_{\sigma+,i} + \sum_{i=1}^{n} H_{\tau+,i} \qquad (14)$$

Added over all wheels we obtain the vehicle weight,

$$G = \sum_{j=1}^{m} V_j \qquad (15)$$

the vehicle motive power,

$$T = \sum_{j=1}^{m} T_j \qquad (16)$$

and the rolling resistance of the vehicle.

$$R = \sum_{j=1}^{m} R_j \qquad (17)$$

The maximum ground slope tan α mastered by the vehicle is calculated as follows:

$$\tan\alpha = \frac{T - R}{G} \qquad (18)$$

The maximum is normally attainded with slip value of approx 40%.

Thus, in the available simulation model, the vehicles are represented by a number of parameters, namely:

wheeled vehicles:
-weight
-center of gravity
-number of axles
-distance between axles
-wheel radius
-contact length tyre substrate

tracked vehicles:
-weight
-center of gravity
-number of bogie wheels
-radius of bogie wheels
-distance between axles of bogie wheels
-contact length track substrate p. bogie wheel

For both types the geometry of the organs of motion is also introduced as parameter. This is possible by dividing the organs of motion into equal members as mentioned above.

In the simulation models presented here the soil models of the upper and lower soil horizon are coupled. Coupling is defined so that for each element of the organs of motion the stresses from both soil models are determined separately and weighted depending on the depth of sinkage. For very slight sinkage the influence of the upper, for very deep sinkage the influence of the lower soil model will prevail.

4.2. Weather/soil humidity simulation model

The soil humidity is calculated as a function of the precipitation, evaporation and time.

The precipitation must be measured directly. The evaporation is derived from the observed variables of temperature, air humidity, cloudiness and wind velocity.

The theoretical fundamentals employed are based on experimental data over many years.

4.3. Databank with mobiliy-relevant terrain data

The mobility-relevant terrain data are soil type, slope, vegetation type and population density. In this work a regular square surface grid was applied and the correspondig terrain data per area were defined.

REFERENCES

[1] BOLLING I. Bodenverdichtung und Triebkraftverhalten bei Reifen - Neue Mess- und Rechenmethoden, Diss. TU München 1987, erschienen in Forschungsbericht Agrartechnik des Arbeitskreises Forschung und Lehre der Max-Eyth-Gesellschaft (MEG), Nummer 133

[2] BOONSINSUK P. and YONG R.N. Soil Compliance influence on tyre performance, 8th International conference ISTVS 1984, Proceedings Vol 1

[3] CHEN W.F. and MIZUNO E. Nonlinear Analysis in Soil Mechanics, Elsevier 1990

[4] CHUNG T.J. LEE J.K. Dynamics of viscoelastoplastic soil under a moving wheel, Journal of Terramechanics 1975 Vol 12 No I pp 15-31

[5] FRITZ P. Rheo-Staub, Users Manual, Departement of Rock Engineering Swiss Federal Institute of Technology, ETH-Hönggerberg, Zürich 1989

[6] FRITZ P. Numerische Erfassung rheologischer Probleme in der Felsmechanik, Institut für Strassen-, Verkehrs-, Eisenbahn- und Felsbau, an der Eidg. Techn. Hochschule Zürich Mitteilung Nr. 47 1981

[7] KARAFIATH L.L. Finite Element Analysis of ground defomation beneath moving track loads, 8th International conference ISTVS 1984, Proceedings Vol 1

[8] KOOLEN A.J. and KUIPERS H. Agricultural soil mechanics. Springer 1983 ISBN 3-540-12257-5

[9] PERDOCK U.D. & ARTS W.B. The performance of agricultural Tyres is soft soil Conditions, Soil & Tillage 1987, 10, 319-330

[10] POLLOK D.PERUMPRAL J.V. KUPPUSAMY T. Finite Element Analysis of multipass effects of vehicles on soil compaction, American soc. of agricultural Engineers 1986 Vol 29 (1)

[11] REGLI G., HANDKE A., BÜTIKOFER M. Material laws as a basis for simulation models for the calculation of wheel-soil interaction, examination using the finite element Method, Journal of Terramechanics, Vol 30. No 3, pp 165-179, 1993

[12] SOEHNE W. Druckverteilung im Boden und Bodenverformung unter Schlepperreifen, in Grundlagen der Landtechnik, Band 5 1953

[13] STEINER M.Analyse, Synthese und Berechnungsmethoden der Triebkraft-Schlupf-Kurve von Luftreifen auf nachgiebigem Boden, DISS. TU München, Söhne Woschni 1979

[14] WONG J.Y. Theory of Ground vehicles, John Wiley & Sons 1978 ISBN 0-471-03470-3

[15] WONG J.Y. On the study of wheel-Soil Interaction, Journal of Terramechanics, No 2, 1984

[16] WONG J.Y Terramechanics and off-road vehicles, Elsevier Amsterdam 1989

[17] YONG R.N. and FATTAH E.A. Prediction of wheel-soil interaction and performance using the finite element method, Journal of Terramechanics 1976 Vol 13 No 4 pp 227-240

[18] YONG R.N. FATTAH E.A. and BOONSINSUK P. Analysis and prediction for tyre-soil interaction and perfomance using finite elements, Journal of Terramechanics 1978 Vol 13 No 3 pp 43 - 63

[19] YOUNG R.N. FATTAH E.A. and SKIDAS N. Vehicle Traction Mechanics, Elsevier 1984, ISBN 0-444-42378-89 April 1989

THEORETICAL CONCEPTS IN SOIL-WHEEL INTERACTIONS

D.R.P.Hettiaratchi
Department of Agricultural & Environmental Science
The University of Newcastle upon Tyne,
Newcastle upon Tyne, NE1 7RU, U.K.

ABSTRACT

The paper presents a preliminary attempt at incorporating some recently developed theoretical concepts into the analysis of soil-wheel interactions. The mechanics of rut formation is quantified in terms of measurable soil constants in the critical state model and the initial bulk density (or specific volume) of the soil. A new form of pressure-sinkage function is presented.

The geometry of the contact patch can be established from known rut depth. Skid or slip regulates the kinematics of motion of these surfaces and these influence the slip-line geometry at this interface. The manner in which this governs the stress distribution between the wheel and the soil is discussed and compared with published experimental observations.

The development of statically admissible slip-line solutions for estimating soil-wheel reactions is outlined. This provides the theoretical basis for simulating soil-wheel performance in terms of soil parameters that can be obtained from standard laboratory tests. Mathematical models required for this can be developed in terms of straightforward closed algebraic and trigonometric expressions.

1. INTRODUCTION

There are many complex processes involved in the interaction of an elastic wheel rolling on deformable soil. In order to facilitate the analysis of these interactions suitable simplifications must be introduced into the following three basic elements of the problem.

(a) *Geometry of the Contact Area*

The shape and proportions of the interface between the wheel and the soil are functions of both the deformation characteristics of the wheel (tyre stiffness) and the soil (compressibility). The former can be simply quantified by the axle load - centre line deflection characteristics of the tyre. This *elastic* characteristic is usually sufficient to arrive at the approximate proportions of the flattened sections of a tyre of given size.

The quantification of the deformation of the soil is less straightforward and in the present context the critical state model will be used to predict the pore volume changes associated with wheel sinkage. Wheel sinkage is an important parameter required in the analysis set out in (c) and is arrived at from an *elastic-plastic* model.

(b) *Kinematics of Motion of Contact Area*

Points on the surface of a slipping or skidding wheel describe cycloidal paths relative to the soil. These movements have a profound influence on the deformation and failure modes of the soil. The effects of slip and skid on soil-wheel interactions are introduced through this element of the analysis.

(c) *Contact Area Stresses*

There is no simple mathematical method currently available for dealing with soil failure induced by rough curved boundary surfaces. There is, however, an acceptable comprehension of the nature of the soil stresses acting on plane rough surfaces failing soil. Furthermore, the influence of the kinematics of motion of such plane components on the stress distribution is also reasonably well understood. It therefore make sense to approximate the complex geometry of the contact surface of a wheel by several plane sections. This analysis assumes the soil is a *rigid-plastic* Mohr-Coulomb material and deals with *plane-strain* (or 2-dimensional) stress fields.

The main argument for proposing such a hybrid model is the need to simplify the analysis to techniques which can be developed in terms of closed form solutions. The simplifying conditions for each model applies to one particular aspect of the problem and does not necessarily nullify those assumed in the others.The use of plane-strain two-dimensional fields are difficult to justify and this approximation is forced on us as no adequate simple model exists for the three-dimensional failure regime induced by a rolling wheel. The inertia loads induced by the motion of the soil is assumed to be small compared with the static stresses, thus reducing the problem to a quasi-static one. Evidently high-speed performance cannot neglect this aspect of soil loading.

2. SOIL DEFORMATION

In broad terms the deformation of the soil induced by a rolling wheel is the cumulative effect of the following three factors:

(a) Settlement due to soil *compaction* resulting from irreversible changes in pore space.

(b) Displacement of the contact surface due to general *shear failure* and *flow* of the soil.

(c) Mechanical *excavation* associated with the motion of lugs and grousers.

The soil deformations due to 2(b) and 2(c) are difficult to quantify. Sideways displacement of soil by a sliding rigid-block bearing capacity type failure can occur in compact soils subjected to high wheel loads. In the longitudinal direction this soil movement takes the form of a bulldozing action ahead of the wheel or at high slip by a rearwards "bucket wheel" excavation. In the present context the main component of wheel sinkage will be attributed to 2(a) and wherever necessary a nominal shear failure sinkage contributed by 2(b) is added to this (see Section 3.5).

To estimate the compaction sinkage 2(a) it is necessary to utilise a model which

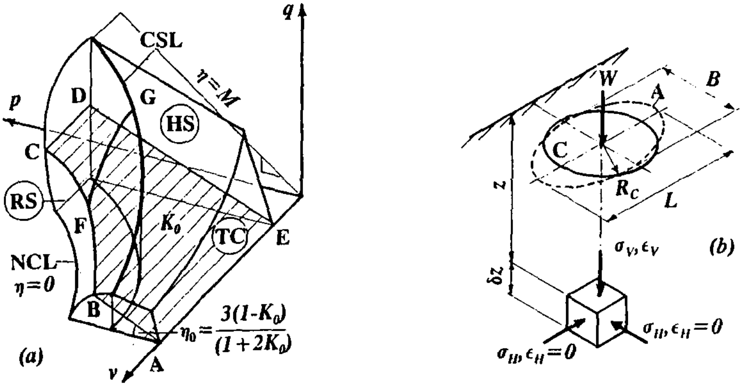

Fig. 1 (a) Main features of critical state space and location of K_0-plane. (b) Soil element below contact patch.

associates soil volume change with applied stress and the Cambridge critical state model (Roscoe *et al*, 1958) provides this connection. For a description of this model see Atkinson & Bransby (1977) or Wood (1990). The application of this model to soil-machine systems is discussed by Hettiaratchi, (1989). A major obstacle in the practical application of this elegant model has been the difficulty in predicting the stresses generated within the soil by the contact area stresses. Two basic stress components p and q are used to formulate the critical state model and these are defined in terms of the principal stresses σ_1, σ_2 and σ_3 ($\sigma_1 > \sigma_3$) thus:

$$p = ⅓(\sigma_1 + \sigma_2 + \sigma_3) \ ; \ q = (\sigma_1 - \sigma_3) \qquad (1)$$

The deformations in item 2(a) are assumed to result from one-dimensional compaction and requires three simplification. Firstly we assume that all horizontal strains are zero ($\epsilon_H = 0$); secondly that σ_2 approximates to the boundary conditions of a triaxial compression test ($\sigma_2 = \sigma_3$); and thirdly that the major and minor principal stresses maintain a constant ratio during loading so that $\sigma_1 = K_0 \ \sigma_3$, where K_0 is the coefficient of earth pressure at rest. Substituting the last two conditions in Equations (1) gives:

$$p = ⅓\sigma_1(1 + 2K_0) \ ; \ q = \sigma_1(1 - K_0) \qquad (2)$$

The implications of these assumptions are illustrated in Fig. 1(a) which shows the familiar three-dimensional plot of critical state space. All one-dimensional compression states lie on the hatched inclined K_0-plane ABCDE. It will be seen from Equation (2) that this plane has a fixed slope $\eta_0 = q/p$ given by:

$$\eta_0 = [3(1 - K_0)]/(1 + 2K_0)$$

The K_0-plane intersects the Roscoe surface in the curve BC and all plastic deformations in one-dimensional compression must follow this path. As BC does not cross the critical state line it is clear that one-dimensional loading does not bring the soil to general shear failure. In the event state paths deviate from the plane ABCDE and follow a path such as FG, general shear failure, stipulated in condition 2(b), occurs at G on the critical state line.

3. WHEEL SINKAGE

Current techniques for predicting wheel sinkage closely follow Bekker's early work (Bekker, 1960) and are nearly all based on the physical analogy between plate sinkage tests and rut formation. This approach leads to empirical relationships between contact pressure, sinkage and plate proportions. The dimensionally correct pressure-sinkage equation proposed by Reece (1966) is:

$$p = (k_1 + k_2 b)(z/b)^n \tag{3}$$

3.1 Soil Stresses

A fresh approach to this problem can be made using the critical state model referred to in Section (2). The typical elliptical wheel contact surface A in Fig. 1(b) has major and minor axes L and B respectively. For the present analysis this surface is substituted by a circular contact surface C of identical surface area. The characteristic radius R_c of this circle is:

$$R_c = \tfrac{1}{2}\sqrt{(LB)}$$

The small element of soil in Fig. 1(b) is located at a depth z on the vertical centre line below the equivalent circular contact surface C. The faces of this element are assumed to be principal planes with $\sigma_1 = \sigma_V$ and $\sigma_H = \sigma_3\ (=\sigma_2)$. As will be seen from Fig. 1(a) the initial deformation on the K_0 plane is indeed entirely elastic until the state path reaches the trace BC on the Roscoe surface. The soil then deforms plastically along BC. The development of such plastic deformations in the absence of lateral strains generate stress-strain characteristics very similar to those obtained in simple tensile tests on metals. Based on this rather tenuous similarity the stress σ_V due to a uniform normal stress f on the contact surface is estimated by the well known Boussinesq's elastic analysis (see for example Poulos & Davis, 1974):

$$\sigma_V = \sigma_1 = f\left[1 - \left(\frac{z^2}{z^2 + R_c^2}\right)^{\frac{3}{2}}\right] \tag{4}$$

Equations (4) and (2) completely define the two critical state stress parameters p and q within the soil at points along the centre line below the contact surface.

3.2 Vertical Deformations

In the critical state model, deformations are characterised by changes in the specific volume v of the soil. The present analysis is concerned mainly with linear displacements, in particular vertical displacements. In one-dimensional compression there is no dimensional

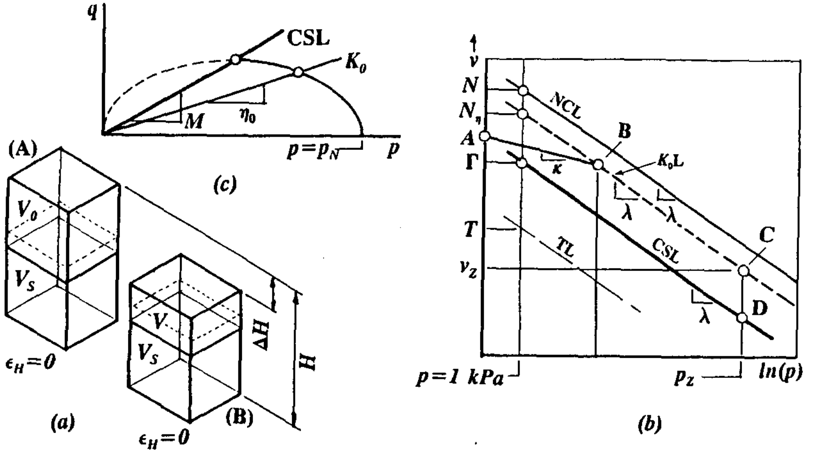

Fig.2 (a) Conversion of volumetric strains to vertical linear strains in one-dimensional compression. (b) Projection of critical state boundaries on $q = 0$ (isotropic) plane. (c) Typical projection on a constant v plane. Elliptical Cam-clay model for Roscoe surface.

change in the horizontal plane. Hence the reduction in the pore space V_0 of element (A) in Fig. 2(a) to V in (B) is entirely accommodated by the vertical contraction ΔH of the original height H of element (A). As the volume of solids V_S remains unchanged it can be shown that:

$$H\, a_s/v_0 \;=\; (H - \Delta H)\, a_s/v \qquad (5)$$

where a_s is the sectional area of the element and v_0 and v are the initial and final specific volumes of the elements. The vertical linear strain in terms of specific volume change is obtained from Equation (5) as:

$$\Delta H/H \;=\; \epsilon_V \;=\; \epsilon_Z \;=\; (1 - v/v_0) \qquad (6)$$

It is important to note that the above analysis is applicable only to partly saturated soils where the volume of the pore water (shown in dotted lines) remains unaltered during the compression. If the pore space V_0 was full (or nearly full) of liquid, then the change from V_0 to V cannot take place without the liquid draining out of the pore space. This is a time dependent consolidation process controlled by the nature of the drainage path available for the dissipation of excess pore pressure. The present analysis does not take such conditions into account.

3.3 State Path Traces

The projections on the $q = 0$ plane of the state boundary junctions between the Roscoe (RS), Hvorslev (HS) and Tension (TC) surfaces shown in Fig. 1(a) are re-plotted on the v -ln(p) diagram shown in Fig. 2(b). The curves in p-q-v-space transform into straight lines in this log-linear presentation. For all practical purposes the normal consolidation line (NCL), the intercept of the K_0-plane with the Roscoe surface (K$_0$L), the critical state line

(CSL) and the tension cut-off line (TL) are assumed to have identical slopes of λ. These lines can be quantified by the following equations:

$$\text{NCL: } v = N - \lambda \ln(p) \ ; \ q = 0 \tag{7}$$
$$\text{CSL: } v = \Gamma - \lambda \ln(p) \ ; \ q = Mp \tag{8}$$
$$\text{K}_0\text{L: } v = N_\eta - \lambda \ln(p) \ ; \ q = \eta_0 p \tag{9}$$

The elastic compression lines (such as line AB) have a fixed slope of κ:

$$\text{EL: } v = E - \kappa \ln(p) \tag{10}$$

In the above equations λ, N, Γ, M and κ are unique soil constants. The parameter E can be derived in terms of these constants. To calculate the coefficient N_η in Equation (9) it is necessary to quantify the shape of the Roscoe surface which is intersected by the K_0-plane. The trace of the Roscoe surface on constant v-planes has been modelled as an ellipse (Cam-clay model, Roscoe & Burland,1968).The equation, $p = p(\eta)$ to this ellipse, which passes through the origin of co-ordinates, is:

$$p = [\mathrm{M}^2/(M^2 + \eta^2)]p_N \tag{11}$$

There are more complicated versions of this equation but this simple form will suffice. The intercept N_η can be obtained from Equations (7) to (11) as:

$$N_\eta = N - (\lambda - \kappa) \ln[(M^2 + \eta^2)/M^2] \tag{12}$$

3.4 Rut Depth Estimation

The value of σ_V estimated from Equation (4) is the peak value on the centre line of the contact circle. This stress falls off as we move off centre. Although it is perfectly feasible to allow for this variations the following analysis assumes that this stress is invariant under the contact surface.

As the wheel rolls on to the soil surface the state path of a typical soil element at a depth z is shown by the trace ABC on Fig. 2(b). The soil is at its initial specific volume v_0 at A and compresses elastically on the K_0-plane to B and then follows the one-dimensional compression trace to C. The value of $p = p_z$ at C can be computed from Equations (2) and (4). This calculated value of p_z is then substituted in Equation (9) to give the final specific volume v_z of this element:

$$v_z = N_\eta - \lambda \ln(p_z) \tag{13}$$

The small elastic volume change from A to B is not included in this simple analysis. Once v_z is known the vertical strain of the element is obtained off Equation (6) as:

$$\epsilon_z = (1 - v_z/v_0) \tag{14}$$

Note that ϵ_z is a complex function of z defined by Equations (2), (4), (12) and (13). The total rut depth Z_R is the cumulative addition of all the vertical displacements ϵ_z given by equation (14), summed down to the depth z_0 where ϵ_z becomes negligibly small or zero, and is given by:

$$Z_R = \int_{z=0}^{z_0} \varepsilon_z \, dz = \int_{0}^{z_0} (1 - \frac{v_z}{v_0}) \, dz \tag{15}$$

In practice it is found that the depth z_0, at which $\epsilon_z \rightarrow 0$, is sensitive both to the initial specific volume v_0 and the magnitude of the contact stress f and increases directly with these parameters. It is interesting to note that the calculation of rut depth for a soil with initial specific volume v_0 from Equation (15) depends on the soil constants λ, κ, M, N, K_0 and the contact surface parameters f and R_C. If elastic deformations are neglected (i.e. $\kappa = 0$) and to a good approximation $K_0 = (1 - \sin \varphi)$ and $M = [6 \sin \varphi/(3 - \sin \varphi)]$, then the three parameters λ, N and φ provide the bare minimum number of soil constants required to evaluate wheel sinkage. The only other soil variable involved is the initial condition of the soil represented by its initial specific volume v_0 or alternatively by its field bulk or dry density.

3.5 Plastic Failure

If the above analysis is required to take account of sinkage due to bearing capacity failure or collapse of the soil beneath the wheel [mode 2(b) in Section 2], then a semi-empirical modification can be carried out by allowing for the additional volume change Δv_f associated with the path FG in Fig. 1(a). This state path departs from the assumed K_0-plane and takes the soil from the K_0 intercept on the Roscoe surface to the critical state line. Point G represents the conditions where structural collapse or flow of the soil beneath the contact surface takes place.

Referring to Fig. 2(b) the reduction in specific volume Δv_f from one-dimensional consolidation up to C and general shear failure at D is the interval CD, which is simply $\Delta v_f = N_\eta - \Gamma$. This interval is constant for all points along the intercept BC of the K_0 plane with the Roscoe surface and can be introduced into equation (13) through equation (12), which now takes the form:

$$v_z = 2N_\eta - \Gamma - \lambda \ln(p_z) \tag{16}$$

Equation (16) can then be used in place of Equation (13) in the solution of Equation (15). This simple expedient assumes that all the soil elements simultaneously reach the critical state line and, in reality, may not be far from the truth.

4. PRACTICAL EXAMPLE

The above analysis can be applied to a vast range of published data on wheel sinkage performance. Not surprisingly, none of the published information contains details of the crucial critical state parameters required for such an analysis. A performance check of Equation (15) for these experimental conditions is therefore not possible.

As a preliminary attempt, the investigations of Febo & Pessina (1987) on tyre contact area are used to calculate *theoretical* rut depths in a local soil whose critical state parameters are known. Table 1 is an adaptation of Febo & Pessina's data on contact area and wheel load for a conventional 520/70R34 radial-ply tyre operating at an inflation pressure of 160 kPa.

Table 1

LOAD (kN)	AREA (m^2)	R_c (mm)	f (kPa)
4	0.040	113	100
7	0.060	138	117
10	0.072	151	139
13	0.100	178	130
16	0.112	189	143
19	0.131	204	145
22	0.152	220	145
25	0.170	233	147
28	0.189	245	148
31	0.210	259	148

The theoretical *compression* sinkage of this tyre on a typical loam soil is estimated from Equation (15). The soil parameters used in the calculations were $\lambda = 0.2$, $M = 1.2$, $N = 3.0$, $\kappa = 0.05$ and $\varphi = 30°$. Five initial void ratios of the soil from very loose ($v_0 = 3.0$, dry density $\approx$ 0.9 Mg/m^3) to dense ($v_0 = 2.2$, dry density $\approx$ 1.23 Mg/m^3) were used in the simulation. The integration of Equation (15) was carried out by simple 5-point Gaussian Quadrature. The upper integration limit z_0 was obtained from a numerical solution of the root of Equation (14) by setting ϵ_z to a small value (or zero).

The predicted sinkages are shown in Fig. 3(a) and a typical stress and strain distribution on the centre line is shown in Fig. 3(b). The load sinkage data in Fig. 3(a) have been plotted on log-linear axes and it is clear that the plots are substantially linear, except at very low contact stresses. This result is in line with the log-linear variation of v with p in the critical state model (see Equations 7, 8 and 9). This indicates that load sinkage data for wheels (and plates) should be of the form:

$$Z = k \ln (f) \tag{17}$$

There is an anomaly in this equation, as in the critical state equations, where the sinkage goes to zero at $f = 1$ and not at $f = 0$, which is as it should be. In the current critical state formulation the parallel problem has be overcome by specifying the intercepts, such as N and Γ, at $p = 1$ kPa and the state space in the interval $0 < p < 1$ is normally ignored. An alternative method is to define the contact stress as $(f + f_0)$ where f_0 is a reference stress which will be unity at $f = 0$ in the system of units used to define f. If f is

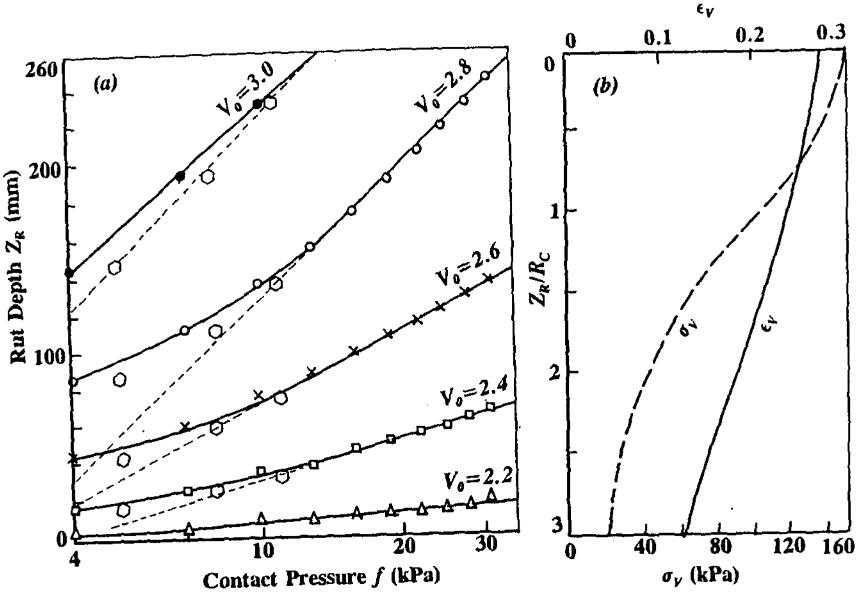

Fig. 3 (a) Theoretical sinkage characteristics of a 520/70R34 radial-ply tyre on a loam soil. V_0 = initial void ratio. (b) Typical vertical stress and strain distribution in soil below contact surface of tyre in (a).

expressed in kPa then f_0 = 1 kPa and Equation (17) can be restated thus:

$$Z = k \ln(f + 1) \tag{18}$$

It is interesting to note that the linearised form of Equation (3), which represents the currently accepted form of pressure sinkage and rut depth formulae, is clearly a log-log variation with pressure as the independent variable. In the light of the analysis in Sections 4 it is probably worthwhile considering whether these equations should be re-cast in the form of Equation (18), which has some theoretical justification. The hexagonal points on Fig. 3(a) are the corrected values according to equation (18). These points appears to eliminate a large part of the deviations from a linear plot at low values of p given by equation (17).

The coefficient k in Equations (17) and (18) is a function of the critical state soil constants λ, M, κ and φ , all of which could be measured by carrying out standard triaxial compression tests. The coefficient k is also dependent on the equivalent contact circle radius R_C and the initial void ratio (alternatively bulk or dry density) of the soil. The former can be obtained from tyre deflection data and the latter is a field variable, also readily measurable.

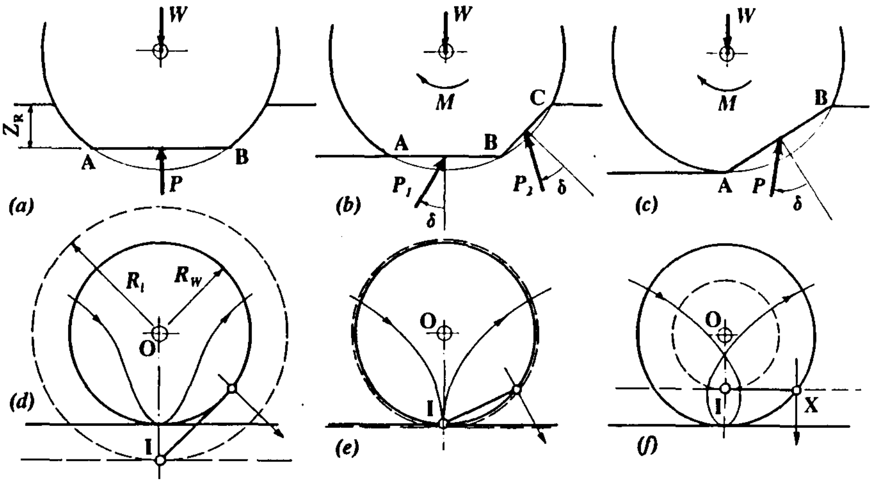

Fig. 4 (a) to (c) Formation of equivalent soil-wheel interface. (d) to (f) kinematics of points on contact surface. I = instantaneous centre of rotation. Broken lines show imaginary non-slipping wheels.

5. CONTACT SURFACE GEOMETRY

The prediction of rut depth Z_R discussed in Sections 3 and 4 provides the basis for a simplified analysis of the geometry of the contact surface. The three basic stages are illustrated in Figs. 4(a) to 4(c). In a static wheel the rut depth is Z_R and the main contact surface AB is *horizontal*. In a rolling wheel we assume that an additional inclined plane surface BC is developed [Fig. 4(b)] and the proportions of AB and BC depend on the magnitudes of the vertical components of the soil reactions P_1 and P_2 required to balance the axle load W. The conditions shown in Fig. 4(c) can occur where the soil reaction P acting on the inclined section AC alone is sufficient for vertical equilibrium. Evidently this is a highly simplified approach and there are more sophisticated analyses such as that proposed by Schmid (1993). The present analysis assumes that the contact surface can be approximated by the conditions set out in Fig. 4(c), which, to all intents and purposes, is a reasonable fit to the contact surface profile proposed by Schmid.

Points on the assumed plane contact surfaces move in cycloidal paths. It is convenient to analyze these motions relative to an instantaneous centre of rotation I shown in Figs. 4(d) to 4(f). This technique was used by Onafeko & Reece (1967) and Wong & Reece (1967). This diagram shows the imaginary equivalent non-slipping wheels and their associated rolling planes (shown in broken lines). The location of the instantaneous centre I is at the contact point of the imaginary system. For any given slip s the distance OI on the vertical diameter of the wheel is given by:

$$R_i = (1 - s)\, R_W \qquad (19)$$

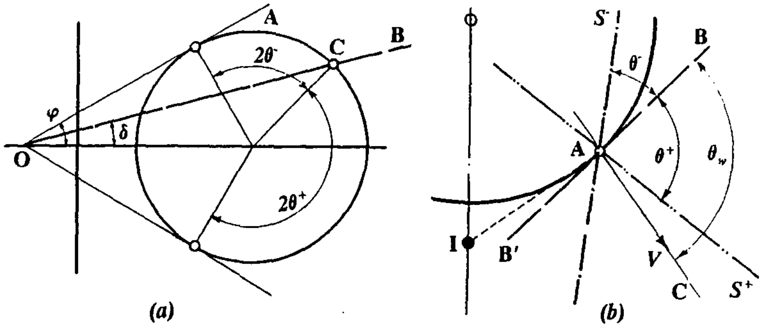

Fig.5 (a) Mohr's diagram for soil-wheel interface stresses. (b) Direction of velocity vector V and slip-line directions at points on a skidding wheel.

Equation (19) shows that for a skidding wheel ($s < 0$) the instantaneous centre I lies below the soil surface and for a slipping wheel ($0 < s < 1$) the instantaneous centre is above the soil surface.

6. SLIP-LINE COMPATIBILITY

A detailed numerical analysis of the stresses on the cylindrical surface of rigid wheels using Sokolovski's method (1960) was carried out by Karafiath (1971). It is proposed to use a simplified version of this method which depends on the development of slip line solutions from which contact stresses can be estimated from closed form solutions [Reece & Hettiaratchi (1989), Hettiaratchi (1993)]. The basis of this method is the construction of statically admissible slip-line fields using logarithmic spirals and straight lines. These fields must be compatible with the stress conditions on *all* the boundaries.

An important boundary is the interface between the wheel surface and the soil and this is quantified by the simple linear law:

$$\tau = c_a + \sigma \tan \varphi \qquad (20)$$

$$c_a = c \cot \varphi \tan \delta \qquad (21)$$

These conditions are shown on the Mohr's diagram in Fig. 5(a) where the Mohr-Coulomb failure line OA and the wheel interface sliding conditions OB pass through the common point O [geometry determined by Equation (21)]. Consider a typical point A on the surface of the wheel shown in Fig. 5(b). The equivalent plane interface at A between the wheel and the soil (the interface for short) is represented by the tangent plane B'AB and the direction of the failure or slip lines at A are AS^+ and AS^-. These slip lines make the angles θ^+ and θ^- with the interface B'AB and these angles can be obtained from the Mohr's diagram in Fig. 5(a) as:

$$\theta^{\pm} = (45° + \tfrac{1}{2}\varphi) \pm \tfrac{1}{2}[\,\sin^{-1}(\sin\delta/\sin\varphi) + \delta\,] \qquad (22)$$

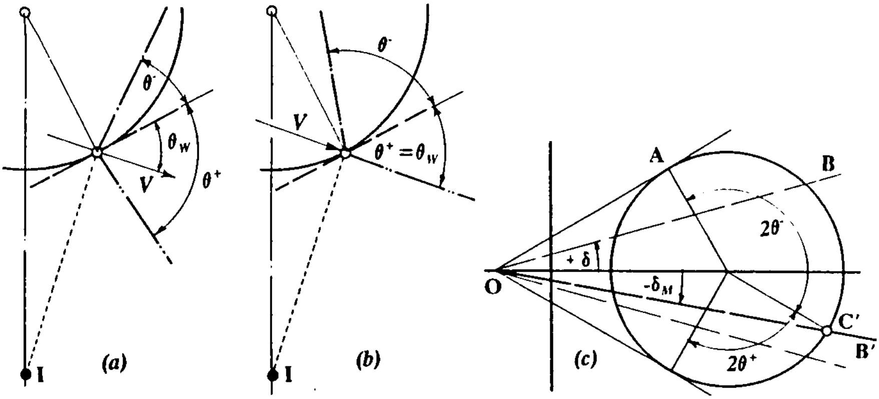

Fig. 6 Influence of kinematics on orientation of slip lines: (a) Soil sliding at interface, (b) Mobilised friction arrests sliding. (c) Mohr's diagram for negative mobilised friction.

Current earth pressure theory caters for such interfaces which move in simple translation (without rotation) into the soil (see Hettiaratchi & Reece, 1974). When the soil slides upwards towards the soil surface the friction conditions are represented by points on OB [Fig. 5(a)] and the angle of friction is the maximum value δ between the interface and the soil. These conditions hold good so long as the direction of motion of the interface B'AB, represented by the velocity vector **V** [AC in Fig. 5(b)] is directed outside the S^+ slip direction with $\theta_W > \theta$ (Hettiaratchi & Reece, 1975). This type of slip-line geometry is associated with a "basic stress field".

If, however, as shown in Fig. 6(a) the local velocity vector **V** points inside the S^+ slip direction ($\theta_W < \theta^+$) then the S^+ slip direction is incompatible with the kinematics of motion of the interface. Under these conditions continuous penetration of the interface forms a failure plane parallel to the direction of motion of the interface (see Hettiaratchi & Reece, 1975). The S^+ slip direction must therefore follow the direction of the displacement vector **V** as shown in Fig. 6(b) so that θ^+ is now constrained to take up the value θ_W. A "kinematic stress field" is associated with these conditions.

The consequence of this kinematically driven change to θ^+, is shown in Fig. 6(c). For the case illustrated, this constraint results in the *reduction* of θ^+ to the kinematic value θ_W. The original point C on the Mohr's diagram in Fig. 5(a) now moves to the position C' in Fig. 6(c) and the friction conditions of the interface now lie on the line OB'. As a result the *mobilised* angle of friction δ_M has become negative and must lie in the range $|\delta_M| < \delta$. The mobilised angle of friction is now less than the sliding value and it therefore follows that the soil element at A has stopped sliding and for the case illustrated its incipient displacement is downwards (δ_M -ve). The slip directions for this case is as shown in Fig. 6(b) where $(\theta^+ + \theta^-) = (90° + \varphi)$ as before. The analysis of this phenomenon is associated with the formation of fixed boundary wedges and the value of the mobilised angle of friction δ_M can be shown to be given by the expression:

$$\xi = 2\theta_W - \varphi - 90°$$

$$\tan \delta_M = (\sin \varphi \sin \xi)/(1 + \sin \varphi \cos \xi) \qquad (23)$$

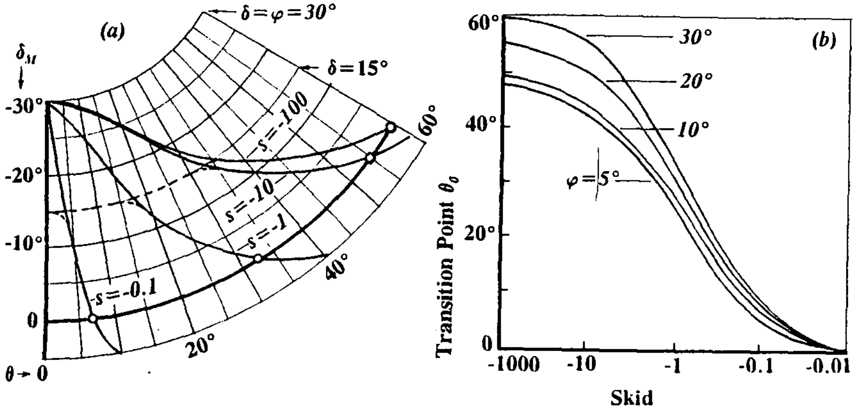

Fig. 7 (a) Variation of mobilised friction angle δ_M on contact surface for a soil with $\varphi = 30°$. s = skid values. (b) Influence of skid on position of transition point where friction reverses.

7.CONTACT SURFACE FRICTION

The change from basic to a kinematic stress fields on the soil-wheel interface takes place when $\theta_W \leq \theta^+$. The angle θ^+ is fixed for any given φ and δ but θ_W depends on the position of the instantaneous centre (and consequently slip or skid) and the particular point on the wheel surface under consideration. Thus for any specified slip (or skid) it is possible to trace the position, if any, where the stress regime changes from basic to kinematic form. It can be shown that this transition occurs only in the case of the skidding wheel ($s \leq 0$) where the instantaneous centre lies within the soil [see Figs. 4(d) to 4(f) and 6(a) and 6(b)].

From geometrical considerations it is possible to estimate the value of θ_W at points along the wheel circumference and the value of the mobilised angle of friction can then be estimated from Equation (23). The results of such a calculation for a skidding wheel rolling on a soil with $\varphi = 30°$ is shown on a polar plot in Fig. 7(a). It is clear that the transition point, where $\delta_M = 0$, is a function of skid. The variation with skid of the central angle θ_0 subtended between the vertical radius and the transition point for a range of values of φ is shown in Fig. 7(b). The transition point is insensitive to φ at low skid (or slip) and the proportion of the contact surface over which shear stresses reverse increase rapidly with skid. In the case of a locked wheel a fixed soil wedge develops over the entire contact surface (see Wong & Reece, 1966, Figs.8A and 10) and accords with the present analysis. At finite values of slip the system is expected to continue to behave as a convex cutting blade with a single sided failure pattern.

The diagram in Fig. 7(a) shows how δ_M varies for two possible values of interface roughness. If the interface were perfectly rough ($\delta = \varphi$) then the variations will follow the full lines. However if the interface is partially rough (say $\delta = \frac{1}{2}\varphi = 15°$), then δ_M cannot exceed δ so the curves flatten off along the dotted lines.

7.1 Skidding Wheel

There is considerable experimental evidence to show that the shear stress distribution on the surface of a skidding wheel shows a characteristic change in direction (see for example Onafeko & Reece, 1967). This directional change is associated with the transition point where the mobilised angle of friction δ_M alters from positive values, through zero to negative values. From the Mohr's circle diagram the magnitude of the shear stress at the soil-wheel interface is:

$$\tau = c \cot \varphi \tan \delta_M + \sigma_N \tan \delta_M \qquad (24)$$

A detailed assessment of the way the shear stress τ varies round the contact circumference of the wheel can be made from Equation (24) if the variation of σ_N is known. Assuming the skidding wheel behaves like a convex cutting surface σ_N is low at the soil surface (zero if $c = 0$) and increases roughly linearly with depth. Qualitatively this predicts a gradual rise in τ to the kinematic stress field point, then falls rapidly to the transition point, then reverses and rises with increasing σ_N and reversed δ_M up to the exit point at the vertical diameter. This variation closely follows observed experimental observations except for the fact that at the theoretical value of τ at the exit point is high, whereas the observed values are usually near zero.

7.2 Slipping Wheel

As shown in Fig. 4(f) the instantaneous centre I for a slipping wheel is located within the wheel radius. The velocity vectors of all points on the contact surface are directed well downwards. It can be shown that in this case θ_W is always greater than θ^+ and the failure is entirely basic. As the wheel is slipping, all points on the wheel move in one direction relative to the soil and the contact shear stress is unidirectional, as found by experiment.

The point on the wheel level with the instantaneous centre I [point X on Fig. 4(f)] is an important delimiter. The horizontal components of the velocity vector of all points on the wheel lying above X are directed forward whilst those lying below point rearwards. Thus the part of the wheel lying above X acts as a forward directed cutting blade whilst the lower part up to the exit point is a backwards-directed cutting blade. Thus the normal contact stress σ_N is expected to rise from a small value at the soil surface towards X. For the rearward failure regime point X becomes the top of the equivalent cutting blade and the contact stress must then fall off towards the exit point. This gives the characteristic rise of σ_N to a peak around X and falls off to zero at the exit point. The shear stresses derived from Equation (24) follow the same pattern and these are once again as observed.

8. SLIPLINE FIELDS

The analysis presented in Sections (6) and (7) provides the basis for the development of the slip-line fields generated by rolling wheels. Elegant solutions to this problem have already been provided by Karafiath (1971) who used a complex numerical solution based on a mathematical technique developed by Sokolovski (1960). These solutions have not allowed for kinematic effects and it may be appropriate to attempt a tentative extension of the simplified version of Sokolovski's method (Reece & Hettiaratchi,1989; Hettiaratchi, 1993) to take account of these effects.

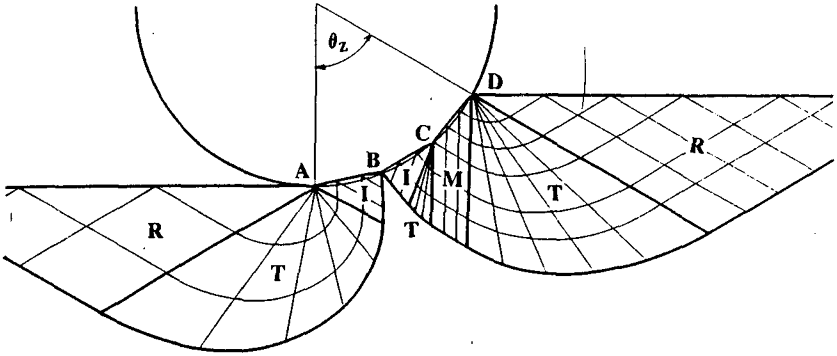

Fig. 8 Slip-line field in the soil beneath a driven slipping wheel. Refer to text for explanation of symbols identifying zones.

In both cases of a slipping and skidding wheel the entry angle θ_z can be estimated once the rut depth Z_R has been obtained from Equation (15):

$$\theta_W = \cos^{-1}(1 - Z_R/R_W)$$

where R_W is the radius of the wheel. The location of the other important delimiting points on the wheel contact surface can be arrived at from the analyses presented earlier.

In the case of a slipping wheel the point B on the contact arc ABCD in Fig. 8 is on a level with I on the vertical radius [corresponding to point X in Fig. 4(f)]. The face BCD fails soil in the direction of travel and AB opposite to it. Although the slip-line field can be constructed with BD as a single plane element a closer approximation can be achieved by subdividing it down to a number of smaller segments. The drawing in Fig. 8 uses two such elements. The single element AB fails soil backward. The interface friction angle is fully mobilised in one direction on all the segments AB, BC and CD.

The development of the curved wheel surface of a skidding wheel by plane segments is shown in Fig. 9. The point C corresponds to the transition point and B in Fig. 8 now coincides with the exit point A. The friction angle, which is fully mobilised over the upper part of CD, goes to zero at C and is mobilised in the reverse direction from C to A(B).

The slip-line fields in Figs. (8) and (9) have been constructed for $\varphi = 30°$ and a wheel-soil roughness angle $\delta = 25°$. Details of the configuration of the various zones are detailed elsewhere (see Sokolovski, 1960; Reece & Hettiaratchi,1989). In outline they are as follows: **I** = interface zone - proportions determined by θ^+ and θ^-; **T** = radial transition shear zone composed of radial straight lines and logarithmic spirals; **M** = modified Rankine zone which is a passive plane shear zone where principal planes are not vertical and horizontal; **R** = Rankine zone where the principal planes are vertical and horizontal; **W** =

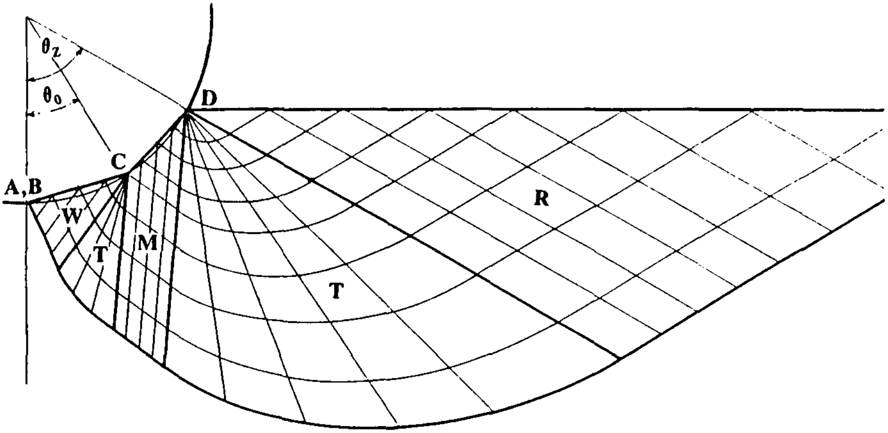

Fig. 9 Slip-line field developed by a towed wheel. A(B)C is the kinematic zone over which sliding ceases. Refer to text for explanation of symbols identifying zones.

boundary wedge determined by kinematic constraints (proportions dictated by θ_W)- soil does not slide and $|\delta_M| \leq \delta$.

The rupture surface enclosing the slip-line fields for a driven slipping wheel agrees closely with the classical glass-box experimental observations presented by Wong & Reece (1966). However there is considerable departure from their findings in the case of the towed skidding wheel. The slip-line theory does not predict a rearward failure regime as observed in the glass-box experiments.

There is an obvious conflict in that the predicted rupture block appears to be disproportionately large. This may be due to assuming the W-zone to be a fully formed "wedge" whereas in practice it may be a (hitherto undefined) blunted version. Salokhe & Gee-Clough (1988) have observed such deformed wedges in cage-wheel lugs. This modification to the wedge zone probably arises when the interface has a major rotational component, as is the case with the wheel segments.

From kinematic considerations the forward failure is acceptable and in the limit the locked wheel ($s = -\infty$) generates complete forward failure. The rearward failure observed in the glass-box experiments may be a artefact generated by soil "escaping" under the wheel as a result of it riding up on the soil failed in the formation of the "bow wave". The glass box photographs of this type of failure are invariably associated with very small sinkages.

In any event, once the rupture boundaries are identified according to a clearly defined set of rules, formulated in conjunction with unambiguous assumptions, then closed equations can be derived to calculate the soil reactions on the interface. The basic steps for these calculations have been presented by Reece & Hettiaratchi, 1989. The axle load, torque, thrust, and rolling resistance can then be obtained from the static equilibrium of the forces acting on the wheel-soil system. This simulation can be based on the readily measurable soil parameters such as c and φ.

9. CONCLUSIONS

The introduction of several bold simplifying assumptions has paved the way for the application of recently developed concepts in critical state Soil Mechanics to the wheel sinkage problem. This analysis is a logical progression from the earlier empirical approach to one in which sinkage can be predicted in terms of soil parameters which can be measured by standard laboratory methods. Admittedly, the experimental procedures required for establishing the critical state parameters required in this analysis are rather involved laboratory procedures, but they are none the less measurable constants for a given soil.

The analysis associates sinkage with the degree of compaction of the soil. Not unexpectedly the looser the soil the deeper the sinkage. This intuitive result can now be quantified in terms of measured soil properties such as initial bulk density [see Fig. 3(a)]. The linearised pressure-sinkage relationship appears to be a log-linear one [$z = k \ln(p)$] and is at variance with the corresponding log-log function [$p = k z^n$) currently assumed. A further departure is that the model proposed has contact pressure as the independent variable. Some caution has to be exercised in applying these revised relationships, particularly in view of the wide ranging simplifications that have been introduced in their derivation. Fresh experimental corroboration is required in terms of measured critical state parameters.

The kinematics of the soil-wheel interface is shown to have a major influence on the boundary conditions governing the slip-line orientation at the interface. Previous explanations have dealt with this problem purely from a kinematic viewpoint. The current analysis blends the Soil Mechanics aspects into this analysis. Slip-line fields can be readily extended into the rupture zones from known interface boundary configurations.

Once the rupture geometry is determinate soil-wheel interface forces can be calculated by considering the static equilibrium of all the boundary forces. Admittedly these calculations are fairly long and involved but they can all be developed in terms of straightforward closed form equations which can then be readily coded for evaluation on a desk-top computer with modest memory requirements. This method is not dependent on the application of advanced mathematical techniques.

The rupture boundaries developed for skidding or towed wheels show considerable variation from those currently accepted. A major criticism of the rupture surface geometry presented here for this case is that the volume of soil brought to shear failure appears to be disproportionately large. In addition the familiar rearward failure segment is absent. This anomaly has been explained on the basis that the available glass-box investigations show too small a sinkage. The single forward failure regime is a logical extension of the failure regime observed with fully braked towed wheels.

REFERENCES

Atkinson, J.H. & Bransby, P.L. 1978. *The mechanics of soils-an introduction to critical state soil mechanics*. McGraw-Hill, London.

Bekker, M.G. 1960 *Off the road locomotion*. University of Michigan Press, Ann Arbor, USA.

Febo, P. & Pessina, D. 1987 *Contact area tests of a new wide section agricultural tyre.* Proc. 9th ISTVS Int. Conf. Barcelona, Spain. 1, 236-243.

Hettiaratchi, D.R.P. 1989 *Critical state soil-machine mechanics.* Proc. Nordiske Jordbruksforskeres Forening Seminar No. 165, Oslo. Agric. University of Norway, N-1432 Ås, Norway.53-68.

Hettiaratchi, D.R.P. 1993 *Modelling soi-machine interactions.* Proc. 11th ISTVS Int. Conf. Lake Tahoe, Nevada, USA. 2, 561-570.

Hettiaratchi, D.R.P. & Reece, A.R. 1974 *The calculation of passive soil resistance.* Géotechnique, 24, 289-310.

Hettiaratchi, D.R.P. & Reece, A.R. 1975 *Boundary wedges in two-dimensional passive soil failure.* Géotechnique, 25, 197-220.

Karafiath, L.L. 1971 *Plasticity theory and the stress distribution beneath wheels.* Journal of Terramechanics,8,49-60.

Onafeko, O. & Reece, A.R. 1967 *Soil stress and deformation beneath rigid wheels.* Journal of Terramechanics, 4, 59-80.

Poulos, H.G. & Davis, E.H. 1974 *Elastic solutions for soil and rock mechanics.* John Wiley & Son, New York.

Reece, A.R. 1965 *Principles of soil-vehicle mechanics.* Proc. Auto. Div. Inst. Mech. Engineers, 180, Pt. 2A, 45

Reece, A.R. & Hettiaratchi, D.R.P. 1989 *A slip-line method for estimating passive earth pressure.* Journal of Agric. Eng. Res. 42, 27-41.

Roscoe, K.H., Schofield, A.N. & Wroth, C.P. 1958 *On the yielding of soils* Géotechnique, 8, 22-53.

Roscoe, K.H. & Burland, J.B. 1968 *On the generalised stress-strain behaviour of 'wet' clay.* in J.Heyman & F.A.Leckie (eds.) Engineering Plasticity, Cambridge University Press, Cambridge.

Salokhe, V.M. & Gee-Clough, D. 1988 *Modes of wet clay soil behaviour under a single cage wheel lug.* Journal of Terramechanics,4,273-285.

Schmid, I.C. 1993 *Inflation pressure control to improve terrain-trafficability-a model for simulation.* Proc. 11th ISTVS Int. Conf. Lake Tahoe, Nevada USA, 1,64-75.

Sokolovski, V.V. 1960 *Statics of soil media* Butterworths, London.

Wong, J.Y. & Reece, A.R. 1966 *Soil failure beneath rigid wheels.* Proc. 2nd. ISTVS Int. Conf. Quebec, Canada. 425-445

Wong, J.Y. & Reece, A.R. 1967 *Prediction of rigid wheel performance based on the analysis of soil-wheel stresses; Part I.* Journal of Terramechanics, 4, 81-98.

Wood. D.M. 1990 *Soil behaviour and critical state soil mechanics.* Cambridge University Press, Cambridge.

THE INTERACTION BETWEEN THE ROLLING TYRE AND THE SOFT SOIL
FEM-SIMULATION BY *VENUS* AND VALIDATION

Thomas Aubel

Institute of Automotive Engineering IKK
- Prof. Dr.-Ing. I. Schmid -
University of the Federal Armed Forces Hamburg, Germany

ABSTRACT

For calculating the processes between the tyre and the soil a new modular FEM simulation concept called ***VENUS*** *is developed at the Institute of Automotive Engineering (IKK). It is composed of a tyre model, a soil model and an interaction model.*

The interaction model couples the both submodels for the tyre and the soil and is able to calculate e.g. the tyre deformation, the sinkage, the contact shape as well as the rolling resistance, the circumferential force and the soil compaction.

For the validation of the interaction model tests had been carried out. In the paper the results of simulation will be compared with the results of these tests. It will be shown, that ***VENUS*** *is a well working FEM-simulation system to investigate the acting processes between the stationary as well as the rolling tyre and the soft soil.*

1 INTRODUCTION

The terrain mobility of a vehicle as well as the soil loading by a vehicle, which is mostly bad for the harvest-yield, are mainly influenced by the parameters acting in the contact area between the tyre and the soil. The important factors are the wheel load, the tyre- and the soil-properties, the size and the shape of the contact area and the rolling process itself.

To calculate these processes two different approaches are known: first, the analytical calculation, which is performed e.g. by BEKKER [1], SÖHNE [2] and SCHMID [3], and second, the calculation using the Finite Element Method (FEM) [4], which is performed e.g. by YONG et al. [5], JARZEBOWSKI et al. [6] and REGLI et al. [7]. The state of the art of modelling the tyre-soil interaction using the FEM is summarized in **fig. 1**.

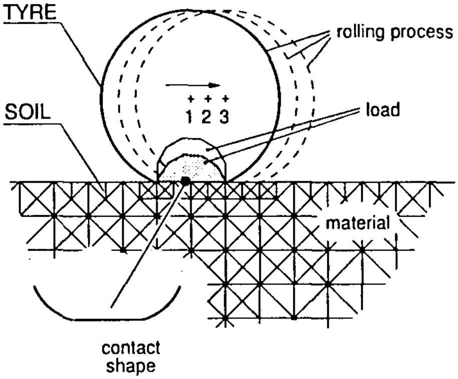

Fig. 1: Structure of tyre-soil interaction models using FEM

The known FEM-models mentioned above are based on a lot of assumptions and simplifications, regarding the following subjects:

Modelling: In any case only the soil is reproduced by finite elements. The tyre is not simulated as an original FEM-body.

Material description: The linear elastic theory is often used as material law. In some case a plastic theory is applicated. But mostly they are so complicated, that they are very difficult to use.

Loading: The wheel load is substituted by stress states in the contact area. Although these stress states are unknown, the values are assumed and used as input data.

Contact Shape: The size and the shape of the contact area is determined by external methods. On one hand it is measured, on the other it is calculated using e.g. the contact theory by HERTZ.

Rolling Process: The rolling of the wheel is replaced by a horizontal displacement of the substituted wheel load on the deformable soil, as shown by the steps 1, 2 and 3.

This utilization makes clear, that the existing FEM models imply a lot of idealizations: especially the material description of soil and tyre, the substitution of the loading procedure, the estimation of the contact contour between the tyre and the soil and the reproduction of the rolling contact. As a result, the FEM-models using these simulation concept will not be able to calculate the interactive processes between the tyre and the soft soil in a realistic way.

2 FEM-SIMULATION MODEL *VENUS*

The theory of the new simulation model *VENUS* is in detail the subject of earlier papers [8,9,10]. In this paper only a short description of the philosophy, the concept and the structure of the model will be given.

2.1 Requirement to the simulation model

Until now a procedure is missing, which only uses known parameters as input data like the elastic tyre attributes as a function of inflation pressure, the physical soil parameters and the wheel load. All other factors like tyre deformation, sinkage, stress distribution in the contact zone, pressure distribution in the ground as well as size and shape of the contact area have to be results of the simulation.

Fig. 2 shows the principal processes happening on the basis of the interaction between the tyre and the soil schematically. As external loads on the system tyre-soil, the wheel load and a driving force in case of the towed wheel or a driving moment in case of the driven wheel, are acting. As a result of the load and the interaction between the tyre- and the soil-parameters, local stresses in the contact zone occur. In case of force balance these stresses involve a radial tyre deformation and a radial sinkage. The integral of these values yields the size and the shape of the contact contour. These calculated processes as a function of the load-input are operating on the mobility factors like the circumferential force and the rolling resistance as well as on the soil load like compaction.

To simulate these processes realistically the most important requirement is to develop a simulation model, which uses only known parameters as input data and which calculates the results of the interaction between the tyre and the soil.

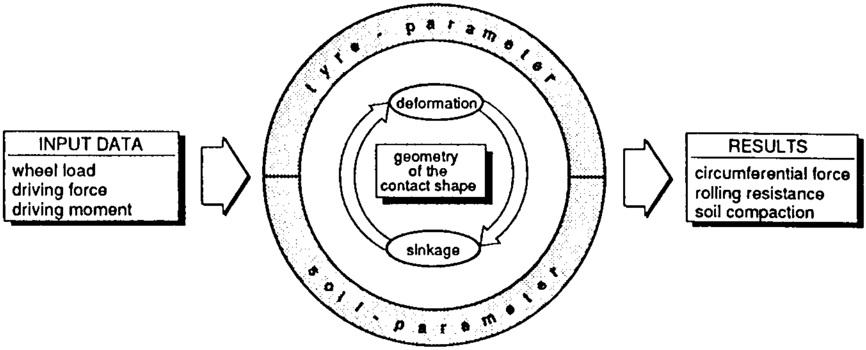
INPUT DATA
wheel load
driving force
driving moment
tyre - parameter
deformation
geometry of the contact shape
sinkage
soil - parameter
RESULTS
circumferential force
rolling resistance
soil compaction

Fig. 2: Principle process caused by the interaction between the tyre and the soil

2.2 Simulation concept

The simulation model is built up by the substructures *tyre*, *soil* and *interaction*. **Fig. 3** shows this concept schematically.

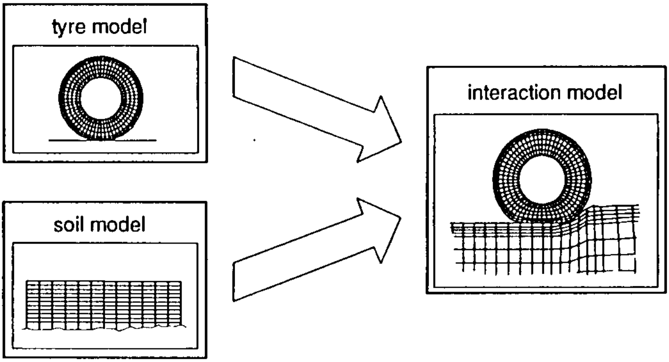
tyre model
soil model
interaction model

Fig. 3: Modular simulation concept

For the tyre it was necessary to develop a new FEM-model. The well known tyre models are very powerful but as well very complicated. And in any case they are only usable for the rolling contact on a rigid road, but not for the interaction with a soft soil. The developed tyre model is built up by different circular rings and uses the linear elastic theory. The application of the model is very easy. The model was verified by different tests on a rigid surface. It fulfils all requirements and is usable for the coupling with the soil model. Applications on different tyre types confirm this statement.

For the soil the extended DRUCKER-PRAGER theory [11] is used as plasticity rule. The theory uses parameters as input data, which are measurable. Namely these are the internal angle of friction and the cohesion. By this way the application of the plasticity model is easy. To validate this submodel, the comparison between simulation and measurement had been carried out. The close agreement of the results had shown, that the soil model is suitable for the investigation of the interaction between the tyre and the soft soil.

The successfully usage of the substructures for tyre and soil opens the way to couple them to the interaction model.

2.3 Structure of the interaction model

The physical processes operating by the contact of two deformable bodies are very complex. The resulting deformations are influencing each other up to the balance of the local forces. This is especially relevant for rolling movements. The contact zone is permanently changing with the rotation. In addition to the normal pressure, there are stresses in radial direction.

The construction of the simulation model is shown in **fig. 4.** In contrast with the known FEM-models, *VENUS* considers these relations in a realistic way:

Modelling: As well as the soil, the tyre is reproduced by finite elements.

Material description: The load-deformation behaviour of the tyre is described by an elastic material law, that one of the soil by an elastoplastic material law. The application and the parameter identification of the submodels are very easy.

Loading: The loads - wheel load F_z, driving force X or driving moment M - are acting in the center of the wheel.

Contact Shape: It is not necessary to assume the contact contour hypothetically. Size and shape of the contact contour are a result of the interactive processes between the tyre and the soil.

Rolling Process: The wheel has a vertical, a horizontal and a rotational degree of freedom. By this way the tyre is a free movable body in the plane, which enables a realistic rolling process.

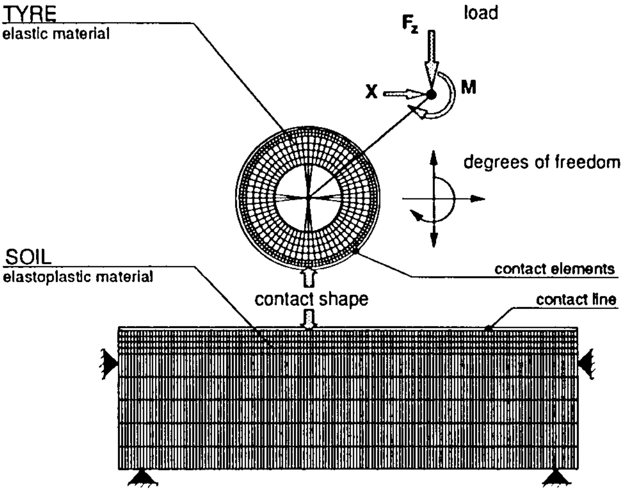
TYRE
elastic material
F_z
load
X
M
degrees of freedom
SOIL
elastoplastic material
contact elements
contact shape
contact line

Fig. 4: Structure of the interaction model

As a function of the external loads as well as of the inflation pressure and the soil resistance, the tyre deformation, the sinkage, the contact shape and a free rolling process of the wheel on the deformable ground are occuring.

The numerical solution is realized by a proper contact algorithm. Special elements on the rolling strip of the tyre and a slideline on the surface of the soil make it possible for every node on the circumference of the tyre to come in contact with every point on the soil surface. Additionally, penetrations of one body into the other are impossible. The friction between tyre and soil is considered by using COULOMB's law.

2.4 Working of the simulation model

Using the new simulation model *VENUS* some application examples will be presented in the following. For the simulation, the FEM-code ABAQUS [12] is applicated.

The first part of the examples shows the interaction between the stationary tyre (type *14.0-R-20mil*) and the soft soil. The sinkage z_0 will be investigated as a main influence factor concerning the vehicle mobility as well as the environmental aspects.

Influence of the soil type on the sinkage: The soil type influences the sinkage very much. A frictional soil reacts more strongly than a cohesive soil, which is influenced by the moisture content significantly. As a result of that, it can be expected, that the sinkage on a sand is generally smaller than on a loam. **Fig. 5** shows the simulation result for the tyre on different soil types. The wheel load amounts $F_z=35kN$, the inflation pressure $p_i=4.5bar$. As different soils a *sand* with a water content of $w=6\%$ and a *loam* with $w=14\%$ are used. It is obvious, that the simulation model shows the influence of the soil type on the sinkage z_0 correctly. The sinkage in the *sand6%* is much smaller than in the *loam14%*.

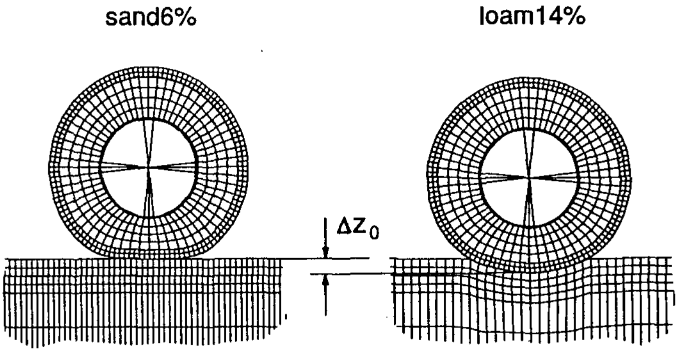

Fig. 5: Influence of the soil type on the sinkage z_0 (F_z=35kN, p_i=4.5bar)

Influence of the wheel load on the sinkage: It is well known, that the sinkage increases with the increasing of the wheel load. **Fig. 6** shows the simulation result of the tyre with the inflation pressure of $p_i=4.5bar$ on the *loam14%*. The wheel load has the value of $F_z=23kN$ in one case and $F_z=35kN$ in the other case. By looking on the sinkage z_0 the correct working of the simulation model considering the influence of the wheel load is obvious. The sinkage of the wheel with $F_z=23kN$ is smaller than that one of the wheel with $F_z=35kN$.

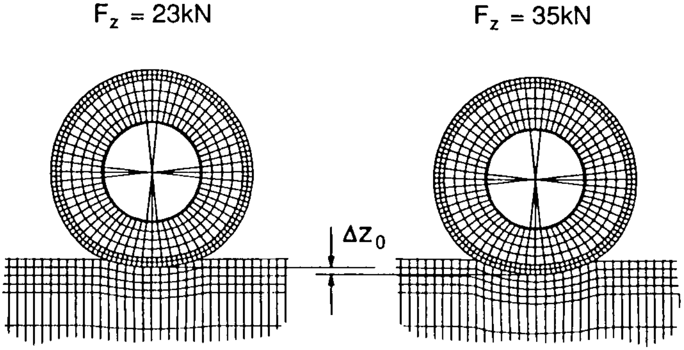

Fig. 6: Influence of the wheel load F_z on the sinkage z_0 (loam14%, p_i=4.5bar)

Influence of the inflation pressure on the sinkage: The inflation pressure has a significant influence on the sinkage. Lower inflation pressure produces a larger contact area and by this a lower sinkage. **Fig. 7** shows the simulation result of the tyre with the different pressures of p_i=*4.5bar* and of p_i=*1.0bar*. The soil is a *loam14%* and the wheel load amounts F_z=*35kN*. It is visible, that the sinkage decreases with lower inflation pressure. Like the soil type and the wheel load mentioned above, the influence of the inflation pressure on the sinkage is correctly reproduced by the simulation model.

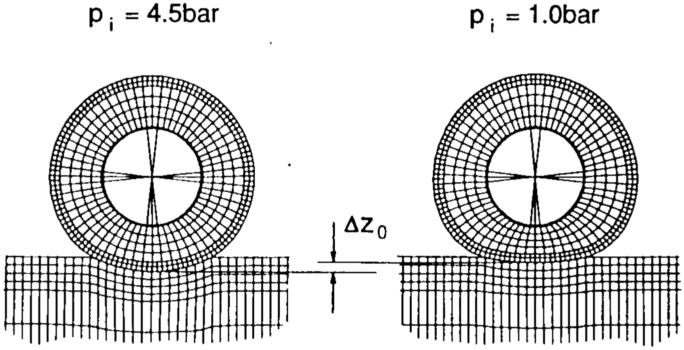

Fig. 7: Influence of the inflation pressure p_i on the sinkage z_0
(loam14%, F_z=35kN)

The second part of the examples shows the interaction between the rolling tyre (type *14.0-R-20mil*) and the soft soil. The physical processes are different from those of the stationary wheel. As a result of the interacting processes caused by the rolling contact, sinkage and tyre deformation are permanently developed to a new balance of local forces.

Influence of the inflation pressure on the rolling process: The experience has shown, that the variation of the inflation pressure represents one of the main control parameters to decrease the rolling resistance and to increase the vehicle mobility. **Fig. 8** shows a simulation result of the *towed wheel* using a *loam14%* and a wheel load of $F_z=23kN$. For $p_i=4.5bar$, the "bulldozing-effect" can be observed, which is well known from driving tests. By reducing the inflation pressure to $p_i=1bar$, a large soil deformation is avoidable. This is a result of the higher deforming ability of the tyre. These results show the realistic working of the simulation model. Especially the reproduction of the bulldozing effect indicates a high capacity of *VENUS*.

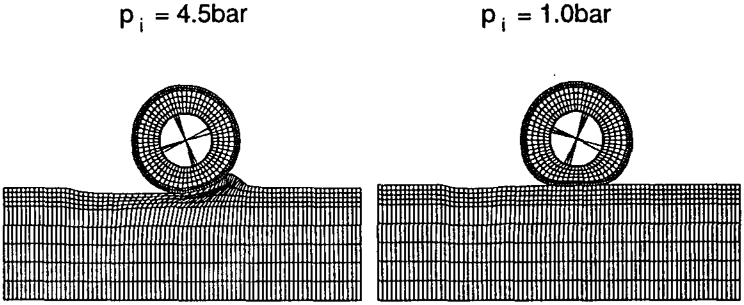

Fig. 8: Influence of the inflation pressure p_i on the interaction between a towed tyre and the soft soil (loam14%, F_z=23kN)

Influence of the moving kind on the rolling process: It is well known, that the processes between a towed and a driven wheel on the soft soil are very differently. In order to investigate the shearing resistance, the driven wheel on the deformable soil is simulated, too. **Fig. 9** shows the simulation result compared with the processes under a towed wheel. The soil is a *loam14%*, the wheel load amounts $F_z=23kN$ and the inflation pressure amounts $p_i=4.5bar$. The effects on

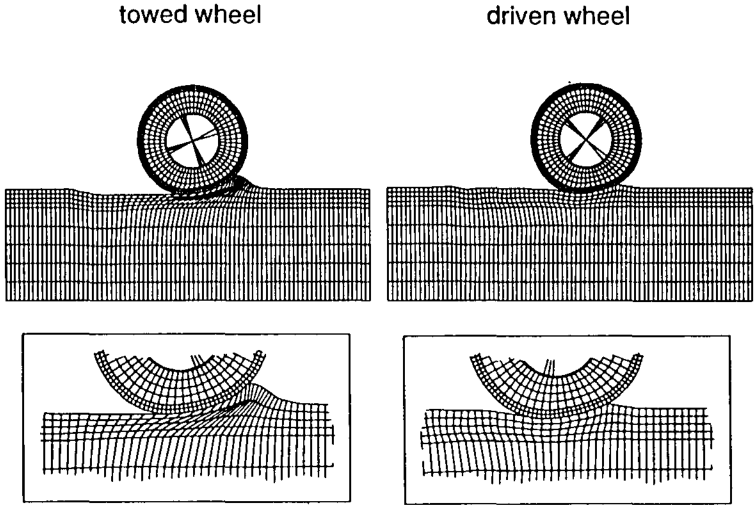

Fig. 9: Influence of a towed and a driven wheel on the interaction between the tyre and the soil (loam14%, F_z=23kN, p_i=4.5bar)

the interaction processes are very differently. In case of the towed wheel an increasing bulldozing effect is obvious. There is a material displacement in direction of the movement only. Because of the shear forces at the driven wheel, the bulldozing effect is smaller. The soil reacts with a material displacement in front of and behind of the tyre, as it is shown in the lower part of **fig. 9**. These results are close to the experiences observed in driving tests.

Influence of the inflation pressure on the ground pressure: The main factors influencing the soil load, which is mostly bad for the harvest yield, are the pressure and the pressure distribution in the soil. To investigate these effects of vehicle movement in a terrain, the rolling driven tyre on a soft ground is simulated. The soil is the *loam14%*, the wheel load amounts $F_z=23kN$ and the inflation pressure has the values of $p_i=4.5bar$ and of $p_i=1bar$. In **fig. 10** the well known effect of inflation pressure influence is obvious. With decreasing inflation pressure the soil load decreases. The value of the ground pressure is less in the case of the inflation pressure of $p_i=1.0bar$ as in the case of $p_i=4.5bar$. Controlling the inflation pressure to lower values, effects higher mobility as well as lower soil load.

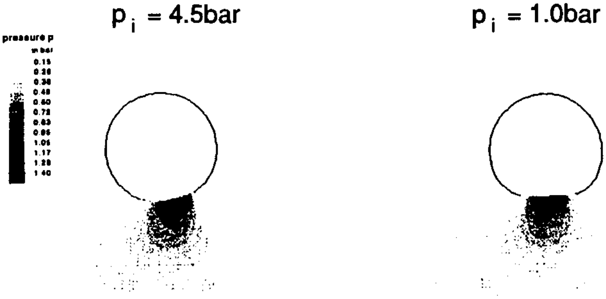

Fig. 10: Influence of the inflation pressure on the pressure distribution in the soil (loam14%, F_z=23kN)

Altogether these results show, that the new simulation model *VENUS* is a well working simulation tool to investigate the terrain mobility as well as the environmental aspects caused by a vehicle.

3 VALIDATION

To validate the new simulation model tests had been carried out. The comparison of these test results with simulation results in the following will give an impression of the quality of the simulation model.

3.1 Test Stand

The test stand for measuring the interaction processes between the stationary as well as the rolling tyre and the soft soil shows **fig. 11** in the basic version. The main parts are the stand, the load system with a control unit, the tyre, the soil bin and the measuring system.

A servo hydraulic cylinder moves vertically the tyre into the soil, at first controlling the way and later on the wheel load. As a function of different soil types and inflation pressures, the wheel load, the tyre deformation, the sinkage and the contact shape had been measured.

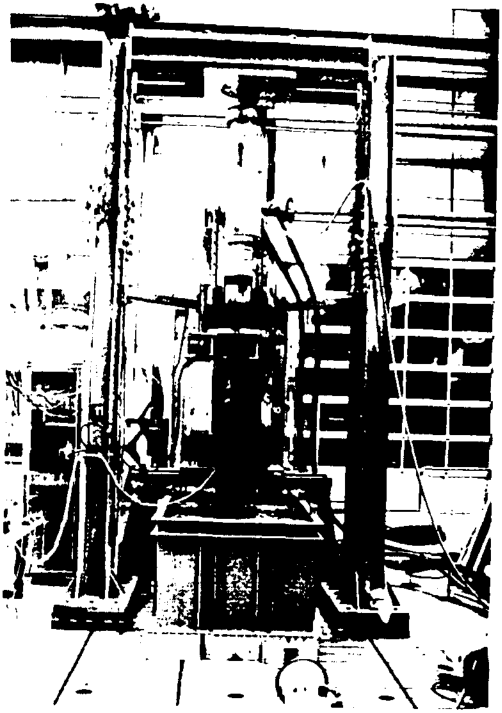

Fig. 11: Test stand for the investigation of the stationary wheel

Fig. 12: Test stand for the investigation of the rolling wheel

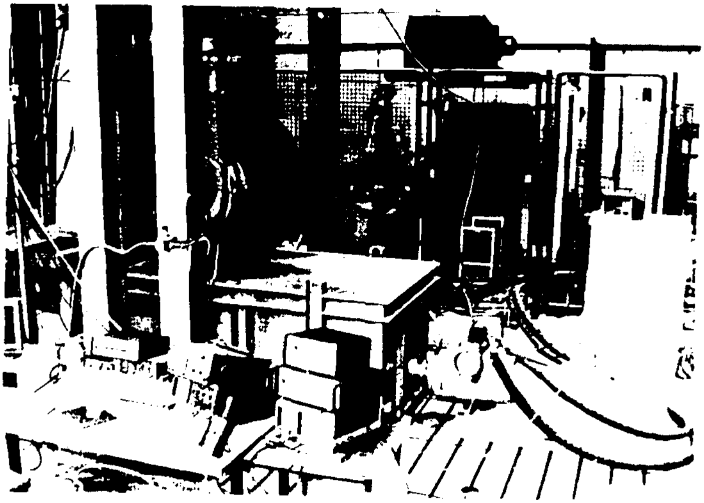

For the investigation of the rolling tyre a second servo hydraulic cylinder is integrated, **fig. 12**. It works in horizontal direction and moves the soil bin. By this way in cinematic inversion the tyre is rolling in the soft ground. Additionally to the conditions of the stationary wheel, the tyre deformation and the sinkage in dependence of the rolling way had been measured.

3.2 Measuring Equipment

To measure the tyre deformation, the sinkage and especially the contact shape, it was necessary to develop a special measuring equipment. The equipments known until now are working by measuring the contact print or by measuring a local point of sinkage and tyre deflection inside the tyre.

The new measuring equipment, **fig. 13**, is built up by a LASER-telemeter, an electromotor, a radial toothed-bar and an external working control unit. The telemeter measures the distance between the measuring head and the inside tyre wall. It is movable about an angle of 60 degrees. The principle of measuring is the triangulation method [13]. By this way it is possible to measure the tyre deformation and the sinkage, if the LASER is positioned in the vertical direction, as well as the complete contact shape, if the measuring head is moved around the working angle. The controlling of the system is realized by the external electronic control unit.

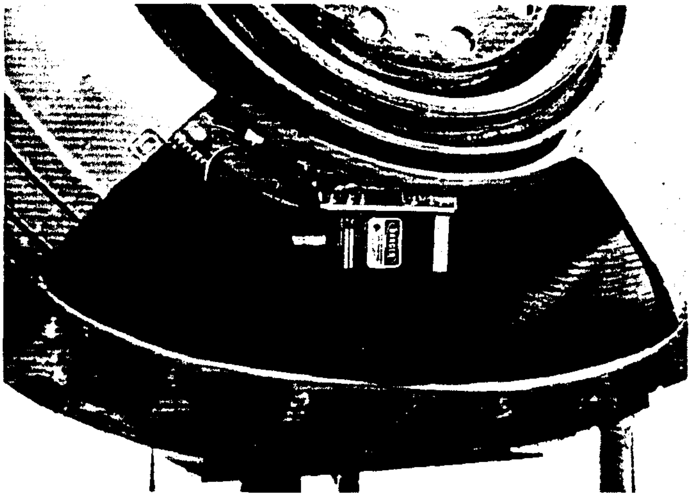

Fig. 13: LASER-telemeter system to measure the contact shape inside the tyre

3.3 Test Conditions

To investigate the interaction processes between the stationary as well as the rolling tyre and the deformable soil, the following test data are realized:

tyre *special version* of the tyre *14.0-R-20mil*
inflation pressures $p_i=1,3,6\ bar$
soil *sand* with $w=5\%$
loam with $w=14\%$
loam with $w=15\%$

The measuring parameters are the tyre deformation, the sinkage, the contact length and the contact shape, regarding the wheel load and the rolling way. In the following the relations will be shown for the *loam14%* as an example.

3.4 Simulation quality investigating the stationary wheel

Fig. 14 shows the tyre deformation f_0 and the sinkage z_0 in regard to the wheel load F_z. It is obvious that the simulation model shows the same relations like the test. The conformity in case of z_0 is very good. The difference in case of f_0, especially for $p_i=1bar$, has its reason in the special version of the test tyre. But altogether it is possible to say, that the submodels for the tyre and the soil as well as the interaction model are working very well.

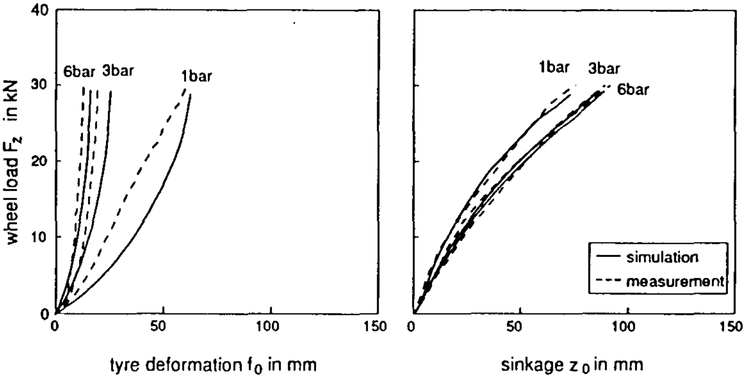

Fig. 14: Tyre deformation f_0 and sinkage z_0 on a loam14% - comparison between simulation and measurement

Fig. 15 shows the contact length *L* between the tyre and the soil plotted against the inflation pressure p_i. It is to observe that the simulation model reproduces the reality very well, especially in case of higher inflation pressures like $p_i=3bar$ and $p_i=6bar$.

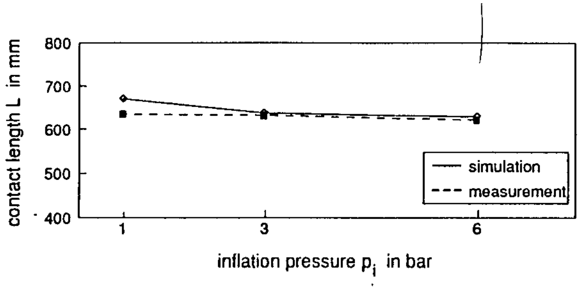

Fig. 15: Contact length L on a loam14% - comparison between simulation and measurement

Fig. 16 shows the contact shape between the tyre and the soil. It is obvious that not only the vertical values of the tyre deflection and the sinkage are reproduced very well. In the same way, the simulated and the measured contact shape regarding the inflation pressure p_i are very close.

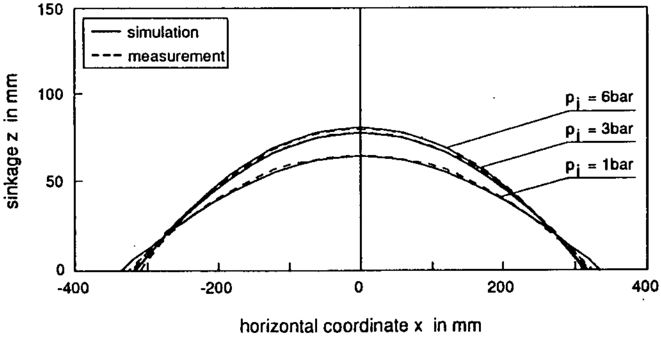

Fig. 16: Contact shape on a loam14% - comparison between simulation and measurement

By this way it is shown, that the new simulation model *VENUS* is able to reproduce the interaction processes between a tyre and a soil like the *loam14%* very well. This statement is valid for the other investigated soil types like the *sand5%* and the *loam15%*, too.

3.5 Simulation quality investigating the rolling wheel

The results of simulation and test for the rolling tyre are shown in **fig. 17**. The tyre deformation f_0 and the sinkage z_0 are plotted against the rolling way x for the different inflation pressures of p_i=*6bar* and p_i=*1bar*.

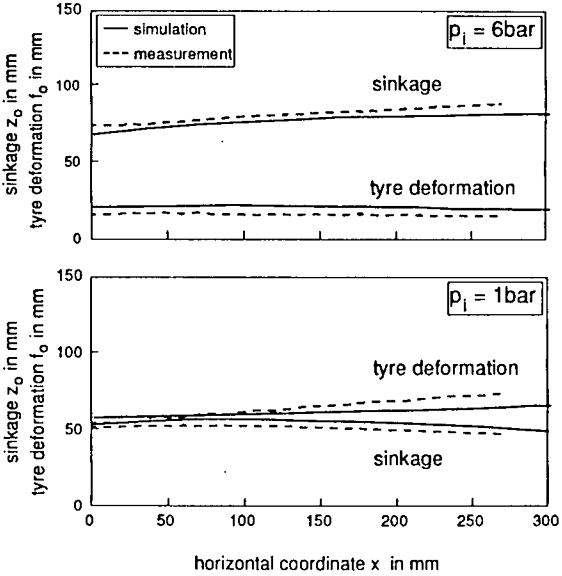

Fig. 17: Tyre deformation f_0 and sinkage z_0 on a loam14% - comparison between simulation and measurement

As well as the processes in case of the stationary wheel, the processes between the rolling tyre and the soft ground are reproduced correctly. For p_i=*6bar VENUS* calculates close to the real conditions the sinkage z_0 larger than the tyre deformation f_0. For p_i=*1bar* the tyre deformation f_0 is larger than the sinkage z_0 obtained from the measurement as well as from the simulation. Especially the phenomenon, that the sinkage at first increases and later on decreases, which is resulting from the high tyre deformation ability, is well reproduced by the simulation model. As well as these effects, the values of tyre deformation and of sinkage resulting from simulation and from test are very similar.

As a conclusion of this validation it can be noticed, that the new simulation model reproduces the effects of interaction between the stationary tyre as well as between the rolling tyre and the deformable soil very well. Here not more discussed, the results from the known analytical models are nearly the same. But especially for the sinkage and the contact length the results calculated by *VENUS* are more close to the reality.

4 INVESTIGATION SPECTRUM

The simulation model *VENUS* opens up a promising field of investigation for the interaction between tyres and soft soils. A listing of the investigation possibilities is given in **Tab. 1**.

Tab. 1: Investigation possibilities concerning the vehicle mobility and the environmental aspects

considerable acting factors	vehicle mobility aspects	environmental aspects
wheel load **tyre type** **inflation pressure** **soil type** **moisture content** **towed wheel** **driven wheel** **soil layers** **inhomogenities of the ground**	circumferential force rolling resistance drawbar pull slip stress distribution in the contact area contact shape tyre deformation sinkage	pressure distribution compaction surface deformation stress on roots harvest yield water balance

Tab. 1 makes clear, that the new simulation model performs a wide investigation spectrum. Factors to increase the terrain mobility can be investigated as well as factors to decrease the environmental influence.

The profile of the tyre is not integrated until now, but as a further more development of *VENUS* first work is done by FERVERS [14]. **Fig. 18** shows an example of integrating the tyre profile. This first result promises a lot of interesting investigations to optimize the profile design increasing the terrain mobility.

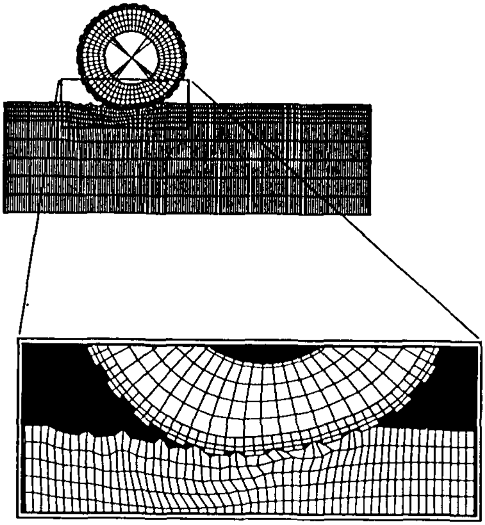

Fig. 18: Rolling process influenced by the tyre profile

5 CONCLUSIONS AND OUTLOOK

Altogether, the new FEM-simulation model *VENUS* opens up a promising field of investigation for the interaction between elastic tyres and soft soils. It reproduces the effects acting between the tyre and the soil in a very realistic way compared with the natural state. Compared with the analytical methods and the existing FEM models, the new system has the advantage, that it is not necessary to estimate any parameters resulting from the interaction between tyre and soil.

On one hand, *VENUS* can be used to optimize the layout of off-road vehicles, e.g. as a tool for the concept of an inflation pressure control system, which can contribute to decrease the rolling resistance and to minimize the fuel consumption. On the other hand, it is also possible to calculate the soil compaction as the result of the vehicle load. This is of particular interest for agricultural applications.

In the future the main part of development will be the considering of the tyre profile.

REFERENCES

[1] **Bekker, M.G.**: Off-the-Road Locomotion. The University of Michigan Press, Ann Arbor 1960

[2] **Söhne, W.**: Rad- und Gleiskettenfahrzeug: Bewertung und Entscheidung aufgrund von Theorie und Forschung. Vortrag SFM Studiedagar, Skövde 1970

[3] **Schmid, I; Ludewig, J.**: Improved Calculation of Sinkage of a Wheel on Soft Ground. Proceedings 5th European Conference of the ISTVS Vol.1 S.318-321, Budapest 1991

[4] **Zienkiewicz, O.C.**: Methode der Finiten Elemente. Carl Hauser Verlag, München 1975

[5] **Yong, R.N.; Fattah, E.A.; Boonsinsuk, P.**: Analysis and Prediction of Tyre-Soil Interaction and Performance using Finite Elements. Journal of Terramechanics Vol.15 No.1 pp.43-63, 1978

[6] **Jarzebowski, A.; et al.**: Numerical Prediction of the Soil Behaviour under a Rigid Wheel. Proceedings 5th European Conference of the ISTVS Vol.1 S.49-56, Budapest 1991

[7] **Regli, G.; Handke, A.**: Simulation der Wechselwirkung Reifen-Boden mit Hilfe der finiten Elemente. VDI/MEG Kolloquium Landtechnik H.7 S.38-45, München 1989

[8] **Aubel, Th.**: Application of the Finite Element Method on Soil Mechanical Processes. Proceedings 5th European Conference of the ISTVS Vol.1 S.9-16, Budapest 1991

[9] **Aubel, Th.**: FEM-Simulation der Wechselwirkung zwischen Reifen und nachgiebiger Fahrbahn. Automobiltechnische Zeitschrift 94 S.662-667, 1992

[10] **Aubel, Th.**: FEM-Simulation of the Interaction between an Elastic Tyre and Soft Soil. Proceedings 11th International Conference of the ISTVS Vol.2 S.791-802, Lake Tahoe 1993

[11] **Drucker, D.C.; Prager, W.**: Soil Mechanics and Plastic Analysis of Limit Design. Quarterly of Applied Mathematics Vol. 10, 1952

[12] **Hibbitt, Karlsson & Sorensen, Inc.**: ABAQUS-Manuals. Version 4.9, Providence Rhode-Island 1989

[13] **Klicker, J.**: Triangulationsmeßtechnik. ZESS-Workshop - Laseroptische und bildgebende Sensorsysteme für die individuelle Meßtechnik, Siegen 1992

[14] **Fervers, C.W.**: FE-Simulation of Tyre-Profile-Effects on Terrain Mobility of Vehicles. Proceedings 6th European Conference of the ISTVS, Wien 1994

Session III B

Sektion III B

Simulation 2

Simulation 2

Ground Vehicle Performance Optimization Using the Genetic Algorithm

James L. Overholt, Ashraf A. Zeid* & Mikell K. Eiler
U.S. Army TARDEC
Mobility Technology Center
Warren, MI 48397-5000

On most vehicle systems there are adjustable parameters which could have profound effects on the vehicle's overall performance. If some quantifiable measure of performance exists, then the natural assumption is to implement some nonlinear optimization scheme that searches the space defined by these variable quantities. In theory, this approach may find at least a local extreme point, but in practice, will prove most difficult due to the complex constraint surfaces formed by these large-scale systems.

A Genetic Classifier System (GCS) attempts to solve this Problem by starting with hundreds of potential solutions and then eliminating and generating new candidates through a "natural selection" process. This "survival of the fittest" approach requires that a performance measure be calculated for every potential solution. After every member of the population has been evaluated for his merit, each solution receives a weighting commensurate with its performance. New candidate solutions are generated by randomly selecting two parents from the available members of the population, and "mating" them to produce new offspring. The premise behind this methodology is that good traits of highly weighted solutions are passed down to their "children". Spawning of new generations continues until a desired Performance level is obtained.

This methodology is used to tune adaptive suspension algorithms for a generic off-road vehicle. The criteria of merit for competing adaptive control routines based on minimizing absorbed power over a variety of terrains and vehicle speeds. The GCS method can be used to optimize the vehicle physical parameters and sensor locations while simultaneously structuring the control algorithms.

---

* Currently with the Army High Performance Computing Research Center (AHPCRC)

This paper will be published in an appendix to the proceedings

THE SIMULATION OF THE PHENOMENA BETWEEN TYRE AND TERRAIN WITH THE SIMULATION SYSTEM *ORIS*

Klaus J. Ruff
Institute of Automotive Engineering IKK
- Prof. Dr.-Ing. I. C. Schmid -
University of the Federal Armed Forces Hamburg, Germany

ABSTRACT

*The program system **ORIS** (Off **R**oad **I**nteractive **S**imulation), developed at the Institute of Automotive Engineering (IKK), simulates interactively the motion of vehicles in the terrain. The simulation model is composed of submodels, which represent the modules **interactive interface driver-vehicle-terrain**, **drive line** including engine, **wheel-soil interaction**, **vehicle** (dynamics) and the **terrain**.*

Concerning the wheel-soil-interaction, the rigid wheel model or a wheel-soil-model for the elastic tyre can be used alternatively. Thereon the contact area is described by a parabola. Furthermore the slip-sinkage and the multipass effect are considered. The motion of the vehicle in the terrain map and its position in the three-dimensional area are shown on a monitor. The structure of the terrain model is presented. Simulation results are presented and discussed.

1 INTRODUCTION

In the automotive industry simulation models are used to examine vehicle concepts, vehicle components and the dynamics of the vehicle on the road. For this purpose the components of the vehicle and the road are reproduced in models. If it is necessary to consider the reaction of the human being, the real driver has to be included, because simulation of a human being is very difficult.

In the terrain mobility the simulation is especially useful, because tests in the terrain can not be reproduced easily by the reason of the inhomogeneity of the terrain and the influence of the weather. Till now especially the interaction between tyre and soil was examined, because in the terrain the resistances increase compared to the road. Therefore the drawbar pull is smaller than on the road.

A model, which on one hand describes the whole system driver-vehicle-terrain and on the other describes in detail the behaviour of the drive line and the interaction with the terrain including the slip and the multipass-effect, did not exist. With such a model it should be possible to examine the influence of steering actions with the accelerator or brake pedal, with the steering wheel and with the gear shift. It should be also possible to examine design parameters like engine and torque converter characteristics, gear ratios, torque distribution, tyre geometry and inflation pressure.

To investigate the interaction between driver, vehicle and terrain a simulation model is presented, which contains these three elements. The human is acting as operator of the computer, and vehicle as well as terrain are simulated.

2 SIMULATION MODEL

The model fulfils the following demands:

- interactive steering of the motion direction, regulation of the engine power and choice of the gear ratio by the operator
- simulation of the interaction between vehicle and terrain in detail
- visualisation of a terrain section with different altitudes and various characteristic soil-values and of the moving vehicle on the monitor.

Interactivity means, that the answer to an action must follow in a very short time, not perceptible for the human being. Therefore precision of the simulation as well as computing time have to be considered. Because the longitudinal dynamics is the important factor for the motion in the terrain, the vertical and lateral dynamics were not fully taken into account.

Fig. 1 shows the concept of the simulation system ***ORIS***.

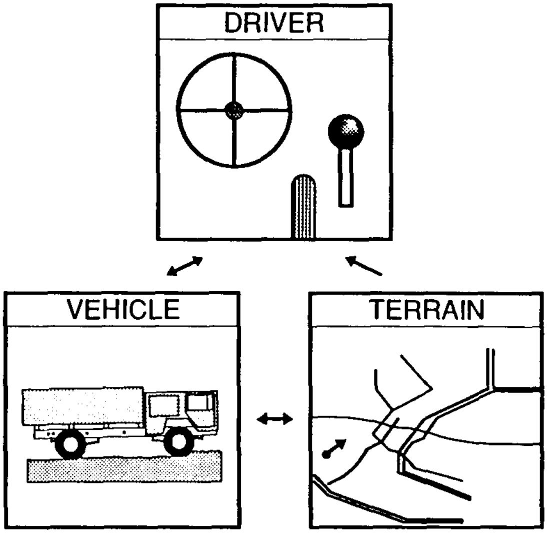

Fig. 1: Concept for the simulation system ***ORIS***

In fig. 2 the structure of the simulation model can be seen.

On the 5th European Conference of the ISTVS the **concept**, the **structure** and the **interaction tyre-terrain** had been introduced, [1]. The models for the **interactive interface**, the **engine**, the **drive line** and the **digital terrain** had been presented on the 11. International Conference of the ISTVS, [2]. In this paper the improvements of the **interactive interface** and the **digital terrain** as well as the new **tyre-terrain-models** are shown. In the **vehicle model** the actual site of the vehicle in the three-dimensional terrain is calculated with the inputs of velocity, driving direction and slope. With this information the wheel loads are determined. For the actual position of the vehicle and of the wheels the information about the terrain (soil, inclination) is obtained from the terrain model.

The simulated subject is a truck MAN type 451, which is used in the Federal Armed Forces as LKW 5t gl. The simulation program is developed in the program language ANSI-C and C++.

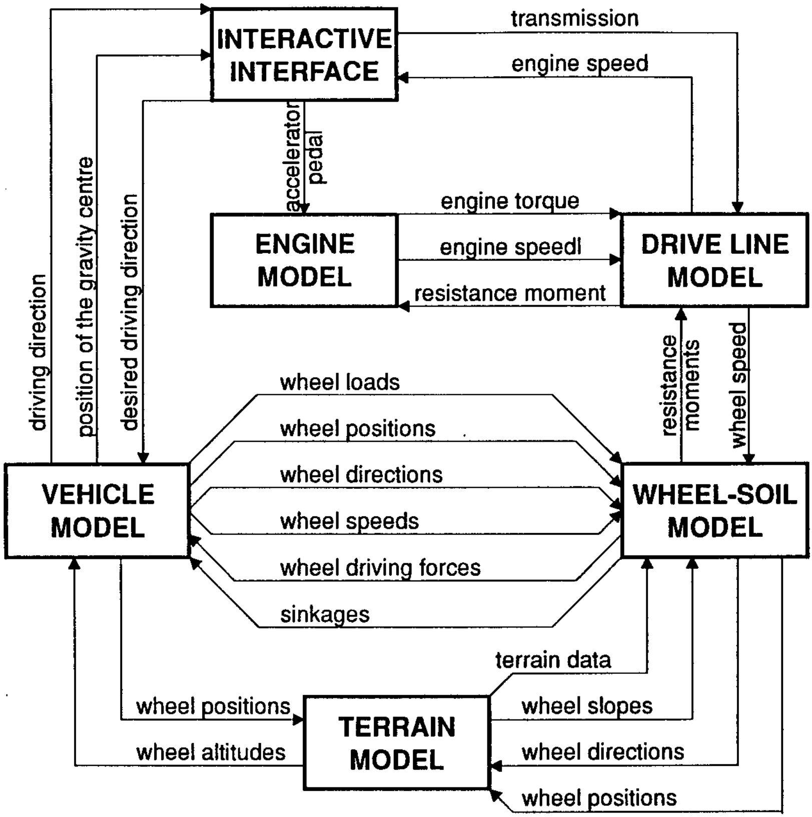
INTERACTIVE INTERFACE
transmission
engine speed
accelerator pedal
ENGINE MODEL
engine torque
engine speedl
resistance moment
DRIVE LINE MODEL
driving direction
position of the gravity centre
desired driving direction
resistance moments
wheel speed
VEHICLE MODEL
wheel loads
wheel positions
wheel directions
wheel speeds
wheel driving forces
sinkages
WHEEL-SOIL MODEL
terrain data
wheel positions
wheel altitudes
TERRAIN MODEL
wheel slopes
wheel directions
wheel positions

Fig. 2: Structure of the simulation model

2.1 Interactive interface

On one hand the interactive interface is used to inform the driver on velocity or engine speed. The instruments are located at the instrument panel as usual and are monitored in the graphical window as it is shown in fig. 3. On the other hand the driver determines the values of the accelerator pedal, of the desired driving direction and of the gear ratio in the interactive interface. This is done with a computer mouse. The actual values are fed in with control spools, push-buttons and a marking point, which moves the steering wheel.

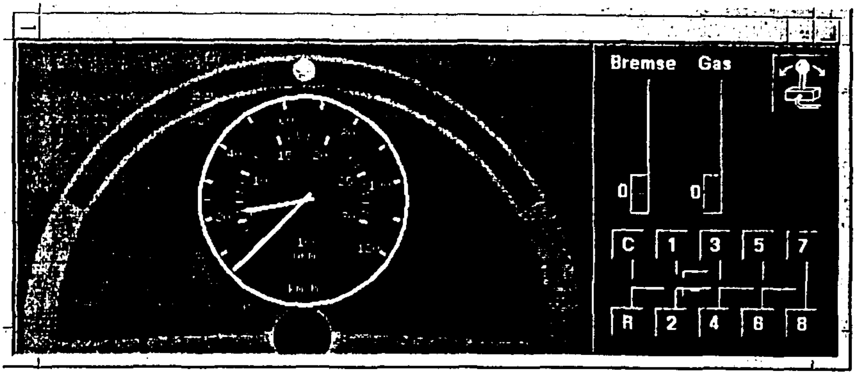
Bremse
Gas
0
0
C
1
3
5
7
R
2
4
6
8

Fig. 3: Graphical window of the interactive interface

The input can also be made with a dial box and a button box, which are represented in fig. 4. There the accelerator pedal and the brake pedal are simulated with one turn regulator, the steering wheel with another turn regulator and the gearbox with push-buttons. The advantage of this control is the simultaneous use, which is impossible with the computer mouse.

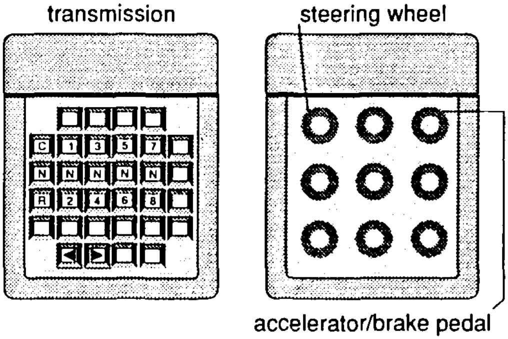
transmission
steering wheel
C
1
3
5
7
N
N
N
N
N
R
2
4
6
8
accelerator/brake pedal

Fig. 4: Dial box and button box as input elements

On the graphical terrain map the driver watches the position of the moving vehicle and with this also the velocity and driving direction, as it is described in chapter 2.2.

2.2 Terrain model

In the digital terrain model [3, 4, 5] the altitude and the characteristics of the soil exist at each coordinate position. The model is realised with layers, which can be shown on the monitor, if required.

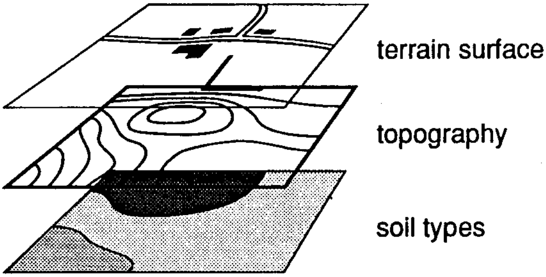
terrain surface
topography
soil types

Fig. 5: Structure of the terrain model

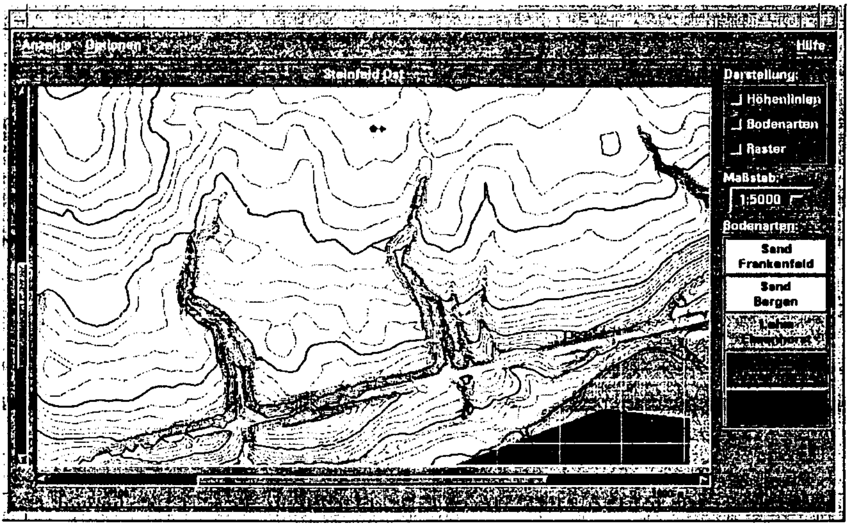
Anzeige
Optionen
Steinfeld Ost
Hilfe
Darstellung:
☐ Höhenlinien
☐ Bodenarten
☐ Raster
Maßstab:
1:5000
Bodenarten:
Sand Frankenfeld
Sand Bergen

Fig. 6: Terrain section with contour lines and classes of soil-values

The terrain net is generated with triangles as basic elements to economise store capacity and computing time. This is important for a possible transfer from a one-dimensional top view to a three-dimensional view for the driver and is of advantage for the presentation of the terrain area.

3 WHEEL-SOIL-INTERACTION

In contradiction to the road the wheels in the terrain develop a sinkage. The rolling resistance is mainly caused by the compacting work of the soil and less by the deformation work of the tyre. The transmission of the circumferential forces on the tyre is limited.

Three different models are used to describe the wheel-soil interaction. One model is the well-known one of the rigid wheel by BEKKER [6, 7]. The second model is derived from the first one with a parabola shape of the contact area [8], and the third one describes the interaction with an elastic tyre, SCHMID [8, 9]. The multipass-effect, which was first systematically examined by HOLM [10], is considered with the assumptions by SCHMID and LUDEWIG [11]. Shear stress is calculated with JANOSI and HANAMOTO [12] with the shear displacement by LUDEWIG [13]. Slip sinkage is considered according to STEINER [14].

3.1 Rigid wheel with circle geometry

The static sinkage z_0 is calculated with a series development, which is finished after the first step [6, 7].

$$z_0 \approx \left[\frac{F_z}{b \cdot k \cdot \sqrt{D} \cdot \left(1 - \frac{n}{3}\right)} \right]^{\frac{2}{2 \cdot n + 1}} \tag{1}$$

with		
	b	wheel width
	D	wheel diameter
	F_z	wheel load
	k	module of soil deformation
	n	sinkage exponent.

The passage of the 2. wheel, the so called multipass-effect, is not considered.

3.2 Rigid wheel with parabola geometry

The advantage of the parabola geometry is the easy mathematical handling of the parabola [8]. The solution of the equation for the static sinkage z_{01} of the 1. wheel can be found without a series development.

$$z_{01} = \left[\frac{F_{z1} \cdot \left(\frac{n}{2} + 1 \right)}{b \cdot k \cdot \sqrt{D} \cdot \sqrt{1 - \frac{z_{01}}{D}}} \right]^{\frac{2}{2 \cdot n + 1}} \tag{2}$$

3.3 The multipass-model for the rigid wheel with parabola shape

The model for the multipass is based on the hypothesis, that the pressure level of the following wheel has to be bigger than that of the 1. wheel to get an additional sinkage. This hypothesis neglects the elasticity of the terrain. Hereby it must be considered, that the integral p(x)dx, that represents the pressure distribution along the contact area, is equal to the wheel load. Fig. 7 explains this multipass model.

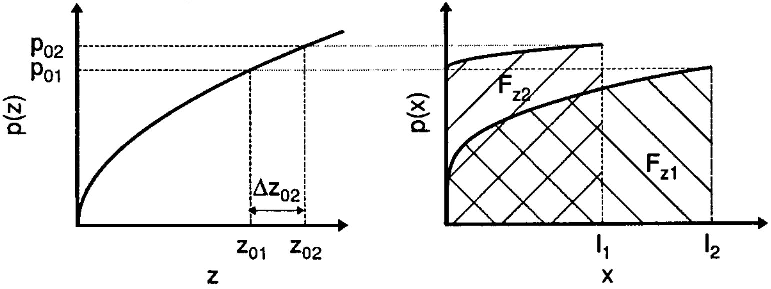

Fig. 7: Model for the multipass-effect

According to this, the static additional sinkage Δz_{02} for the 2. wheel can be calculated.

$$\Delta z_{02} \approx \left[\frac{F_{z2}}{b \cdot k \cdot \sqrt{D} \cdot \sqrt{1 - \frac{\Delta z_{02}}{D}} \cdot z_{01}^{n} \cdot \left[1 + \frac{2 \cdot n}{3} \cdot \frac{\Delta z_{02}}{z_{01}} \right]} \right]^{2} \qquad (3)$$

3.4 Elastic tyre with parabola geometry

The parabola model for the elastic tyre on soft soil exists since 1990, [8], and was first presented in 1993 on the 11. th International Conference of the ISTVS, [9]. If the assumptions for the wheel diameter D^*

$$z_0 << D^*, \qquad f_0 << D, \qquad z_0 + f_0 << D$$

are true, the wheel diameter ratio D^*/D can be calculated as follows.

$$\sqrt{\frac{D_1^*}{D}} \approx \sqrt{1 + \frac{f_1}{z_{01}}} + \sqrt{\frac{f_1}{z_{01}}} \qquad (4)$$

$$\text{with} \quad f_1 \approx \frac{2 \cdot \sqrt{\frac{f_1}{z_{01}}} \cdot \sqrt{\frac{D_1^*}{D-1}}}{\frac{D_1^*}{D}} \cdot f_{k1} \qquad (5)$$

$$z_{01} \approx \left[\frac{F_{z1} \cdot \left(\frac{n}{2} + 1 \right)}{b \cdot k \cdot \sqrt{D} \cdot \sqrt{\frac{D_1^*}{D}}} \right]^{\frac{2}{2 \cdot n + 1}} \qquad (6)$$

and	D_1^*	equivalent wheel diameter
	f_1	tyre deformation
	f_{k1}	tyre deformation on a flat road.

The tyre deformation on a flat road f_{k1} is derived from the spring characteristics of the tyre depending on the inflation pressure and the wheel load.

3.5 The multipass-model for the elastic tyre with parabola shape

The 2. wheel, which drives in the track of the 1. wheel, rolls on the pre-compacted terrain. The extreme condition of the pre-compacted terrain is similar to the condition on the flat road. For this limit condition the contact length l_{k2} can be determined with the formula for the circular segment and with this result the medium pressure on terrain $\overline{p}_2$ can be calculated.

$$l_{k2} = \sqrt{f_{k2} \cdot (D - f_{k2})} \tag{7}$$

$$\overline{p}_2 = \frac{F_{z2}}{l_{k2} \cdot b} \quad . \tag{8}$$

The pressure along the contact length $p_2(x)$ can be supposed with

$$p_2(x) = p_{2\max} \cdot \left[1 - \left(\frac{x - \frac{l_{k2}}{2}}{\frac{l_{k2}}{2}} \right)^m \right] \tag{9}$$

and $p_{2\max}$ maximum pressure
$m \geq 1$

It has been found, that m = 4 meets the reality sufficiently.

The integral over the contact area is equal to the wheel load. The solution of this integral can be solved to the maximum pressure

$$p_{2\max} = \frac{m+1}{m} \cdot \frac{F_{z2}}{b \cdot l_{k2}} \quad . \tag{10}$$

The maximum pressure can be also expressed as a function of the maximum track depth $z_{02} = z_{01} + \Delta z_{02}$.

$$p_{2\max} = k \cdot (z_{01} + \Delta z_{02})^n \quad . \tag{11}$$

If the formula (11) and (10) are equalised, the static sinkage of the 2. wheel results.

$$\Delta z_{02} = \left[\frac{m+1}{m} \cdot \frac{F_{z2}}{k \cdot l_{k2} \cdot b} \right]^{\frac{1}{n}} - z_{01} \quad . \qquad (12)$$

4 SIMULATION RESULTS

Tests with variation of different parameters were made to show especially the working of the different wheel-soil models. To make clear these differences, other influences like slip-sinkage and different soils were neglected. In the following only a small part of the research spectrum of ***ORIS*** is shown by some examples.

The data of the vehicle are given in [15]. The characteristics of the soil are listed in table 1.

Table 1: Characteristics of the used soil

soil	k	n
loam IKK	6,75	0,51

Fig. 8 shows the static sinkage for a loaded vehicle. For the rigid wheel the different sinkage is only caused by the distribution of the axle load for the loaded truck, which is 45 % on the front axle and 55 % on the rear axle. For the rigid wheel with the parabola shape, multipass-effect results in a smaller sinkage on the 2. wheel. For the elastic tyre the sinkage is reduced on the 1. wheel and also on the 2. wheel, which is caused by the longer contact area.

In fig. 9 the sinkage for the unloaded truck can be seen. The distribution of the axle load is 55 % on the front axle and 45 % on the rear axle. In case of the elastic tyres there is no additional sinkage for the 2. wheel, because the pressure below the 1. wheel is not reached with the smaller load of the following wheel at the inflation pressure of 4,5 bar.

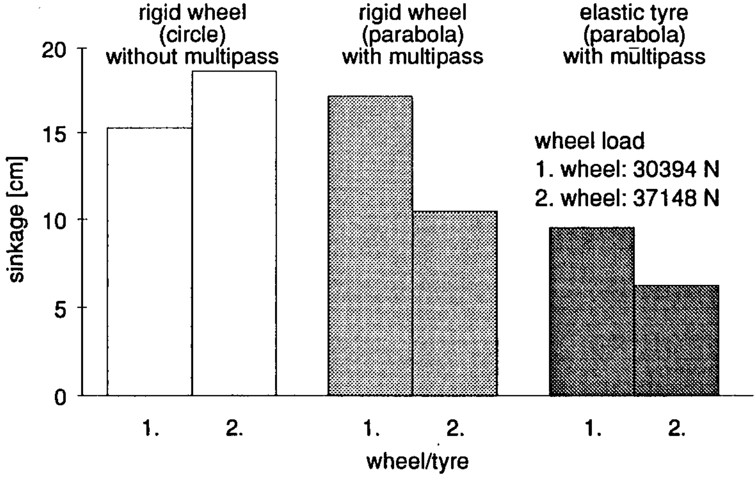

Fig. 8: Static sinkage for the 1. and 2. wheel of the loaded vehicle for different wheel-soil models on loam

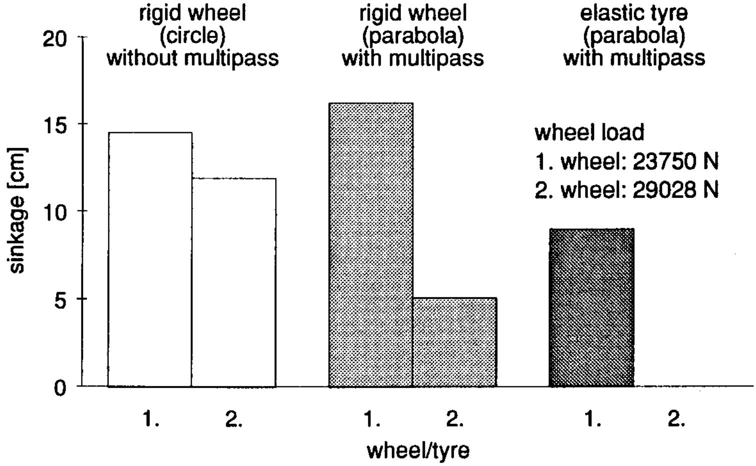

Fig. 9: Static sinkage for the 1. and 2. wheel of the unloaded vehicle for different wheel-soil models on loam

Fig. 10 shows the static sinkage and the soil pressure along the contact length for the loaded vehicle computed with the two models using the parabola geometry. Here it can be seen, that the rigid wheel has a bigger sinkage and a shorter contact length. The static sinkage of the 2. wheel remains as long at the level of the 1. wheel as the actual pressure is smaller than the final pressure under the 1. wheel.

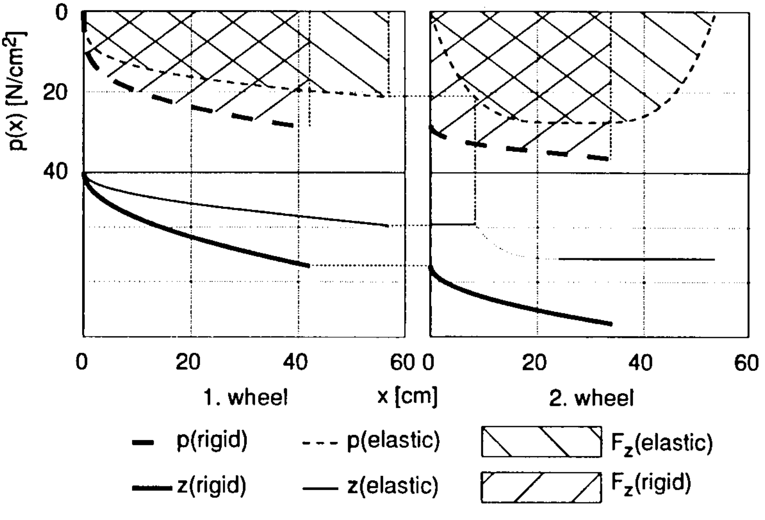

Fig. 10: Static sinkage and pressure distribution along of the loaded vehicle the contact length for the parabola models on loam

The results for the unloaded vehicle are shown in fig. 11. In the case of the elastic tyre there will be no additional sinkage for the 2. wheel caused by the axle load distribution (see also fig. 9).

Fig. 12 shows the sinkage and the tyre deformation on the tyre 14 R-20 mil filled with three different inflation pressures at the loaded vehicle. For the elastic tyre the rolling resistance consists of the soil compacting work and the tyre deformation work. Therefore sinkage and tyre deformation are represented together. With increasing inflation pressure the tyre becomes harder, deforms less and has a larger sinkage caused by the smaller contact length. The sum of sinkage and tyre deformation is at the same level for the three inflation pressures.

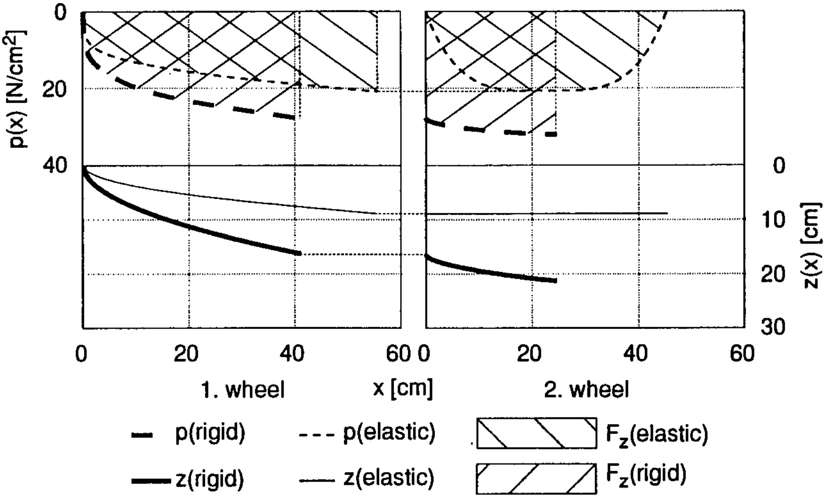

Fig. 11: Static sinkage and pressure distribution along the contact length of the unloaded vehicle for the parabola models on loam

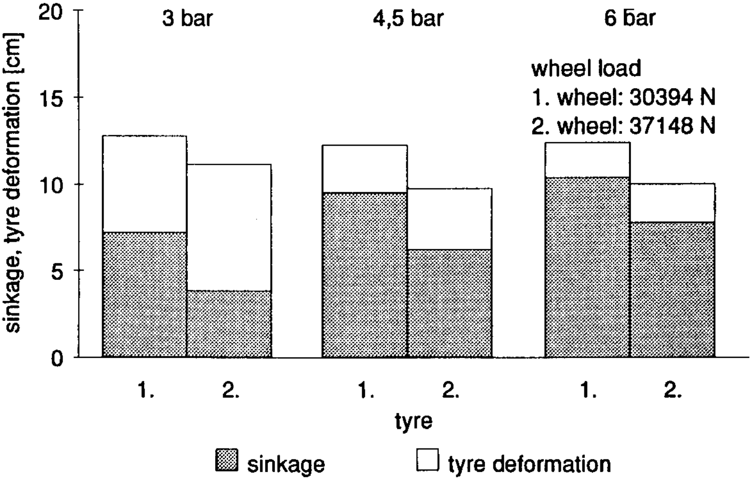

Fig. 12: Comparison of three inflation pressures for the elastic tyre for the loaded vehicle on loam

Fig. 13 shows the same results for the unloaded vehicle. An additional sinkage for the 2. wheel can be seen only for the inflation pressure of 6 bar, whereas for lower inflation pressures the level of the soil pressure from the 1. tyre is not reached with the 2. tyre.

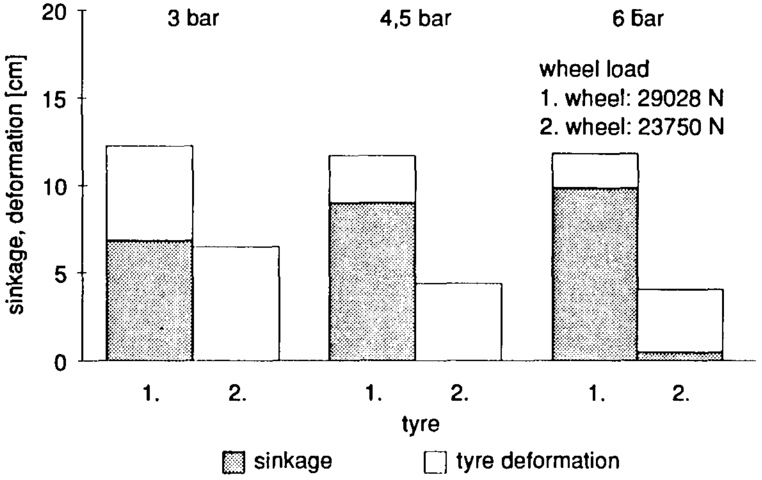

Fig. 13: Comparison of three inflation pressures for the elastic tyre of the unloaded vehicle

5 CONCLUSIONS

The program system ***ORIS***, which was developed at the Institute of Automotive Engineering (IKK) in Hamburg, simulates the terrain mobility of vehicles with driver interactively. It is the main feature of the model, that it is able to simulate the complete vehicle in a terrain comprehensively and to reproduce the horizontal dynamics in detail.

The vehicle-terrain-system is divided in modules, which describe the drive line including the engine and the wheel-soil interaction. Different wheel-soil models are integrated, which are based on the theory by BEKKER and permit, compared with the basis, an essential better simulation of the wheel-soil interaction considering the elastic wheel, the multipass-effect and also the slip-sinkage.

The operating elements and the terrain are simulated in an interactive interface driver-vehicle-terrain and in a digital terrain model and are shown in graphical windows.

The main application spectrum is in the research and the development of terrain vehicles. The complete vehicle as well as its components can be optimized in regard to their terrain mobility. Time and costs can be economized. Not only the design parameters like wheel width and diameter as well as wheel load can be examined, but also the influences of

- the engine,
- the characteristics of the torque converter,
- the gear ratios including gear shift algorithms,
- the torque distribution in the distribution gear and differential gears
- the tyre pressure including inflation pressure control and
- the wheel slip including slip control.

Also the influence of the weather and the atmospheric conditions on the soil strength can be considered [16]. Therewith the simulation system ***ORIS*** is a useful tool also for the optimization of tasks in the military, the agricultural and the environmental subject.

REFERENCES

[1] RUFF, K.: Interactive Simulation of the Driver-Vehicle-Terrain-System. Proceedings of the 5th European Conference of the International Society for Terrain-Vehicle Systems. Budapest, 1991

[2] RUFF, K.; JAKOBS, R.: Interactive Simulation of Vehicle Movement in Terrain. Proceedings of the 11th International Conference of the International Society for Terrain-Vehicle Systems. Lake Tahoe, 1993

[3] JAKOBS, R.: Digitales Geländemodell des Simulationssystems ORIS - Konzept und Realisation. Hamburg, Universität der Bundeswehr, Institut für Kraftfahrwesen und Kolbenmaschinen, 1993. Forschungsbericht Nr. 93-04

[4] JAKOBS, R.: Digitales Geländemodell für die Simulation der Fahrzeugbewegung auf nachgiebigem Boden. Tagungsband des 9. Arbeitstreffens der Auftragnehmer vom BMVg - Rü T II 1, 1993

[5] JAKOBS, R.: Digitales Geländemodell des Simulationssystems ORIS - Weiterentwicklungen und Ergänzungen. Hamburg, Universität der Bundeswehr, Institut für Kraftfahrwesen und Kolbenmaschinen, 1993. Forschungsbericht Nr. 93-09

[6] BEKKER, M. G.: Theory of Land Locomotion : The Mechanics of Vehicle Mobility. Ann Arbor: The University of Michigan Press, 1956

[7] BEKKER, M. G.: Introduction to Terrain-Vehicle System. Ann Arbor: The University of Michigan Press, 1969

[8] SCHMID, I. C.: Grundlagen der Geländegängigkeit - Wechselwirkungen zwischen Rad und weichem Boden : Vorlesungsumdruck. Universität der Bundeswehr. Hamburg, 3. Aufl., 1990

[9] SCHMID, I. C.: Inflation Pressure Control to Improve Terrain-Trafficability - a Model for Simulation. Proceedings of the 11th International Conference of the International Society for Terrain-Vehicle Systems. Lake Tahoe, 1993

[10] HOLM, C.: Das Verhalten von Reifen beim mehrmaligen Überfahren einer Spur auf nachgiebigem Boden und der Einfluß auf die Konzeption mehrachsiger Fahrzeuge. VDI-Fortschrittsberichte Reihe 14 Nr. 17, Düsseldorf: VDI-Verlag, 1972

[11] LUDEWIG J.: Dual-Mode-Modell für den Multipass elastischer Räder auf nachgiebigem Boden. Hamburg, Universität der Bundeswehr, Institut für Kraftfahrwesen und Kolbenmaschinen, 1994. Interner Bericht.

[12] JANOSI, Z.; HANAMOTO, B.: Analytical Determination of Drawbar Pull as a Function of Slip for Tracked Vehicles in Deformable Soils. In: Proceedings of the 1st International Conference on Terrain-Vehicle Systems. Turin, 1961

[13] LUDEWIG, J.: Vergleich berechneter Triebkräfte von Rädern mit gemessenen Werten. Hamburg, Universität der Bundeswehr, Institut für Kraftfahrwesen und Kolbenmaschinen, 1989. Forschungsbericht. IKK-Nr. 89-20

[14] STEINER, M.: Analyse, Synthese und Berechnungsmethoden der Triebkraft-Schlupf-Kurve von Luftreifen auf nachgiebigem Boden. München, Technische Universität, Dissertation, 1979

[15] Technische Dienstvorschrift 2320/043-12. Teile 1 und 2. : LKW 5 t gl. Bad Neuenahr, 1979

[16] HINTZE, D.: Einfluß der Witterung auf die Bodenfestigkeit als Kriterium der Geländebefahrbarkeit. Hamburg, Universität der Bundeswehr, Fachbereich Maschinenbau, Dissertation, 1992

6th European ISTVS Conference

4. ÖVK Symposium
"Off Road Vehicles in Theory and Practice"

Vienna, Austria
27-30 September 1994

Calculated and Experimental Simulation of Off Road Trucks

Dr. Wilfried Eichlseder
Dipl.-Ing. Gottfried Raab

Steyr Daimler Puch AG
Technology Centre
A-4400 Steyr, Austria

1. Summary

Simulations applied to the development of offroad-vehicles prior to the cross-country test phase are described. The analytical and experimental methods are presented by

- finite element analyses
- fatigue life prediction
- process simulation, as driving simulation
- field data acquisition and processing
- servo-hydraulic tests of vital parts and subsystems

By means of the methods shown, and their systematic application the developing time and expenses can be reduced and the weights minimized. In many projects these methods have been applied by the Steyr-Daimler-Puch / Technology Centre for the development of trucks. Based on this experience a new fleet of offroad-trucks was developed in an extremely short time. During this time only data of the loading on components of the trucks could be recorded, there was no time for extensive fatigue tests on the proving ground. The special requirements on the vehicles could only be met by the comprehensive application of computerized methods, which allow the simulation of systems, the dimensioning of components and the effective testing of parts and subsystems.

2. Introduction

The dimensioning of the axle-suspension-system, the chassis frame and the driving components of off road vehicles, regarding material and weight reduction yet maintaining safety and reliability, takes a considerable part of the developing expenses. In this field extensive calculations, tests on benches, and on the road, are a vital part of the developing process. During the design phase the calculated and experimental simulation of the vehicle and its components means a considerable potential for the reduction of costs and time.

3. Calculated simulation

Some of the computer based methods used for the development are shown on the following examples. On the one hand, the methods range from the simulation of systems to the dimensioning of components, on the other hand, from the calculation to experimental investigations on test benches. All these computer based methods allow a detailed and flexible study of functions, stresses, fatigue life, dynamic behaviour etc. and the optimization of components and complete vehicles.

3.1 Structural analysis

By means of the finite element method the stress distribution in components is calculated. Stress concentrations can be identified and modified at an early stage. As off road vehicles under their extreme service conditions are loaded above the fatigue limit, the prediction of the fatigue life is necessary. With a special finite element postprocessor the life time of components can be determined.

Stress analysis

Chassis frames of trucks are the components which have to endure the vehicle weight and the pay load. The stiffness of the vertical bending is determined by the long bars, while the horizontal and torsional stiffnesses are essentially influenced by the cross members and their link to the long bars. In this function, as the central element, the frame carries the cab, the engine, the transmission, the body, fuel tank, etc. The forces of these components are transferred through the frame to the springs and axles.

The loads acting on the frame result from inertias of the components mentioned, and from deformations at the driving manouvers, respectively. One of the highest loadings result from torsion, implied by the unevenness of the ground.

To obtain the loadings of the frame a finite element analysis offers best possiblities. The structure is modelled by shell elements (see Fig. 1), the body as well as the axle system are simulated by beam elements, which describe the centres of gravities and the masses. The loads are described by basic loadcases, as vertical and horizontal bending, torsion, driving in curves, braking etc.. The total loads result as a combination of these basic load cases.

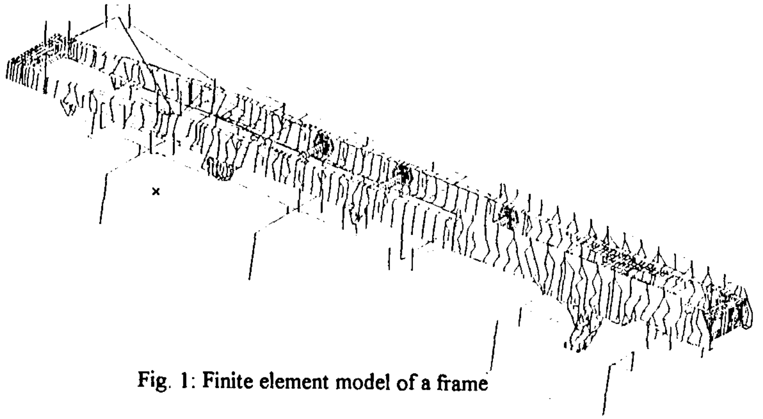

Fig. 1: Finite element model of a frame

Dynamic analysis

The base for fatigue life calculations are load spectra generated by measurements or calculations of the dynamic behaviour. On an axle system the simulation of the dynamics is done with the finite element method (Fig. 2). To determine the dynamic forces in the axles and linkages the impacts are simulated in 3 directions: vertical, longitudinal and lateral. A simplified beam model is used for the dynamic analysis of impacts. The forces of this simulation are the base for the detailed stress analyses on finite element structures of volume or shell elements.

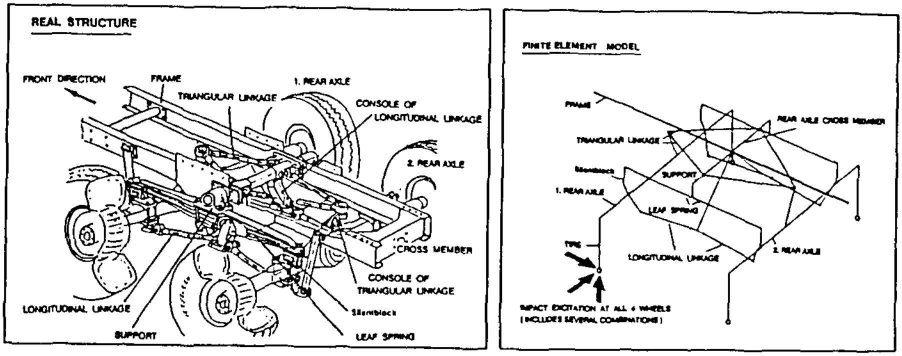
REAL STRUCTURE
FRONT DIRECTION
FRAME
1. REAR AXLE
TRIANGULAR LINKAGE
CONSOLE OF LONGITUDINAL LINKAGE
2. REAR AXLE
CROSS MEMBER
CONSOLE OF TRIANGULAR LINKAGE
Silentblock
LEAF SPRING
SUPPORT
LONGITUDINAL LINKAGE
FINITE ELEMENT MODEL
FRAME
REAR AXLE CROSS MEMBER
TRIANGULAR LINKAGE
Silentblock
SUPPORT
1. REAR AXLE
LEAF SPRING
TIRE
LONGITUDINAL LINKAGE
2. REAR AXLE
IMPACT EXCITATION AT ALL 4 WHEELS
(INCLUDES SEVERAL COMBINATIONS)

Fig. 2: Rear axle system - real structure and beam model

Fatigue analysis

The calculation of the fatigue life with traditional concepts are difficult to put directly into practice with the finite element method because the initial values of the calculation are often much more complex than their treatment in theory would indicate. For example, an FE calculation produces stress and elongation tensors although most of the published concepts of operating strength are limited to the representation of single-axis stress and elongation situations. The practical investigator has plenty of scope here to influence the correlation of the result with reality positively or negatively.

For the automated assessment of finite element structures in respect of the fatigue life a method and a postprocessor (FEMFAT) was developed, which is especially adapted for requirements and possibilities of the FEM /4/. FEMFAT permits the assessment of the operating strength of structures calculated by the finite element method by the incorporation of a lifetime calculation. In this way statements about the height of stresses in the stationary condition can be supplemented by one about the influence of loading spectra and stress patterns on the durability of the component loaded with vibrations on the FE structure. In this the whole loading spectrum is taken into account in the strength assessment and not simply the height and pattern of the stresses. The program processes stresses from membrane, shell and 3-D solid elements. On the basis of strength data and s/n curve data from unnotched test rods, s/n curves in relation to FE nodes are calculated for components taking into account the most varied influencing factors, such as amplitude stress tensor, mean stress tensor, relative stress gradient, surface roughness, technological influences, local plastic deformations and statistics. The loading information required for the accumulated damage is taken on the one hand from the FE stress analysis and on the other hand from rain-flow spectra or other data reduction procedures mappable in them.

As an example the calculation of the fatigue life of a cross member of a frame is shown. The cross member is welded and mounted at the long bars with bolts, which are simulated by a conjunction of beam and rod elements. In the FE-run the static stresses of the various load cases are calculated. Next FEMFAT takes these stresses and calculates according to Miner's rule the damage for each load case, which is finally summated to get the total damage and life time in each node of the structure. The distribution of the total damage is shown in fig. 3. As can be seen from the stress and damage distribution in this fig. the spot with the highest stresses does not always correspond to the area with the highest damage. The damage distribution shows the sum of all load cases, while the stress plot shows one temporary loading only. One of the advantages of the procedure presented is that damage which occur at different times can be summated.

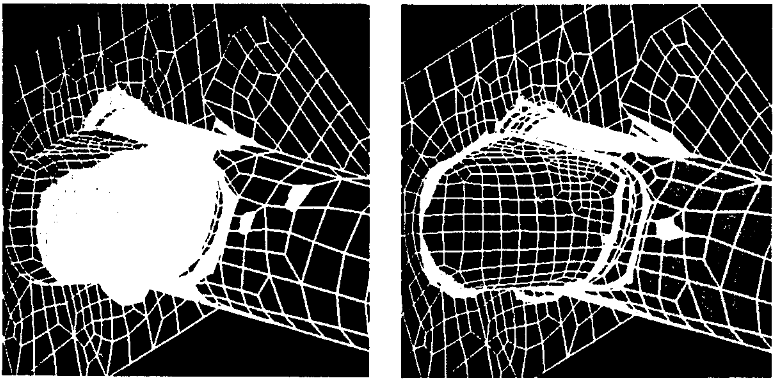

Fig. 3: Fatigue analysis of a cross member: stresses (left) - damage (right)

3.2 Multibody systems

The comfort of vehicles is influenced by low frequency movements of the vehicle and by high frequency noise emissions. The noise emissions are mainly investigated by means of measurements, the low frequencies by calculations and tests.

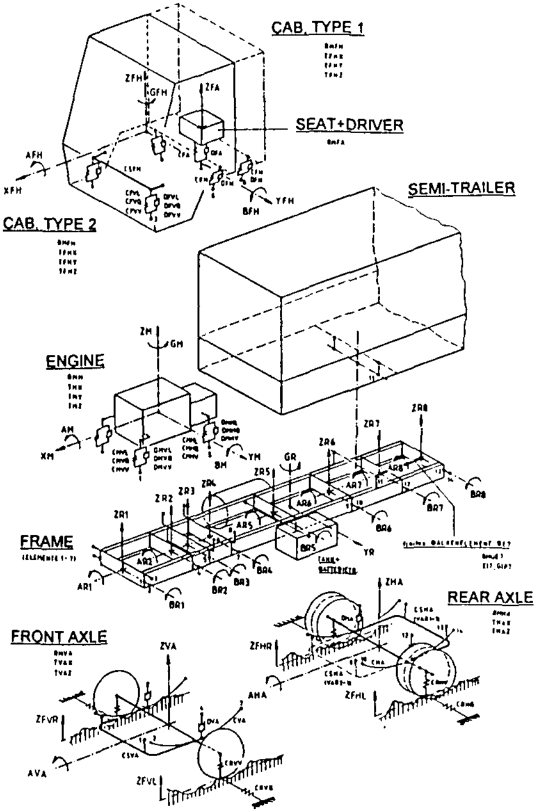
CAB. TYPE 1
SEAT+DRIVER
SEMI-TRAILER
CAB. TYPE 2
ZFH
GFH
ZFA
AFH
XFH
YFH
BFH
ENGINE
ZH
GH
AH
XH
YH
BH
GR
ZR1
ZR2
ZR3
ZR4
ZR5
ZR6
ZR7
ZR8
AR1
AR2
AR5
AR6
AR7
AR8
BR1
BR2
BR3
BR4
BR5
BR6
BR7
BR8
YR
FRAME
ZHA
AHA
REAR AXLE
ZFHR
ZFHL
FRONT AXLE
ZVA
ZFVR
ZFVL
AVA

Fig. 4: Model of a Truck

The optimization of the comfort of trucks is a lot more difficult compared with personnel cars, since trucks have a wide range of unloaden/loaden-ratios, and trucks can be supplied with a wide variety of bodies. Furthermore, the dominant components, such as springs and dampers, have to fulfil the requirements for the transport of high payloads. However, by variation of the suspension system of the cab the comfort can be optimized. For the evaluation of the driving comfort of trucks the accelerations of the cab and the driver's seat are decisive, the driving safety is based on the dynamic load of the wheel related to the static wheel load. For the determination of these values *multibody systems*, which combine relatively rigid bodies (engine, axles, cab) with elastic structures (chassis frame), are used. With such a simulation model influences on the comfort of a vehicle can be studied quickly and cost-effectively. The principal model of such a vehicle is shown by Fig. 4, which has 47 degrees of freedom.

3.3 Process simulation

By simulation of complex processes influences by parameters on the system can be easily studied. For the design of the components, as cooling system, brake system, leaf spring, etc. simulation models are presented:

Cooling system

For the dimensioning of the cooling system a software package is used, which enables the simulation of cooling processes in vehicles under service conditions.
The model allows to a large extent to optimize the cooling system without extensive tests on the road or in labs. Various combinations of different cooling components can be simulated and optimized. The following parameters can be investigated rapidly:

- CAC, oil cooler and radiator sizes,
- types of radiators, CAC's and oil coolers
- diameters of fans,
- fan speed,
- combination of radiator, CAC and oil cooler,
- influence of glycol,
- ambient temperature and
- build in situations.

The model is based on the characteristics of the water- or oil-radiator, the CAC , fan performance and air-resistance measured in the vehicle. This model segments the area of the radiators into parts (see Fig. 5), which are described by the mass flows, temperatures and component characteristics These parts are described by equation systems, its results are fed into the basic equation for the cooling circuit. Under consideration of the mass flows of the cooling media, like air, water and oil, the program then solves the nonlinear equation system for the determination of the service point of the cooling system (see Fig. 6). For this specific service point the mass flows, temperatures, pressures and the actual power requirement for the fan are calculated.

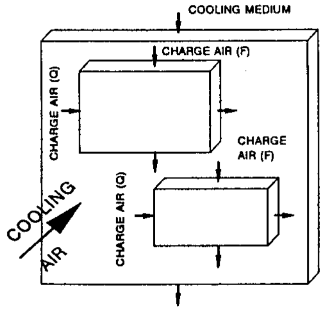

Fig. 5: Analysis model

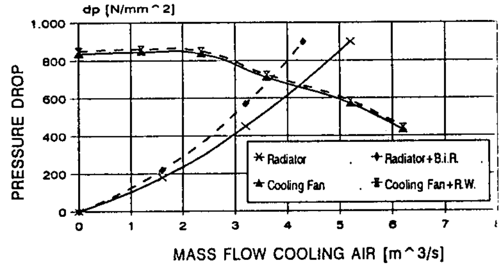

Fig. 6: Operating point

Offroad trucks must operate on the severe climatic operating conditions. Calculated are the temperatures of the cooling media before and after the radiator, charge air cooler and converter cooler. Different types of radiators, fans, dimensions etc. are investigated to find the optimized design of the cooling system. Most cost-intensive measurements of the cooling system can be sharply reduced. This is a result of less tests needed and less mechanical components used to change the layout of the cooling system. All of this helps to save time and expenses during the developing phase.

Driving simulation

To be able to make predictions about the fuel consumption, the engine loading and the life time of drive components in certain kinds of roads, driving conditions and vehicle types computer simulation of the driving offers an essential aid. The gradients and an outline of the track are fed into the program. The driving simulation takes into account

- engine, tyre, gearbox and general vehicle data
- height and outline profiles of the route
- visibility
- permissible transverse acceleration
- speed limits, stops
- legal maximum speed
- wheel-braking, exhaust brake

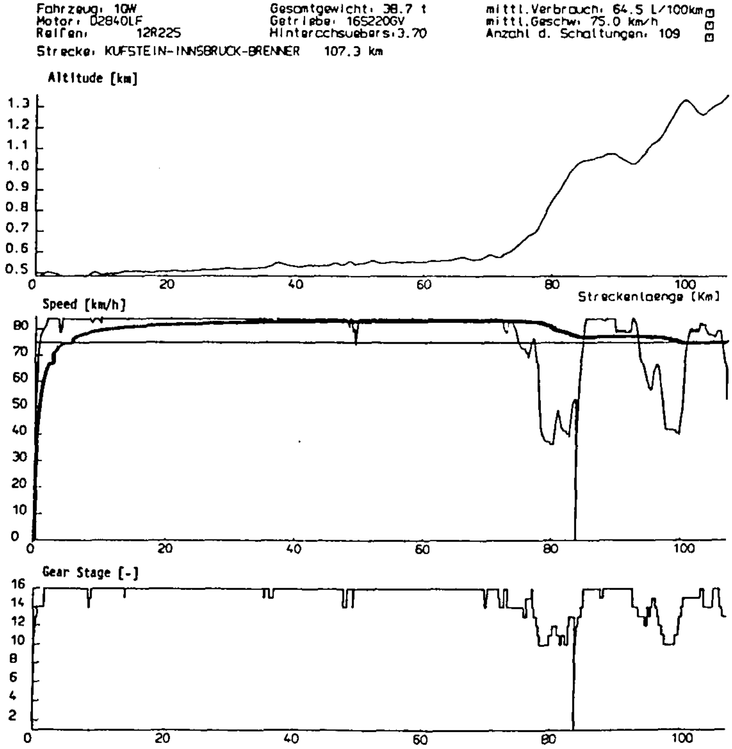

Fig. 7: Computing Driving Simulation

The run of the vehicle is simulated incorporating engine, vehicle and drive train data, it being possible to feed in various strategies for the driver. The speed of the vehicle is calculated with the engine situation, such as r.p.m., torque and consumption, at each speed. In this the loads in the individual drive elements produced by the gear engaged and the torque transmitted in each case are vital for calculating the driveline.

Fig. 7 shows the result of such a driving simulation. For the length of the track both the course of the vehicle speed, the fuel consumption and the gear engaged in the gearbox are shown.

One aim of the simulation calculations is to find the optimum overall economy for given operating conditions by co-ordinating the individual elements of the total system of engine-transmission-vehicle. By the variation of the data of the engine, the weight, the gear-ratios etc. the optimum can be found in a very early stage of the development.

3.4 Dimensioning of Components

Brake system

In order to achieve high efficiency the vehicles have to be tuned to special operation conditions. Based on serial vehicles more and more trucks are produced with special chassis and bodies which have to meet the regulations for the brake system. The diagrams depicting the adhesion, the braking and the force distribution of the brakes are very useful for the development of the brake system and frequently demanded by authorities for the homologation. When these values are calculated, their dependence on the pressure in the coupling head, the axle loading, the centre of gravity and the deceleration is considered:

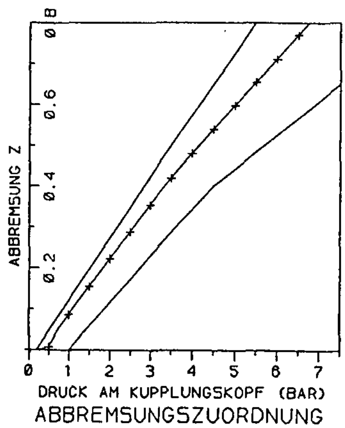

Fig. 8: Braking vs. pressure

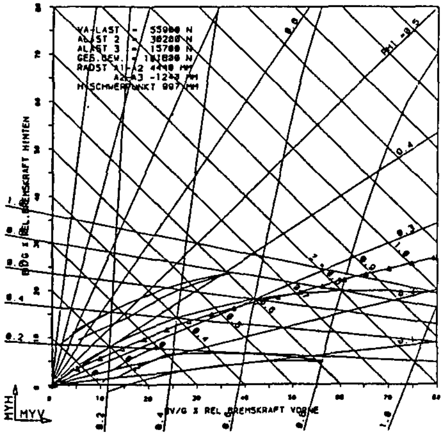

Fig. 9: Brake force distribution

By the computerised design the control of the braking forces at the front- and rear-axle can be quickly optimized. The calculation model takes into account the following criteria for the calculation of the braking forces :

- multi axle vehicles, with and without axle load compensation
- hydraulic and pneumatic pure and combined brake systems
- static and dynamic governors
- distance or pressure controlled governors

Leaf springs

For the dimensioning and design of leaf and parabolic springs an CAE-CAD integrated system has been created, to calculate their deflections, stresses, natural frequencies and weights. From the data of the analysis a drawing of the spring is generated automatically (Fig. 10). Different springs can be investigated and designed extremely fast. If some of the free parameters are prescribed, the program also allows an automatic optimization of springs. As soon as the calculation is done and the geometry is checked on the screen, the drawing is transferred to the CAD-system.

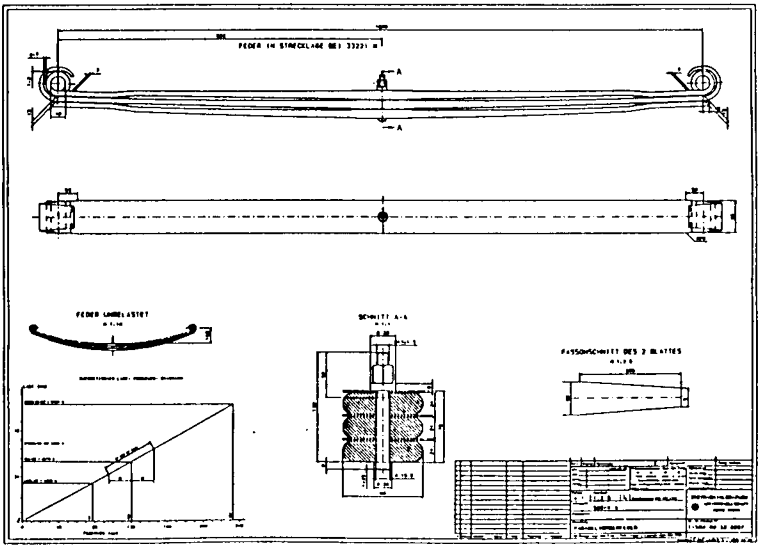

Fig. 10: Automatically generated drawing of a spring

4. Experimental simulation

Before components are installed in prototype vehicles a high level of development standard can be gained by preliminary tests of the components on dynamic test benches. Investigations of a cab and an axle show the possibilities of servohydraulic tests. Starting with the field data acquisition and the data processing the procedure on the test bench is explained.

4.1 Data acquisition

Measurements are performed and recorded by mobile data recording and analysis systems, which are able to record 32 or more channels simultaneously. The software is running on Laptop PC's, the data are stored preferably on optical disks. During the measurements the data can be checked on the screen of the PC as on oscilloscopes. Problems during the data acquisition can be detected very early by this method.

During data processing the first stage is the calculation of the statistics and plotting of sections of the signals in the time domain. Then frequency spectra and rainflow classifications are done (Fig. 11). The measured signals are shortened for the test program by eliminating low damage sections, thus the duration of the tests on the test bench is reduced. This operation is done manually by checking the time plots and defining the cutting points. With special programs, where only the starting and ending points of the signal sections are entered, new spectra are created. Therefore the whole life of truck components and subsystems under service conditions can be simulated on the test bench in only 200 - 400 hours. This reduction is based on fatigue life calculations done on the measured signals and the test bench loadings.

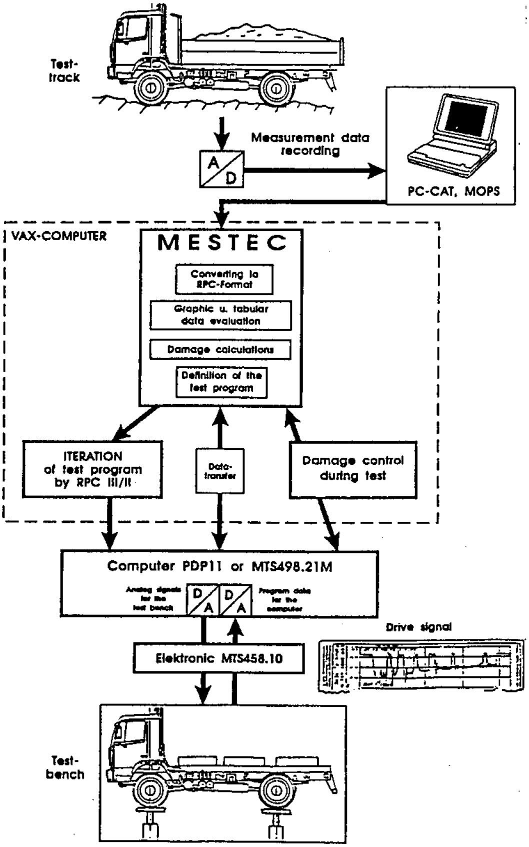
Test-
track
Measurement data
recording
A
D
PC-CAT, MOPS
VAX-COMPUTER
MESTEC
Converting to
RPC-Format
Graphic u. tabular
data evaluation
Damage calculations
Definition of the
test program
ITERATION
of test program
by RPC III/II
Data-
transfer
Damage control
during test
Computer PDP11 or MTS498.21M
Analog signals
for the
test bench
D
A
D
A
Program data
for the
computer
Drive signal
Elektronic MTS458.10
Test-
bench

Fig. 11: From data recording to test bench control

4.2 Servo-hydraulic tests

Fig. 12 shows a cab on the test bench with 3 vertical actuators. Four vertical acceleration sensors on the floor mountings and longitudinal and lateral acceleration sensors on the top of the cab are used to control the excitation of the actuators. The signals are generated by a special software system which controls the actuator drive signals by iterations.

Another Test on a servohydraulic test bench shows fig. 13. The tests are done to prove the strength and durability of radiators. The fig. shows a test bench with a combination of a water and charge air cooler. To simulate the vertical and horizontal vibrations with only one servohydraulic actuator a special configuration has been developed. The test conditions for a typical radiator system are

- vertical sinusoidal accelerations up to +/- 5 G,
- frequencies of 15 to 36 Hz, sweeping up and down,
- inner pressure pulsating from 0 to 0.7 bar,
- coolant temperature of 95° C.

The tests are completed by thermo shock tests with coolant temperatures of 18 to 95°C in a cycle of 6 minutes.

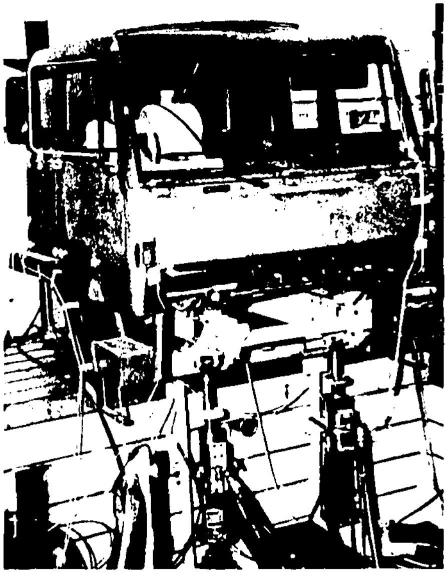

Fig. 12: Cab on the test bench

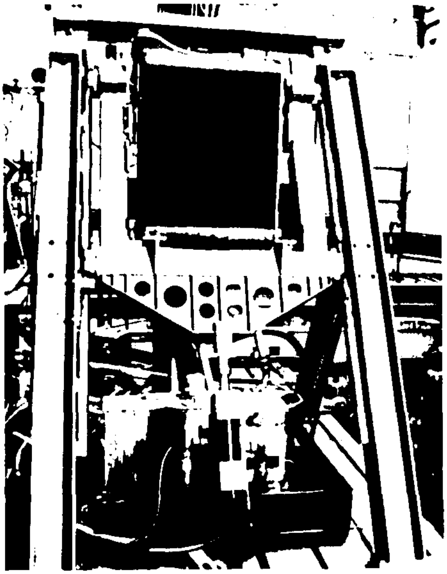

Fig. 13: Radiator test bench

Session IV
Sektion IV

Off Road Tyres

Geländereifen

INVESTIGATIONS ON TRACTOR TYRES TEST STANDS AND RESULTS

Heinz Dieter Kutzbach
University of Hohenheim, Germany
Institute of Agricultural Engineering

ABSTRACT

At the Institute of Agricultural Engineering main research activities concentrate on investigations on farm tractor and implement tyres running on rigid and soft surfaces. For measuring the damping coefficients and spring rates of rolling tyres, which influence ride safety and ride comfort during transport at higher speeds a flat-belt tyre test stand is available. The vertical behaviour of the tyres can precisely be described by a non-linear tyre model. For a detailed description of the horizontal tyre behaviour the relation between lateral and longitudinal forces, slip and slip angles has to be known. Lateral forces on rolling tyres are measured with a single axle trailer with angled tyres. With a single wheel tester the investigations are extended to driven and braked tyres. For registration of the soil properties a cone penetrometer and a linear shear tester have been developed. The test stands and some general results are described in this paper.

1. INTRODUCTION

In contrast to other motor vehicles tractors and self-propelled farm implements often are not spring suspended. Thus the tyres of these vehicles represent their only spring and damping elements. Therefore ride safety and comfort are critically influenced by spring and damping characteristics of the tyres. Due to the increasing maximum travelling speed for on-road transportation purpose and the pay load in agricultural use the knowledge of the spring and damping characteristic becomes more important. The values of these dynamic tyre characteristics are influenced by inflation pressure and the construction of the tyre (biased ply or radial ply), the rubber mixture, the tyre size, the tread design and the rolling speed. To improve the tyres in respect to ride safety and ride comfort accurate, repeatable measurements of the dynamic tyre characteristic are necessary. These values depend very much on the tyre rolling speed.

Research on horizontal forces of agricultural tyres has been concentrated on the tractive and rolling resistance performance. Compared to vertical and longitudinal forces, lateral force characteristics have received less attention though they are very important.

Driving on slope, ploughing or working with side attached implements leed to a constant slip angle. In contrast to this cornering operations of tractors and trailers with tandem (or tridem) axle units have to be considered as situations with instationary slip angle. Lateral forces are acting on free rolling tyres (tractor front wheels and tandem trailer wheels) as well as on driven wheels, e.g. tractor rear wheels driving on a slope.

2. VERTICAL DYNAMIC TYRE FORCES

2.1 Flat-belt tyre test stand

There are various methods to determine dynamic tyre characteristics. Investigations of tyres mounted on vehicles or with particular measuring trailers show, among other things, the disadvantage that the stimulations from the street, which is not exactly even, are not reproducible. Due to the size of tractor tyres it is rather difficult to work with cylindrical test stands in the laboratory as the diameter of the drum should be greater than 10 m to adequatly simulate even surfaces.

This fact led in 1978 to the development of the flat belt tyre test stand [1,2], shown in fig. 1. At this laboratory test stand the tyre to be investigated is rolling on an even supported steel belt, which is welded endlessly. The thickness is 1 mm and it is stretched over two steel drums. The first drum is driven by a direct current motor and the second is supported traversably round a lateral axis to control the course of the belt. The technical data are given in table 1.

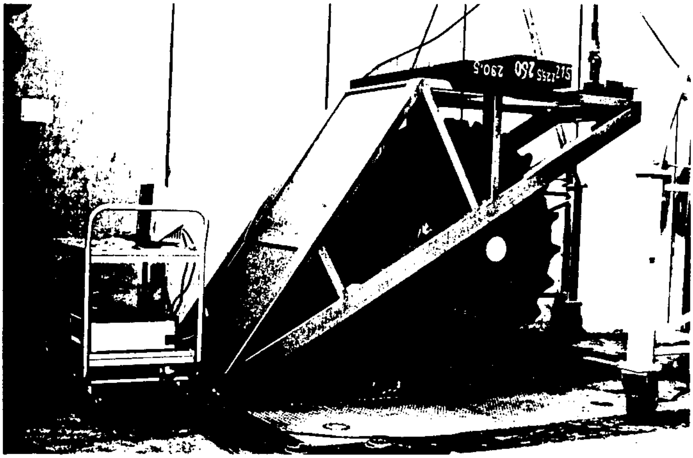

Fig.1: Flat-belt tyre test stand

engine power	22	kW
maximum vertical load	60000	N
maximum longitudinal load	16000	N
braking moment	0 - 5000	Nm
braking period	0 - 20	s
speed of the wheel	0 - 50	km/h
diameter of the rolls	1000	mm
width of the rolls	645	mm
axle base of the rolls	2000	mm
width of the belt	600	mm
thickness of the belt	1	mm
maximum tyre width	600	mm
maximum tyre diameter	2000	mm

Table 1: Technical data of the flat-belt tyre test stand

At the tyre contact area the flexible steel belt is supported by a teflon-coated steel plate. This plate is perforated by a lot of drill-holes through which an oil-water-emulsion is pumped into the space between belt and plate for lubrication and cooling. The steel plate is mounted on pressure gauges in three points, so it is possible to measure the contact forces of the tyre on the support. Plesser [3] presents a paper about the installation of a tyre braking device.

The tyre is guided horizontally by a rocker, which can be easily lifted with a crane. The loading of the tyre is adjusted with metal weights, installed over the tyre. The tyre motion is measured by an inductive displacement transducer, which is attached at the axle.

To start the tests of the free oscillating tyre it is lifted so far that the contact force remains at about 100 N. After having been accelerated the tyre is released from the block and tackle and oscillates towards its steady position.

Later on a similar test stand has been built in Berlin which could be oscillated as a whole. Kising [4] showed that the measured dynamic tyre characteristics are the same no matter whether the tyre is free oscillating or the whole belt surface is oscillated.

2.2 Spring rate and damping coefficient

For the calculation of the dynamic behaviour of tyres a simple equivalent model for the elastic viscous behaviour of the tyre material is generally taken as fundamental mathematical description. The simpliest of these models is the Voigt-Kelvin-Model (fig. 2a) consisting of a spring with parallel damper. The spring characteristic is assumed to

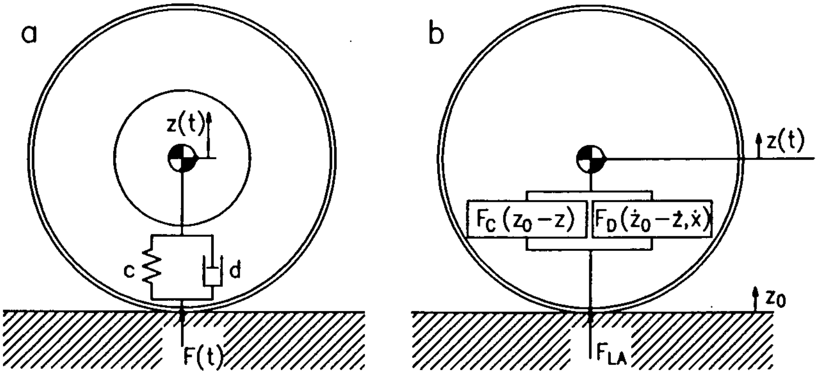

Fig. 2: Tyre models
a. Voigt Kelvin model b. Non-linear model

be linear and the viscous damper force to be proportional to deflection speed. Assuming that it is possible to reproduce the tyre behaviour accurately enough with this model, the tyre can be considered as a damped harmonic spring-mass oscillator. Thus the homogeneous differential equation of second order is valid for the deflection z(t):

$$\ddot{z} + 2 \cdot \delta \cdot \dot{z} + \omega^2 \cdot z = 0 \qquad (1)$$

With: ω^2 standardized spring constant (square of the natural circular frequency)

$2 \cdot \delta$ standardized damping

Together with the tyre deflection amplitude ratio f_n/f_{n+1} and the oscillation time T_s the damping constant

$$\delta = \frac{1}{T_s} \ln \left(f_n / f_{n+1}\right) \qquad (2)$$

and the dimensionless damping factor according to LEHR is obtained

$$D = \frac{\ln(f_n / f_{n+1})}{\sqrt{4\pi^2 + (\ln(f_n / f_{n+1}))^2}} \qquad (3)$$

With the oscillation time T_s and the knowledge of the mass m of the oscillator the dynamic spring constant c_{dyn} can be determined.

$$c_{dyn} = \frac{4\pi^2 \cdot m}{T_s^2 \, (1 - D^2)} \qquad (4)$$

It is also possible to calculate the spring constant c_{roll} staticly by measuring the tyre deflections $f = z - z_0$ and the tyre load F.

$$c_{roll} = \frac{F}{f} \qquad (5)$$

Investigations showed that the tyre deflection decreased with increasing rolling speed, which can be explained by the hardening of the tyre due to centrifugal forces reacting on the single tyre elements. Calculating the spring rate from the tyre loading and the deflection with equation (5) would result in interpreting this behaviour as an increase of the spring rate c_{roll} with increasing rolling speed.

Calculating the dynamic spring rate c_{dyn} of the oscillating tyre with equation (4) results in a decrease of the stiffness with increasing rolling speed, shown in fig. 3.

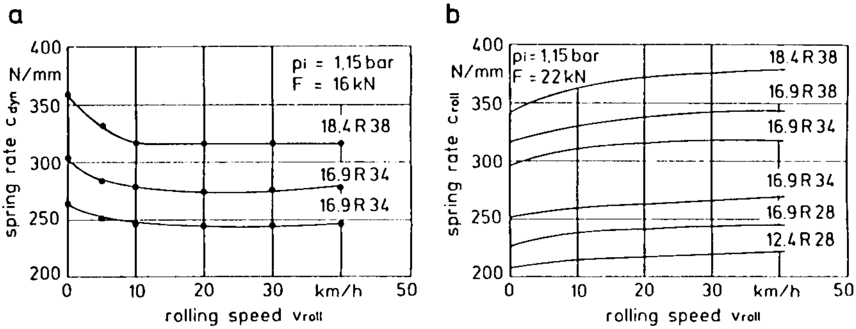

Fig. 3: Spring rates versus rolling speed
a. Dynamic spring rate b. Static spring rate

Plotting the dimensionless damping factor D (equation 3) shows the decrease of the tyre damping with higher speed very clearly (fig. 4). A large decrease of the damping occurs between 5 and 15 km/h. For higher rolling speeds the curves seem to approach a limit asymptotically. Besides that, analysing the various tyres being investigated leads to the fact that the damping decreases with increasing tyre pressure and decreasing load, respectively, which means less distortion of the tyre. According to that, diagonal tyres show a higher damping than radial tyres, because the contact surface of the latter is not distorted as much as that of diagonal tyres.

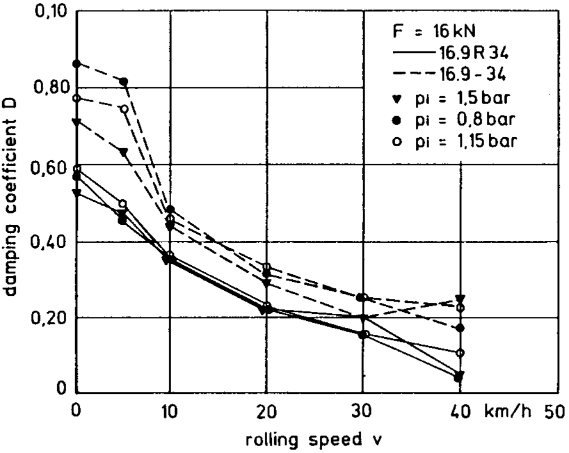

Fig. 4: Damping coefficient versus rolling speed

2.3 Non-linear tyre model

As the Voigt-Kelvin tyre model leads as example for the calculation of the forces not to very good results, Langenbeck [5] determined with the flat-belt tyre test stand parameters for a new non-linear tyre model (fig. 2b). In vertical direction simular to the Voigt-Kelvin tyre model the damping forces and spring forces are used. The spring characteristic is not linear but approximated by a power function, the decreasing of the damping coefficient with rolling speed is approximated by a linear function of speed up to a value of 12 m/s.

For the non-linear model a spring characteristic according to the equation

$$F_C = c_1 \cdot f^{C_2} \qquad (6)$$

and a damping force proportional to the deflection speed

$$F_D = d_v \cdot \dot{f} \qquad (7)$$

is applied, where f is the tyre deflection.

For the relationship between the damping coefficient and the rolling speed the following equation is applied

$$d_v = d_1 - d_2 \cdot v \qquad (8)$$

With the equations (6) - (8) the whole tyre load in vertical direction is

$$F = F_C + F_D = c_1 \cdot f^{c_2} + (d_1 - d_2 \cdot v) \cdot \dot{f} \qquad (9)$$

The influence of the rolling speed, of the tyre parameters and the tyre construction on the model parameter has been investigated with the test stand. Only one parameter has been varied, the other parameters have been kept at their norm-value. Table 2, for example, shows the model parameter for two different surfaces.

	c_1 [kN]	c_2 [-]	d_1 [kNs/m]	d_2 [Ns^2/m^2]
Steel	634	1,19	3,10	124
Sand Paper	617	1,18	3,69	213

Table 2: Non-linear model parameter for two surfaces (Standard conditions: 16.9 R 34, 1,5 bar, 18 kN)

The swinging behaviour of the farm tractor tyre is better described by this non-linear tyre model as by the Voigt-Kelvin-Model, though the model parameter for low rolling speed up to ≈ 3 m/s differ from the "real" values (fig. 5). This figure illustrates, that the linear approximation of the decrease of the damping coefficient with the rolling speed can be improved by a hyperbolic approximation. Because of its simplicity the non-linear tyre model can be used favourably for complex three dimensional tractor/trailer dynamic simulations.

3. HORIZONTAL TYRE FORCES

3.1 Registration of soil properties

To measure soil penetration resistance cone penetrometers, devices made of a thin rod with a cone tip, are used. By means of penetrometer measurements information on soil characteristics such as compaction and trafficability can be easily and quickly found. The amount of penetration resistance varies with soil characteristics such as soil type, moisture content and density. With automation of penetration and electronic registration of data, penetrometer measurements have become more accurate.

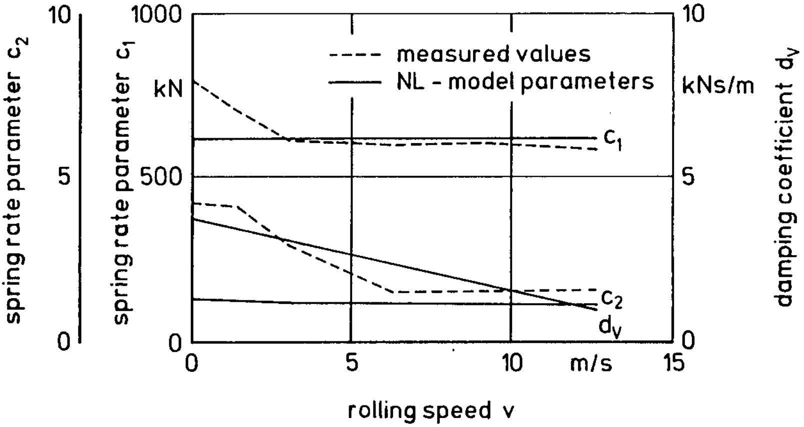

Fig. 5: Non-linear model parameter (standard conditions: 16.9 R. 34, 1,5 bar, 18 kN)

The penetrometer used at Hohenheim University has a shaft length of 800 mm (fig. 6). To get the standardized, constant penetration speed the shaft is driven by a direct current motor. Depths and cone force are registered electronically.

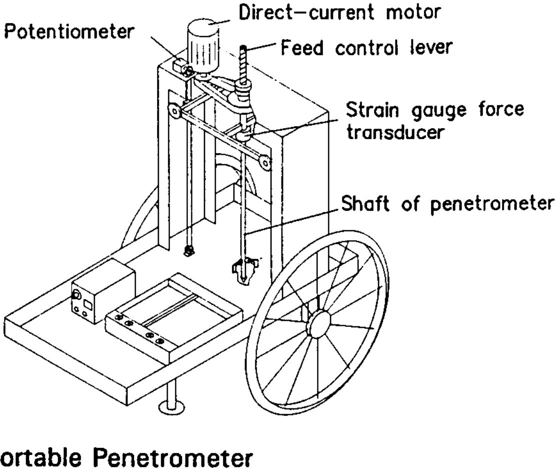
Direct-current motor
Potentiometer
Feed control lever
Strain gauge force transducer
Shaft of penetrometer

Fig. 6: Portable Penetrometer

Cone index measuring devices are located at the upper end of the penetrometer shaft. The measured cone index includes an unknown amount of friction that occurs between the penetrometer shaft and the soil.

To avoid this shaft friction the penetrometer is equipped with a force transducer directly behind the cone tip (fig. 7). To show the influence of friction, the output of a strain gage force transducer, mounted at the upper end of the shaft, and the output of the quartz pressure transducer were recorded simultaneously during a measurement [6]. Fig. 8 shows the penetration pressure recorded by each system and the difference of the signals. It becomes obvious that the friction increases with increasing depth of penetration.

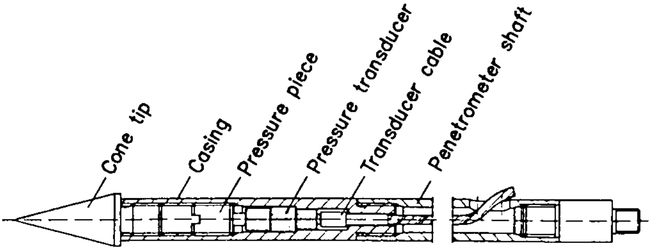

Fig. 7: Penetrometer cone tip with integrated force transducer

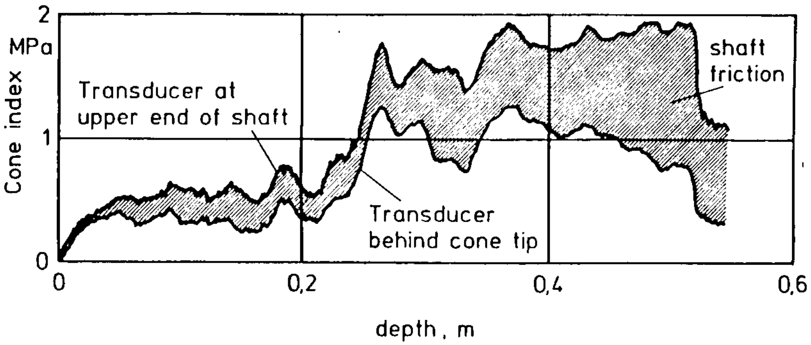

Fig. 8: Cone Index measured with both force transducers and shaft friction

To measure shear stresses on soft soil surfaces which might influence the traction forces of tyres a linear shear tester was developed [7]. The frame of this shear tester is mounted in the three point hitch of a farm tractor (fig.9). The shearplate holder is guided by 4 plastic rollers in the frame and driven by a hydraulic cylinder which is supplied from the hydraulic system of the farm tractor. The shear speed can be set to different values up to 0,45 m/s by a hydraulic flow control valve. This shear speed is equivalent to the shear speed of tyres running with 15% slip at 10 km/h.

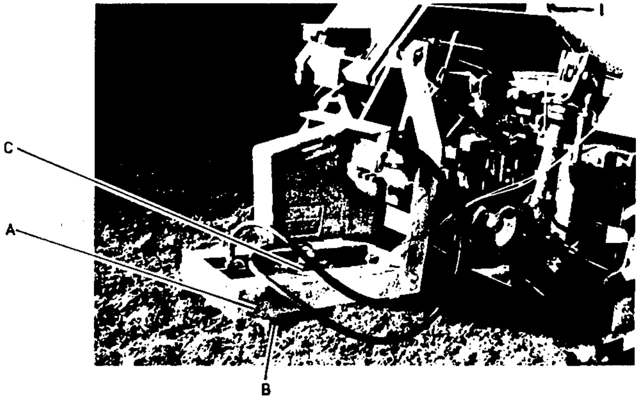

Fig. 9: Linear shear tester
A. Frame B. Shear plate C. Hydraulic cylinder

The shear tester can be equipped with different shear tools. Measurements have been carried out with a simple metal plate and a metal plate on which a rubber is glued. Both plates have a size of 500 cm^2. Furthermore a metal plate with a grouser has been investigated whereby the grouser heigth can be verified. The vertical and horizontal force is measured with an octagonal force transducer. To measure only the forces under the shear tools and not in front of them the shear carriage is equipped with a bulldozer plate.

For a constant normal stress σ the increase of the shear strength τ_{max} against shear speed can approximated to be linear (fig. 10). This relation can be described by the equation

$$\tau_{max} = 0{,}025 \cdot v_s + 0.387 \cdot \sigma + 0.018 \qquad (10)$$

which is valid only for this special soil type and the range of covered shear speed. Of course for shear speed $v_s = 0$ the shear stress should be $\tau = 0$ too. Some more results will be shown in the following paper of Barrelmeyer [8].

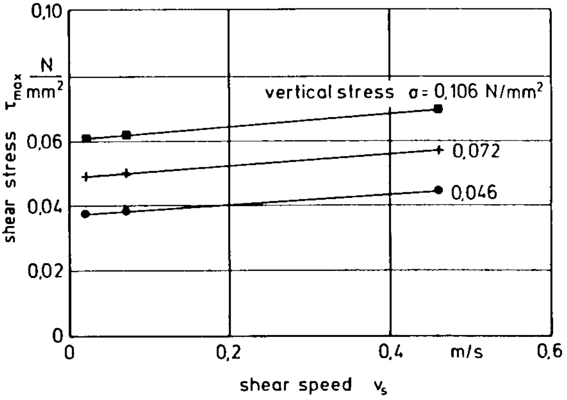

Fig. 10: Maximum shear stress versus shearing speed (silty clay, moisture content 23%, 40 days after scarifying and recompacting)

3.2 Single axle trailer

To enable investigations about the reaction of instationary angled tyres, a trailer has been developed, (fig. 11), equipped with a hydraulic steering of the free rolling tyres and a five-component wheel-dynamometer for one wheel [9,10]. With this test trailer investigations have been carried out with constant angled tyres during the test procedure as well as instationary angled tyres. The steering of

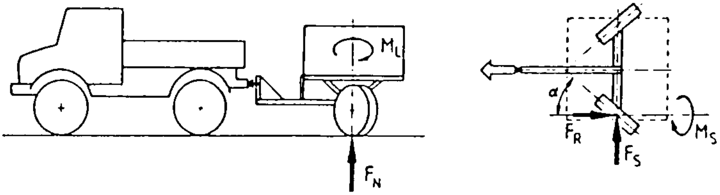

Fig. 11: Single axle trailer

wheels against each other proved to be a good presupposition to perform the investigations without the trailer leaving the straight rut. Steering angle, mean forces (wheel load F_N, lateral force F_S, rolling resistance F_R), aligning (M_L) and camber torque (M_S) are measured with a self developed, compact designed wheel-dynamometer, fitted centrically in the left wheel.

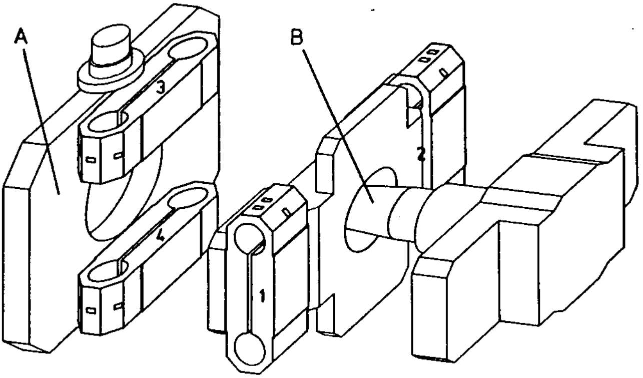

Fig. 12: Five-component wheel dynamometer
A. Plate with steering knuckle B. Wheel bearing pivot

The wheel-dynamometer consists of 4 octagonal force transducers (fig. 12) which are assembled as a pair crosswise. Force transducers 1 and 2 are measuring wheel load, lateral force and camber torque, force transducers 3 and 4 rolling resistance and aligning torque. With a special calibriation equipment the linear characteristic of the dynamometer and a low cross talk between the force channels could be shown. Only the rolling resistance value was remarkably increased by the lateral force. This could be eliminated by the following data analysis and processing. The technical data of the single axle trailer are presented in table 3.

3.3 Instationary slip angles

The results of the investigations on rigid and soft surfaces are presented as an example for the tyre 14.5 R 20 with AS-farmer tread. Fig. 13 shows the comparison of stationary and instationary angled

max. diameter of the test wheel	1400	mm
max. vertical load on test tyre	20	kN
max. lateral force on test tyre	18	kN
max. slip angle	45	°
total length of the trailer	3200	mm
total width of the trailer	2100	mm
total height of the trailer	2400	mm

Table 3: Technical data of the single axle trailer

tyres on concrete. The dotted line connects the points measured in stationary manner. Compared to the dotted line with a steep tangent at zero slip angle the measurements proved a delayed increase of lateral forces with increasing slip angle, characterized by a horizontal tangent at zero slip angle. The reason lies in the deformation of the tyre when the slip angle increases. This reaction is influenced in particular by the steering velocity. The more steering velocity increases, the greater the horizontal distance between stationary and instationary measured lines gets.

This different reaction is recognizable as well on soft surfaces like meadow and stubble with the difference, that gradient of the lateral force versus slip angle curve and the maximum side forces on soft surfaces are smaller than on concrete.

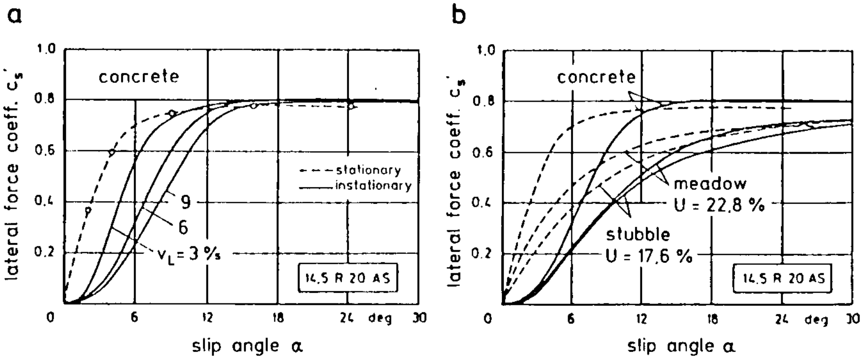

Fig. 13: Lateral force coefficient versus slip angle
a. Influence of shearing speed b. Influence of surface
(tyre load: 10 kN;inflation pressure: 110 kPA;speed: 1m/s)

3.4 Single wheel tester

To extend the investigations on the lateral force/slip angle relations to driven and braked wheels, a single wheel tester has been developed [7,11,12]. The test rig is a four-wheel trailer towed by a tractor (fig.14). The data of the single wheel tester are given in table 4.

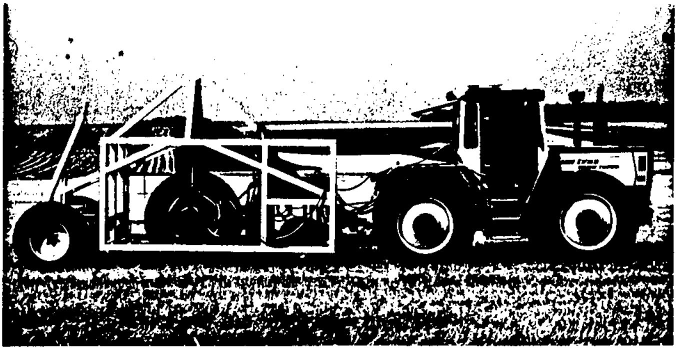

Fig. 14: Single wheel tester for driven angled wheels

min. diameter of the test wheel's rim:	520	mm
max. diameter of test wheel:	2000	mm
max. width of test wheel:	1200	mm
min. vertical load on test tyre:	0	kN
max. vertical load on test tyre:	40	kN
max. slip angle	20	°
max. propulsion power at test wheel:	52	kW
max. rotation of test wheel:	45	$/min^{-1}$
total length of test rig:	4700	mm
total width of test rig:	2500	mm
total height of test rig:	3200	mm
total weight of test rig:	5300	kg

Table 4: Technical data of the single wheel tester

In order to prop the lateral forces of the test wheel, the rig is coupled into the lower links of the towing or braking tractor during the test run. To maneuver in the field the rear axle can be steered with a hydraulic cylinder. The test wheel runs in the middle of the tractor's trac. It is fixed to the rig by four hinge bearings to enable a vertical movement of the test wheel to follow to the uneveness of the ground. To compensate different test wheel diameters the whole linkage can be lifted with a hydraulic cylinder.

The independent hydraulic circuits on the test rig are powered from the PTO of the braking tractor by a mechanical power devider and a cardan shaft. The vertical load on the test tyre is applied by a double acting hydraulic cylinder. To maintain constant load, even when crossing undulate ground, the pressure is regulated by an automatic control system and a pilot valve. A very high oil flow necessary to cross a ground wave with constant vertical load is supplied by an accumulator. The hydraulic drive system consists of an axial piston pump with adjustable displacement and a multistage hydraulic control motor. A planetary drive is used to reduce the speed of rotation. By using an electromagnetic variation of the pump's delivery volume the slip of the test wheel is infinitely variable during a test run.

The key part of the whole test rig is a 6-component-wheeldynamometer. It allows measurements of three forces in all main co-ordinate directions and as well the three relating moments. The dynamometer is mounted between the wheel bearing and the linkage to the rig. All tyre forces are transmitted by the piezo-electric force transducers. The data are registrated via an A/D-converter by a computer. Data analysis follows directly after the test run. The test results are shown on a monitor in the tractor cab.

3.5 Tyre force characteristic

Stationary measurements of lateral and longitudinal forces have been carried out by Armbruster [7]. During these measurements the speed of the test wheel has been increased continuously. At the beginning of a test run the wheel runs with negative slip at the end of the test run with maximum positiv slip (about 60%).

Most interesting is the combined lateral and longitudinal force generation of the tyres. It can be observed, that the lateral forces are diminished as the tractive forces increase, especially at higher slip angles. The maximum lateral force was found at little negative tractive force, corresponding with small negative wheelslip, (fig. 15). Even at very high slip and high tractive forces the lateral forces did not decrease to zero, but to approximately half of their maximum. On the scarified surface the measured side forces have been higher than on the hard surface, probably because sinkage was possible and the lugs became influential. Bigger tyres generated higher side forces. Higher slip angles caused higher lateral forces. But a range of constant lateral forces was not reached even at slip angles of 16°.

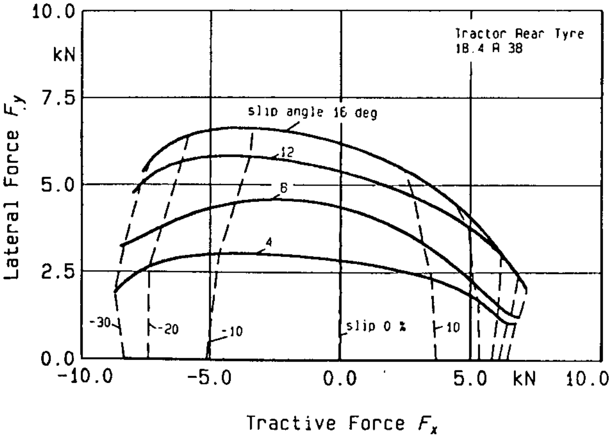

Fig. 15: Tyre force characteristic
(18.4 R 38, wheel load 10 kN, inflation pressure 130 kPa, on a stubble field, moisture content 18,3%)

To make experimental results usable for vehicle users and design engineers the observed behaviour of the tyres must be described numerically. Especially in the field of agricultural tyre performance different mathematical models have been developed to calculate lateral and longitudinal forces. After collecing an extensive amount of measured data over a wide range of different conditions, existing models will be verified either to confirm or to improve them.

4. CONCLUSIONS

At the Institute of Agricultural Engineering of the University of Hohenheim several test stands have been developed to measure dynamic tyre properties in laboraty tests (flat-belt type test stand) and force characteristics on rolling, driven or braked tyres in field tests (single axle trailer; single wheel tester). The soil properties are registrated with appropriate equipment (penetrometer, linear shear tester).

The encouraging results demonstrate the capability of this equipment. The research activities will be continued.

REFERENCES

[1] Schrogl, H.: Dynamische Eigenschaften von Ackerschlepper-Treibradreifen bei höheren Rollgeschwindigkeiten. Dissertation Hohenheim, Forschungsbericht Agrartechnik, MEG, Nr. 159, 1989

[2] Kutzbach, H.D. and H. Schrogl: Dynamic Behaviour of Rolling Tractor Tires. Proceedings 9. Intern. Conference ISTVS, Madrid, 1987, S. 457-464

[3] Plesser, J.: Longitudinal Dynamics of Agricultural Tyres. Proceedings 6th European Conference ISTVS, Wien 1994

[4] Kising, A.: Dynamische Eigenschaften von Traktorreifen. Dissertation Berlin, VDI-Fortschritt-Berichte, Reihe 14, Nr. 40, VDI-Verlag Düsseldorf, 1988

[5] Langenbeck, B.: Untersuchungen zum Fahrverhalten von Ackerschleppern unter besonderer Berücksichtigung der Reifeneigenschaften. Dissertation Stuttgart, VDI-Fortschritt-Berichte, Reihe 14, Nr. 55, VDI-Verlag Düsseldorf, 1992

[6] Armbruster, K.A., A. Hertwig und H.D. Kutzbach: An improved design of cone penetrometer. J. Agric. Enging. Res. (1990) 46, S. 219-222

[7] Armbruster, K.A.: Untersuchung der Kräfte an schräglaufenden angetriebenen Ackerschlepperrädern. Dissertation Stuttgart, VDI-Fortschritt-Berichte, Reihe 14, Nr. 53, VDI-Verlag Düsseldorf, 1992

[8] Barrelmeyer, Th.: Forces Acting on Driven Tractor Tyres with Stationarey and Instationary Slip Angles. Proceedings 6th European Conference ISTVS, Wien 1994

[9] Heine, A.: Experimenteller Beitrag zum Schräglauf- und Lenkmomentverhalten rollender Reifen landwirtschaftlicher Fahrzeuge auf starrer und nachgiebiger Fahrbahn. Dissertation Stuttgart, Forschungsbericht Agrartechnik, MEG, Nr. 199, 1991

[10] Heine, A. and H.D. Kutzbach: Comparison of steady and unsteady cornering experiments with free rolling Agricultural tyres. Proceedings 4th European Conference ISTVS, Wageningen 1989, Volume 1, S. 92-99

[11] Armbruster, K.: Development of a single wheel tester for measurements on driven angled wheels. Proceedings 4th European Conference ISTVS, Wageningen 1989, Volume 1, S. 8-14

[12] Armbruster, K.H. and H.D. Kutzbach: Combined lateral and longitudinal forces on driven angled tractor tyres. Journal of Terramechanics, 28 (1991), H. 4, S. 331-338

FORCES ACTING ON DRIVEN TRACTOR TYRES WITH STATIONARY AND INSTATIONARY SLIP ANGLES

Thomas Barrelmeyer
University of Hohenheim, Germany
Institute of Agricultural Engineering

ABSTRACT

At the Institute of Agricultural Engineering at Hohenheim University a single wheel tester has been developed to investigate power transmission from tractor tyres to ground. For the description of the horizontal tyre behaviour four characteristic values are of main interest. These values are longitudinal and lateral tyre force, slip and slip angle. Results are presented as drawbar pull/slip and as tyre carpet plots (lateral force versus drawbar pull). Eventually the applicabilty of horizontal tyre models is discussed.

1. INTRODUCTION

Evaluating the performance of self-propelled farm machinery power transmission from tractor tyres to ground is of fundamental importance. There are various demands to be met by the tractor tyre. High drawbar pull should be achieved on yielding ground (ploughing, tilling), as well as on solid ground (transport). Furthermore good directional stability, ride safety and ride comfort are of fundamental importance. There is an interaction between the forces in the tyre-soil contact area. If, for example, high lateral forces are necessary to keep the tractor on its contour line on a slope this results in decrease of drawbar pull and tractive efficiency. The paper deals with the description of this interaction.

2. SINGLE WHEEL TESTER

The Single Wheel Tester built at Hohenheim University has already been presented [1,2,3]. This paper concentrates on further developments. During a test run a four wheel trailer is towed by a tractor at constant speed, fig. 1. The gauge wheel is mounted in a frame and can be moved vertically.

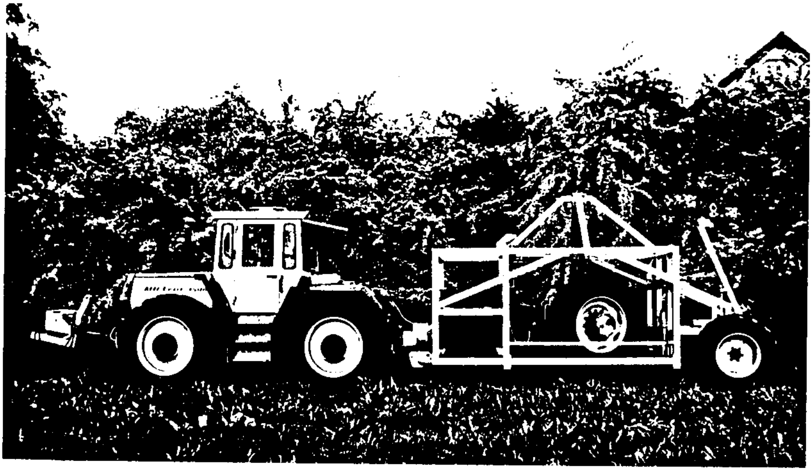

Fig. 1: Single wheel tester

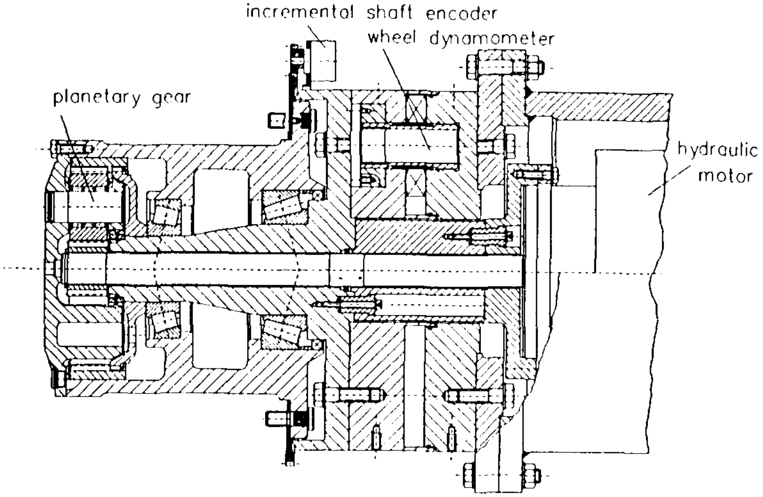
incremental shaft encoder
wheel dynamometer
planetary gear
hydraulic motor

Fig. 2: Cutaway view of the gauge wheel

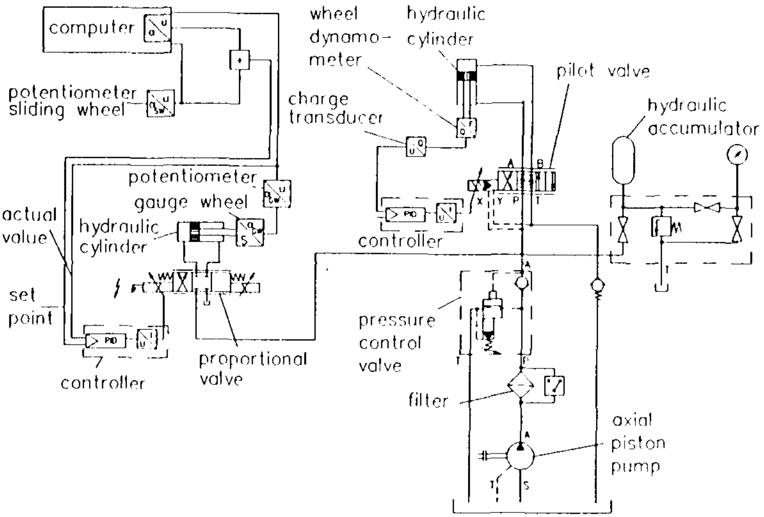
computer
potentiometer sliding wheel
potentiometer gauge wheel
actual value
hydraulic cylinder
set point
controller
proportional valve
wheel dynamometer
hydraulic cylinder
charge transducer
controller
pilot valve
hydraulic accumulator
pressure control valve
filter
axial piston pump

Fig. 3: Hydraulic circuits automatically controlling tyre load and slip angle

Figure 2 shows a cutaway view of the gauge wheel. All forces can be measured by a six-component piezoelectric wheel dynamometer. Steering, camber and propulsion torque can be calculated. The trailer is equipped with three hydraulic circuits. A closed hydrostatic circuit is used to brake or propel the wheel by means of an adjustable radial piston pump. The second circuit controls the tyre load. The third circuit, finally, serves to control the slip angle, i.e. the steering of the wheel, fig. 3. Thus, lateral tyre forces can be investigated which are engendered by stationary and instationary slip angles. Though the gauge wheel is connected to the frame of the trailer by very rigid upper and lower links there is a certain deformation when the tyre load increases which in turn causes cambering of the wheel. This is the reason why the platform the links are mounted on is allowed to rotate whereby the camber angle can be adjusted from zero to twenty degrees, fig. 4.. The measuring of all characteristic values is depicted in fig. 5. The tyre forces are measured by the wheel dynamometer

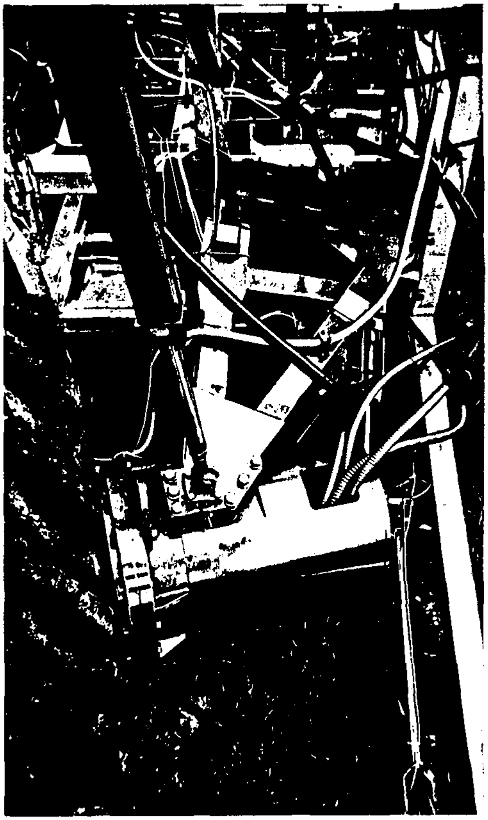

Fig. 4: Gauge wheel, α and $\gamma > 0°$

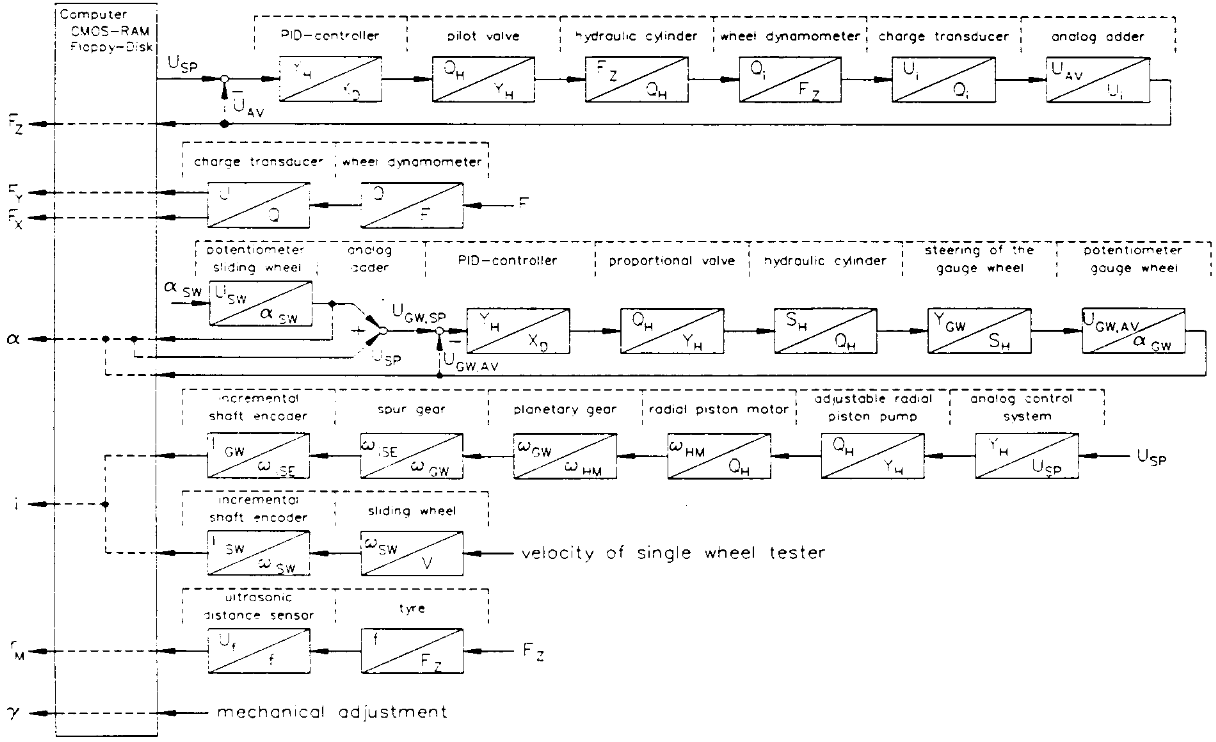
Computer
CMOS-RAM
Floppy-Disk
PID-controller
pilot valve
hydraulic cylinder
wheel dynamometer
charge transducer
analog adder
U_{SP}
$\bar{U}_{AV}$
Y_H X_D
Q_H Y_H
F_Z Q_H
Q_i F_Z
U_i Q_i
U_{AV} U_i
F_Z
charge transducer
wheel dynamometer
U Q
Q F
F
F_Y
F_X
potentiometer sliding wheel
analog adder
PID-controller
proportional valve
hydraulic cylinder
steering of the gauge wheel
potentiometer gauge wheel
α_{SW}
U_{SW} α_{SW}
$U_{GW,SP}$
U_{SP}
$U_{GW,AV}$
Y_H X_D
Q_H Y_H
S_H Q_H
Y_{GW} S_H
$U_{GW,AV}$ α_{GW}
α
incremental shaft encoder
spur gear
planetary gear
radial piston motor
adjustable radial piston pump
analog control system
I_{GW} ω_{ISE}
ω_{ISE} ω_{GW}
ω_{GW} ω_{HM}
ω_{HM} Q_H
Q_H Y_H
Y_H U_{SP}
U_{SP}
i
incremental shaft encoder
sliding wheel
I_{SW} ω_{SW}
ω_{SW} V
velocity of single wheel tester
ultrasonic distance sensor
tyre
U_f f
f F_Z
F_Z
r_M
γ
mechanical adjustment

Fig. 5: Measured and controlled physical values

mentioned above. Whereas the tyre load is automatically controlled the lateral and the longitudinal force result from the tyre-soil interaction. During a test run the single wheel tester is coupled to the three-point hitch of the towing tractor. The front axle of the trailer is lifted so that only the tyres of the steerable trailer-rear axle touch the ground. Great slip angles of the gauge wheel make the trailer move sidewise, which leads to a decrease of the original slip angle as shown in fig. 6. The decrease can be measured by the sliding wheel when

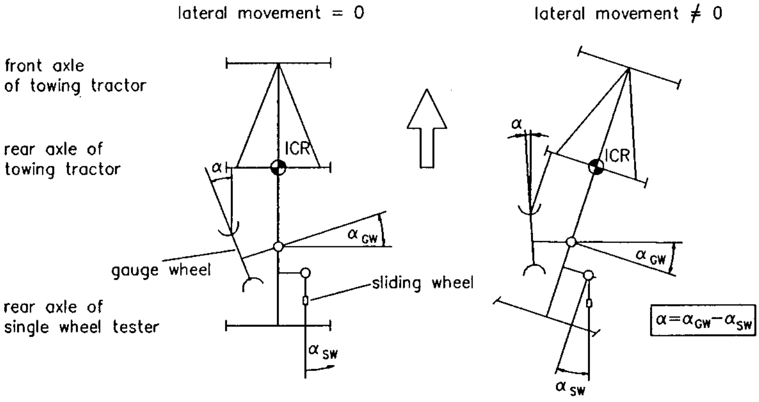
lateral movement = 0
lateral movement ≠ 0
front axle of towing tractor
rear axle of towing tractor
ICR
α
α GW
gauge wheel
sliding wheel
rear axle of single wheel tester
α SW
ICR
α
α GW
α SW
α=α GW−α SW

Fig. 6: Determination of the actual slip angle

assuming point ICR as the test rig's instantaneous centre of rotation (see fig. 6). Using the control circuit (fig. 5) the deviation of the slip angle can be controlled presuming that 20°- $\alpha_{GW} < \alpha_{SW}$.

Counting the impulses of the incremental shaft encoders mounted on the gauge and sliding wheel the slip of the tyre can be calculated according to different slip definitions, Table 1 eq. 1-3. As far as on-the-road vehicles are concerned ride safety is of great importance and therefore vehicle braking operations are in the focus of interest. Here the special case of a completely slipping wheel is of no practical importance. For off-road vehicles the tractive efficiency ought to be optimized and the special case of a blocking wheel is of little interest. The single wheel tester of Hohenheim University, however, offers the opportunity to simulate all driving situations mentioned above. That is the reason why Armbruster proposed a combination of both definitions [2]. Fig. 7 shows a comparison of definitions (1),

slip definition	e.g.used by	blocking wheel	completely slipping wheel
$i=\frac{s_{th}-s_{a0}}{s_{a0}}$ (1)	Haken [4]	-100%	+ ∞
$i=\frac{s_{th}-s_{a0}}{s_{th}}$ (2)	Grečenko [5]	-∞	+100%
$i_B=\frac{s_{th}-s_{a0}}{s_{a0}}$ $i_T=\frac{s_{th}-s_{a0}}{s_{th}}$ (3)	Armbruster [2]	-100%	+100%
s_{th}... theoretically travelled distance s_{a0}... actually travelled distance when $\alpha=0°$			

Table 1: Slip definitions

(2) and (3) applied at a tyre test with zero slip angle. Slip definition (3) is useful when high negative and positive slip values obtained during one test run have to be plotted in one diagram. The unsteadiness of the slip definition at zero slip, however, has to be considered as a disadvantage [4,5]. If the slip angle α is greater than zero it has to be taken into account that the vector of tyre circumferential velocity does not coincide with the vector of vehicle travel or sliding wheel circumferential velocity, fig.8. Since all forces and other physical values are presented in the tyre coordinate system the actual distance s_a, measured by the sliding wheel, has to be projected on the tyre x-axis. Consequently the slip can be calculated as

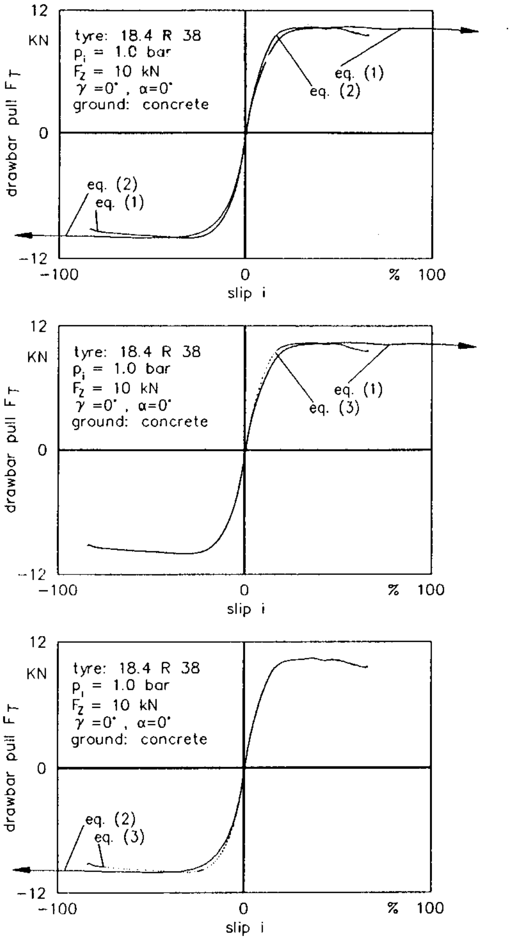

Fig. 7: Comparison of different slip definitions (F_{Ri} neglected)

$$i_B = \frac{s_{th}}{s_a \cdot \cos\alpha} - 1 \; ; \qquad i_T = 1 - \frac{s_a}{s_{th}} \cdot \cos\alpha \tag{4}$$

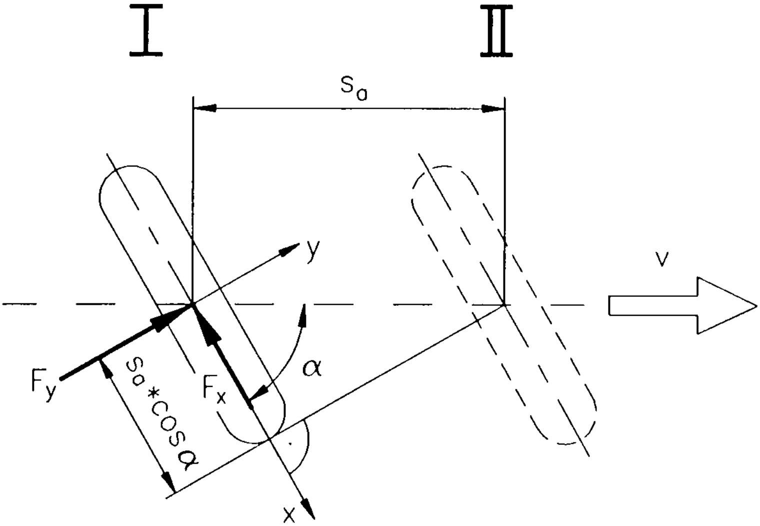

Fig. 8: Travelled distances of a wheel with slip angle $\alpha > 0°$

Fig. 9 gives an impression of how far the slip is influenced by the slip angle.

Since a lot of measurements have been carried out on soft soil the rolling resistance has to be taken into account when determining the slip zero. In fig. 10 the longitudinal forces acting on a tyre are plotted against slip. The relationship between these forces has already been described by Schüring [6]. After having replaced the planetary gear of the gauge wheel the rolling resistance of the tyre can be measured directly. The rolling resistance on an asphalt road is assumed to be the interior rolling resistance of the tyre due to its flexing work.

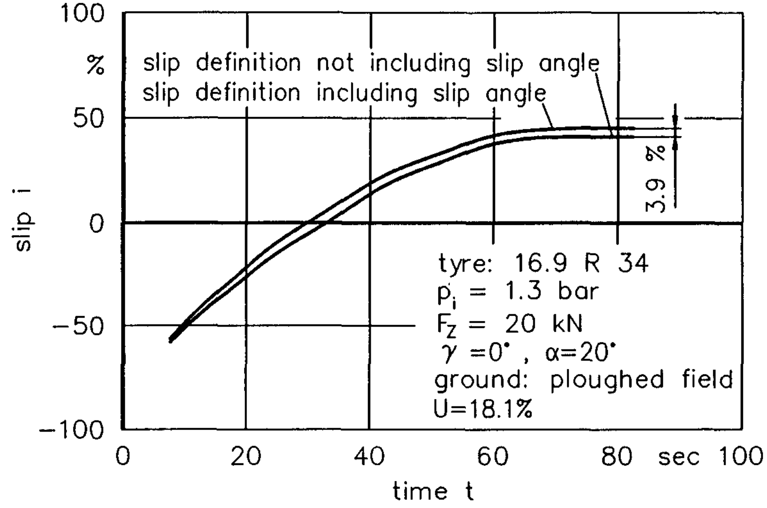

Fig. 9: Slip definition including slip angle α

$$F_{Ri} = F_R \quad \text{on asphalt, concrete} \tag{5}$$

As a next step the rolling resistance on soft ground is measured. With the simplifying assumption that the interior rolling resistance on solid ground is of the same value as on yielding ground the exterior rolling resistance can be calculated from

$$F_{Re} = F_R - F_{Ri} \tag{6}$$

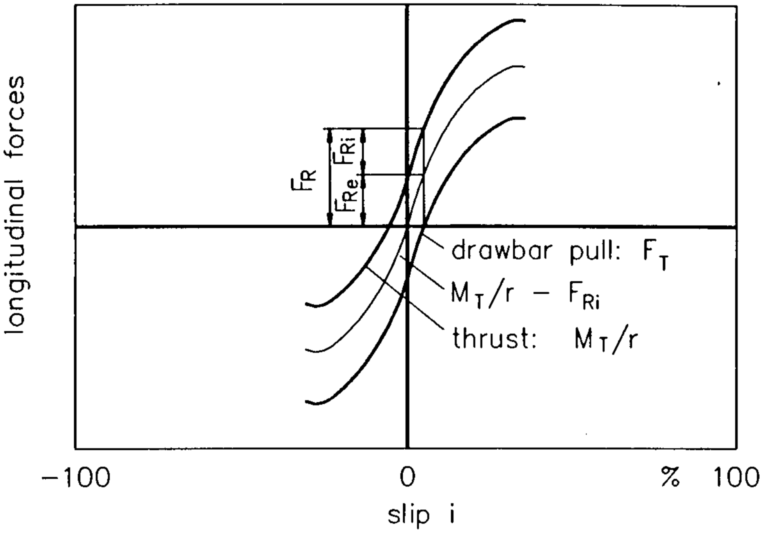

Fig. 10: Longitudinal forces acting on a tyre

The above mentioned assumption does not really reflect reality because the tyre deformation depends on the resilience of the ground [7].

During a calibration test run a slip calibration factor

$$scf = \frac{I^*_{GW}}{I^*_{SW}} \qquad (7)$$

is determined at zero slip. For this reason the test wheel's velocity is increased until the measured drawbar pull which is displayed on-line on the computer screen equals the negative exterior rolling resistance. As long as the resilience of the ground does not change during the following test runs the slip can be calculated from

$$i_B = \frac{I_{GW}}{I_{SW}} \cdot \frac{1}{scf \cdot \cos\alpha} - 1 \; ; \qquad i_T = 1 - \frac{I_{SW}}{I_{GW}} \cdot scf \cdot \cos\alpha \qquad (8)$$

3. PARAMETERS UNDER INVESTIGATION

3.1 Steering Cycle

During the test runs the slip angle can be changed as illustrated in fig.11. The parameters α_{t1}, α_{t2}, α_{t3}, Δt_1, $\dot{\alpha}_{t2}$, $\dot{\alpha}_{t3}$ can be chosen freely

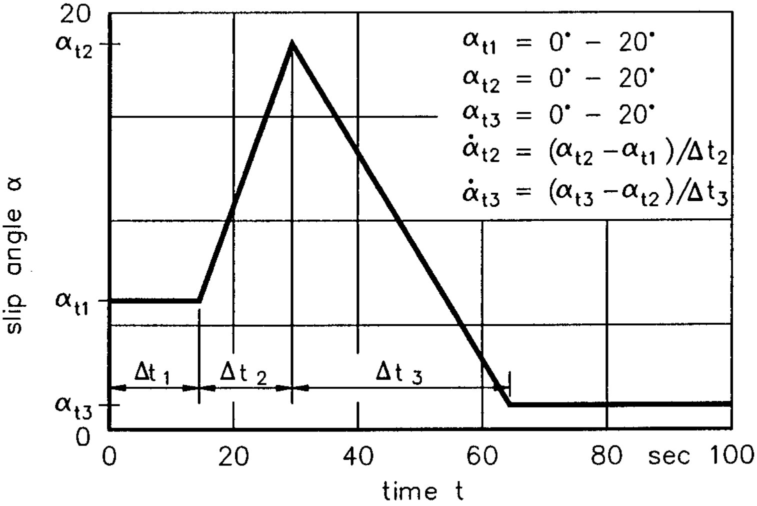

Fig. 11: Steering cycle

before the test run starts. Only three steering cycles, however, have been investigated:

Cycle 1: $\alpha_{t1} = 0°$, $\alpha_{t2} = 20°$, $\alpha_{t3} = 0°$
$\Delta t_1 = 20$ sec, $\dot{\alpha}_{t2} = \dot{\alpha}_{t3} = 1°$/sec, 2°sec, 4°/sec, 8°/sec, 10°/sec

Cycle 2: $\alpha_{t1} = 0°, \alpha_{t2} = \alpha_{t3} = 20°$
$\Delta t_1 = 20$ sec, $\dot{\alpha}_{t2} = 1°$/sec, 2°/sec, 4°/sec, 8°/sec, 10°/sec

Cycle 3: $\alpha_{t1} = \alpha_{t2} = \alpha_{t3} = 0°$, 5°, 20°, 15°, 20°

Cycle 3 does not describe a real steering cycle but a wheel which runs with stationary slip angle. There are two ways of measuring the tyre forces and of depicting them in a tyre carpet plot. Applying one method the slip angle is adjusted to a certain level and kept constant and the slip is changed during the test run. Applying the other method the slip is kept constant and the slip angle is changed during the test run, i.e. the wheel is steered. Because of the automatic control circuit it is much easier to keep the slip angle at a constant level than the slip because in this case the influence of the slip angle on the slip (see equation (4)) has to be neglected. This is due to the fact that up to now the propulsion of the gauge wheel has been controlled by an analog system and not by a computer.

3.2 Travel Surface

Tyre forces have been measured on a solid concrete and asphalt roadway. As a soft travel surface a stubble field has been chosen. After first measurements it has been ploughed and used again.

Table 2 gives an overview of mechanical soil properties which have been measured with a translational shear tester described in [2]. Due to soil compaction parts of the ploughed field showed a very uneven surface finish, the crumb was very coarse. The clods generated by a three-furrow-mouldboard plough often covered a hollow space which collapsed when charged with the metal plate of the shear tester. This is the reason for the high value of Φ on the ploughed field. It can be concluded from this that high shear strength values are obtained only for high vertical stress values or that a tyre has to do a lot of compaction work before it can transmit high longitudinal forces. Compared to literature the cohesion measured on the stubble field seems to be too great.

soil	surface	moisture content U [%]	cohesion c [N/mm²]	angle of internal friction Φ [°]
silty loam	stubble	20,1	0,051	25,1
silty loam	ploughed	19,6	0,018	44,6

Table 2: Mechanical soil parameters

4. RESULTS

4.1 Rolling Resistance

As a basic investigation the rolling resistance of a standard tyre has been measured on different grounds. In fig. 12 the rolling resistance is plotted versus speed. On the ploughed field the maximum speed has not been chosen greater than 9 km/h because the ride on the clods of the cohesive soil has been very unsteady. Only on the ploughed field the rolling resistance increases with speed. On the stubble field and the asphalt road, however, it remains almost constant. The greater the resilience of the ground the greater the rolling resistance. Increasing tyre load leads to greater sinkage and tyre

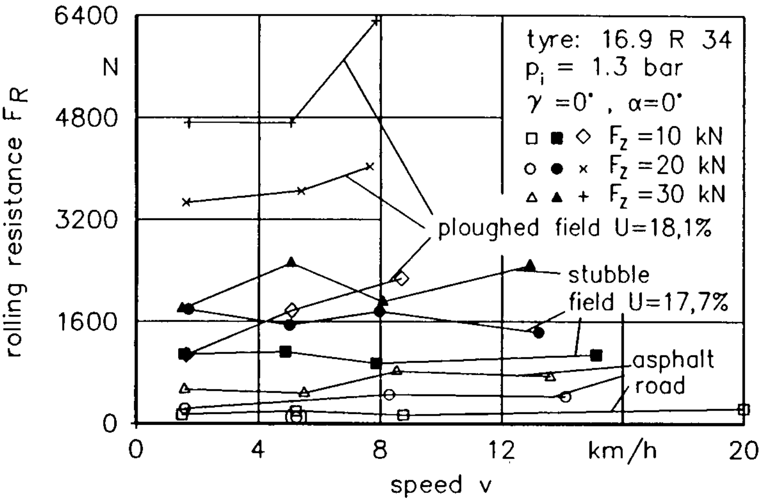

Fig. 12: Rolling resistance on different grounds

deflection which in turn causes much more soil deformation and tyre flexing work.

In [2] Armbruster compares the performance of different tyres and reveals that the forces depend very much on tyre parameters such as width, diameter and inflation pressure. This can be observed as well in fig. 13 which compares the rolling resistance of two different tyres. Due to the greater rut width of the wide-base tyre the exterior rolling resistance is greater compared to the tyre 16.9 R 34.

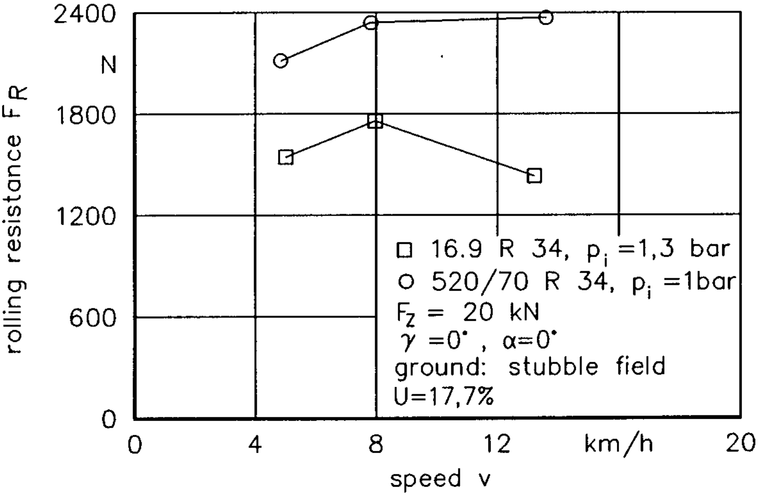

Fig. 13: Rolling resistance of different tyres

Since the number of test runs increases very rapidly when investigating different tyres with different tyre parameters the test runs reported about have been carried out only with the standard tyre

16.9 R 34. The measurements on yielding ground revealed that there are a lot of disturbing factors in the soil of the test field which made it difficult to reproduce measurements. Nevertheless each set of test parameters has been measured only once as far as no mistake became obvious directly after the test run. This, however, made it possible to investigate a great variety of parameters as described in the following. The curves of the tyre carpet plots discussed in the next chapter are cubic splines based on mean values calculated from measured data. Slip was calculated with eq. (4).

4.2 Tyre Forces On Different Grounds

The horizontal tyre forces, shown in fig. 14, have been measured during test runs with constant slip angles and increasing slip. The general shape of the curves is in good accordance with the results published in [2]. Lateral forces of a braking wheel are greater than those of a driving wheel as far as slip angles $\alpha > 10°$ are concerned. The tyre carpet plots are not symmetrical. The slip and drift theory of Grečenko explains this behaviour analytically [8]. On the stubble field the lateral forces are greater than on a ploughed field. The lateral force of a tyre running on yielding ground consists of two components as described by Schwanghardt [9]. The first component is the lateral force acting in the horizontal tyre contact area which can be geometrically added to the longitudinal tyre force. The amount of the resultant force is limited by the soil strength. The second component is the normal force of the earth wall acting on the tyre side wall. On a ploughed field the earth wall generated by a tyre running with slip angle is higher than on a stubble field but the

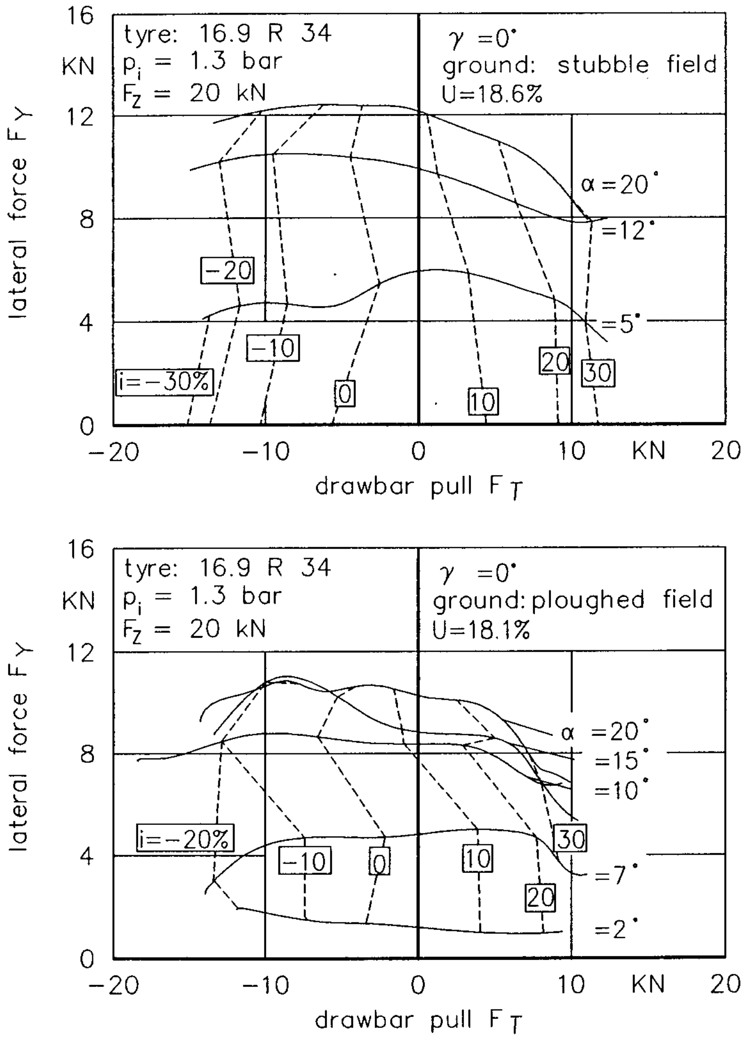

Fig. 14: Horizontal tyre forces on different grounds

soil strength is less. Obviously the influence of the lateral force in the horizontal tyre contact area is of main importance.

4.3 Tyres Running With Instationary And Stationary Slip Angles

Further measurements have been carried out during which the slip has been kept constant and the slip angle has been continuously changed. Fig. 15 shows a comparison of tyre carpet plots of a steered (instationary slip angle) and a non-steered wheel (stationary slip angle) with the interesting result that the lateral tyre forces of the steered wheel are smaller compared to the wheel running with stationary slip angle. Similar effects have been reported by Heine

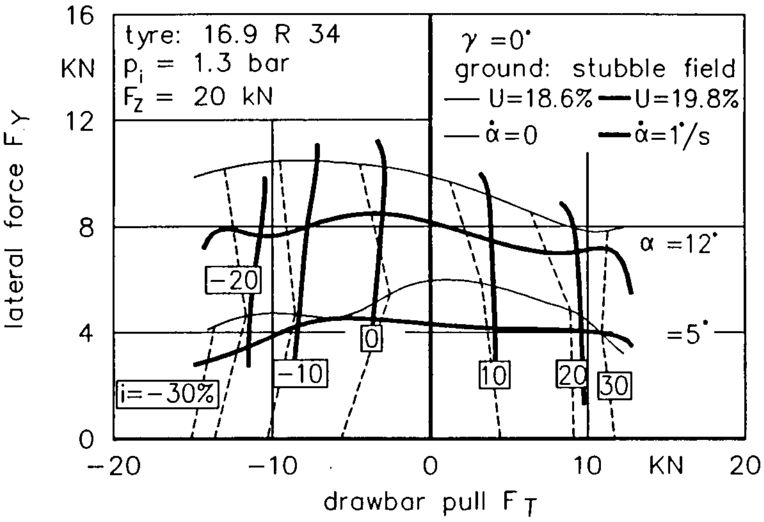

Fig. 15: Wheel running with stationary and instationary slip angle

[10] who concludes from his measurements that the generation of lateral guiding forces is time-dependant.

4.4 Rolling and steering speed

In fig. 16 different steering and rolling speeds are compared. It becomes obvious that lateral tyre forces decrease with increasing rolling and steering speed. Especially the lateral forces of a braking wheel will be greater if the wheel is moved slowly. This result is surprising because soil strength increases with growing shear velocity [11]. However, it needs some time to generate the lateral tyre force due to tyre deflection and furthermore it needs some time to build the earth wall which acts on the tyre side wall. This effect becomes obvious especially in diagram d and even more in fig. 17 which illustrates that the lateral force does not grow to its stationary value if the tyre is steered back immediately after having reached its maximum slip angle.

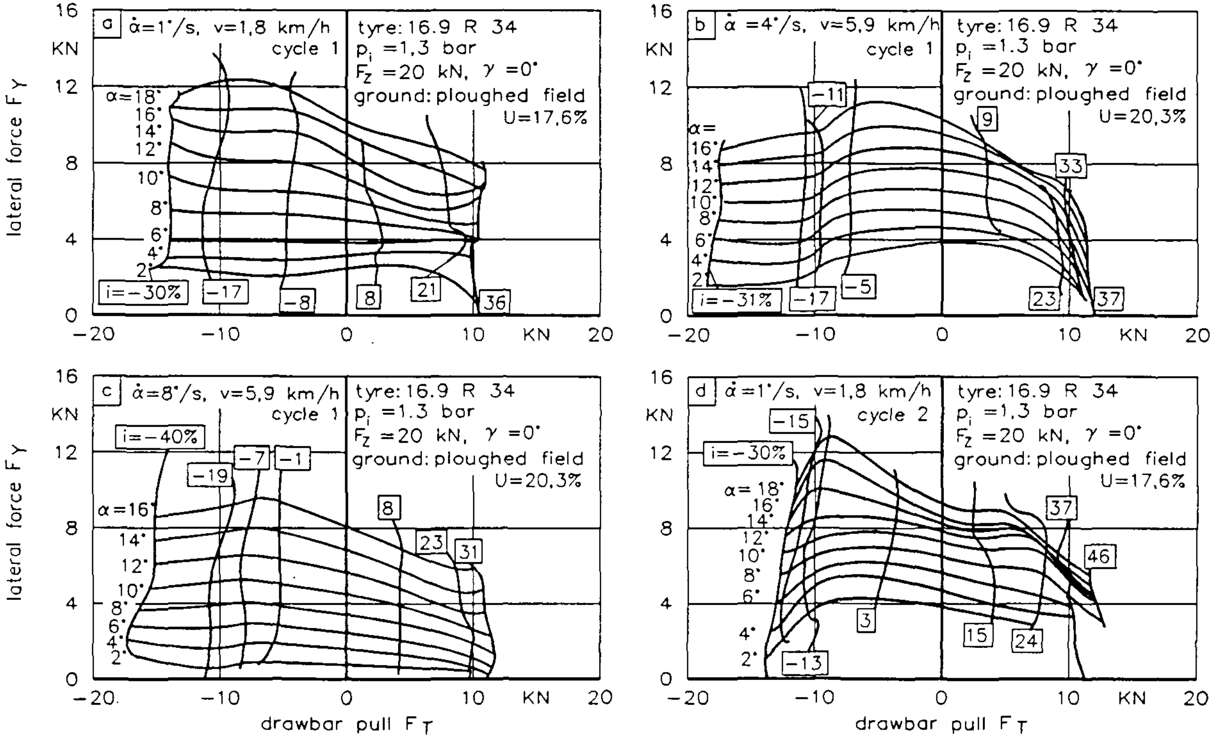

Fig. 16: Rolling and steering speed influence

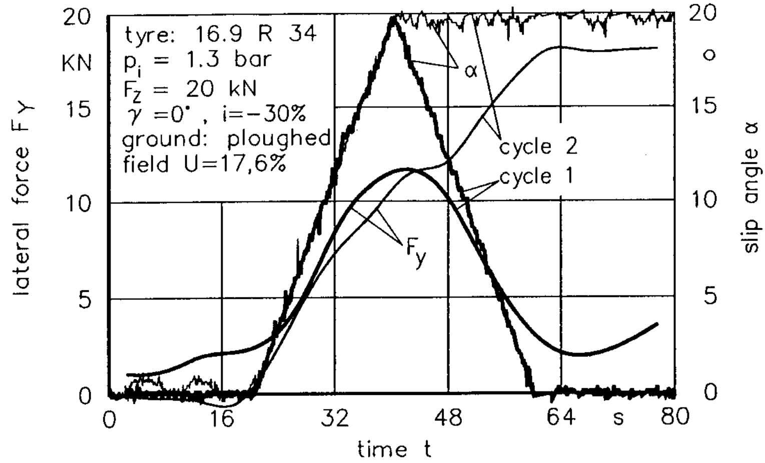

Fig. 17: Lateral tyre forces with different steering cycles

5. APPLICABILITY OF HORIZONTAL TYRE MODELS

The results presented reveal that the generation of horizontal tyre forces on yielding ground is time-dependant. Horizontal tyre models published up to now have not taken into account these effects but have only described the stationary behaviour. In this case good accordance between measurement and calculation can be achieved [2]. Further research should investigate the influence of instationary slip angles which is of at least the same practical importance.

6. LIST OF SYMBOLS

c	N/mm²	cohesion
F	N	force

F_R	N	rolling resistance
F_{Re}	N	exterior rolling resistance
F_{Ri}	N	interior rolling resistance
F_T	N	drawbar pull
f	m	tyre deflection
i	%	slip
M	Nm	torque
p_i	bar	inflation pressure
Q	c	electric charge
scf	1	slip calibration factor
t	s	time
U	V	fig. 5: voltage
	%	otherwise: moisture content
v	m/s	speed
α	°	slip angle
$\dot{\alpha}$	°/s	steering speed
γ	°	camber angle
Φ	°	angle of internal friction

Indices:

a0	actually, $\alpha = 0°$
AV	actual value
B	braking
D	difference
GW	gauge wheel
H	hydraulic
iSE	incremental shaft encoder
SW	sliding wheel
SP	set point

th	theoretically
T	driving
x	tyre longitudinal coordinate
y	tyre lateral coordinate
z	tyre vertical coordinate

7. REFERENCES

[1] Armbruster K. und H.D. Kutzbach: Development of a single wheel tester for measurements on driven angled wheels. Proceedings 4th European Conference ISTVS, Bd. 1 (1989) Wageningen/Holland, S. 8-14

[2] Armbruster, K.: Untersuchung der Kräfte an schräglaufenden angetriebenen Ackerschlepperrädern. Dissertation 1991, Universität Stuttgart, veröffentlicht VDI-Fortschritt-Berichte, Reihe 14: Landtechnik/Lebensmitteltechnik, Nr. 53

[3] Barrelmeyer, Th., B. Langenbeck, K. Armbruster und H.D. Kutzbach: Tyre model for vertical, longitudinal and lateral forces on driven angled tractor wheels. Proceedings of the 11th International Conference ISTVS. Incline Village, Lake Tahoe, 27-30 September 1993, S. 54-63

[4] Haken, K.: Konzeption und Anwendung eines Meßfahrzeugs zur Ermittlung von Reifenkennfeldern auf öffentlichen Straßen. Dissertation 1993, Universität Stuttgart.

[5] Grečenko, A.: The slip and drift model of a wheel with tyre

compared to some other attempts in this field. Journal of Terramechanics, Vol. 29 (1992) pp. 599-604

[6] Schüring, D.: Zur Theorie des Geländerades. Forsch. Ing.-Wes. Bd. 34 (1968) Nr. 6, S. 165-176 und Bd. 35 (1969) Nr. 1, S. 7-11

[7] Schmid, J.C.: Inflation pressure control to improve terrain-trafficability. A. model for simulation. Proceedings of the 11th International Conference ISTVS. Incline Village, Lake Tahoe, 27-30 September 1993, S. 64-75

[8] Grečenko, A.: Das Slip-Drift-Modell des Rades anwendbar für weiche oder starre Fahrbahn. VDI-Berichte Nr. 1082, 1993, S. 99-108

[9] Schwanghart, H.: Seitenkräfte an gelenkten Luftreifen in lockerem Boden. Grundlagen der Landtechnik 17 (1967) 3, S. 105-114

[10] Heine, A.: Experimenteller Beitrag zum Schräglauf- und Lenkmomentverhalten rollender Reifen landwirtschaftlicher Fahrzeuge auf starrer und nachgiebiger Fahrbahn. Dissertation (1991) Universität Stuttgart, veröffentlicht Forschungsbericht Agrartechnik des Arbeitskreises Forschung und Lehre der Max-Eyth-Gesellschaft, Nr. 199

[11] Beretitsch, S.: Kräftespiel im System Schneidwerkzeug-Boden. Dissertation 1992, Universität Karlsruhe

LONGITUDINAL DYNAMICS OF AGRICULTURAL TYRES

Joachim Plesser
University of Hohenheim, Germany
Institute of Agricultural Engineering

ABSTRACT

The increasing speed of normally unsuspended agricultural vehicles results in problematic situations with regard to ride safety and ride comfort. With a flat-belt tyre test stand, developed at the University of Hohenheim, it is possible to investigate the dynamic behaviour of tractor tyres especially in the vertical and longitudinal direction.

The tyre and the whole vehicle is activated to vibrations by the uneveness of the road and the difference of the tyre-diameter over the circumference. The dynamic behaviour will be shown and the interaction between vertical and longitudinal vibrations will be discussed.

With a wheel brake it is possible to generate longitudinal forces in the contact area. The resulting dynamic behaviour is investigated by varying inflation pressure, driving speed, vertical load and the temperature of the tyre.

1. INTRODUCTION

During the last years the use of agricultural tractors has been in steady change. Years ago the tractor was only used for cultivation of the field. Nowadays the part of transportation work increases more and more. Today a maximum speed of 40 - 50 km/h for agricultural tractors is quite customary. With the increase of transportation speed the problematic ride conditions of unsuspended vehicles gain in importance. In particular the standard-trac could not provide sufficient ride comfort and only a insufficient ride safety.

The dynamic behaviour and therefore ride safety and ride comfort depends due to the missing suspension on the spring- and damping characteristics of the tyres. Because of the big low-pressure tyres with small damping values the vehicle is activated to vibrations by the uneveness of the road and the difference in the diameter over the circumference of the tyre itself.

The ride condition becomes problematic when the tyre loses tread mat. In this case the tyre cannot transmit any forces from the vehicle to the ground. Especially when the steering front wheels lose ground contact, dangerous driving situations might occur.
On one side the tyre is used on greenland and soil and on the other side on solid roadways. By formulating the demands for an optimum tractor-tyre some points are incompatible.

The demands are minimum rolling resistance, good traction properties, low wear, good spring comfort, optimal soil protection and a safe handling performance.
Because of that, the construction of an agricultural tyre is a compromise of the demands mentioned above [4]. One cannot optimize the tyre only for good vibration behaviour. Therefore one has to find other possibilities to isolate the vehicle from vibrations.

Examples are:
- suspension of the cabin
- suspension of the axles (in particular the front axle)
- use of devices like plough or other masses to absorb the vibrations

The suspension of the seat serves to improve the comfort of the driver. It has only a secondary influence on the behaviour of the whole vehicle.

To optimize the possibilities of vibration-isolation for the whole vehicle, the knowledge of the damping and spring characteristics of the tyres is necessary. These characteristic values can also be used as input-data for simulation programmes to describe the dynamic performance of the vehicle.

In former works the dynamic behaviour in the vertical direction was investigated at the University of Hohenheim [5]. Now, in addition to the vertical forces, the longitudinal forces are investigated at a tyre test stand.

2. Tyre Test Stand

The test stand developed at the Institute of Agricultural Engineering is a flat-belt tyre test stand (fig.1). The test tyre rolls on an endless steel belt and is led in a rocker in the longitudinal direction of the belt [1].
The axis of rotation of the rocker is positioned in the tread level of the tyre. The axis lies in the right-angle to the rolling direction of the tyre and the belt. To simulate a real street roughness, sand paper with grain size 40 is sticked on the belt.

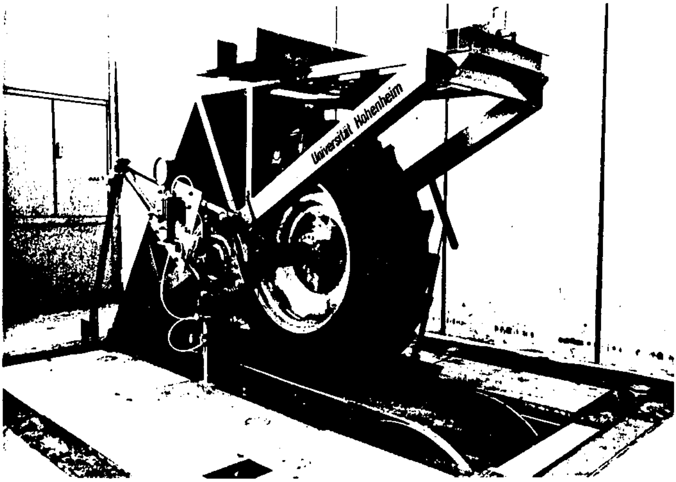

Fig. 1. Flat-belt tyre test stand

Under the contact area the belt is supported by a fixed steel plate. The plate is coated with teflon. There are a number of drillings in the plate where a water-oil-emulsion is pumped through. By this method, the arrangement is becoming a slide bearing.

On top of the rocker, weights can be fixed to vary the load of the tyre.

With a wheel brake it is possible to act peripheral forces into the tyre (fig.2). In the contact area these forces work as longitudinal forces.
The brake is a disk-brake with a disk diameter of 400 mm. The whole brake is attached to the wheel shaft by two feather-keys at the free end of the shaft.

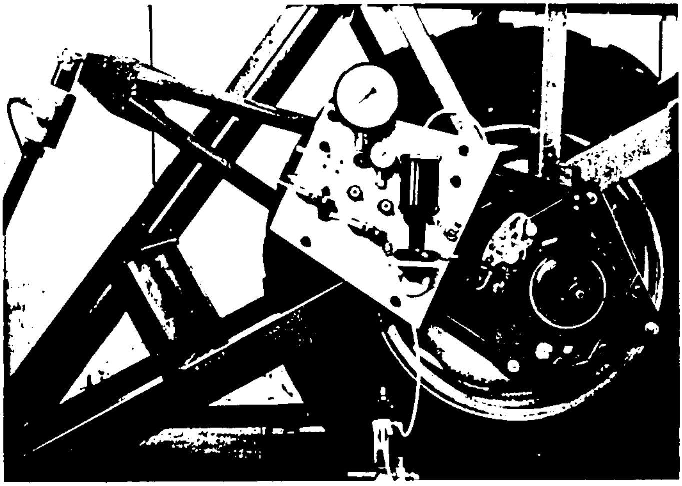

Fig. 2. Wheel brake of the tyre test stand

The two steel plates of the brake frame are supported by two roller bearings to the brake hub. The brake disk is connected form-fit to the hub in a special arrangement, so that thermal expansion of the disk has no influence on the operability of the brake.

The braking moment is supported by a torque converter bearing with a crank of a lever of about 1300 mm to the frame of the test rig. In the vertical part of the torque converter there is a load cell to measure the force in this direction. With the part of the force that works in a right-angle to the rotation axis and the well known distance to the axle (1300 mm), the braking moment can be determined.

By two turning knuckles, one in the connection of the torque converter to the frame of the test rig and the other above the load cell (see fig. 2), the brake can join in every movement of the rocker.
The maximum braking moment of one caliper is 5000 Nm. To enhance the braking moment it is possible to install a second caliper at the brake.

To get a continuous variation of the braking moment and the braking period, a pneumatic control system is used (fig. 3).
By the 3/2 - directional control valve the air pressure of the compressed-air ductwork system, which is about 8 - 9 bar, is cut in or out.

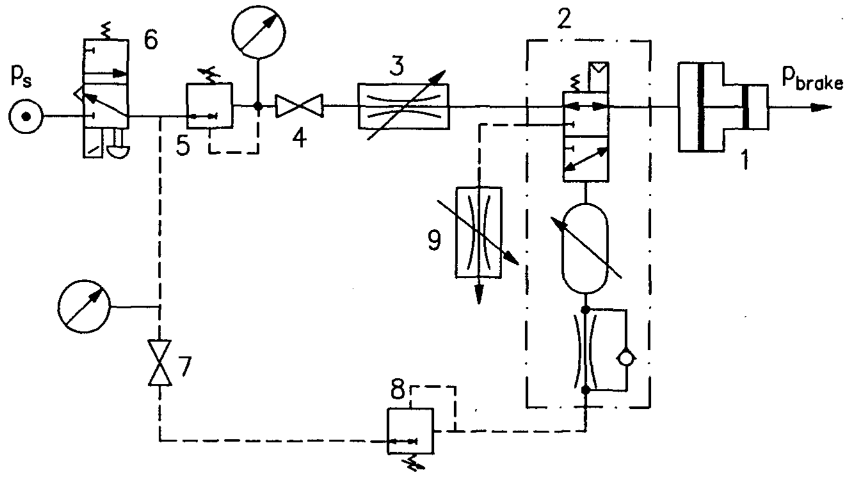

Fig. 3. Pneumatic control system of the brake

With the two pressure controller 5 and 8 the braking pressure (5) an the actuating pressure (8) of the time delay valve can be adjusted. Both pressures are displayed on a manometer. The braking time is controlled by the time-delay valve 2.
The pressure intensifier 1 works with a ratio of 1:16. So the maximum pressure is about 130 bar. With the flow control valve 9 the pressure reduction can de delayed.

By this arrangement the braking moment can be varied between 0 and 5000 Nm and the braking time between 0 and 20 seconds.

Because of the low acceleration level of agricultural vehicles it is close to the actual usage to employ a brake for passing longitudinal forces into the tyre. At the real vehicle dynamic longitudinal forces can be acted into the contact area by a brake or by pushing-forces of a trailer.

To stimulate the tyre to vibrations, the whole rocker is lifted up with a crane. At a definable height one can open the releasing gear and the tyre falls down and oscillates with its natural frequency. The initial height is reached when the vertical load is just yet high enough to run the wheel with the belt velocity. Investigating the dynamic behaviour of a tyre, the technique of measuring is very important. At the tyre test stand one can measure with ten sensors the physical values: vertical load, longitudinal force, rotation angle of the wheel, deflection of the tyre, braking moment and speed of the wheel and the belt.

The longitudinal forces mentioned above are measured with load-transducer-pins in the bearing of the rocker.

With the exception of the incremental shaft encoders for measuring the speed of the belt and the tyre, which deliver TTL-signals, all sensors supply analog signals between 0 and 10 volts (the sensors based on strain measurement are amplified with a carrier frequency amplifier to the range of 0 - 10 volts). These signals are read in by a A/D-converter in a PC-486. After the measurement the data are saved on the hard disk of the computer.

The maximum sampling frequency per channel is 670 Hz. In a special sample-and-hold mode it is possible to measure all seven variables simultaniously. This is a requirement for measuring high dynamic processes. Fig.4 shows the principle set-up of the measuring instrumentation.

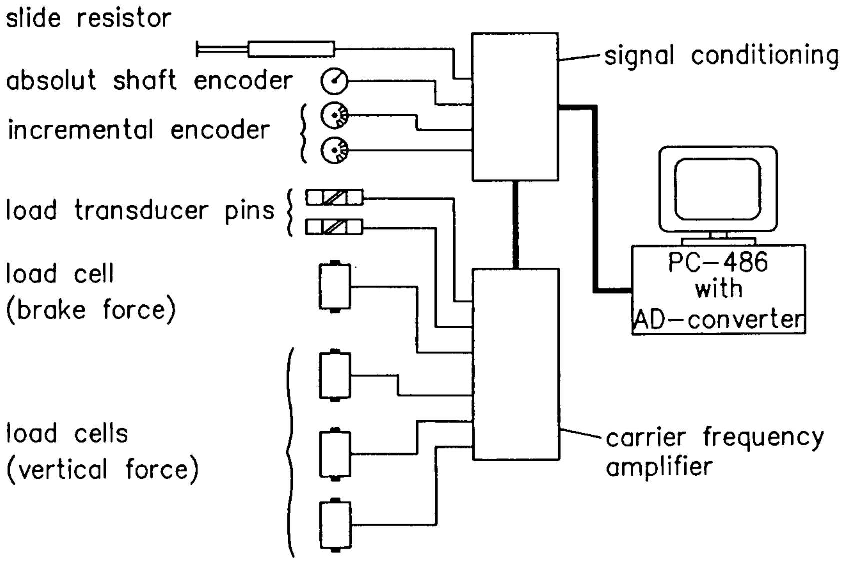
slide resistor
absolut shaft encoder
incremental encoder
load transducer pins
load cell
(brake force)
load cells
(vertical force)
signal conditioning
PC-486
with
AD-converter
carrier frequency
amplifier

Fig. 4. Set-up of the measuring instrumentation

3. LONGITUDINAL FORCES

A longitudinal force is a peripheral force which works in the contact area of the tyre in the rolling direction of the wheel.
With a wheel that rolls free, without any acceleration torque, the longitudinal force correspond to the rolling resistance of the tyre.

When the wheel is driven or braked, the resulting longitudinal force consists of the rolling resistance and the propulsive or the brake force (fig.5). Equation 1 shows the sum of all moments for the arrangement at the tyre test stand. In this case, the bearing friction is neglected.

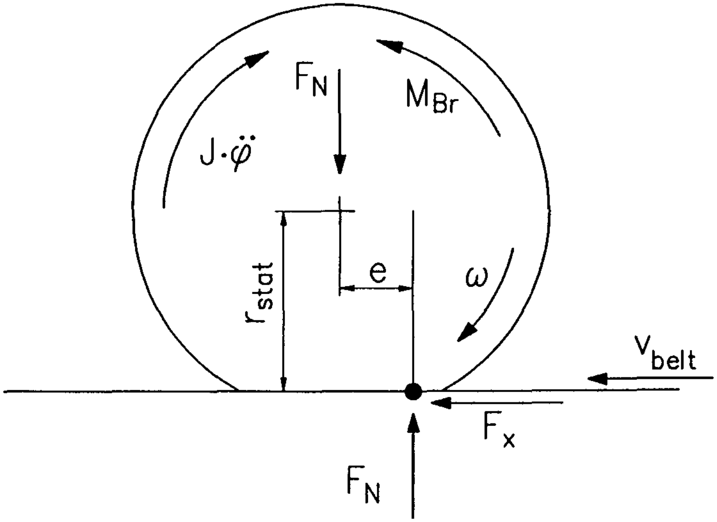

Fig. 5. Forces and moments of a wheel

$$M_{Br} = F_x \cdot r_{stat} - F_N \cdot e + J \cdot \dot{\omega} \qquad (1)$$

At this point it should be mentioned that for calculating the forces and the moments of a tyre the static load radius is used [3], which is the distance between the middle of the axle and the surface of the roadway. The dynamic load radius, resulting of the rolling circumference of the wheel, is employed for kinematic reflections.

Longitudinal forces are shearing forces in the tyre stock which can be outlined over the contact area [6]. Fig. 6 shows the qualitative course of those forces. Between inlet and outlet there is a change in the sign. The place of the zero crossing depends on the so called "lever-arm of the rolling friction" e [3]. (see fig. 5)

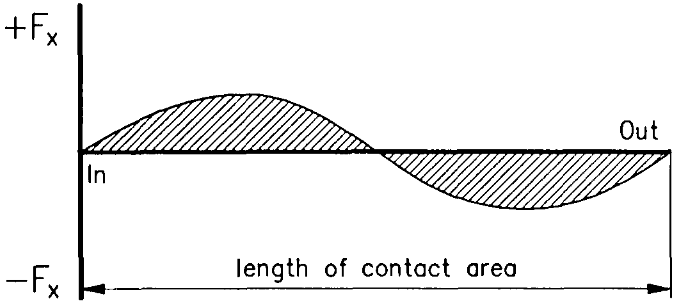

Fig. 6. Shearing forces in the contact area

One aim of the work at the tyre test stand is to obtain the longitudinal forces and to determine the spring- and damping characteristics in the longitudinal direction. The ride conditions of agricultural tractors should be described by numerical simulation programmes where the spring and damping values can be used as input data.

The longitudinal forces described in this article are yielded from the conditions of the tyre on even roadways. Another type of longitudinal forces are led into the tyre by driving on bad roadways with potholes or queren of obstacles. The stimulation of those forces is stochasticly. In particular, for agricultural vehicles these outer conditions exist very often, but in the context of this paper they will not be dealt with.

Investigations on longitudinal forces of agricultural tractors on solid roadways have not been published yet. Literature reports of investigations on this subject carried out in Silsoe [2] in the seventies but results have not been published.

4. MEASURING RESULTS

With the described test rig and the set-up of the measuring instruments, it is possible to get all relevant values in the vertical and longitudinal direction. In this paper only some important values for the longitudinal direction will be discussed.

You can see in equation 1 and fig. 5, that the lever-arm of the rolling friction is important for determining the forces and the moments of a wheel. To determine the lever-arm for all different tyres in every running state the special arrangement of the three load cells for measuring the vertical load is used (fig.7).

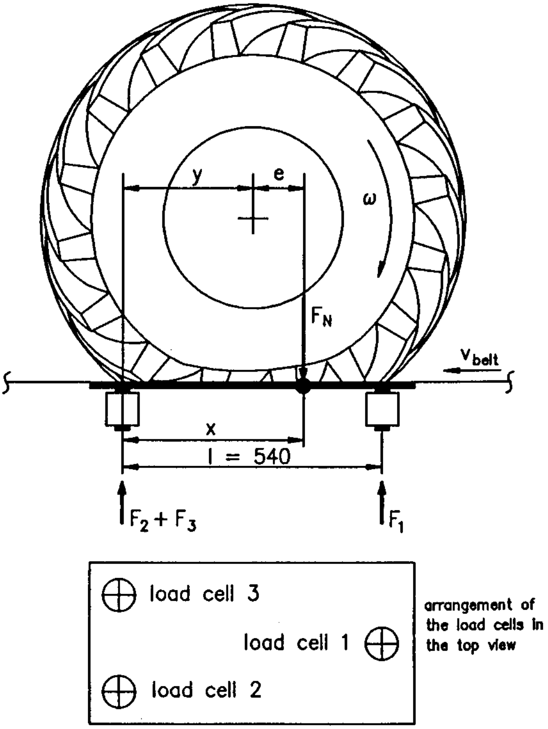
y
e
ω
F_N
v_{belt}
x
l = 540
$F_2 + F_3$
F_1
load cell 3
load cell 1
load cell 2
arrangement of the load cells in the top view

Fig. 7. Measurement of the vertical forces

$$F_N \cdot x = F_x \cdot 540 \qquad (2)$$

The three load cells support statically defined the steel plate where the belt slides over. The front load cell is positioned in the middle, in front of the contact area of the tyre. The two rear load cells are positioned behind the contact area in a right-angle to the rolling direction of the tyre. The front and both rear load cells are calibrated separately and can be recorded separately as well.

The sum of the signals from all three load cells equals the total vertical load. With a simple reflection of the moments by the force of the vertical load F_N and the force at the front load cell F_1 and with the well known distance between the front and the rear load cells the distance x (equation 2) can be determined. The distance between the middle of the axle and the rear load cells can be calculated from geometrical relations. The difference between y and x is the lever-arm of the rolling friction e.

For a free rolling wheel without any acceleration, equation 1 is reduced to

$$F_x = F_R = F_N \cdot \frac{e}{r_{stat}} \qquad (3)$$

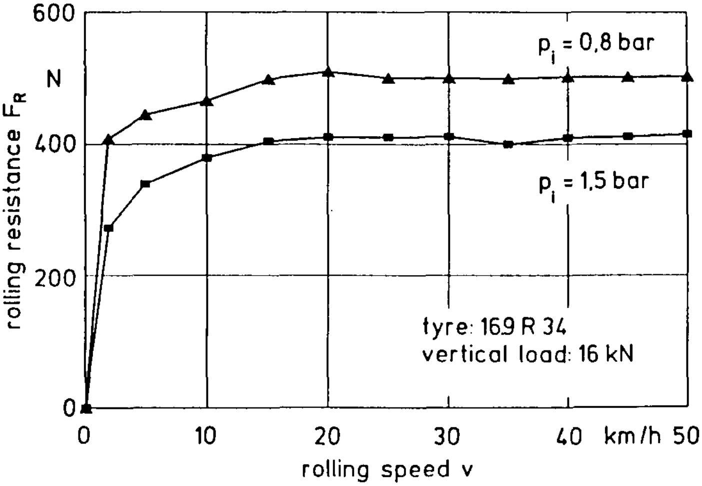

Fig. 8. Rolling resistance of a free rolling tyre

With the principle of measuring explained above and with equation 3, fig. 8 shows the rolling resistance of an agricultural tyre for the speed-range of 0 - 50 km/h. Every point is a mean value of three revolutions of the tyre.

Fig. 9 shows the real course of the rolling resistance over the same three revolutions at a speed of 25 km/h. The rolling resistance depends on the static load radius r_{stat}. At this speed, the axle oscillates up and down in a harmonic motion. The rolling resistance de- and increases with the same frequency.

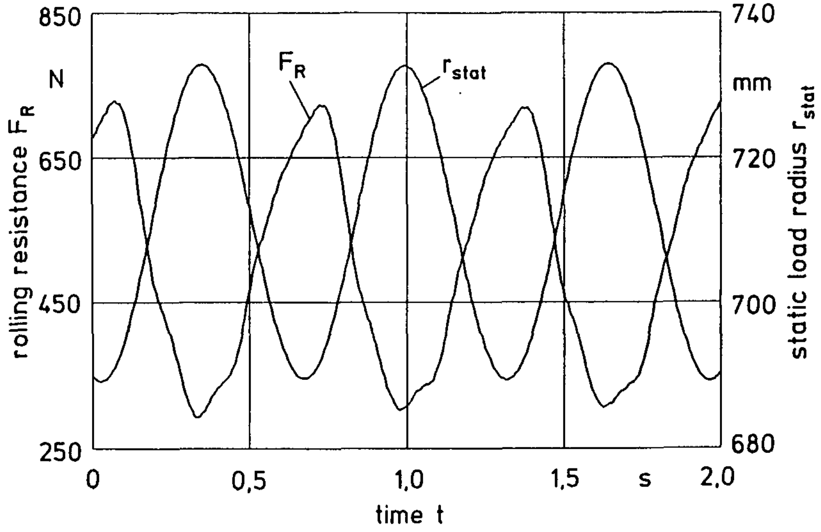

Fig. 9. Rolling resistance depending of the static load radius

The lever-arm of a free rolling tyre at a speed of 25 km/h is about 20 mm (fig. 10). If you decelerate the wheel with the brake (see fig. 10) , the lever-arm decreases to 8 - 10 mm and after releasing the brake the lever-arm goes up to the original value again.

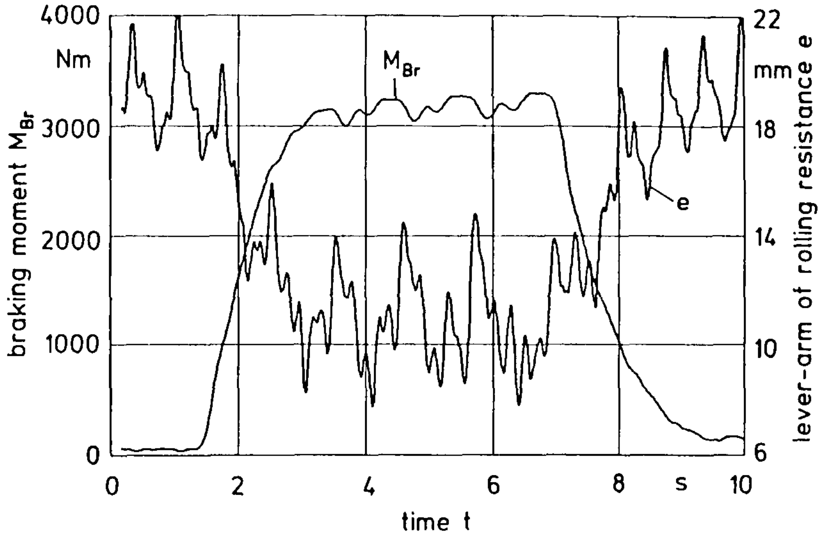

Fig. 10. Braking of a tyre 16.9 R 34, p_i = 1.5 bar, v = 25 km/h

The peaks in the measuring signals for the lever-arm indicate the revolutions of the wheel. Due to the difference in the diameter over the circumference, every revolution the tyre oscillates periodically up and down. With the same period the lever-arm de- and increases.

In equation 1 all moments of a braked wheel are described. With the sensors used at the tyre test stand it is possible to measure all values of this equation. The rotation mass of the wheel, the wheel shaft and the brake disk were determined in tests to 58 kgm^2.

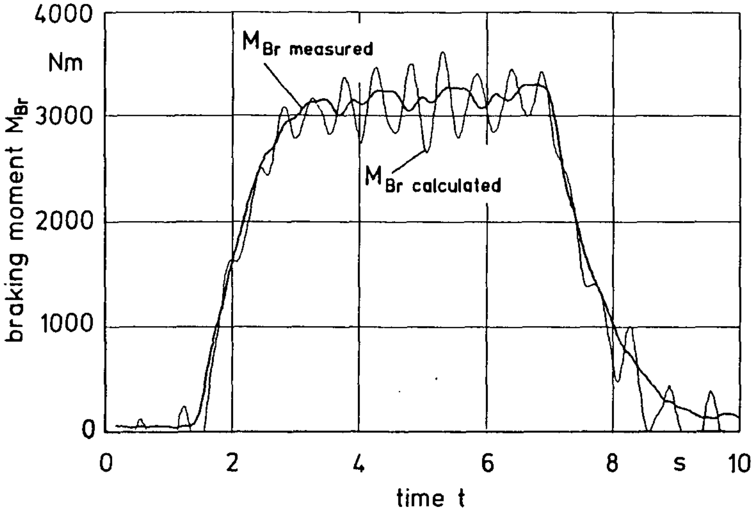

Fig. 11. Measured and calculated braking moment

Fig. 11 shows the shape of the measured braking moment curve and the braking moment curve calculated by the separate values of the other side of the equation. When you take into account that the signals of seven sensors are used to calculate the braking moment, the correspondence between the two curves is quite good.

5. CONCLUSIONS

With the flat-belt tyre test stand and the set-up of measurement instruments it is possible to measure all relevant values in the vertical and longitudinal direction. The lever-arm of the rolling resistance can be determined for all ride conditions and for the tyre-sizes which can be put on the test stand.

With a wheel brake it is possible to act definable longitudinal forces into the contact area.
The spring and damping characteristics can be calculated and used as input data for simulation programmes to predict the ride behaviour of agricultural tractors.

6. REFERENCES

[1] LANGENBECK, B.: Untersuchungen zum Fahrverhalten von Ackerschleppern unter besonderer Berücksichtigung der Reifeneigenschaften. Dissertation VDI-Fortschritt-Berichte
Reihe 14: Landtechnik/Lebensmitteltechnik 1992, Nr.55, S. 1-99.

[2] LINES, J.A.: Predicting the ride vibration of an unsuspended tractor using the dynamic characteristics of rolling tyres.
Journal of Terramechanics, Vol. 29, No. 3, pp. 307-315, 1992.

[3] MITSCHKE, M.: Dynamik der Kraftfahrzeuge, Band A: Antrieb und Bremsung. Springer-Verlag, Berlin, 1984.

[4] PICKEL, P.: Simulation fahrdynamischer Eigenschaften von Traktoren. Dissertation VDI-Fortschritt-Berichte
Reihe 14: Landtechnik/Lebensmitteltechnik 1993, Nr. 65, S. 1-160.

[5] PLESSER, J., KUTZBACH, H.D.: Modelle zur Beschreibung des Schwingungsverhaltens von Ackerschlepperreifen. Vortrag, TAE-Tagung 1992, Proceedings II, S. 437-442, 15.-18.9.1992, Prag

[6] REIMPELL, J.: Fahrwerktechnik 1. Vogel-Verlag, Würzburg, 1982

Session V
Sektion V

Tyre Inflation Pressure Systems

Reifendruckregelanlagen

Effect of Reduced Tire Inflation Pressure on Agricultural Tires

Helmut Schwanghart*
Technical University Munich, Germany
Institute of Agricultural Machinery

ABSTRACT

In the last decades agricultural vehicles and tractors increased in size and weight. These machines are compacting the soil and subsoil in the field severely. This causes environmental damage and decreasing yields. The on-road running tire with high inflation pressure sinks deeply when moving in soft soil. This leads to high rolling resistance, reduced drawbar pull and heavy compaction. With the same load like on road the tire inflation pressure can be reduced by 1 bar if the vehicle moves from the road with reduced speed into the field. This effects greater contact area with decreased pressure, higher drawbar pull, smaller sinkage with smaller rolling resistance and lower soil compaction. Measurements and results of performance are shown.
For using lower tire inflation pressure in the field the so-called Central Tire Inflation (CTI) system in the vehicle is necessary for good performance. The present available CTI systems are reported about.

1. INTRODUCTION

The number of heavy tractors over 3.5 tons permissible total weight have increased considerably in the last years (**Fig. 1**). Today the weight of more than 42 % of all tractors in Germany is over 3.5 tons.

---

* apl. Prof. Dr.-Ing. H. Schwanghart is head of the section Terramechanics in the Institute of Agricultural Machinery, Techn. University Munich/Germany

The tires of these tractors overroll and compact during plowing with 4 bottoms up to 66 % of the total field area and during sowing, cultivating and harvesting between 40 and 50 % respectively. Therefore every spot in the field is overrun by tractor tires at least 2 to 6 times per year. This causes partly the loss of the soil's living space and its transfer function. Animals and microorganisms in the soil are disturbed [1].

By numerous overrunnings the fields can be compacted so heavily, that the yield decreases, because it is very difficult for the roots to penetrate the dense soil layers. This must be counterbalanced by larger energy expense at soil loosening as well as by more fertilizer application.

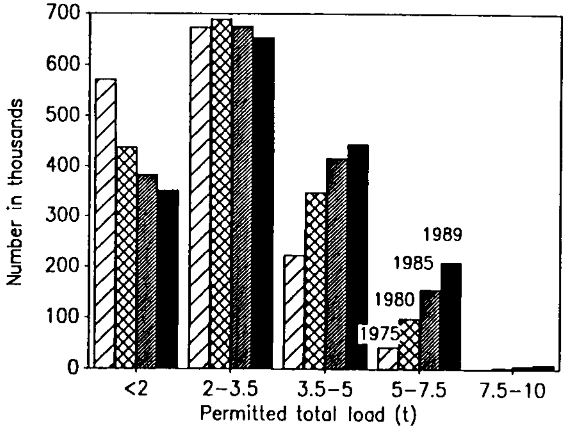

Fig. 1: Amount of tractors in relation of permitted total weight in the years 1975 to 1989.

Furthermore the rainwater can only slowly seek through the condensed ground to the subsoil. That is the reason why in many places investigations are made how far smaller tire inflation pressure with larger contact areas cause smaller rut depths at the surface and less compaction in the subsoil. To change tire inflation pressure in the field, one needs vehicles with so-called central tire inflation (CTI). Such facilities and soil reaction is reported about [2, 3, 4, 5, 6, 7, 8].

2. TERRAMECHANIC RELATIONSHIPS

The tire load capacities, for instance the rated loads, must be observed according to the catalogues for different inflation pressures (Fig. 2). They rise with higher inflation pressure and with decreasing speed. For carrying the same load on the field at a speed of 10 km/h compared to driving on the road with 50 km/h, the inflation pressure of modern tires can be reduced by about 1 bar. On the other hand the low field tire inflation pressure must be increased for the road traffic at the transport of loads from the field to the street (sugar beet). This is only possible if there is a compressor on the tractor.

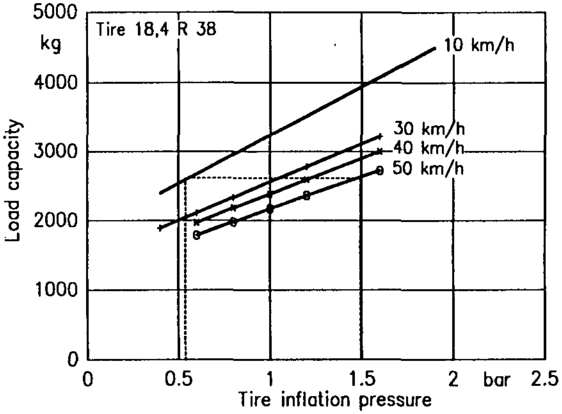

Fig. 2: Load capacity (rated load) of the tire 18,4 R 38 in relation to tire inflation pressure at different speeds.

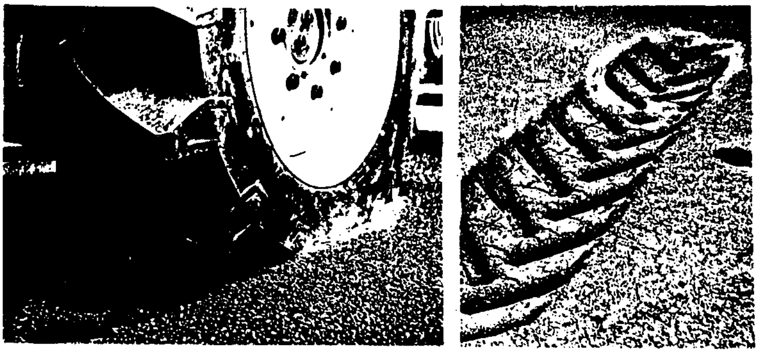

Fig. 3: Rut and marking of the contact area of a tire on soft soil.

Contact areas of agricultural tires were measured in the soil bin of the Institute of Agricultural Machinery, Technical University of Munich. After a short ride the test rig is stopped and the soil surrounding the tire track is powdered with white calcium carbonite (**Fig. 3**). After removing the tire vertically the projection of the line bordering the contact area is drawn on a transparent foil and afterwards the area is determined by a planimeter. Lugs and lug interfaces produced the loaded contact area.

By reduction of inflation pressure of about 1 bar at constant load the contact areas of the tires increase more on hard ground (20 to 35%) than on soft soil (5 to 20%). **Fig. 4** shows the areas of a tire 360/70 R 24 on concrete and in soft soil.

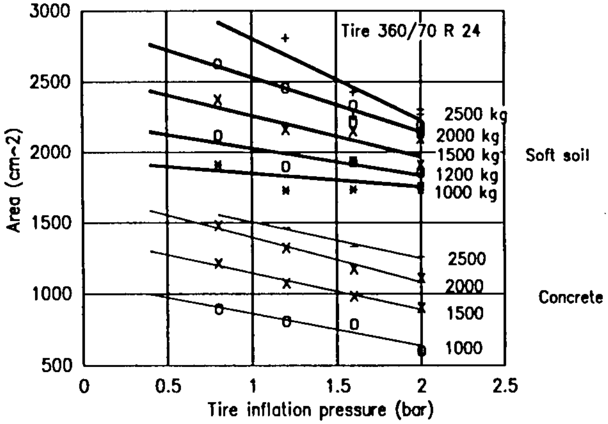

Fig. 4: Measured contact area of the tire 360/70 R 24 in loose soil.

At a rated load of 1200 kg there results an increase of contact area on loose loamy sand of about 16% from 1850 to 2150 cm^2. In this case the road inflation pressure of 1.6 bar is reduced to 0.6 bar field inflation pressure.

There are some models to calculate the mean contact area under a tire, but they are very complicated. With some simplifying assumptions one can calculate the contact area A and the pressure in the contact area p_g under the tire on loose soil [9]. According to **Fig. 5** the length of the contact area is:

$$r^2 = l_1{}^2 + (r - \delta - z)^2$$

$$l_1 = \mathrm{SQR}\,[2 \cdot r \cdot (z + \delta) - (z + \delta)^2]$$

$$l_2 = \mathrm{SQR}\,(2 \cdot r \cdot \delta - \delta^2)$$

$$l = l_1 + l_2 = \mathrm{SQR}\,[D \cdot (z + \delta) - (z + \delta)^2] + \mathrm{SQR}\,(D \cdot \delta - \delta^2) \qquad (1)$$

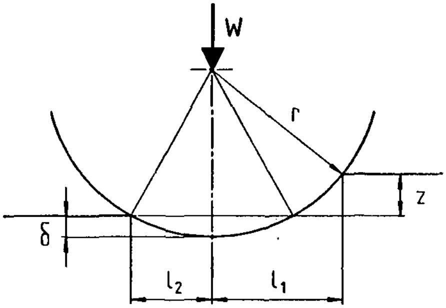

Fig. 5: Geometrical data of a tire on soft soil including tire- and soil deformation.

Assuming that 80% of the total load is supported on the plain part of the contact area with the length $2 \cdot l_2$ the tire deformation can be calculated with the spring rate c_o at an inflation pressure p_i. The ballance will be supported by the length $l_1 - l_2$.

$$\delta = 0.8 \cdot W / c_o \qquad (2)$$

c_o is known by measurements on concrete or it can be determined by the tire volume [11, 8]. By the simplified Bekker-equation the sinkage z results to:

$$p = (k_c/b + k_\phi) \cdot z^n$$

with $$k_c/b + k_\phi = k$$

is $$z = (p/k)^{1/n} \qquad (3)$$

$$p = W/A \qquad (4)$$

$$A = b \cdot l \cdot \beta \qquad (5)$$

According to experiments in the loamy sand the ellipticity coefficient β of the area is approximately 0.75 - 0.80. The value l_w, the percentage rate of the load on the rated load W_{rated} according to the inflation pressure p_i, determines the tread width with the rated tire width b_o:

$$l_w = W/W_{rated} \qquad (6)$$
$$b = b_o + b_1 \cdot l_w \qquad (7)$$

Thereby b_1 becomes the value 3 to 5 (cm/load part in percent). With the given values W, D, b_o, p_i, c_o, k, n, β and W_{rated} the unknown values of l, z, δ, p, A, b and l_w can be expressed by the equations (1) to (7). The shortest way for a solution is to calculate the length l (equation 1) by an iteration.

The mean contact pressure of the tire 13,6/12-28 was determined by this calculation. The measured and calculated values are shown in **Fig. 6** [9]. In spite of great simplifications, the quoted values agree well with the measured ones. **Fig. 7** shows the measured mean contact pressure of different agricultural tires for rated loads at 20 km/h in relation to the tire inflation pressure [10, 11]. The Terra low inflation pressure tire produces as expected the lowest mean pressure in the contact area. The contact pressure rises with size and load capacity of tires. It gets up also with increasing tire inflation pressure. All these contact pressures are in the range of 0.5 to 1.2 bar. According to **Fig. 8**, the larger contact pressures are not caused by tractors, but by combines, trailers and forage wagons with heavy loads [12, 13]. These tires should be investigated urgently. They are of greater importance concerning the soil compaction.

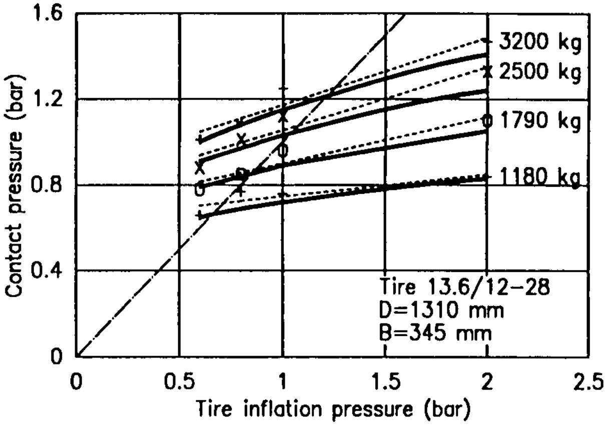

Fig. 6: Contact pressure in relation to tire inflation pressure. (Full line according to calculation, dotted line according to measurement)

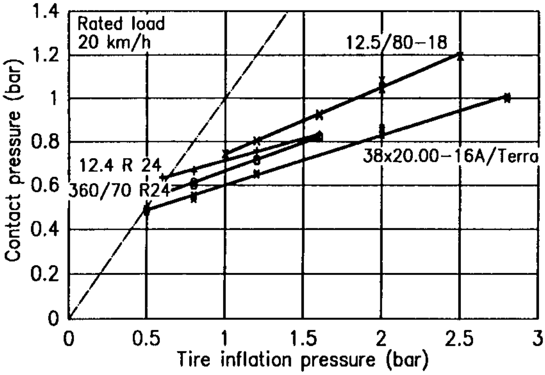

Fig. 7: Contact pressure of some agricultural tires for rated loads at 20 km/h in relation of tire inflation pressure.

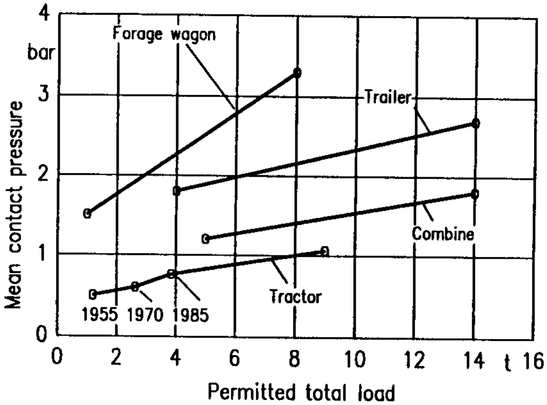

Fig. 8: Mean contact pressure of agricultural vehicles in loose soil at permitted total loads.

For the compaction of the soil in the upper layers the contact pressure is relevant. Smaller contact pressure causes smaller sinkage and less soil damage. For the compaction in deeper layers the total load is of great importance. **Fig. 9** shows the influence of tire inflation pressure of an 18,4 R 38 tire on compaction of a loose loamy sand in different depths. The tire load was 3000 kg. The rut depth was 10 - 12 cm.

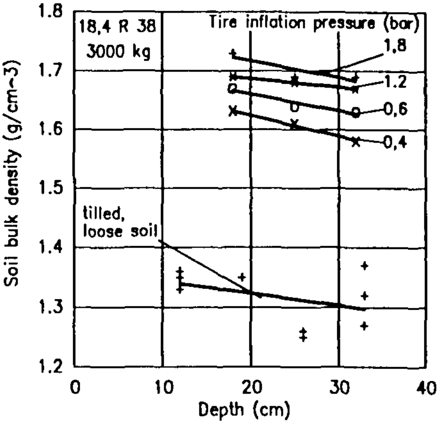

Fig. 9: Soil density in the loose soil after overrolling of a tire 18,4 R 38 with constant load and different inflation pressure.

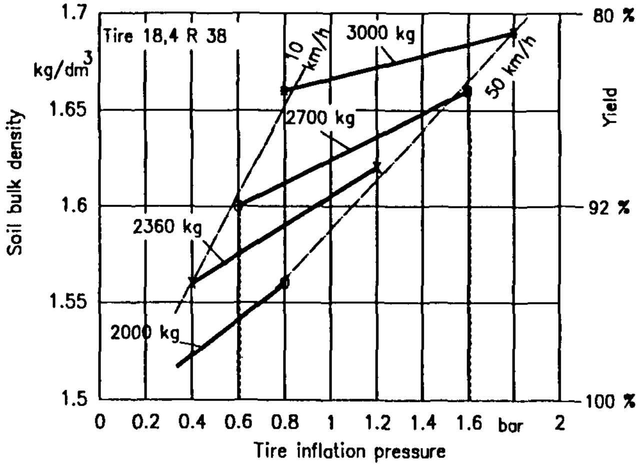

Fig. 10: Soil density in a depth of 25 cm after overrolling of the tire 18,4 R 38 in loose soil and yield in relation of tire inflation pressure with rated loads for different velocities.

The loose soil had a density of about 1.32 kg/dm^3. It increased in 25 cm depth with an inflation pressure of 0.4 bar to 1.6 with 1.8 bar to 1.7 kg/dm^3. That shows a clear relationship of the density on tire inflation pressure. **Fig. 10** shows the soil density after an overrolling by a tire 18,4 R 38 with different loads. With a wheel load of 2700 kg and by the reduction of the inflation pressure from 1.6 bar (road) to 0.6 bar (field) the tire compacts the soil only up to 1.6 kg/dm^3 and not up to 1.65 kg/dm^3. The yield of this loamy sand depends on density and attains its upper limit at a density of 1.5 kg/dm^3 [14]. The corresponding yield is registered in Fig. 10. From this results that with 1.6 bar tire inflation pressure the harvest is reduced to 86% of the maximal attainable yield, with 0.6 bar however to 92% of the maximal attainable yield. This means a yield increase of about 6% with smaller inflation pressure.

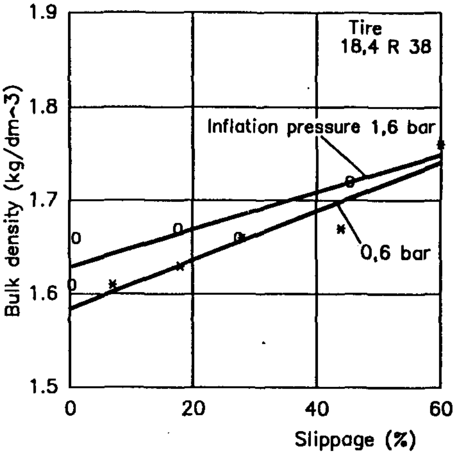

Fig. 11: Soil density after overrolling in relationship of slippage.

With a driving wheel the soil density at a wheel load of 2670 kg increases with rising slippage from aproximately 1.6 kg/dm^3 to 1.75 kg/dm^3 (**Fig. 11**). Also in this case with smaller slippage the lower tire inflation pressure gives a considerable advantage.

The draught, respectively the drawbar pull of the tire increases also with reduced inflation pressure. **Fig. 12** shows an increase of drawbar pull coefficient at 20% slippage from 40% to 50%, that is about 25 %, if the tire pressure is reduced from 1.6 to 0.6 bar. So also the rolling resistance coefficient decreases. For a number of tires the percentage drawbar pull increase in relation to slippage is recorded in **Fig. 13**. With a slippage of 20% a reduction of inflation pressure gives an increase of drawbar pull from about 20% to 40%.

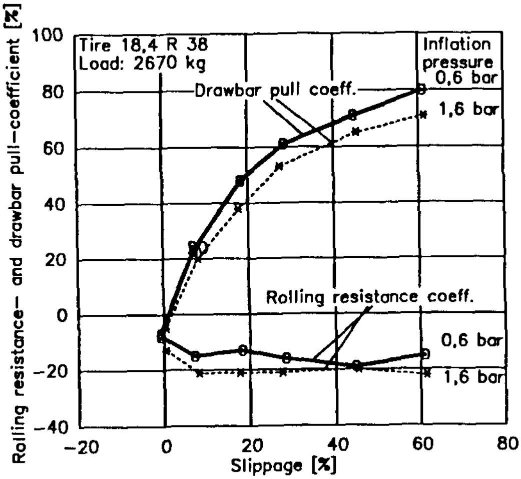

Fig. 12: Drawbar pull- and rolling resistance coefficient in loose soil.

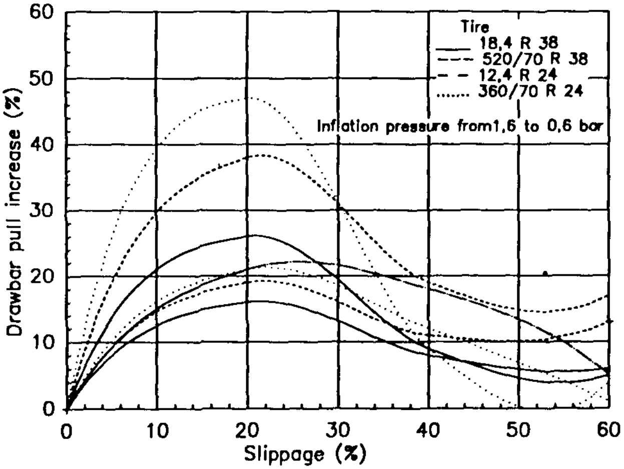

Fig. 13: Drawbar pull increase in percentage in relation to slippage with various tires at different load in soft soil.

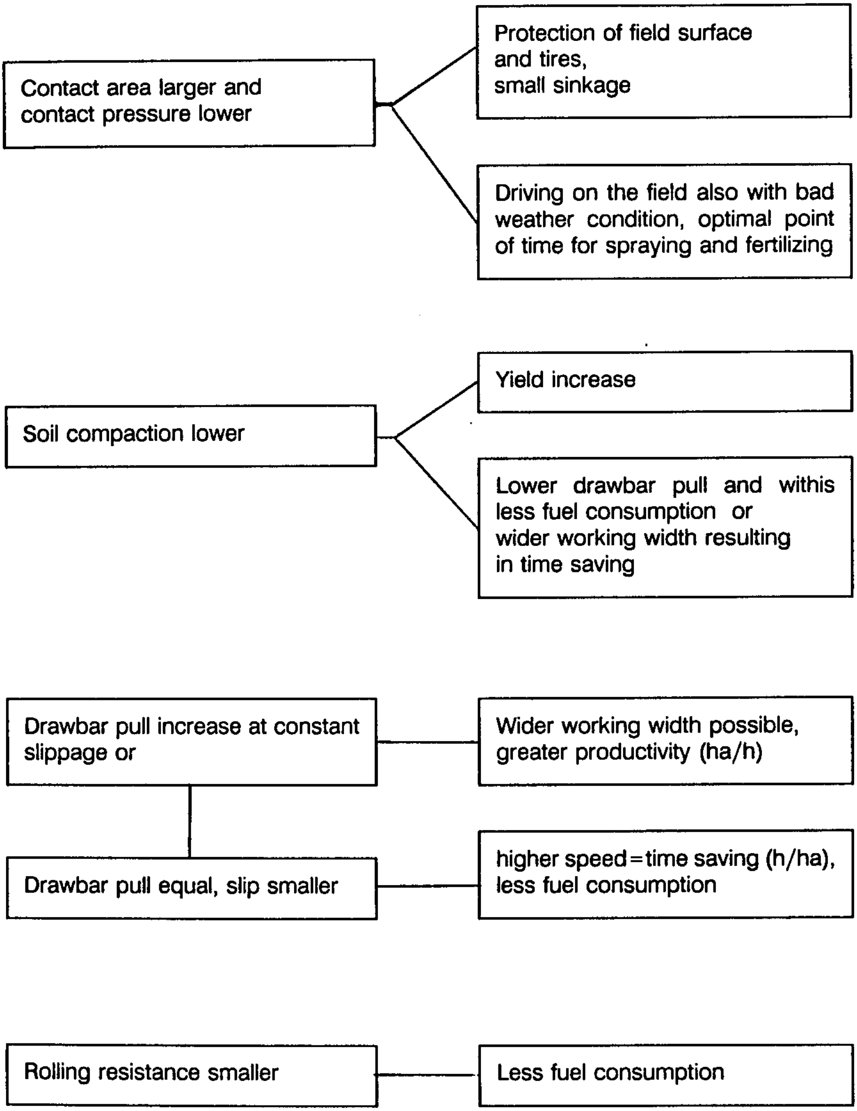
Contact area larger and contact pressure lower
Protection of field surface and tires, small sinkage
Driving on the field also with bad weather condition, optimal point of time for spraying and fertilizing
Soil compaction lower
Yield increase
Lower drawbar pull and withis less fuel consumption or wider working width resulting in time saving
Drawbar pull increase at constant slippage or
Wider working width possible, greater productivity (ha/h)
Drawbar pull equal, slip smaller
higher speed=time saving (h/ha), less fuel consumption
Rolling resistance smaller
Less fuel consumption

Fig. 14: Effect of reduced tire inflation pressure.

3. EFFECTS OF REDUCED TIRE INFLATION PRESSURE ON FIELD OPERATION.

Fig. 14 shows the summarized effect of reduction of tire inflation pressure by about 1 bar for agricultural tires. The lower inflation pressure produces bigger contact areas and therewith less contact pressure. This takes care of the soil and the tires and achieves larger striking power. The smaller compaction increases the yield and supports fuel- and time saving at the following tillage.

The drawbar pull increase results in higher acreage and lower fuel consumption and it saves working hours.

These advantages can only be achieved, if there is a tire control system installed in the tractor. The structure of these systems is briefly described below.

4. STRUCTURE OF CENTRAL TIRE INFLATION PRESSURE SYSTEMS

A central tire inflation consists of following parts [15]:

- a compressor with/without pneumatic accumulator,
- air tubes to valves with/without rotating transfer element
- measurement of pressure with recording device
- control of the pressure increase respectively reduction

When a compressor in the vehicle is available, one can use it also for tire inflating. When an installation of a new compressor is necessary, it can be driven by the crankshaft, by the PTO or by the hydraulic equipment. Factory mounted compressors require no additional costs, but need long time for inflation due to their small capacity. They need 2 to 6 minutes for inflating 4 tractor tires. A time less than 2 minutes would be desirable. The tires are filled up by air which is pumped from the compressor through unflexible tubes into the tire. Thereby the air must go from the stationary part of the tractor to the rotating wheel. There are different possibilities:

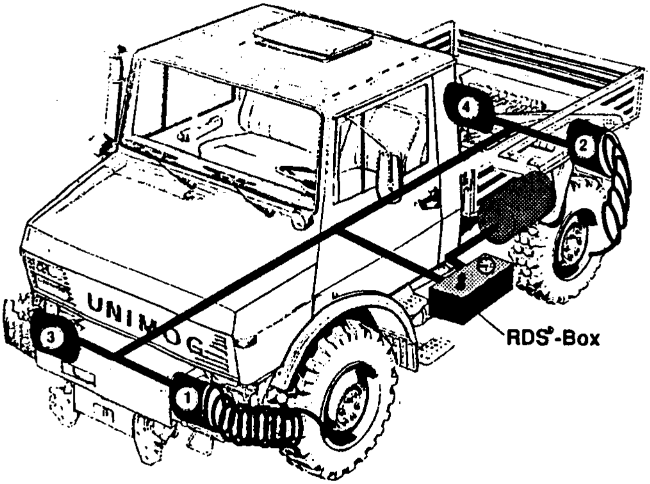

Fig. 15: Changing of the tire inflation pressure in a stationary vehicle. RDS-Box with 4 tubes [16].

a.) The air reaches the air-valves through flexible tubes mounted by hand while vehicle is stopped (**Fig. 15**).

b.) For filling up the tires during driving a rigid tube leads the air over the mudguard to the axle center at the outlying part of the wheel. Then the air goes through a rotational transfer element (saleable finished product) from the stationary tube to the valve on the rotating wheel.

c.) Also for filling up during driving, but from the inside of the wheel, there are two versions of air tranfer:

The first version is used for replacing equipment. A fixed tube leads from the cabine to the axle shaft to an individually designed part of transfer between fixed axle shaft and rotating axle. This consists of two concentric cylindric parts, one connected with the axle shaft (stator) and another connected with the wheel (rotor). The air is fed from a canal in the stationary part over a slot tightened by radial- and axial packings to the turning wheel.

With newly designed and produced vehicles the air is fed from boreholes in the fixed housing of axle bearings between the wheel bearings into a canal of rotation, which is packed up by seals. From there the air runs through several boreholes in the rotating hub to the felloe and to the valve.

d.) At reduction gear axles the air comes through a fixed tube to the inside of the axle housing. Using a rotational transfer element (finished product) the air goes first in the axle and furthermore through an axial bore hole in the center of the shaft to the tire.

The best way for measurement is to record the pressure by a manometer in the pipe connected with the tire, shortly after filling up or discharge. It is more difficult, to measure the tire inflation pressure with a sensor directly on tire valve and to transmit it by of a transfer ring or inductive equipment to the vehicle cab.
There are two groupes of pressure control systems to be distinguished: Manual and automatic control. Using manual control the operator starts the procedure of changing inflation pressure and finishes it after the desired pressure has been achieved.
In automatic control the pressure increase or decrease is actuated by a pressure preselection. Then the system adjustes the pressure automatically.

5. AVAILABLE TYPES OF AGRICULTURAL CENTRAL TIRE INFLATION SYSTEMS.

RDS-Box of the company Pösges and Tigges (41468 Neuss): Can be installed in all tractors for increasing or reducing the tire inflation pressure after stopping the vehicle. The driver gets out, selects the desired pressure on the box and connects each tire with a flexible tube. A compressor (390 l/min) needs 2 minutes to inflate 4 tires 16,9 R 24 from 1.6 to 2.4 bar. Price: ca. 2500.- DM.
Nowadays this equipment can be bought as an implement called Air box. In this case the small control support is mounted on a well accessible position, the bigger pneumatic unit can be mounted elsewhere in the vehicle.

Another innovation of the same company is the Airmaster. After stopping the tractor the driver connects the accumulator of the pneumatic brake with the single wheels by a tube of 4m length with built-in manometer. The normal air valves of the 4 wheels are replaced by bigger ones to accelerate in- and deflation (Price 400.-DM).

Agropneu is also manufactured by the company Pösges and Tigges (41468 Neuss). Both new and elder tractors can be equipped with this implement. The equipment works during the ride too.
The transfer of compressed air from fixed axle shaft to rotating axle takes place in an individually designed part between axle house and hub on the inside of the wheel. The system is manually controlled by the driver, whereas the actual pressure is permanently indicated. When the nominal pressure is attained, the driver has to switch off. With a compressor of 200 l/min the equipment needs 5.5 minutes to inflate 2 tires 18,4 R 38 from 0.8 to 1.6 bar (Price about 6000.- DM.)

Tirecontrol of Mercedes Benz (70302 Stuttgart) is designed for the Unimog. The transfer of the compressed air from the fixed to the rotating part is inserted in the axle bearing house and works in the stand and during the ride. The driver selects pressure increase or decrease. The equipment switches off, when all the 4 tires have an inflation pressure of 1.6 respectively 4.1 bar. With the Unimog compressor (290 l/min) all the 4 tires of the Unimog are filled in about 4.8 minutes from 1.6 to 2.5 bar. The price is about 6000.- DM.

Terragator of Kurstjens (Grubbenvorst/Netherlands). The changing of tire inflation pressure acts on the tractor rear axle and on various trailer axles during the ride. The transfer of the compressed air via mudguard to the outside axle center is manually controlled by the tractor driver. An additional high capacity compressor in the range of 867 to 1200 l/min needs 8-10 minutes to inflate 6 tires 20,5 R 24 from 1 to 4 bar. Price 15-20000 DM.

Equipments made by farmers themselves:
a) with additional compressor and air accumulator, transfer part from fixed to rotating outside on the wheel center. Price of material for 4 wheels 1200.-DM.
b) during the ride the air is led from an available compressor by a trans-

fer part from fixed to rotating on the reduction gear axle to the wheel valve. Price of material for 3 axles about 5000.-DM.

c) during the ride the air is led from 5 accumulators (every accumulator contents 90 l) upon the tractor roof via tubes outside of the mudguards and via a rotational transfer element on the axle center to the valve. In only 20 seconds the pressure of 2 tires 20,8-38 is increased from 0.6 to 1.4 bar. Total costs about 4000.-DM.

6. SUMMARY

The load capacity of agricultural tires rises with decreasing speed and increasing inflation pressure. At constant load and with lower speed on the field the tire inflation pressure may be reduced by about 1 bar in the most cases. This enables soil protecting during operation on the field. Moreover the contact area rises with decreasing contact pressure. The soil compaction becomes less and the drawbar pull increases, while the rolling resistance is reduced.

The resulting advantages like soil protection, increase of field performance, yield increase, reduced fuel consumption and economy with working hours are shown. The necessary central tire inflation systems are described. The prospect of the presently obtainable equipments is shown.

7. REFERENCES

[1] Schwanghart, H. und R. Hedderich: Reifenluftdruckverstellanlagen. Landtechnik 47 (1992) H. 7/8, S. 341-344.

[2] Brenndörfer, M.: Variable Luftdruckeinstellung - eine echte Alternative zum Niederquerschnittreifen. Landtechnik 42 (1987) H. 10, S.408-409.

[3] Neunaber, M.: Richtig ballastiert - mindestens 20 % mehr Zugkraft. Profi 3 (1991) H. 12, S. 84-88.

[4] Renius, K.TH.: Traktoren. Landtechnik 47 (1992) H. 1/2, S. 12-15.

[5] Theißen, G.: Luft rein - Luft raus. Profi 2 (1990) H. 1, S. 42-45.

[6] -,-: Neues Reifendruck-Regelsystem. Profi 3 (1991) H. 11, S. 122.

[7] -,-: Variable Luftdruckverstellung. Landtechnik 47 (1992) H. 3, S. 149.

[8] Schwanghart H. u. R. Hedderich: Reifenluftdruckverstellung an Fahrzeugen. Landtechnik 47 (1992) H. 1/2, S. 57.

[9] Schwanghart, H.: Measurement of contact area, contact pressure and compaction under tires in soft soil. Proceed. 10th Intern. Conf. ISTVS Kobe/Japan 1 (1990), S. 193-204.

[10] Schwanghart, H.: Bodendruck und Verdichtung unter landwirtschaftlichen Reifen. Proceed. 5th Europ. Conf. ISTVS Budapest (1991), S. 163-170.

[11] Schwanghart, H.: Measurement of contact area, contact pressure and compaction under tires in soft soil. J. of Terramechanics 28 (1991) H. 4, S. 309-318.

[12] Schwanghart, H.: Bodenverdichtung unter einem rollenden Rad. VDI-MEG Kolloquium "Reifen landwirtschaftlicher Fahrzeuge", München (1989) H. 7, S. 129-137.

[13] Schwanghart, H.: Soil compaction under a rolling tire. Proc. 4th Europ. Conf., Int. Soc. Terrain Vehicle Syst., Wageningen (1989) Vol. 1, S. 179-186.

[14] Petelkau, H.: Ertragliche Auswirkungen technologischer Schadverdichtungen der Ackerkrume. Agrartechnik 41 (1991) H. 2, S. 54-57.

[15] Schwanghart, H. und R. Hedderich: Reifenluftdruckverstellanlagen, Auswirkungen und technischer Stand. BML-Arbeitstagung (Göttingen), KTBL-Arbeitspapier 167 (1992), S. 29-34.

[16] -,-: Produktinformation Pösges & Tigges, Reifendruckregelsystem RDS-Box.

Design and Performance of Central Tire Inflation Systems

H.–P. Schlechter, Ing. (grad)
Proving Ground of the German Armed Forces, Trier

Abstract

The following presentation tries to briefly illustrate the influence of tire pressure reduction on the mobility of wheeled vehicles on the basis of measurement and calculation results.

Significant characteristics and the differences of various central tire inflation systems installed in series production vehicles and prototypes are demonstrated.

Deflation and inflation times of regulation devices serve as performance characteristics for a system comparison.

1. Introduction

It is well-known that one possibility to enhance the mobility on soils with limited load-carrying capacity is the reduction of the tire pressure. This measure helps to increase the transferable tractive force. This is due to the enlargement of the tire tread area, an improved adaptation of the tire footprint to the soil, an enlargement of the effective tire diameter and thus a reduction of rolling resistance.

The great influence of tire pressure on the transferable tractive force was confirmed by measuring results (figure 1). A tire pressure reduction from 3.5 bar to 2,o bar resulted almost in a duplication of the tractive force (net tractive force).

As a reference of how critical the traficability of the soil was during measuring, it may be noted that the vehicle operating on soil with a high friction coefficient and high load-carrying capacity reaches approx. 1oo kN at a speed of approx. 1o km/h.
Calculations also show the great importance of tire pressure (figure 2).

A tire pressure of 4.3 bar may possibly permit a vehicle to travel only 65 % of a selected and measured terrain. If the tire pressure is reduced to 1.3 bar the same vehicle may travel approx. 9o % of the same terrain under the same marginal conditions.

Measurements on agriculturally used soils consisting of sand and clay with different states of preparation show that, besides the drive system, the tire pressure plays a decisive role (figure 3). On soils with low load-carrying capacity, e.g. dune sand, the propulsion formula and tire pressure are even more important factors.

As a result of this experience the wheeled vehicles of the former Warsaw-Pact states, and thus the vehicles of the former East German Army NVA, were almost entirely equipped with central tire inflation systems.

2. Configuration Examples of Central Tire Inflation Systems

To date, the Federal Armed Forces do not have a fielded wheeled vehicle equipped with a central tire inflation system. Inflation/deflation of tires is only possible with the vehicle stopped by using the on-board equipment (tire inflation hose, screw driver, tire pressure gauge) (see figure 4). Every cross-country vehicle, however, is equipped with an air supply valve. A simple, trouble-free and cost effective method to change the tire pressure, which is not often used, since it is cumbersome to handle and since pressure changes are not required due to a very dense network of roads in the Federal Republic of Germany.

A relatively simple central tire inflation system is installed in the light Russian truck type GAZ 66 (Gorki Automobile Factory) (figure 5).

The device can be controlled by means of a turning handle in the vehicle cab, and it can be used with the vehicle moving or stationary. The pressure can be checked on a manometer in the dashboard.

The turning handle controls a pressure control valve which can be engaged in three positions.
The pressure control valve permits connecting the air compressor and the tires via an annular chamber seal and a shutoff valve, and the tire with the enviroment by an integratet outlet.

The pressure control valve (figure 6) is a piston valve with three air chambers, which are separated by seals

- from the compressed air pressure system
- to the tire
- to the ambient air

In order to change the tire pressure, the piston with the constriction is brought into a position, where the air between sealing ring and constriction can either flow from the compressed air system to the tire or from the tire to the ambient air.

Piston valves of this type or of similar design are used in all non-armored trucks of Soviet production. Operation of the piston valves is carried out with a turning handle, or very often with a three position slide (figure 7) or with a pull handle (fig. 8), as is the case in the KRAZ 255 B. In this vehicle the pressure control valve is connected with a pressure limit valve so that a minimum pressure is preserved in the remaining compressed-air system (air brake).

Figure 9 shows, as an example, the pressure control valve of the MAZ 543, the design of which is different from other pressure control valves described before.

In older vehicles and the armored wheeled vehicles of the former Warsaw Pact states the pressure control valves are often followed by junction blocks (fig. 1o). The junction blocks represent a combination of cutoff valves allowing to separate individual wheels/axles from the pressure regulating device with open wheel cutoff valves from the vehicle cab, without stopping the vehicle to open or shut the cutoff valves of the wheel.

This advantage, however, requires some additional technical equipment. This additional equipment is shown in figure 11, representing the truck ZIL 157 which was built with a junction block until 1963 (top) and later without junction block (bottom).

The older vehicles by manufacturer Tatra were also equipped with junction blocks. In the Tatra 813 (8x8) the pressure control valve is directly screwed to the junction block, and the bearing of the operating handle is also located in the junction block housing. As is shown in figure 12, the driver can connect to and disconnect from the tire pressure regulation device individual wheels while the vehicle is moving.

Deflation or inflation of tires of the armored personnel carrier SPW 4o P2 is carried out semi-automatically via a pressure reducer valve in the fighting compartment. This reducer valve is positioned between the emergency line and the junction block (figure 13).

The pressure reducer valve (fig. 14) is made up of two housing halves which are separated by a membrane with a valve seat. In the lower part of the casing there is a solid valve seat. Both valve seats are connected by a double valve. To increase the tire pressure the spring (5) is preloaded with the hand wheel (1) so that the membrane and thus the double valve moves down. This movement opens a connection from the air reservoir to the tires. Pressure balance between spring and tire pressure causes the membrane, and thus the double valve, to return to the original position, thus interrupting the link from the reservoir to the tires.

In order to reduce the tire pressure the spring (5) is released so that the membrane is moved up due to the air pressure in the lower casing half, thus uncovering the valve seat. Now the air can escape from the tires via the valve seat in the membrane and through connection A in the upper part of the housing.

Pressure balance causes the membrane to return to the original position and to rest again on the double valve with the valve seat. This is a simple and sufficiently accurate semi-automatic regulation device for practical use.

The armored personnel carrier SPW 7o is equipped with a dump valve (fig. 15) in addition to the pressure reducer valve. This dump valve is directly connected to the air duct in the junction block, so that operation of the dump valve will cause the pressure reducer valve to the bypassed and the drain time to be reduced. When operating the dump valve the pressure has to be monitored on the manometer in the vehicle cab during the deflation process, which is not necessary when the pressure reducer valve is used.
Change of the tire pressure of truck W5o manufactured by the IFA automobile works, Ludwigsfelde, is carried out using four mechanical valves in the vehicle cab, which are operated with toggle handles (fig. 16). The tire pressure is monitored on a double-manometer in the dashboard.

Inflation and deflation of tires is carried out per axle (front and rear axle wheels have different tire pressures). For inflation the central valves are opened so that the air flows from the compressor to the wheels of the pertinent axle. For deflation the external valves are opened so that the air is bled from the tires of the pertinent axle through the valve block. This device is a simple manually controlled mechanism with acceptable bleed time.

The IFA L6o, the successor truck of the IFA W5o, has two rocker switches with indicator lights for the operation of the central tire inflation system and also a double manometer in the dashboard to monitor the tire pressure (fig. 17). The rocker switches control solenoid valves opening a connection per axle from the pressure reservoir to the tires or from the tires to the ambient air.

Regarding the bleed time performance the device installed in the L6o is comparable to the device in the IFA W5o. A prototype of an amphibious engineer reconnaissance vehicle (APE) contained a time controlled system (fig. 18).

The pressure control valve was manually operated and had three latch-in positions, where each position corresponded to a tire pressure level. When operating the pressure control valve, a 3/2 directional solenoid valve and a timing element were electrically triggered.

The 3/2 directional valves triggered relay valves at the axles which, according to their preselection, opened a line from the reservoir to the tires or from the tires to the 3/2 dirctional valve. After elapse of the preselected time, the inflation or deflation process was terminated by the timing element which triggered the directional valve. The central tire inflation system was designed as a single line device. Regarding reliability, accuracy and performance is was in no way convincing.

Another APE prototype also contained a single-line tire inflation system which was simply controlled by the driver (fig. 19).

After opening of the mechanical wheel cutoff valve the driver could change the tire pressure per axle. By means of a rotary switch the driver could operate solenoid valves, which on their part affected relay valves (relay valves were joined per axle in on valve block).

The relay valves either opened the connection from the reservoir to the tires of one axle or from the tires to the bleed valve in the valve blocks. The manometers in the operation panel showed the pressure per axle dynamically. After the inflation or deflation process the driver had to turn the rotary switch to "test" position to check the static air pressure and carry out adjustments, if necessary.

The bleed time performance of this device can be considered as just about sufficient. A central tire inflation system of this design is offered by Mercedes Benz for their truck model LA 1117.

The M3 amphibian about to be fielded in the Federal Armed Forces is equipped with a combined pressure and time controlled regulation device by EWK/WABCO (fig. 2o). A characteristic feature of this device is the double-line design. On line serves for filling the tires and the other for triggering the valves. The bleed valves of this system are located on the wheels so that a short bleed time is achieved. The fact that two rotary couplings are required is a disadvantage of this device since they need considerable space per wheel.

Another type of central tire inflation system is the double line device (fig. 21) presented by the company of Sondertechnik (Linz). Here, the bleed valves are also located on the wheels. A particular feature is a pressure sensor for each wheel. Transfer of sensor measuring data is carried out inductively via a moving coil. The advantage of this configuration lies in the fact that the tire pressure is continuously monitored and the data are available to the on-board computer so that a separate measuring process is not required prior to a pressure change. The drawback lies in the space required to install the pressure sensor, coil and cables on the wheel.

The central tire inflation system of the new 5 t truck M 925 (fig. 22) for the US forces is designed as a single line device. It is a construction of Steyr-Antriebstechnik. A special feature of this design, which is also pressure and time controlled, is a quick-release valve per axle. During normal travel the wheel valves are closed and the air tubes are vented through a valve at the pneumatic control unit (fig. 23).

In order to check the tire pressure the tire valve is opened with a pressure impulse via the dump valve at the axle, so that the tire pressure is present at the pressure sensor within the pneumatic control unit.

For inflation, the tire valve is opened with a pressure impulse (fig. 24) as is for measuring. Subsequently, the tire is filled through a solenoid valve over a time based on the measured tire pressure and the available reservoir pressure.

To vent the tire the tire valve is opened via a pressure impulse, as is used for measuring. By means of a sudden venting of the air tube to the quick release valve at the axle this valve is placed in a position where the air of the tire can flow to the ambient air through the valve. After another pressure impulse the venting process is terminated after a specified time.

In an experimental wheeled vehicle (8x8) by Mercedes Benz, developed and built within the scope of a study, the central tire inflation system by Labinal (fig. 25) was installed. The device is made up of an operating and display unit in the vehicle cab, a central control unit with solenoid valves and pressure sensors, a computer and the tire valves. During normal travel the air tube to the tire valves is vented through a solenoid valve in the central control unit (fig. 26). To measure the tire pressure the tire valve is opened with a high pressure impulse. The solenoid valve for venting of the feeding tube to the tire valve is closed so that the tire pressure is present at the sensor in the central control unit.

To vent the tires, the tire valve is triggered with a low pressure impulse and opens to the outside (fig. 27). For inflation, the tire valve is triggered with a high pressure impulse, as is for measuring; subsequently the solenoid valve to the pressure reservoir opens and the tire is inflated.

The fill and bleed times are calculated for each tire on the basis of the existing tire pressure data and the reservoir pressure, so that during the first bleeding or filling process approx. 8o to 9o % of the desired value can be obtained (fig. 28). Assuming that for cross-country travel the tire pressure is normally reduced (here: 4,o bar), the minimum pressure (here: 1,1 bar), can almost be obtained in less than 6o seconds, if required. The subsequent measuring and control procudures of the device serve only to adjust the pressure to the precise value.

3. Performance of Central Tire Inflation System

As a rule, the bleed times should be so short that the time from the detection of a difficult topography to the moment the vehicle reaches that terrain is sufficient to achieve the required low tire pressure without stopping the vehicle. Based on this requirement, the bleed times shall range from 1 to 2 minutes, the desired value being less than 1 minute. Vehicles where the quick release valve is installed at the wheels are capable of reaching these bleed time values (fig. 29).

The fill times are less important, but with regard to the velocity requirements of the vehicle they should not exceed 1o minutes when the vehicle is moving. The enclosed table gives the vehicle related fill and bleed times. The evaluation performance should as well consider the air volume to be handled by the systems, as is shown in the following figure (fig. 3o).

To complete the presentation the last figure (fig. 31) correlates the sizes of the tires, the bleed volumes and, as far as they are known, the bleed and fill times, pressures for road travel and minimum pressure values for different vehicles as well as the specific bleed and fill time values.

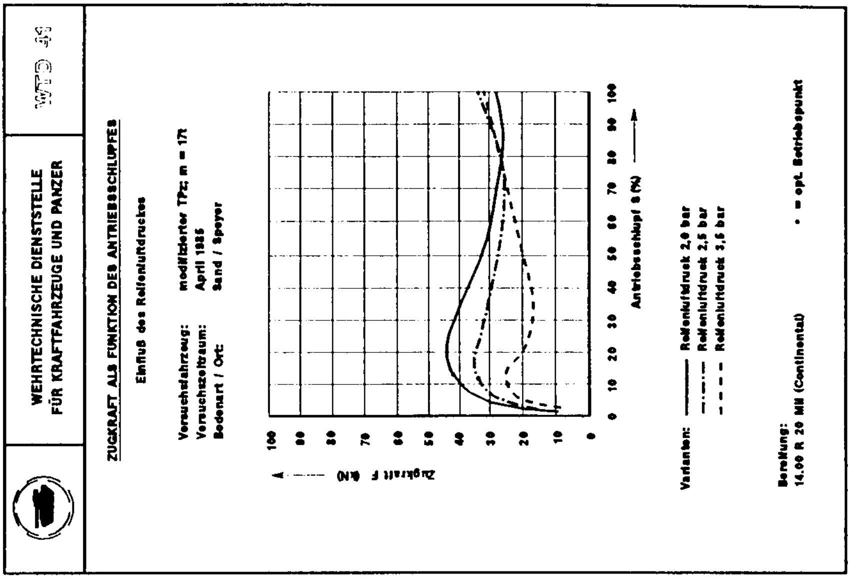

Abb.: 01

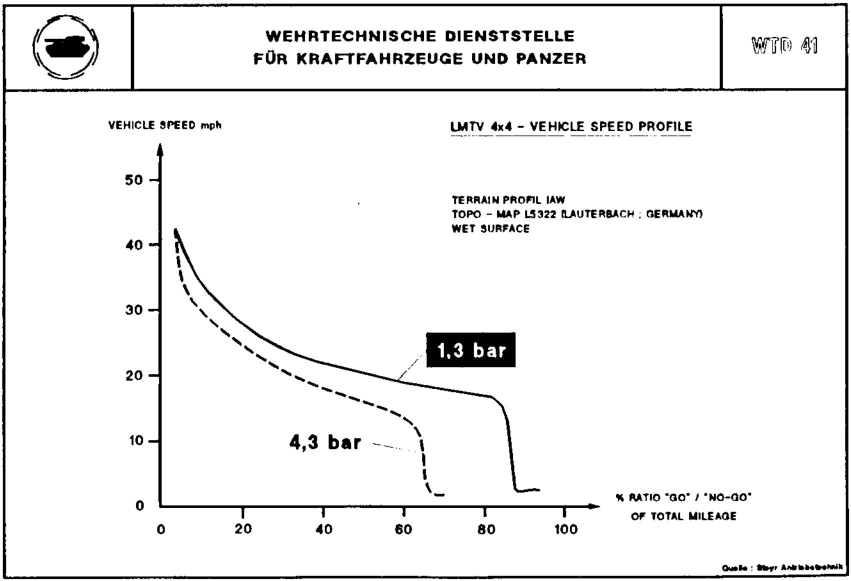

Quelle : Steyr Antriebstechnik

Abb.: 02

WEHRTECHNISCHE DIENSTSTELLE
FÜR KRAFTFAHRZEUGE UND PANZER
WTD 41

Einflußgröße		ermittelte Zugkraft ($F_{z\ opt.}$)			
		$\bar{x}$ Sand / Lehm		Dünensand	
		kN	%	kN	%
Reifengröße	13.00 R 20 XL	63	93 ↓	-	-
	14.00 R 20 Mil	62	91	32	66 ↓
	14.00 R 20 XL	58	85	-	-
	16.00 R 20 XL	68	100	48	100
Profilhöhe	0 %	54	92 ↓	44	100 ↑
	30 %	55	93	39	89
	60 %	55	93	33	75
	100 %	59	100	31	73
Antriebsformel	AF 1 (6x6)	63	100 ↑	32	100 ↑
	AF 4 (4x4)	43	68	20	63
	AF 3 (6x4)	35	57	16	50
Reifenluftdruck	2,0 bar	72	100 ↑	43	100 ↑
	2,5 bar	66	92	33	77
	3,5 bar	63	88	24	56
	4,5 bar	60	83	-	-

Abb.: 03

WEHRTECHNISCHE DIENSTSTELLE
FÜR KRAFTFAHRZEUGE UND PANZER
WTD 41

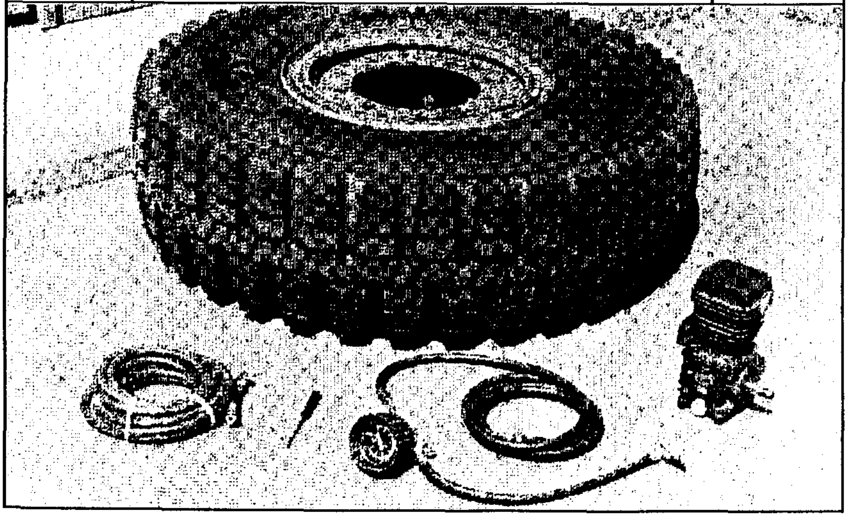

Abb.: 04

WEHRTECHNISCHE DIENSTSTELLE
FÜR KRAFTFAHRZEUGE UND PANZER

WTD 41

Reifendruckregelanlage GAZ 66

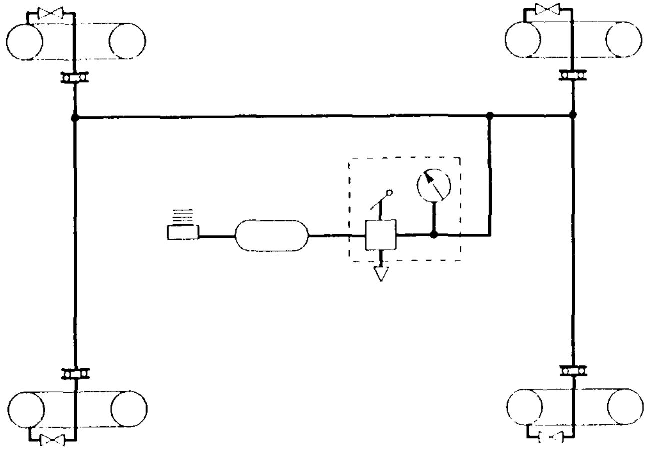

Abb.: 05

WEHRTECHNISCHE DIENSTSTELLE
FÜR KRAFTFAHRZEUGE UND PANZER

WTD 41

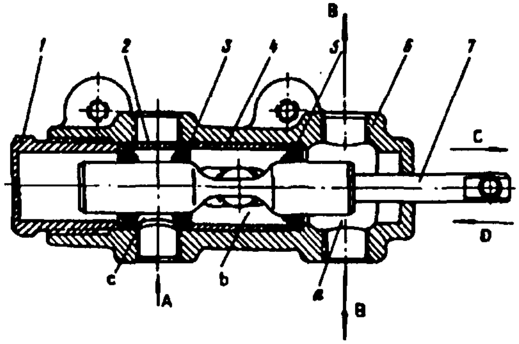

1 - Deckel; 2, 4 - Abstandbuchse; 3 - Führungsscheibe; 5 - Dichtmanschette; 6 - Gehäuse; 7 - Schieber; A - von der Druckluftanlage; B - zur Außenluft; C - Ablassen der Luft; D - Aufpumpen; a, b, c - Räume

BAZ 5937 / 5939	Drucksteuerventil

Abb.: 06

WEHRTECHNISCHE DIENSTSTELLE
FÜR KRAFTFAHRZEUGE UND PANZER

WTD 41

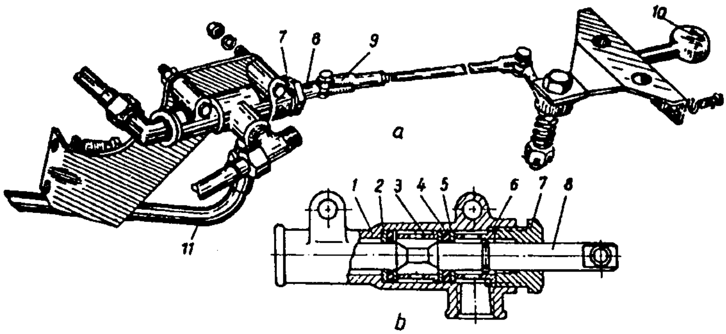
1
2
3
4
5
6
7
8
9
10
11
a
b

Drucksteuerventil der Reifendruckregelanlage

1 — Ventilgehäuse; 2 — Abstandring des Dichtringes; 3 — Ventilbuchse; 4 — Dichtring; 5 — Lagerscheibe; 6 — Sicherungsring; 7 — Kolbenführung; 8 — Kolben; 9 — Stellgabel; 10 — Ventilbetätigungshebel; 11 — Luftableitungsrohr

Abb.: 07

WEHRTECHNISCHE DIENSTSTELLE
FÜR KRAFTFAHRZEUGE UND PANZER

WTD 41

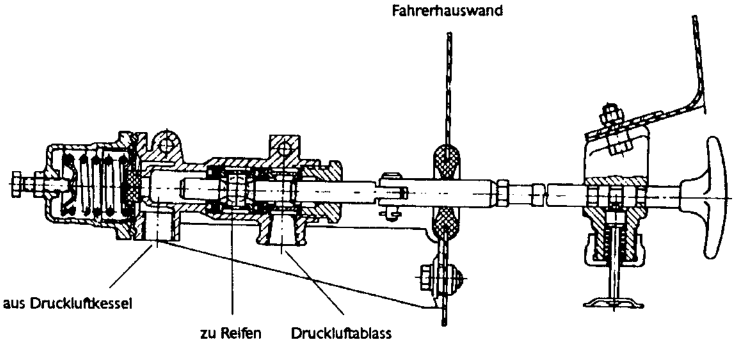
Fahrerhauswand
aus Druckluftkessel
zu Reifen
Druckluftablass

KrAZ 255 B	**Drucksteuerventil**

Abb.: 08

WEHRTECHNISCHE DIENSTSTELLE
FÜR KRAFTFAHRZEUGE UND PANZER

WTD 41

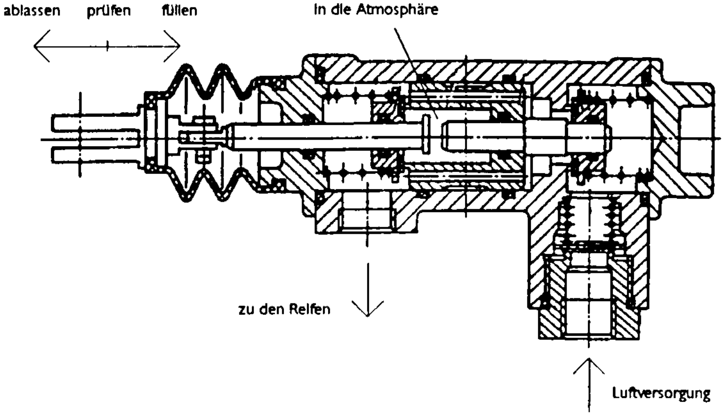
ablassen
prüfen
füllen
In die Atmosphäre
zu den Reifen
Luftversorgung

MAZ 543 | **Drucksteuerventil**

Abb.: 09

WEHRTECHNISCHE DIENSTSTELLE
FÜR KRAFTFAHRZEUGE UND PANZER

WTD 41

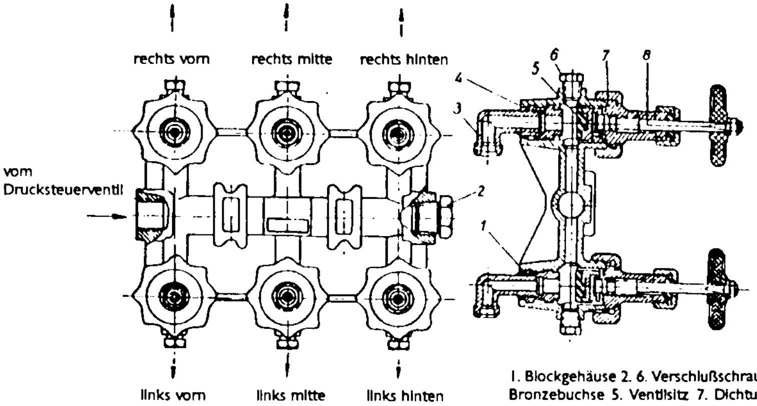
rechts vorn
rechts mitte
rechts hinten
vom
Drucksteuerventil
links vorn
links mitte
links hinten
1
2
3
4
5
6
7
8

1. Blockgehäuse 2. 6. Verschlußschrauben 4. Bronzebuchse 5. Ventilsitz 7. Dichtung der Spindelführung 8. Spindel 9. Winkelstutzen

ZIL 157 | **Luftverteilerblock**

Abb.: 10

WEHRTECHNISCHE DIENSTSTELLE
FÜR KRAFTFAHRZEUGE UND PANZER

WTD 41

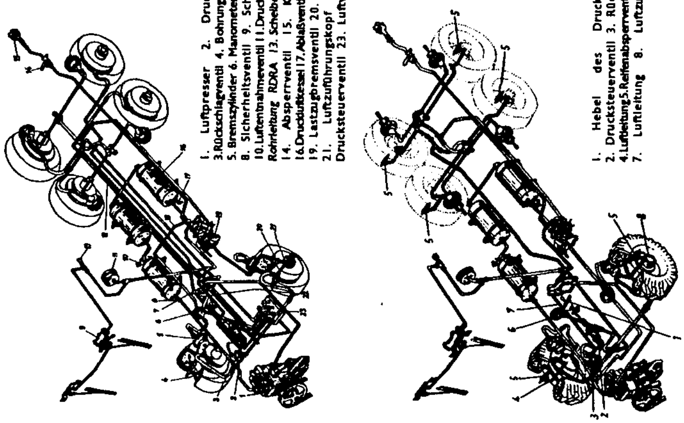

1. Luftpresser 2. Drucksteuerventil 3. Rückschlagventil 4. Bohrung für Luftzufuhr 5. Bremszylinder 6. Manometer 7. Druckregler 8. Sicherheitsventil 9. Scheibenwischer 10. Luftentnahmeventil 11. Druckmanometer 12. *Rohrleitung RDRA* 13. Scheibenwischerhalter 14. Absperrventil 15. Kupplungskopf 16. Druckluftkessel 17. Ablaßventil 18. Bremsventil 19. Lastzugbremsventil 20. Absperrventil 21. Luftzuführungskopf 22. Hebel Drucksteuerventil 23. Luftverteilerblock

1. Hebel des Drucksteuerventils 2. Drucksteuerventil 3. Rückschlagventil 4. Luftleitung 5. Reifenabsperrventil 6. Manometer 7. Luftleitung 8. Luftzuführungskopf

ZIL 157 K **Reifenluftdruckregelanlage (alt/neu)**

Abb.: 11

WEHRTECHNISCHE DIENSTSTELLE
FÜR KRAFTFAHRZEUGE UND PANZER

WTD 41

Reifendruckregelanlage TATRA 813 (8x8)

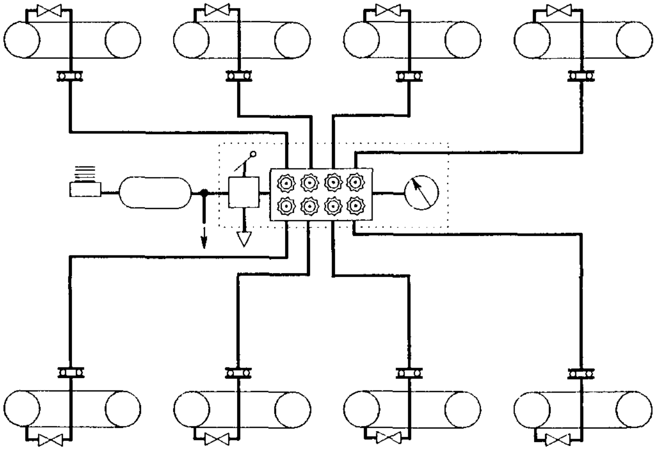

Abb.: 12

WEHRTECHNISCHE DIENSTSTELLE
FÜR KRAFTFAHRZEUGE UND PANZER

WTD 41

Reifendruckregelanlage SPW 40 P2

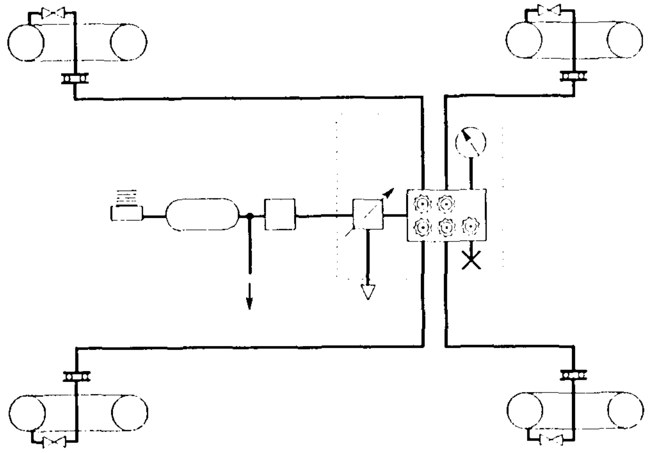

Abb.: 13

WTD 41

WEHRTECHNISCHE DIENSTSTELLE
FÜR KRAFTFAHRZEUGE UND PANZER

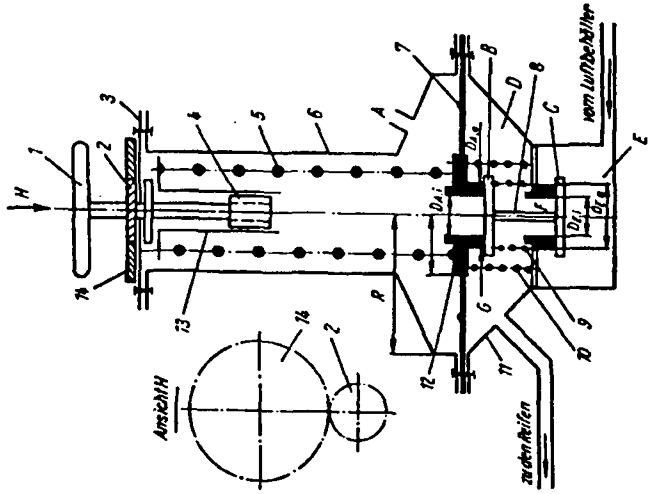
H
1
2
3
4
5
6
7
8
9
10
11
12
13
14
A
B
C
D
E
G
R
$D_{a,a}$
$D_{a,i}$
$D_{i,i}$
$D_{i,a}$
vom Luftbehälter
zu den Reifen
Ansicht H

Abb.: 14

WEHRTECHNISCHE DIENSTSTELLE
FÜR KRAFTFAHRZEUGE UND PANZER

WTD 41

Reifendruckregelanlage SPW 70

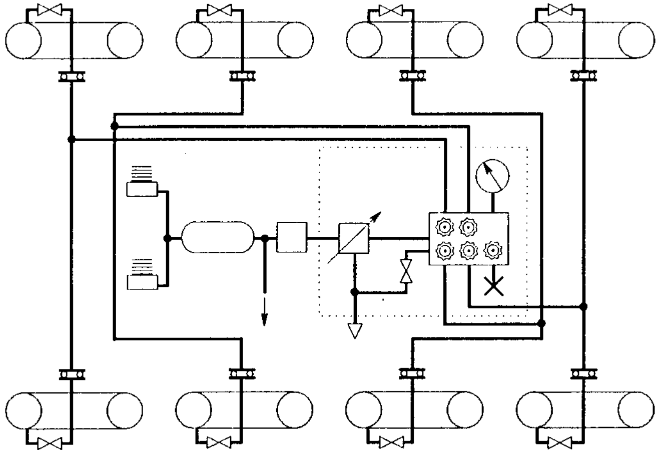

Abb.: 15

WEHRTECHNISCHE DIENSTSTELLE
FÜR KRAFTFAHRZEUGE UND PANZER

WTD 41

Reifendruckregelanlage IFA W50

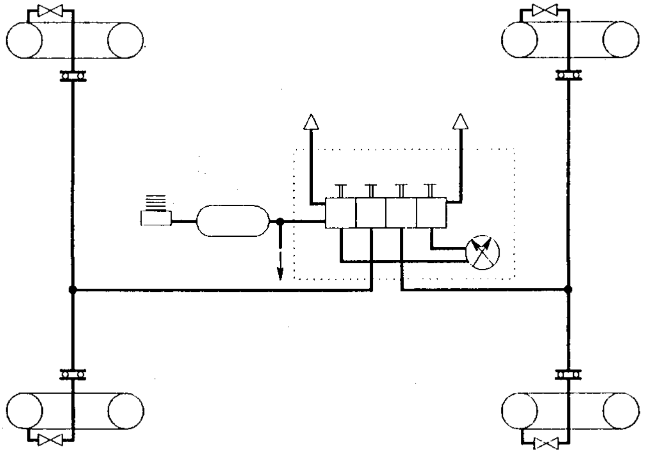

Abb.: 16

WEHRTECHNISCHE DIENSTSTELLE
FÜR KRAFTFAHRZEUGE UND PANZER

WTD 41

Reifendruckregelanlage IFA L60

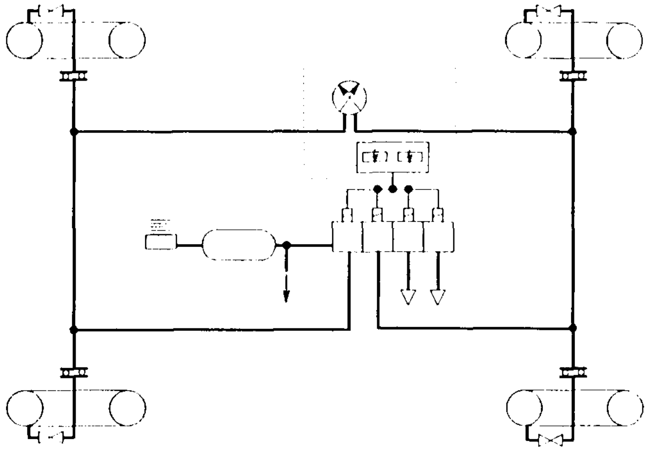

Abb.: 17

WEHRTECHNISCHE DIENSTSTELLE
FÜR KRAFTFAHRZEUGE UND PANZER

WTD 41

Reifendruckregelanlage APE

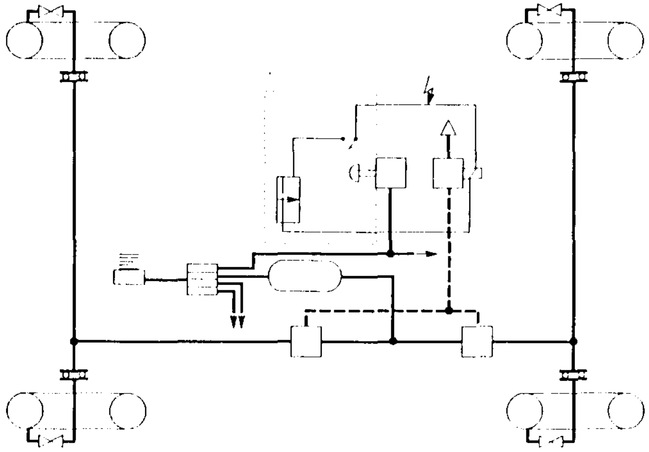

Abb.: 18

WEHRTECHNISCHE DIENSTSTELLE
FÜR KRAFTFAHRZEUGE UND PANZER

WTD 41

Reifendruckregelanlage APE

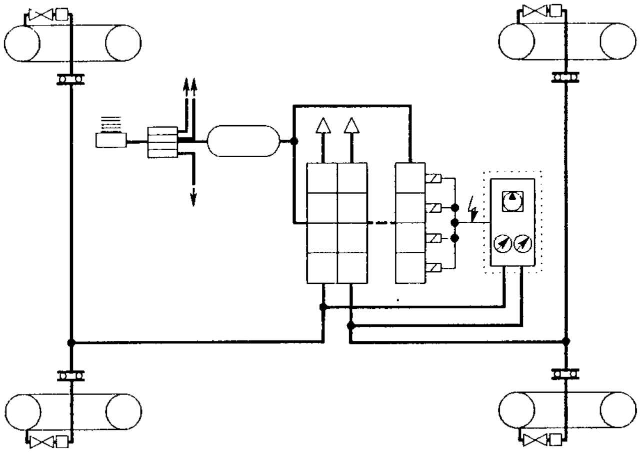

Abb.: 19

WEHRTECHNISCHE DIENSTSTELLE
FÜR KRAFTFAHRZEUGE UND PANZER

WTD 41

Reifendruckregelanlage SSB (M3)

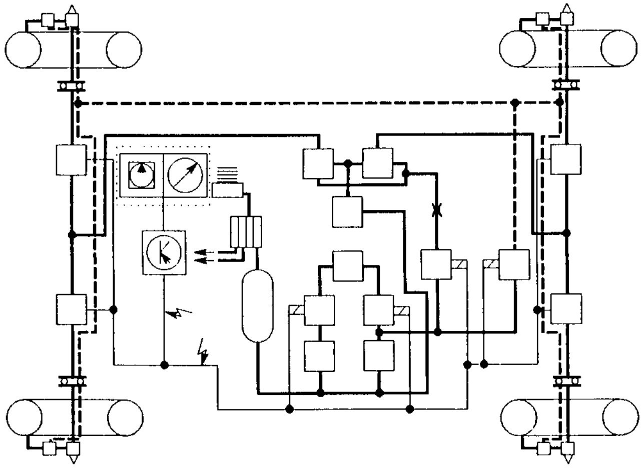

Abb.: 20

WEHRTECHNISCHE DIENSTSTELLE
FÜR KRAFTFAHRZEUGE UND PANZER

WTD 41

Reifendruckregelanlage CATS (Fa. Sondertechnik)

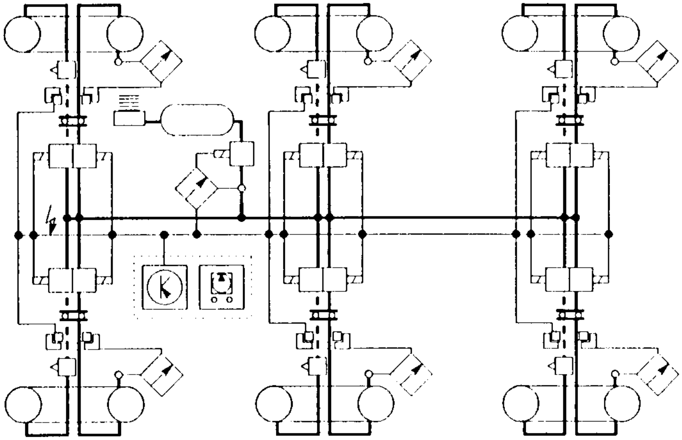

Abb.: 21

WEHRTECHNISCHE DIENSTSTELLE
FÜR KRAFTFAHRZEUGE UND PANZER

WTD 41

Reifendruckregelanlage CTIS / LKW 5t M925 A2

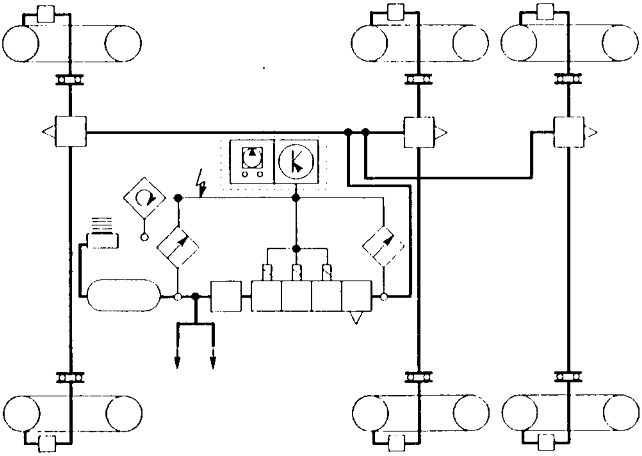

Abb.: 22

WEHRTECHNISCHE DIENSTSTELLE FÜR KRAFTFAHRZEUGE UND PANZER

WTD 41

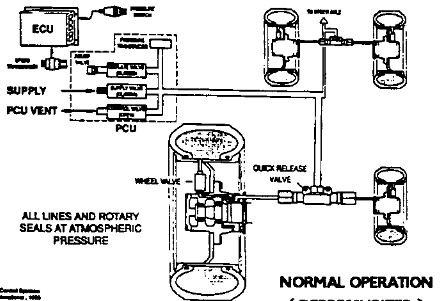
ECU
SUPPLY
PCU VENT
PCU
WHEEL VALVE
QUICK RELEASE VALVE

ALL LINES AND ROTARY SEALS AT ATMOSPHERIC PRESSURE

NORMAL OPERATION
(DEPRESSURIZED)

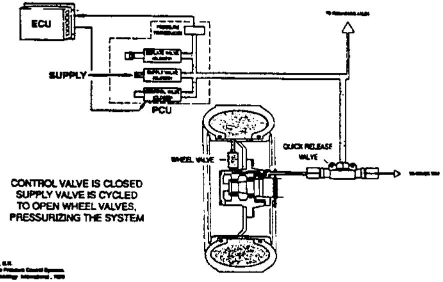
ECU
SUPPLY
PCU
WHEEL VALVE
QUICK RELEASE VALVE

CONTROL VALVE IS CLOSED SUPPLY VALVE IS CYCLED TO OPEN WHEEL VALVES, PRESSURIZING THE SYSTEM

MEASURE

Quelle: Steyr Antriebstechnik

Abb.: 23

WEHRTECHNISCHE DIENSTSTELLE FÜR KRAFTFAHRZEUGE UND PANZER

WTD 41

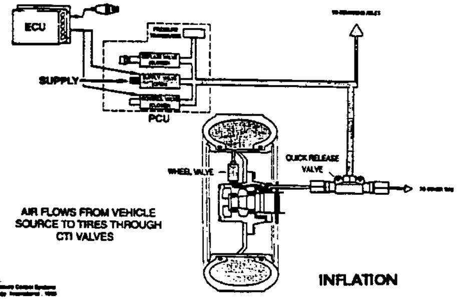
ECU
SUPPLY
PCU
WHEEL VALVE
QUICK RELEASE VALVE

AIR FLOWS FROM VEHICLE SOURCE TO TIRES THROUGH CTI VALVES

INFLATION

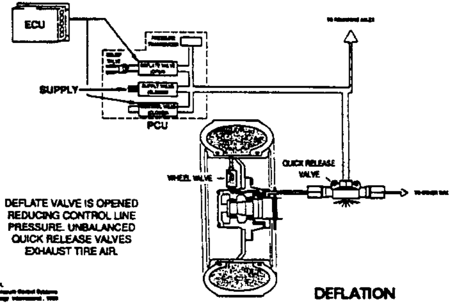
ECU
SUPPLY
PCU
WHEEL VALVE
QUICK RELEASE VALVE

DEFLATE VALVE IS OPENED REDUCING CONTROL LINE PRESSURE. UNBALANCED QUICK RELEASE VALVES EXHAUST TIRE AIR.

DEFLATION

Quelle: Steyr Antriebstechnik

Abb.: 24

WEHRTECHNISCHE DIENSTSTELLE
FÜR KRAFTFAHRZEUGE UND PANZER

WTD 41

Reifendruckregelanlage Fa. Labinal im ExF Rad (8x8) DB

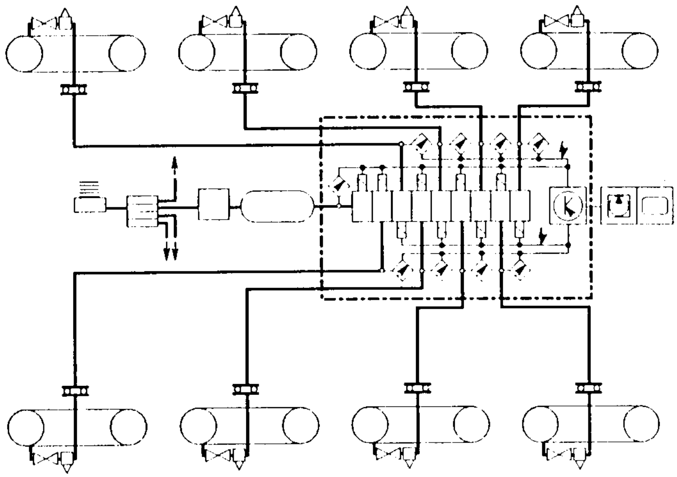

Abb.: 25

WEHRTECHNISCHE DIENSTSTELLE
FÜR KRAFTFAHRZEUGE UND PANZER

WTD 41

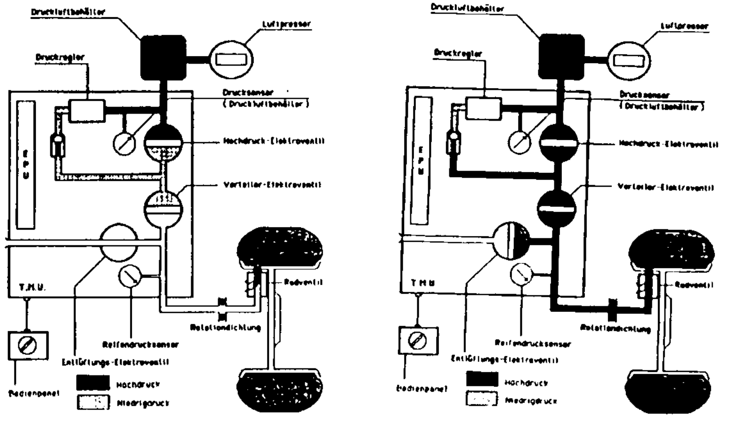
Druckluftbehälter
Luftpresser
Druckregler
Drucksensor
(Druckluftbehälter)
Hochdruck-Elektroventil
Verteiler-Elektroventil
EPU
T.M.U.
Radventil
Rotationdichtung
Reifendrucksensor
Entlüftungs-Elektroventil
Bedienpanel
Hochdruck
Niedrigdruck
Druckluftbehälter
Luftpresser
Druckregler
Drucksensor
(Druckluftbehälter)
Hochdruck-Elektroventil
Verteiler-Elektroventil
EPU
TMU
Radventil
Rotationdichtung
Reifendrucksensor
Entlüftungs-Elektroventil
Bedienpanel
Hochdruck
Niedrigdruck

Normalfahrt

Messen

Abb.: 26

**WEHRTECHNISCHE DIENSTSTELLE
FÜR KRAFTFAHRZEUGE UND PANZER**

WTD 41

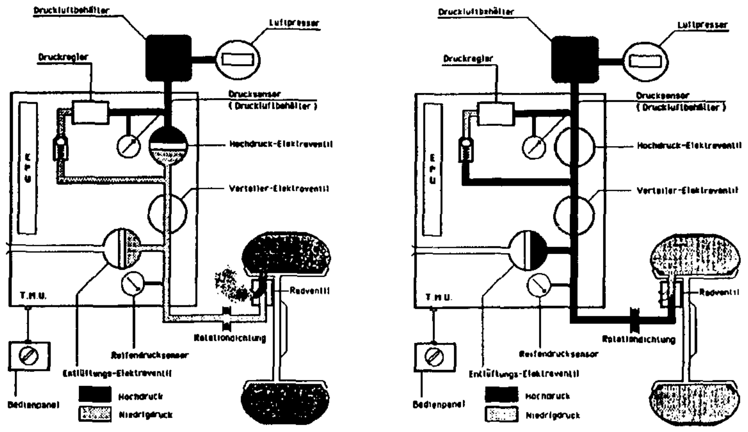
Druckluftbehälter
Luftpresser
Druckregler
Drucksensor
(Druckluftbehälter)
Hochdruck-Elektroventil
Verteiler-Elektroventil
E P U
T.M.U.
Radventil
Rotationdichtung
Reifendrucksensor
Entlüftungs-Elektroventil
Bedienpanel
Hochdruck
Niedrigdruck

Entlüften

Befüllen

Abb.: 27

**WEHRTECHNISCHE DIENSTSTELLE
FÜR KRAFTFAHRZEUGE UND PANZER**

WTD 41

Ablasszeit ExF Rad (8x8) DB ; RDRA Fa. Labinal

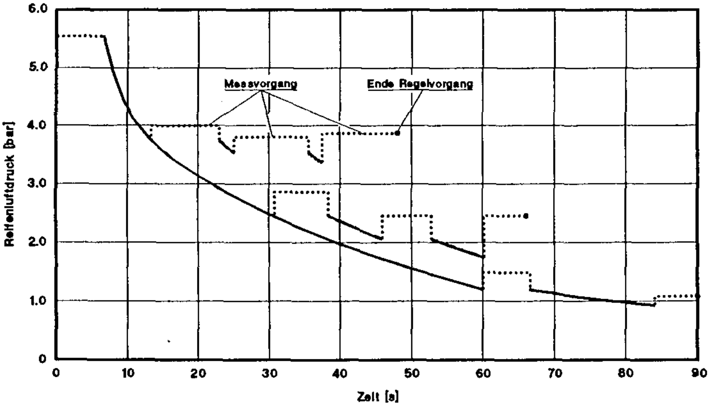

Abb.: 28

WEHRTECHNISCHE DIENSTSTELLE FÜR KRAFTFAHRZEUGE UND PANZER

WTD 41

FÜLLZEITEN	ABLASSZEITEN
I. < 10 min ExFz Rad (8x8) APE TM 01 APE EM 02 SPW 40 IFA L60	I. < 1 – 2 min ExFz Rad (8x8) SSB (M3) CATS
II. 10 – 12 min SPW 70 TATRA 815 (6x6/8x8)	II. 3 – 5 min M 925 A2 APE EM 02 SPW 70 SPW 40 BAZ 5937/5939
III. 15 – 25 min M 925 A2 TATRA 813 KAMAZ 4310 URAL 4320 IFA W50 ZIL 157 u. ZIL 131 GAZ 66	III. 7 – 10 min APE TM 01 MAZ 543 TATRA 815 (6x6/8x8) KAMAZ 4310 URAL 4320 u. Ural 375D IFA L60 IFA W50 ZIL 157 u. ZIL 131 GAZ 66
IV. 26 – 35 min MAZ 543 BAZ 5937/5939 KRAZ 255 URAL 375D	IV. ≥ 10 min TATRA 813 (8x8) KRAZ 255

Abb.: 29

WEHRTECHNISCHE DIENSTSTELLE
FÜR KRAFTFAHRZEUGE UND PANZER

WTD 41

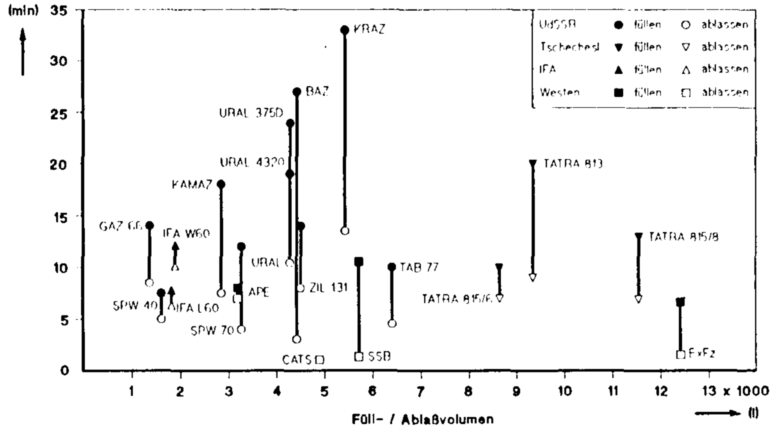

Abb.: 30

Fahrzeug bzw. System	Reifen			Volumen (dm³)	Gesamt	Zeiten (min)	2000 min⁻¹	Spez. Vol. (m³/min)	
	Stk.	Größe	Luftdruck (bar)	1 Reifen	$p_{max} \rightarrow p_{min}$	Ablaß	Füll	Ablaß	Füll
GAZ 66	4	12.00-18	2,8 - 0,5	150	1380	8,5	14	0,162	0,099
ZIL 157	6	12.00-18	3,5 - 0,5	150	2700				
ZIL 131	6	12.00-20	4,5 - 0,5	185	4440	8	14	0,555	0,317
URAL 375D	6	14.00-20	3,2 - 0,5	265	4293	10,5	24	0,409	0,179
URAL 4320	6	14.00-20	3,2 - 0,5	265	4293	10	19	0,429	0,226
KAMAZ 4310	6	1220x400-533	3,0 - 0,7	205	2829	7,5	18	0,377	0,175
KRAZ 255B	6	1300x530-533	3,5 - 1,0	360	5400	13,5	33	0,400	0,164
BAZ 5939	6	1200x500-508	4,0 - 1,0	245	4410	3	27	1,470	0,163
MAZ 543	8	1500x600-635	4,3 - 1,3			8,5	32		
SPW 40 P2	4	13.00-18	2,8 - 0,5	175	1610	5	7,5	0,322	0,215
SPW 70	8	13.00-18	2,8 - 0,5	175	3220	8 (4)	12	0,403 (0,805)	0,268
TAB 77	8	14.00-20	3,5 - 0,5	265	6360	9 (4,5)	10	0,707 (1,413)	0,636
TATRA 813 (8x8)	8	15.00-21 ND	4,0 - 0,8	365	9344	9	20	1,038	0,467
TATRA 815 (6x6)	6	15.00-21 ND	4,75 - 0,8	365	8650	7	10	1,236	0,865
TATRA 815 (8x8)	8	15.00-21 ND	4,75 - 0,8	365	11534	7	13	1,648	0,887
IFA W50 LA/A	4	16-20 ND	2,5 - 0,8 VA 5,0 - 1,8 HA	195 195	663 1248	7,5 12	7 15	0,191	0,159
IFA L60 AP-N	4	18/70-20	2,75 - 1,3 VA 5,0 - 2,75 HA	250 250	725 1125	4,5 9	3 11	0,257	0,231
APE - EM	4	20,5 R 25	2,4 - 0,7	445	3026				
APE - TM	4	20,5 R 25	2,5 - 0,7	445	3204	7	8	0,458	0,401
SSB (M3)	4	23,5 R 25	3,5 - 1,0	570	5700	1,3	10,5	4,385	0,543
CATS	6	12 R 22,5	8,0 - 1,5	125	4875	1			
CTIS (M925)	6	14.00 R 20	4,1 - 0,85	260	5070				
ExFz (Labinal)	8	17,5 R 25	5,5 - 1,1	350	12320	1,5	6,5	8,213	1,895

Abb.: 31

LIST OF SYMBOLS USED IN THE SCHEMATIC DRAWINGS

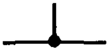	PRESSURE LINE / CONNECTION	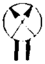	DUAL PRESSURE GAGE
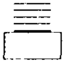	AIR COMPRESSOR	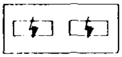	ROCKER-TYPE SWITCH, ELECTRIC
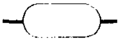	COMPRESSOR TANK	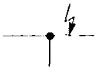	ELECTRIC WIRE / CONNECTION
	VALVE	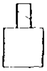	MAGNETIC VALVE
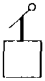	VALVE, OPERATED BY LEVER	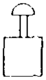	VALVE, OPERATED BY PUSH BUTTON
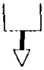	OUTLET, WITH PIPE ADAPTER	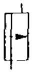	TIMER
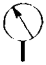	PRESSURE GAGE	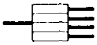	FOUR CIRCUIT SAFETY VALVE
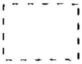	DRIVER'S CAB LIMITS	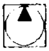	ROTARY SWITCH
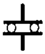	ROTARY AIR TRANSMISSION	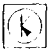	ELECTRONICAL CONTROL UNIT / COMPUTER
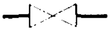	SHUT OFF VALVE	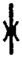	THROTTLE
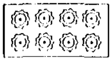	AIR DISTRIBUTOR, COMBINATION VALVE		OUTLET WITHOUT PIPE ADAPTER
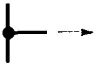	TO OTHER CONSUMERS	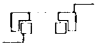	ROTATING SUSPENDET COIL / INDUCTIVE TRANSMISSION
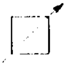	PRESSURE REDUCTION VALVE, SEMI AUTOMATIC	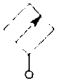	PRESSURE SENSOR
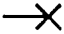	AIR CONNECTING PIECE	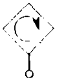	IMPULSE TRANSMITTER FOR REVOLUTION INDICATOR
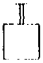	VALVE, MECHANICALLY OPERATED BY ROCKER ARM	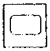	DISPLAY

Influence of advanced chassis technology on off-road mobility, determined by means of the 8x8 experimental vehicle

Werner Sünkel
Mercedes-Benz AG, Stuttgart

After development of the 2nd generation of wheeled vehicles for the the German Federal Army (the Bundeswehr), Mercedes-Benz entered into considerations on a potential 3rd generation of wheeled armoured vehicles.

Various studies for overall vehicles and vehicle systems were drawn up to define the following requirements placed on future chassis:

- Increase in gross weight by at least 50% corresponding to 10 tons to
  - o enhance the degree of protection and the survival capability of armoured vehicles and
  - o increase the payload.

- The generally accepted good mobility of the 2nd generation of wheeled armoured vehicles must be exceeded. An off-road mobility comparable to that of modern tracked vehicles must be aimed for.

- The robustness of today's chassis with rigid axle or individual wheel location must be increased.

- Concept of a modular vehicle family with
  - o standardised major components and assemblies
  - o using as many commercially available components, assemblies, parts and manufacturing procedures as possible

- Minimising life-cycle cost (LCC) during
  - o development
  - o purchasing and
  - o operation.

By commission of the Federal Ministry of Defence, an experimental vehicle was built up and has been tested since 1986 at the Federal Armed Forces Technical Center 41 (WTD 41) to verify the forecast performance data of the 8x8 chassis with

- individual wheel location
- all-wheel drive and steering
- new combat wheel based on the Continental Tire System (CTS)
- tyre pressure control system
- suitable driver's operating panel with multi-function display.

The hull, chassis, steering system, drive train, combat wheel, tyre pressure control system and driver's place with operating panel had to be designed in a near-standard form.

For cost and time reasons, existing components or parts were used as an interim solution for the other assemblies. The Mercedes-Benz V12-engine with 612 kW and the Renk HS 226 flanged-on manual transmission with higher output was used for the first time.

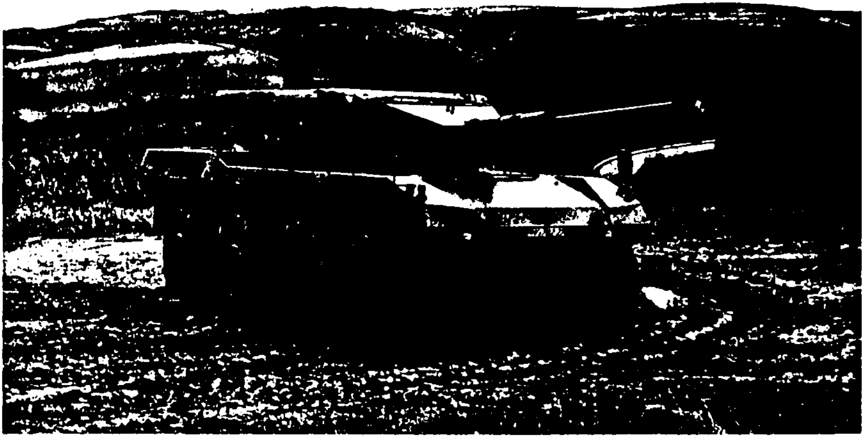

In the past, design measures taken to improve certain performance characteristics and components were the usual means to enhance the performance of wheeled vehicles and to reduce the construction-related disadvantages.

Since the defined requirements exceeded the capacity of commercially available chassis components, new solutions had to be found taking the vehicle's system and family capability into account; this means that it was not possible to concentrate on partial problems or develop partial solutions only.

o **Wheel location**

When determining a suitable wheel location system, the following wheel location methods proved incompatible with the system for the envisaged application:

- single or dual-joint swing axle
- diagonal swing axle
- single or dual-crank axle
- rigid portal axle
- De Dion rigid axle

Therefore, only the link-located rigid axle with transverse location by means of a Watt linkage, McPherson wheel location with hydropneumatic spring damper strut and a double wishbone axle were eligible for further consideration.

The new individual wheel location in accordance with the double wishbone principle was chosen. It features a triangular link at the bottom and a semi-trailing arm at the top which does not take up a lot of space.

The standardised halfshafts have been designed in such a way that the wheel location and drive elements are the same for all vehicle variants. The axle is adapted to the relevant installation site by means of bearing brackets with steering arms.

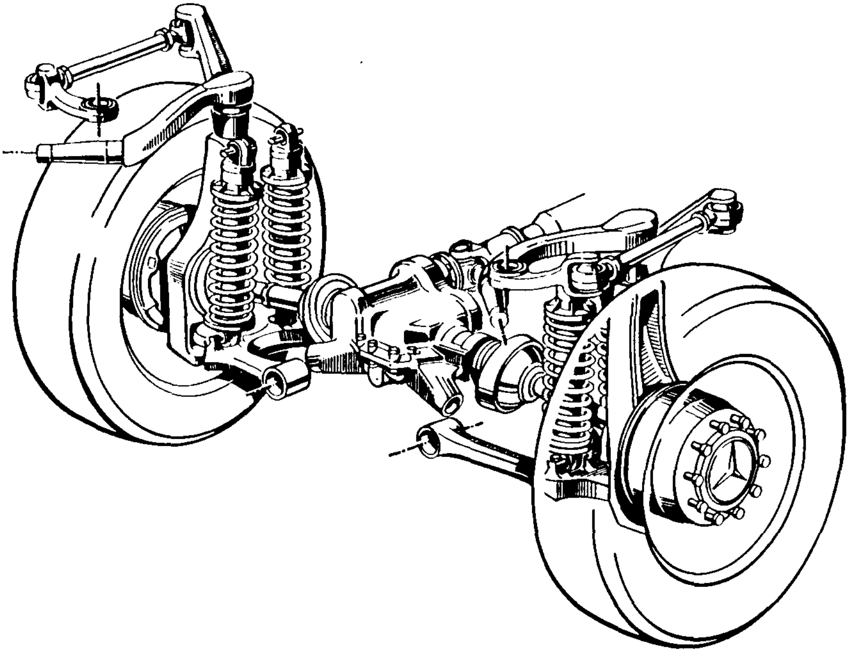

Fig. 1 Double wishbone axle with steering and wheel drive

The vehicle with all-wheel steering is characterised by a large spring travel and only slight changes in toe-in and camber, providing high ride comfort on off-road terrain on the one hand and - on the other hand - optimum traction also on soft ground due to low dynamic wheel load fluctuations. Because of the smaller unsprung masses, individual wheel suspension is advantageous as compared to the rigid axle in terms of higher average speeds and lower body accelerations. Robustness vis-à-vis mechanical damage under aggravated conditions and under the impact of weapons has been considerably enhanced.

- Suspension and damping

The mechanical interfaces of the standardised halfshafts have been designed such that either hydropneumatic or active spring elements can be installed on the basis of conventional coil spring/damper elements. The installation space does not project above the tangent surfaces on the wheel envelope.

Particular importance must be attached to damping on vehicles with high off-road capability. The dynamic wheel load can be a multiple of the static wheel load which necessitates the use of appropriately large and well matched vibration dampers. This prevents hard impacting of the limit stops and thus reduces the stresses and strains on the wheel location elements. The damper work is a multiple of the spring work, which inevitably leads to a high thermal load on the dampers.

In addition, the wheel considerably contributes to increasing the energy absorption capacity of the chassis.

The following diagram shows the projected energy absorption capacity of a halfshaft resulting from driving over a ramp. The wheel is at full rebound when the vehicle touches ground again. The overall kinematic spring travel of 480 mm consists of 200 mm spring deflection and 280 mm rebound. With a tyre deflection of approx. 160 mm, the useful spring travel is 640 mm.

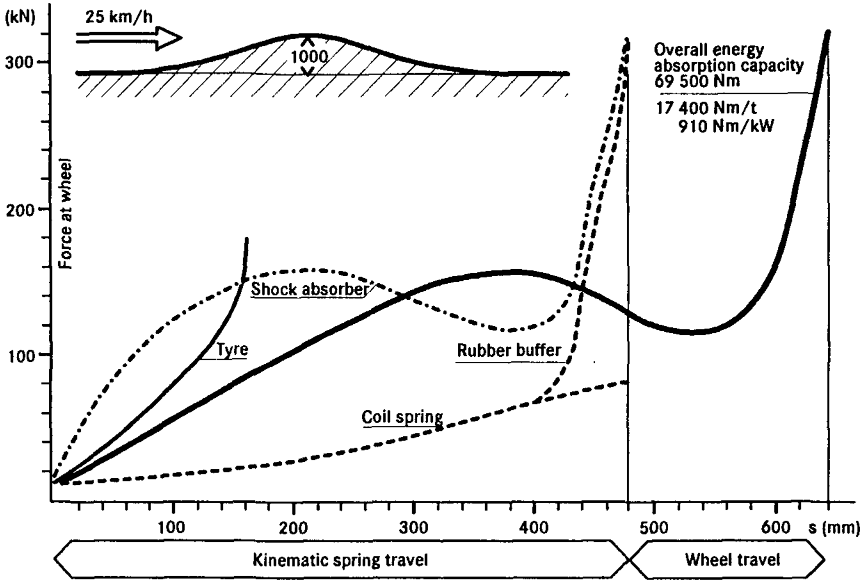

Fig. 2 Projected energy absorption capacity
EXF 8x8 half shaft; ramp

The overall energy absorption capacity of 69,500 Nm is based on

- the two coil springs with 14,100 Nm
- the dampers installed in the springs with 39,700 Nm
- the rubber limit stop with 6,200 Nm and
- the tyre with 9,500 Nm.

The assumed maximal forces of the spring/damper system have been confirmed when determining the load data with the EXF 8x8.

By way of example, the consistency with the assumed values for driving over the round obstacle at a speed of 30 km/h is shown.

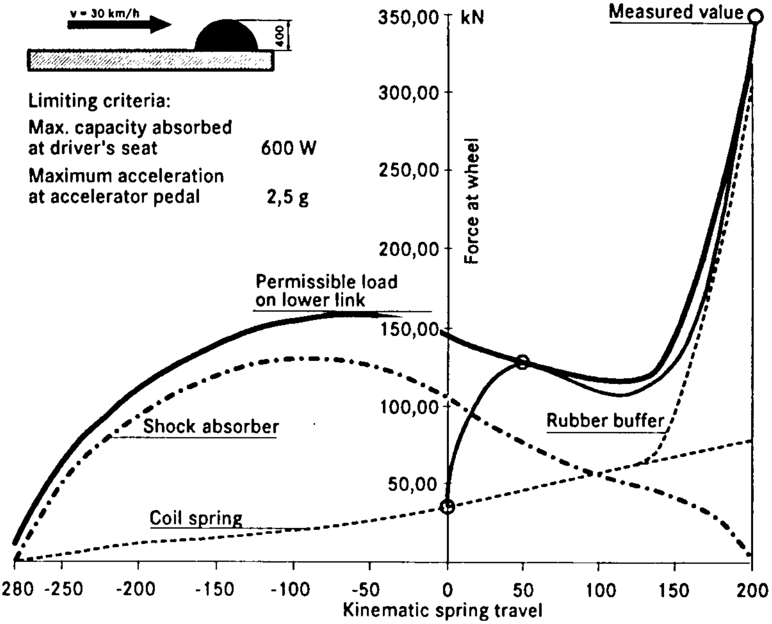

Fig. 3 Checking the load assumptions

The "relative functional chassis performance" of the EXF 8x8 was determined at the Federal Armed Forces Technical Center (WTD 41); an improvement of 54% as compared to the Leopard 2, a modern tracked vehicle, was found in the process.

To determine the relative functional chassis performance, the vehicle drives several times over the sinus wave at a constant speed until it reaches the load limit of 2.5 g at the driver's place. In addition, the possible ramp approach speed for 2.5 g at the driver's seat is determined for ramp gradients of 20% to 50%. The relative functional chassis performance is determined from the two partial performances "driving over the sinus wave" and "ramp approach speed".

o Steering

Manoeuvrability is of decisive importance for the mobility of a wheeled armoured vehicle in wide-area applications. The LUCHS armoured reconnaissance vehicle, with its all-wheel drive and all-wheel steering and a turning circle diameter of 12 m, continues to be the yardstick for a new generation of wheeled vehicles.

To increase the useful volume, the wheel turning angles were to be reduced. Because of the disadvantages in terms of driving dynamics, skid steering was excluded as an alternative.

Possible steering axle combinations were investigated with the 8x8 LUCHS vehicle; at the same time, a reduction in track circle diameter by braking the inner wheels was demonstrated.

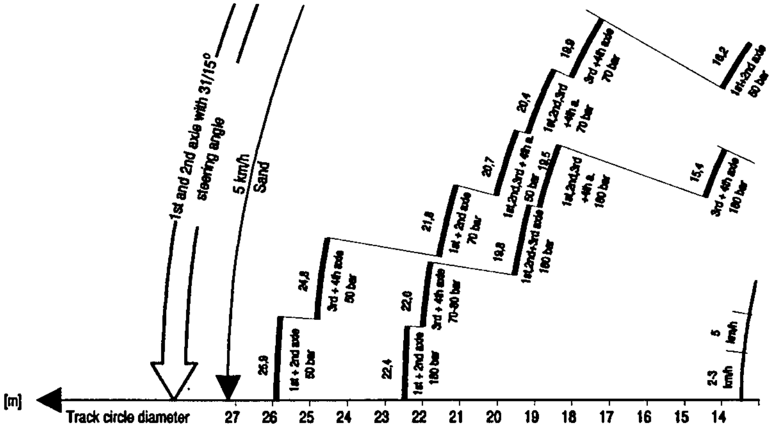

Fig. 4 Track circle diameter of LUCHS armoured reconnaissance vehicle with superimposed wheel brake steering

For example, a reduction in track circle diameter by 2 to 3 m was determined on sand at a speed of 5 km/h. On a concrete surface, a track circle of 15.4 m was achieved with two steered axles, and a diameter of 11.3 m was achieved with three steered axles.

The unacceptably extreme tyre deformation, the high tyre wear and the different turning circles depending on ground conditions and speeds led to an all-wheel steering system with reduced turning angles on the 2nd and 3rd axles.

Tests have shown that despite smaller turning angles on the 1st and 4th axle and deliberate acceptance of steering kinematics faults on the 2nd and 3rd axle, a turning circle of approx. 12 m can be achieved with all-wheel steering. It was demonstrated that the EXF vehicle needs the same time to turn around on a 6 m wide road as a modern tracked vehicle.

This means that no cross-drive steering system is required; therefore, it will not be installed on future highly mobile wheeled vehicles to prevent unnecessary complexity, and the Ackermann steering principle will be retained.

o Wheel system

The CTS wheel system developed together with Continental consists of a rim with emergency running surface and control valve, tensioning rings and tyres. It features the following positive characteristics for off-road operation when compared with traditional wheel systems:

- less structural load on the tyre when driving with reduced tyre pressure
- enhanced traction because of larger contact patch than on conventional tyres
- transfer of high torques at low tyre pressure due to clamping of the tyre bead
- very good driving dynamics due to the high transfer ability for lateral forces
- no additional emergency operation element required
- less overall weight
- lower cost.

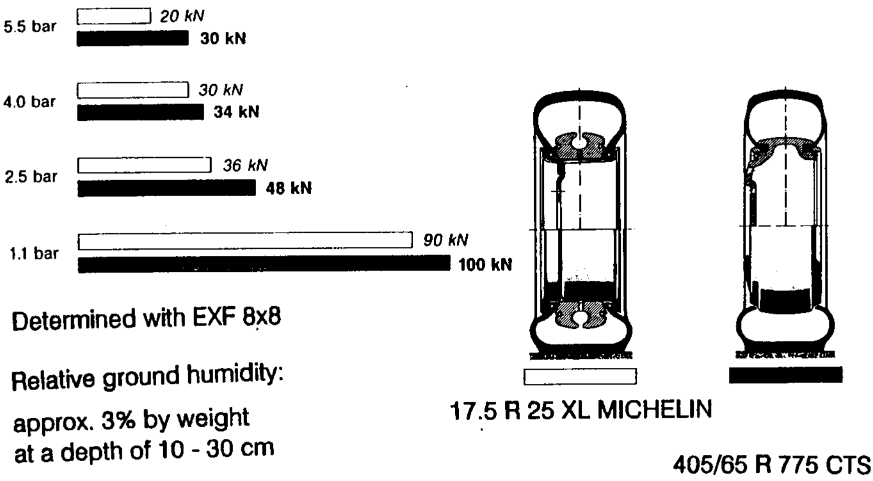

Determined with EXF 8x8

Relative ground humidity:

approx. 3% by weight
at a depth of 10 - 30 cm

Fig. 5 Comparison of tractive forces on sandy ground (dune)

Tests performed to date with hand-made tyres have shown that it is worthwhile to continue developing this wheel up to production standard.

o Tyre pressure control system

In order to make it possible to drive both at high speeds and on soft terrrain, it is essential that the tyre pressure can be adjusted. In other words, the wheeled vehicles with high off-road capability must be fitted with a tyre pressure control system. Reducing the tyre pressure while on the move enlarges the tyre contact area and reduces the amount of pressure on the ground while the ability to drive over soft ground is greatly improved.

Basic investigations verified the tyre deflation time for 17.5-R25 XL tyres:
- 70 seconds from 5.5 bar road-driving pressure to 1.1 bar self-freeing pressure

This significant advance is based on modern electronic control technology and on rapid expulsion of air via a new kind of control valve into the atmosphere.

As soon as the critical terrain has been left, the drive-dependent maximum speed can be resumed while the tyre pressure is being increased again.

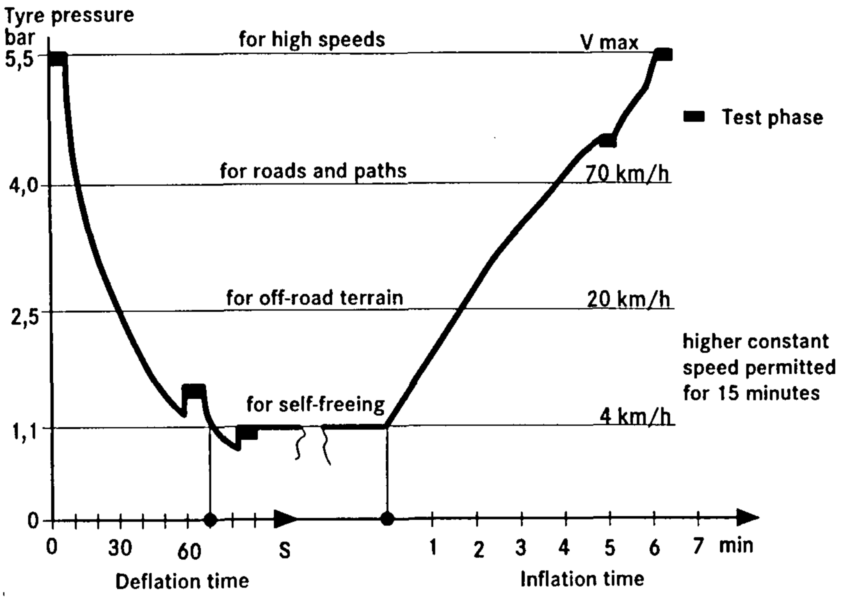

Fig. 6 Deflation and inflation times of the tyre pressure control system

o Crown wheel and pinion

Standard-production parts from the tried and test Mercedes-Benz axle range are used in the newly designed housing of the crown wheel and pinion with throughdrive.

o Propshaft

Wheel location kinematics have been laid out in such a way that only small longitudinal displacements occur in the main sprung area in the flexible shaft between the joints. The resulting lower axial forces make for a much longer service life of the joint bearings.

Mounting the dual propshaft in a protective tube offers itself for use in military applications. The cost-efficient universal-joint propshafts from the commercial vehicle range have now also reached a standard which allows their use in this highly stressed axle.

Mobility

Off-road mobility is one of the major characteristics of an off-road vehicle, especially in military applications.

Verification of mobility during the concept phase is mainly based on empirical values and comparisons with known vehicles since the resources and data available for simulation are limited at this early stage.

For the first time, theoretical mobility investigations were performed parallel to the concept layout phase, using the NRMM NATO Reference Mobility Model.

In our view, the standardised NATO model provides the following advantages for both developers and customers:

- The required vehicle data is not too sophisticaed and can be generated without too much effort.
- The ground data is available for standard terrains.
- The linear elements such as ditches, embankments etc. have been defined.
- It is usually possible to estimate and finance the cost of simulation and evaluation.
- Comparisons of various crossings of large terrains can be easily made and presented.

The 8x8 Luchs armoured reconnaissance vehicle with 20 t and the Leopard 2 tracked vehicle were defined as reference vehicles for a first assessment of the projected 8x8 vehicle with a gross vehicle weight of 26 t.

The mean accumulated speed in open terrain was calculated. The open terrain does not incorporate any linear obstacles, paths or roads.

Despite an increase in weight by 6 t, the enhanced mobility of the 26 t vehicle with tyre pressure control system in up to 84% of the terrain is clearly positive.

Between 84% and 90% of the terrain, the specified target was not achieved. Since it was mainly the soft ground which causes immobilisation, the situation can only be improved by enlarging the tyre contact patch.

The part of the terrain the vehicle was not able to negotiate amounted to approx. 9%.

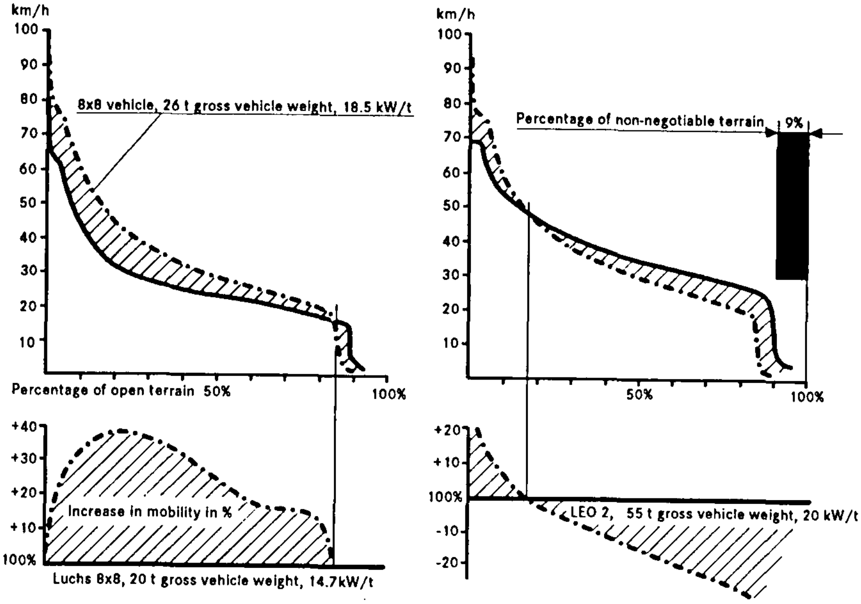

Fig. 7 Comparison of mobility of 26 t vehicle and reference vehicles in open terrain

As compared to the tracked vehicle, the wheeled vehicle was at a disadvantage as early as of 17% of the terrain. It was only possible to make up for this shortcoming by increasing the tyre size from 15.5 R 25 to 17.5 R 25 and using a six-speed manual transmission.

The following diagram shows the effect of the gross vehicle weight and the larger tyres with a width of 405 mm and 455 mm in comparison to the tracked vehicle.

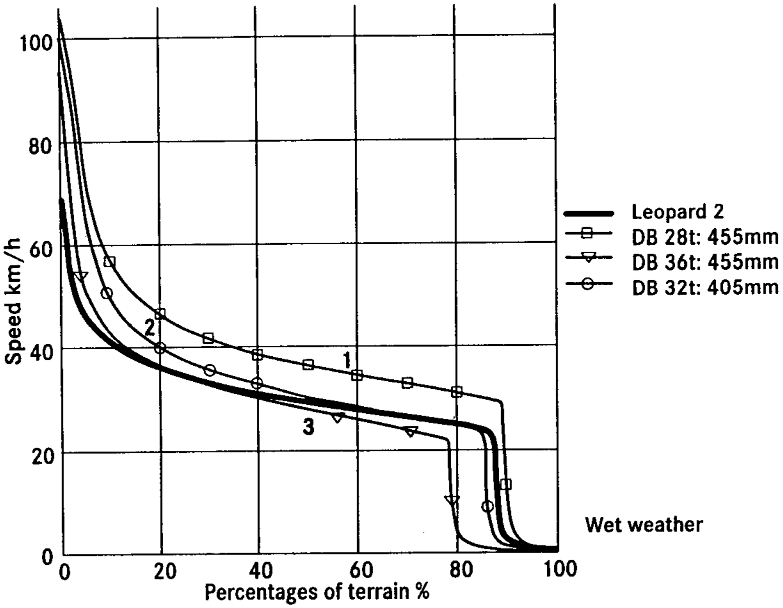

Fig. 8 Mobility profile in open terrain

It can be clearly seen that curve 2 of the 32 t vehicle with 405 mm wide tyres meets the specifications. Therefore, a gross weight of approx. 30 to 32 t and a tyre width of 405 mm for the CTS wheel was specified. The performance data of the CTS tyre were oriented towards the Michelin 17.5 R 25 XL tyre with a reduction in dimension of approx. 10%.

The following simplified presentation of part of the NRMM shows that the real terrain consists of three elements:

- open terrain with composition of the ground, inclines, unevennesses, vegetation and range of vision
- roads and paths with rolling resistance, inclines, unevennesses, curves and range of vision
- linear elements: rivers, rivulets, ditches, embankments, walls etc.

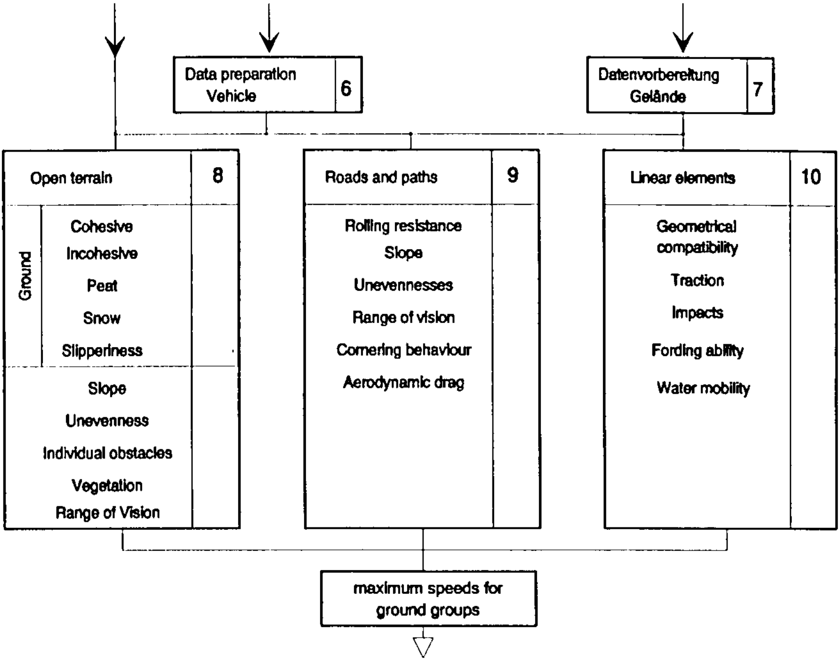
Data preparation Vehicle
6
Datenvorbereitung Gelände
7
Open terrain
8
Ground
Cohesive
Incohesive
Peat
Snow
Slipperiness
Slope
Unevenness
Individual obstacles
Vegetation
Range of Vision
Roads and paths
9
Rolling resistance
Slope
Unevennesses
Range of vision
Cornering behaviour
Aerodynamic drag
Linear elements
10
Geometrical compatibility
Traction
Impacts
Fording ability
Water mobility
maximum speeds for ground groups

Fig. 9 Simplified presentation of part of the mobility model

Comparative simulations under the same conditions have helped us in arriving at a trend statement to decide on a concept. However, it must be pointed out that in open terrain

- only straight-ahead driving is taken into account
- cornering - especially on soft ground - and cross slope driving are not taken into account
- lateral forces are not taken into account.

Since due to its design, the wheeled vehicle can reach higher speeds on paths and roads while at the same time the noise and vibration load on the crew and tyre wear is lower, this element must also be included in the mobility considerations.

The following diagram shows the much higher attainable speed of the wheeled vehicle as compared to the tracked vehicle in wet weather.

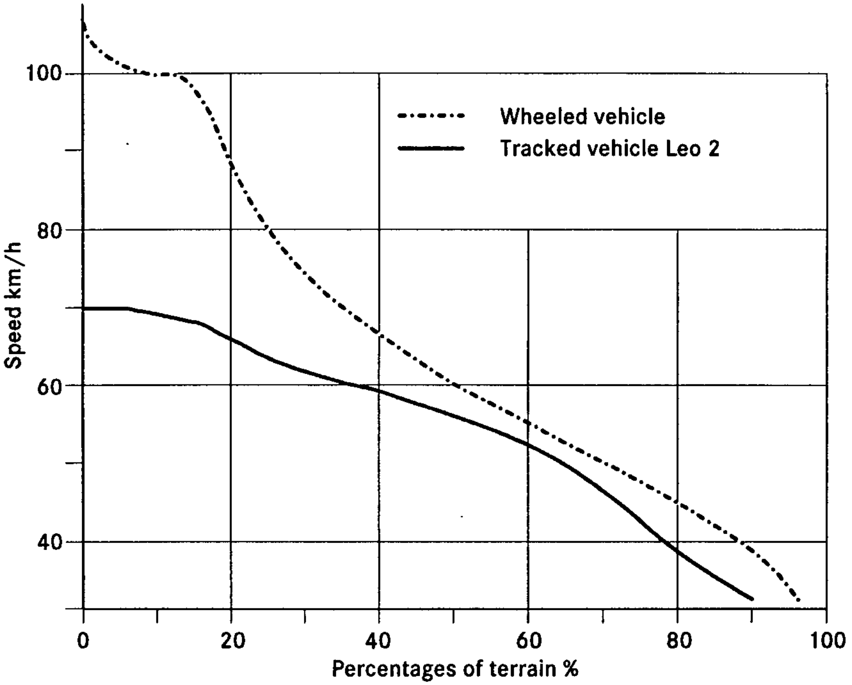

Fig. 10 Mean accumulated speed on the path and road network

The simulation results may be sufficient for the developers with their expertise and experience and the possibility to discuss things with the analysers; they are, however, not sufficient for the customer - in this case the tactical expert - who is interested in the vehicle's mobility in wide-area applications.

Even though reality cannot be fully shown by the relatively low-cost simulations, a trend statement can be made if the same boundary conditions apply.

The map of isochronous lines shows in an illustrative manner the time required in wet weather by the tracked vehicle (lines) and the wheeled vehicle (areas) to reach an optional point from the same starting point.

The class interval shown is 5 minutes.

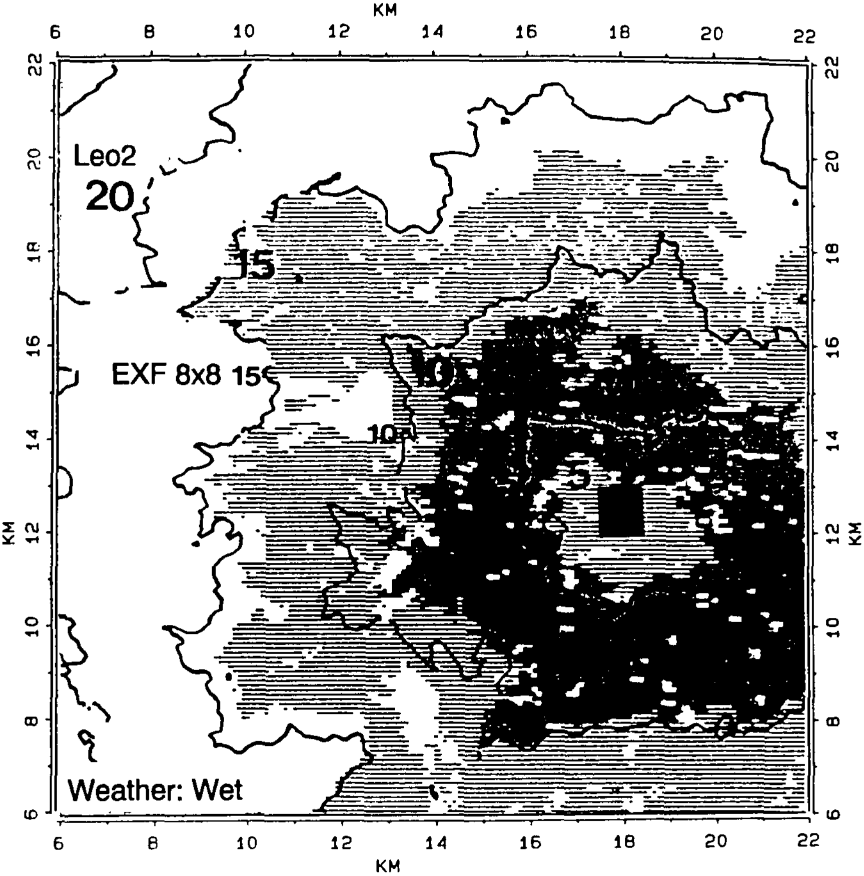

Fig. 11 Map of isochronous lines: open terrain, roads and linear elements

Verification of simulation results

The discussions about the mobility exhibited by wheeled and tracked vehicles, the appropriateness of the simulation programme used and the characteristic tyre data resulted in a verification of the NRMM on a training area close to the standard terrain.

A representative circuit with a length of 24 km was determined, the terrain data was acquired, and the theoretical lap times of the Leopard 2, Marder and EXF 8x8 reference vehicles were calculated for dry, moist and wet weather.

The mobility profiles were calculated for dry and wet weather.

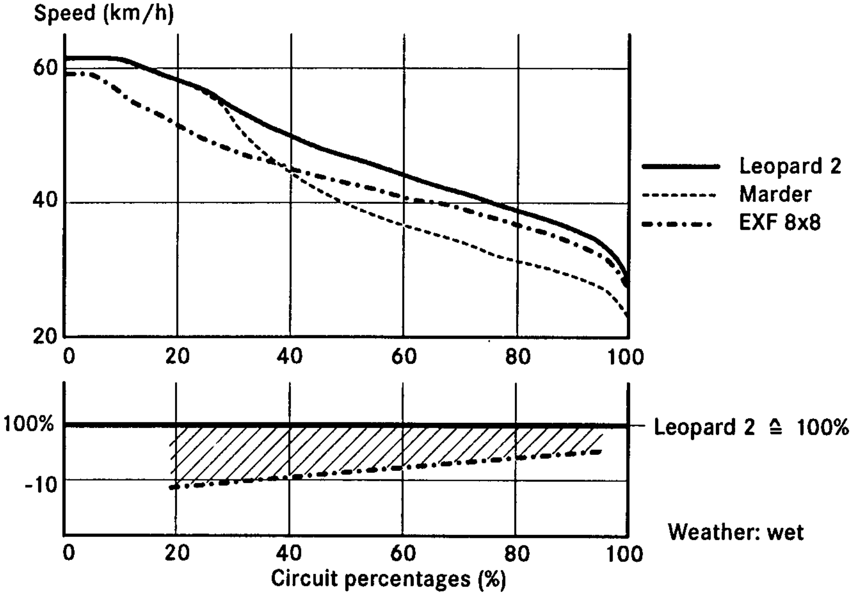

Fig. 12 Mobility profiles: Marder, Leo 2, EXF 8x8

Due to its design, the wheeled vehicle reaches higher speeds in dry weather on 40% of the circuit. For the rest of the circuit, the Leopard 2 and the EXF 8x8 are at the same level.

In wet weather, the speed attained by the wheeled vehicle is below that of the tracked vehicle. The reason stated for this phenomenon which was incomprehensible to us was a different interaction between the ground and the track pad and the tyre respectively. In contrast to the tyres, the track rests on the ground, which means there is static friction and the road wheels roll over the stationary track.

The actual driving time deviates from the calculated lap time by + 8.3% to - 9.8%. A forecast result below ± 10% is sufficient for the analyst.

The lower performance of the wheeled vehicle as compared to the tracked vehicle between 11% and 6% is within the pessimistic range of the simulation.

	Driving time in min:sec		
Weather	Calc..	actual	Dev.
Leopard 2			
dry	44:22	43:26	-2,1 %
	44:22	48:00	7,6 %
moist	45:45	45:33	-0,5 %
wet	52:20	-	
Marder			
dry	57:36	62:48	8,3 %
moist	60:13	-	
wet	62:01	-	
RKW-EXF			
dry	43:57	41:53	-4,9 %
moist	44:44	40:45	-9,8 %
wet	58:30	-	

Source of data: Battelle Institut

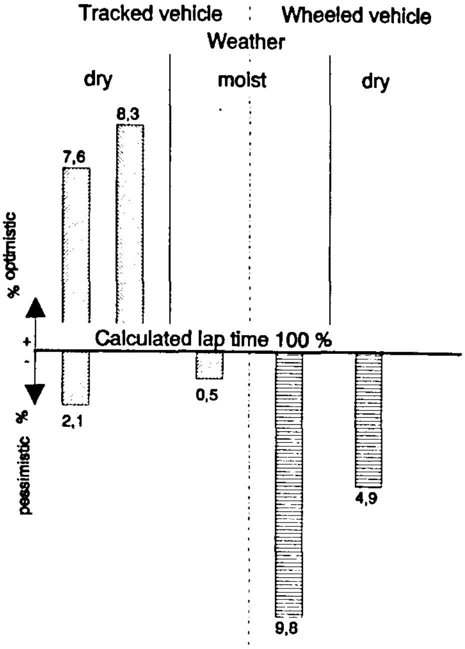

Fig. 13 Deviation of actual lap times and calculated lap times

Even though it was not possible to drive under all weather conditions, the deviations show nevertheless that rather optimistic calculations were performed for the tracked vehicle whereas the calculations for the wheeled vehicle were only pessimistic.

Extensive comparison drives with wheeled and tracked vehicles on different types of terrain all led to the general statement that the EXF 8x8 with a gross weight of 32 t has reached the Leopard 2's level of off-road mobility. On paths and roads, the gross weight can even be increased to 36 t without any loss in mobility.

An assessment of the results available illustrates four aspects:

1. A simulation analysis of mobility can only be reasonably performed on the basis of close cooperation between vehicle developers, customers and the user of the analysis programmes.

2. Some of the results of the most recent calculations are considerably more favourable for wheeled vehicles than in the past.

3. The significance of theoretical mobility investigations is limited due to the current state of simulation technology.
   Further verifications by means of practical tests are indispensable.

4. The characteristic data of new tyre designs must be determined and incorporated in the analysis model.

Results proven with the EXF 8x8

Since 1986, proof has been furnished in more than 10,000 km tough test operation of the EXF 8x8 that the forecast performance data and the robustness of the new assemblies were obtained and in some cases even exceeded.

The following is a list of objectives and proof furnished in the meantime:

- The increase in gross weight from 20 t to 36 t was verified by production of the EXF with 30 t and the subsequent increases in gross weight.

- The basic concepts and basic components required for a modular vehicle family have been defined.

- The basic components were designed together with leading manufacturers, some of them were built and pre-testing was carried out.

- Mobility was demonstrated in comprehensive simulations, comparison and verification drives.

- Robustness and thus reliability have been considerably increased by raising the load assumption and by installing the following new parts some of which are based on more cost-efficient standard parts.

- o stress and strain-optimised wheel location
- o elastic support of triangular links and crown wheel and pinion
- o elastic design of upper links
- o spherical rubber joints on track rod
- o rack and pinion steering for heavy-duty vehicles
- o clamped tyre bead
- o protected propshaft
- o curved teeth couplings in drive train
- o slide ring seal for air ducting

- The lifecycle cost was reduced on an ongoing basis parallel to the design work by drawing up input data for LCC analyses such as
  - o failure rates for reliability analyses
  - o accessibility, time required and replacement part/reconditioned part prices for maintenance and repair analyses
  - o purchasing prices.

- o A cost/benefit analysis was drawn up for the new standardised axle which says that per ton of axle load on the axle with individual wheel location, the performance is increased by approx. 100 % as compared to the commercially available rigid axle while the price is only approx. 20 % higher.

Session VI
Sektion VI

Vehicle Dynamics

Fahrzeugdynamik

DYNAMIC SIMULATION
COST BENEFITS & DESIGN ADVANTAGES

S. F. Storey
Simatics Limited, Cambridge, UK

ABSTRACT

Dynamic simulation is a cost effective way to determine the best design characteristics of physical systems. Three main reasons for simulating systems over experimental testing are:

1) **Cost Benefits** - Set-up, material, personnel and site costs of experimental trials often run into tens of thousands of Dollars, if not over $100,000. Several trials are usually required to prove a design or design changes. Using Simulation, the number of trials needed is reduced, often just to prove the final design.

2) **Practical Benefits** - It is usually difficult to determine the operating limits that a system can be subjected to before failure. With simulation, design limits can safely be exceeded and failure mechanisms studied without physical testing restrictions. A more comprehensive understanding of systems can be gained.

3) **Performance Benefits** - Before 'cutting metal' designs and design changes can be thoroughly exercised by simulating the behaviour and performance of components, sub-systems, or complete vehicles.

Having decided to take advantage of the benefits of simulation, a choice of methods has to be made. There are two main categories, in-house code development or commercially available packages.

I) With in-house development, time and cost are generally the limiting factors to produce a reasonable simulator. The result is often sparsely documented, difficult to use and restricted in application.

II) Commercially available packages are either all embracing and direct. The suppliers of these packages often offer software development and consultancy facilities in addition to the software licences. All embracing packages are designed for a wide range of applications. They are time consuming to learn and use and design modifications can result in having to completely re-model from scratch. Direct packages are usually designed to be easy and quick to learn and use, removing much of the basic model building, by offering a structure to build from. Many design changes can be studied in a few hours.

Dynamic Simulation
Cost Benefits and Design Advantages

S. F. Storey

Simatics Limited
Cambridge, United Kingdom

Dynamic Simulation
Benefits

Financial

Practical

Performance

Financial Benefits

Reduce the number of experimental trials

Many design changes can be assessed;
- in days, even hours instead of months
- without manufacturing and experimental costs

Prototyping is used to prove the design, not the concept as well.

Comparative designs can be easily studied.

Practical Benefits

- Comprehensive understanding of systems
- Study failure mechanisms
  - Design limits can be exceeded to study:
    - Vulnerable areas
    - Under or over designed components
  - Safety Limits can be determined:
    - Without potentially dangerous experiments
    - In extremes of operating environments

Performance Benefits

- Exercise designs and design changes:
  - Before ‘cutting metal’
  - In hours, even minutes compared to days
- Determine dynamic characteristics of:
  - Complete systems
  - Sub-systems
  - Individual components

Simulation Approach

- Start with a simple model
- Generally refine the model
- Focus on particular areas of interest
- Refine these areas
- Study convergence of results
- Change various parameters to look for particular sensitivities of the model

Simulation - Why ?

- Saves
  - Time
  - Money
- Increases
  - Efficiency
  - Understanding

Simulation studies

- Comparative analysis
  - trends
  - design improvements
- What-if ? scenarios
  - change parameters
  - add or remove components
  - operate outside the design limits

Simulation techniques

- Individual run
  - Study a number a defined parameter effects
- Multiple run
  - Iterative parameter changes
- Monte-Carlo analysis
  - Study the effects of multiple parameter changes
    - for example:
    - Examining a range of suspension stiffnesses
    - Changing masses and moving mass centres

Simulation options

All embracing

- eg Language based
  - ACSL
- Icon based
  - Sim-u-Link

Direct

- eg SIMTRAK
  - Flowmaster

All embracing packages

Offer a wide range of applications

Non-specific, mainly equation or Icon based

Require much model building time

Often require complete re-modelling for even small model changes

Usually complex and difficult to use

Data input and results output have to be specifically defined by the user

Direct packages

Structured for particular tasks

Generally parameter based and menu driven

Require limited, if any, model building

Quick and simple to analyse model changes

Simple to use and often comprehensive in the features offered in their subject area

Data input and results output are configured to the requirements of the analyses

Tracked Vehicle Suspensions

SIMTRAK

- Input parameters
  - Terrain profile
  - Vehicle masses and inertia's
  - Track properties
  - Suspension characteristics
  - Initial conditions

Simatics Limited

Military Systems Analysis

Vehicle analysis

SIMTRAK

Tracked Vehicle Suspension Analysis

SIMDRIVE

Vehicle Drive Line Performance Analysis

Gun Dynamics

SIMBAD

Barrel, Shot and Mounting Dynamic Analysis

SIMBIB

Internal Ballistic Analysis

RIDE DYNAMICS OF TERRAIN VEHICLES

Horst Göhlich
Technical University of Berlin, Germany
Institute of Agricultural and Construction Machinery

ABSTRACT

The optimization of the dynamic behaviour of terrain vehicles follows basically two aims. These are the measures for the increase of driving comfort and those of driving safety.

While driving on a street or a terrain vibrational movements occur on the vehicle, mainly because of the unevenness of the ground. Those vibrations are transferred through the vehicle into the driver, who can be submitted to a strong load.

The dynamic behaviour of non-suspended vehicles is a function of many factors. The geometry of the vehicle, the quality of the tires, and the spring and damping behaviour of these tyres are of major importance for driving safety and comfort. An evaluation of the suspension displacements, the forces, the accelerations, etc., is needed to make a statement about the driving behaviour of a vehicle.

1. INTRODUCTION

One of the most well known terrain vehicles is the tractor, mostly used in agriculture. It's development during the last decade is characterised by the enhancement of size and power as well as by the improvement of the dynamic behaviour and comfort.

A first approach for the decrease of vibrational loads was the improvement of the seat suspension, especially air-suspended seats. However the main disadvantage of any seat suspension is the fact, that an ergonomically accepable damping is limited and relative movements between the seat and the controls occur, which in any case causes discomfort for the driver particular when high amplitudes of the vehicle body become effective.

2. GENERAL ASPECTS OF DRIVING DYNAMICS

While driving on a track, vibrational movements occur on the vehicle, mainly because of the unevenness of the ground. Additionally, the "non-ideal" form of the tyres (excentricity, non-circularity) and the unbalanced masses of the wheels create selfexcited vibrations.

Those vibrations are transferred through the vehicle into the driver, who can be submitted to a strong load. Furthermore, dynamic stresses in the constructional components of the vehicle are created. Simultaneously, the wheel loads can differ considerably. The loads on single wheels may be temporarily nil, which is especially dangerous when the steering front wheels are concerned, in which case the steering ability of the vehicle is temporarily lost.

Among the most important characteristics of the vibrational behaviour of unsuspended tractors are the natural frequencies of the vertical vibrations, the pich and the roll. The value of these frequencies, as well as the amplification of the excitation in the resonance points is determined mainly by the weight and the moments of inertia and the properties of resilience of the tyres, because in general other suspension elements do not exist. The natural frequencies for tractors lie between 2,0 and 3,5 Hz. The maxima of the frequency response functions are in general high, because the only suspension elements - the tyres - possess a very low damping coefficient.

3. THE INFLUENCE OF THE TYRE ON THE RIDE DYNAMICS

The dynamic behaviour of non-suspended vehicles on public roads is a function of many factors. The geometry of the vehicle, the quality of the tyres and the wheel rim, and the spring and damping behaviour of these tyres are of major importance for driving safety and comfort.

For die vibrational charcterisation of tyres, a distinction beetween the quasi-static and the dynamic condition has to be made. The following considerations refer to the spring and damping properties, as well as to the transfer and the amplification of the distortion influences.

Nonuniformities, unbalanced masses and inhomogenities of the wheel and tyre material create vertical dynamic forces on the rolling tyre, which are repeated with every revolution. If the excitation frequency is equal the natural frequency of the vehicle, then considerable vertical amplitudes can create in the resonance region - a very frequent case. Fig. 1 shows this behaviour in the case of a rear tyre (18.4 x 38) with a radial run-out of ± 2 mm.

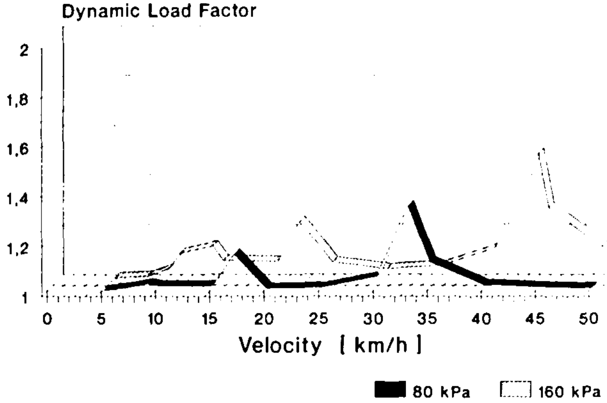

Fig. 1: Dynamic load factor as a function of velocity and inflation pressure (m = 1550 kg, tyre size 13.6 x 38). Dynamic load factor = $1 + F_{z\,dyn\,max} / F_{z\,stat}$

Because of the impulses caused by the lug contact and lug separation of the deeply lugged agricultural tyres, high frequency excitations are introduced into the chassis of the vehicle. Those vibration screate additional stresses in the structure of the vehicle and reduce the driving comfort.

Wear is in general an amplifying factor for the high-frequency vertical vibrations. With continious wear the vibration exitation of the system tyre-vehicle increases and the driving comfort decreases in consequence.

The research to date indicates, that for a complete investigation of the properties of tyres as well as the entire vibration behaviour of the vehicle, not only the new tyres but also the used worn tyre must be investigated. Measurements on agricultural tyres show that the intensity of the excitation will increase strongly, even with minimal wear.

Recent investigations of principles on tyre wear on our new band test stand showed among other the dependance of the average friction coefficient at various wheel speeds, Fig. 2. More detailed measurements on different areas of a lug explored the following friction values of a finite profil element, Fig. 3. Fig. 4 represents the slip distance covered along the contact area.

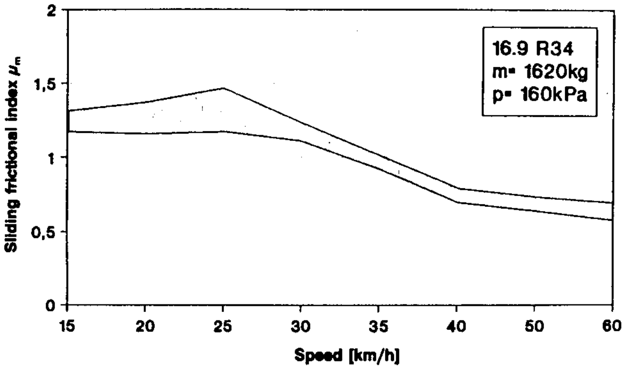

Fig. 2: Average frictional index, resulting from the inertia forces of a lug part as a function of the wheel speed (after Siefkes, 1993).

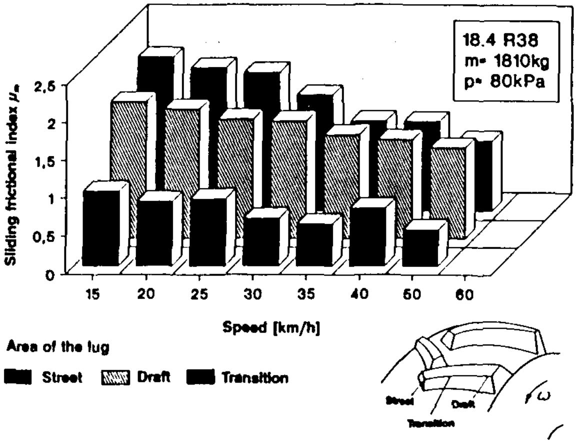

Fig. 3: Average frictional index, related to inertia force of a finite profile element depending on the area of the lug (after Siefkes, 1993).

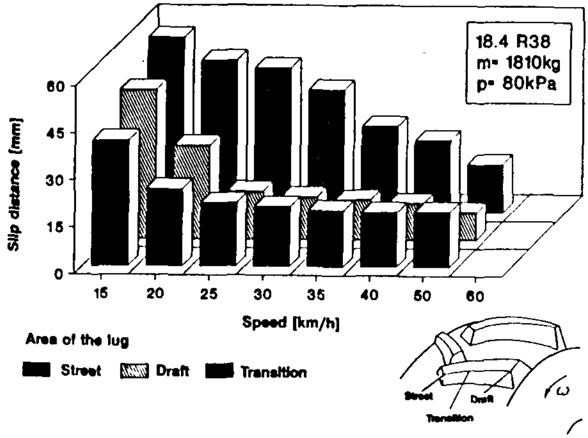

Fig. 4: Total slip of a finite profil element during wheel contact on the different lug areas (after Siefkes 1993).

4. DYNAMIC STIFFNESS AND DAMPING OF TYRES

As already shown for the low-frequency vibrational behaviour, the stiffness plays a major role for a tyre under load. It influences the frequency with which the vehicle vibrates. Furthermore, the stiffness determines the maximal possible load. The damping influences the maximal possible amplitudes of the vibrational system tyre - chassis mass.

A significant difference is drawn between the static and the dynamic stiffness and betwe~~n~~en the static and the dynamic damping. The static parameters are measured with simple force-displacement experiments, where the wheel-axle is fixed. Contrarily the dynamic parameters are determined with a preloaded, freely vibrating tyre.

The vertical stiffness and the damping of the tyre are to a high extent non-linear. They depend on the physical values load, inflation pressure, velocity and temperature. They also change with the excitation frequency, caused by the roughness of the route. Furthermore, differences in stiffness and damping can be determined that are due to the different ways of tyre construction, Fig. 5.

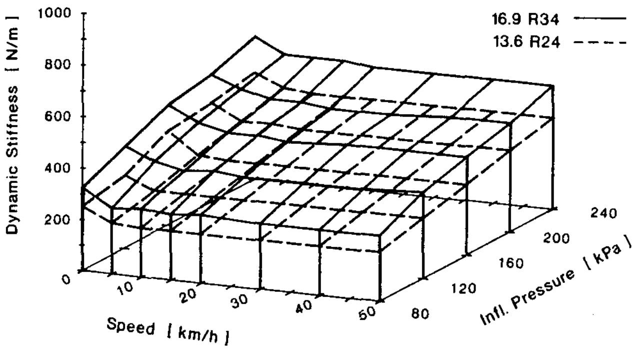

Fig. 5: Dynamic stiffness of a front and rear tyre as a function of the velocity and of the inflation pressure (front: m = 958 kg, tyre size 13.6 x 24; rear: m = 1560 kg, tyre size 16.9 x 34).

The stiffness of agricultural tyres has the following typical characteristics:

- Between 0 - 10 km/h the stiffness decreases by approximately 20% to 25%.
- Above 10 km/h the stiffness is constant.
- Increasing the inflation pressure will result in an increase of the stiffness.
- For higher work loads the stiffness will increase.
- Diagonally braced carcass tyres possess a 10% to 20% higher stiffness then comparable dimension radial tyres.
- With increasing excitation frequency the tyre stiffens.

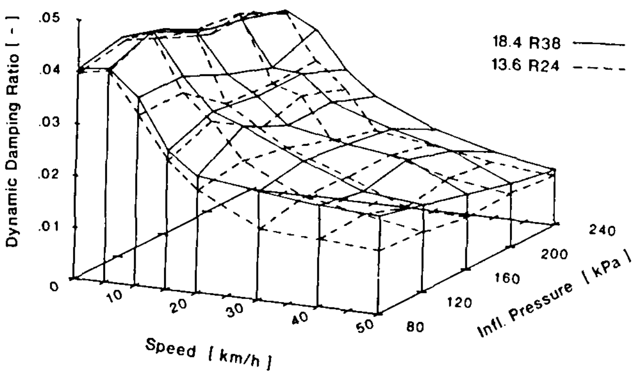

Fig. 6: Dynamic damping constant of a front and rear tyre as a function of the velocity and cf the inflation pressure (front: m = 970 kg, tyre size 13.6 x 24; rear: m = 1620 kg, tyre size 18.4 x 38).

Typical characteristics can also be identified in the behaviour of the dynamic damping of large volume tyres shown in Fig. 6.

- Often the damping increases slightly between 0 - 5 km/h about 5%.
- Above 5 km/h the damping declines asymptotically. For 50 km/h the limit with 30% of the original value is reached.
- With increasing inflation pressure the, damping declines.
- Higher workloads to an increase of the damping.
- Diagonal braced carcass tyres show higher damping for low inflation pressures than comparable radial tyres. For high inflation pressures no differences can be found.

5. TECHNIQUES FOR VIBRATION ISOLATION

Because of the limited time, I can not go deeper into the evaluation of vibration. You may find it in the book titled "Progress in Agricultural Physics and Engineering" edited by John Matthews - CAB International

Besides the "classic" measures for the isolation of vibrations, i.e. the suspended seat, other solutions have to be considered. Threee basic systems can be named, possessing specific advantages and disadvantages:

- suspended cabin
- front axle suspension
- implements as dynamic vibration absorbers.

(Fully suspended vehicles are not discussed at this place, because their application is still limited for agricultural and simular purposes).

The cabin suspension uses the principle of the vibrational isolation of the driver workplace. One important advantage of this solution is the much higher total suspended mass compared to the system seat/driver, leading to considerably lower natural frequencies. In such a case, a simplification of the driver seat's suspension system becomes possible. A further improvement of driver comfort results from the avoidance of relative movement between the driver body and the controls. Due to further progress in the utilisation of electric and hydraulic transmission elements on the tractor, the connections of the operating controls to the unsuspended parts of the tractor will become less difficult.

A stable suspension construction is needed to ensure kinematically exact guidance of the cabin as well as to fulfill the requirements of the law, concerning overturning and resistance to continued rolling of the vehicle. Fig. 7 shows a relatively simple construction of a cabin suspension.

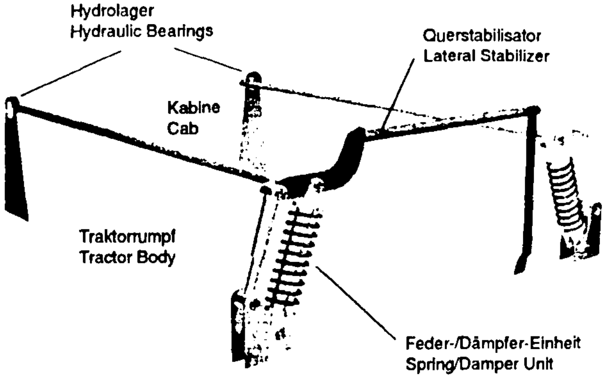
Hydrolager
Hydraulic Bearings
Querstabilisator
Lateral Stabilizer
Kabine
Cab
Traktorrumpf
Tractor Body
Feder-/Dämpfer-Einheit
Spring/Damper Unit

Fig. 7: Cabin Suspension FENDT Favorit 800 Series (Schematic).

A suspended front axle will lead to an amelioration of the driving stability and safety because of the decrease in the dynamic front axle forces (Fig. 8). The vibration stresses on the driver depend to a considerable extent on the position of the seat with reference to the axles. A mid-mounted cabin normally represents an optimum position also with respect to the suspended front axle. Furthermore, such a cabin position will result in an increase of the front-axle load, which will consequently stabilise the front part of the vehicle.

The third solution is represented by an absorber system using mounted implements. The absorption principle presupposes a simple spring-mass system, which will normaly be effective for one specific operating frequency. Under these conditions the system will be completely calm (front wheel loads). Because of the varying implement masses and the vehicle excitation frequency range the system will be broadband and need additional damping (Fig. 9).

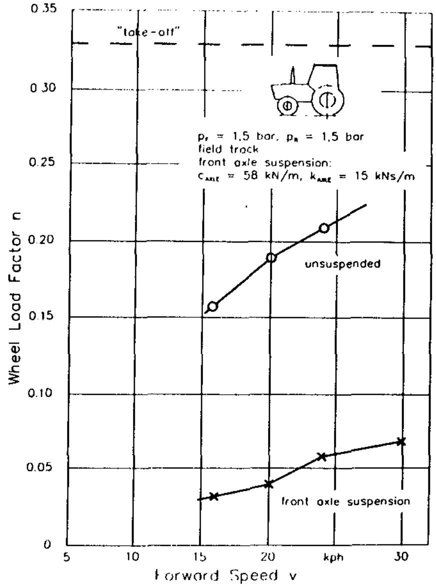

Fig. 8: Measured curves of the wheel load factor. (After Weigelt, 1987).

Much more practicable is an active system, allowing a complete absorbtion by automatic control of the electro-hydraulic lift. A digital controller reduces the dynamic front-axle loads, leading to considerable increase in driving comfort. It has been proved that the use of control systems of this kind will permit doubling the speed while maintaining the same vibrational loads.

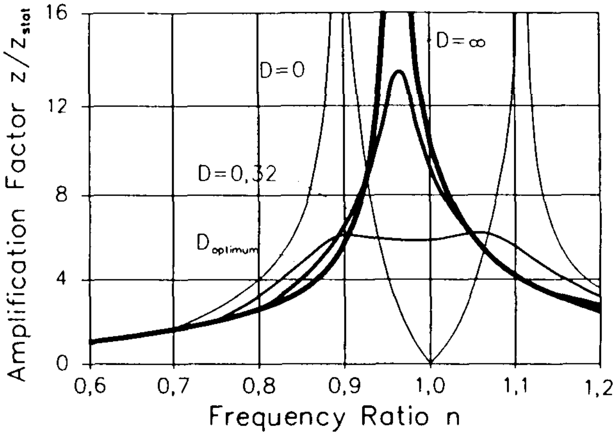

Fig. 9: Transfer function of an absorber for different dampings.

The use of mounted masses for the absorbtion has a decisive significance for the exclusion of critical driving conditions during the transport of mounted implements. However, such a device does not solve the vibration problems of empty tractors or tractors towing trailers.

Together with our investigations on the electronic control of diesel-injection-pumps and their advantage for an complete engine-transmission-management-system, we also investigated the pitch and longitudinal vibrations damping by a fast change of the engine speed with reasonable success.

As a result of our computer simulation works, Fig. 10, gives the vertical acceleration value of the different concepts on the vehicle vibration of the front axle (DX 86, SIMPACK, Hussey Highway, 27 km/h).

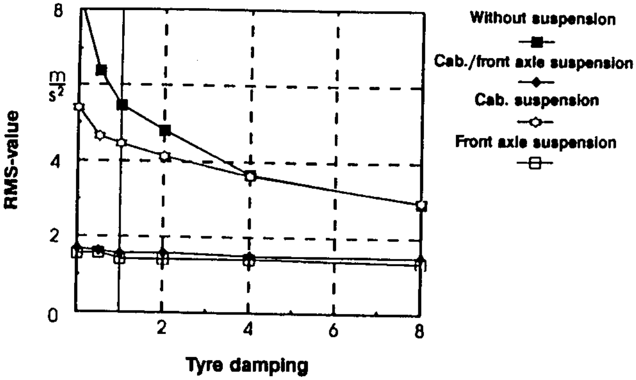

Fig. 10: Influence of different spring systems of the vibration at the front axle (after Pickel, 1994).

CONTROLLED SUSPENSION FOR OFF-ROAD VEHICLES

D. A. Crolla

Department of Mechanical Engineering
The University of Leeds
Leeds LS2 9JT

Abstract

The topic which has dominated vehicle dynamic studies over recent years is that of suspension systems. These have been variously described by a wide variety of names, such as 'active', 'intelligent', 'adaptive', etc. However, they all have one feature in common - they incorporate some **controlled** element. Public attention has been drawn to these developments through the glamour of Formula 1 racing, although ironically, advanced suspensions offer greater potential for much more practical vehicles. The technology behind the various types of advanced suspensions is not, however, well understood, with much of the literature containing dramatic comments and ambitious claims for the potential improvements in performance.

The first aim of this paper is to describe the alternative systems that have been proposed. The second is to address two fundamental questions:

- What are the potential benefits offered by these alternative systems?
- What are the practical implications in terms of costs and power requirements?

The final aim is to tailor the above the above comments to off-road vehicle design. Work to date (see, for example Sharp and Crolla, 1987) has concentrated on road vehicles, mainly passenger cars, and some additional interpretation is required before existing measured and predicted results can be applied to off-road conditions.

Background

To set the scene some comments on current practice in passive suspension design are appropriate. The fundamentals of the suspension problems are reasonably well understood and good design requires an effective compromise between:

- passenger (and cargo) ride comfort
- suspension working space usage
- tyre/ground contact force variation
- vehicle attitude control

The quarter car model, shown in Fig. 1, provides a good framework for considering the first of these key aspects of performance (Sharp and Crolla, 1987). For example, designers recognise that low spring stiffnesses and hence low natural frequencies lead to good isolation, but such suspensions then require large dynamic deflections, and conflict, therefore, with other demands on space. Selection of damper settings, often the subject of an immense amount of practical testing, is a compromise between ride vibration isolation and control of wheel hop resonance.

Choice of the best suspensions settings would be difficult enough if the problem were really as simple as implied in Fig. 1, but the real vehicle has a wheel at each corner and it relies on the suspension to control body roll when cornering. Roll behaviour is of key importance in dictating the handling behaviour of the vehicle and, in general, a soft suspension which provides good isolation also allows significant body roll which is undesirable for good handling and stability. Hence, yet another set of design compromises must be reached. Although a somewhat over-simplified view, this arrangement is weighted towards handling (stiff suspensions) for most European cars, towards ride (soft suspensions) for American and some French cars, and towards soft suspensions (for both ride and ground following ability) for off-road vehicles.

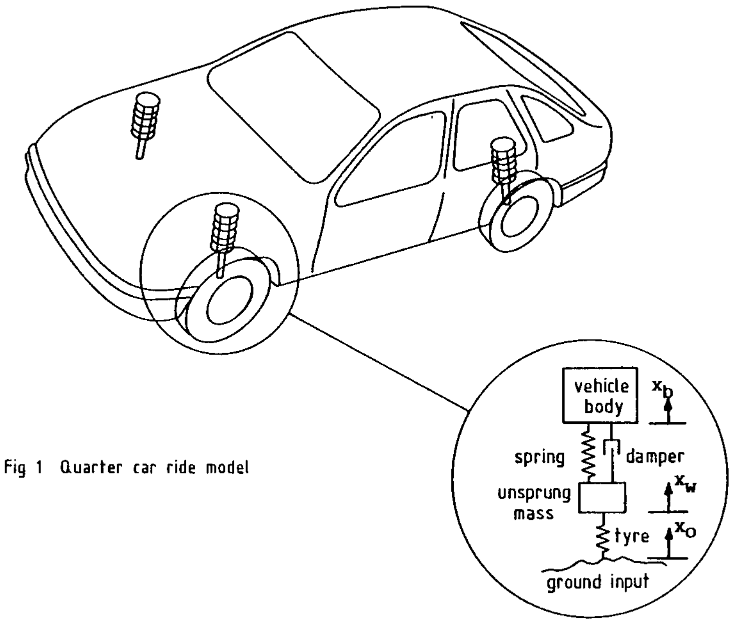

Fig. 1 - Quarter car ride model

The potential for an intelligent suspension which can do better in relation to this compromise is now clear, but there is one more important issue. Real vehicles operate over a wide range of running conditions (i.e. surfaces and speeds). If one were simply able to pick the passive spring and damper settings for each condition, then significant performance improvements could be gained without the need for any of the expensive actuators that are often associated with intelligent or active suspensions. This principle, that the suspension adapts to the particular running condition, offers another potential source of improvement and discussion of it will form an important part of this paper.

For off-road vehicles, there are some additional constraints to be considered (Crolla *et al*, 1987). First, the range of surfaces over which an off-road vehicle must operate is normally much wider than for a road vehicle. Second, for agricultural applications, the vehicle may have an implement attached which requires accurate control relative to the ground surface (e.g. plough, sprayer boom). Third, the constraints imposed by the requirements for all wheel drive and high transmitted torques further restrict the design freedoms for advanced suspensions. Finally, although controlling the dynamic tyre/ground load remains an important feature in maintaining good on-road handling, it is also important off the road for controlling the generation of tractive forces.

Suspension systems compared

Table 1 outlines the main features of different suspension systems. The principle of operation of the fully active, slow-active and semi-active systems is similar and is summarised in Figs. 2 and 3. Transducers mounted on the body and wheel measure information about the system 'states', i.e. x_o, x_b, x_w, $\dot{x}_b$ and $\dot{x}_w$. This information is monitored by a microprocessor which then acts according to some pre-programmed control law and issues a demand signal. The actuator and associated control hardware attempts to track this force or displacement demand signal faithfully, operating in the conventional closed loop manner.

The main analytical difficulty lies with obtaining a suitable control law. Mathematical techniques are available for this; the most straightforward, but unfortuantely the most impractical because of the need to measure the gound profile, comes from classical optimal control theory. This 'full state feedback approach' requires transducers to measure x_o, x_b, x_w, $\dot{x}_b$ and $\dot{x}_w$. The force demand signal (U) is then simply,

$$U = k_o x_o + k_1 x_b + k_2 x_w + k_3 \dot{x}_b + k_4 \dot{x}_w$$

The optimum k values are those which minimise a specified Performance Index, which in this case contains body acceleration, suspension working space and dynamic tyre load with weighting factors controlling their relative importance.

For the more practical case in which not all the state information is measured, iterative techniques for obtaining a reduced set of control gains are available (Wilson *et al*, 1986). In particular, measuring the ground profile height, x_o, is not an attractive proposition from a practical viewpoint. The same operating principle applies to the semi-active and switchable damper systems, except that the force demand can only be dissipative since such systems cannot put power into the suspension.

Basic design factor is working space requirement

Comparing the performance of competing systems is not a straightforward matter and until recently resulted in great confusion reflects the designer's basic approach to the problem; i.e. given this amount of working space, what is the 'best' suspension in terms of the performance criteria already discussed?

Using this approach, the relatively simple addition of self-levelling offers substantial advantages over conventional passive systems, the percentage gains being related to the laden/unladen mass ratio of the vehicle. The benefits arise simply from the fact that if there is no static deflection associated with adding the load, then more suspension working space is available and this can be exploited by using a softer spring than conventional (Fig. 4). Results for a 12 t prototype farm transport vehicle (FTV) with 6 t payload (Crolla et al, 1987) indicate that just by adding a self-levelling facility, ride improvements of more than 50% can be achieved.

Table 1 - Suspension Systems Defined

Passive - A system comprising only springs and dampers. Neither the rates of the springs nor the dampers are capable of being changed by external signals. The suspension is only capable of storing, restoring and dissipating energy; there is no means of supplying external energy to the system.

Passive, self-levelling - This operates exactly as a passive suspension except that external energy is provided to maintain constant ride height of the vehicle in response to changes in *static* loading. Typically, such systems would be pneumatic or hydro-pneumatic and have a delay time of several seconds before any levelling corrections were made.

Dissipative semi-active - A system with the ability to continuously vary the rate of energy dissipation. Typically, this involves controlling the orifices of a damper or the force across some equivalent actuator. A minimal amount of energy is required because the damper or actuator never has to supply energy to the suspension system, it only has to dissipate energy but in a more intelligent way than a passive damper.

Limited bandwidth or slow-active (Fig. 2). - A system in which an actuator acts in series with the passive suspension spring. Such an actuator may be based on hydraulic or electrical components and would have typically a bandwidth of around 3 Hz. It is this limitation in frequency response which distinguishes the slow active system form the fully active system described next.

Active (Fig. 3). - A system in which an actuator either totally replaces the conventional spring and damper elements or acts in parallel with a spring. The actuator works according to a force demand signal typically generated from a microprocessor on the basis of measured information about accelerations and displacements of the vehicle body and wheel. This type of system requires a significant amount of energy and the bandwidth is limited only by the frequency response of the actuator and control components, which would typically be hydraulic aerospace quality with a bandwidth of 60-100 Hz.

Adaptive - An adaptive system is one in which some suspension parameters can be altered in response to a change in the vehicle operating condition (e.g. different road surface for forward speed). So, for example, a passive system could be adaptive if a number of discrete spring and damper rates was provided. The adaptive control would select the 'best' spring and damper settings for the particular condition. Thus, for smooth roads it may select soft springs and low damper settings and then switch to high spring and damper settings when the vehicle is on a rough road or track. Equally, an active system can (and in fact almost certainly would) be adaptive. In principle, the active system only has to change some feedback constants used in the control law in order to be adaptive and since these are stored in the microprocessor, it is a relatively simple operation to vary them according to some predetermined plan.

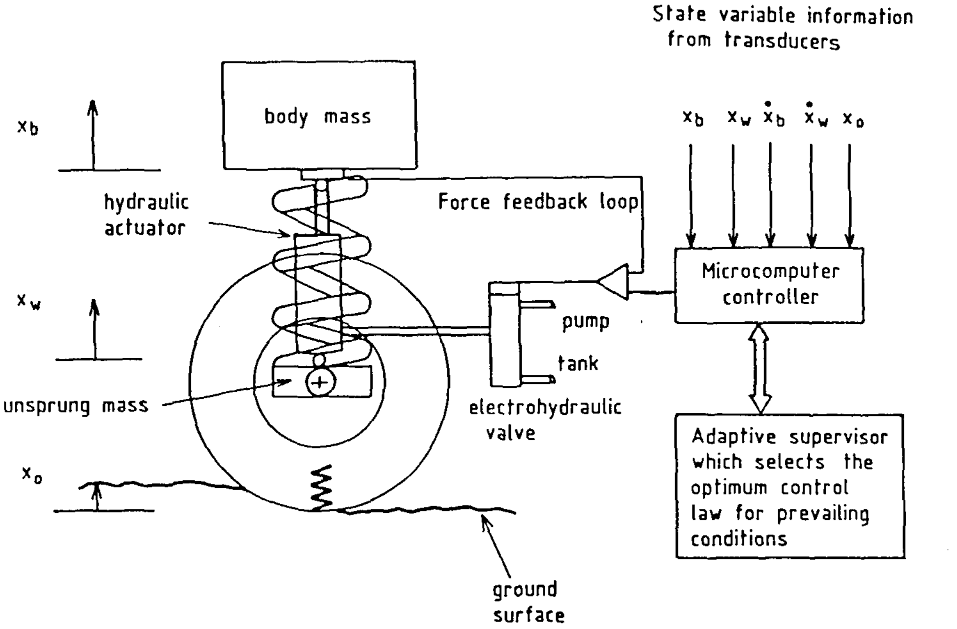
State variable information
from transducers
x_b
x_w
$\dot{x}_b$
$\dot{x}_w$
x_o
body mass
x_b
hydraulic
actuator
Force feedback loop
Microcomputer
controller
x_w
pump
tank
unsprung mass
electrohydraulic
valve
Adaptive supervisor
which selects the
optimum control
law for prevailing
conditions
x_o
ground
surface

Fig. 2 - Fully active suspension system with a spring in parallel to carry the static load

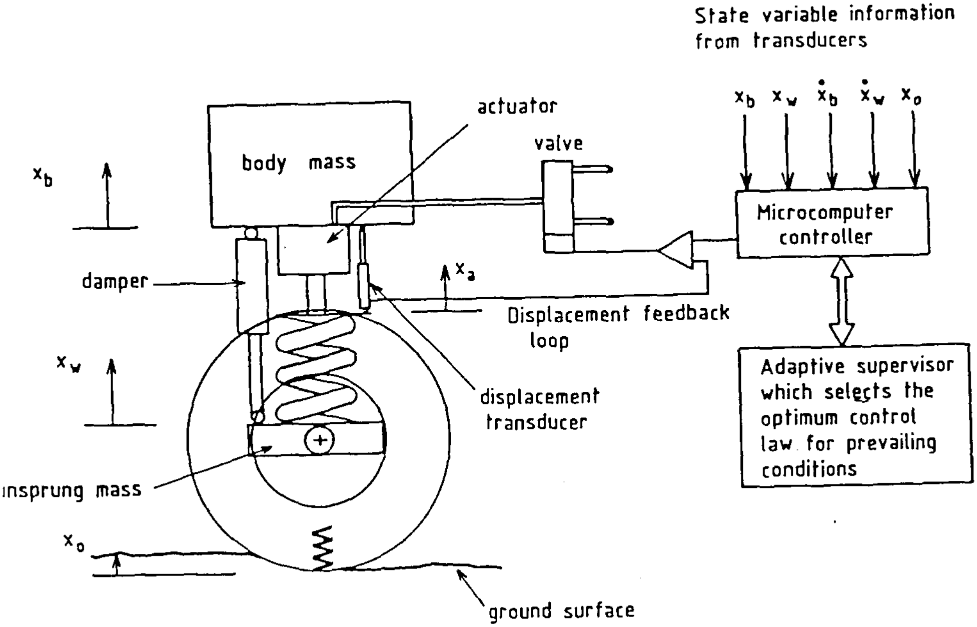
State variable information
from transducers
x_b
x_w
$\dot{x}_b$
$\dot{x}_w$
x_o
actuator
valve
body mass
x_b
Microcomputer
controller
damper
x_a
Displacement feedback
loop
x_w
displacement
transducer
Adaptive supervisor
which selects the
optimum control
law for prevailing
conditions
nsprung mass
x_o
ground surface

Fig. 3 - Limited bandwidth active (or slow active) suspension system with a spring in series with the actuator

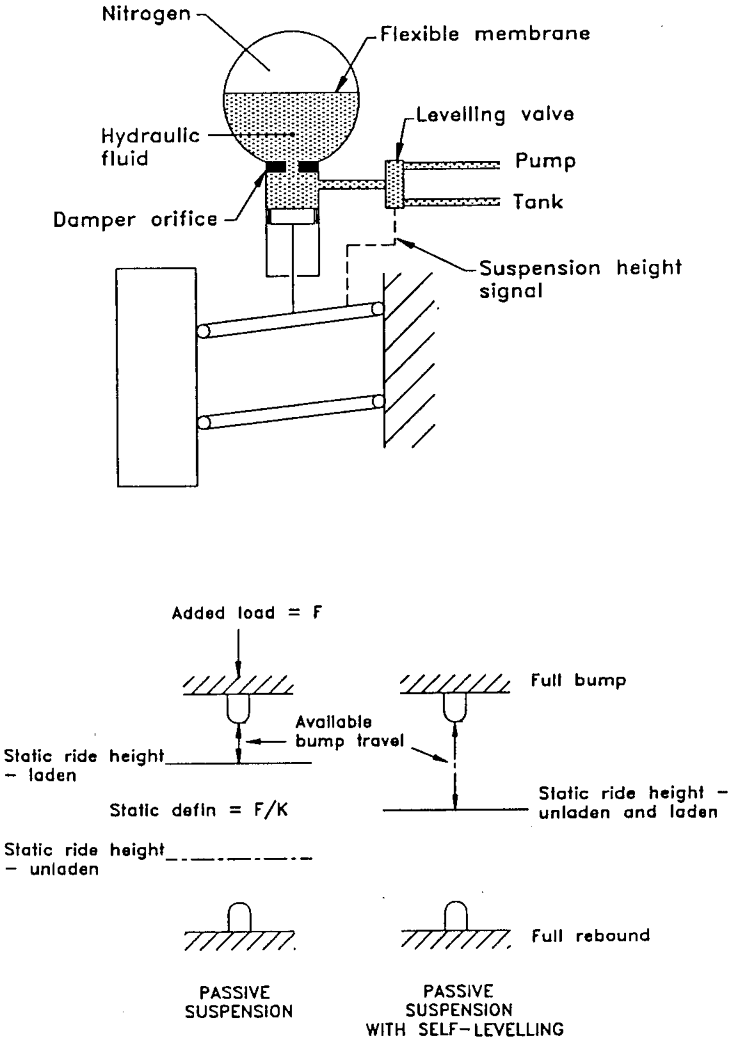
Nitrogen
Flexible membrane
Levelling valve
Hydraulic fluid
Pump
Tank
Damper orifice
Suspension height signal
Added load = F
Full bump
Available bump travel
Static ride height - laden
Static defln = F/K
Static ride height - unladen and laden
Static ride height - unladen
Full rebound
PASSIVE SUSPENSION
PASSIVE SUSPENSION WITH SELF-LEVELLING

Fig. 4 - A hydropneumatic implementation of a self-levelling suspension (upper) and the resulting improved use of the available working space (lower)

Thus, there are some significant potential gains available from modest changes to passive systems; the drawback is that vehicle attitude is less well controlled by the softer suspension. However, one method of counteracting roll and pitch angles arising from cornering and braking manoeuvres was proposed many years ago by Automotive Products (Crolla *et al*, 1987). This hydropneumatic system incorporating a hydromechanical valve arrangement has proved to be successful on prototype vehicles although it has never achieved commercial success.

The next level of sophistication involves the **controlled** suspensions already described. Predicted results using data for a single wheel station of a typical passenger car (Sharp and Hassan, 1989) are shown in Fig. 5. Results calculated using data for the farm transport vehicle have revealed similar trends (Crolla and Aboul Nour, 1988). These predicted results shown in Fig. 5 were obtained from calculations in which the quarter car model traversed a random ground profile at three different speed/roughness conditions. The suspension working space usage was exactly the same for all the systems shown. For the active and passive systems, the lines indicate that there are a number of systems with different stiffness, damping or feedback gain values which satisfy this working space requirement.

Advantages of active systems

These condensed results contain several interesting findings which are contrary to some of the folklore surrounding active suspensons. First, although active suspensions show clear advantages over passive arrangements, the potential improvement in terms of ride performance is at best only about 25%.

Second, the biggest improvements arising from the active suspensions occur on the roughest sufaces. A more strict intepretation of this is that the biggest improvements are shown when the ratio of road roughness to available working space is greatest. At the other end of the spectrum on the smooth main road surface, a purpose-designed passive system can achieve similar performance to the active system. However, there are other factors to be considered in addition to these ride results. The passive system which achieves this performance is extremely soft by comparison with conventional systems so that static deflection and body attitude control would pose insurmountable problems. The comparable active system, however, would overcome both these problems.

A third conclusion is that the slow active system provides similar performance to the fully active one. This appears to be extremely significant from a practical viewpoint because the components associated with the limited bandwidth, slow active system are much cheaper than those for the fully active system, which requires high bandwidth, (aerospace quality) components. Although the layout shown in Fig. 3 looks rather impractical, the same principle can be achieved using a hydropneumatic system with a valve controlling the oil flow to the struts, as discussed later.

Fourth, the semi-active system based on a continuously variable damper which is able to track a dissipative force demand shows worthwhile advantages. Such systems, which are currently of great interest in passenger car design because of their negligible power requirement, would almost certain be used with self-levelling control and some form of roll control system. This would allow softer suspension spring rates to be exploited.

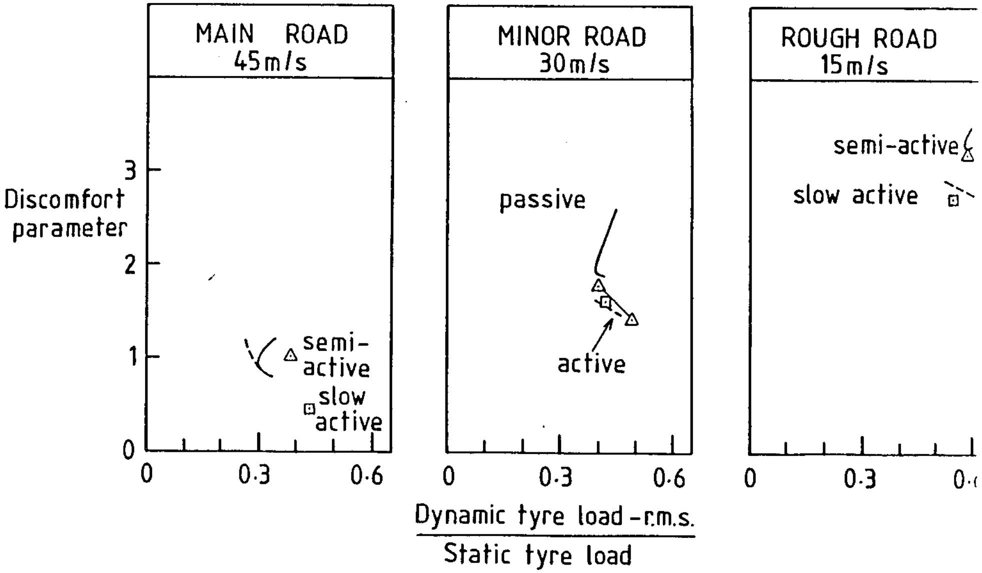

Fig. 5 - Benefits available from controlled systems over passive (solid line) for 3 surfaces (constant workspace = 180 mm)

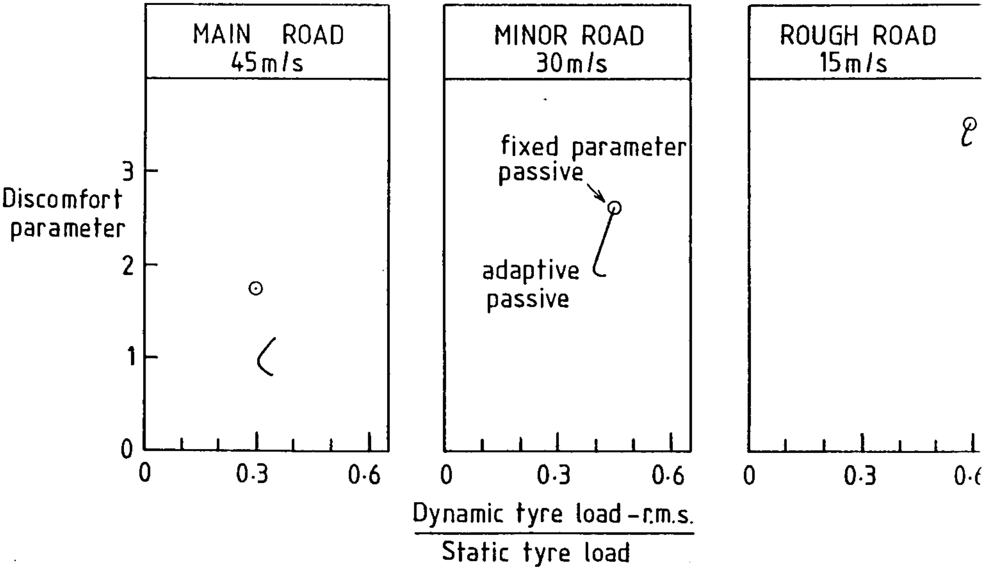

Fig. 6 - Benefits available from an adaptive system over a conventional, fixed parameter passive system over 3 surfaces (constant workspace = 180 mm)

The fifth, and most important, advantage of active systems is a more subtle one. Returning to conventional passive systems, the main weakness is that the designer must choose parameter values, whereas what he would like to adapt the stiffness and damping values to each road/speed conditions. The benefits of being able to do this are shown in Fig. 6.

There are, however, significant practical problems associated with altering the suspension stiffness over the required range. With the active systems, however, they have the additional advantage that there is no problem in building in an adaptation strategy. The 'parameter values' are essentially a set of control gains held in a microprocessor and these could easily be updated as the vehicle speed or road conditions change.

Special considerations for off-road operation

There are several features which are specific to operation off the road and which influence the aforegoing comments.

Rough surfaces - Off-road vehicles operate over the roughest surfaces and find themselves, therefore, at the very end of the operating spectrum where the biggest percentage improvements are available from active systems. Thus, as an overall guideline, bigger potential benefits are available to off-road vehicles compared to on-road vehicles.

Range of surfaces - The main design constraint on off-road vehicles arises from the requirement to operate off the road. However, in most applications (e.g. agricultural, military, earthmoving, forestry etc.) the vehicles must also operate for substantial periods on roads at ever increasing speeds. Thus, the range of surfaces over which they must travel is far wider than for other vehicles and large benefits are available from exploiting the principle of adaptation discussed previously.

Large working space - Passive suspension designs for off-road applications require relatively low spring stiffness and large wheel travels. This, in turn, means that control of roll angles and static deflections is often more of a problem than for road vehicles. However, it also means that the addition of relatively simple enhancements, such as self-levelling or slightly more complicated ones like roll angle control result in substantial improvements. This has already been shown for the prototype FTV (Crolla *et al*, 1987) and military vehicles (Maclaurin, 1983). Similar hydropneumatic suspension systems to those used on those vehicles are now beginning to appear on other off-road vehicles (e.g. Chafer SSV spraying vehicles).

Power usage - Recent calculations of power usage are summarised in Tables 2 and 3. These results refer to a single wheel station for a FTV, and all the components are assumed to be 100% efficient (Crolla and Aboul Nour, 1988). This provides a basis for comparing the fundamental differences between the various control schemes. Also, for both the fully and slow active systems, a conventional passive spring is assumed to act in parallel with the actuator to take the static vehicle load. Although this modifies the values of the control gains, it does not compromise the overall performance of either system.

Three main points emerge. First, for the power-consuming systems, there is very little difference in mean power usage. Second, the mean powers dissipated by all the systems are remarkably similar. Of course, the detailed way in which the power is dissipated must be different in each case to account for the different performances. Finally, because there is an order of magnitude difference between power dissipated and demanded, it suggests that the way in which intelligent suspensions gain most of their advantage is in controlling the dissipation of power.

Hydropneumatic system promising for future

Fully active systems appear to have little commercial future. The costs associated with high quality actuators and servo-valves are likely to remain prohibitive for many years.

Table 2 - Comparison of mean power demand with active and slow active systems - at equal dynamic tyre loads

Suspension working space, rms cm	Dynamic tyre load parameter %	Mean power demand W	
		Active	Slow Active
2.5	23	36	39
3.5	23	128	158
4.5	27-29	380	490

Table 3 - Comparison of mean power dissipation with different systems - compared at a dynamic tyre load of 23%

Suspension working space, rms cm	Mean power dissipation, kW				
	Passive	Active	Semi-active	Slow active	Switchable damper
2.5	1.48	1.43	1.41	1.53	1.40
3.5	1.40	1.40	1.27	1.54	1.35
4.5	1.31	1.51	1.31	NA	1.29

Switchable dampers are currently available commercially and more sophisticated, controllable dampers look a possibility for the near future. However, on their own, they do not offer enough advantages for off-road applications. They must be combined with self-levelling control and probably roll control, in order to exploit the use of low spring stiffnesses.

Slow active systems look attractive in terms of performance providing they can be engineered at reasonable cost. Although there are many possibilities involving the use of electrical, pneumatic or hydraulic elements (Sharp and Hassan, 1989), a system based on hydropneumatic components looks most promising.

Many of the components required for a hydropneumatic system have already been proven on off-road vehicles, so the key to extending the capabilities of the system further lies with the development of an electro-mechanical valve to control oil flow. The mechanical valves used in

the Automotive Products system which only control body attitude have never found favour commercially. However, if this valve were replaced by an electrically-driven flow control valve then all the benefits offered by the slow active system could be exploited as shown in Fig. 7 (upper); methods of reaching the static load could be engineered as shown in Fig. 7 (lower).

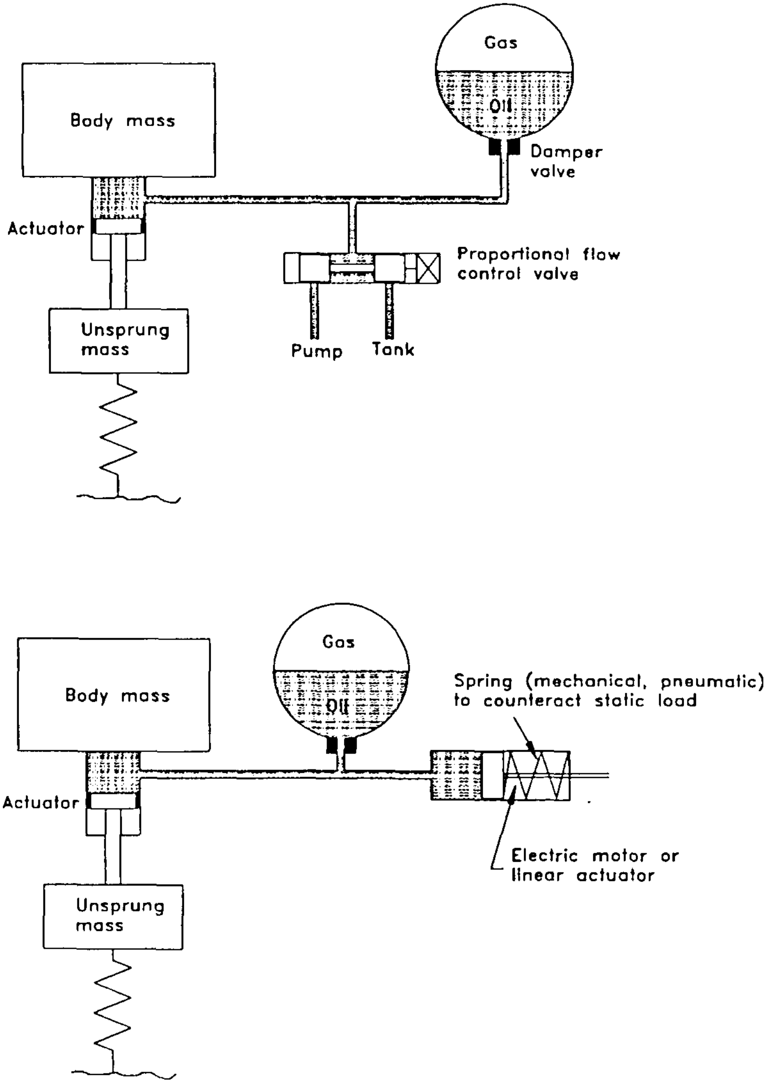
Gas
Oil
Body mass
Damper valve
Actuator
Proportional flow control valve
Unsprung mass
Pump
Tank
Gas
Body mass
Oil
Spring (mechanical, pneumatic) to counteract static load
Actuator
Electric motor or linear actuator
Unsprung mass

Fig. 7 - Hydropneumatic implementations of the limited bandwidth active system

Recent theoretical research has been carried out to investigate the potential of even more advanced active systems which incorporate preview information of the road ahead of the front wheels. There are various ways (see Karnopp and Heess, 1991) of tackling the controller design to exploit this information assuming it is available and undoubtedly significant performance improvements - of the order of 30% reduction in acceleration levels - are available. However, the problem of whether a height sensor (ultrasonic or laser based) can be made to perform adequately in this role has not yet been overcome and even then, cost and reliability issues remain.

On any vehicle which has a front and rear axle, a degree of preview exists - commonly referred to in the literature as "wheelbase preview" - arising from the fact that the input at the rear wheels is precisely a delayed version of that at the front. Control laws have been devised (Abdel Hady, 1991) to exploit this information and substantial performance improvements of around 25% are available - but only at the rear axle - if this wheelbase preview effect is embodied in the controller design.

Conclusions

Controlled suspensions offer substantial potential benefits to off-road vehicle performance. In several respects these potential advantages are greater for off-road vehicles than for passenger vehicles which have been the focus of attention of developments to date. In particular, the potential for making the suspension adaptive (i.e. selecting the optimum set of parameters for each road roughness and speed condition) looks particularly advantageous.

Two systems merit further detailed development for future advanced vehicle designs. The cheaper of these involves soft passive springs, adaptive dampers plus self-levelling (and possibly roll/pitch) control. The more expensive and sophisticated system involves hydropneumatic components operating according to the slow active strategy. The key to the future of this approach is in a low cost, electrically-driven control valve.

References

- **Sharp R S, Crolla D A** (1987). Road vehicle suspension design - a review. *Vehicle System Dynamics,* 16, (3), pp 167-192.
- **Crolla D A, Pitcher R, Lines J, Horton D N L.** (1987). Active suspension control for an off-road vehicle. *Proc I Mech E.* 301, D1, pp 1-10.
- **Wilson D A, Sharp R S, Hassan S** (1986). On the performance capabilities of active automotive suspension systems of limited bandwidth. *Vehicle System Dynamics*, 1986, 15, pp 105-118.
- **Sharp R S, Hassan S A** (1987). On the performance predictions of active automotive suspension systems of limited bandwidth. *Vehicle System Dynamics*, 16, pp 213-225.
- **Crolla D A, Aboul Nour A M A** (1988). Theoretical comparisons of various active suspension systems in terms of performance and power requirements. *Proc I Mech E Conf* on "Advanced Suspensions", London, pp 1-10.
- **Maclaurin E B** (1983). Progress in British tracked vehicle suspension. SAE Paper 830442.
- **Karnopp D, Hess G.** (1991). Electronically controllable vehicle suspension. Vehicle System Dynamics, 20, pp 207-218.
- **Abdel Hady M B A, Crolla D A** (1992). Active suspension control algorithms for a four wheel model. Int. J. Vehicle Design, 13, pp 144-158.

Session VII
Sektion VII

Vehicle Design

Fahrzeugkonstruktion

Latest Developments in Superstructures for All-Terrain Logistic Support Trucks

Dkfm. Dr. E. PRANCKL, Ing. W. WIESER
STEYR Nutzfahrzeuge AG, Steyr

ABSTRACT

The desire for simplified transport solutions and the rationalisation process being carried out all over the world including in the military sphere in respect of troop strength and the procurement of armaments have brought for military supplies a clear trend towards interchangeable bodies on cross-country military trucks.

The experience of the Golf War and our own projects already realised indicate increased transport capacity, simple and safe handling, personnel, material and time savings and the advantages of direct supply in operations.

Cross-country supply trucks and interchangeable body systems adapted for military operations are a precondition which will be more closely described in what follows.

1. The Historical Development

Military supplies have in the past been and are still today largely loaded and unloaded by hand onto and from standard military trucks.

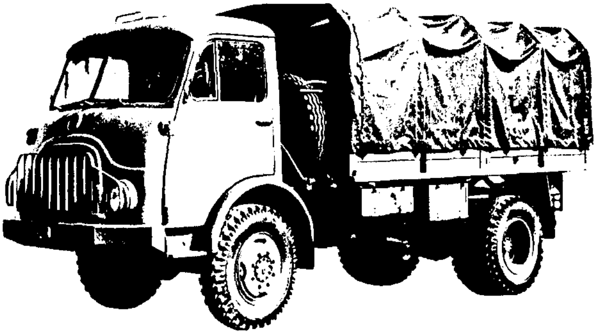

Figure 1. STEYR 680M/4x4, 4.5 tonnes

In recent decades considerably easier and simpler handling has become standard practice with the use of loading-aids such as tail-lifts, fork-lift trucks and loading-cranes.

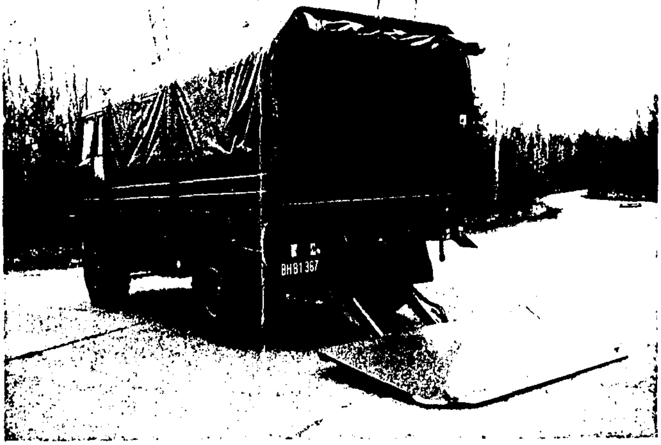

Figure 2. STEYR 12M18/4x4 with an electrohydraulic tail-lift able to lift up to 1500 kg

The next big step in the direction of further simplification, increased performance and relief for the crew was the introduction of vehicle-bound self-operating demountable bodies.

The American corps of engineers had vehicles with set-down facilities for transporting track boards and bridge-building equipment for on- and off-road operations as early as the end of the forties, beginning of the fifties.

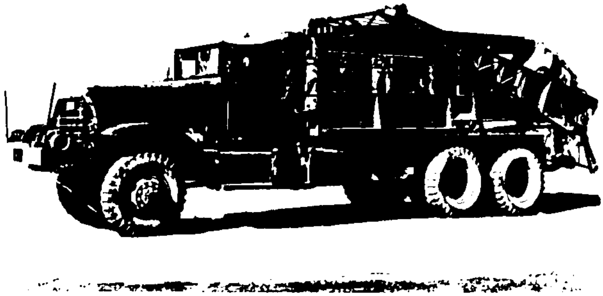

Figure 3. Cross-country bridge truck

Hydraulic lifting-devices of the US companies HEIL and DAYBROOK with a permissible load of 3600 kg were mounted on American BROCKWAY 6x6 chassis.
These vehicles were also used for many years by the engineering corps of the Austrian army.

The widespread use of hook devices in the non-military field above all for the transport of containers and bottle-banks brought further development.

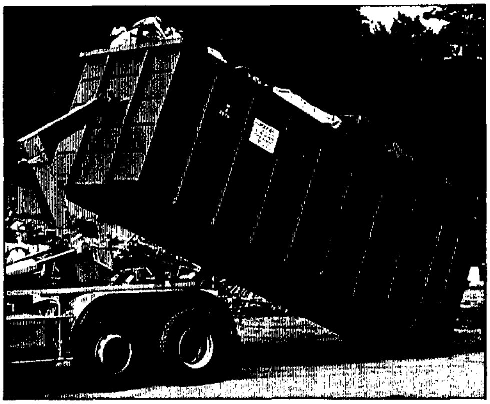

Figure 4. Commercial hook device with a rag-container

The first projects in the large armies of the Western world had begun by the middle of the eighties. Thus there has been a programme in the US army to procure a total of 5000 8x8 and 10x10 vehicles of the HEMTT series with 3-axle trailers.

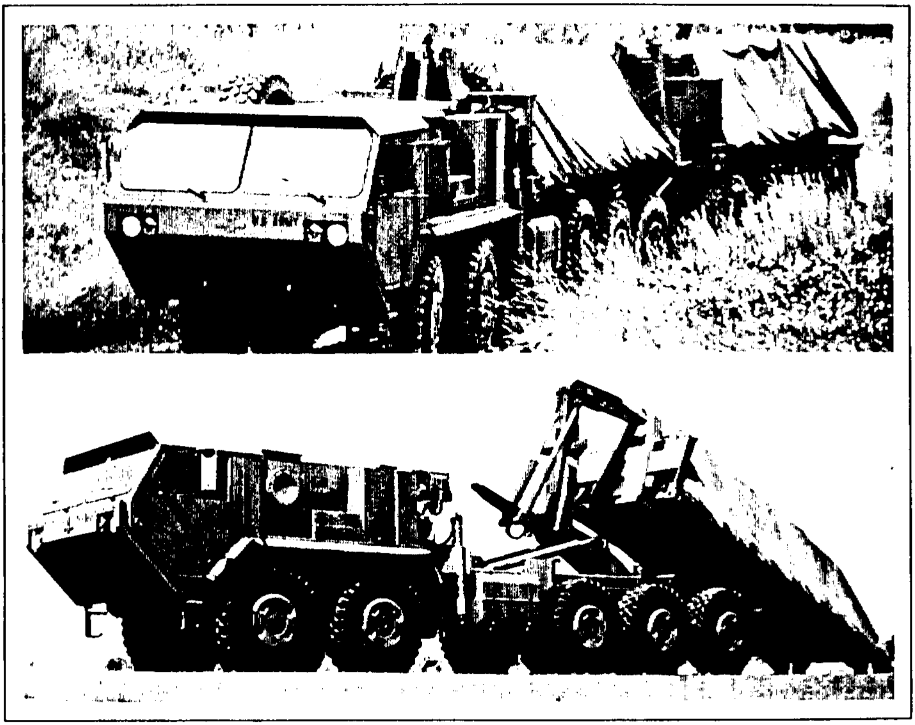

Figure 5. OSHKOSH HEMTT PLS truck with trailer

The British have also put a high-performance system into service with DROPS. This is mounted on the British 8x6 chassis of Leyland-DAF and the FODEN company.

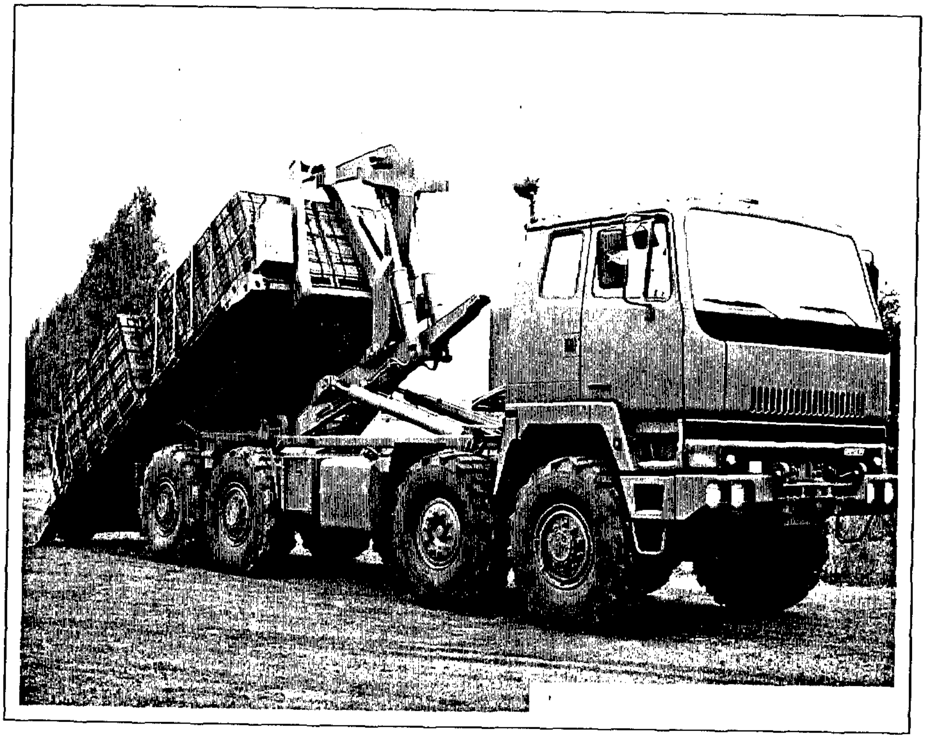

Figure 6. LEYLAND-DAF with DROPS

In both cases the set-down systems come from the British/Finnish company MULTILIFT. These vehicles have a payload of around 16 tonnes and are designed to transport loads in pallet form on so-called "flat racks".

2. The Experience of the Golf War

After the Golf War the British reported highly positive experience with this transport system used for the first time in active military service.

The result was a dramatic reduction in the loading- and unloading-time required and a rapid turn-round of goods with relatively few vehicles operating continuously.

Thus a platform can be loaded in around 33 seconds and set down in little more, i.e. 37 seconds.

The Commander-in-Chief of the British troops, General Sir Peter de la Billiere, reported that each vehicle of the Tenth Transport Regiment covered 400 miles per day transporting a total of 30 million litres of fuel and 50000 tonnes of material in a very intensive 3-week build-up in January, 1991, to supply the attacking troops. The number of PLS transport vehicles required was - and this is naturally not a cause for rejoicing for us as vehicle-manufacturers - only about 20 % of the number of standard vehicles.

3. Own Projects

When the Canadian armed forces placed an order with STEYR in the spring of 1988 for the delivery of 1200 320-hp 6x6 vehicles, a so-called BTS/DFRS variant was among the 8 different bodies. The abbreviation stands for Bridge-Transporter and Dismountable Flat Rack System. A total of 180 vehicles in this version were delivered.

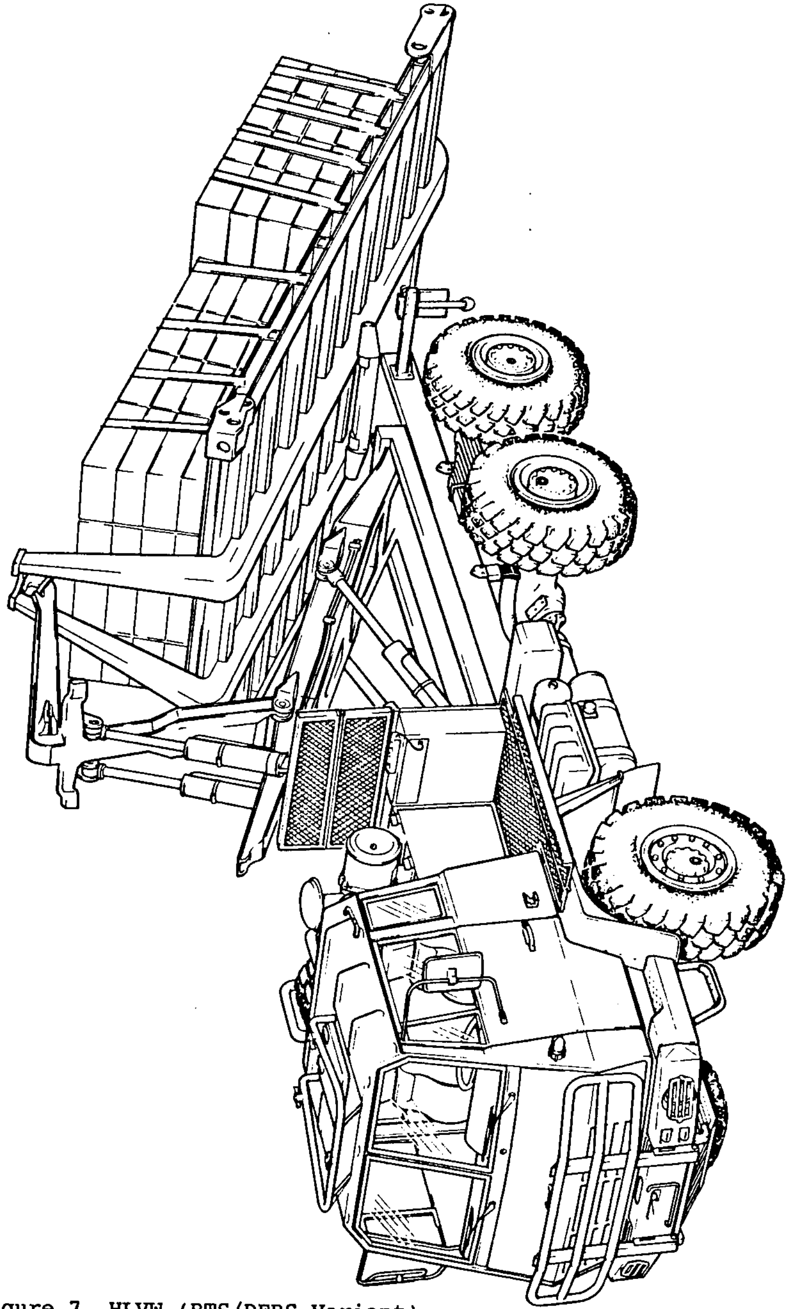

Figure 7. HLVW (BTS/DFRS Variant)

This is suitable for the transport of loads in pallet form on so-called flat racks, i.e. platforms and by means of a special adapter pallet

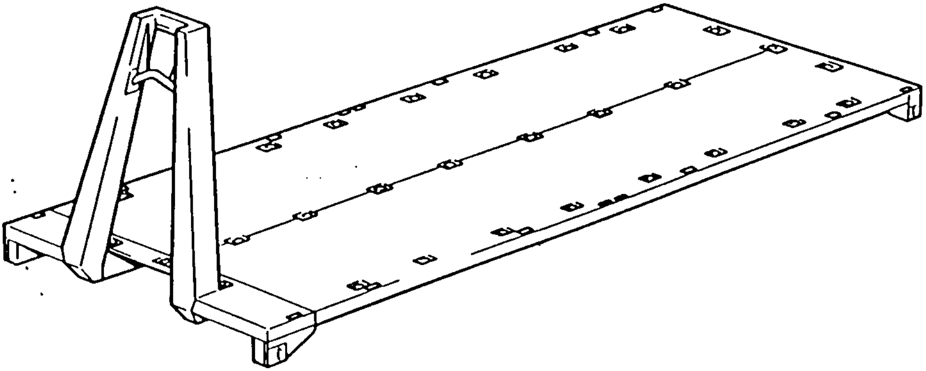

Figure 8. Depositable platform

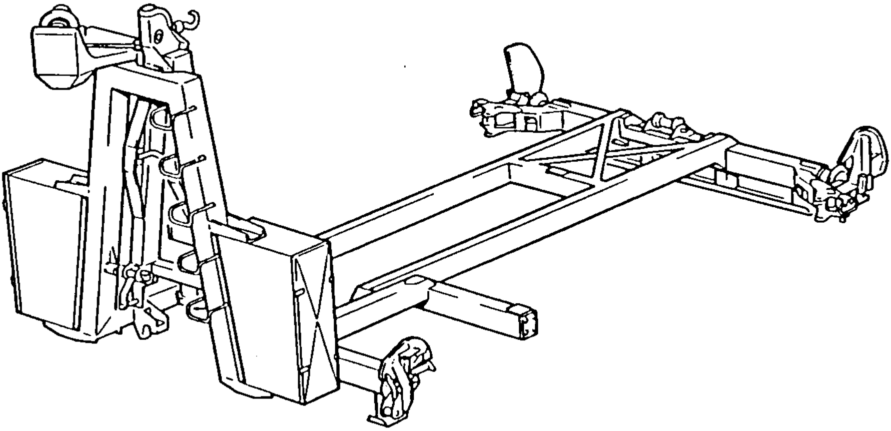

Figure 9. Bridge adapter pallet

for the transport of pontoon sections up to a payload of 10 tonnes.

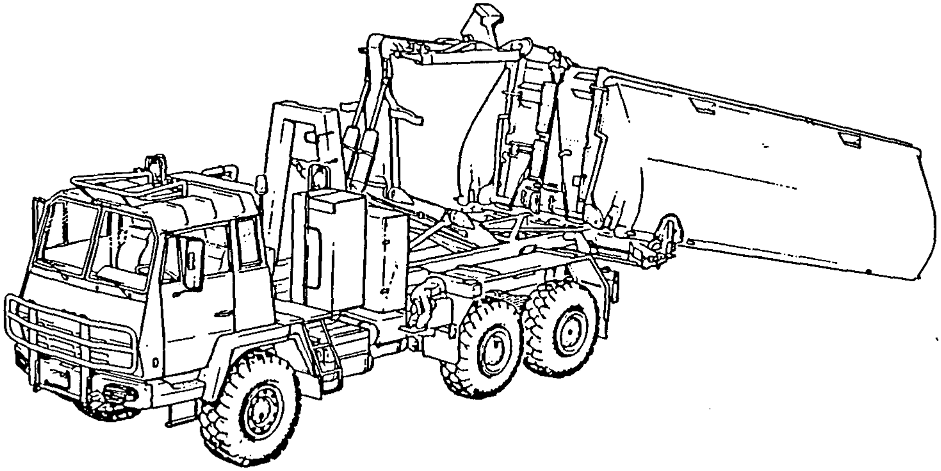

Figure 10. Canadian HLVW as a pontoon-transporter

When used as a bridge-transporter the vehicle can be driven with its rear end into water as deep as 1.5 metres, from which position the bridge section can be slid into the water where it unfolds by itself to the width of a two-lane road.

Figure 11. HLVW setting down an "Interior Bay"

The two different bridge sections are formed as a so-called interior bay with which a pontoon-bridge can be extended at will and as a ramp bay for driving on and off at each bank and have different lengths, i.e. the ramp bay is about 1 metre shorter.

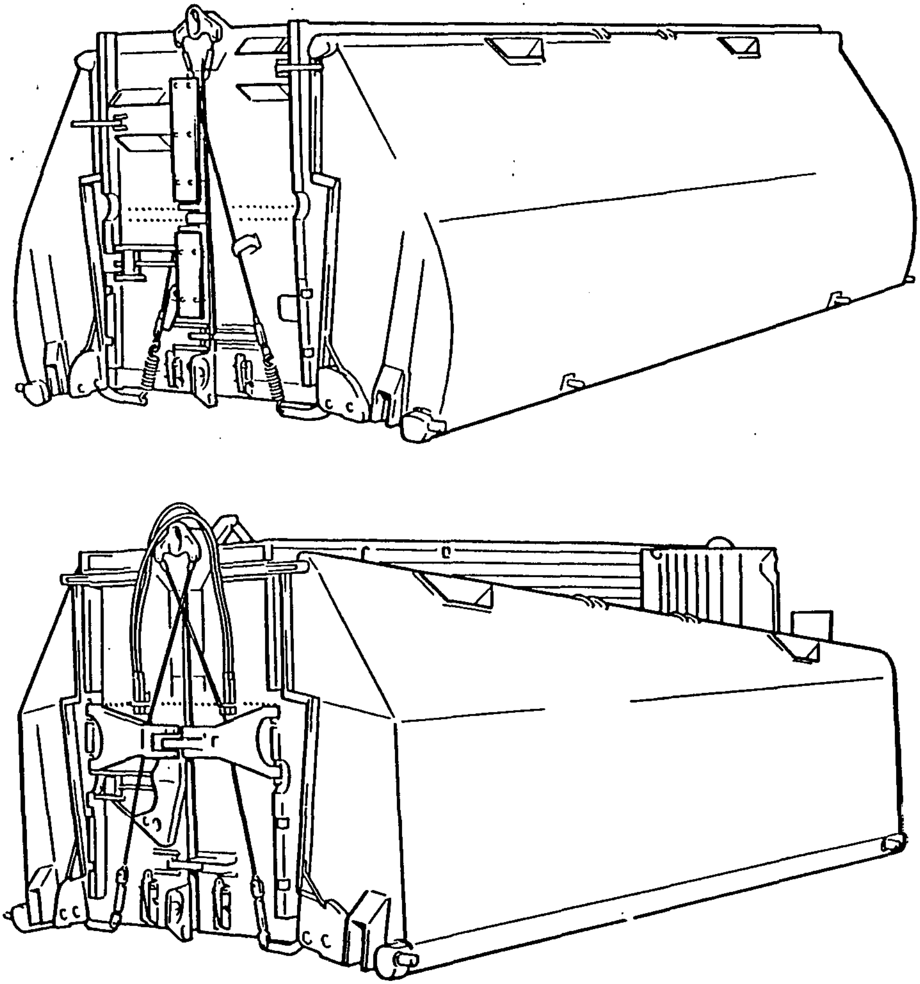

Figure 12. "Interior and Ramp Bays"

A hydraulically operated winch is mounted on the front vertical part of the adapter frame for pulling out and folding together the bridge sections and is connected with the hydraulic system of the carrier vehicle by means of quick couplers.

Figure 13. HLVW pulling out an interior bay

A blocking-device was provided for the second rear axle for lifting heavy loads and for pulling bridge sections onto banks.

Two hydraulic cylinders acting on the rear ends of the swivel springs and so on the axle body prevent too great a shifting of the weight away from the front axle while the centre of gravity of the load is behind the centre of the rear axle.

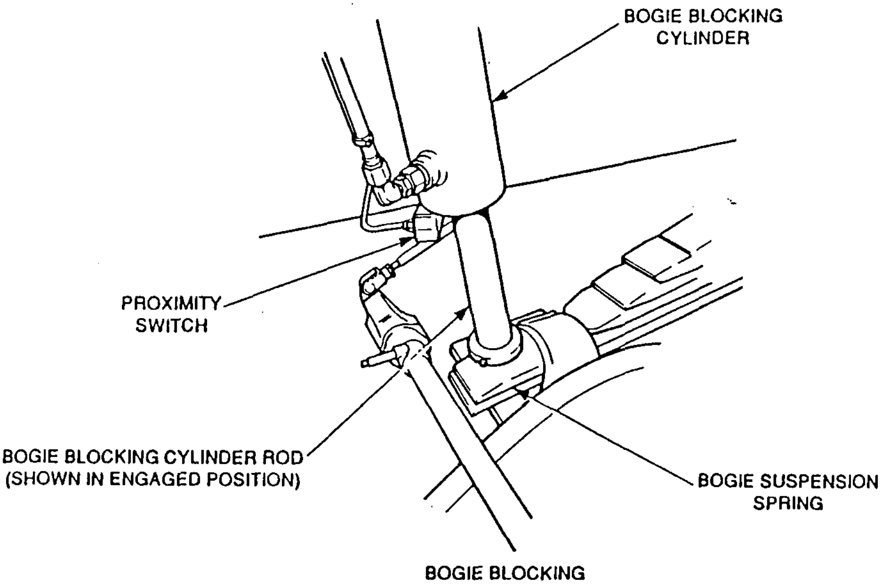
BOGIE BLOCKING CYLINDER
PROXIMITY SWITCH
BOGIE BLOCKING CYLINDER ROD (SHOWN IN ENGAGED POSITION)
BOGIE SUSPENSION SPRING
BOGIE BLOCKING

Figure 14. Blocking-device for the second rear axle

The dangerous situation of the vehicle leaving the ground at the front can in this way be effectively prevented. The loading of the second rear axle rises as a result to twice the nominal value, i.e. from around 10 to 20 tonnes.

Because there are no sudden impacts, this brief rise is possible without any plastic deformations on the axle body.

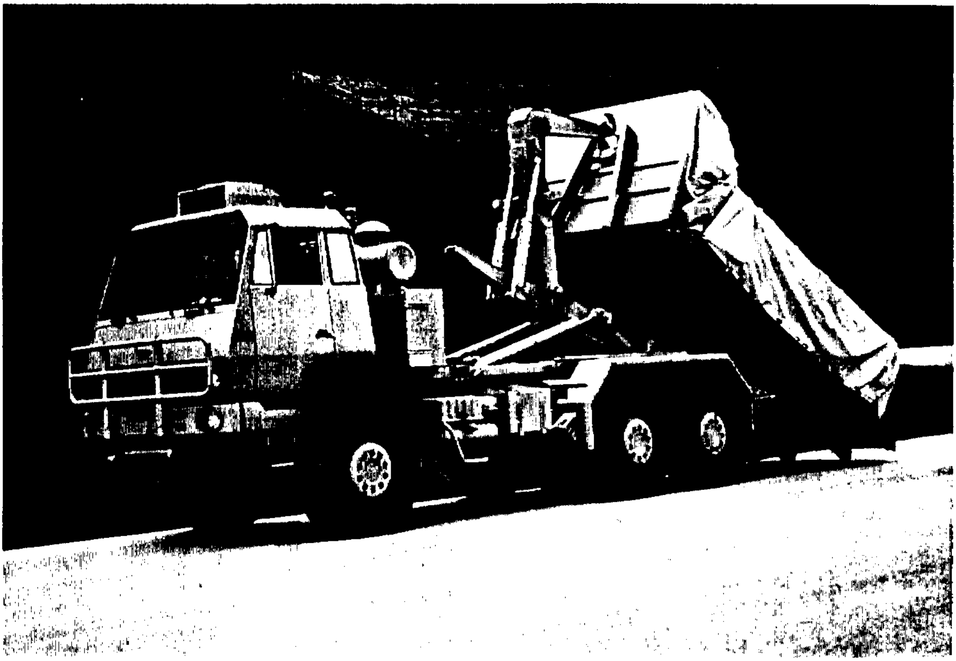

Figure 15. STEYR 26M42/6x6 taking on a platform

4. Further Developments

The MULITLIFT company has developed a so-called CONTAINER-HANDLING UNIT so that ISO containers can also be managed by these systems.

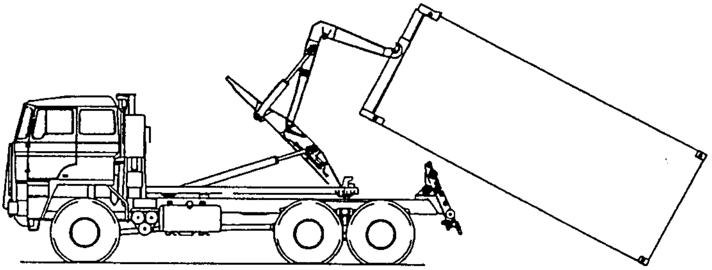

Figure 16. MULTILIFT hook device with a container-handling unit

An "H-frame" is bolted at the front on the face of the container on its corner brackets and every standard 20-foot ISO container can be loaded and unloaded with the normal hook system by means of roller blocks arranged to swivel.

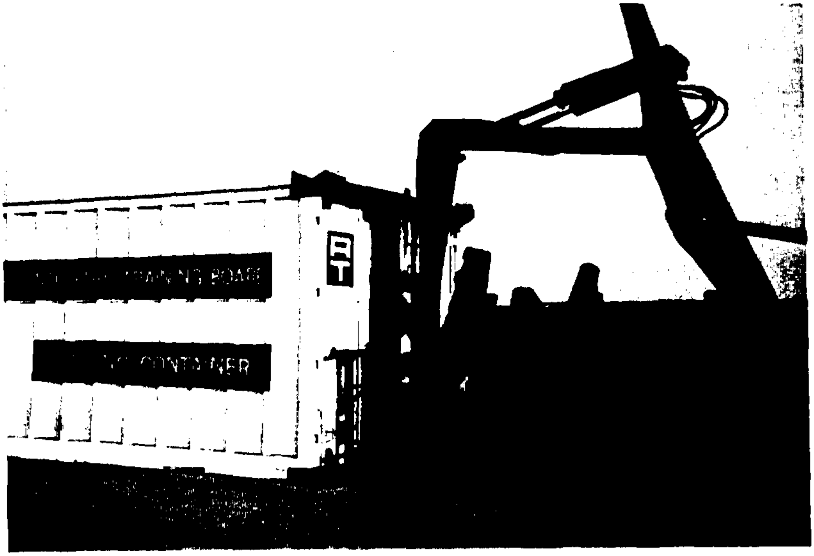

Figure 17. "H-frame" on a standard 20-foot ISO container

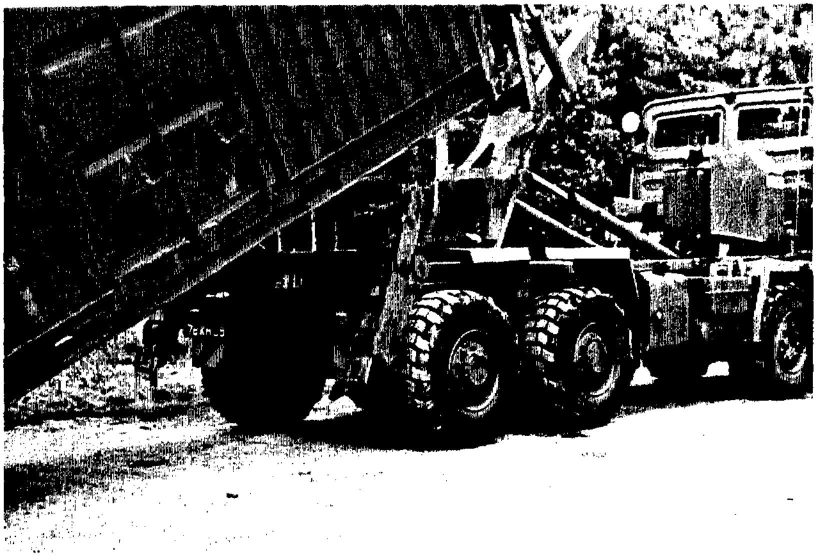

Figure 18. Roller assembly

One disadvantage of the ISO container is, however, that the load of the container can never be seen from the outside. This fact also proved to be a great disadvantage in the Golf War. For this reason thousands of containers had to be opened to find out what was inside them.

The "sideless container" or platforms with foldable front and rear walls are a solution to this problem. An insertable lifting-bow makes it possible to stack the folded platforms in a small space.

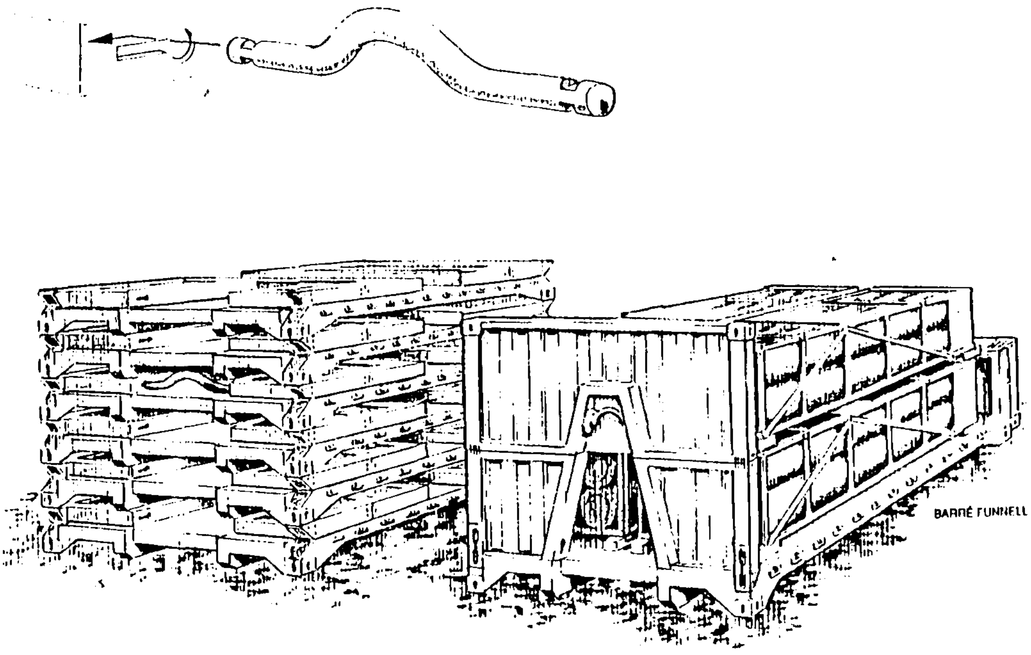

Figure 19. Foldable platforms with lifting-bows

The Norwegian HÄGGLUNDS MOELV company has presented an interesting innovation with a trailer that is loadable independently of the truck.

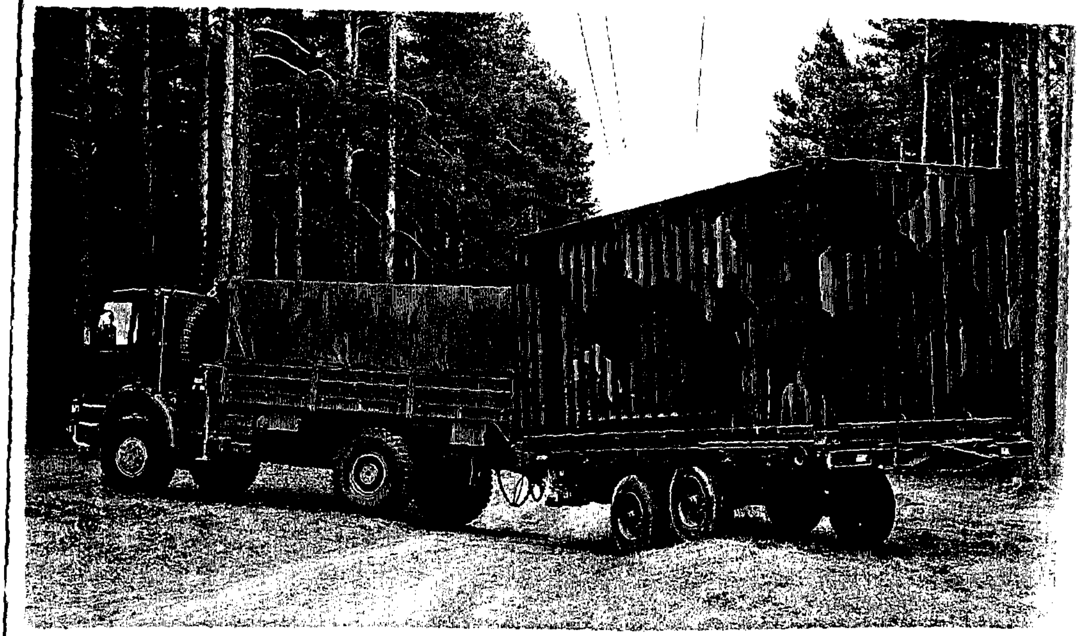

Figure 20. MB 63 MULTI 2-axle trailer

The hydraulic container platform, swivellable and movable towards the rear and with unfolding ramps,

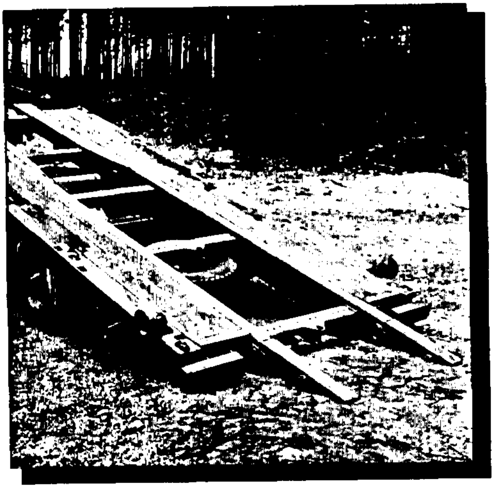

Figure 21. Platform and folding ramps

makes it possible to pull on a 20-foot container, this being done with the aid of a hydrowinch mounted on the trailer bar.

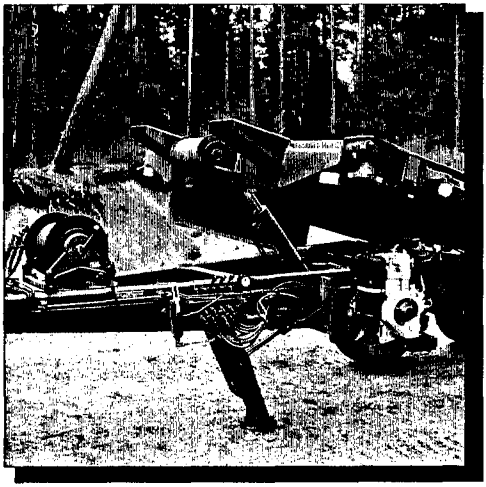

Figure 22. Winch, hydraulic drive with a diesel engine

The winch is driven by a diesel/hydraulic unit mounted on the side of the chassis frame and so can be operated independently of the truck.

A transverse beam with swivellable guide rollers is fitted on the corner brackets of the container at the front to make the pulling-on easy and the pulling-cable is fixed to this beam.

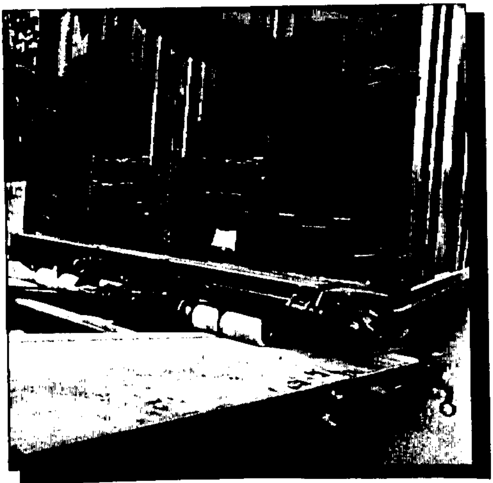

Figure 23. Transverse beam with swivellable guide rollers

Hydraulically extendable running-rollers are fitted next to the rear container locks to guide the rear part to the container. These rollers are retracted before the container is locked.

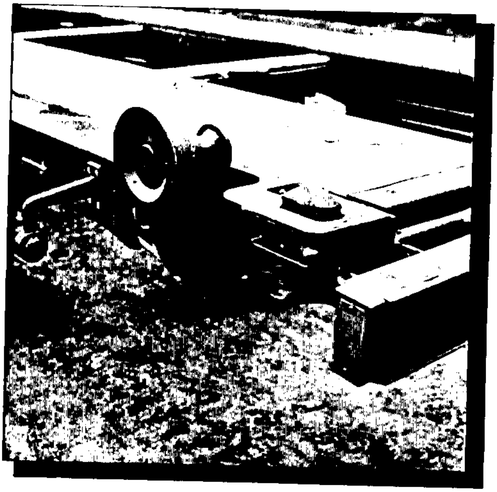

Figure 24. Hydraulically extendable running-rollers and container locks

5. Summary

The preceding explanations clearly indicate that a modern army cannot in future do without PLS vehicles. Above all for reasons of saving expense and time.

The very varied applicability is an additional advantage.

The Austrian army is also already thinking about introducing these systems and is in the happy position of being able to draw on the experience of others.

THE NEW MAN TRANSFER CASES FOR DEPLOYMENT IN ON-ROAD AND OFF-ROAD VEHICLES

Dr.-Ing. Karl Viktor Schaller
MAN Nutzfahrzeuge AG, Munich, Germany

ABSTRACT

In 1988 Zahnradfabrik Friedrichshafen (ZF) and MAN Nutzfahrzeuge AG concluded an agreement to develop a new family of transfer cases for commercial vehicles. The first series-production transfer case left the assembly line at the end of 1992 (see figure 1).

The family of transfer cases comprises four models of different sizes, all orientated to MAN's vehicle range:
The G 1000-2R (nominal torque 5,000 Nm) for the L 2000 range, the G 1000 (9,000 Nm) for the M 90 range, the G 1700 (16,000 Nm) for the F 90 range and the G 2500 (22,000 Nm) for heavy-duty operation.

The objectives of the development work were reduced costs and weight, improved performance, lower noise levels and low power divider losses.

Thanks to the application of the latest techniques in design (e.g. computation of housing with FEM), testing (e.g. holographic examination of noise radiation) and production (rotary friction and electron-beam welding), all development objectives have been achieved. The development process will be presented in the paper.

4,000 transfer cases have been installed to date.

INTRODUCTION

This paper is divided into the chapters:

1) Transfer case family
2) New design characteristics
3) Development examples

1) TRANSFER CASE FAMILY

Figure 2 shows the new transfer cases in comparison to the old.

Why was there a need to replace the old and reliable transfer case family?

First of all, the newly designed trucks have a higher torque spectrum in the drive-train and reach the limits of the old transfer cases.

Secondly, in 20 or 30 years of component life manufacturing and design methods change. This results generally in new components with fewer but more complex parts. The total of assembling and manufacturing leads to better costs for new components.

Thirdly, application profile changes. For example, the noise legislation led to new design objectives.

The above mentioned facts led to a development contract with Zahnradfabrik Friedrichshafen (ZF) in 1988. The first series-production transfer cases with new design left the assembly line in 1992.

The old and the new ranges of transfer cases were structured with regard to the MAN vehicle range.

Our heavy weight truck - the F 2000 - has a G 1700 instead of the old G 801 for standard applications. Heavy duty applications in excess of 60 t have now a special transfer case - the G 2500-2.

G 1000-1/-2, G1700-1/-2, G2500-2

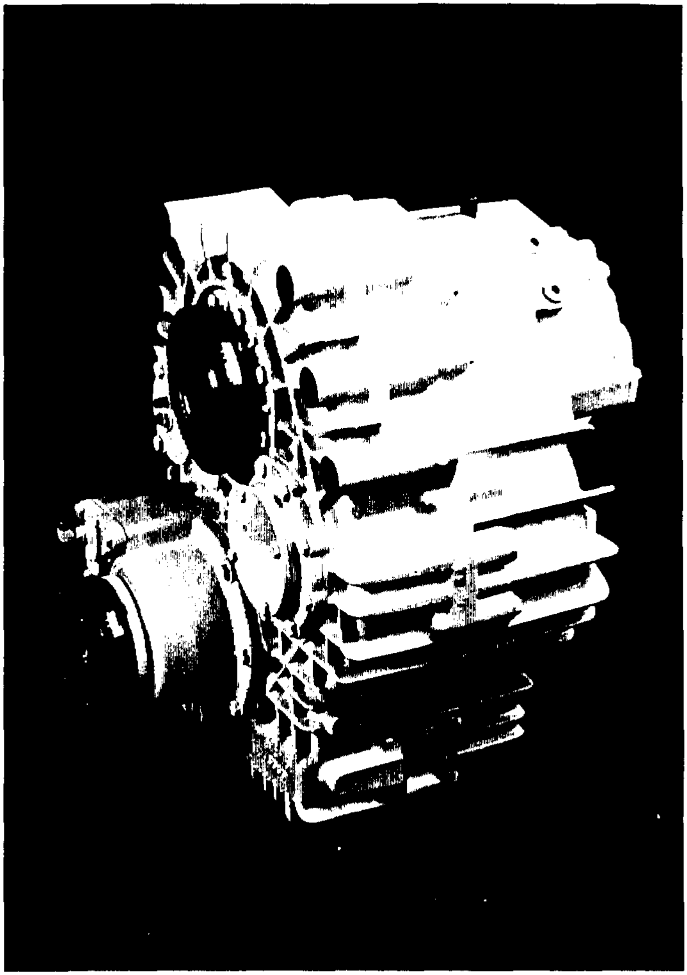

TKA

Figure 1

New Range of Transfer Cases

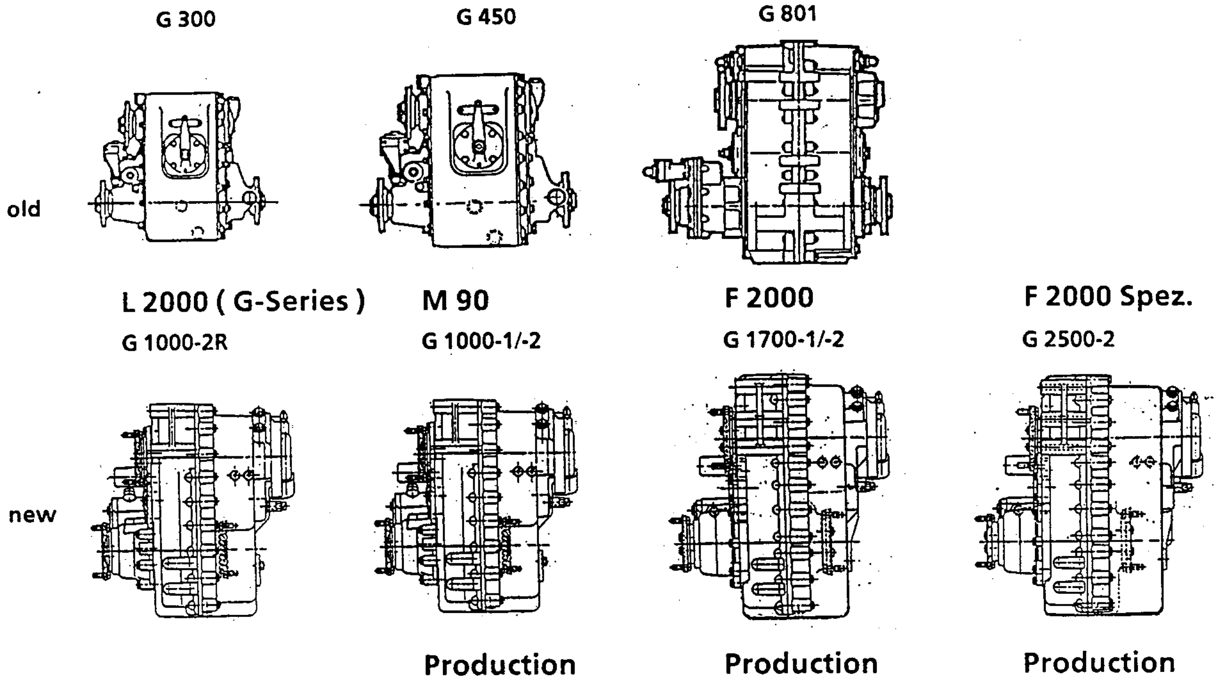
G 300
G 450
G 801
old
L 2000 (G-Series)
G 1000-2R
M 90
G 1000-1/-2
F 2000
G 1700-1/-2
F 2000 Spez.
G 2500-2
new
Production
Production
Production

TKA

Figure 2

New Range of Transfer Cases

Medium-weight trucks in the M 90 range will have the new G 1000 instead of the 30 year old G 450.

The L 2000 (light-weight) will start its all-wheel-driven life with the new G 1000-2R. The 'R' in the name of the transfer case means 'reduced' torque capacity. The gearbox design incorporates many parts of the stronger G 1000 to reduce the number of parts for the family.

Figure 3 shows an overview with technical data for all members of the transfer case family. In addition to figure 2 you can see that there are two more transfer cases - G 1000-1 and G 1700-1. These transfer cases are single-speed and have the same data as their twin-speed brothers. Why we are manufacturing single-speed transfer cases is shown later.

All transfer cases can be equipped either with permanent all-wheel drive with differential and a torque distribution of 1 : 2.2 - 3.2 or with an engageable front-wheel drive without differential. This gives the customer the opportunity to select the right transfer case for his requirements and to save costs if a transfer case without differential is suitable.

The G 2500-2 is the strongest transfer case with a rated torque of 22,000 Nm. This allows a GCW of more than 100 t on-road and 55 t off-road.

As mentioned before, G 1700-1 and G 1700-2 are standard for the F 2000 up to a GCW of 60 t on-road and 42 t off-road. The rated torque is 16,000 Nm.

G 1000-1 and G 1000-2 allow 36 t and 24 t on/off-road with a rated torque of 9,000 Nm.

The G 1000-2R is reduced to 25 t and 12 t with a rated torque of 5,000 Nm.

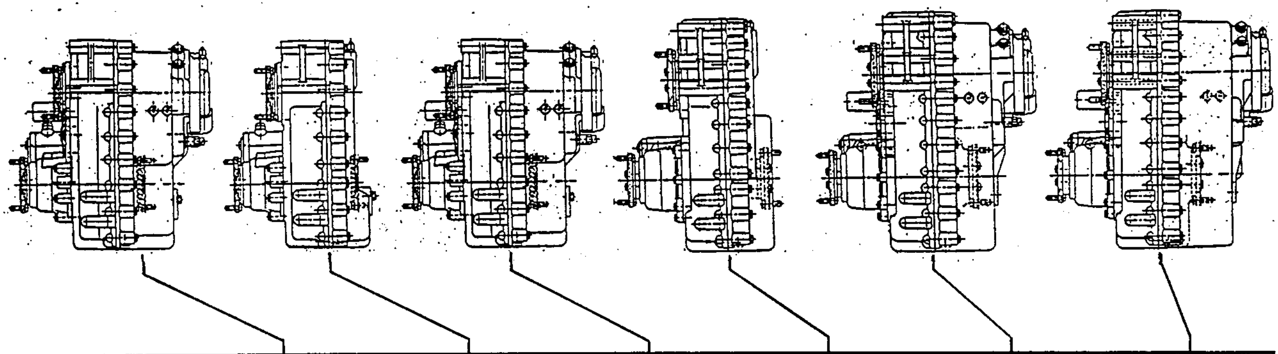

		G1000-2R	G1000-1	G1000-2	G1700-1	G1700-2	G2500-2
ratio	on road	1,031	1,000	1,031	1,055	1,007	0,981
	off road	1,608	-----	1,608	-----	1,652	1,583
weight in kg		150	163	201	268	337	370
rated torque in Nm		5.000	9.000	9.000	16.000	16.000	22.000
max. torque PTO		-----	-----	8.000	-----	8.000	8.000
max. GCW in t	on road	25	36	36	60	60	100
	off road	12	24	24	42	42	55

TKA

Figure 3

New Range of Transfer Cases

MAN

All twin-speed transfer cases can be equipped with a PTO. It is the front-axle drive part of the G 1000 and fits to all cases. The maximum torque is 8,000 Nm.

Figure 4 shows a photograph of the G 1700-1 single-speed transfer case.
As you can see single-speed transfer cases allow a very slim an light-weight design.

Why single-speed transfer cases can be used is shown in figure 5.

There are two different kinds of reasons:

The first kind is related to drive-train design. Over the last 20 years the overall ratios of manual gearboxes have increased - as an example from 9 (ZF S 6-90) to 17 (ZF 16 S-151). This makes it much easier to start a fully loaded truck in an off-road situation without transfer case (6×4). In addition the turbo-charged and intercooled engines gained - after some development - even at low speeds significantly in terms of torque.

The second kind of reasons is related to service. For some tasks all-wheel-drive but no off-road ratio is needed. A snowplow is an example.
The inspection of old transfer cases in some cases showed no use of the off-road gearing.

All of the above mentioned reasons gave us confidence that the development of single-speed transfer cases was a correct step to take. The current sales figures proved this decision to be right.

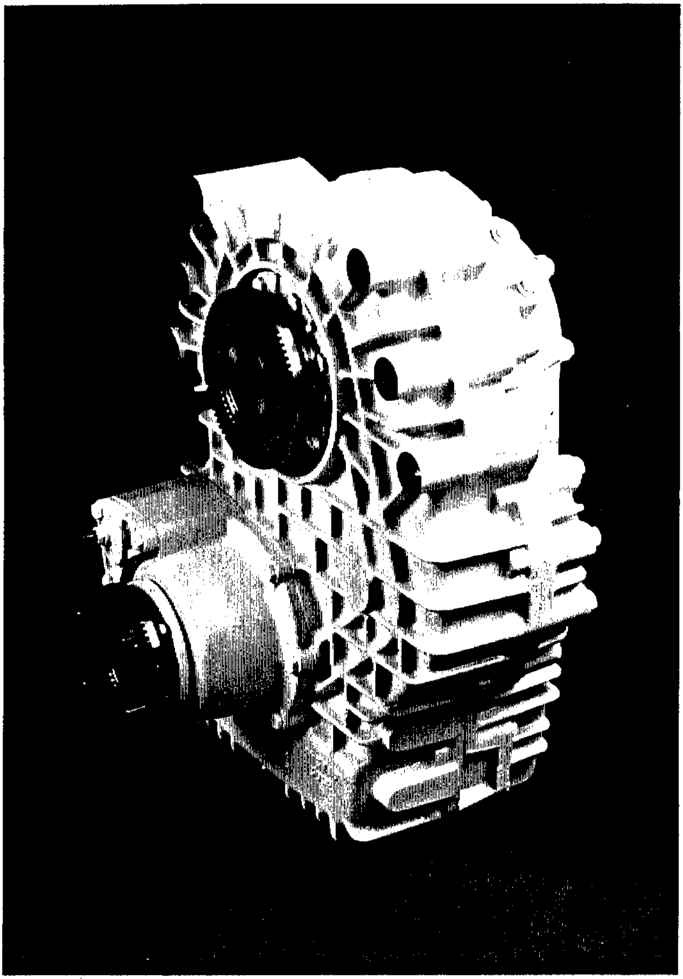

TKA

Figure 4

New Range of Transfer Cases
Single Speed G1700-1

MAN

Why Single Speed Transfer Cases?

V
E - The over-all ratios of manual gearboxes have
H increased over the last 20 years (i.e. : S6-90 : 9
I 16S-151 : 17)
C
L - Engines gained torque (50....100%)
E

S
E - For some service all-wheel-drive
R but no off-road ratio needed (snowplow)
V
I - Inspection of old transfer cases showed in some
C cases no use of off-road gearing
E

TKA

Figure 5

New Range of Transfer Cases

MAN

2) NEW DESIGN CHARACTERISTICS

Figure 6 shows a section through the G 1700-2.

The power flow for on-road and off-road is marked. On-road operation uses two gear-trains which yields advantages in noise behaviour and gear strength. Off-road operation uses the intermediate shaft as an idler gear.
The intermediate shaft is made out of two drop-forged and friction-welded parts. On one end it has the speedometer sensor and on the other end an optional steering pump.
For a good oil supply all twin-speed transfer cases are equipped with an integral oil pump.
This section shows a transfer case with PTO. The pneumatic shifting is on-road/neutral/off-road only for PTO cases, otherwise on-road/off-road.

The front view in figure 7 shows the position of input, intermediate and output shaft within a triangle. This design gives a good distance between input and output shaft centres, low bearing forces at the intermediate shaft and space for vehicle parts such as a spare wheel.

For a permanent all-wheel drive a differential as shown in figure 8 is needed. In general a planetary gearset gives the torque distribution between front and rear axle(s). The pitch diameter of sun and internal gear define the ratio of torque distribution. The G 1700-x, for example, is available with the ratios 1 : 2.2 and 1 : 3.2. The first ratio is selected for 4×4 and 8×8, the second for 6×6 vehicles.
A special design problem is a short distance between front and rear axle flange. This was achieved by a special bearing system for the internal gear/flange unit and electron-beam welding for the planet carrier. The two-point bearing system uses the planetary gearset and a journal bearing to compensate the propshaft forces.

Figure 9 shows in a rear view of a G 1700-2 with PTO the most important parts of the oil supply system in an 'x-ray' picture. The

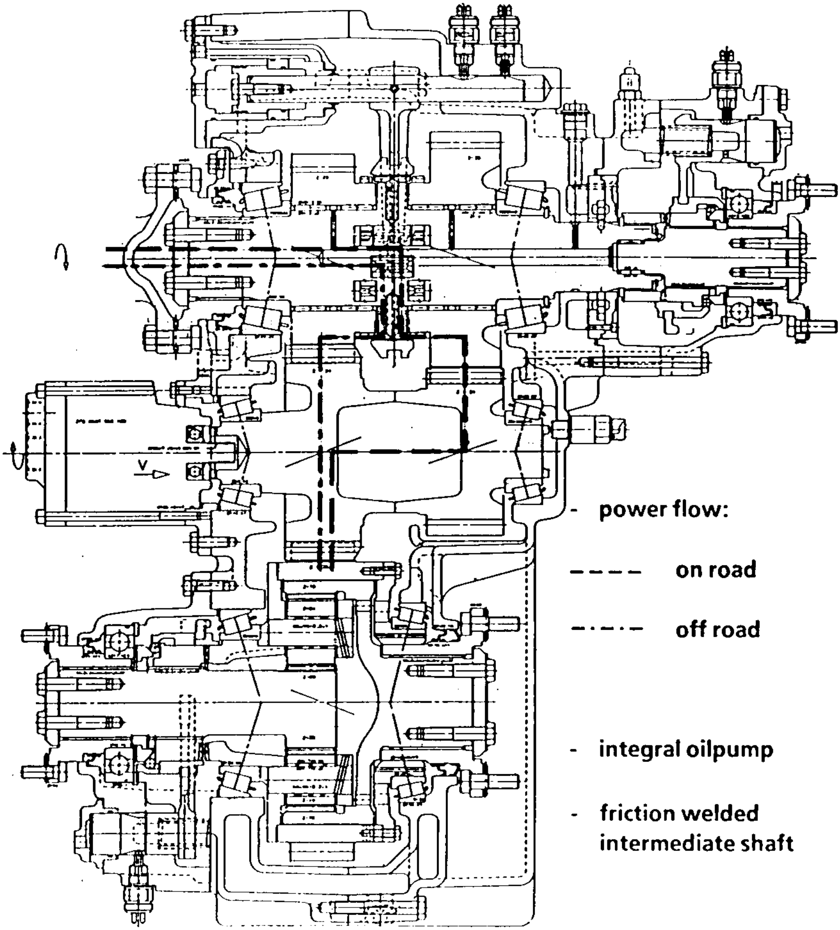

- power flow:

---- on road

-·-·- off road

- integral oilpump
- friction welded intermediate shaft

TKA

Figure 6

New Range of Transfer Cases

Section G1700-2

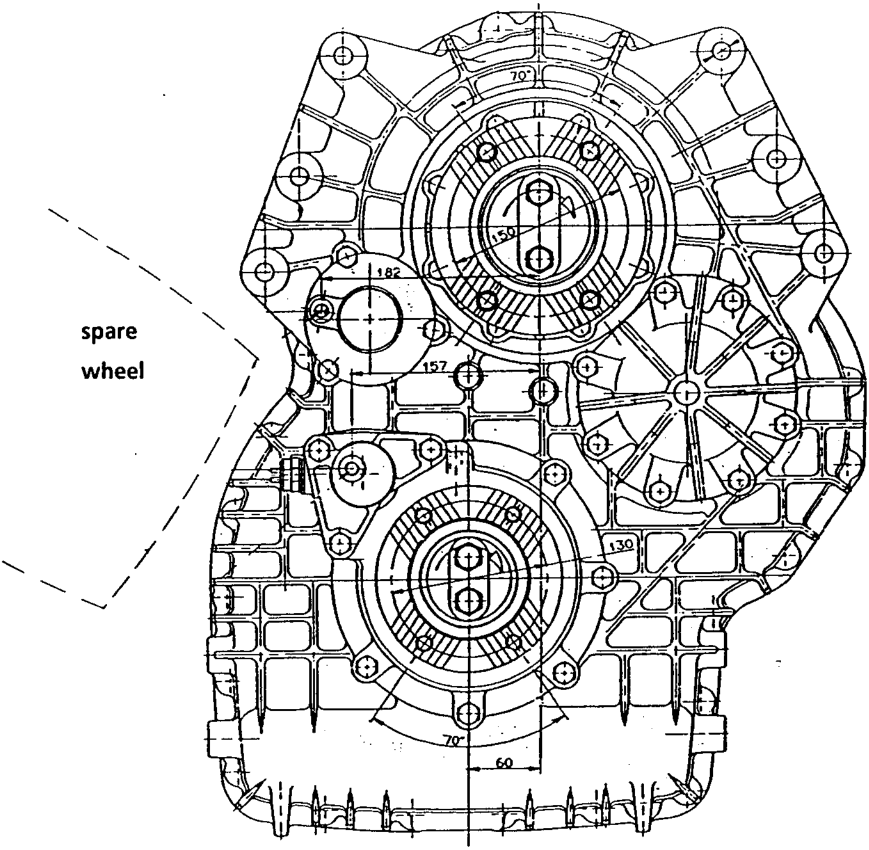
spare
wheel
70°
150
182
157
130
70°
60

G1700-2

TKA

Figure 7

New Range of Transfer Cases

Front View G1700-2

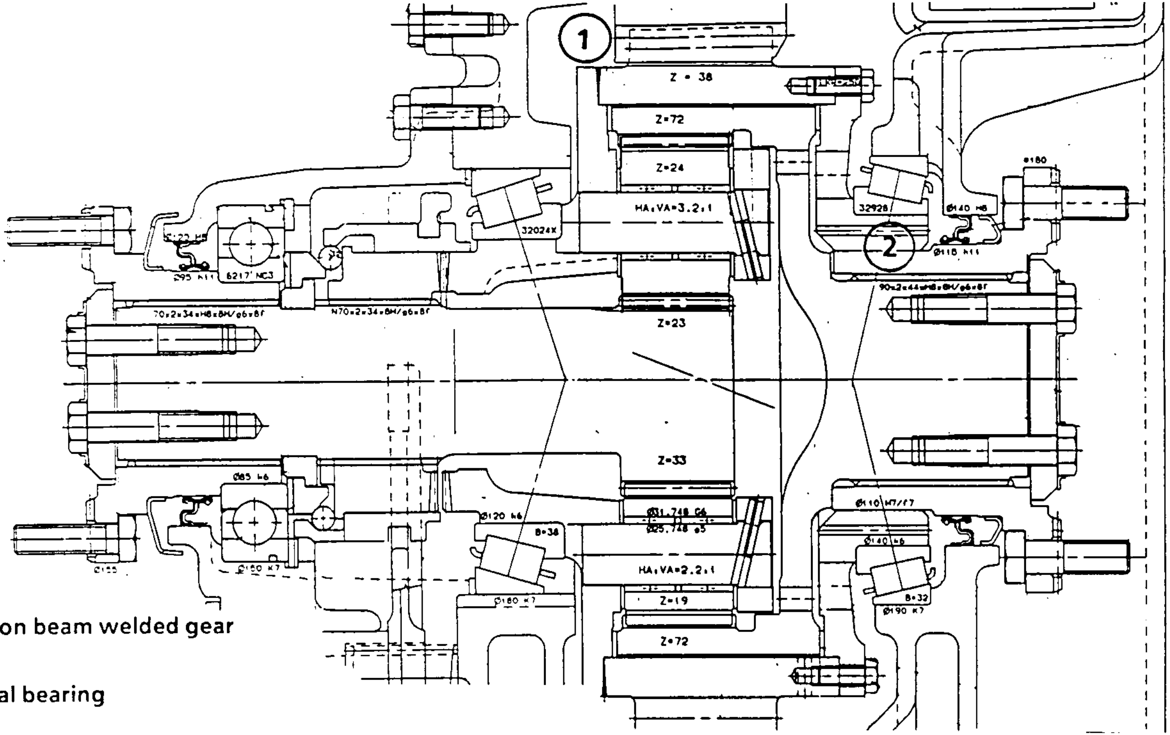
1
Z = 38
Z=72
Z=24
HA:VA=3.2:1
32024X
Z=23
Z=33
Ø31.748 G6
Ø25.748 e5
HA:VA=2.2:1
Z=19
Z=72
32928
2
Ø140 H8
Ø118 h11
ø180
90x2x44xH8x8H/g6x8f
70x2x34xH8x8H/g6x8f
N70x2x34x8H/g6x8f
Ø95 h11
6217' NC3
Ø85 h6
Ø160 K7
Ø155
Ø120 h6
B=38
Ø180 K7
Ø110 H7/f7
Ø140 h6
B=32
Ø190 K7

① electron beam welded gear

② journal bearing

TKA

Figure 8

New Range of Transfer Cases
Differential

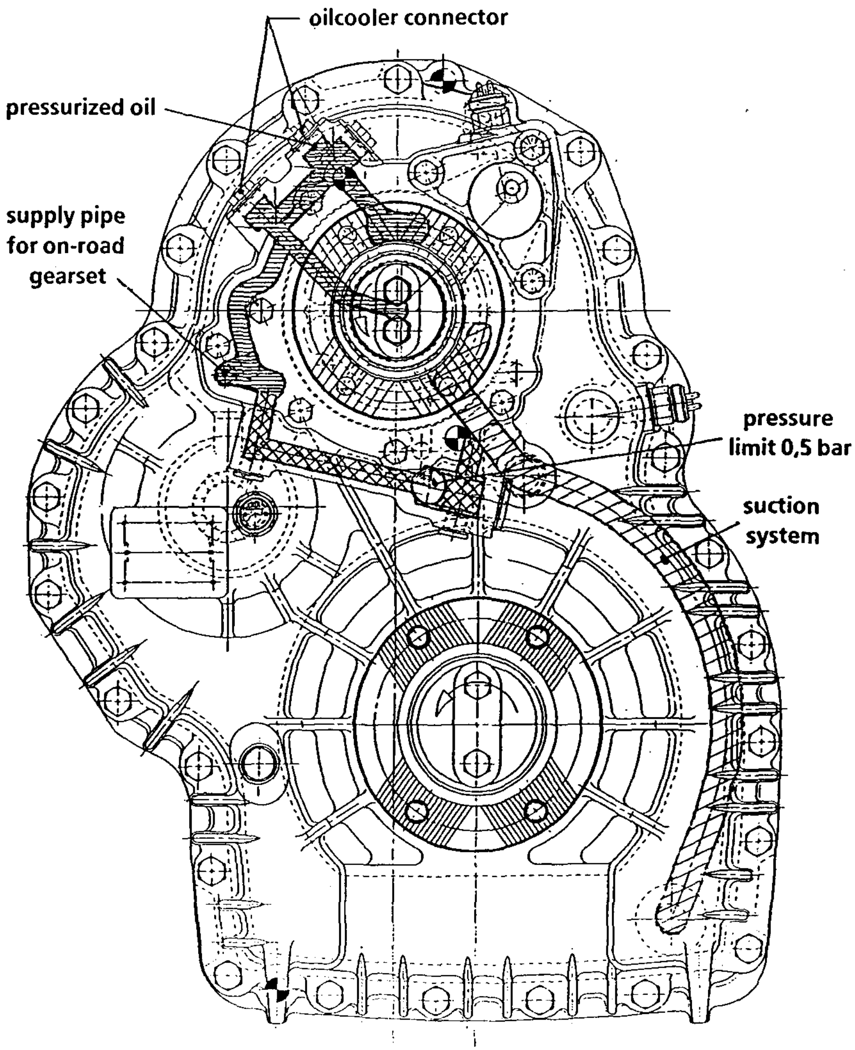
oilcooler connector
pressurized oil
supply pipe for on-road gearset
pressure limit 0,5 bar
suction system

TKA

Figure 9

New Range of Transfer Cases

Oil Supply System

MAN

suction system consists of a filter at the oil sump and a pipe. After the oil pump, which is located at the input shaft, pressurized oil can optionally be routed to the oil cooler. A radial feed system routes the oil to the centre bore at the input shaft to supply the idler gear bearings. The on-road gearset is supplied by a pipe.
Power losses due to oil splash and, related to them, high oil temperatures at high speeds are a major problem for truck transfer cases. The oil supply system limits the amount of circulating oil at high speeds. At 1,000 rpm approximately 0.5 bar oil pressure is reached and a pressure limiting valve starts to open. Pressurized oil is led back to the suction system. Torque loss at 2,500 rpm was limited by this to 23 Nm (G 1700-2).

3) DEVELOPMENT EXAMPLES

Figure 10 shows a rear half of a single-speed transfer case under 17 % grade downhill (coast) operation in a finite element stress analysis. As you can see especially at the intermediate shaft bearing high stresses show up. Housing thickness and ribs were designed in accordance with the FEM-results. In addition bump tests showed the same high stress zones as FEM.

In figure 11 a graphic way of showing gearing deflections is presented. A prototype transfer case was loaded with 20,000 Nm output torque on a static test rig.
Dial gauges measured housing, shaft and gear deflections. A computer programm helped to visualize the measured deflections.
The upper picture shows poor gear contact for the off-road geartrain in the first prototype transfer case. The second prototype showed much better contact behaviour.

Figure 12 shows a holographic picture of the lower half of a G 1700-2 transfer case installed in a vehicle on a rolling road test bed. The upper half is covered by the frame rail.
Two holographic pictures taken with a short time delay provide the interference pattern shown in figure 12. A pattern structure with a high density of lines helps to identify vibrating parts of the housing.

These parts were modified in stiffness and/or mass to reduce the noise radiation from the housing.

The last three figures constitute a selection from the development work done. All other tests on rigs or in vehicles showed a significant improvement compared to our old transfer cases. Due to a closed-loop development with design, test and manufacturing departments quality and cost objectives have been achieved.

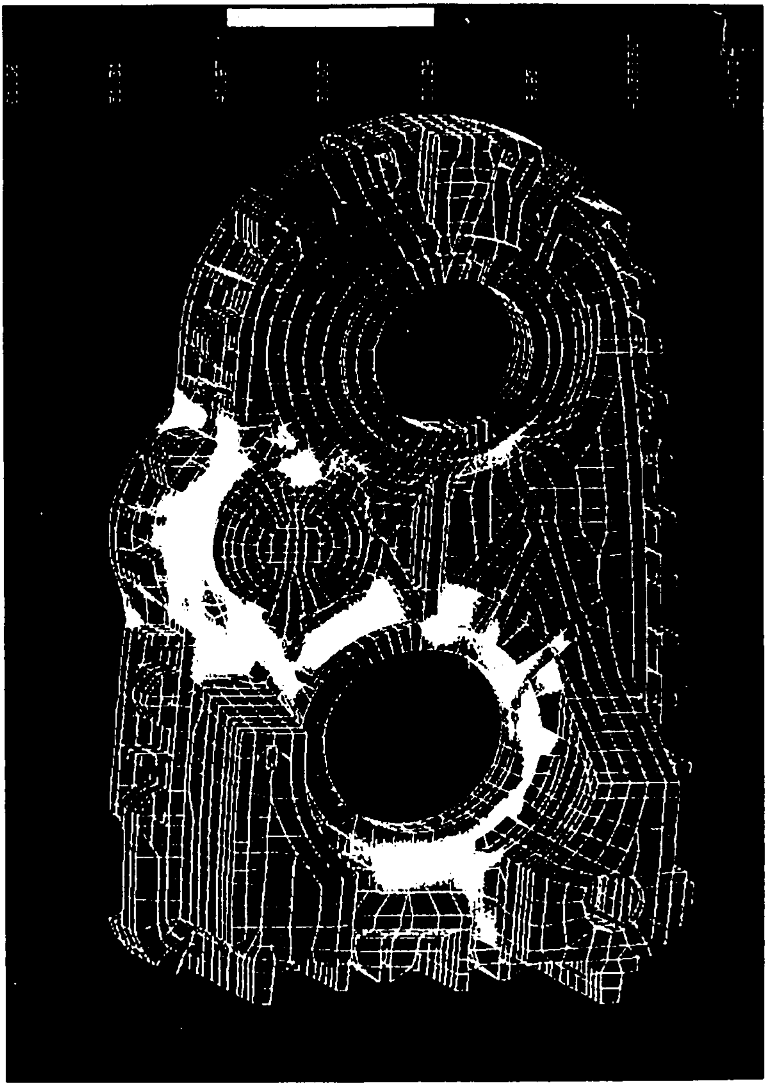

TKA

Figure 10

New Range of Transfer Cases

FEM - Analysis

MAN

Prototyp I

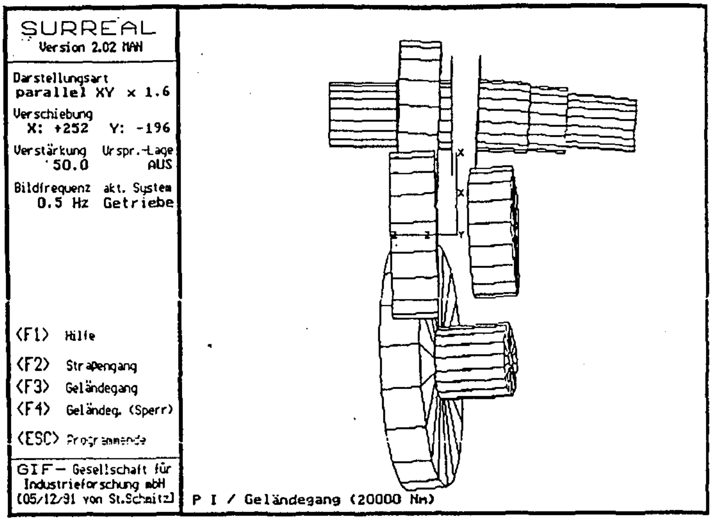

SURREAL
Version 2.02 MAN

Darstellungsart
parallel XY x 1.6

Verschiebung
X: +252 Y: -196

Verstärkung 50.0
Urspr.-Lage AUS

Bildfrequenz 0.5 Hz
akt. System Getriebe

<F1> Hilfe
<F2> Straßengang
<F3> Geländegang
<F4> Geländeg. (Sperr)
<ESC> Programmende

GIF – Gesellschaft für
Industrieforschung mbH
[05/12/91 von St.Schmitz]

P I / Geländegang (20000 Nm)

Prototyp I - Abtriebsmoment = 20 000 Nm

Prototyp II

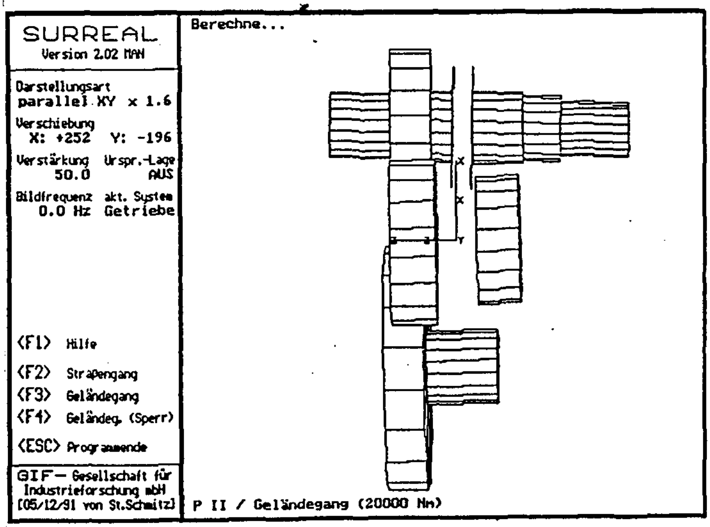

SURREAL
Version 2.02 MAN

Berechne...

Darstellungsart
parallel XY x 1.6

Verschiebung
X: +252 Y: -196

Verstärkung 50.0
Urspr.-Lage AUS

Bildfrequenz 0.0 Hz
akt. System Getriebe

<F1> Hilfe
<F2> Straßengang
<F3> Geländegang
<F4> Geländeg. (Sperr)
<ESC> Programmende

GIF – Gesellschaft für
Industrieforschung mbH
[05/12/91 von St.Schmitz]

P II / Geländegang (20000 Nm)

Prototyp II - Abtriebsmoment = 20 000 Nm

TKA

Figure 11

New Range of Transfer Cases

Gearing Deflections

MAN

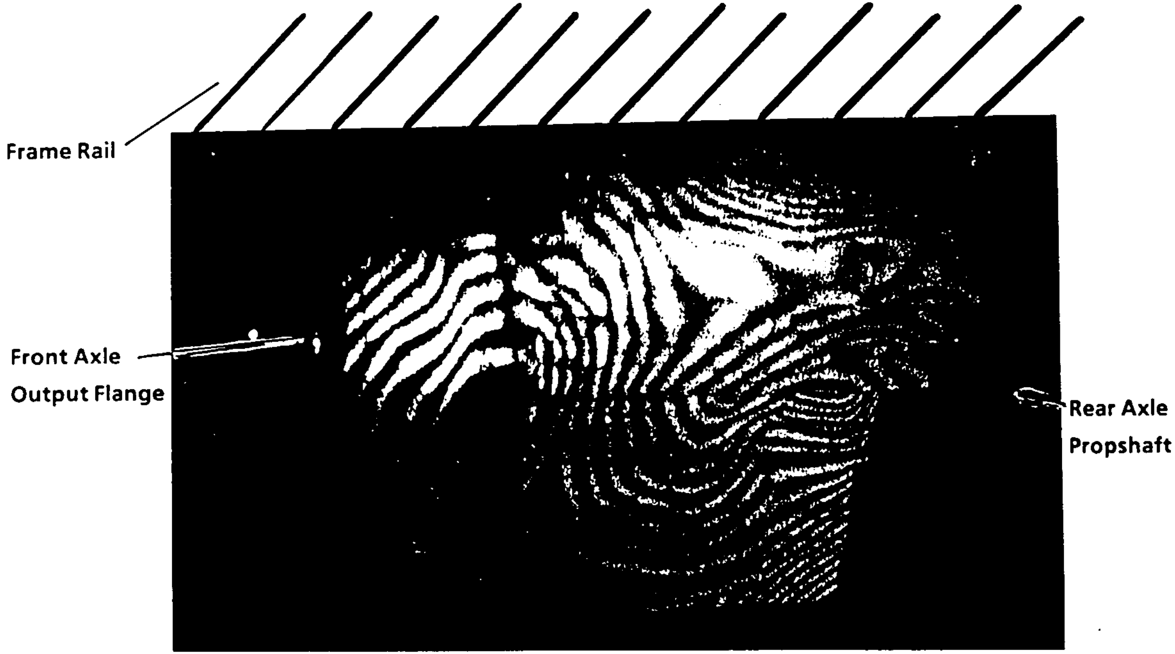
Frame Rail
Front Axle
Output Flange
Rear Axle
Propshaft

TKA

Figure 12

New Range of Transfer Cases
Holographic Investigation in Vehicle

DEVELOPMENT AND EXPERIMENTAL EVALUATION OF ALL-WHEEL STEER ON A 6X6 OFF-ROAD VEHICLE

Dr S Nell Pr Eng, Manager: Test, Evaluation & Technology
Ermetek, P O Box 8323, Elandsfontein
South Africa 1406

ABSTRACT

This paper describes the development, implementation and experimental evaluation of the all-wheel steer principle on a heavy 6x6 off-road vehicle. The study was necessary to establish the influence of all-wheel steer on the high speed stability and the low speed manoeuvrability of the aforementioned vehicle, as work in the field of all-wheel steer has mainly concentrated on *4x2* passenger vehicles.

The second and third axles of the vehicle were steered by using two hydraulic actuators controlled by a computer from within the driver's compartment, resulting in a first order 'steer by wire' system. All the wheels can be turned through the same angle, or the front and rear wheels can be steered in opposite directions. Additional unsophisticated strategies were developed to improve handling and stability at high speeds.

The ISO double lane change test was chosen to evaluate handling, while a new method was developed and a special track laid out to evaluate low speed manoeuvrability, both on sand and on a concrete surface. Results indicated that the turning circle of the vehicle was reduced by *71%*; whilst the high speed stability and low speed manoeuvrability were significantly increased.

1. INTRODUCTION

The manoeuvrability and handling performance of wheeled vehicles can be enhanced by actively steering all the wheels of the vehicle by mechanical, hydraulic or electronic means according to a predetermined control strategy. A vast amount of literature in this field is available, concentrating primarily on *4x2* passenger vehicles and the mathematical derivation of control laws.

The principle of all-wheel steer dates back to around *1915*, when the German company ***Büssing*** developed a prototype *4x4* vehicle which could be steered either from a conventional position in the front of the vehicle, or from a second backwards facing position in the rear (Oswald, 1975, p 35).

Work in this field commenced again in *1930*, when various reconnaissance and light armoured vehicles were developed and built in Germany. The all-wheel steer capability could, in most cases, be manually disconnected by a mechanical clutch at speeds above ± *30 km/h*, while some vehicles, such as the German ***Schwere Spähpanzer Sd. Kfz 234 (8x8) Typ ARK*** reconnaissance vehicle, had a permanent all-wheel steer capability. At the present time, the ***Spähpanzer Luchs (8x8)*** reconnaissance vehicle of the German Army still has an all-wheel steer capability at speeds under *20 km/h*, while companies such as ***Oshkosh*** (United States) and ***ZF*** (Germany) offer packages to modify existing commercial heavy vehicles to include all-wheel steer.

This paper describes the development and experimental evaluation of all-wheel steer on a heavy *(18 500 kg) 6x6* off-road vehicle, as a requirement existed to quantify the increase in the performance and mobility of heavy off-road wheeled vehicles when an all-wheel steer capability is implemented. The purpose of the study can be summarized as follows:

a. To evaluate the principle of all-wheel steer, taking into account low speed manoeuvrability and high speed handling.

b. To evaluate and compare the performance of the vehicle on sand and on a concrete test track with and without the all-wheel steer capability.

c. To develop a test procedure and identify evaluation parameters which can be used to determine and compare the low speed manoeuvrability of different vehicles.

2. THEORY

2.1 Background

Sano et al (1986) utilised basic dynamics and a thought experiment to determine a control strategy for a *4x2* passenger vehicle with an all-wheel steer capability. A steering ratio, which is the ratio between the steering angle of the rear wheels and the steering angle of the front wheels, was calculated as a function of speed using a two dimensional bicycle model. This ratio steered the vehicle in such a way as to keep the centre line of the body tangential with the path that the centre of gravity follows during a steady-state turn.

The control strategy required the wheels to be steered in the opposite direction at low vehicle speeds, and in the same direction when the speed is greater than a specific value. The authors then came to the conclusion that the following alternative strategy, based on the steering wheel angle and not on the vehicle speed, can provide the same effect:

a. In order to manoeuvre the vehicle at low speeds, the front wheels are normally turned through a greater angle in comparison with higher speeds. The manoeuvrability can then be increased if the rear wheels are turned out-of-phase with the front wheels, thereby decreasing the turning circle and increasing the manoeuvrability of the vehicle.

b. At higher speeds, the front steering angles are usually limited to a few degrees. It is then desirable to steer the rear wheels in-phase with the front wheels, as this tends to reduce the phase delay in the lateral acceleration and yaw velocity response to a steering input, thereby increasing handling at high speeds.

2.2 Control strategies

For the purpose of this study, the following two unsophisticated control strategies were developed:

2.2.1 Strategy 1

Strategy 1 is based on the aforementioned alternative approach. The relationship between the front, middle and rear wheels was calculated in the following manner:

a. Determine the mathematical relationship between the rotation of each idler arm and the steering angle of the adjacent wheels. The idler arm is situated in the middle of the axle, and connects the two tie-rods to the wheelhubs.

b. Specify the rear idler angle as a function of the front idler angle by the following three parameters (refer to **Figure 1**):

   1. The so-called ***cross-over point*** is defined as the maximum front idler angle (*14°* in this case) that can occur under normal driving conditions at high speeds. This value has been determined by simulation, using the ***DADS*** simulation package to simulate the behaviour of the vehicle performing a double lane change manoeuvre at different speeds.

   2. The rear wheels are steered in phase with the front wheels to a ***maximum value*** for the idler angle of approximately *2°*. This point is assumed to be halfway between *0* and the cross-over point. As was the case with the previous parameter, this value was determined by simulation as well.

   3. The ***maximum allowable idler angle*** of the rear wheels. This value is a function of the type of axle used.

c. Fit a curve (dotted line, **Figure 1**) through the three points.

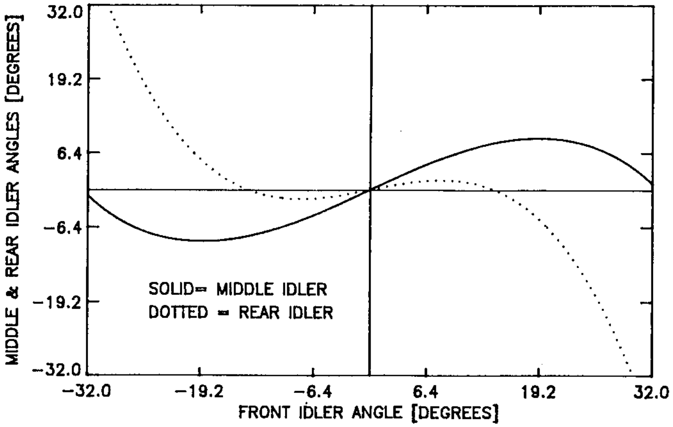

Figure 1: Middle and rear idler angles as a function of the front idler angle

d. Relate the middle idler angle to the front and rear idler angles, using the Ackermann principle.

e. Fit a curve through the relationship as determined in d.

The following polynomials were fitted to represent the mathematical relationships between the middle and rear idler angles as a function of the front idler angle:

Middle idler:

$$\beta = c_1\alpha + c_2\alpha^3 + c_3\alpha^5 + c_4\alpha^7 \qquad (1)$$

with

α = front idler angle;
β = middle idler angle;
c_1 = *7.10E-01;*
c_2 = *-7.10E-04;*
c_3 = *1.50E-07;*
c_4 = *-1.00E-10.*

Rear idler:

$$\gamma = c_5\alpha + c_6\alpha^3 \tag{2}$$

with

γ = rear idler angle;
c_5 = *3.03e-01*;
c_6 = *-1.55E-03*.

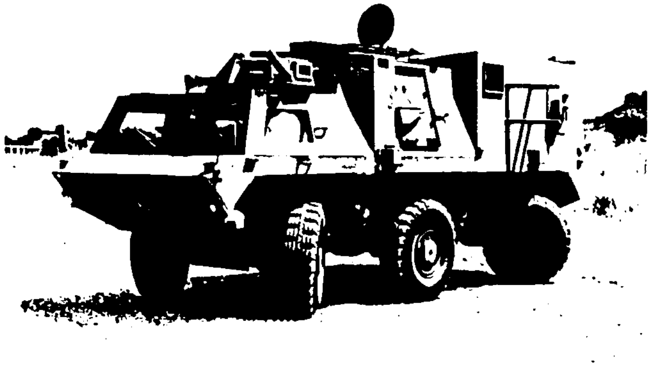

Figure 2: Out-of-phase steering to increase low-speed manoeuvrability

The rear wheels are therefore steered in phase with the front and middle wheels for front idler angles less than *14°*, thereby increasing the high speed handling characteristics of the vehicle as discussed.

In addition, the low speed manoeuvrability can be increased as well, as the rear wheels are steered out of phase for front idler angles greater than the cross-over point. **Figure 2** shows the vehicle turning at low speed.

2.2.2 Strategy 2:

The low speed manoeuvrability can be increased by reducing the turning circle as previously discussed, as well as by providing the capability to move the vehicle in a combination of a lateral and a longitudinal direction. This can be accomplished by turning all the wheels in a similar direction through identical angles, in other words:

$$\alpha = \beta = \gamma \tag{3}$$

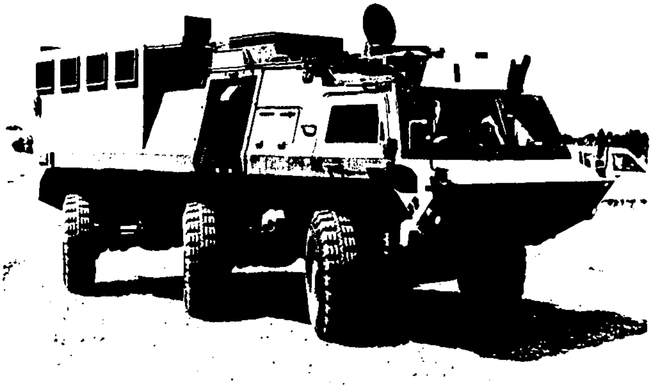

Figure 3: In-phase or crab steering

The crab steer mode can be seen in **Figure 3**. This strategy was evaluated at low speeds only, as subjective results indicated that drivers became disorientated, especially when the vehicle was travelling in reverse.

3. IMPLEMENTATION

3.1 Vehicle modifications

For the purpose of this study, a prototype *6x6* mine resistant vehicle, fitted with *14.00x20* cross-ply tyres, was used. The 'V' shaped hull made the implementation of all-wheel steer possible, especially at the rear of the vehicle, where the third non-steerable axle was replaced by a front axle which was rotated through *180°* in order to maintain the *6x6* drive capability.

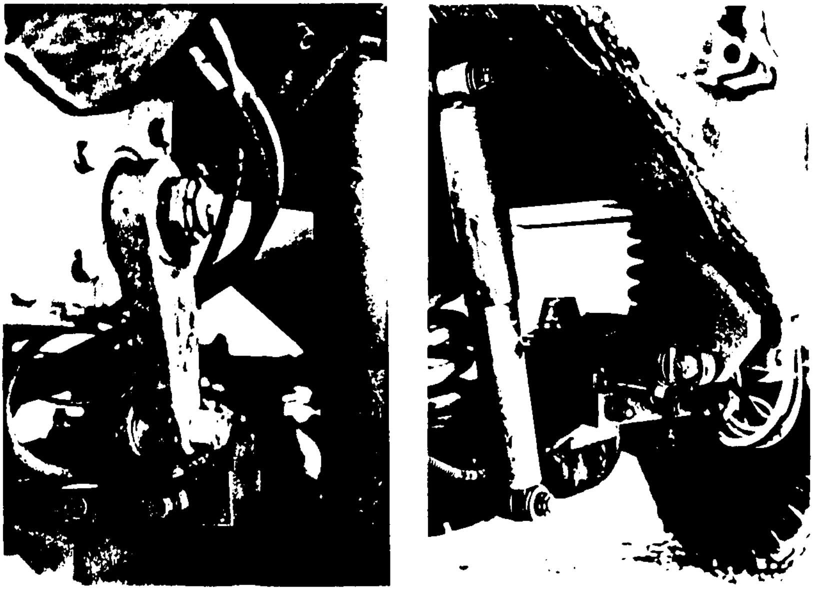

Figure 4: Hydraulic cylinders for middle (a) and rear (b) axles

In order to mount the suspension and axle locating components, small modifications were carried out on the vehicle hull in the proximity of the third axle.

An additional pump and hydraulic system were fitted to supply pressure to two hydraulic cylinders, which were used to steer the second and third axles. The first cylinder (total travel *254 mm*) used to steer the second axle, was mounted in place of a steering rod (**Figure 4(a)**) between the idler and pitman arms, whilst the second cylinder (total travel *284 mm*) was mounted on a predetermined position on the vehicle hull (**Figure 4(b)**).

3.2 Control system

The electronic control system (**Willemse, 1993**) consisted of sensors to measure the three idler arm rotations, electronics to perform signal conditioning and to execute control algorithms, as well as control cards to control the hydraulic actuators. The control system is shown diagrammatically in **Figure 5**, and the main components are discussed in the following paragraphs.

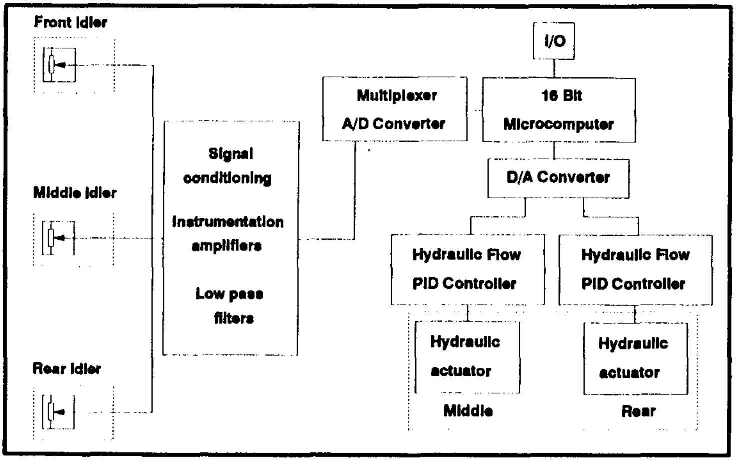
Front Idler
Middle Idler
Rear Idler
Signal conditioning
Instrumentation amplifiers
Low pass filters
Multiplexer A/D Converter
I/O
16 Bit Microcomputer
D/A Converter
Hydraulic Flow PID Controller
Hydraulic Flow PID Controller
Hydraulic actuator
Hydraulic actuator
Middle
Rear

Figure 5: Control system

a. Sensors and signal conditioning

A wirewound track servo potentiometer was mounted inside a plastic housing (**Figure 4 (b)**) on the idler arm of each axle to measure the steering angle. Cables were directed through the vehicle hull to the drivers compartment where the controller was situated.

Potentiometers were connected to differential instrumentation amplifiers with screened twisted pair wire. This was done to improve noise and common mode signal rejection. In addition, each of the signals from the potentiometers was filtered with a second order Butterworth low pass filter.

b. Multiplexer, A/D and D/A Converters

A *RTD406* datamodule board was used to provide a *16* channel analog multiplexer and a *12* bit resolution analog-to-digital converter to digitise the three analog inputs. A two channel *12* bit digital to analog converter was provided to generate control voltages for the hydraulic controller cards.

c. Inputs and outputs

Four toggle switches were mounted on the controller (Figure 6) to allow the driver to select a control algorithm. A 7 segment LED was provided to present mode feedback and error messages, while a knob was fitted to perform calibration tasks.

When no power is supplied, the two hydraulic actuators remain locked in position and the vehicle can be steered in the conventional way using the first two axles.

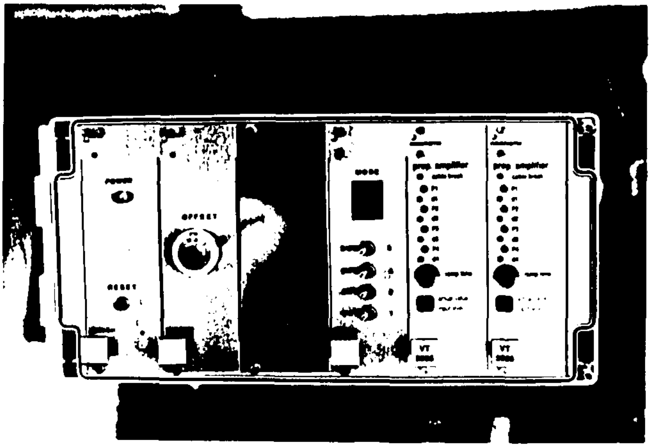

Figure 6: Controller, showing toggle switches and hydraulic control cards

d. Hydraulic Controller Cards

Two ***Mannesmann Rexroth*** *VT5005* hydraulic controller cards were used to control the proportional directional valves with spool position feedback, as mounted on the hydraulic actuators. These cards can be seen on the right hand side of the controller (Figure 6).

e. Software

An ***Ampro 286 Coremodule*** microcomputer with a *80287* co-processor was used in this study. The purpose of the software, which was written in ***Turbo Pascal 6***, was the following:

1. Digitise inputs

The three input channels were digitised and scaled at a sampling rate of *10 ms*. The required middle and rear idler angles are then calculated using **Equations** (1), (2) and (3).

2. Mode control

The mode control software allows switchover between modes (such as between **Strategy** 1 and **Strategy** 2) only when the idler angles are close to zero or close to the idler angles where the mode was first selected. This is done to minimize switchover transients which could surprise the driver and lead to accidents.

3. Position control

The position loop between wanted and actual angles is closed in real time by utilizing a proportional controller.

4. Error management

Error management is limited to checking angles for plausibility. In the case where one or more of the angles is not plausible, an error message is displayed and the position loop is opened. A zero signal is supplied to the hydraulic actuator cards which will lock the actuators in their current state.

Due to the fact that the middle and rear wheels are steered by a control system without any linkages connecting the idler arms with the steering wheel or the front idler arm, a first order 'steer-by-wire' system has been implemented. The control system can be extended to include various overriding capabilities, such as restricting counter-steer at high speeds.

4. EXPERIMENTAL EVALUATION

4.1 Low speed turning performance

The low speed turning performance of the vehicle was evaluated on a concrete test track and in sandy desert conditions. Two aspects were considered, namely the effect of the all-wheel steer capability on the turning circle and on the manoeuvrability of the vehicle.

4.1.1 Turning circle

The turning circle between kerbs was measured by driving the vehicle at a very slow speed in a circle with the steering wheel locked in the maximum position. Cones were placed next to the tyre marks, after which the maximum diameter of the turning circle was determined.

The average cone index for the sandy desert soil was measured as *12 018 kPa/m*, and the moisture content ranged from *0.4%* on the surface to *1.1%* at a depth of *350mm*. Results are tabulated in **Table 1**.

Table 1: Turning circle [m]

	Concrete surface		Sandy desert soil	
Strategy	**Left**	**Right**	**Left**	**Right**
Conventional	18.45	18.65	19.31	19.32
Strategy 1	10.95	11.22	11.30	11.75

From the table it can be seen that the turning circle has been substantially decreased by making use of all-wheel steer, ranging from a reduction of *68.49* % on the hard surface to *73.18* % on the sandy terrain. These values where calculated by using the following relationship:

$$\% = \frac{value, conventional - value, strategy}{value, strategy} \qquad (4)$$

Turning circles on the sand are higher than on the concrete surface, due to the lateral sliding movement of the tyres on the sand.

4.1.2 Manoeuvrability

In order to quantify the low speed manoeuvrability of the vehicle, an appropriate test procedure and accompanying evaluation parameters were developed and identified.

A test course (**Figure 7**) was laid out and marked with cones at *10m* intervals. The vehicle was then driven, using three different drivers with varying driving experience, through the course, following a route as indicated in the figure. The duration of the following was measured, using stopwatches:

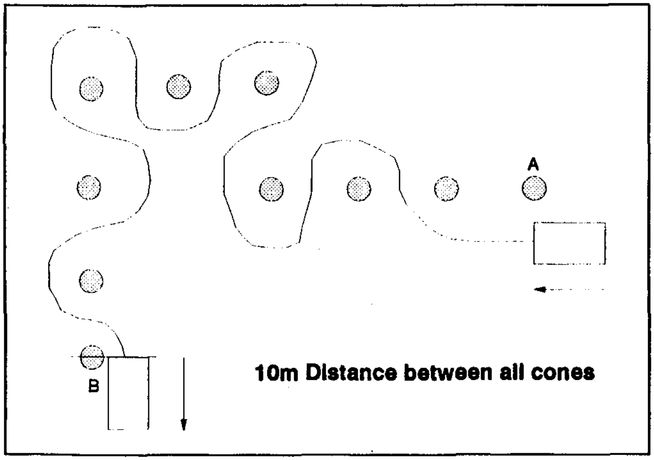

Figure 7: Course for manoeuvrability tests

a. The time from the start of vehicle movement at point A until the line at point B was crossed. This period is defined as T_1.

b. The time span measured as the vehicle was moving forward. If the driver was unable to follow the path and has to stop, turn the steering wheel in the opposite direction and then reverse, time measurement was delayed until the vehicle was able to move forward again. This period is defined as T_2.

The difference between the two times ($T_1 - T_2$) can be used as a measure of the manoeuvrability of the vehicle. If the difference is *0s*, the vehicle is then able to complete the course without stopping and thus has adequate manoeuvrability. Results are tabulated in **Table 2** for tests carried out on a concrete surface and in **Table 3** for tests carried out on sandy desert soil.

Table 2: Manoeuvrability on concrete surface [s]

	Conventional steer			**All-wheel steer**		
Driver	T_1	T_2	$T_1 - T_2$	T_1	T_2	$T_1 - T_2$
1	91.85	67.38	24.47	37.10	37.10	0
2	101.20	74.46	26.74	38.93	38.93	0
3	93.48	74.63	18.85	36.63	36.36	0

Table 3: Manoeuvrability on sandy desert soil [s]

	Conventional steer			**All-wheel steer**		
Driver	T_1	T_2	$T_1 - T_2$	T_1	T_2	$T_1 - T_2$
1	120.4	89.58	30.82	42.12	42.12	0
2	122.9	81.29	41.61	51.01	51.01	0
3	110.0	90.62	19.38	49.39	49.39	0

From these results it can be clearly seen that the manoeuvrability of the vehicle with an all-wheel steer capability is significantly higher when compared to the conventional steering. For example, the total time to complete the course has been reduced by between *123%* (driver 3, sandy conditions) and *186%* (driver 1, sandy conditions).

4.2 High speed handling

The ISO double lane change test procedure **(Anon, 1975)** was used to evaluate the high-speed handling of the test vehicle with and without all-wheel steer. The following variables were measured and used as evaluation parameters (unweighted RMS values):

a. The yaw velocity, as measured by a gyroscope.

b. The lateral acceleration in the vicinity of the drivers seat.

c. The steering wheel angle.

Tests were carried out at a constant velocity of *60 km/h.* Results are tabulated in **Table 4** and are shown graphically in **Figures 8 - 10.**

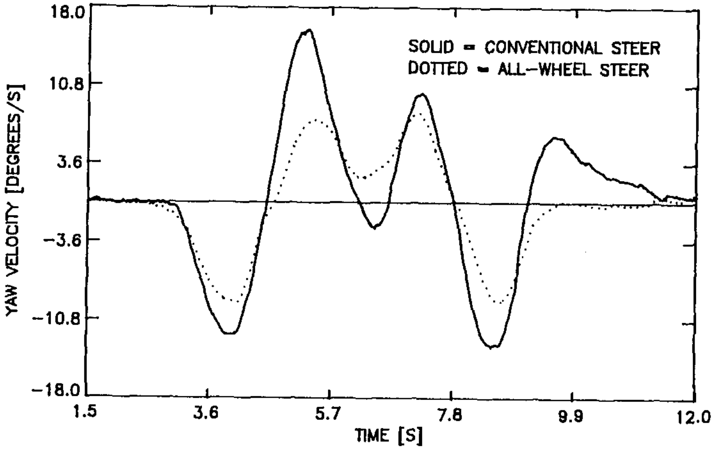

Figure 8: Yaw velocity, double lane change test

Table 4: Unweighted RMS-values, double lane change test

Parameter	Conventional steer	All-wheel steer	% difference
Yaw velocity [°/s]	6.72	4.42	52.04
Lateral acceleration [m/s^2]	2.02	1.77	14.12
Steering wheel angle [°]	67.16	59.19	13.47

From **Table 4** and **Figures 8 - 10** the following observations can be made:

a. A significant reduction (> *10%*) in the values of all the evaluation parameters has been achieved by the implementation of all-wheel steer. These values could be considerable higher if more sophisticated strategies were used.

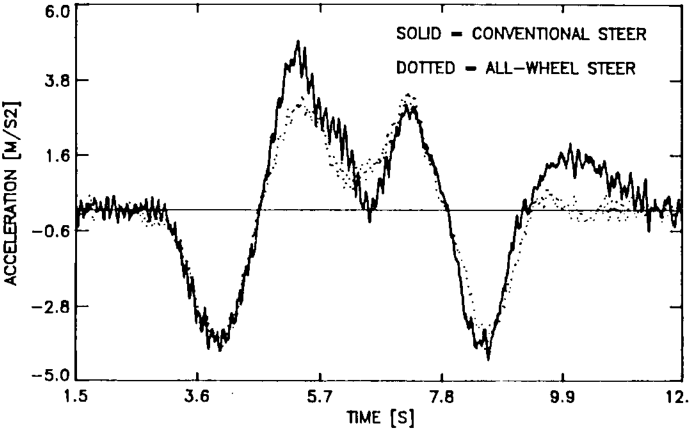

Figure 9: Lateral acceleration, double lane change test

b. The all-wheel steer values diminished more rapidly from around *9s*, in comparison with the values of the conventionally steered vehicle. Less correction to the steering wheel is thus required, the vehicle is more stable and handling is increased.

This is due to the fact that the phase delay in the lateral acceleration and yaw velocity response to the input from the steering wheel was reduced. Slip angles and lateral forces are developed at all the tyres the moment the steering wheel is turned. This is in contrast to when the vehicle is conventionally steered, and slip angles only occur at the rear tyres when a vehicle side-slip angle has been developed.

After completion of the constant forward velocity tests, a maximum or critical speed of *73.65 km/h* was obtained passing through the double lane change course when steering the vehicle in the conventional way, whilst a speed of *81.37 km/h* (*10.5%* difference) was measured using **Strategy** 1. It is therefore clear that the principle of turning all the wheels in the same direction for small steering angles, increases the high speed stability of the vehicle.

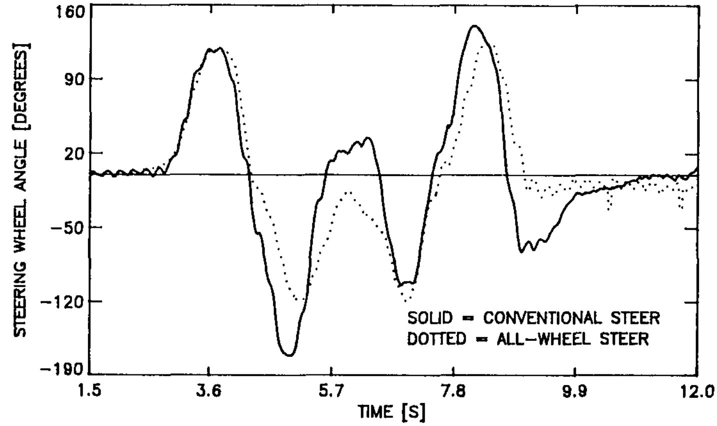

Figure 10: Steering wheel angle, double lane change test

5. SUMMARY, CONCLUSIONS AND FUTURE WORK

In this paper, the principle of all-wheel steer was evaluated on a heavy *6x6* off-road vehicle. The second and third axles of the vehicle were steered by two computer controlled hydraulic cylinders. Unsophisticated control strategies were developed to increase the low-speed manoeuvrability and the high-speed handling of the vehicle. The latter was evaluated by using the ISO double lane change manoeuvre, while for the former a newly developed test specification was used.

Experimental results indicated an increase in the low-speed manoeuvrability and high-speed handling characteristics of the vehicle.

The following conclusions can now be made:

a. The principle of all-wheel steer is not new, but the technology used to implement the capability has become more readily available. Computers and electronically controlled hydraulic cylinders replaced the mechanisms and rods as was used in past systems.

b. An increase in the handling and manoeuvrability of the vehicle can be obtained by unsophisticated control strategies, which are based on the principle that in-phase steering should occur at high speeds (small steering angles), and out-of-phase steering should take place at lower speeds (large steering angles). No additional sensors, other than those required to measure the idler angles, are therefore required. An additional advantage is that these strategies can be tailored and refined by using advanced simulation packages.

Present work includes an experimental programme to establish the influence of all-wheel steer on tyre wear, while more advanced handling and 'steer-by-wire' control algorithms will be developed.

6. REFERENCES

Anon; **Road Vehicles - Test Procedures for a Severe Lane Change Manoeuvres**, ISO/TR3888, International Organization for Standardization, 1975.

Oswald W; **Kraftfahrzeuge und Panzer der Reichswehr, Wehrmacht und Bundeswehr**, Motorbuch Verlag, 8. Auflage, Oktober 1975.

Sano S et al; **Four Wheel Steering System with Rear Wheel Steer Angle Controlled as a Function of Steering Wheel Angle**, SAE 860625, Society of Automotive Engineers, Warrenton, 1986.

Willemse J B; **Project All-wheel Steer Design File**, Work Authorisation FCLADE, Ermetek, January 1993.

****

'Personal Data of the Lecturer'

1. **Name of Lecturer (Christian and Surname, Academic Title):**

   Stefan Nell, Dr.

2. **Name of Company:**

   Ermetek (Pty) Ltd

3. **Position in company:**

   Manager: Test, Evaluation & Technology

4. **Professional Career**

4.1 Academic qualifications

B Eng (Mechanical Engineering), University of Pretoria, 1985.

M Eng (Mechanical Engineering), University of Pretoria, 1987.

Diploma in Datametrics, University of South Africa, 1991.

PhD (Mechanical Engineering), University of Pretoria, 1993.

Registered as a Professional Engineer with the Engineering Council of South Africa.

Associate Member of the South African Institute of Mechanical Engineers.

4.2 Career

Engineer-in-training, Ermetek, 1988 - 1990.

Project Manager: Technology, Ermetek, 1991 - 1992.

Manager: Test, Evaluation & Technology, 1993 -.

4.3 Special Expertise

Vehicle Dynamics, Suspensions, Test and Evaluation of off-road vehicles.

****

Session VIII
Sektion VII

Soil Machinery

Baumaschinen

OPTIMIZATION OF EXCAVATOR BOOMS OPERATING LOADS, STRUCTURAL DYNAMICS

Ertugrul Güner, Wolfgang Poppy, Matthias Weid
Berlin University of Technology (TU Berlin), Germany
Construction Machinery - Design and Engineering

ABSTRACT

Hydraulically operated equipments of excavators are still predominantly calculated with statistically insufficiently secured design loads. Over- and undersizing cannot be excluded reliably this way.

For a safe and at the same time light-weight-oriented design of the equipment, load spectra have to be determined under realistic operating conditions and analyses of the structure must already be carried out during the phase of designing. The basis for this was developed in close cooperation with several manufacturers, aimed to achieve results in a generally applicable form. The development of suitable mechanical models and methods for the derivation of design spectra was prerequisite. Extensive investigations to optimize the structure referred to kinematics, load capacity, vibration characteristics and operating strength of the equipment as well as to stability of the whole machine.

1 Introduction

During the last forty years, remarkable improvements in the technology of construction machinery have been achieved mainly due to multiple operating experiences. Meanwhile this process has reached a level, where growing demands to power, cost and safety can only be met by scientifically secured methods of optimization.

Hydraulically operated equipments of excavators are still predominantly calculated with statistically insufficiently secured design loads. This is because of the very high expenses for experimental determination of representative conditions for load and stress under operating conditions. Over- and undersizing, causing detrimental effects to realizable reaches and payloads or to load capacity and operating life of the equipment, cannot be excluded reliably this way.

Designing of construction machinery optimized to operating life by principles of operating strength and light-weight design, needs the determination of load spectra under real operating conditions. For this the typical operating conditions of construction machines have to be analysed and specified in an operating schedule. In accordance with this analysis, suitable mechanical models and easily usable methods for the measurement of operating loads as well as statistical methods for the derivation of design spectra have to be developed.

These investigations have been performed exemplarily at TU Berlin within the scope of the research project "construction machinery - load spectra" with a hydraulic excavator doing earth work and with an industrial excavator. The aim was to develop the mechanical models and the measuring methods based on them in a way which makes them applicable to similar structures of construction machinery [1].

Besides the optimal designing, the vibration characteristics of the equipment, too, influence the operating life of the machine. At present, investigations on structure-dynamical features of construction machinery are performed at TU Berlin within the scope of the research project "construction machinery - structural dynamics". Aim of this project is to develop models which simulate realistically the dynamical operating characteristics of construction machinery.

With such models, extensive variations in parameters to optimize the structure-dynamical features can already be done economically during the phase of design.

2 Operating conditions and schedules of hydraulic and industrial excavators

Hydraulic excavators are used in earth work to break out, load and remove earth and rock as well as in handling of bulk goods, industrial excavators are used for handling on wood- or junkyards. Excavators consist of a basic machine and an equipment (figure 1 on the next page), which, on hydraulic excavators, normally consists of a boom (one or two part boom and arm) and an attachment with hydraulic adjustment, for example a grab, a bucket, a loading shovel or a hydraulic breaker. The equipment of industrial excavators consists of a monobloc boom, an industrial arm and an unattached tool.

The operating schedules of the investigated machines vary considerably in operating range and field of task, depending on the operator. The design spectra do not have to be based on all possible operating schedules, but only on those representative ones which are substantial for the failure of the high-duty structural parts. According to the list of construction machinery [2], the economical working life of hydraulic excavators totals seven years. However, in some cases the actual working life can total more than ten years. For a one year operating period, 1,500 to 2,500 h can be achieved. Backacting excavators are characterized by a cyclical procedure with a cycle time of 20 to 30 s. With up to 1,000 cycles/day, 250,000 cycles can be performed yearly.

Impacts and strong accelerations cause especially high stresses. Above all backhoe work can be characterized by high load amplitudes. The operating loads an excavator can bear are limited by the response of the pressure relief valves in the hydraulic system, by the tilting of the machine when exceeding the stability and by the sliding of the undercarriage when exceeding the static friction between undercarriage and subsoil because of too high crowd forces when operating the shovel.

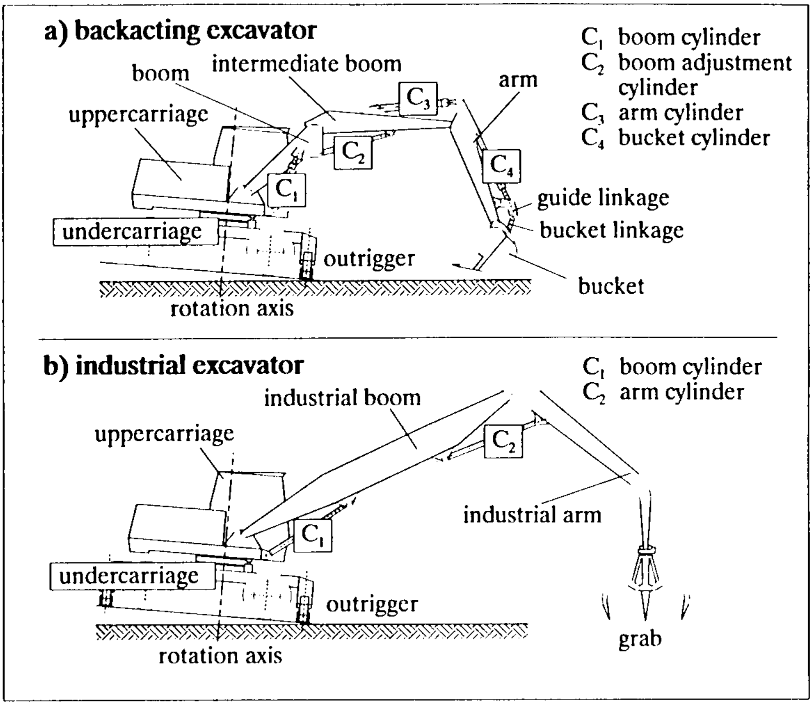
a) backacting excavator
boom
intermediate boom
uppercarriage
arm
C_3
C_2
C_1
C_4
undercarriage
outrigger
guide linkage
bucket linkage
bucket
rotation axis
C_1 boom cylinder
C_2 boom adjustment cylinder
C_3 arm cylinder
C_4 bucket cylinder
b) industrial excavator
industrial boom
uppercarriage
C_2
C_1
industrial arm
undercarriage
outrigger
grab
rotation axis
C_1 boom cylinder
C_2 arm cylinder

Figure 1: Terms of the test machines

The crowd force and the breakout force of backacting excavators or of shovel excavators respectively, are created according to DIN 24 086 in certain positions of the equipment by actuating the arm cylinder and the bucket cylinder or the shovel cylinder with statistically maximum cylinder loads. The closing force of the grab defined in DIN 24 086 does not stress the boom. Therefore the weights lifted or carried are substantial as nominal loads for equipments with a grab (DIN 24 083). Under real operating conditions the operating loads can vary in a wide range regarding magnitude and direction.

Industrial excavators are used as power machines on wood- and junkyards. On junkyards they predominantly move car bodies and light scrap parts. They feed scrap presses or load and unload transport vehicles. During about 10 % of their operating period they are used for handling heavy scrap parts (castings, forgings and big steel plate parts). According to the list of construction machinery the entire period of operation totals in double or triple shift to more than 20,000 h in seven years of working life. High periods of operation with 4,000 h/year are the extreme. For most of the junkyard operations 2,000 to 3,000 hours of operation yearly can be assumed. A cycle for feeding a scrap press with car bodies lasts about 115 s, so 60,000 to 90,000 cycles can be done yearly. Especially high stresses can occur during crushing or tambing of scrap parts by impact motions as well as during strong acceleration periods and during "sweeping" of scrap parts scattered across the site with the help of a dozer blade attached to the grab.

3 Determination of operating loads and stresses

3.1 Modeling and measuring methods

Operating loads and stresses of construction machinery equipments, caused by their function, working motions and service weight, can be determined with the help of mechanical models. These models have to be built in a way that the load components substantial for the failure and their distribution over the boom can be determined from as few as possible measured quantities. The operating loads of the test machines have been determined with a measuring system like shown in figure 2 on the next page.

For the determination of operating loads and stresses of the equipments their positions have to be known in every operating condition. The positions and motions of the equipments are determined kinematically clear by cylinder travelings which can be measured by spool travel gauges. The measurement of the path is preferable to the measurement of the angle at a swivel joint, because the measuring arrangement is easier to calibrate and can also be used when the cylinder does not cause a rotation but a linear motion of the boom parts (for example telescopic arms).

In the first place, equipments of excavators are stressed highly by bending. External operating loads result from weight carried and digging load, internal operating loads result from service loads and acceleration loads of the

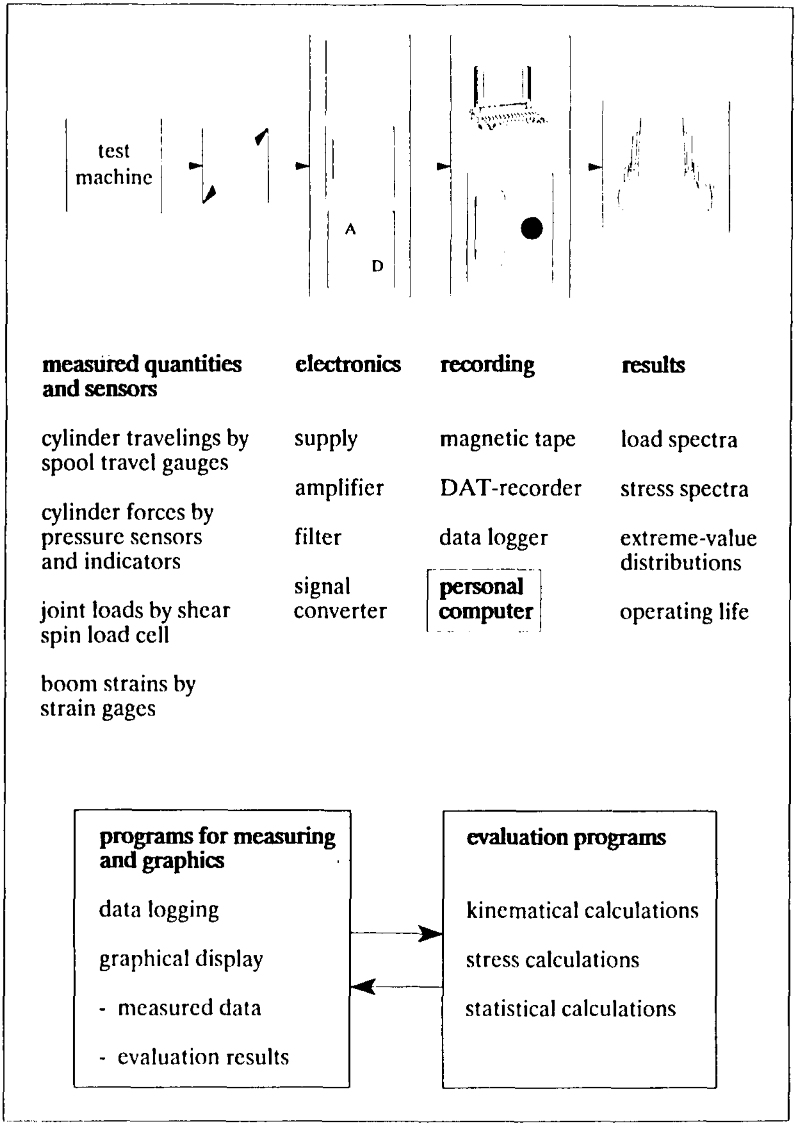
test machine
A
D
measured quantities and sensors
electronics
recording
results
cylinder travelings by spool travel gauges
cylinder forces by pressure sensors and indicators
joint loads by shear spin load cell
boom strains by strain gages
supply
amplifier
filter
signal converter
magnetic tape
DAT-recorder
data logger
personal computer
load spectra
stress spectra
extreme-value distributions
operating life
programs for measuring and graphics
data logging
graphical display
- measured data
- evaluation results
evaluation programs
kinematical calculations
stress calculations
statistical calculations

Figure 2: Measuring and evaluation system for the determination of operating loads and load spectra

equipment. The equipment can be modeled as a framework, attached to the basic machine, consisting of bending beams for the boom arms as well as of push/pull rods for the hydraulic cylinders and the linkages. When reducing the complex load conditions with external and internal operating loads at different work spots to a simplified substitute load system, especially the course of bending section loads must not be affected inadmissibly. By this reduction of the load system, equivalent operating loads are defined which are divided in main and shear loads. The main loads describe the force components in the motion plane of the equipment and the moments to the normal (z axis) of this boom plane. The shear loads describe all the other force and moment components of the six components relating to a cartesian coordinate system at the reduction spot. They can be recorded by measuring the joint forces by shear pin load cells at the swivel joints of the arms or by measuring the strain at the web plates of the arms (in direction of the longitudinal axis). The principle of the shear pin load cells is based on the measuring of the strain due to shear forces between the bearing bushings. With the couples of forces at two shear planes on two measuring axis orthogonal to each other, it is possible to determine the moments to the x and y axis of the pin.

3.2 Operating measurments

For the derivation of design loads for a strong designing of the equipment, extensive operating measurements have been performed under typical and as hard as possible operating conditions during several days. Furthermore impact and acceleration events for the investigation of extreme loads and structure-dynamical features have been recorded in separate measurements. The measuring program was of following extent:

Hydraulic excavator:	Quarry operation (class of soil 6 to 7 according to DIN 18 300) and operation in soft soil (class of soil 3 to 4),
Industrial excavator:.	Junkyard operations with different handling materials (light scrap parts, heavy castings, steel plate parts and forgings, car bodies).

When working in soft soil with the hydraulic excavator, high loads can occur, too. For this, the physical system-caused load limits for tilting and the hydraulic pressure reliefs are substantial. The higher failure when working in a quarry is caused by superposed impact events and higher load cycle numbers compared to working in soft soil. Working with light scrap parts can be substantial for the failure of industrial excavators, too, because of higher accelerations as when working with heavy scrap parts.

To be able to transmit the design loads derived from this operating measurements to other machines or to similar fields of application, they were compared with machine data. For this the determination of dynamic coefficients or load factors respectively between the different operating conditions is suitable, too. The conclusion report of the research project "construction machinery - load spectra" contains further details on the measurements and their evaluation [1].

4 Investigations on operating strength

4.1 Methodology

The fatigue assessment of a structural part can be done experimentally or analytically. Experimental fatigue assessment procedures need more efforts and are more expensive, therefore they are used mainly for structural parts of productions on a large scale with low part costs or for safety parts which have to meet extreme demands in light-weight design, conditional to their function [3]. For construction machinery with bigger and more complicated structural parts, an analytical fatigue assessment, based on nominal stress Wöhler curves for samples similar to the structural parts, is recommended by following method:

- Preparation of an operating schedule based on operating experiences with probabilities of occurence of different operating conditions, as well as on market demands,

- Determination of operating loads and stresses under typical as well as under hardest possible operating conditions according to the operating schedule,

- Derivation of the design loads substantial for the operating strength in the form of design spectra which contain the statistical frequency by suitable classification methods of all the essential load cycles to be expected during the design period,

- Determination of operating strength data (which means the permissible time strength and fatigue limit values of stress amplitudes from Wöhler curves or operating life curves) from codes or own systematical laboratory tests considering the influence of material, shape, production and stress characteristics (for example fluctuation of average load, spectrum form),

- Calculation of operating life to quantify the operating strength by suitable cumulative damage calculations in which the stress spectra are compared with Wöhler curves (analogous to the comparison of structural part stresses to tolerable structural part stresses in statistical strength assessment procedures),

- Check of the assumptions on which the fatigue assessment is based by comparison with prototype tests or with operator knowledge of the actually reached operating lifes and operating schedules.

For very big and complex single designs, only an analytical fatigue assessment based on local stresses and on Wöhler curves from tests with notch rods or shape elements makes sense, because of time and cost reasons. The problem of the application of this data to real structural parts has to be solved considering the influence of shape, production, and type of stress. One substantial prerequisite for the designing by principles of operating strength is the derivation of design loads decisive for the failure. They have to contain as design spectra the extreme loads and stresses which can cause a forced failure, as well as the operating load and stress cycles relevant to and representative for the fatigue.

4.2 Statistical basis

For the determination of the load spectra the load cycles of a load course are classified into pre-set load cycle ranks or classes with suitable counting methods. This means their class frequency and - from the amount of the class frequencies - their amount frequency is determined. It is common to display the load spectra - like the Wöhler curves - in a graph with logarithmical axis for the load cycle ranks and the load cycle coefficients (amount frequencies) belonging to them.

Of the classification methods known in operating strength research, the Rainflow counting method based on material mechanics supersedes more and more. This method counts the stress-strain hysteresis substantial for the failure and allows the classification of two parameters important for the operating strength, like amplitude and average of a vibration, into a matrix. Out of this matrix, spectra according to orthodox counting methods can be won, too, at any time, like the counting of class exceedings and of range couples which is known from many investigations on operating strength of motor vehicle chassis. These classification methods are explained in detail in DIN 45 667 as well as in [1, 4, 5].

The load spectra for different load phases (like cycles of hydraulic excavators) determined by classification methods, can show variations under constant operating conditions, too. The probability of exceeding the load spectra can be determined with the help of the distributions of extreme-values which show the statistical distribution of the maximum values of the spectrum for several load phases in a probability net [1, 5].

For the determination of the probability of survival for a structural part, the probability of survival of the Wöhler curves has to be considered as well as the probability of exceeding the load spectra [5]. The later is gained by the probability of occurence of different load conditions according to the operating schedule as well as by the variation of the load spectra during these operating conditions. The probability of survival for a structural part only depends on the probability of exceeding the design spectra, if the probability of survival for the Wöhler curves is very high (more than 90 %). The Wöhler curves are usually derived from vibration strength tests up to breakage. For the prediction of the operating life until a crack occurs, a very low probability of failure has to be set up or a very high probability of survival respectively, if the operating life is calculated by Wöhler curves for breakage.

4.3 Operating strength data from codes and operating life calculations

To consider the influence of shape, material, and production on the calculation of operating life for a structural part by the nominal stress scheme, Wöhler curves or operating life curves from tests with samples similar to the structural part are necessary. The Wöhler curves of Eurocode 3 (for big welded steel constructions in the widest sense) are more suitable compared to DIN 15 018 (for steel trusses in crane manufacturing with usual steel suitable for welding) and DASt 011 (for high-strength fine-grained steel suitable for welding), because they are determined from tests on samples similar to the structural parts [6]. The orthodox methods of DIN 15 018 and DASt 011 are based on permissible reference stresses determined in dependency of pre-set fields of stress tolerance, spectrum forms and stress groups. In contrast to these methods, Eurocode 3 additionally recommends to judge the operating strength by a cumulative damage calculation. For boxlike welded structural parts, usual for construction machinery equipments, detail category 100 is specified in Eurocode 3. For higher detail effects caused by additional reinforcements, the lower categories up to about 40 are recommended. This means less bearable stress amplitudes of about 60 %.

The operating life of a structural part can be calculated with the help of the linear cumulative damage theory by Palmgren and Miner [7]. In this theory the load cycle coefficients of a stress level ΔN_{Ki} in the field of time strength of the Wöhler curve are put in proportion to the load cycle coefficient of this Wöhler curve N_{Wi} on the same stress level and are added up over all stress levels. The modified Miner rule is characterized by the consideration of a failure contribution below the curves of fatigue strength [7]. For this, the curve of time strength is extended fictitiously with a lower inclination in the field of fatigue strength. The load cycle coefficients on different load levels are put in proportion to this modified Wöhler curve and the single failure contributions are added up. If the growing failure sum depending on the operating time reaches the pre-set failure criterion (like $D = 1$) then the operating time belonging to it corresponds to the operating life expectancy. Figure 3 on the next page shows an example of cumulative damage calculation with the modified Miner rule.

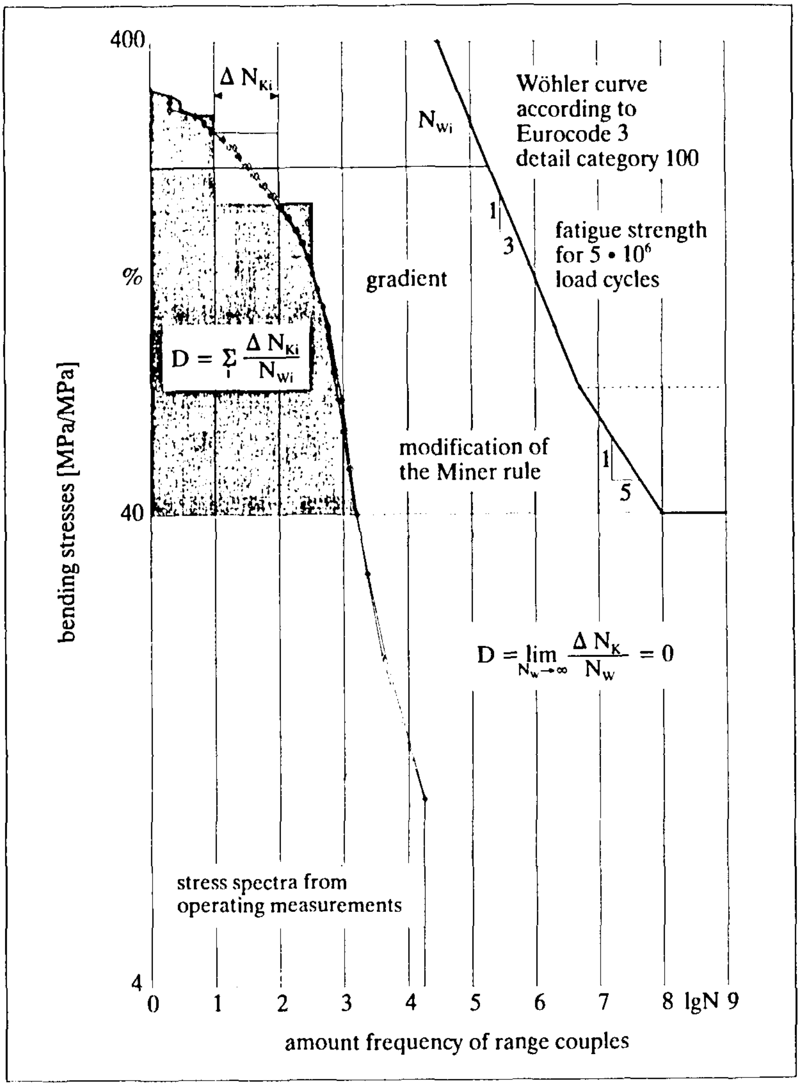

Figure 3: Cumulative damage calculation according to the modified Miner rule for a backacting excavator working in a quarry

The operating life predictions by cumulative damage theories according to the Miner rules described before can show wide variations. To increase the accuracy of predictions, in the literature a failure criterion different from D = 1 is often used. It has to be determined according to the application. Help is provided by the relative Miner rule which allows the comparison between the failure sum of a design spectrum with known operating life and the failure sum of a design spectrum with unknown operating life. The failure of both spectra has to be calculated against the same Wöhler curve. In both cases the proportion of the failure sums is conversely proportional to the proportion of operating life. This means that the failure sum of the reference spectrum with known operating life can be used as a failure criterion for the design spectrum with unknown operating life, if both spectra were determined under similar operating conditions. A statistical analysis of failure occurences of construction machines operated under similar conditions, would supply the substantial failure sum as a design or failure criterion.

5 Simulation of operating loads and structural part stresses for the structure optimization

Numerical simulations for structure analysis or structure optimization respectively, are of increasing importance in the field of construction machinery design. As analytical methods for the determination of operating loads and structural part stresses, they are an important aid in structure optimization regarding kinematics, lifting capacity, stability, vibration characteristics, and operating strength. They support the developing or optimization process by allowing extensive parameter studies already in an early phase of developing - even before building a prototype. By this the costs of developing are reduced. In structure optimization, different computer-supported analytical methods can be used which complement one another.

Design programs are used for quasi static calculations in pre-designing as to kinematics, lifting capacity, stability, and strength according to the nominal stress concept. In cooperation with different manufacturers of construction machinery they were made in consideration of their practical demands and developed further continuously. By now they are a fixed component in their design practice and are used with success. With the help of Multi-Body-System (MBS) simulation programs the dynamical features of construction machines can be investigated and the vibration characteristics of the whole machine can be optimized by parameter variations. Finite-Element-Method (FEM) simulations are in close context with structure-dynamical simulations of mechanisms able to vibrate. They can be used on the one hand for the determination of the stiffness and natural frequency of structural parts for the vibration analysis of the mechanism and on the other hand for the investigation of influences of discontinuities to structural part stresses with dynamical loads of the vibration analysis.

5.1 Design programs with quasi static simulation models

With the help of design programs, the effects of basic structure changes to substantial design parameters can be investigated and documented quickly. Besides, the limiting conditions of the machine - like working area limits, dead center points of the joint drives, hydraulic pressure reliefs, interlockings of the arms among each other or by collisions with external objects, stability and tilting angle when working on a slope - and their exceedings are quantified, so that the necessary design steps for the compliance of certain limiting values can be initiated specifically.

To build a numerical simulation model the body-system-coordinates of the structure points, of the centres of gravity of the equipment and of the cross sections to be investigated as well as the joint drives, the variations of the position of the equipment and the load assumptions belonging to them, are configurated interactively and filed in ASCII data files. The structure points can be indicated freely depending on the equipment. Kinematics of equipments can be configurated in any way with the help of only few parameters for different types of joint gears, for example hydraulic cylinders and their combination with a linkage in bottom or overhead installation position.

To allow the determination of the loads of sectioning and the nominal stresses of the arms, any sections can be configurated at the equipment. For this the position of the cross section centre and the orientation of the cross section normal vector is defined in relation to an arm-body-system. The loads of sectioning at these cross sections are calculated from static conditions of equilibrium at the sectioned part of the equipment with the operating loads belonging to it. Depending on the cross section position, the forces of sectioning of the cylinders, of the bucket linkage, or of the arm swivel joint have to be considered, too.

For the simulation of work cycles by position variations of the equipment, cylinder travelings or arm position angles and their field of variation can be set alternatively for every joint drive. In this, it is distinguished between the arm position angles in relation to the horizontal (relating to the global system) and in relation to the neighbouring arm-body-system. When setting the arm position angles the cylinder travelings belonging to them are calculated, checked for plausibility and corrected if necessary. The plausibility check contains the traveling limits and the exceedings of dead center points of the joint gear which changes the translational motion of the cylinder into a rotation.

For every simulation step the loads of the joint drives, the forces of sectioning and the nominal loads of the arms at freely selectable cross sections are calculated as well as the stability and nonskid security and the tilting angle when working at a slope. The results are documented in ASCII data files.

5.2 Modeling for structure-dynamical investigations

The dynamical loads from natural resonance, caused by working motions with high accelerations as well as by irregular or periodical load functions, can be determined with vibration models only. For this the whole machine is portrayed mechanically as a discrete multi-body-system able to vibrate. It consists of mass elements, spring and damping elements and their kinematical bonds among each other, and is stimulated to natural resonance by external load functions or motion guide functions (kinematical stimulation).

The mass distribution has great influence to the structure dynamic of a machine. It can be approximated by discrete bodies in the form of geometrical mass elements, for example box-formed beams for the arms or cylindrical rods for the hydraulic cylinders and swivel joints (figure 4).

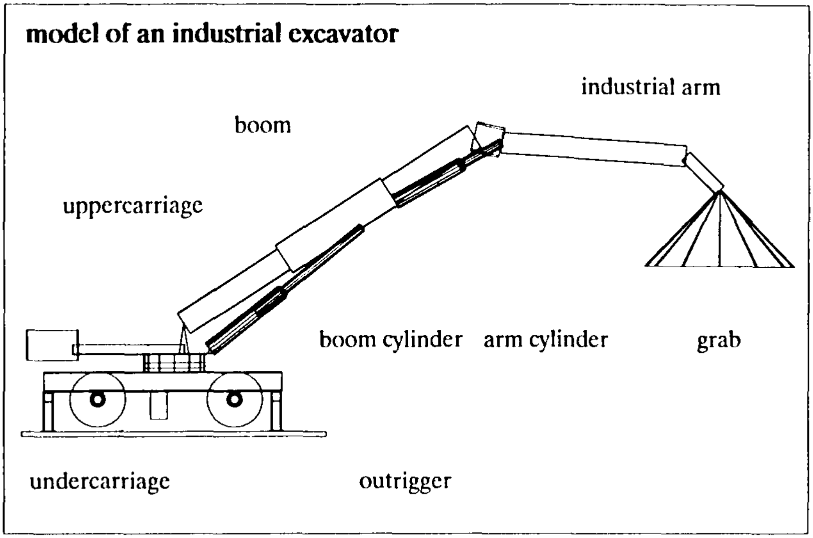

Figure 4: MBS simulation model of an industrial excavator

For the verification of the mass distribution in the model, the resulting position of the centre of gravity and the weight of the body from the measurements (or from CAD-models) are used. First the mass elements have to be spread for this in a way, that the known position of the centre of gravity of the structural part is kept, for example by thicker box profiles in the mass-concentrated joint areas. After this the density of the used mass elements of the structural part model is adapted to the known weight of the structural part. For the bonds between the bodies a large library of joints with different degrees of freedom is available. At the industrial excavator the individual structural parts are connected with each other by swivel joints or translational joints for example.

The elasticity or softness respectively of the system of hydraulic construction machinery equipments depends mainly on the hydraulics. The modulus of compression E for hydraulic oil is between 1,400 and 3,300 N/mm^2 [8, 9, 10] and is smaller by the factor 64 to 150 related to the modulus of elasticity for steel with 210,000 N/mm^2. For the softness - or the reciprocal stiffness - the dimensions of the vibrating components are substantial, too, besides the modulus of compression or elasticity. These are the dimensions of the hydraulic components (cylinders, axial piston pumps and motors, tubes and valves [11]) which determine the loaded pressurized oil volume as well as the dimensions of the steel parts (figure 5 on the next page).

The influence of body elasticities related to the influence of hydraulics on system stiffness and on natural frequencies has to be checked in every single case, for example with the frequencies from measuring the relevant natural resonance conditions or from FEM-modal analyses of the arm-bodies. A pragmatic way to do so is to build the simulation model with rigid bodies and elastic hydraulic cylinders first and then to compare the natural resonance from the simulation and from the measurement with each other. From great differences of the essential natural frequencies can be judged, that the influence of body elasticity cannot be neglected. If the natural frequencies from simulation and measurement correspond, the modeling with rigid arms and elastic hydraulic cylinders is obviously enough to investigate the load parameters substantial for operating strength - like frequency and amplitude. The natural frequencies are known to depend on system stiffness only, when the mass distribution is equal.

System damping is mainly influenced by hydraulic components (viscous fluid damping, viscous/dry cylinder friction) additionally by joint friction and material damping at big body deformations. In contrast to stiffness, damping of construction machinery equipments is hard to determine analytically from the decay characteristics of measured natural resonances. A measure for the size of damping forces by viscous/dry friction is provided by hystereses of measured cylinder forces at successive slow lifting and lowering motions of the equipment or at load and unload events with constant position of the equipment. In any case a minimum of damping in the simulation model is necessary just for the numerical stabilization of the integration of differential equations with strong parameter alternations.

For the analytical determination of dynamical operating loads from wanted working motions, kinematical stimulation functions or motion guide functions are necessary for the vibration system, for example controlling the cylinder

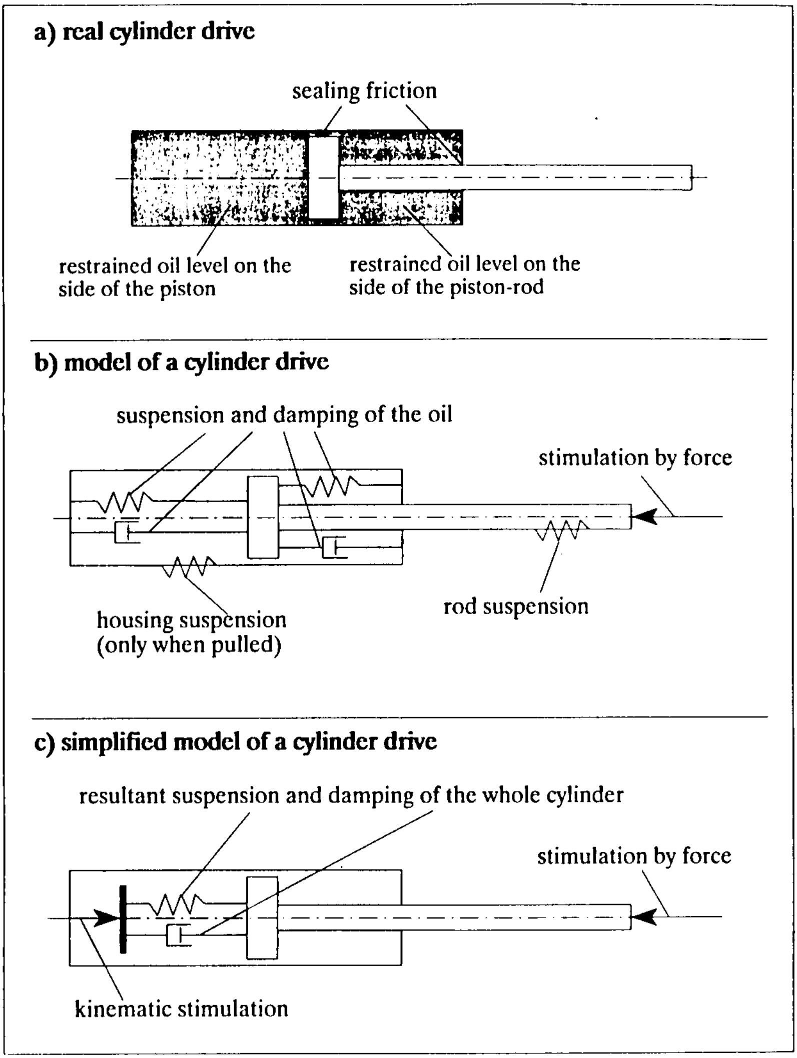

a) real cylinder drive

sealing friction
restrained oil level on the side of the piston
restrained oil level on the side of the piston-rod

b) model of a cylinder drive

suspension and damping of the oil
stimulation by force
housing suspension (only when pulled)
rod suspension

c) simplified model of a cylinder drive

resultant suspension and damping of the whole cylinder
stimulation by force
kinematic stimulation

Figure 5: Hydraulic cylinder model for MBS simulations

motions of hydraulic equipments. For dynamical operating loads, base load cycles, caused by guiding functions (without acceleration loads) as well as additional load cycles caused by natural resonances around this guiding functions are essential. To verify the simulation model, such guiding functions and natural resonances can be gained from operating measurements including high accelerations or rapid payload changes, for example abrupt lifting and lowering motions of the equipment or rapid loading or unloading of payloads. If the motion guide functions are defined in the form of measured data, which are normally approximated by a spline function when fed into the simulation program, special attention has to be payed to the dissolution of natural resonances and therefore to the input frequency. The guide function data files must not reproduce the natural vibration. Otherwise artificial resonances are created in the simulation model which do not correspond to reality.

The method of structure-dynamical modeling presented so far has been tested with an industrial excavator. Comparisons of natural frequencies between the simulation model with rigid arms and elastic hydraulic cylinders on the one hand and the structure-dynamical measurements on the other hand confirm the model designs for lifting vibrations. According to this the influence of body elasticity of the arms on the loads in the boom plane can be neglected related to the influence of cylinder stiffness. This verification of system stiffness by natural frequencies is allowed [12], because with weak damping and exact modeling of mass inertia the sensitiveness of natural frequencies only depends on system stiffness.

Dynamical operating loads which are caused mainly by natural vibrations can be reduced, in contrary to functional operating loads, and by that either the operating life or the payload can be increased. The structure-dynamical optimization is complicated by the multitude of machine parameters to be investigated and the complexity of real operating conditions. Therefore improvements reducing the natural vibrations for a few typical vibration conditions have to be striven for. These improvements do not necessarily lead to equal improvements for real complex operating conditions.

5.3 Basics for structural part modeling with the help of FEM

After determining the operating loads experimentally or analytically by quasi-static and dynamic models, the shape of the structural part can be optimized regarding constant stress. For this, continuum models of the structural parts (for example by FEM) which can approximate the increase in stress at detail spots exactly enough are necessary. This can only be done in the sense of the structure-stress-concept or of the structure-strain-concept respectively [13], while detail spots caused by production like weld seam faults or heat-affected zones cannot be modeled at all.

When doing FEM-modeling the structural parts are made of continuum basic elements like beam, rod, shell, or volume elements whose deformation characteristics can be described mathematically in dependence on the element knot loads or in general on the boundary conditions. The necessary continuum equations of the element are formulated by differential methods (equilibrium at material spots by angular momentum equations) or energetical variation methods (principle of virtual work or principle of the minimum of potential energy) in consideration of material laws and solved with the help of suitable design functions for element deformations. In general the energetical variation principles are preferred because the design functions do not have to meet all the boundary conditions. Therefore a wider range of design functions can be used for the approximate solution of the continuum differential equations.

With the help of continuum models not only local increases in stress caused by shape can be determined analytically, but also body elasticities for structure-dynamical simulation. More and more MBS simulation and FEM programs offer interfaces to exchange load assumptions for the structural part as well as stiffness and mass matrices of the stuctural part and by this reduce the number of optimization iterations.

The modal analysis of structural parts by FEM continuum models can also provide a criterion to what extent body elasticities have to be considered in MBS simulations. In structure-dynamical simulations of car chassis for example, structural parts with natural base frequencies of more than 30 Hz are modeled as rigid bodies [14]. The greater the difference between the natural frequencies of the body and the natural frequencies of the whole vibration system substantial for the operating strength is, the smaller is the influence of body elasticities on system vibrations. So structural parts can be modeled as rigid bodies in MBS simulation then.

6 Summary

Methods for determining operating loads developed within the scope of the research project "construction machinery - load spectra" provide basics for a better covering of design loads for operating strength design of construction machinery. The mechanical models as well as the measuring and evaluation methods can be used for similar designs very easily. Exemplarily performed calculations of operating life explain the correlation between the influence of structural part shape, material, production, and, above all, load.

Fatigue assessments are full of wide variations. The exact determination of operating schedules and the correct derivation of design loads have great influence on the quality of a fatigue assessment. Therefore the importance of statistical investigations of operating conditions and loads which can only be specified by observations over many years and by systematical collection of operating data has to be pointed out especially. For this, manufacturers and operators of the machines have to work in close cooperation.

The operating strength of construction machinery can be increased mainly by improving the detail cases caused by design or production as well as by reducing the bending stresses of the boom arms by "framework-like" designs. For this, arm swivel joints and cylinder joints should be brought together. Because this step influences also kinematical and structure-dynamical features of the machine, extensive parameter studies are necessary about the vibration characteristics of construction machinery which can only be mastered economically with the help of numerical simulation.

At present these investigations are performed within the scope of the research project "construction machinery - structural dynamics" with the aim of optimizing the structure-dynamical machine parameters (dimensions, mass distribution, stiffness, and damping) already during the phase of design in a way, that system vibrations and thus operating loads can be reduced in the sense of fighting the causes. This also improves operating strength.

7 Literature

[1] Güner, E.; Poppy, W.: Baumaschinen-Lastkollektive. Schriftenreihe der Forschungsvereinigung Bau- und Baustoffmaschinen (FVB), Heft Nr. 1, Frankfurt/M., Oktober 1992

[2] Baugeräteliste 1991. Hrsg.: Hauptverband der Deutschen Bauindustrie. Wiesbaden, Berlin: Bauverlag, 1991

[3] Schütz, W.; Vormwald, M.: Betriebsfestigkeit im modernen Maschinenbau. Landtechnik 49 (1991) 12, S. 586-589

[4] Clormann, U. H.; Seeger, T.: Rainflow-HCM - Ein Zählverfahren für Betriebsfestigkeitsnachweise auf werkstoffmechanischer Grundlage. Stahlbau 55 (1986) 3, S. 65-71

[5] Buxbaum, O.: Betriebsfestigkeit; Sichere und wirtschaftliche Bemessung schwingbruchgefährdeter Bauteile. Düsseldorf: Verlag Stahleisen, 1986

[6] Schütz, W.: Die Übertragbarkeit von Werkstoffkennwerten auf Bauteileigenschaften. VDI-Berichte Nr. 852, S. 167-188; Düsseldorf: VDI-Verlag, 1991

[7] Haibach, R.: Betriebsfestigkeit; Verfahren und Daten zur Bauteilberechnung. Düsseldorf: VDI-Verlag, 1989

[8] Backé, W.: Servohydraulik. Vorlesungsumdruck, RWTH Aachen, 1986

[9] Matthies, H. J.: Einführung in die Ölhydraulik. Stuttgart: Teubner, 1991

[10] Melchinger, U.: Simulation der Arbeitsbewegungen und Antriebssysteme von Hydraulikbaggern. Dissertation, TU Berlin, 1992

[11] Heckelmann, V.: Steifigkeit hydraulischer Vorschubantriebe. o + p 21 (1977) 6, S. 441-443

[12] Trapp, H.-J.: Beitrag zum rechnerischen Betriebsfestigkeitsnachweis für Bauteile in Krantriebwerken. Konstruktion 27 (1975), S. 142-149

[13] Radaj, D.: Gestaltung und Berechnung von Schweißkonstruktionen; Ermüdungsfestigkeit.
Düsseldorf: Deutscher Verlag für Schweißtechnik DVS, 1985

[14] Willumeit, H.-P.: Computergestützte Berechnungsverfahren in der Fahrzeugdynamik. Düsseldorf: VDI-Verlag, 1991, S. 383-457

DIN 15 018 Teil 1: Krane; Grundsätze für Stahltragwerke, Berechnung

DIN 18 300 VOB Verdingungsordnung für Bauleistungen,
Teil C: Allgemeine Vorschriften für Bauleistungen, Erdarbeiten

DIN 24 083 Erdbaumaschinen; Hydraulikbagger; Angabe der Tragfähigkeit

DIN 24 086 Erdbaumaschinen; Hydraulikbagger; Grabkräfte, Begriffe, Nennwerte

DIN 45 667 Klassierverfahren für das Erfassen regelloser Schwingungen

DASt 011 Hochfeste schweißgeeignete Feinkornbaustähle mit Mindeststreckgrenzenwerten von 460 und 690 N/mm^2; Anwendung für Stahlbauten

Eurocode 3 Chapter 9: Design of Steel Structures. Commission of the European Communities; Edited Draft Issue 3, April 1990

GROUND VIBRATION BY MOTION OF CONSTRUCTION VEHICLES

K.Kogure, M.Aoyama and Y.Miyata
Department of Civil Engineering, National Defense Academy
1-10-20 Hashirimizu,Yokosuka,Kanagawa,Japan

ABSTRACT

This paper deals with the vibration of peaty soft ground by the motion of dump trucks and bulldozers. On the peaty soft ground, a gravel road, a steel running-panel road and a temporary asphalt-paved road were constructed for test running of vehicles. From the measurements of ground vibration, it was seen that vehicle's weight and speed much affect peaty soft ground vibration. Largest vibration was recorded when vehicles ran on the gravel road, followed by running on panels and on the temporary asphalt paved road in this order.

Keywords : ground vibration, dump truck, bulldozer, peaty soft ground

1. INTRODUCTION

The ground vibration by motion of construction vehicles is one of the typical public nuisances caused by construction works. In Japan, many complaints have been filed by neighboring residents over the ground vibration caused by construction works as the scale of each work has grown larger and the land utilization has been densified. These complaints can be classified into three types; damage to houses, psychological(mental) disturbance and physiological(physical) disturbance. Recent trend is the increase of complaints about psychological disturbances, which occur on lower vibration levels than those of two other types of nuisances.

Most of the past studies on ground vibration caused by construction vehicles were devoted to the vibration of hard ground[1][2]. This paper reports and evaluates the results of the measurement of ground vibration caused by dump trucks and bulldozers running on the soft ground. The measured ground was peaty and soft. Principally, the following subjects were considered. (1) The difference of ground vibration levels by weight of dump trucks and bulldozers, (2) difference of ground vibration levels by three types of road surface conditions on the soft ground, (3) damping characteristics of soft ground vibration, and (4) influence of weight and running speed on ground vibration.

Vehicle's weight and speed much affect soft ground vibration. The vibration of soft ground quickly increases as the weight and speed increase. As for road surface conditions, largest vibration was recorded when a vehicle ran on a gravel road, followed by running on running panels and on a temporary asphalt pavement in this order. The distance from a vibration source to a measurement point and the vibration level has a linear relation on semi logarithmic scale.

2. EXPERIMENTS

The test was carried out on the soft peaty ground located in the suburbs of Tokyo. The composition of soil strata at the test site is shown in Fig.1. A ultra-soft peaty stratum extends from the ground surface to the depth of 2.6 m. It had the water content of approximately 600 %, wet density of roughly 1.1 t/m^3 and density of solid portion of about 1.6 t/m^3 and contained almost no soil particles. There is a thick layer of silty clay underneath the peaty stratum. Void ratio of the peaty stratum was 5 to 20 and its unconfined compression strength was approximately 2.0 t/m^2. On this soft peaty ground, a gravel road, a steel running-panel road and a temporary asphalt-paved road were constructed for test running of vehicles.

Construction vehicles used in the test were dump trucks weighing 4 t and 11 t and bulldozers weighing 7 t, 14 t and 17 t. Dump trucks were tested in two load conditions, with and without load. The specifications of tested vehicles are summarized in Table1.

Vibration levels (VL, unit:dB) was directly measured by a vibration level meter, which is designated in the Japanese Industrial standard (JIS) as a measuring instrument of vibration nuisance[3]. Direct measurement of vibration level in decibel (dB) facilitates easy comparison with vibration nuisance limits adopted by local governments.

3. VIBRATION LEVEL

A phenomenon that vibration propagates using ground as a medium is represented as wave motion. Vibration is represented by waveform, displacement, velocity, acceleration, etc[4]. To measure and assess a vibration nuisance, the vibration level (VL) is used. This is derived from acceleration value after taking human sensitivity for vibration into consideration and defined as follows.

$$VL = 20 \log \frac{A}{Ar} \tag{1}$$

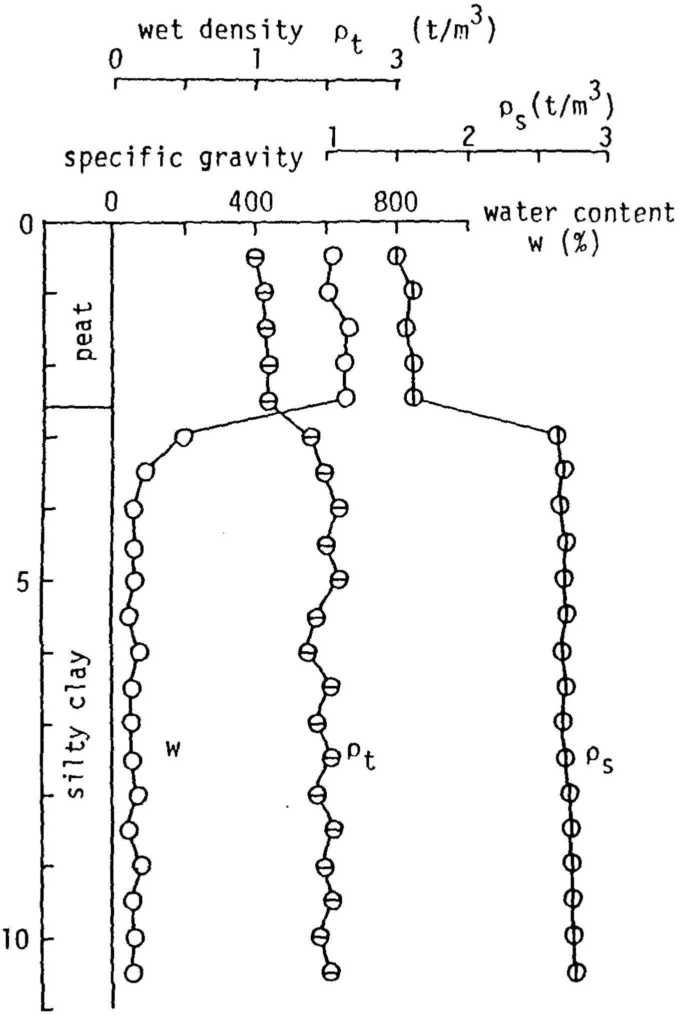

Fig.1 Soil strata and physical properties of test site

Table 1 Parameters of test vehicles

		weight (kg)
11 t dump truck	unload	9000
	load	20000
4 t dump truck	unload	3500
	load	7500
17 t bulldozer		17140
14 t bulldozer		12300
7 t bulldozer		6800

where, Ar: Reference value of vibration acceleration ($10^{-5}m/s^2$)

A : Effective value of vibration acceleration

$$A = \sqrt{\Sigma (A' \cdot A)}$$

A_n: Acceleration at each frequency

A_s: $A_s = \frac{1}{\sqrt{2f}}$ (for $1 \leq f \leq 4$ Hz)

$A_s = 1$ (for $4 \leq f \leq 8$ Hz)

$A_s = \frac{1}{0.125f}$ (for $8 < f < 90$ Hz)

f : Frequency

The vibration level meter used incorporates an electric circuit to adjust the measurement to human sensitivity for vibration as mentioned above and is capable of recording a vibration level directly in decibel (dB). Table2 shows the relationships between vibration level (VL) and acceleration, etc. Though vibration levels fluctuate irregularly and widely, uppermost values in the 80 % range were used as evaluation indices. It is referred here that the regulated limit of vibration nuisance for the test area is 60 dB.

Table 2 Relationship between vibration parameters

acceleration (cm/s^2)	acceleration level (dB)	vibration level (dB)	vibration velocity (mm/s)
- 0.8	- 55	- 49	- 0.1
0.8 - 2.5	55 - 65	49 - 58	0.1 - 0.3
2.5 - 8.0	65 - 75	58 - 67	0.3 - 0.8
8.0 - 25.0	75 - 85	67 - 77	0.8 - 2.4
25.0 - 80.0	85 - 95	77 - 86	2.4 - 6.2
80.0 - 250.0	95 - 106	86 - 96	6.2 - 17.2
250.0 - 400.0	105 - 109	96 - 99	17.2 - 25.7
400.0 -	109 -	99 -	25.7 -

4. RESULTS AND DISCUSSIONS

Fig.2 shows the relationship between vibration level (VL:dB) and vehicle speed (Vt:km/h) at a point 7.5 m away when dump truck runs on the temporary asphalt pavement. It is shown that the vibration level rises as the vehicle speed increases. Also, the weight increase results in larger vibration. In order to suppress the vibration level below 60 dB, the regulated limit of vibration nuisance in this area, the loaded 11 t dump truck has to be slowed down below 5 km/h.

Figs.3 and 4 show the relationships between vibration level and vehicle speed when the vehicle runs on the gravel road and the running panels, respectively. The result of gravel road running test shown in Fig.3 indicates that there was no difference between loaded and unloaded 11 t dump trucks. Compared with the paved road running, however, vibration level rose by about 1.3 times. The test on the running panels shown in Fig.4 reveals that the rate of change of vibration level by vehicle speed is smaller than the cases shown in Figs.2 and 3. It also shows that there was no significant difference in the level of vibration caused by the 11ton dump truck, whether it was load or unload. The vibration level of the running-panels is rated similar to that of the paved road.

It is understood that it is effective to use the temporary paved road to move construction vehicles on such soft peaty ground as the test site. When constructing the temporary road, it is important to determine its route in consideration of a permanent road to be built in future.

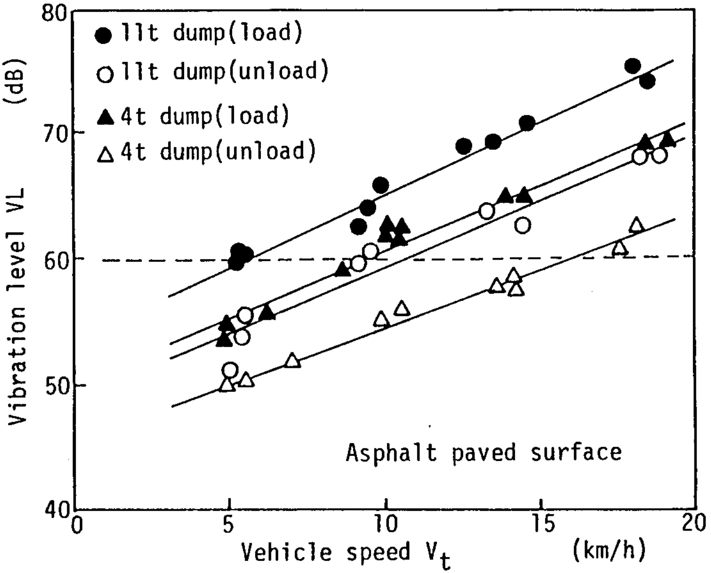

Fig.2 Relationship between vibration level at a point 7.5 m away and vehicle speed(asphalt surface)

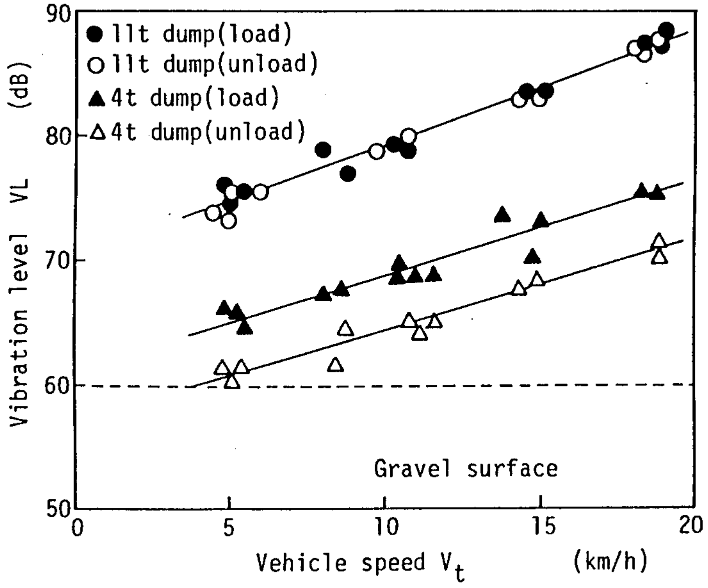

Fig.3 Relationship between vibration level at a point 7.5 m away and vehicle speed(gravel surface)

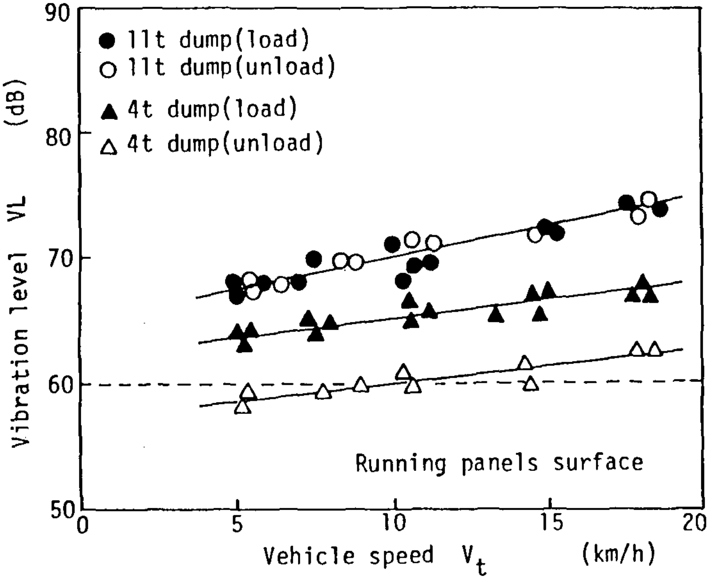

Fig.4 Relationship between vibration level at a point 7.5 m away and vehicle speed(panels surface)

Fig.5 is an example showing damping of vibration levels in accordance with distance from the vibration source. It is shown that vibration levels fall quickly as the distance increases. Fig.6 shows the data in Fig.5 expressed on semilogarithmic paper. The relations are almost linear and the empirical formulas are derived as shown below.

VL = 111 - 28 log R (for gravel road) (2)
VL = 96 - 24 log R (for panels road) (3)
VL = 92 - 25 log R (for pavement road) (4)

The value derived by dividing the difference of vibration levels between a measurement point and a 7.5m point by a vibration level at the latter point is defined as a damping rate of vibration level (Dr). Fig.7 shows the relationship between Dr and distance R. Irrespective of the road surface type, the relationship can be approximated by a straight line on semilogarithmic paper. Although absolute values of the vibration levels differ depending on the road surface type, damping rates of vibration levels remain almost unchanged as shown in Fig.7.

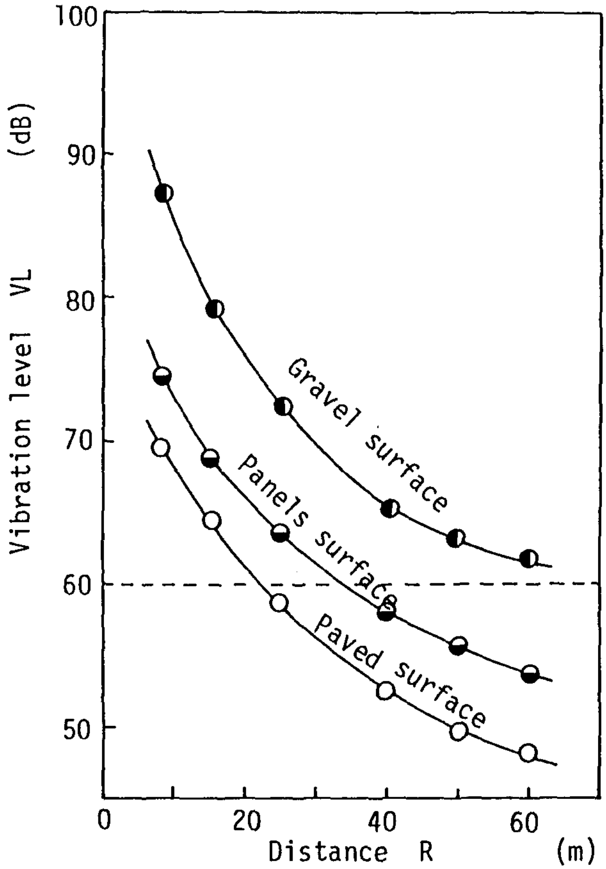

Fig.5 Damping of vibration levels with distance from vibration source

The straight line in Fig.7 can be expressed as follows.

$$Dr = 0.32 \log R - 0.28 \tag{5}$$

where, R is expressed in terms of meters.

Figs.8 and 9 show the relationships between vibration levels in vertical and horizontal directions and distances when various bulldozers run on the gravel road. No difference of vibration levels due to bulldozer weight was observed and levels were plotted on a straight line. Vibration levels of the bulldozer in the horizontal direction are higher than those in the vertical direction. In the case of the dump truck, however, vibration levels did not change much direction–wise.

As the regulated limit of vibration nuisance applicable to the test area is 60 dB, bulldozers have to be used roughly 25 m or more away from private houses. Figs.8 and 9 also contain relational expressions between both. Comparison of vibration levels by dump trucks and bulldozers shows that larger vibration is caused by dump trucks on such soft ground as the test site and points to the necessity to pay sufficient attention to the selection of dump trucks' route and their operational mode.

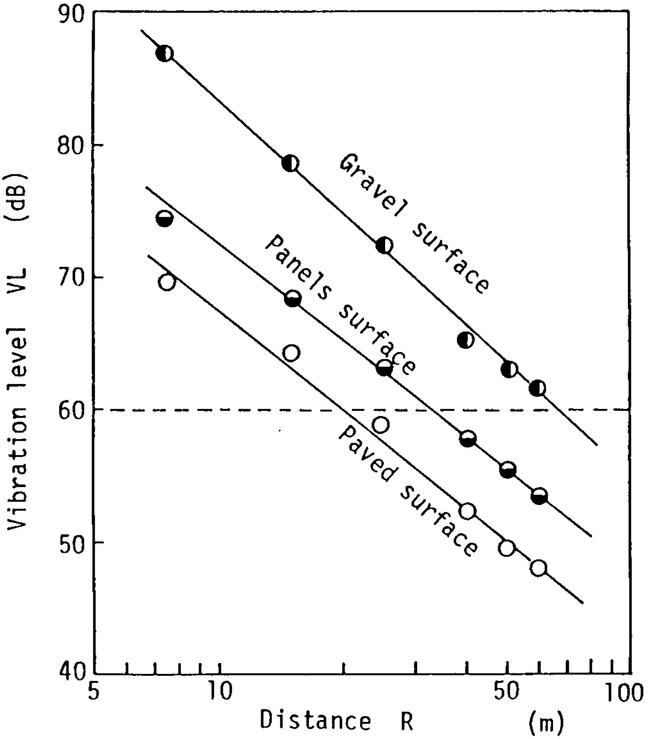

Fig.6 Damping of vibration levels with distance from vibration source

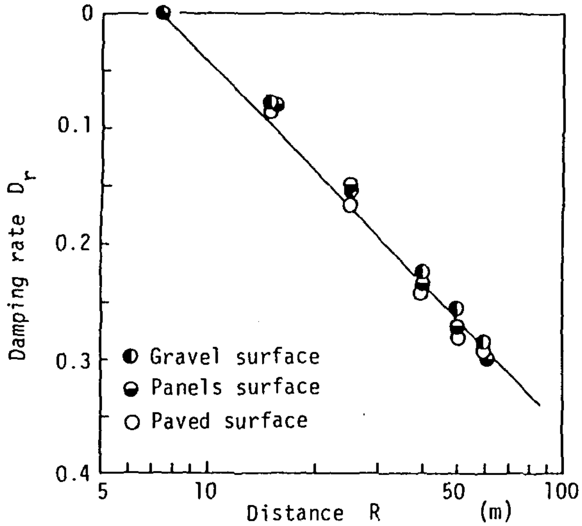

Fig.7 Relationship between damping rate and distance from vibration source

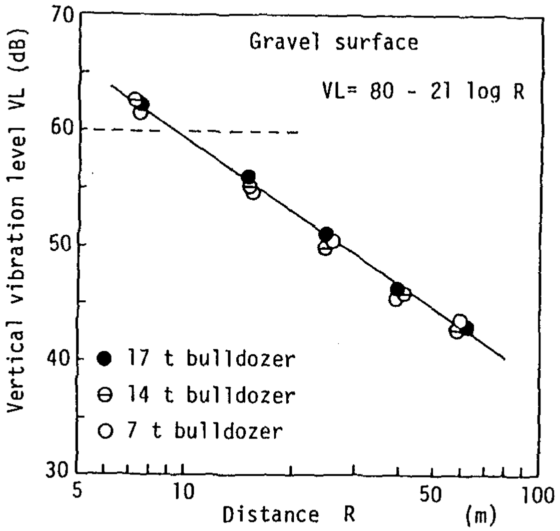

Fig.8 Relationships between vibration levels in vertical and distance(gravel surface)

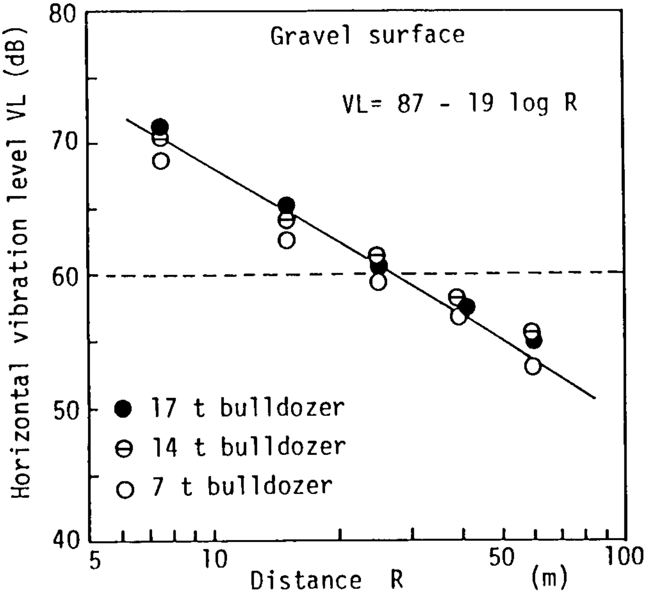

Fig.9 Relationship between vibration levels in horizontal and distance(gravel surface)

5. CONCLUSIONS

This study was devoted to the experimental review of ground vibration characteristics presented when dump trucks and bulldozers run on the soft peaty ground. The research findings can be summarized as follows.

Speeds of construction vehicles influence resultant levels of vibration to a great extent. The relationship between running speeds and vibration levels can be expressed in a straight line. To meet the vibration nuisance limit requirement applicable to this test area of less than 60 dB, a loaded 11 t dump truck, for example, has to keep its speed at around 5 km/h or lower. Smallest ground vibration is generated by vehicles running on the temporary asphalt pavement and vibration levels grow larger when they run on running panels and a gravel road in this order. Dumping rate of vibration level does not change by the road surface type. Regardless of the road surface type, the relationship between a damping rate and distance can be approximated by a straight line on semilogarithmic paper. Ground vibration caused by the running dump truck shows no difference between vertical and horizontal vibration levels, but the bulldozer shows higher vibration level in the horizontal direction than in the vertical direction. A difference in weight of bulldozers does not produce the difference in the vibration level. Larger ground vibration is generated by the dump truck than by the bulldozer on such soft ground as the test site.

REFERENCES

[1] Nakagawa,K. and Watanabe, S.(1975): Vibration pollution and its counter plan, Thuchi to Kiso,Vol.30, No.1, pp.65–71.

[2] Enami, A et al.(1983): Pollution by construction and counterplan, Japanese Society of Soil Mechanics and Foundations Engineering, pp.149–260.

[3] Sakai,T.(1986): Loudness and noisiness of construction noise, Civil Engineering Journal, Vol.28, No.6, pp.308–313.

[4] Fukuda, T.(1994): Traffic Engineering, Asakura Publication, pp.138–141.

COMPACTION EFFECT OF VIBRATORY SOIL COMPACTORS MODELING, SIMULATION, OPERATING TESTS

Dipl.-Ing. Michael Tettke, Prof. Dr.-Ing. Wolfgang Poppy
Institute for Machine Construction
Construction Machinery - Design and Engineering
Berlin University of Technology

ABSTRACT

The field of soil compacting has experienced a rather drastic change during the last few decades. While the machinery involved has grown to greater and greater complexity, the industry these days yields reliable and sensitive field measuring devices for supervising and documenting the compaction progress which are more and more gaining market power.

Increasing performance and output can be achieved by running vibratory rollers in automatic operation as well as by means of Automatic Data Processing in order to control compaction results in situ.

Basic inquiries on this subject have recently been implemented at the Technical University of Berlin.

1. SOIL COMPACTION USING VIBRATORY ROLLERS

As a quality-forming completion of any digging job, soil compaction asks for the highest grade of performance of the equipment used. The majority of all compaction work is performed by various types of vibratory rollers such as rollertrains, single (trailertype) or tandem rollers. Their compaction power results from both static and dynamic effects, depending on vibratory system parameters like roller mass, excitation mass and -frequency, but also on the driving speed.

According to a given type and state of the soil, the operator has to adjust (and frequently readjust) his machine so as to achieve the desired compaction grade with as few passes as possible, yet garanteeing stable and homogenous results.

Modern state-of-the-art powering and controlling technologies in these rollers already offer means of infinitely variably setting driving speed and excitation frequency. Further developments in hydraulics and microelectronics will also enable a continuous setting of the excitation mass during operation. Thus, vibratory rollers will be adjustable to a wide variety of different jobs and operating conditions.

Yet even today, the roller operator often enough finds himself hopelessly overcharged by trying to optimally adjust his machine to a given job or actual compaction state, and to finally guess the right time to terminate his efforts. Depending on the soil type and its actual properties, any misapplication or machine maladjustment may even lead to grain shatterings or reloosening of the ground surface.

Therefore, any further development should lead to an automatisation of roller operation and compaction result control. This calls for automatic identification of the actual compaction state and appropriate setting of the machine parameters.

2. MODELING AND COMPACTION ANALYSIS

In order to examine all the parameters important to vibration behavior and compaction results, and for deriving new strategies for an automatic adjustment of all necessary machine parameters, no empirical inquiry would alone be sufficient since the individual parameters can but very inadequately be adjusted independently. So, a simulation model for representing the dynamic behavior of any vibratory roller corresponding to a given soil type has been developed [1].

Using a mathematical description on the interactions between roller behavior and actual ground compaction state, single compaction parameters can be examined as they are. To do that, the simulation model must be able to represent every possible state of operation. So the model consists of two separate systems representing the roller and the soil in their compaction-relevant properties.

In its simplest form, the roller part of the model consists of the elements frame mass m_f, roller (or drum) mass m_d, and roller suspension with a stiffness c_f and damping rate d_f. The roller drum is forced to oscillate by the excitation force F_e, which rotates at the speed of Ω **(Fig. 1)**. The influence of the larger frame inertia found in rollertrains or tandems must be compensated by using an equivalent frame mass m_f* instead of m_f.

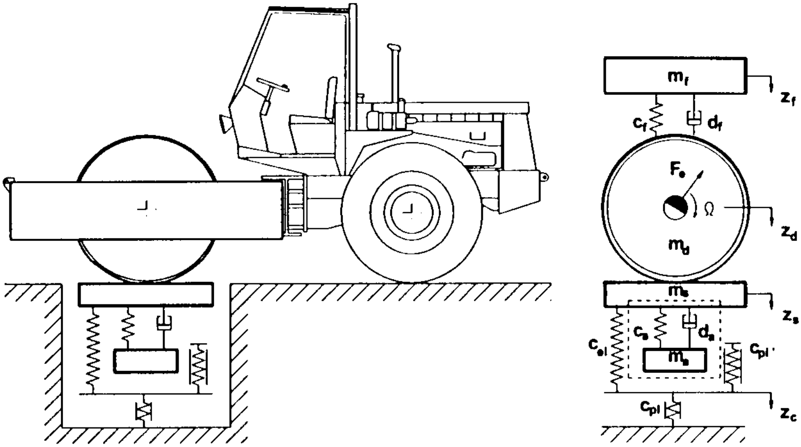

Fig. 1: Model of the roller/soil system

The most important claim to the soil model is for it to be able to represent both elastical and elasto-plastical deformations. Its synthetisation follows the thesis that any increase in plastic deformation (i.e. compaction) can only be achieved by increasing the forces induced. This concept has been realised by a soil model consisting of a combined three-spring-system [2].

In order to model the soil's properties, and to be able to correlate the empirical parameters of the roller/soil system with the ones computed for the model system, the vibrating part of the soil (right underneath the roller) must be modeled as a limited (or lumped) mass element m_s. Together with the spring element c_{el}, this mass m_s constitutes an undamped oscillator system. To control the system's elastic vibrations, its vibration energy has to be drained by an absorber mass m_a coupled to m_s via absorber elasticity c_a and damper d_a.

During the compaction process, roller behavior has to be separated into contact operation and bounce operation. The roller's motion state at a given time depends upon the momentary surface force, i.e. the total force forwarded from the roller into the soil surface. The question of whether the roller leaves ground contact or no cannot be answered by simply computing the ratio between maximal excitation force vs. total roller weight, since it is also influenced by the spring/damper systems involved in the roller suspension and the vibrating part of the soil.

During the leap phase of operation the roller body is completely airborn, so that roller mass and soil mass are discoupled. The following contact phase will begin with the roller's impact onto the soil.

The contact phase has to be separated into two different states of soil deformation which in normal operation occur at different times and frequencies. While in elasto-plastic deformation, all springs of the model are stressed, i.e. springs c_{pl} and c_{pl}' are deformed irreversibly while c_{el} is stressed elastically. In case of predeformed soil, all static and dynamic loads are charged only to the elastic element c_{el}. In this state, the stop springs c_{pl} and c_{pl}' are no more deformable.

3. EVALUATION OF THE MODELING PARAMETERS

In order to simulate the roller/soil system's behavior, all the modeling parameters have to be evaluated.

Roller Parameters

Based on the roller's technical data, the following values of the model's elements must be computed:

- Frame (Load) mass m_f, or equivalent frame mass m_f^*
- Vibrating mass (roller drum) m_d
- Unbalance $m_u \cdot r_u$
- Suspension spring rate (stiffness) c_f
- Suspension damper rate d_f

These data can only be computed after assuming the proposed vibration behavior of roller and frame. While the masses of frame and roller body can easily be measured for trailertype rollers, the effective inertia m_f* of automotive vibratory rollers such as tandems or trains calls for a rather complicated evaluation process considering their respective lumped-element inertiae and their geometry. The mass inertia Θ_{yR} of a given roller can be experimentally tested by suspending the whole machine to freely oscillate and then taking the period time of its free (natural) oscillation.

$$m_f* = \frac{\theta_{yR} + m_f \cdot (l_h^2 + h_s^2)}{l_r^2}$$

m_f	Frame mass
l_h	Distance mass center / rear axle
l_r	Distance drum center / rear axle
h_s	Height of mass center / surface
Θ_{yR}	Moment of inertia

Roller drum and machine frame are connected via elastical elements. Their main tasks are isolating the frame from the roller drum's vibrations while still transmitting supporting, steering and traction forces and torques. Commercially available rollers are usually equipped with rubber/metal elements (silentblocks) in these places. The necessary data which are essential for any modeling process include the dynamic stiffness (spring rate) c_f and damping rate d_f of these elements, which are not constants, but depend on the frequency of their actual oscillating stress and on the actual displacement amplitude.

Soil Parameters

The soil part of the model considers the mass m_s of the soil's vibrating range (simplified to a lumped, rigid element), the stiffnesses c_{el}, c_{pl} and c_{pl}' and of course the parameters m_a, c_a and d_a of the supplementary absorber system. Contrary to the roller part of the model, these parameters are much harder to obtain since there's no direct mathematical relation between them and the soil's actual properties. Another problem is that any interdependences between modeling and operational parameters are unknown and liable to change during operation.

For computing the soil model parameters, real soil properties like grain size distribution, water content or cohesiveness cannot be used. Instead, analysing the dynamic properties of the complete roller/soil system may lead to restrictions and regularities which allow a parameter evaluation.

4. RESULTS

Using a rollertrain/soil system as shown in Fig. 1 as an example, oscillating behavior and compaction effect of the roller can be simulated. The modeling parameters as listed in **Tab. 1- Tab. 3** are based on experimental results as well as on what could be gathered from the manufacturer's data sheets.

Table 1: Technical Data of the roller and preset data

Self-propelled vibratory roller 2310 (HAMM)		
Technical data provided by the manufacturer		
Operating weight	m_{tot}	6500 kg
Static weight (drum)	m_{stat}	3500 kg
Excitation frequency	f_e	30 Hz
Excitation force (f_e=30 Hz)	F_e	105 kN
Nominal amplitude of drum displacement	A_0	1.4 mm
Experimental data		
Distance mass center - rear axle	l_h	1.33 m
Distance drum center - rear axle	l_r	2.44 m
Height of mass center - soil-surface	h_s	0.79 m
Moment of inertia of roller	Θ_{yR}	$16.6 \cdot 10^3$ kgm^2
Preset data		
Frequency ratio	η	3.0
Damping rate	D	0.06
Natural frequency of roller/soil system	f_{0ep}	15 Hz
Natural frequency of additional system	f_a	23 Hz

Table 2: Parameters of roller model

Drum mass	m_d	2110 kg
Frame mass (resting on drum)	m_f	1390 kg
Equivalent frame mass	m_f^*	2800 kg
Static weight vs. Excitation force	γ	0.33
Frame mass vs. Drum mass	α	0.66
Moment of unbalance	U	2.96 kgm
Natural frequency of frame mass	f_{0f}	15 Hz
Spring stiffness of frame suspension	$c_{f\,stat}$	$5.48 \cdot 10^6$ N/m
Damping factor of frame suspension	d_f	10480 Ns/m

Table 3: Parameters of soil model

Soil mass	m_s	700 kg
Additional mass	m_a	70 kg
Elastic spring stiffness	c_{el}	$87 \cdot 10^6$ N/m
Plastic spring stiffness	c_{pl}	$49.3 \cdot 10^6$ N/m
Plastic spring stiffness	$c_{pl'}$	$75.8 \cdot 10^6$ N/m
Spring stiffness of additional mass suspension	c_a	$1.46 \cdot 10^6$ N/m
Damping factor of additional mass suspension	d_a	3440 Ns/m

The simulated vibration behavior of this primitive model would be checked by means of animation software and then rated afterwards, based on time laps of the different outcome variables.

The simulation, which at first is valid only for the given operating point of the roller, will then be extended to excitation frequencies ranging from $f_e = 1$ Hz to 50 Hz to allow further parameter variation. The characteristics of the resulting variables are fixed in their amplitude and frequency distribution as well as in the typical shape of their time laps.

4.1 VARYING THE ROLLER DRUM SUSPENSION

In vibratory roller design, the frequency ratio η is a variable which can be chosen out of a range between $\sqrt{2} < \eta < \eta_{max}$. In this chapter, the effect of varying the frame's vibratory isolation grade on roller drum behavior will be presented.

Results are plotted as effective values (RMS) vs. excitation frequency in a range up to $f_e = 50$ Hz. By reducing the time domain data, single values of the outcome found at a given point of the frequency domain (e.g. at an operating frequency of $f_e = 30$ Hz) can be compared, allowing to extrapolate the effect of varied frequencies on the result.

On a real machine, the ratio of excitation frequency and the frame's natural frequency can be varied simply by using silentblocs of different Shore grades in the roller suspension. **Fig. 2** shows the effective frame acceleration amplitude (response) at various frequency ratios η plotted on the excitement frequency domain.

Increasing the value for η obviously reduces the amplitude at operating frequency. Frame acceleration resonance shows up in a range between the frame's respective natural frequency and the excitation frequency. The closer the last two get to each other on the frequency axis, the wider gets the resonance range and the larger

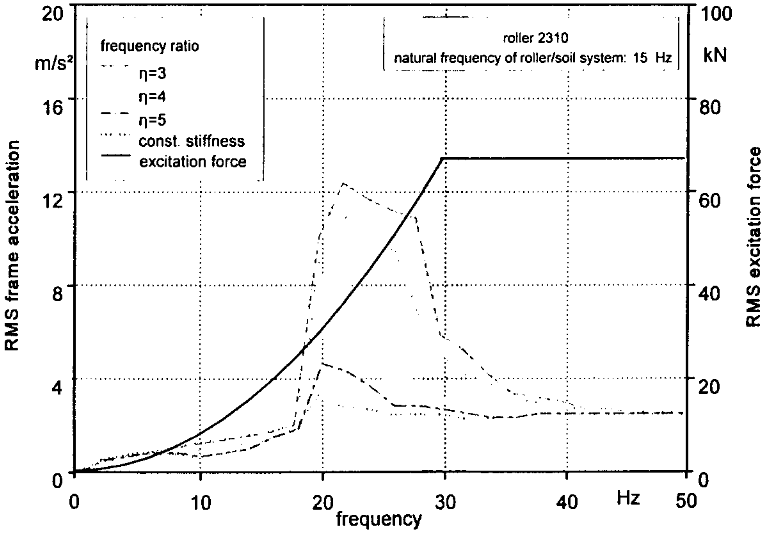

Fig 2.: Frequency analysis of RMS frame acceleration at various frequency rates

grow the resonant amplitudes. In Fig. 2, the hatched areas are enclosed by acceleration values based on constant (dotted lines) or frequency dependent silentbloc spring rates. The response curves vary mainly within the resonant range of the frame, where the ones based on frequency dependent spring rates rise about 20 % higher than the accelerations computed using constant spring rates.

4.2 VARYING THE EXITATION FORCE

Another characteristic of vibratory rollers is found in the rate Υ between static drum load and excitation force equivalent:

$$\gamma = \frac{m_{stat} \cdot g}{\hat{F}_e}$$

As can be extracted from data sheets, machines of a certain type independently of brand or gross weight all show more or less the same γ values. For example, rollertrains average at $\gamma = 0.3$, which means that their excitation force amplitude F_e during normal operation is about three times as high as their static drum load m_{stat}.

The γ rate can be changed by varying either static drum load or excitation force amplitude. For investigating the influence of a variable excitation force amplitude on the roller drum's vibratory behavior, the static drum load is kept at constant.

Fig. 3 shows the effective (RMS) vertical roller drum accelerations for various excitation force amplitudes plotted on the excitation frequency domain. It is evident that within the operating frequency range around 30 Hz, accelerations are fairly constant and thus independent of excitation speed changes. Growing excitation amplitudes, however, are apt to move the acceleration graph's noticeable rise into direction of lower frequencies, since the minimum accelerations needed to change over to bounce operation will be reached earlier.

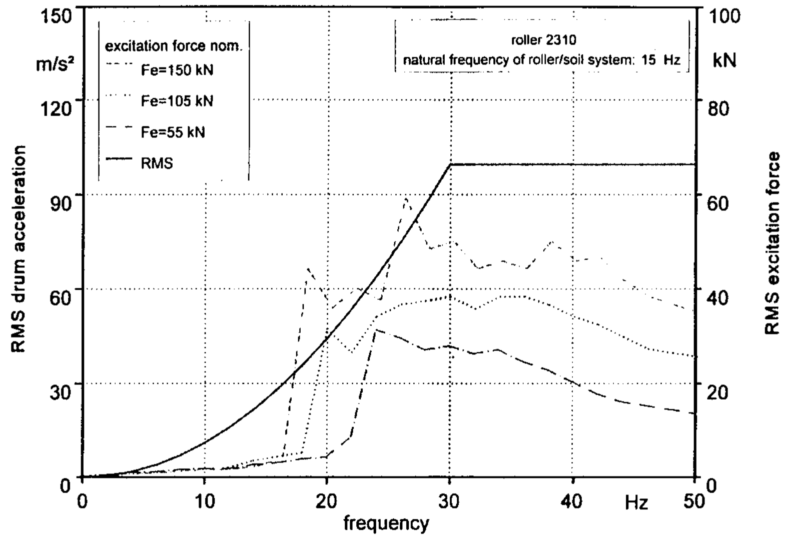

Fig. 3: Frequency analysis of RMS drum acceleration at various excitation forces

In previous investigations [3] on this subject, Luther's efforts to correlate singular parameters (e.g. gross roller weight, roller drum weight and -amplitude, excitation frequency and -force) with compaction results (Proctor density, E-moduli) did not lead to any useful evidence. However, by combining roller drum weight, vertical drum amplitude and excitation frequency into Luther's capacity product V, a positive relation between roller data and compaction success can be stated:

$$V = m_{stat} \cdot g \cdot \hat{z}_d \cdot f_e$$

The higher the value of V, the better the outcome of the compaction process will be. The value of V can be increased by raising the excitation force amplitude in relation to the roller's static drum load. Thus, either raising a rollertrain's excitation amplitude or reducing its drum load will improve its compaction effect. This relation is valid for the whole range of excitation frequencies. Keeping the frequency at constant, any given machine's capacity will depend exclusively on the oscillation amplitude of its roller drum. Further, the drum's theoretical (or nominal) amplitude A_0 depends on weight and displacement of the excitation mass. It follows that the value of the excitation force depends on the rated nominal amplitude A_0 of the drum.

For reasons of fairly good traction, tandem rollers have to get by with lesser amplitude ratings than rollertrains and trailertype rollers, which allow greater excitation forces compared to their respective drum load. The layout-related differences of the Υ-parameter with significantly lower values for trailertype rollers and rollertrains can be verified on commercially available rollers.

5. EXPERIMENTAL VERIFICATION OF THE MODEL

The system properties of the soil model can be extracted partly from physical laws (e.g. impact theory), partly from soil mechanics. As a verification of the system parameters found so far, accompanying compaction experiments are necessary.

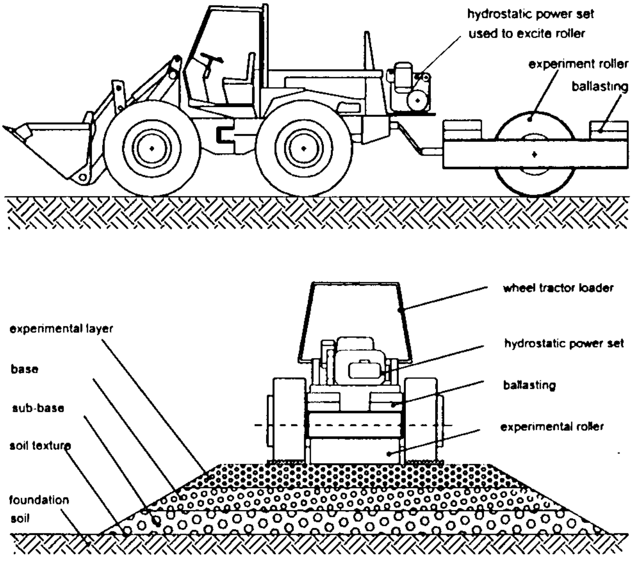
hydrostatic power set
used to excite roller
experiment roller
ballasting
wheel tractor loader
experimental layer
hydrostatic power set
base
ballasting
sub-base
experimental roller
soil texture
foundation
soil

Fig. 4: Compaction test run on an embankment fill probe track using experimental downscaled trailertype roller

Since commercially available rollers aren't designed to flexibly and independently set all the parameters needed (i.e. excitation amplitude, frequency and ballasting), a downscaled model of a trailertype roller as shown in **Fig. 4** has been built. It also reduces the expense in time and material for preparing test runs. In order to increase the range of ballasting, the roller's dieselhydraulic vibration engine has been mounted separately on the towing vehicle (wheel tractor).

Test runs were lead on an experimental track which guarantees realistic vibration behavior of the whole roller/soil system. An embankment fill has proven best suited for that purpose.

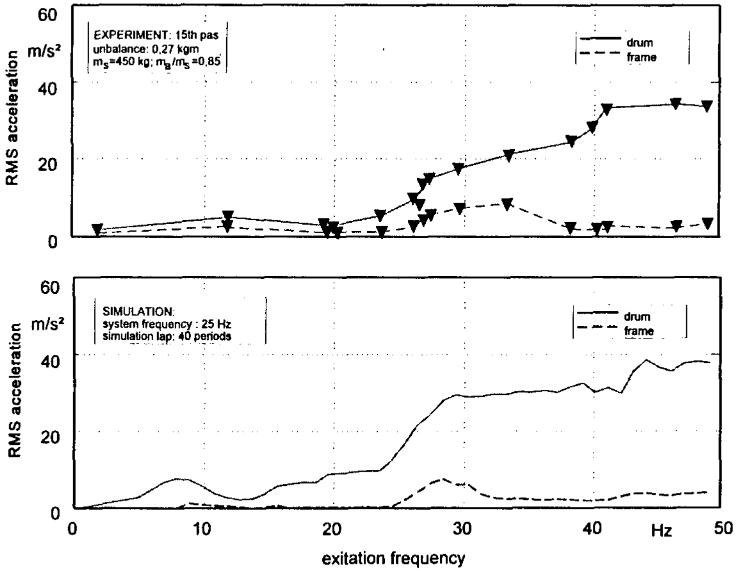

Fig. 5: Frequency domain RMS roller acceleration;
above: test run on highly compacted sand;
below: simulation over 40 periods per single frequency.

The system frequency forms a basis for evaluating the soil model parameters. This natural frequency of the whole roller/soil system must be evaluated experimentally. Usually, it ranges from 15 to 35 Hz [4]. For instants, a test run on precompacted sand with variable excitation frequency, but constant drum load and amplitude brought up a natural frequency of 25 Hz.

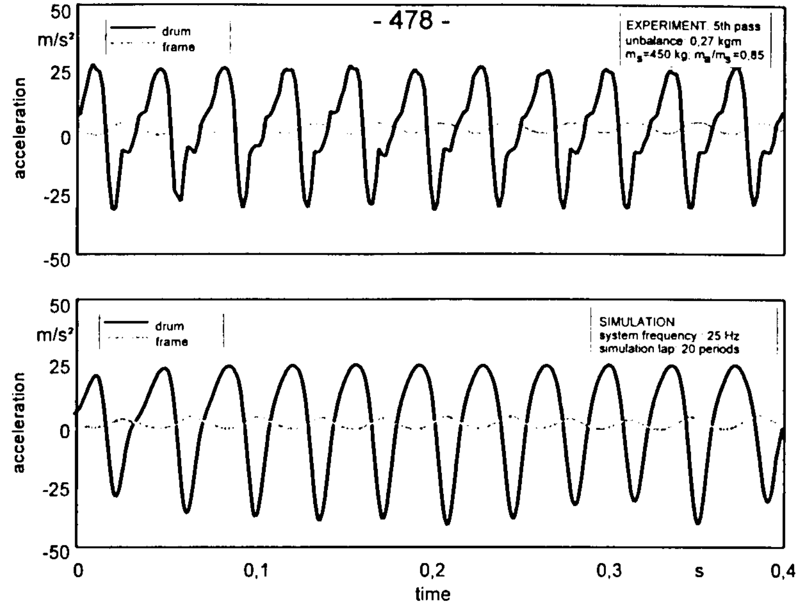

Fig. 6: Time domain RMS roller acceleration;
above: test run on precompacted sand;
below: simulation over 20 periods per single frequency.

Before computing any simulation results, it's necessary to guess the vibrating soil mass m_s, which we have set to 10 % of the static drum load [5]. **Fig. 5** shows an example of the vertical accelerations of each frame and drum, plotted as RMS in frequency domain. The upper plot also marks the actual measuring points. The simulation presented in the lower plot has been computed applying frequency steps of 1 Hz at a simulation length of 40 periods each.

In the frequency range below 10 Hz, a natural roller/frame resonance has a much greater influence on the simulated acceleration courses than on the experi mental ones, where a stable resonant operation couldn't be kept up. Therefore the distance between testing frequencies has been widened in this range.

Looking at frequencies above 25 Hz now, there is a fairly good resemblance between experimental and simulation results. Although the excitation force grows by square of the excitation frequency, the induced drive power cannot be transmitted properly any more at higher speeds, so drum accelerations increase but slowly. Furthermore, the range close to the system's natural frequency isn't suited as normal state of operation because of a significant rise in frame acceleration which results in severe stress to the whole machine.

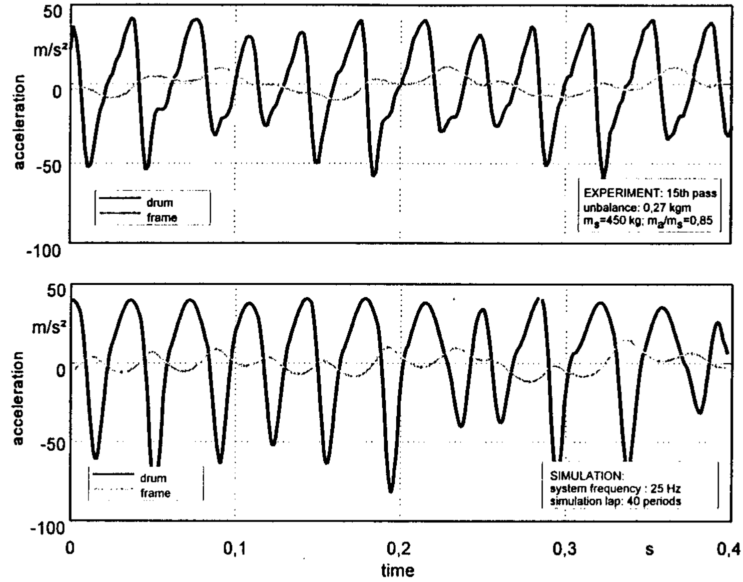

Fig. 7: Time domain RMS roller acceleration;
above: test run on highly compacted sand;
below: simulation over 40 periods per single frequency.

Time courses of drum and frame accelerations at different compaction states are shown in **Fig. 6 and 7.** The simulation settings are the same as in Fig. 5. Based on the presimulation agreements in Fig.1, roller acceleration gets negative (i.e. directed upward) during compression- and rebound phase, while it'll be positive during the leap phase when there is no ground contact. The frequency is set to 30 Hz, which makes the excitation force strong enough to operate the roller in bounce mode.

Due to the hard impact combined with high soil stiffness, the amounting roller acceleration during touchdown phase reaches much higher than its counterpart during leap phase. The frame acceleration comes up to about 10 to 15 per cent of the drum acceleration. The operating frequency lies far above the drum/frame system frequency. This puts up a phase difference of 180° between both acceleration time laps.

During the first four passes of precompacting (Fig.6) there is only a short leap phase which lasts less than one excitation period. After a few more passes the soil stiffness has grown high enough for the roller to stay in the air as long as two rotations of its unbalance shaft (Fig.7). In this case, the leap phase drum acceleration runs symmetrically to its zero position, but during the following impact phase it reaches much higher maximum values than in the beginning of the compaction process. Looking at frame acceleration, the frame/drum natural frequency returns as a beat (or pulsation) started by the impact.

6. PRACTICAL USE IN CONSTRUCTION WORK

Comparing the outcome of both simulation and experiment it is evident that the chosen model is fit to give a good enough image of a complex roller/soil system's oscillating behavior considering the soil's elasto-plastical deformation tendencies as well as the roller suspension's nonlinear elasticity. Moreover, simulation has proven its ability to help systematically design a new vibratory roller even before building a first prototype for testing on a trial- and-error basis. Parameters like frame and drum masses, unbalance, suspension stiffness and operating frequency can be optimally matched. Critical states of operation during leap phases can be computed in relation to soil stiffness to be considered while running the roller. Controller structures for automatically adapting the roller's parameters to compaction progress can be developed, tested and optimised using simulation.

Thus, simulating vibration and compaction behavior of vibratory rollers represents an important contribution to systematically designing new machines and improve the performance of existing ones.

REFERENCES

[1] Pietzsch, D.:
Untersuchungen zum Schwingungsverhalten und zur Verdichtungswirkung von Vibrationswalzen; VDI Fortschritt-Berichte, Reihe 4, Bauingenieurwesen 104
Düsseldorf: VDI-Verlag, 1991
[2] Bathelt, U.:
Das Arbeitsverhalten des Rüttelverdichters auf plastisch-elastischem Untergrund; Bautechnik Archiv, Heft 12, Berlin: Verlag Wilhelm Ernst & Sohn, 1956
[3] Luther, G.:
Die Wirkungsweise und kennzeichnenden Merkmale von Vibrationswalzen
Straße und Autobahn 16 (1967) 3 pp. 80-96
[4] Jurecka, W.:
Das Bewegungsverhalten und die Wirkungsweise von Rüttelverdichtern, Baumaschine und Bautechnik 18 (1971) 11, pp. 461-466
[5] Dimpfl, G.:
Untersuchungen über den Enegieaustausch bei der Bodenverdichtung mit Sprungrüttlern, Dissertation, RWTH Aachen, 1965

Session IX
Sektion IX

Special Topics

Sonderthemen

THE FEA WAY TO AN OCTAGONAL RING TRANSDUCER DESIGN OPTIMIZATION

Ferretti G., Paoluzzi R. & Rigamonti G.
CEMOTER - C.N.R.
Institute for Earth-Moving Machinery and Off-Road Vehicles of the Italian National Research Council
Via Canal Bianco, 28
44044 CASSANA-FERRARA, Italy

1. Introduction

The design of soil-tilling machines of any type would be impossible without considering the physomechanical properties and other characteristics of soils. In particular it results very important to measure the force system acting on the plow during the soil failure that, in the case of symmetrical failure, consists of two mutually perpendicular force components (a horizontal force Fx and a vertical force Fy) and of the moment Mz in the plane of the two forces. These measurements have been carried out for a long time using a series of single dynamometers even if it was difficult to evaluate the accuracy of such a system.

A new measurements method based on the use of an extended octagonal ring transducer was proposed in 1975 by J. Goldwin [1]. This new method offers some advantages such as the simultaneous monitoring, alleviation of the frictional problems arising from the dynamometer suspension bushes, no difficulties caused by the single component construction. A finite element analysis has been carried out in order to optimize the dimensions of the dynamometer with the general objective function of minimum measurement error.

2. The Measurement Method

The original Goldwin dynamometer is shown in Figure 1. Its particular shape allows a linear relationship between the output and the applied load. The values of the two mutually perpendicular forces component and of the moment are evaluated using twelve strain gauges connected four by four in order to form three full bridge circuits BC_{Fx}, BC_{Fy} and BC_{Mz} as shown in Figure 1. The positions of the strain gauges are fixed and chosen in order to minimize the cross sensitivity beetwen the force component channels

Previous experiments [2] showed good performance of the original dynamometer under actual loading condition both in terms of overall resistence and stress distribution even if it was dimensioned only on the base of very restrictive approximations and empirical consideration. The next step towards an improved accuracy therefore required the use of more refined techniques.The optimization of the dimensions of the internal clearances to minimize the measurement error was the strightfoward first attempt made to apply structural optimization techniques to the design of a better transducer. The result obtained were encouraging with a reduction of the measurement error of about 10% [5].

In this first phase of the study the FEM was the fundamental tool used to evaluate the deformations

Figure 1: The Extended Octagonal Ring Dynamometer as proposed by Goldwin in 1975. Design variables used throughout the paper are listed together with the original dimensions.

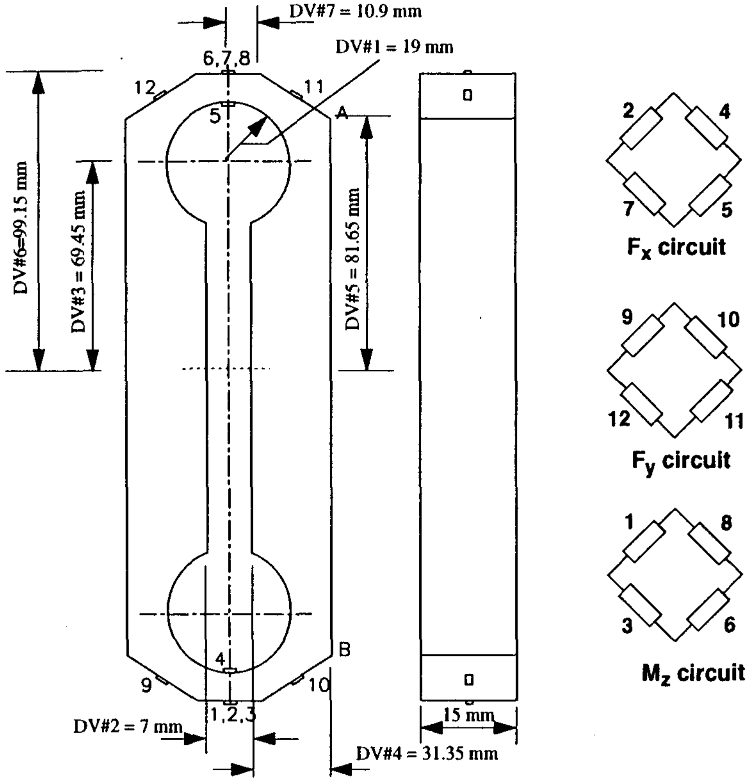

of every single transducer under different load conditions in order to compare the performance of the dimensionally different dynamometer. Strain values are computed at locations close to the measurement points and combined four by four to obtain values proportional to the actual Wheatsone bridge readings. Undesidered responses to ideal loading conditions can thus be used as a measure of the transducer accuracy in order to make an optimization function available.

3. The Ansys Program And The Design Optimization Characteristic

The ANSYS program is a general-purpose computer program for finite element analysis and design that could be used in a high number of disciplines of engineering such as structural,mechanical,thermal, magnetics a.s.o..

Generally speaking, a design optimization procedure is based on a constrained minimization. The performance of the design is somehow described by a single-valued objective function that should be minimized with respect to a set of design variables [6], provided that a set of constraints expressed by inequalities is satisfied. In formal notation it means to find the vector of design variables $\underline{x}$ that minimizes:

$$y = f(\vec{x}, \vec{\alpha}) \qquad \text{with} \quad \begin{cases} a_1 \le x_1 \le b_1 \\ \dots \\ a_n \le x_n \le b_n \end{cases} \tag{1}$$

Where $\vec{x}$ and $\vec{\alpha}$ represents design and state variables respectively.

The solution methods applicable to the problem can be of different kinds, some of them requiring the computation of the derivatives of the objective function, some other not. To calculate an optimum design, the ANSYS program performs a series of analysis-evaluation-modification cycles. That is, an analysis of the initial design is performed, the results are evaluated against specified design criteria, and the design is modified as necessary.

In the analysis we carried out the design variables are the seven geometrical dimensions represented in Figure 1 that fully characterize the dynamometer itself, all the others dimensions are expressed as functions of these base variables. Both the design variables and the state variables are defined in ranges depending on their characteristics and are subjected to conditional substitution[1] in order to avoid dynamometers shaped not congruently with the original one.

The initial user-defined design vector was obtained from the original Goldwin instrument.

As state variables also the displacement of the nodes located at the extremities of the strain gauges and the deformation of the strain gauges themselves are chosen. Conditions have been imposed to avoid strain gauges deformations higher than 10% to be sure of the linear behaviour of the material. The dynamometer is tested with three different load conditions (Table 1) with F_x, F_y, M_z equal to zero, the values read respectively by the bridge circuits BC_{Fx}, BC_{Fy} and BC_{Mz} are the values of the undesidered deformations. A fourth load condition is imposed in order to evaluate the behaviour of the instrument under realistic working conditions characterized by the simultaneous presence of F_x, F_y, M_z. It is worth nothing that to simplify the load step generation the forces had been applied directly to the points shown in Figure 1 and not in a distributed and more realistic way. In spite of obvious local error caused by the application of concentrated forces, deformations in the measurements points are not significantly affected because of the distance from the load application nodes.The objective function to be minimized in the optimization process is the global measurement error defined as the quadratic mean of the sum of the undesidered deformation signal[2], ε_{Fy1}, ε_{Fx2},

Table 1: Load cases

	F_x (N)	F_y (N)	M_z (Nm)
Load case 1	400	0	210
Load case 2	0	150	210
Load case 3	400	150	0
Load case 4	400	150	210

---

[1] Conditional substitution is a feature offered by Ansys Parametric Design Language (APDL) which allows for the assignment of bounded values to design and state variables of the optimizer. From a computational point of view it is equivalent to a series of nested *if...then* structures.

[2] Every single component is the value of the overall deformation read by the bridge devoted to the measure of the unloaded component. Subscripts refer to the unloaded component and to the correspondent load case number.

ε_{Mz3}, read by the bridge circuits in load case 1, 2, 3, divided by the quadratic mean of the sum of the deformation signals, ε_{Fx4}, ε_{Fy4}, ε_{Mz4}, read by the bridge circuits in load case 4.

This way the objective function is defined as follows:

$$OBJ = \frac{\sqrt{{\varepsilon_{F_{y1}}}^2 + {\varepsilon_{F_{x2}}}^2 + {\varepsilon_{M_{z3}}}^2}}{\sqrt{{\varepsilon_{F_{x4}}}^2 + {\varepsilon_{F_{y4}}}^2 + {\varepsilon_{M_{z4}}}^2}} \cdot 100 \qquad (2)$$

This objective function does not really express the measurement error but a value proportional to it. This definition in fact is a simple combination of individual objective functions that could be defined for single load cases. This characterizes the overall analysis as a multi-objective design optimization that represents a considerable complication to the general design optimization problems, as the mutual effects of design changes on different load steps are to be taken into account by the optimization algorithm, and generally those effects are strongly coupled.

Usually problems of the kind proposed are ill-conditioned or, even if they are not, require a robust optimization algorithm to be used. The ANSYS design optimization algorithm is outlined in Figure 2. It converts the constrained optimization problem to an unconstrained one by adding penalties to the objective function approximation to account for the imposed constraints, the search for a minimum is then performed using the Sequential Unconstrained Minimization Technique (SUMT).

It is clear that as the number of the design variables was increased trying to optimize the whole dynamometer, some convergence problems appeared and became really hard to overcome. Therefore very restrictive feasibility limits to the design variables had been imposed and it was also necessary to periodically reselect only the best design to force better curve fit approximation and to reduce the possibility of program convergence onto a local minimum.

4. The Optimization Program

The optimization program is divided into three fundamental sections:

1) the preprocessing one in which the dynamometer geometry is created, the parameters are defined, the load conditions are imposed, and the system is meshed. This last operation is critical because the Ansys version used is limited for educational purpose and so meshes with too high number of elements have to be avoided, but at the same time at least three nodes in each area corresponding to the location of a strain gauge should be generated in order to be able to evaluate the deformation of the strain gauge itself. Mapped meshing with only quadrilateral elements was then impossible to realize because of the great dimensional variations occurred during iterations, so the element used was a 2-D 6-node triangular structural solid that is well suited to model irregular meshes.

2) the postprocessing one in which the displacements of selected nodes are stored and summed in order to measure the deformations of the strain gauges under different load conditions. The maximum stress is also evaluated for a load step representative of actual operating conditions, in order to put constraints on the linearity of the stress/strain relationship in the actual component;

3) the optimization section in which the range of the design variables and of the state variables are defined, in particular the deformation of the transducers are defined as state variable and the corresponding constraints are chosen in order to avoid strain gauges deformation higher than 10%.

The resulting code has been assembled in order to have a proper optimization loop coding within ANSYS which could run in batch mode.

Figure 2: Outline of the general optimization loop within ANSYS. The hatched block identifies the role played by the FE analysis.

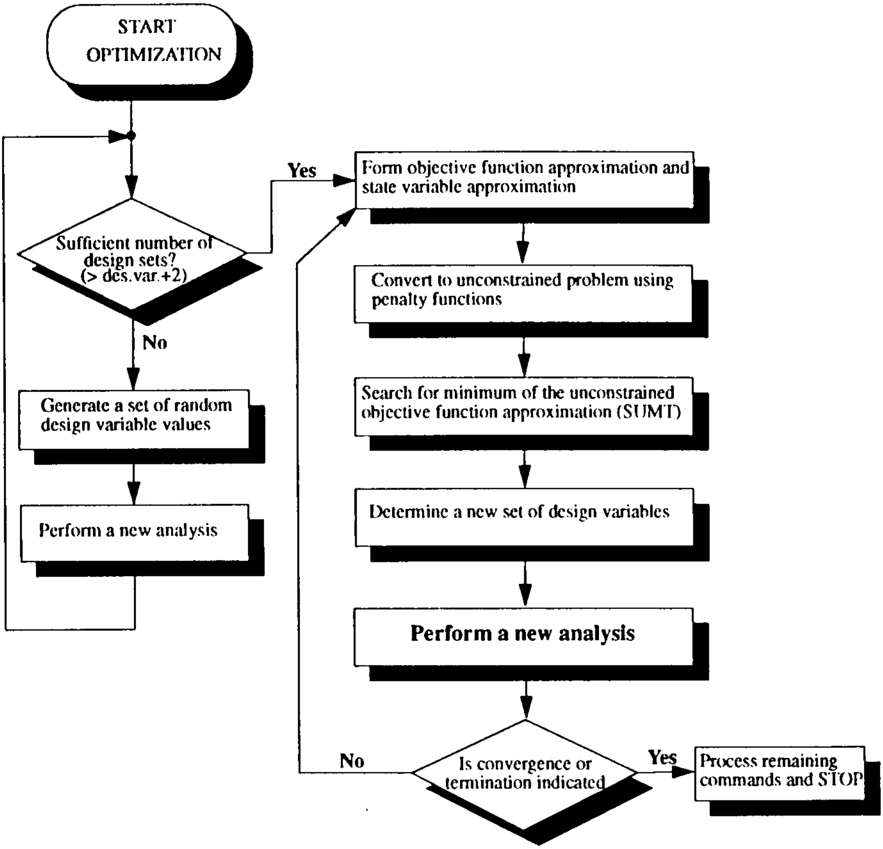
START
OPTIMIZATION
Sufficient number of design sets? (> des.var.+2)
Yes
No
Generate a set of random design variable values
Perform a new analysis
Form objective function approximation and state variable approximation
Convert to unconstrained problem using penalty functions
Search for minimum of the unconstrained objective function approximation (SUMT)
Determine a new set of design variables
Perform a new analysis
Is convergence or termination indicated
No
Yes
Process remaining commands and STOP

5. Results

The final run was executed within a reasonable number of loops, each of them requiring four complete solutions of the FE analysis. Computations were carried out on a MicroVAX II GPX computer and the complete solution of the final batch run required approximately 7 days to be completed.

The plot of the objective function (Figure 3) shows the difficulties encountered by the algorithm to converge even if it is also deeply characterized by the estensive use of the reselection done. In fact a first local convergence occurred after 47 loops (left), then we used the obtained geometrical values as starting point and 18 more loops (right) were performed. The final result is an objective function reduced 80% from about 31 to 6.

The behaviour of individual design variables during the two iterations phases is shown in Figure 4. Design variables never approach feasibility limits, however the analysis of computed maximum equivalent stress, as defined above, shows that the final design is almost at the imposed linearity limit (Table 2). This result is in accordance with the intuitive consideration that less rigid structures should be more sensitive in strain measurement.

Figure 3: Behaviour of the objective functions during the optimization loops. Initial 47 (left) and final 18 (right).

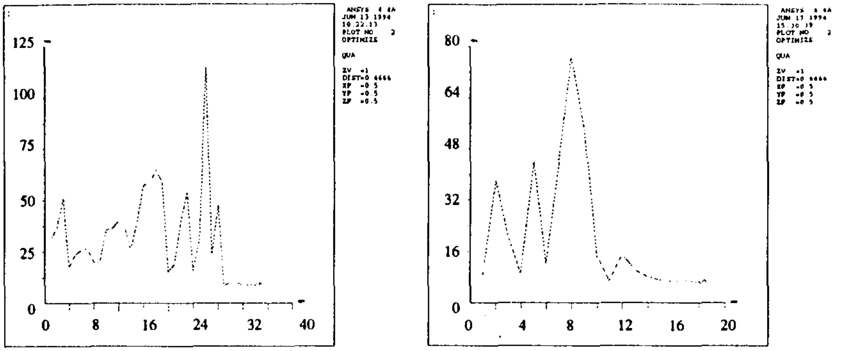

The final shape of the modified octagonal ring transducer is shown in Figure 5. The overall apppearance does not differ considerably from the original one, however the performance does. Figure 5 also shows the deformed shape of the dynamometer as resulting from the application of loads representative of actual operating conditions, which, although amplified by plot magnification, confirm the result of a more flexible structure.

Table 2 compares original and final values of the design variables. The quantitative data show that the dynamometer shape was not affected considerably, however the FE analysis show how its overall accuracy should have been considerably increased. The last row of Table 2 shows the difference in the recorded values of the maximum equivalent stress in the model for the two design options; the imposed limit of feasibility was 180 N/mm^2, and the tendency to the generation of a less rigid structure with reduced transversal sensitivity is confirmed.

The optimized model equivalent stress distribution under combined loads (load step 4 of Table 1) as depicted in Figure 6, shows a much more distorted shape in comparison with the Goldwin one, but, nevertheless, the deformation are, as imposed, in the linear field. This is of course a result of the simplified assumptions necessary in the original traditional design process, and a proof of how FEM analysis tools could be of great aid in the design of better special-purpose transducers.

Apart from the obvious consideration of the reduction in the value of the objective function, other figures of merit can be used to evaluate the solution obtained, namely:

a) the distribution of stress and strain components;

b) the direction of principal stresses;

c) strain gradients at the strain gauges locations.

All of the above evaluations show a better response of the optimized dynamometer with respect to the original one. For instance, Figure 7 shows the stress distribution along the directions of measure of the strain gauges, evidencing the presence of the highest values in the locations of the strain gauges themselves.

Also the comparison between the original and modified dynamometer shows the better performance of the optimized model in terms of direct sensitivity to individual loads, whilst the value of the objective function gives indications on the reduced cross-sensitivity of the transducer.

6. Conclusions

The optimization of a extended octagonal ring transducer has been carried out based on the finite element analysis that showed to be a powerful tool for the geometrical optimization of multi-objective problems provided that they are not ill-conditioned. The ANSYS 4.4A optimization module has been

Figure 4: Individual behaviour of the design variables in the two optimization phases: initial (left) and final (right).

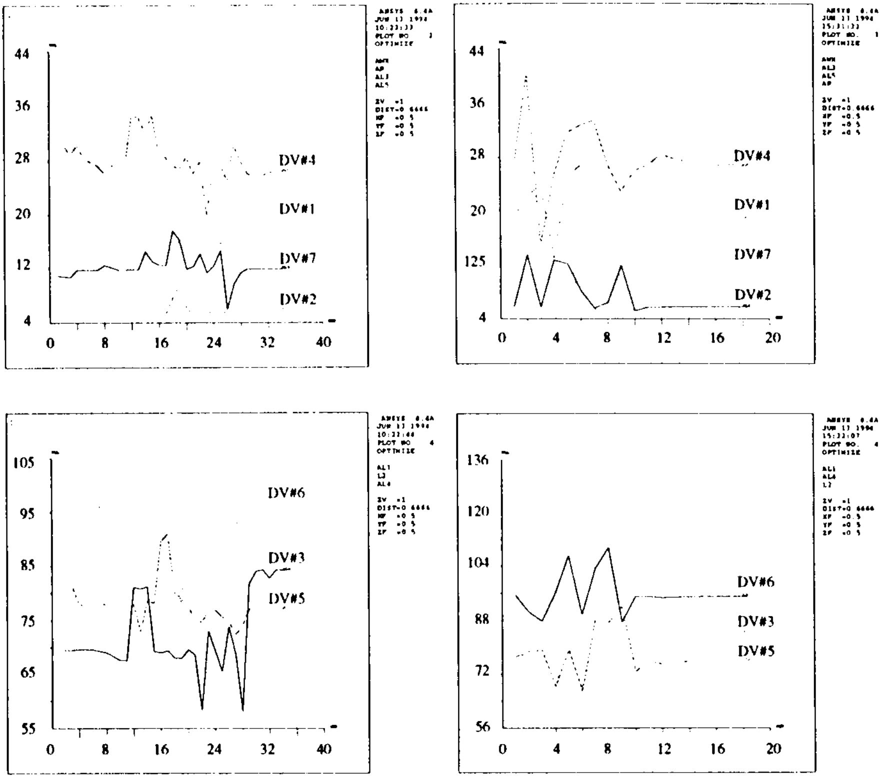

used and constraints were imposed in order to generate a dynamometer shape congruent with the original one. The imposition of multiple load conditions allowed us to evaluate the performance of the dimensionally different dynamometers and in particular the deformations read by each bridge circuit. The global error indicator of the measurement system was chosen as objective function, and final comparison showed a reduction of 80% in the optimized model.

The overall indications coming from the procedure allows a number of considerations:

a) structural optimization techniques can be used, together with FEM analysis, to improve the accuracy of transducers;

b) multi-objective functions can be handled by rather simple algorithms with a certain difficulty, especially when the number of design variables is high;

c) although practical approximations allowed an empirical design of the transducer very close to the optimum, the improvement in terms of accuracy attainable with more refined methods can be considerably high.

Figure 5: Final shape of the optimized dynamometer. The deformed geometry is shown as resulting from the application of a combined load.

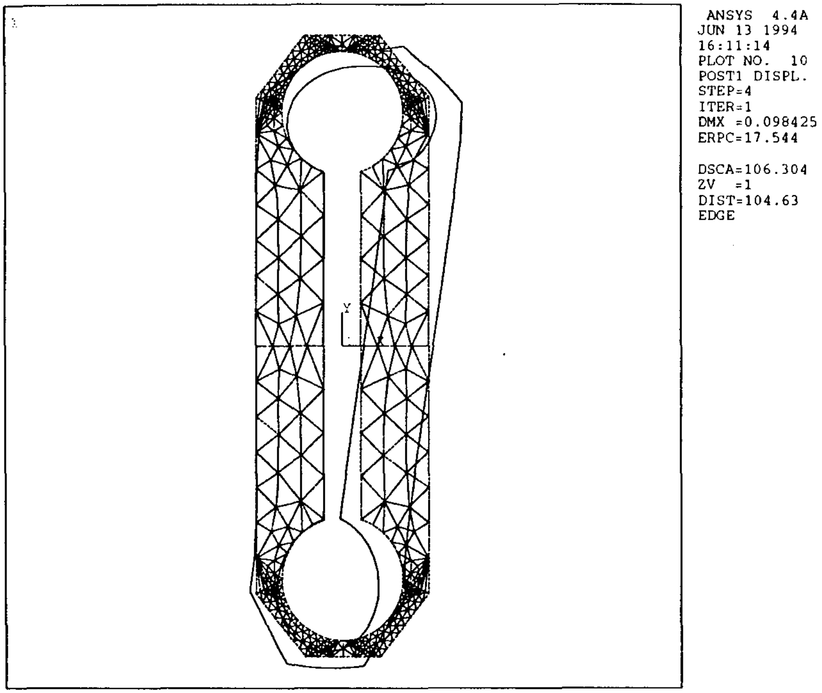
ANSYS 4.4A
JUN 13 1994
16:11:14
PLOT NO. 10
POST1 DISPL.
STEP=4
ITER=1
DMX =0.098425
ERPC=17.544
DSCA=106.304
ZV =1
DIST=104.63
EDGE
Y

Table 2: Design variables comparison

Design Variable	Original Value (mm)	Final Value (mm)	Variation (%)
DV#1	19	18.8	-1.05
DV#2	7	5.75	-17.85
DV#3	69.45	84.18	21.21
DV#4	31.35	26.72	-14.77
DV#5	81.65	75.91	-7.03
DV#6	99.15	95.11	-4.07
DV#7	10.9	11.91	9.26
Max. Equivalent Stress (N/mm^2)	59.743	160.05	167.90

Figure 6: Equivalent Von Mises Stress distribution in the final dynamometer (load step #4)

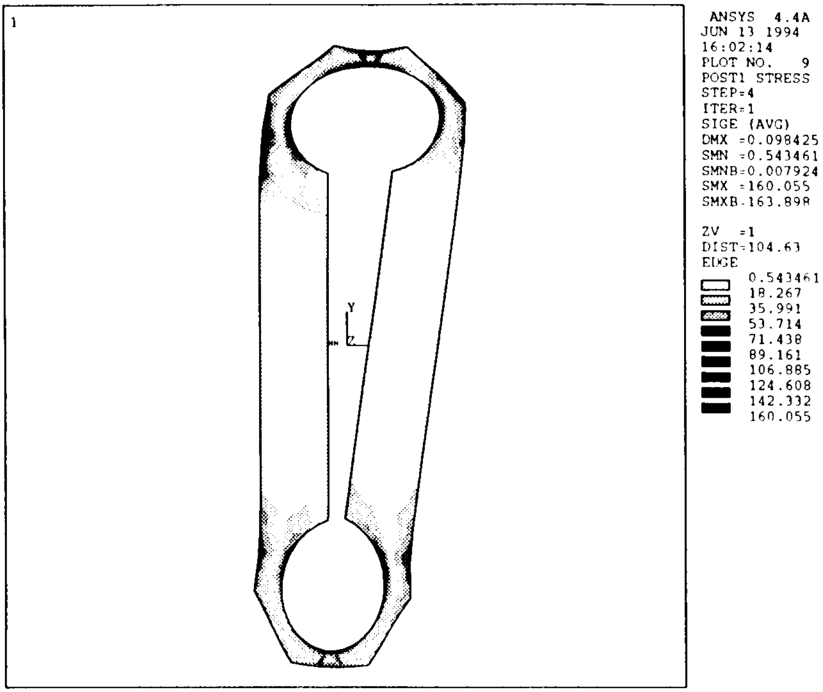
1
ANSYS 4.4A
JUN 13 1994
16:02:14
PLOT NO. 9
POST1 STRESS
STEP=4
ITER=1
SIGE (AVG)
DMX =0.098425
SMN =0.543461
SMNB=0.007924
SMX =160.055
SMXB=163.898
ZV =1
DIST=104.63
EDGE
0.543461
18.267
35.991
53.714
71.438
89.161
106.885
124.608
142.332
160.055
Y
Z
MN

7. References

[1] Goldwin, R.J., 'An Extended Octagonal Ring Transducer for Use in Tillage Studies', J.agric.Engng Res., 20, pp. 347-352, 1975.

[2] Boccafogli, C., Busatti, G., Gherardi, F., Malaguti, F., Paoluzzi, R., 'Experimental Evaluation of Cutting Dynamic Models in Soil Bin Facility', Journal of Terramechanics, Vol. 29, N. 1, 1992, pagg 95-105.

[3] Ansys 4.4 Users Manual, Swanson Analysis System Inc., Houston, PA, 1989.

[4] Ansys 4.4 Users Manual, Swanson Analysis System Inc., Houston, PA, 1989.

[5] Ferretti, G., Paoluzzi, R., 'An Extended Octagonal Ring Transducer Design Optimization', Proc.s of the 6th ANSYS International Conference and Exhibition, Pittsburgh, PA, USA, 1994, vol. 3, pag 14.21.

[6] Carmichael D.G, 'Structural Modelling and Optimization', Ellis Horwood, 1981.

Figure 7: Stress distribution in the direction tangent to the strain gauge for direct loads. F_x (upper), F_y (lower).

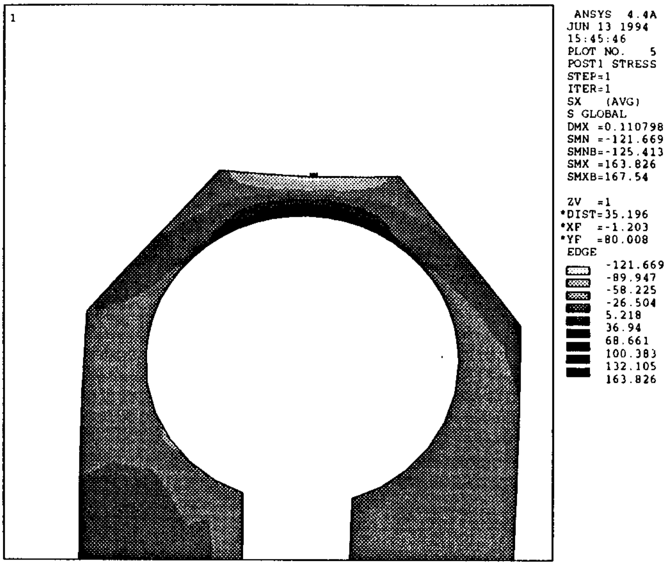

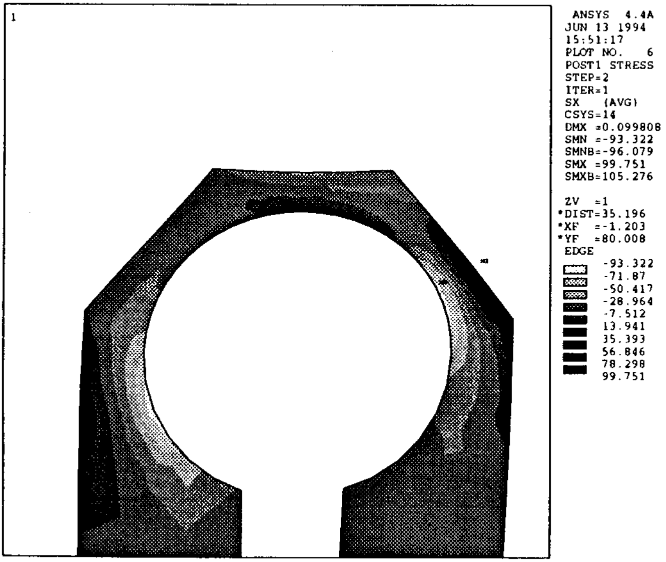

RELIABILITY AND MAINTAINABILITY EVALUATION OF OFF-ROAD VEHICLES

Leon K. Jokubaitis
Director, Reliability Programs
U.S. Army Tank-Automotive Command
Warren, Michigan, U.S.A.

ABSTRACT

This paper presents a new methodology being utilized at the Tank-Automotive Command, United States of America, to determine the reliability and maintainability features of both the tracked and wheeled off-road vehicles. This methodology combines the design evaluations of the vehicles performed by engineers with the shock and vibration results obtained during dynamic tests to arrive at numerical reliability and maintainability predictions. The methodology is cost-effective since it requires only one sample vehicle, very short test time, and a limited amount of funding. The methodology is especially useful to evaluate foreign equipment where only a single sample without sufficient spare parts is available for evaluation. The results of the analysis are useful to design engineers in order to consider improvements to existent hardware, and also wargaming specialists who need foreign equipment reliability and maintainability values to insert in their models.

The paper presents actual examples of two projects performed using this type of methodology. One is for the Russian T-72 Main Battle Tank, and the other is for the Czechoslovakian TATRA 815 8x8 Truck.

INTRODUCTION

Historically, the reliability and maintainability evaluations of the United States materiel have been accomplished by conducting extensive tests with a number of prototypes in order to assess the R&M values, to compare their status against the established requirements, and to identify pattern failures and weak links in design and quality. The methodology and statistics exist to accomplish this evaluation as long as there is an availability of test vehicles, funds, and time.

A different situation exists, however, if it is desired to evaluate a system from an R&M viewpoint with only one prototype, without any spares, and with distinct limitations in funding and available time. A solution to this type of dilemma was developed by the Reliability Office at the U.S. Army Tank-Automotive Command. By this method, a single sample receives extensive design evaluations in consideration with shock and vibration dynamic tests to identify its terrain energy attenuation capabilities. The results of these evaluations are then compared to the known reliability and maintainability values of equivalent vehicles, and the noted percent differences are used to modify the known equipment values to arrive at reliability and maintainability predictions of the vehicle under evaluation with satisfactory confidence in the results.

The body of this paper describes the unique methodologies used for the evaluations with the actual results obtained for the Russian T-72 Main Battle Tank and the Czechoslovakian 815 8x8 (TATRA) Truck.

METHODOLOGY

The basic concept of the developed methodology is the same for both the T-72 and the TATRA, i.e., design evaluation of the systems combined with the shock and vibration results obtained during dynamic tests. However, the T-72 methodology consists of a teardown of the T-72 and detailed engineering comparison with the baseline United States M1A1 MBT components. The TATRA design evaluation was conducted in more general terms. Therefore, the detailed description of the methodology will be separated and discussed in this paper.

T-72 METHODOLOGY

The developed methodology consists of the following steps (See Figure 1).

1. Develop a RAM block diagram of a comparative United States baseline system, and compile R&M values based on previous test data for the major components (or subsystems) of the block diagram. The number of selected components depend on the complexity of the system, but as a general rule, may range from 100 to over 200.

2. Formulate matrix teams of engineering and maintainability experts familiar with the particular components of the baseline systems.

3. Tear down the foreign system and analyze each component in terms of:

a. Its reliability and maintainability strengths and weaknesses. Especially highlight the features for potential reverse engineering activity.

b. Compare the component in terms of its design, use of materiel, manufacturing techniques, etc., with its United States baseline counterpart and subjectively assign a failure rate to the component.

c. Record the times required to remove, diagnose and replace the component (by using the foreign system's maintenance manuals).

d. By the use of the RAM block diagram, sum up the failure rates and compute the total system failure rate and convert it into a mean-mile-between-failure designator. The failure is defined as any unscheduled maintenance action. The components not broken out for specific consideration are treated together under "other" category and are equated to the "other" category established for the baseline system.

e. Record the mean time to remove, diagnose, and replace the T-72 components. Identify it as MTTR. Multiply this value by the previously estimated T-72 failure rate value to arrive at each component's Maintenance Ratio (MR) value.

4. Conduct a short test (less than 100 miles) with the foreign and baseline systems on selected test courses that provide significant shock and vibration environments. With the aid of accelerometers positioned in critical component locations, measure the shock/vibration differential between the two systems. Use the percent differential values to modify failure factors determined in "d" above.

TATRA

The TATRA methodology and the work conducted consisted of the following stages:

1. Identify the design differences between the TATRA 815 and the United States HEMTT system.

2. Conduct a component R&M evaluation to compare the two vehicles from our R&M viewpoint.

3. Conduct an instrumented dynamic evaluation between the two systems to assess the attenuation of terrain energy at the axles, payload area and seat.

4. Identify the systems which offer the greatest potential for R&M technology transfer to the United States.

RESULTS

1. T-72

a. Teardown Analysis - The initial step of the teardown analysis was to prepare a subsystem and major component block diagram.

The second step was to use this block diagram to identify the performance of the baseline M1A1 system. This was done by identifying the particular failure modes causing the nonperformance of the components and the percent of each failure mode contributing to the components' failure rate.

The third step was to investigate the available M1A1 test data bases and to record the failure rates, mean time to repair, and maintenance ratios applicable to each of the block diagram components. Obviously, if a particular component did not exist for the T-72, or if there were differences on design, it was so noted on the record.

These steps constituted the complete M1A1 baseline record to be used by the engineering and maintenance matrix teams in evaluating and predicting the reliability and maintainability of the T-72. This was done by tearing down the T-72 and evaluating each component and its parts in terms of design complexity, manufacturing techniques, use of reliable parts, and particular R&M innovations. This analysis resulted in the prediction of specific reliability and maintainability values for over 200 critical components.

b. Dynamic Test - In November 1993 the Waterways Experiment Station (WES) conducted several field tests with the M1A1 and T-72 battle tanks at Yuma Proving Grounds. These tests were conducted for the Tank-Automotive Command to determine dynamic test shock and vibration differences in the tanks while operating over ride and shock test courses.

Vehicle ride courses were 1,000 ft. long and each course represented a different terrain surface roughness. The surface roughness of each course tested was 1.3, 1.9, and 3.0 root-mean-square (rms) inches. The half-round shock bumps were 8 and 16 inches high. The test courses were used for both two and three dimensional testing. Two dimensional tests were conducted by encountering the same terrain elevation changes simultaneously in both left and right vehicle tracks. This form of testing produces predominately vehicle pitch, front to rear motion, with limited roll, side to side motion. The same test courses were used to create three dimensional testing by only riding one vehicle track on the test course. This allowed one track of the vehicle to encounter terrain elevation changes while the other track rode on a smooth flat surface. This form of testing produced both pitch and roll. Each test sequence was conducted at a different forward velocity, but each forward velocity was held as constant as possible throughout the test sequence. Each test sequence was conducted at an increased forward velocity until energy levels on the driver's seat exceeded safe levels indicated by vertical absorbed power calculations or the maximum forward velocity of the vehicle was achieved. Both tanks were instrumented with 14 vertical accelerometers and one rate transducer at similar stations along each tank. Vertical accelerometers were mounted at the center of the first 6 and the last 4 roadwheels for a total of 10 vertical accelerometers, 5 on each side of the tank. Vertical accelerometers were mounted on each vehicle chassis; 1 on the driver's seat, 1 under the driver's seat, 1 at the vehicle's center, and 1 on the gunners optics. Both tanks were tested at the vehicles' curb weight and exposed to similar test conditions.

Terrain induced vibrational energy was determined by monitoring the instrumentation during each vehicle performance test. The test data were recorded as time histories of each instrumentation device for each test sequence. Typical ride test results of the vehicles' vertical acceleration time history is presented in Figure 2. The root-mean-square data reduction technique was employed for all ride testing to more easily represent a time history test result with a single value quantity. A peak value analysis was used to represent discrete impact loadings from shock tests. Each instrumentation channels' time history data for each ride and shock test sequence was represented using either an rms (for ride tests) or peak value (for shock tests) analysis technique. Between vehicle comparisons were then made using rms and peak values from similar data channels and test sequences. The resulting values are in the form of rms vertical accelerations (g_{rms}), peak vertical accelerations (g_{peak}), rms rotational velocities (0_{rms}), and peak rotational velocities (0_{peak}).

The ride and shock time histories were also transformed into the frequency domain using a Fast Fourier Transformation (FFT). The FFT results of the vertical accelerations in Figure 2 are presented in Figure 3. The data in Figure 3 represents the average vertical acceleration and the corresponding frequency at which it occurred. As shown, the largest average acceleration occurs at approximately 1 hertz which is the dominate frequency from 0 to 10 hertz. This corresponds to the natural frequency of the vehicle's chassis. The area under each test sequence's time history FFT transformation curve was calculated for ranges from 0 to 10 to 100 hertz. This was done to better represent each data channel and test sequence with a single value quantity between these ranges. The frequency ranges were selected based on the natural frequency of the vehicle's chassis, suspension, and track noise. The dominate terrain induced frequencies (those frequencies where the largest average amplitudes occur) in the vehicles' chassis occur between 0 and 10 hertz with engine noise occurring above 10 hertz. The dominate terrain induced frequencies in the vehicles' suspensions occur from 10 to 20 hertz. The dominate frequencies caused by the vehicles' tracks are dependent on the vehicle's speed and range from 20 and 60 hertz. Comparisons of the average acceleration were then made using the FFT values of vertical accelerations (g_{FFT}) and rotational velocities (0_{FFT}) for the 0-10 hertz and 10-100 hertz ranges for both ride and shock test results.

In order to compare the single value representations of the original time histories in reference to the different tests terrains, both the time and frequency results were transformed into a single dimension by dividing the single value representations of the measured accelerations and velocities by the vehicle's average forward test velocity. This produced quantities of (g_{rms})/mph, (g_{peak})/mph, (0_{rms})/mph, (0_{peak})/mph, (g_{FFT})/mph, and (0_{FFT})/mph, which will be called energy, for each ride and shock test sequence. These results were then averaged for all tests on a given terrain surface roughness and obstacle height. Figure 4 presents the time domain results of the two dimensional testing over the ride courses. As shown, the energy levels remain fairly constant as the terrain roughness increases. This indicates that the vehicles' were operated from their minimum to their maximum operational envelope on each terrain roughness. The resulting plots show how the relative energy levels in each tank remains fairly constant for each surface roughness and obstacle height for both the time and frequency domains.

A ratio between the T-72 and M1A1 tanks' energy levels for a given surface roughness and obstacle height were calculated producing a performance index. The performance index shown in Figure 5 indicates which vehicle realized higher energy levels after testing over similar conditions. If the performance index value is larger than 1, the T-72 experienced higher energy levels. It should be noted that a suspension system which measures higher energy levels while operating within its design range is the better performing suspension for this study. Therefore, in the performance index plots, if the values are less than 1, the T-72 experienced lower energy levels. The performance index results were then averaged to produce energy levels representative of all terrains and obstacle heights. The resulting quantities represent the average vibrational and shock energy each tank experienced in its chassis and suspension during all ride and shock testing. The results presented in Figure 6 show the performance index of all ride tests. The plot in Figure 6 shows the T-72 experiencing higher terrain induced energy levels in the chassis for both the time and frequency domain data. The plot also shows the M1A1 experiencing higher energy levels in the suspension except in the 0-10 hertz frequency range. This means the T-72 experiences higher energy levels in this range. But by comparing the two quantities, chassis and suspension, it is evident that the M1A1's suspension absorbs more terrain induced energy than the T-72s resulting in lower energy levels in the vehicle's chassis. The results of all shock tests are presented in Figure 7 showing the T-72 experiencing higher energy levels in most categories. The suspension results indicate that the shock tests were conducted to a level beyond the T-72's suspension design capabilities. This is evident in the performance index for the vehicle's suspension and chassis. The suspension results indicate the T-72 experienced higher shock induced energy levels than the M1A1. This should result in lower chassis energy levels, but the opposite occurs. Therefore, the energy levels in the suspension exceeded the vehicles design capabilities causing the shock induced energy to be passed to the vehicle's chassis.

The above analysis reveals that the M1A1 is 1.8 times better than the T-72 at dissipating continuously induced terrain vibrations, and 3.1 times better at dissipating discrete impact loadings (Figure 8). It should also be noted that this form of analysis is not limited to just these two vehicles. This type of analysis can be made between any group of vehicles. This analysis also offers a realistic method for measuring terrain induced shock and vibration levels, which when done in parallel with reliability and maintainability testing, would result in the capability to monitor energy levels in a vehicle and determine more accurate maintenance schedules based on the amount of energy the vehicle has been exposed to instead of the hours of operation or milage. This analysis technique is also very applicable to current mobility models for predicting component failures caused by terrains.

c. Numerical Analysis - as Modified by the Dynamic Test - Based on the above, the subjective R and M analysis obtained during the teardown portion was modified to compensate for the shock and vibration differential. By analyzing the failure modes of the M1A1 components, it was determined that approximately 13% of the failure modes are affected by the vibration phenomenon. Since the T-72 experiences 80% more continuous terrain induced vibration than the M1A1, it was estimated that the total impact on the T-72 system would be a 10% increase in the failure rate or a 10% decrease in the Mean Miles Between Unscheduled Maintenance Actions. It was decided at this time not to compensate for the instantaneous shock impact differential. However, Waterways Experiment Station and TACOM are investigating this phenomenon and will consider it during future evaluations.

The final reliability and maintainability component analysis between the Russian T-72 and the United States M1A1 MBT is as shown in Figure 9. Here all the factors of the methodology, i.e., teardown and dynamic test results are combined to arrive at the shown values. A benefit of the evaluation was the identification of certain R&M features which could be used for technology transfer.

2. TATRA

a. Design Evaluation - The design evaluation and the dynamic test of the TATRA were performed by Nevada Automotive Test Center (NATC), a Division of Hodges Transportation, under contract to the Tank-Automotive Command.

The evaluation of the TATRA concentrated on the following components:

(1) Backbone tube (TATRA frame)

(2) Independent, swing arm suspension

(3) Powertrain (from transfer case to wheel-end)

Other TATRA components were considered for the evaluation, but were not included because their RAM was either less or equal to their U.S. counterparts.

The general design evaluation of the TATRA indicated that the chassis is simple, robust, and is designed for limited maintenance over the life of the vehicle. Compared to a typical U.S. tactical truck, the TATRA chassis does not utilize:

(1) Walking beams, torque rods or track bars and the associated cross member mounts and rubber bushings that can crack or deteriorate over the life of the vehicle.

(2) Traditional frame rails, cross-members or body pillars.

(3) U-joints, slip yokes and ball joints at each differential.

(4) Spring hangers, hanger bolts/bushings, spring shackles, spring clips.

(5) Complex seals (o-rings are used for the majority of the seals in the chassis). There are a limited number of grease fittings, primarily restricted to steering components.

The only rubber mounts in the TATRA 815 are the engine mounts. The transmission is mounted directly to the transfer case which is mounted to the backbone tube. This reduces the number of rubber mounts that can fail while starting out with heavy load/high torque applications, or deteriorate over time due to vibration and environmental effects. There is no cross member required to support the transmission. Because of the stiff chassis design, the air lines and fuel lines are hard mounted to the chassis.

The TATRA has an intricate arrangement of seven differentials (planetaries) which allows a wide range of driver-selectable axle drive configurations (intra- and inter-axle locks). This system of differentials allows the operator to better match the performance of the vehicle to the adverse terrain conditions, provide a smooth application of power to the ground, and reduce tractive hop.

The powertrain has torque multiplication at the transmission, differential and wheel-end gear reduction with an equal split of each in low range. This reduces the requirement for large driveline components and the extreme interaction between driveline torque and mobility under high loads. When the TATRA chassis is under load, due to the axle off-sets left-to-right, there is no frame twist, axle windup and rotation or torsional pickup on the chassis. The TATRA chassis will not traction hop under high drawbar loads or on grades and will not develop washboard in roads. In U.S. vehicles, traction hop and washboard results in detrimental powertrain and structural loadings.

All driveline components are encased in the backbone tube and are directly in the center of vehicle. Driveline angles and driveline vibrations are not design or maintenance concerns. The enclosed driveline components have less chance of damage and environmental contamination.

Shocks and bump stops are not required. On the TATRA 8x8, shocks may be installed on front to improve ride quality to cab, if necessary. Similarly, bump stops may be installed to limit the 23.5 inches of wheel travel, when necessary.

Finally, when one of the chassis components fail, the TATRA chassis has expanded self-recovery capability and can continue the mission with combinations of failed tire/wheel/hub/axle/spring at more than one location (but not two on same side of the tandem).

b. Dynamic Test - Nevada Automotive Test Center performed a full ride quality analysis between TATRA and a number of United States tactical vehicles. Figure 10 shows speed versus RMS roughness for a constant 6 watt input at the base of the driver's station. Figure 11 shows speed versus half round height for a constant 2.5 g's at the driver's station.

In order to arrive at reliability comparison, the following equation based on speed and road roughness was utilized:

$$L_t = L_e \frac{V_t}{V_e} \left[\frac{V_t \, G_{ee} \, (n_{1e})}{V_e \, G_{tt} \, (n_{1t})} \right]^{b/2}$$

where:

L_t = Length of travel on the test course (miles)
L_c = Length of travel in service (miles)
$G_{tt}(n_{1t})$ = wave number spectral density of test course at $n_{1t} = f_1/V_t$;(ft^2/cycles/ft)
$G_{cc}(n_{1c})$ = wave number spectral density of service road at $n_{1c} = f_1/V_c$;(ft^2/cycles/ft)
V_t = vehicle speed over the test course (ft/sec)
V_c = vehicle speed over the service road (ft/sec)
b = fatigue parameter from S-N curve
n = wave number (cycle/ft)
f_1 = the vehicle's critical frequency

For the instrumented RAM analysis between the TATRA and the Heavy Expanded Mobility Tactical Truck (HEMTT), the "test" subscripts were replaced with "TATRA" and the "service" subscripts were replaced with "HEMTT," as follows:

$$L_{TATRA} = L_{HEMTT} \frac{V_{TATRA}}{V_{HEMTT}} \left[\frac{V_{TATRA}\ G_{HEMTT}\ (n_1)}{V_{HEMTT}\ G_{TATRA}\ (n_1)} \right]^{b/2}$$

The following values show an example of the speed and road roughness inputs to the above equation for the TATRA and HEMTT negotiating a hilly cross-country course:

Parameter	HEMTT	TATRA
Hilly Cross-Country (Butte)		
Speed (MPH)	9.6	16.8
Roughness (FT^2/CYCLE/FT for 1 Hz)	0.02	0.03

$$10{,}719 = 3{,}500 \ x\ \frac{16.8}{9.6} \ x \left[\frac{16.8 \ x\ 0.02}{9.6 \ x\ 0.03} \right]^4$$

Given that the TATRA 815 negotiated the hilly cross-country course at a speed 1.8 times faster than the HEMTT for approximately the same amount of energy input indicates that the TATRA would travel 3.1 times further for the same level of structural fatigue miles. Further assume that the Mean Mile Between Mission Failure (MMBMF) for "fatigue related" items was 3,500 miles for HEMTT. Based on that, the TATRA would have a 10,719 MMBMF rate for proportional fatigue related items.

In instrumented testing of the U.S. Marine Corps Advanced Technology Transition Demonstrator (MCATTD) with the TATRA suspension versus the standard U.S. 5 Ton M939A1 Truck, a similar result was calculated. Results show that the MCATTD would go twice as fast as the M939A1 over the same severity of road roughness with approximately equal dynamic response, ride quality and control. When run at equal speeds, the MCATTD RMS acceleration levels at the sprung mass are approximately 40 percent less than the M939A1.

The equation allows the calculation of the reduction in life due to varying the parameters critical to vehicle fatigue, namely road roughness and vehicle speed.

In the previous example with the MCATTD, if an independently sprung vehicle is able to travel twice as fast as a solid axle vehicle over the same level of road roughness, this strain difference can be equated to a life difference. This assumes that the response on the sprung mass is equal between the two vehicles (i.e., the stresses at the frame are the same and the independently sprung vehicle is traveling twice as fast to achieve the same levels of stress as the solid axle vehicle). Given these assumptions, the life reductions for varying wave-number spectra slopes are as follows:

W	Life Reduction
1.8	5:1
2.0	8:1
2.2	14:1

A large percentage of natural road roughness on gravel roads and off-highway terrain has a wave-number spectrum slope of approximately two. This would indicate a difference in fatigue related RAM of 8:1. The final results of the TATRA analysis are shown on Chart 12.

c. Conclusions - The conclusions drawn from this study and the two specific projects are as follows:

(1) It is feasible to conduct a cost-effective, quick reliability and maintainability evaluation of combat and tactical vehicles with a single sample by using comparative techniques with similar equipment.

(2) The methodology requires an integration of static design evaluations and dynamic shock and vibration attenuation measurements over various off-road terrain.

(3) The methodology provides information for technology transfer considerations and also data (for foreign materiel) for inclusion in wargaming models.

(4) The Tank- Automotive Command in Warren, MI, U.S.A., will continue to use this unique methodology to evaluate other foreign materiel and certain United States equipment in order to conserve funding and personnel resources.

REFERENCES

1. Jokubaitis, Leon K. and Capouellez, Jim, "Reliability and Maintainability Evaluation of the Russian T-72 MBT," December 1993, RAM/Assessment and Data Division (AMSTA-QR), Product Assurance Directorate, Warren, MI 48316, U.S.A.

2. Ashmore, Colin and Hodges Jr., Henry C., "Phase II Reliability and Maintainability (RAM) Evaluation of the TATRA 815," 1993-1994, Nevada Automotive Test Center, P.O. Box 234, Carson City, NV 89702, U.S.A., TACOM Contract No: DAAE07-92-C-R096

3. Jones, Randolph A., "A Limited Study of Terrain Induced Vibration in the M1A1 and T72 Battle Tanks," 1994, U.S. Army Engineer Waterways Experiment Station, Geotechnical Laboratory Mobility Systems Division (CEWES-GM), Vicksburg, MS 39180-6199

4. Ashmore, S.C. and H.C. Hodges, Jr., "Dynamic Force Measurement Vehicle (DFMV) and its Application to Measuring and Monitoring Road Roughness," Vehicle, Tire, Pavement Interface, ASTM STP 1164, J.J. Henry and J.C. Wambold, Eds., American Society for Testing and Materials, Philadelphia, 1992, pp. 69-96

Methodology

STEP 1

M1A1 baseline

STEP 2

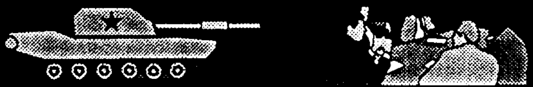

Teardown &
comparison with
M1A1

STEP 3

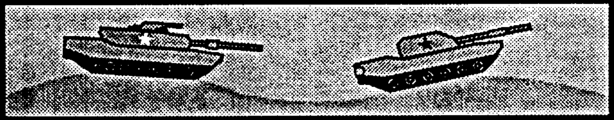

Dynamic short test
for shock/vibration
Δ determination

STEP 4

Adjustment of Step 2 by Step 3

TAC-1433-94

Chart 1

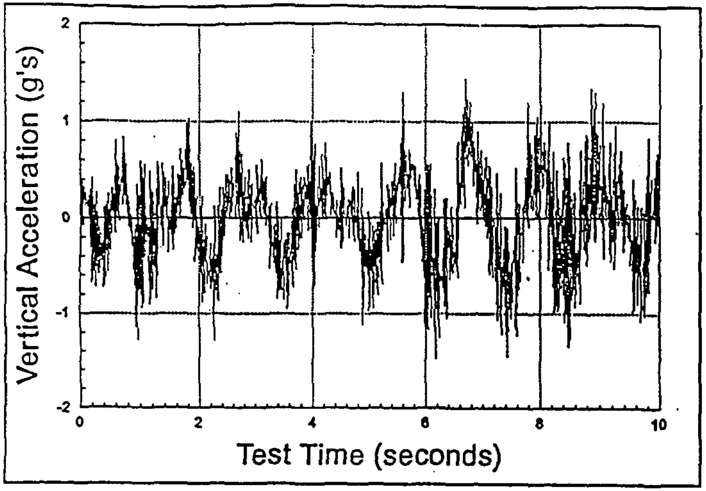

Figure 2. Typical vertical acceleration time history.

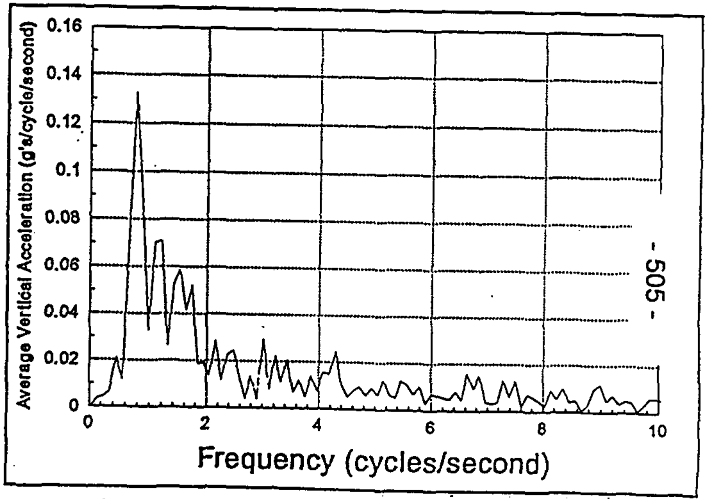

Figure 3. FFT of typical vertical acceleration time history.

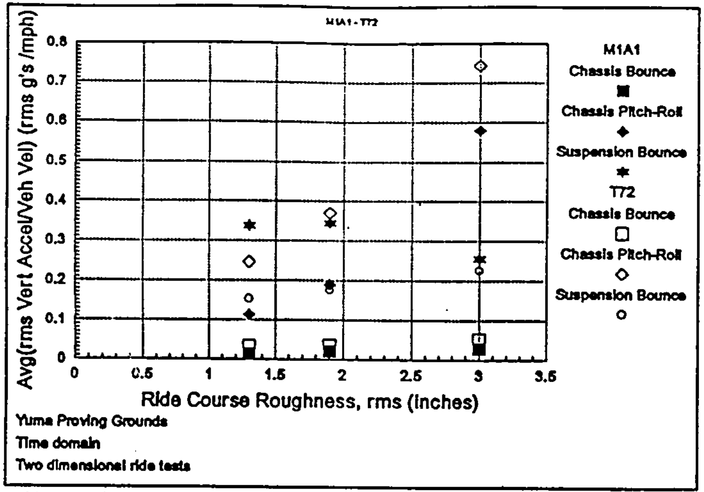

Figure 4. Average of two dimensional testing over different ride courses.

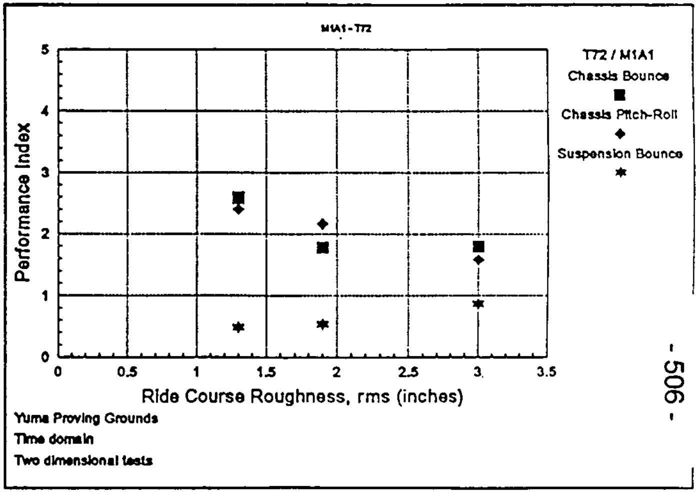

Figure 5. Vehicle performance index for two dimensional ride courses.

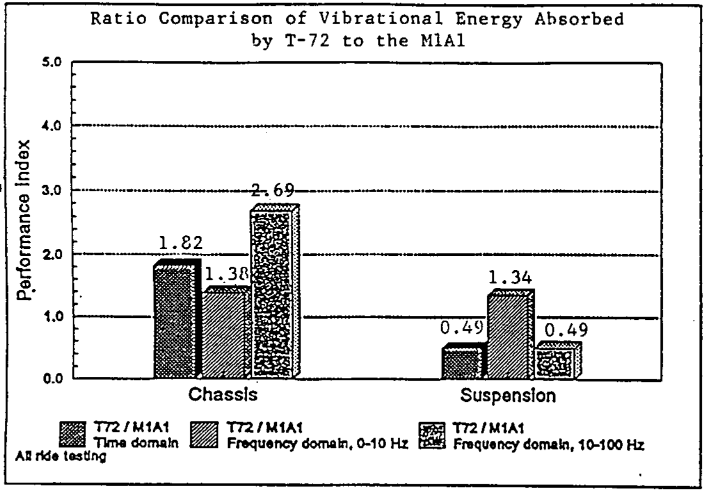

Figure 6. Performance index of the chassis and suspension for all ride tests.

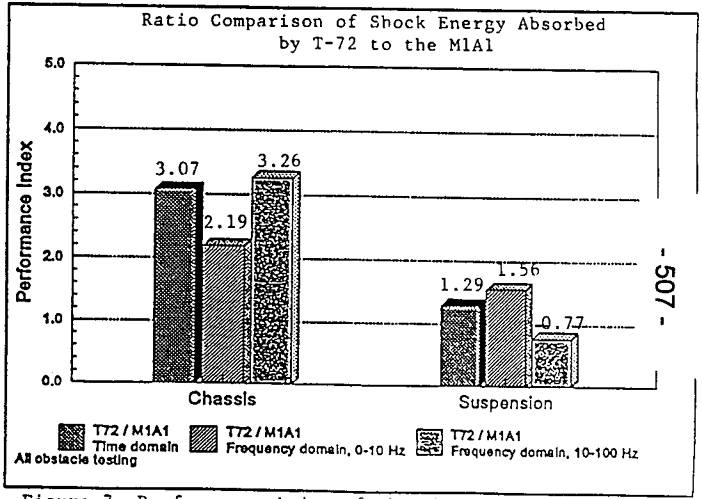

Figure 7. Performance index of the chassis and suspension for all shock tests.

Dynamic Test Results

		M1A1 Chassis
Continuous vibration absorption	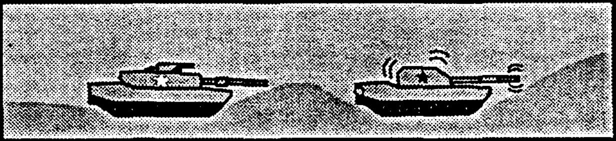	80% Better
Instantaneous shock energy absorption	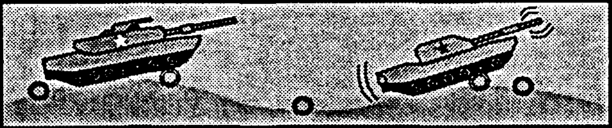	200% Better

TAC-1433-94

Chart 8

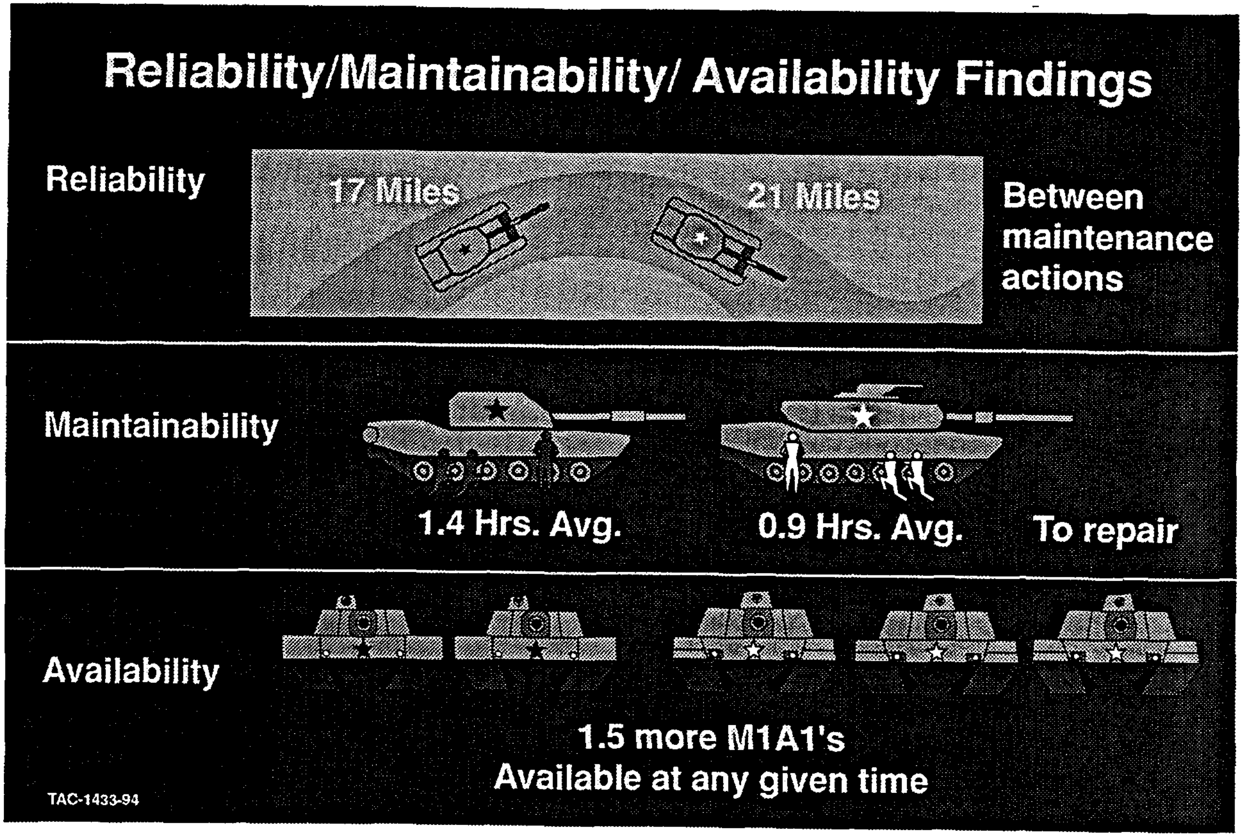

Reliability/Maintainability/ Availability Findings

Reliability

17 Miles

21 Miles

Between maintenance actions

Maintainability

1.4 Hrs. Avg.

0.9 Hrs. Avg.

To repair

Availability

1.5 more M1A1's
Available at any given time

TAC-1433-94

Chart 9

RIDE QUALITY
SPEED VS. RMS FOR CONSTANT 6 WATTS AT DRIVER STATION

TATRA VERSUS U.S.A. VEHICLES

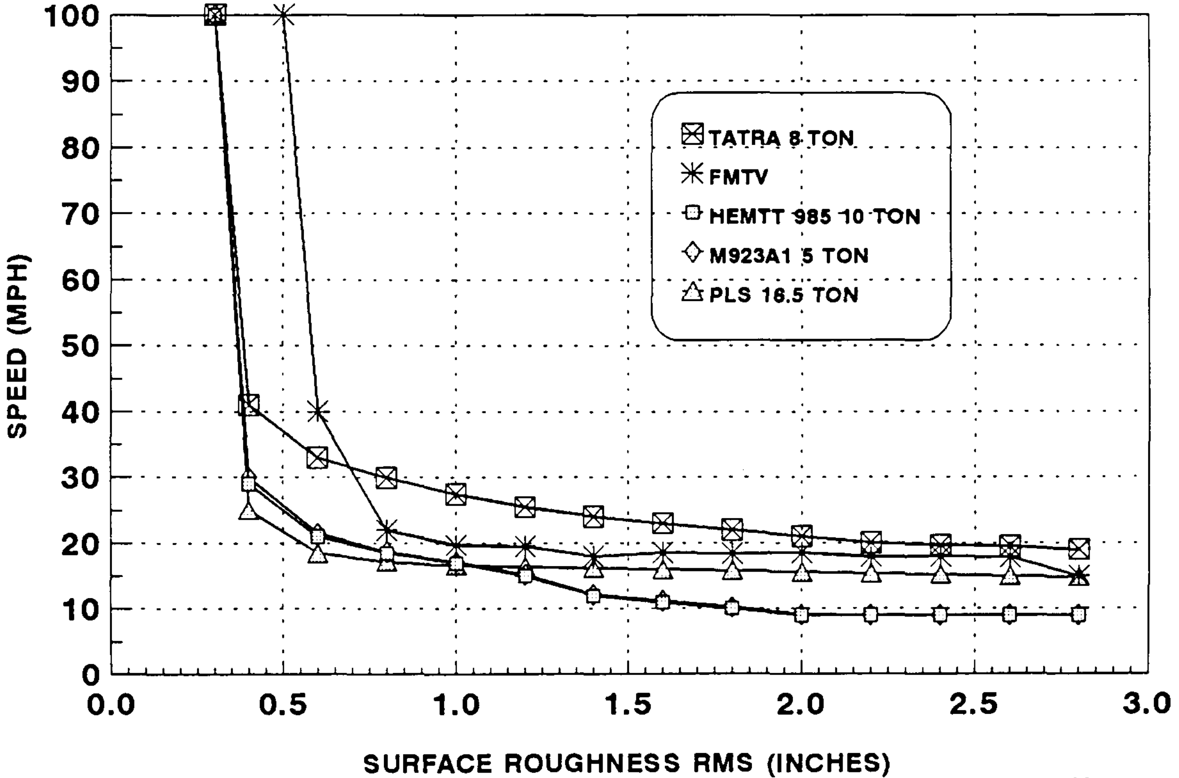

Chart 10

RIDE QUALITY

SPEED VS. OBSTACLE HEIGHT FOR 2.5 G's AT DRIVER STATION

TATRA VERSUS U.S.A. VEHICLES

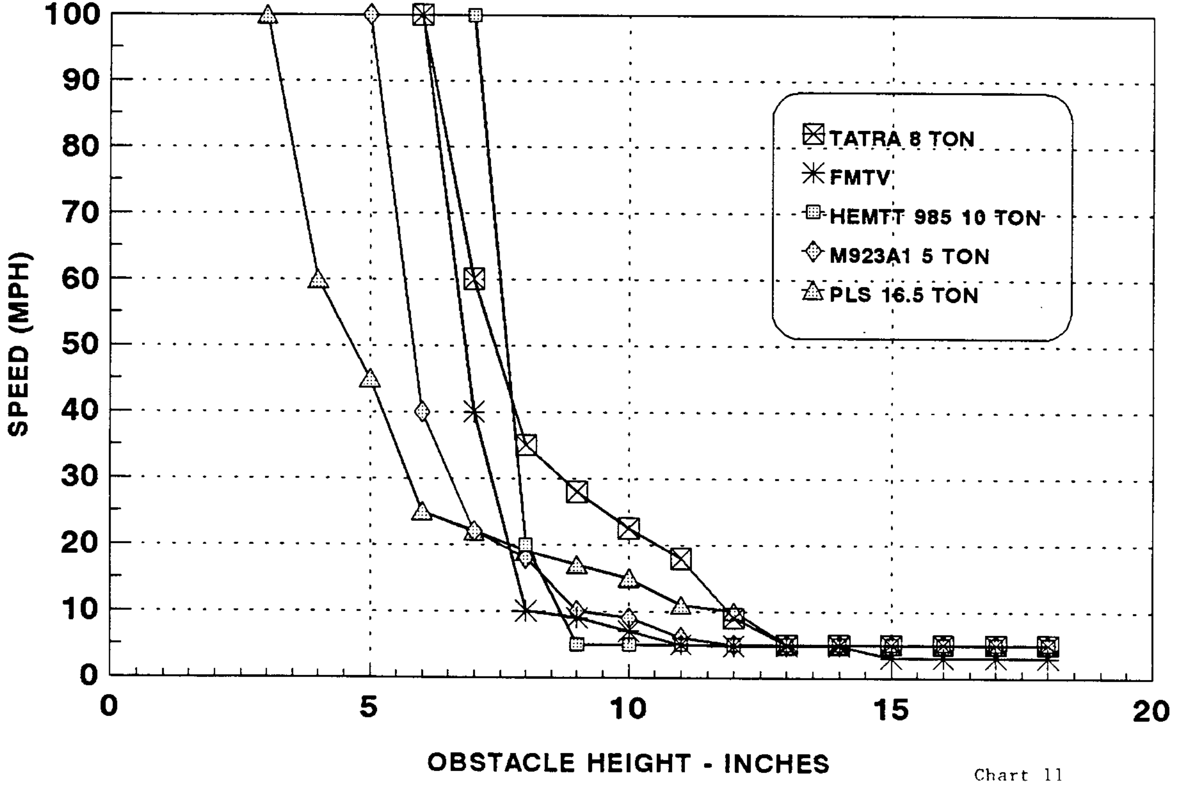

Chart 11

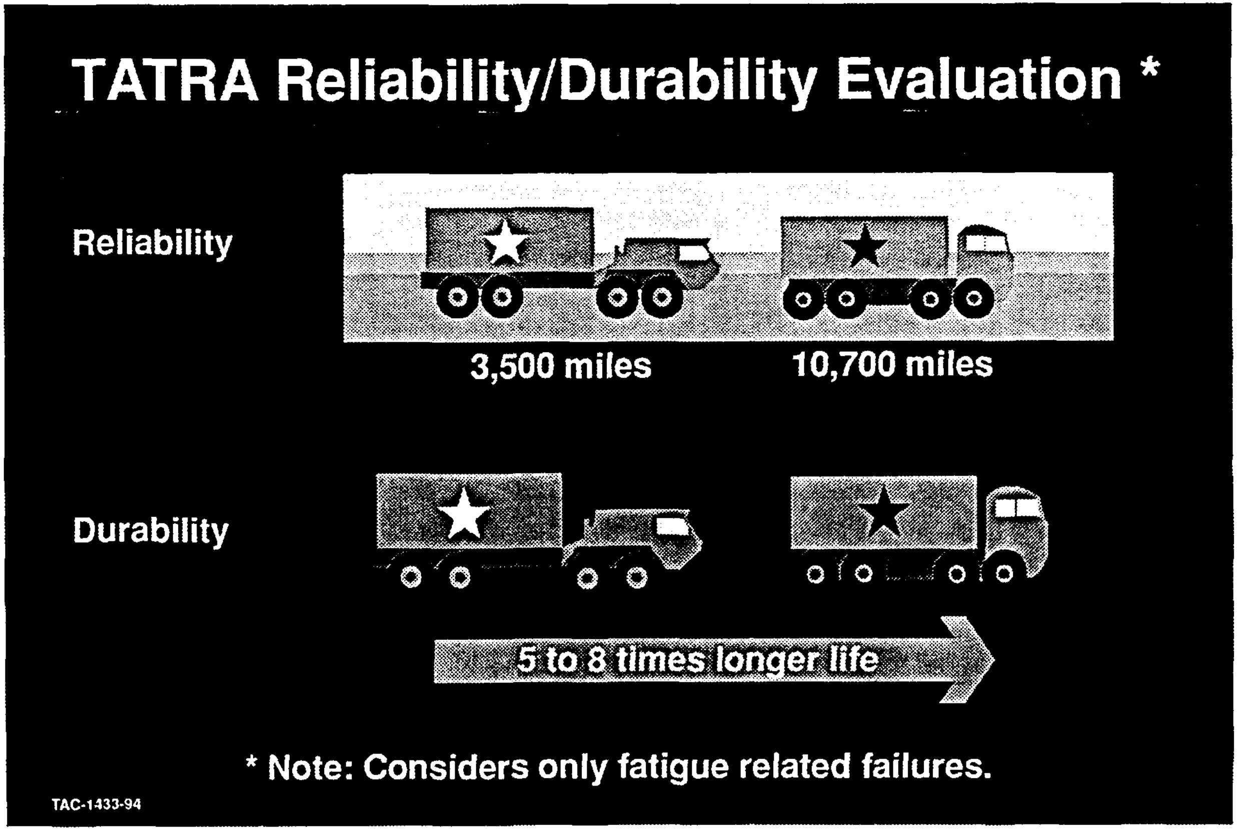

TATRA Reliability/Durability Evaluation *

Reliability

3,500 miles

10,700 miles

Durability

5 to 8 times longer life

* Note: Considers only fatigue related failures.

TAC-1433-94

Chart 12

Off Road Vehicles Marketing

Helmut Moser
4WD-Magazin, Wels, Austria

In order to discuss all-terrain vehicle marketing, we must first look briefly at the past. And here we notice that the popularity and the marketing of various four-wheel and all-terrain vehicles was made easier by the fact that the army made these vehicles acceptable in the civilian sector at an early stage. Many former US, Allied and German army vehicles were converted after the Second World War into municipal and emergency vehicles and served for many years with local district authorities, fire brigades and other users.

And it was again Jeep who, in the years after the war, made the first attempts at advertising all-terrain vehicles to a wider public in the civilian sector by canvassing a civilian version of their own original all-terrain vehicle to farmers, doctors and the users of poor-surface roads. Shortly afterwards, in the late 1940s, Landrover, too, entered this sector of the market, with their very rustic-look adverts for the civilian-purpose Landrover.

At the time, Landrover was the first company that attempted to set up a dense network of dealers across the world in the various Commonwealth countries as well as in Austria. Even then, Landrover applied the recipe for success that should be a feature of modern all-terrain vehicle marketing.

This recipe means a separate section in the company, the section known as applications technology, in which experienced test drivers and all-terrain vehicle specialists demonstrate all the advantages of four-wheel drive on an appropriate terrain, mastering conditions that would be utterly impossible for the average driver.

Since the early 1950s, Mercedes has also been represented in this sector with the Unimog. Excellent test drivers and experienced specialists at the wheel (and at the levers of the differential lock) demonstrated, things on the original Unimogs 401 and 411 that had previously been impossible with ordinary tractors. When the Austrian all-terrain vehicle, the Puch Haflinger AP 700, was developed and appeared on the market at the end of the 1950s and in the early 608, the then Steyr Daimler Puch AG also applied the same marketing and presentation strategy. They displayed the Haflinger in practical use for the civilian purchaser, primarily in the agricultural and forestry sector, at weekend events, or at trade fairs by demonstrating over logs and other obstacles the all-terrain capabilities of this wheeled vehicle, capabilities that in many ways have never been equalled to today. Leaving aside the fact that all manufacturers of all-terrain vehicles and multi-axle-driven lorries presented their vehicles to very critical eyes in the military sector, the wider public was excluded from such four-wheel drive displays until the 1970s. Only genuine insiders know what an all-terrain vehicle was capable of achieving. Information was available on film, in books and brochures, but the civilian user was generally excluded from genuine demonstrations of their all-terrain capabilities. When the off-road boom broke out in the late 1970S (I refer here to the Austrian situation), it was thanks to a company that had recourse to the tried and tested marketing methods in the form of demonstrations in the terrain.

The Wolfgang Denzel KFZ AG, the importer of Mitsubishi vehicles, employed for instance the then off-road national champion and four-wheel trials expert Christian Karlberger, putting a number of demonstration cars at his disposal and arranging a date with every authorized Mitsubishi dealer at which this four-wheel drive professional demonstrated the benefits and advantages of the Pajero.

The competitors on the Austrian market unfortunately missed their opportunity and lost valuable market shares that they have still to make up. It is no accident that Denzel achieves roughly 50 % of new registrations in the heavy off-road segment, roughly 1,800 to 2,100 vehicles per year. If we remember that the second in this sector sells around 700 vehicles, it is clear that this is due not only to the superiority and the excellent price of the Pajero, but also to the company's correct marketing strategy.

I myself have been present at these events and witnessed how the demonstration driver, with the assistance of a good salesman, was able to sell at least one or two vehicles directly at these. demonstrations and presentations.

Thankfully, the Austrian manufacturer, Steyr Fahrzeugtechnik GesmbH and its subsidiary, Steyr AutomobilvertriebsgmbH, has also realized the advantages of this modern marketing method, and is now increasingly using four-wheel drive professionals from its testing department for customer demonstrations of the Puch G range. A regional Mercedes Puch G dealer from Upper Austria informed -us that, thanks to an excellently organized four-wheel drive event and demonstration, he was able to sell 5 Puch Gs in one weekend,

If we now move up two storeys into the heavy lorry sector, the Austrian lorry manufacturer, Steyr Nutzfahrzeuge AG, is a perfect example for excellent marketing in the four-wheel drive sector. For instance, the application technology department presents its four-wheel drive know-how not only to the military sector, but also to fire brigades, building contractors and other users of four-wheel drive lorries, thereby demonstrating the all-terrain capabilities of these Austrian products. It is no accident that almost 35 % of Steyr Nutzfahrzeuge AG sales are accounted for by four-wheel drive vehicles. Unfortunately many other companies have still not decided to present their all-terrain vehicles in practical demonstrations.

The off-road boom of the 1970s and 1980a made the selling of all-terrain vehicles easy. Unfortunately, 80 % of all-terrain vehicle owners do not even know what their vehicles are capable of achieving. And 90 % of the users c)f standard-drive cars are ignorant of the driving characteristics and capabilities of all-terrain vehicles. This failure to demonstrate the vehicles is in practice currently being paid for by those importers of four-wheel drive vehicles who as yet do not employ an applications technology department or a demonstration team.

The time when an all-terrain vehicle could be sold from the shop window for its visual effect is past. The exception is the Jeep Grand Cherokee, a vehicle with a very car-like exterior and excellent driving characteristics on the road. However, many users of this vehicle do not know what the lever marked 4 L means (reducing gear).

What strategies can Austrian industry and importers apply in order to place new accents in the all-terrain vehicle market:

1. If you are an importer or dealer with an all-terrain vehicle in your programme, organize a test terrain (gravel or clay pit) or a hilly site near your premises, preferably free of rocks to avoid damage to the vehicles.
2. Select the target group of users of all-terrain vehicles, and also self-employed professionals who as yet do not own an all-terrain vehicle, and invite them to a presentation of your product. Send invitation cards and start an advertising and PR campaign in your local newspaper.

3. Make a special effort to ensure that the whole family takes part at this demonstration. Women and children are major factors for a sale.
4. In your invitation underline the safety of four-wheel drive vehicles (protection for the family) and the passive and active safety features of the all-terrain vehicle.
5. Try to train a salesman as all-terrain specialist in your company, who should not only be able to handle perfectly the car to be sold, but also know every detail about rival products.
6. Let your customer or casual caller steer the vehicle himself through an easy chicane under the supervision of the salesman or the test driver. Get-his wife to do it as well! Women are much more sensitive in a first test of an all-terrain vehicle, and much the better drivers as compared with men. This is confirmed by the Miss Off Road elimination competitions that Nissan used to hold. In easy trial contests, women who have never driven an all-terrain vehicle are always superior to men who likewise have never driven these vehicles. Woman are also an important factor in making purchasing decisions.
7. Hold a small dexterity test for your customers and anyone interested, with the day's victor winning a small cup. These tests do not depend on speed but on skill. This can work wonders on your sales efforts.
8. Put an all-terrain vehicle user instructions booklet in your customer's glove compartment, preferably a 4-wheel drive guide Such as "Driving correctly off-road", containing illustrated practical tips.

These are just a few ideas and suggestions that are important and vital when selling all-terrain vehicles. I hope that this short talk on all-terrain vehicle Marketing and sales has contained tips that you can use to improve your sales figures.

Session X
Sektion X

Tracked Vehicles

Kettenfahrzeuge

STABILITY OF TRACKED VEHICLES ON INCLINED GROUND

M. KITANO, K. WATANABE and T. KAKINO
Department of Mechanical Engineering
The National Defense Academy
Hashirimizu Yokosuka, Japan

ABSTRACT

Handling and stability of tracked vehicles on inclined ground are strongly affected by the lateral component of gravitational force and terrain conditions. The objectives of this paper are to develop a numerical model for the sliding behavior of tracked vehicles in cross motions along the ground contour line and to improved the handling of the vehicles on a slope. An analytical model that involves soil-track interaction, running conditions and vehicle parameters such as the position of the center of gravity, aspect ration and suspension parameters, is proposed and verified experimentally by using scale model tests. Using the dynamic analysis model, sliding and handling behaviors of the vehicle on a slope are analyzed for an example tracked vehicle, and the optimum steering inputs to maintain the vehicle on a contour line are disclosed.

1. INTRODUCTION

Many studies on the mobility of tracked vehicles, such as trafficability on soft grounds and stability at high speeds, have long been performed. A mathematical model that predicts plane motions of tracked vehicles on a level ground has been presented by Kitano and his colleagues [1, 2]. It was found from these analysis that a tracked vehicle has peculiar steering characteristics, such as over steering and delayed response at high speeds [3, 4].

Tracked vehicles in construction, agriculture and military are operated widely on steep land. It has been pointed out that the mobility of a tracked vehicle on a side slope is affected considerably by lateral forces as compared to wheeled vehicle. Therefore, not only does the handling of the vehicles on a slope become worse due to the lateral slip, but accidents often result when the frictional forces interacting with the track and the ground are no longer sufficient to maintain an equilibrium with the lateral force. In the previous paper, a mathematical model for plane motions of tracked vehicles involved the effects of the track width was developed [5].

In this paper, a mathematical model to predict the motions of tracked vehicles has been developed in order to increase the out-put efficiency of works by improving the handling characteristics of the vehicle on a slope. Particular attention was paid to disclose the effects of the vehicle and operating parameters, and terrain conditions on the lateral slip of the vehicle; and to find the optimum steering input for the vehicle to maintain the trajectory on a contour line of an inclined ground.

2. MATHEMATICAL MODELING

2.1 Kinematics of the vehicle and coordinate systems

Figure 1 shows the coordinate systems used to describe the vehicle behaviors on inclined ground. The X, Y, Z coordinate system as a reference axis is fixed on an inclined surface on which the axes X, Y and Z are mutually perpendicular and the inclined angle of Y axis is defined by η. The x, y, z coordinate is fixed on the geometric center of the vehicle and its origin coincides with the origin of reference axis at time zero. In order to develop a computer simulation model for general use, the position of the center of gravity is assumed to be displaced S_x and S_y from the body center in longitudinal and lateral directions, respectively.

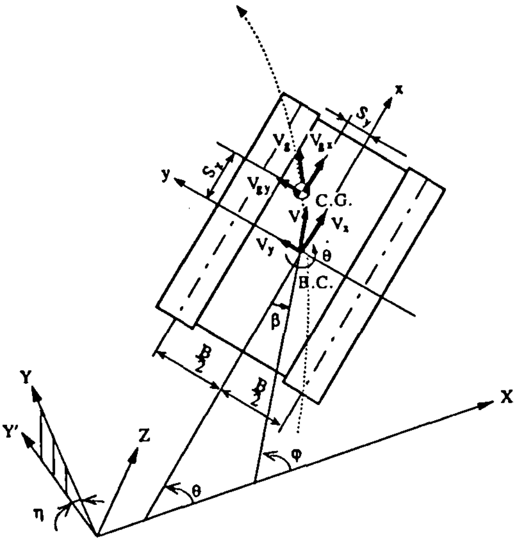

Fig.1 Coordinate systems for tracked vehicle on inclined ground

The motions of a tracked vehicle are analyzed under the following main assumptions:

(1) The model has 7 degrees of freedom; longitudinal and lateral directions, pitch, roll and yaw, together with the rotation of each track mass.

(2) The vehicle configuration is symmetrical with reference to the x and y axes, respectively.

(3) The vehicle has n road wheels with various independent suspensions on both sides. The suspension stiffness and damping coefficients are varied arbitrarily.

(4) The vehicle travels on an inclined plane, and the ground pressure is concentrated under each road wheel.

Kinematics of the vehicle, load distribution under the road wheels, tracked slip, and friction forces when the vehicle has the same independent suspensions were described in the previous papers [1, 2].

2.2 Load distribution with different independent suspensions

Schematic diagrams of the independent suspensions are illustrated in Fig. 2. The stiffness and damping properties of the suspensions are inclined in the model using curves plotted from measured data.

The equations for equilibrium of forces acting on the body, and moments about roll and pitch axes are written as follows:

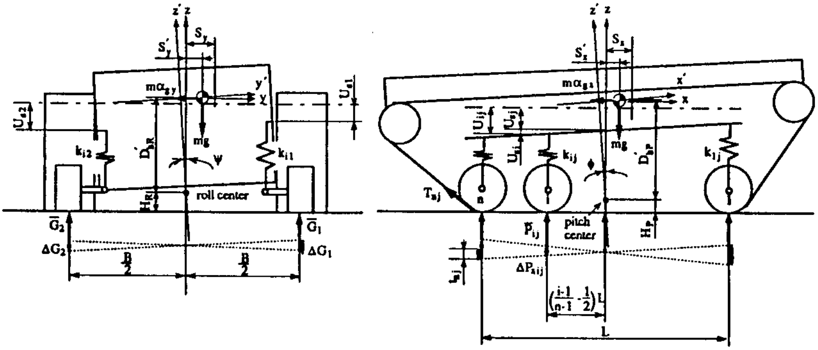
z'
z
S'_y
S_y
$m\alpha_{gy}$
y'
y
U_{e2}
U_{e1}
mg
D'_{gR}
k_{i2}
k_{i1}
ψ
H_R
roll center
$\bar{G}_2$
$\bar{G}_1$
ΔG_2
ΔG_1
$\frac{B}{2}$
$\frac{B}{2}$
z'
z
S'_x
S_x
$m\alpha_{gx}$
x'
x
U_{ij}
U_{sj}
U_{ij}
mg
k_{ij}
k_{1j}
ϕ
D'_{gP}
T_{nj}
n
$\bar{P}_{ij}$
pitch center
H_P
ΔP_{sij}
$\left(\frac{i-1}{n-1}-\frac{1}{2}\right)L$
L

(a) y-z plane

(b) x-z plane

Fig. 2 Suspension systems for tracked vehicles and load distribution

$$mg = \sum_{i=1}^{n} \sum_{j=1}^{2} P_{ij} \tag{1}$$

$$m\alpha_{gy}(D'_{hR} + H_R) - mgS'_y = \frac{B}{2}\sum_{i=1}^{n} \left(P_{i2} - P_{i1}\right) \tag{2}$$

$$m\alpha_{gx}(D'_{hP} + H_P) - mgS'_x = \sum_{i=1}^{n} \sum_{j=1}^{2} P_{ij}\left(\frac{1}{2} - \frac{i-1}{n-1}\right)L \tag{3}$$

where $P_{ij}=k_{ij}U_{ij}$, k_{ij} is the spring constant and U_{ij} defines the deflections of independent suspensions. $m\alpha_{gx}$ and $m\alpha_{gy}$ are the longitudinal and lateral inertia forces acting on the mass center (C.G.). D_{hr} and D_{hp} represent the roll and pitch center heights of the suspension, respectively.

The ground pressure distributions under each road wheel with various independent suspensions can be predicted by calculating the equations (1), (2) and (3).

2.3 Equation of motion on inclined ground

Considering the equilibrium of all forces, such as inertia forces, track tractive forces and rolling resistances, and moments acting on the vehicle, the equations on motions of tracked vehicles on an inclined ground are written as follows [5]:

$$m\alpha_{gx} = \sum_{i=1}^{n} \sum_{j=1}^{2} Q_{xij} - \left(R_1+R_2\right) \tag{4}$$

$$m\alpha_{gy} = \sum_{i=1}^{n} \sum_{j=1}^{2} Q_{yij} \tag{5}$$

$$\begin{aligned} I_z\ddot{\theta} = {} & \sum_{i=1}^{n} \frac{B}{2}\left(Q_{xi2} - Q_{xi1}\right) + \sum_{i=1}^{n} \sum_{j=1}^{2} \left\{\left(\frac{1}{2} - \frac{i-1}{n-1}\right)LQ_{yij}\right\} + \frac{B}{2}\left(R_1 - R_2\right) \\ & - m(\alpha_{gy}S_x - \alpha_{gx}S_y) \end{aligned} \tag{6}$$

$$I_x\ddot{\psi} = m_s\alpha_{gy}(D_{hR}\cos\psi + S_y\sin\psi) - D_\psi\dot{\psi} - K_\psi\psi \tag{7}$$

$$I_y\ddot{\phi} = - m_s\alpha_{gx}(D_{hP}\cos\phi - S_x\sin\phi) - D_\phi\dot{\phi} - K_\phi\phi \tag{8}$$

where

$$\alpha_{gx} = \dot{V}_{gx} - V_{gy}\,\dot{\theta} + g\sin\theta\sin\eta \tag{9}$$

$$\alpha_{gy} = \dot{V}_{gy} + V_{gx}\,\dot{\theta} + g\cos\theta\sin\eta \tag{10}$$

m_s is the spring mass, α_{gx} and α_{gy} are the longitudinal and lateral accelerations. Q_{xij}, Q_{yij} are the tractive forces and lateral friction forces of the

track under the i-j road wheel. R_1 , R_2 are the rolling resistances. The moments of inertia of a body about each axis are defined by I_x, I_y, I_z, respectively. ψ, ϕ and θ are the roll, pitch and yaw angles. K_ψ , K_ϕ are roll and pitch stiffness. D_ψ, D_ϕ are roll and pitch damping coefficients.
The details of developing procedure of the equations have been presented in previous papers [1, 2].

3. EXPERIMENTAL EQUIPMENTS AND METHOD

In order to verify the numerical simulations and to evaluate the behaviors of tracked vehicles on an inclined ground, the scale model tests were carried out. Figure 3 shows the overall view of the one-tenth scale model on the tilt table. The scale model has two separate DC servo motors to control the driving speeds of each side sprocket. The five road wheels with independent suspensions are arranged on each side at the same interval. The maneuver tests surface, 10m×10m wide plane, is made of a wooden plate covered with a hard resin film, and the slope of the tilt table can be increased arbitrarily up to 45 degrees. The trajectories of C.G. , yaw and side slip angles are observed by the optical method as shown in Fig. 4. The optical device can be record the positions of two lights mounted on the front and rear points in the same distance from the body center in 1/60 second interval. The trajectories of the center of gravity, yawing angle, yawing rate and side slip angle can be calculated from the observed data.

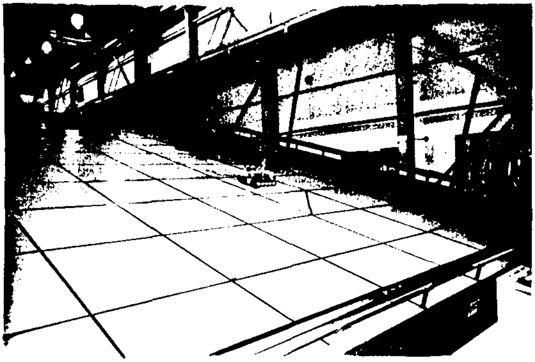

Fig.3 General view of inclined ground

The specifications of a scale model, the basic parameters for dynamic analysis, such as the height of C.G., the moment of inertia about three axes, the height of roll and pitch center, stiffness and damping coefficients of roll and pitch of the suspensions are measured and shown in Table 1. The relationships between slip and tractive forces developing at each portion of the track-ground contact area are essential factors for the lateral stability of tracked vehicles. The dynamic friction coefficients with respect to track slippage were measured using a scale model specially designed for this purpose and the typical results are shown in Fig. 5.

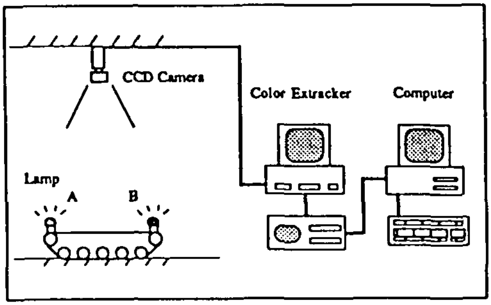

Fig.4 Schematic of optical method to measure turning trajectory

Table 1 Parameters of scale model

Mass	49kg	I_x	1.60kgm^2
Cotact length	0.435m	I_y	4.55kgm^2
Tread	0.295m	I_z	2.34kgm^2
Track width	0.06m	k_{ij}	7900N/m
C.G. height	0.11m	D_ϕ	58Nms/rad
Road Wheel	5	D_ψ	52Nms/rad

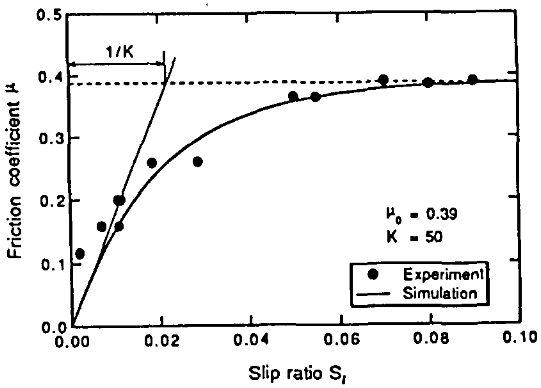

Fig.5 Typical measured μ-slip curve

4. EXPERIMENTAL RESULTS AND NUMERICAL SIMULATION

4.1 Lateral stability in cross slope

The traverse tests were carried out on a side slope of tilt angle, η=10, 20 degrees at a constant speed. Two crawlers with different friction coefficients were used. Figure 6 (a) and (b) show the experimental trajectories of the body center as compared with the computed results. The arrows on the computed trajectories describe the attitude of the vehicle at two second intervals. Good agreement has been found between measured and predicted results of the vehicle behavior on side slopes.

Figure 7 and 8 show the computed results of the yaw angles and the side slip angle under the same running conditions shown in Fig. 5. It was found that the yaw angle increases steadily with running distance, but the side slip angle is kept at the constant value.

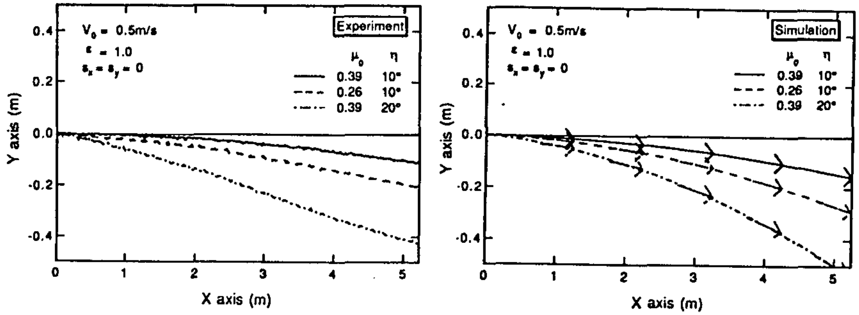

(a) experimental data

(b) numerical data

Fig.6 Influence of inclined angle and frictional coefficient on trajectory

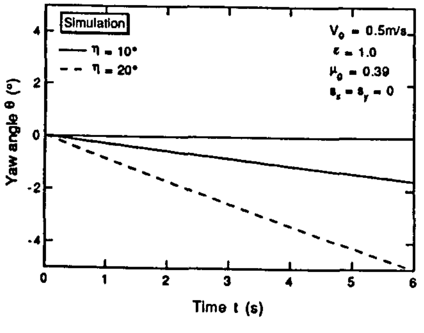

Fig.7 Influence of inclined angle on yaw angle

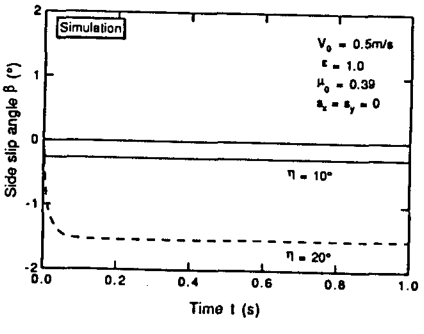

Fig.8 Change of side slip angle

The effects of the forward and backward displacements of the C.G. location on lateral stability of tracked vehicles in acrossing the slope are illustrated in Fig. 9 (a) and (b). It is clear from those results that the lateral slip of the vehicle increases gradually as the C.G. is displaced to forward. By contrast, the influence of the lateral displacement of the C.G. was scarecely found from the numerical results.

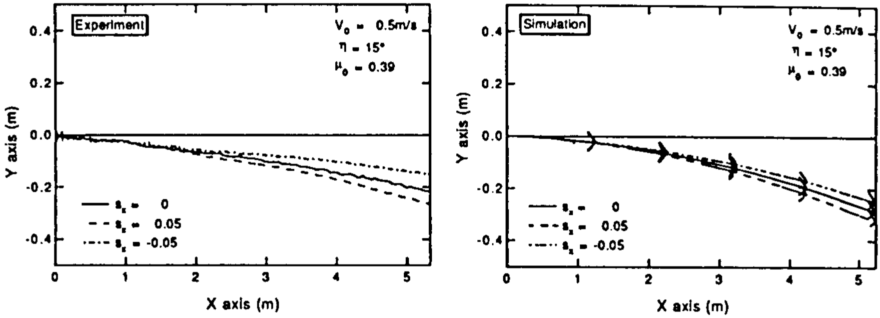

(a) experimental data (b) numerical data

Fig.9 Influence of shift of C.G. location on trajectory

4.2 Simulations for an example vehicle

By using the numerical method developed here, the effects of vehicle parameters such as the load distributions and friction forces in the track-ground interface, the height of the C.G., the characteristics of independent suspensions and others on the vehicle behavior on side slope are investigated. The basic parameters of the example vehicle are shown in Table 2.

The numerical results indicate that there is hardly any effect on the height of the C.G. and the aspect ratio on the vehicle behavior on slope. Figure 10 (b) shows the effects of the load distribution under track rollers on the vehicle behavior.

Table 2 Parameters of example vehicle

Mass	37993kg	I_x	114660kgm^2
Cotact length	4.0m	I_y	45670kgm^2
Tread	2.63m	I_z	109760kgm^2
Track width	0.55m	k_{ij}	993000N/m
C.G. height	1.09m	D_ϕ	592900Nms/rad
Road Wheel	5	D_ψ	705600Nms/rad

The lateral slip of the vehicle from the contour line is increased as the vertical load at the front and rear portions of the track-ground contact area is increased. It can generally be considered that the vehicle behavior depends considerably on the adhesion force at a certain portion of the contact area in which the normal load is the maximum attainable. In the case of the trapezoidal pressure shown in Fig. 10 (a) , the slip of the front portion of a vehicle larger than the rear because of the adhesion force at the front edge is smaller than the rear as shown in Fig. 5.

Figure 11 (a) shows the relationships between the friction coefficient and track slippage at the track-laying area for three types of soft ground. Figure 11 (b) illustrates the lateral slip behavior of the vehicle for three kinds of the modulus K. These results suggest that the vehicle lateral slip increases significantly on softer grounds, because side slip of the front portion of the track increases as the modulus K becomes smaller, as shown in Fig. 11(b).

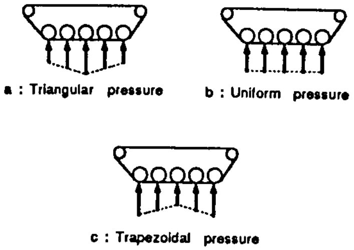

Fig.10(a) Typical load distribution models using a simulation

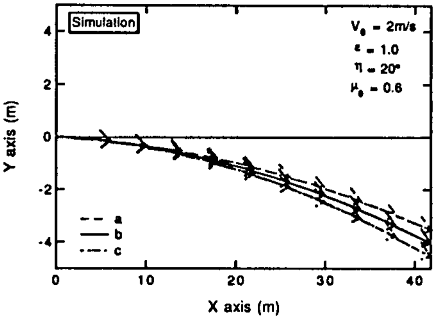

Fig.10(b) Influence of load distribution on trajectory

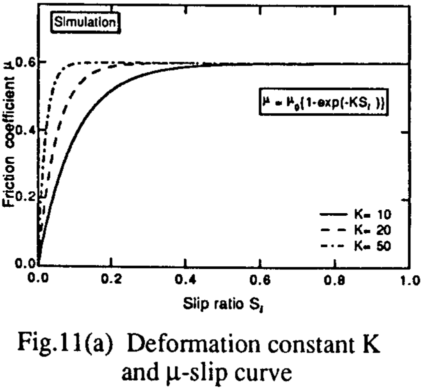

Fig.11(a) Deformation constant K and μ-slip curve

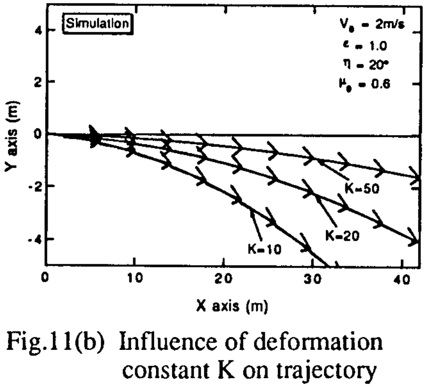

Fig.11(b) Influence of deformation constant K on trajectory

4.3 Steering inputs for runnning on contour line

The optimum steering inputs for a tracked vehicle to cross along a contour line of an inclined ground are investigated using the mathematical model which has been verified in the previous section. As shown in Fig.12, considering the case of a tracked vehicle traverses along a contour line of a slope at a constant speed with a constant side slip angle, the conditions of the restriction for the numerical analysis are given as follows;

$$\varphi = 0\ ,\ \dot{V}_x = 0\ ,\ \dot{V}_y = 0\ ,\ \ddot{\theta} = 0\ ,\ \dot{\theta} = 0 \tag{11}$$

The equations of the cross motion are written as follows:

$$\sum_{i=1}^{n}\sum_{j=1}^{2} Q_{xij} - \left(R_1+R_2\right) - mg\cdot\sin\theta\cdot\sin\eta = 0 \tag{12}$$

$$\sum_{i=1}^{n}\sum_{j=1}^{2} Q_{yij} - mg\cdot\cos\theta\cdot\sin\eta = 0 \tag{13}$$

$$\sum_{i=1}^{n}\frac{B}{2}\left(Q_{xi2} - Q_{xi1}\right) + \sum_{i=1}^{n}\sum_{j=1}^{2}\left\{\left(\frac{1}{2} - \frac{i-1}{n-1}\right)LQ_{yij}\right\} + \frac{B}{2}\left(R_1 - R_2\right) = 0 \tag{14}$$

The relationship between the vehicle speed and both track speeds is defined as:

$$2V_0 - \left(V_{t1} - V_{t2}\right) = 0 \tag{15}$$

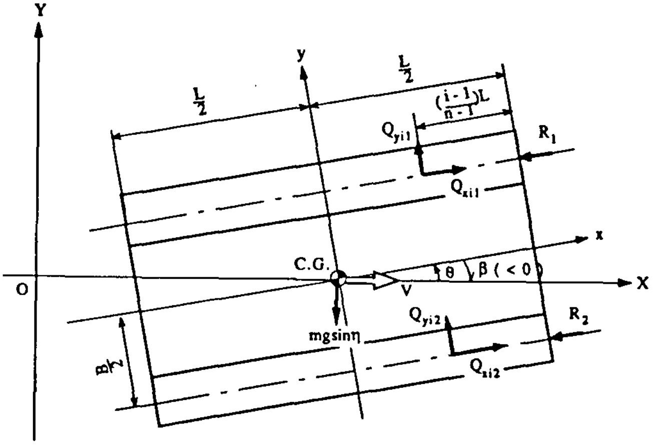

Fig.12 External forces acting on a tracked vehicle under contour line travel

From the predicted results, the optimum steering inputs such as the steering ratio and yaw angle for an example vehicle to cross along a contour line of various kinds of soft terrain are plotted against the inclined angle in Fig. 13 (a), (b), respectively. It is evident from these results that the optimum steering ratio and yaw angle are greater with the increase in slope but there is a decrease of friction force at the track-ground contact area.

The predicted optimum steering inputs were employed to simulate the vehicle behaviors in traversing on a slope. Figuer 14 shows an example of the simulations on the trajectory and attitude of the vehicle with the optimum steering inputs. It was disclosed here that the tracked vehicle can be traversed on a contour line of inclined terrain without lateral slip downward, if the optimum steering inputs are found.

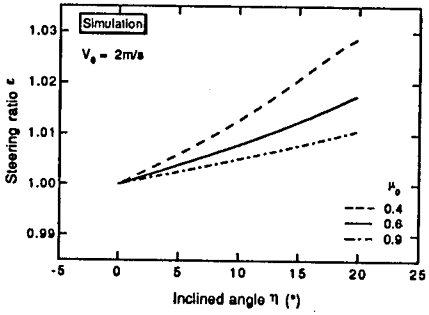

Fig.13(a) Relationships between inclinedangle and steering ratio

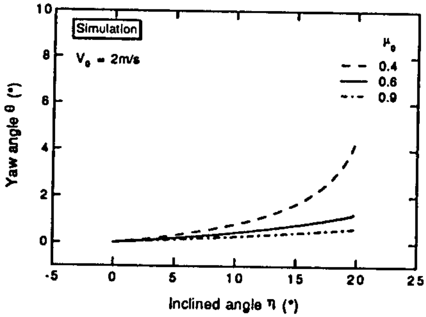

Fig.13(b) Relationships between inclined angle and yaw angle

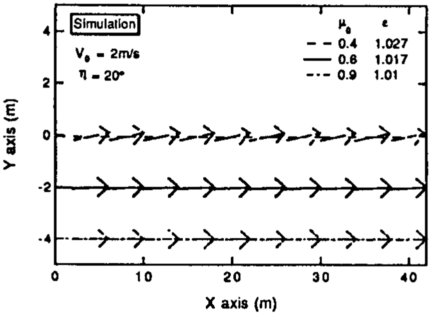

Fig. 14 Vehicle trajectory under contour line travel

5. CONCLUSIONS

A mathematical model has been developed in order to predict the stability of tracked vehicles with different independent suspensions on inclined grounds and the validity of the model was confirmed by using scale model tests. From the results of the numerical analysis and the scale model tests the following vehicle behaviors are disclosed:

1. The effects of the parameters and characteristics of the vehicle and the terrain conditions on the vehicle behaviors in crossing a slope are summarized as follows:
(a) As the position of the center of gravity is moved forward, the lateral slip of the vehicle on a slope is greater, but the effects of lateral and upward displacements are insignificant.
(b) Although the effects of the aspect ratio L/B are small, the lateral slip is slightly increased with track-ground contact length.
(c) The vehicle behavior on a slope is affected considerably by load distribution in the track-ground contact area. The lateral slip is smaller as there is an increase in the normal load in central part of the contact area.
(d) The grouser shape has significant effects on inisotropic tractive forces in longitudinal and lateral directions. The lateral slip is smaller as the lateral friction forces are increased.
(e) The lateral stability of tracked vehicle on a slope is significantly influenced by the terrain factors, especially the relationships between tractive forces and slip ratio. On a soft ground, the initial tangent modulus K is small, the lateral slip of track at the front edge is greater than that of the rear track. This is the reason why the lateral slip of a tracked vehicle is greater on a soft ground.
2. It was found that the optimum steering inputs for the tracked vehicle to run along a ground contour line on a slope terrain could be obtained by using the proposed model.

REFERENCES

[1] M. Kitano, H. Jyozaki: A Theoretical Analysis of Steerability of Tracked Vehicles, Journal of Terramechanics, Vol.13, No.14(1976), pp.241-258.

[2] M. Kitano, M. Kuma: An Analysis of Horizontal Plane Motion of Tracked Vehicles, Journal of Terramechanics, Vol.14, No.4(1978), pp.211-225.

[3] M. Kitano, F. Eiyo: Study on Transient Steering Characteristics of Tracked Vehicles, JSAE Review, No.18(1985), pp.90-97.

[4] M. Kitano, K. Watanabe, Y. Takaba: Lane-Change Maneuver of High Speed Tracked Vehicles, Proceedings of 9th ISTVS, Vol.2(1987), pp.592-593.

[5] K. Watanabe, M. Kitano and T. Katahira: Controllability and Stability of Tracked Vehicles on Inclined Ground, Proceedings of 11th Conference of ISTVS, Vol.2(1993.9), pp.426-435.

Transmission System for Tracked Vehicles

Yesterday - Today - Tomorrow

St. Bollmann

ZF Friedrichshafen
Germany

The history of tracked vehicles for Military Applications in Germany started in 1935 with the Panzer No. I. The engine power at this time was only 100 hp and the maximum possible speed was 40 km/h. But even at this time the use of synchromashed transmissions was a must to make the driving as simple as possible. These vehicles had already a transmission with 5 speeds forward and 1 reverse. The steering was a clutch type steering where the inner curve track was braked by a means of a conventional brake.

In the same year in 1935 the Panzer No. II came in production and here the engine power went up to 140 hp. The number of gears was increased to 6 forward and 1 reverse. To increase the mobility of the vehicle the steering system was changed to a single radius type where one fixed ratio was used to drive the curves.

In the following years from 1938 to 1944 the engine powers went up to 700 hp for the Tiger in 1944. In this vehicle a so called semi-automatic transmission was installed and a twin radius steering working on the regenerative principle was installed. The number of gears was increased up to 8 forward and 4 reverse.

In the years from 1935 to 1944 six different kinds of tracked transmission systems have been developed and went into series production. The biggest progresses have been made by the different kinds of steering systems to increase the mobility of tracked vehicle especially in off-road conditions.

Picture 1 and 2

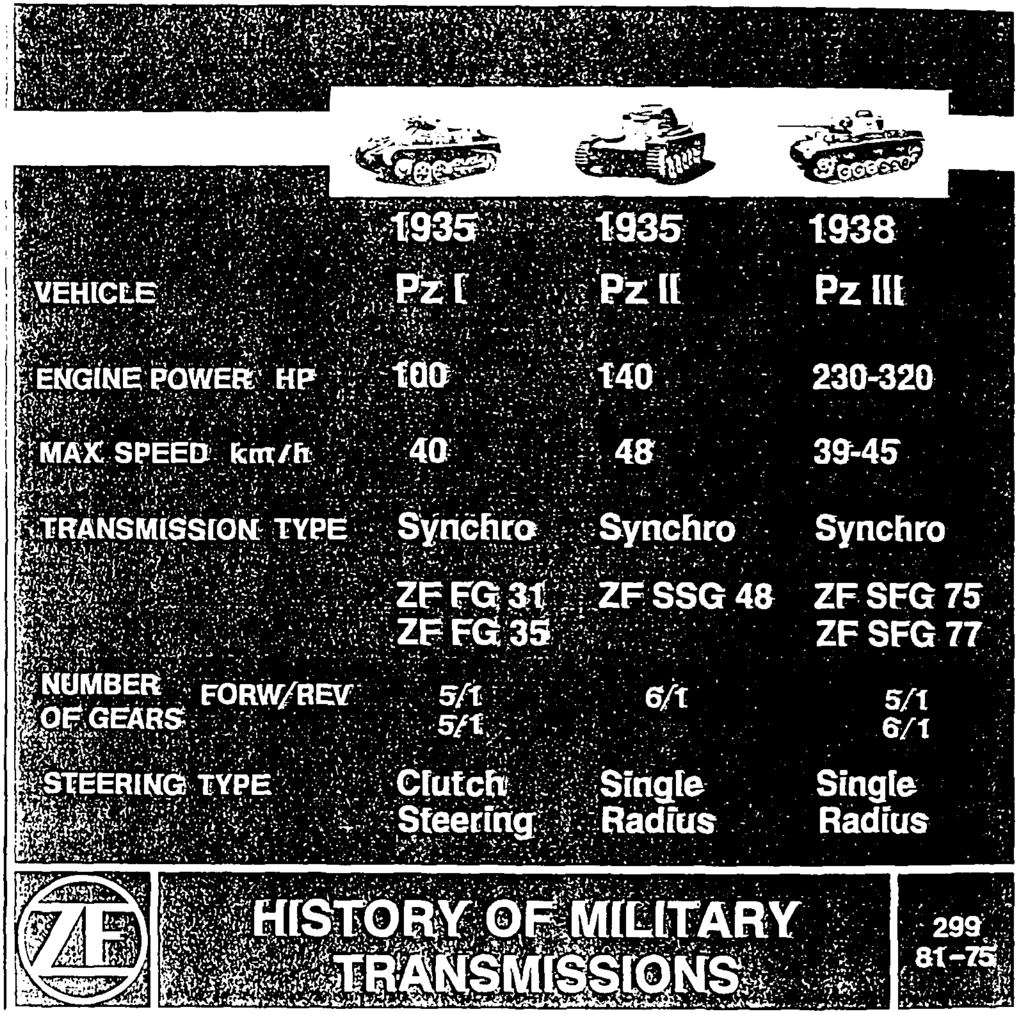

	1935	1935	1938
VEHICLE	Pz I	Pz II	Pz III
ENGINE POWER HP	100	140	230-320
MAX. SPEED km/h	40	48	39-45
TRANSMISSION TYPE	Synchro	Synchro	Synchro
	ZF FG 31 ZF FG 35	ZF SSG 48	ZF SFG 75 ZF SFG 77
NUMBER OF GEARS FORW/REV	5/1 5/1	6/1	5/1 6/1
STEERING TYPE	Clutch Steering	Single Radius	Single Radius

HISTORY OF MILITARY TRANSMISSIONS

299
81-75

	1938	1943	1944
VEHICLE	Pz IV	Panther	Tiger
ENGINE POWER HP	300-320	650-700	700
MAX SPEED km/h	40	55	37-41
TRANSMISSION TYPE	Synchro	Dog-Clutch	Pre -Select (IN PREP)
	ZF SFG 75 ZF SSG 76 ZF SSG 77	ZFAK7-200	Olvar
NUMBER OF GEARS FORW/REV	5/1 5/1 6/1	7/1	8/4
STEERING TYPE	Single Radius	Overlap Steering	Twin Radius

HISTORY OF MILITARY TRANSMISSIONS

Todays Transmission Systems

Due to the different targets of tracked vehicles, resulting on different weights and consequently different mobility, the power to weight ratio defers from approximately 13 hp/ton for Howitzers up to 25 hp/ton for high mobility vehicles.

The military requirements for gradability are at least 60 % vertical slope and up to 40 % side slope. Maximum vehicle speeds are actually going up to 75 km/h. The tractive force is depending on the vehicle weight and should be in the range of 0.7 times vehicle weight to be run with closed lock-up of torque converter. These requirements lead in generally to multi speed transmissions with an overall ratio up to 9. On chart no. 3 a typical example of 2 different transmissions is shown, the dotted line is a 4 speed version, the other one is a 6 speed version with ratio 9.6. On a 14 tons vehicle the 60 % slope can be run with closed lock-up. The 4 speed version already on a 20 % slope starts working on torque converter mode. This results in a higher heat rejection and consequently in a bigger cooling system which not only results in bigger space requirements but also in higher fan power and in last consequence less driving power available on the sprocket.

Picture 4

Modern transmission systems have to follow the requirements of modern vehicles and therefore installation flexibility is one of the most important targets starting already in the development face.

Picture 5

L-configuration is in generally used for front driven vehicles where the driver sits beside the engine.

Picture 6

For rear driven vehicles the side-by-side arrangement has substituted the T-configuration by using the whole width of the hull for the engine transmission block.

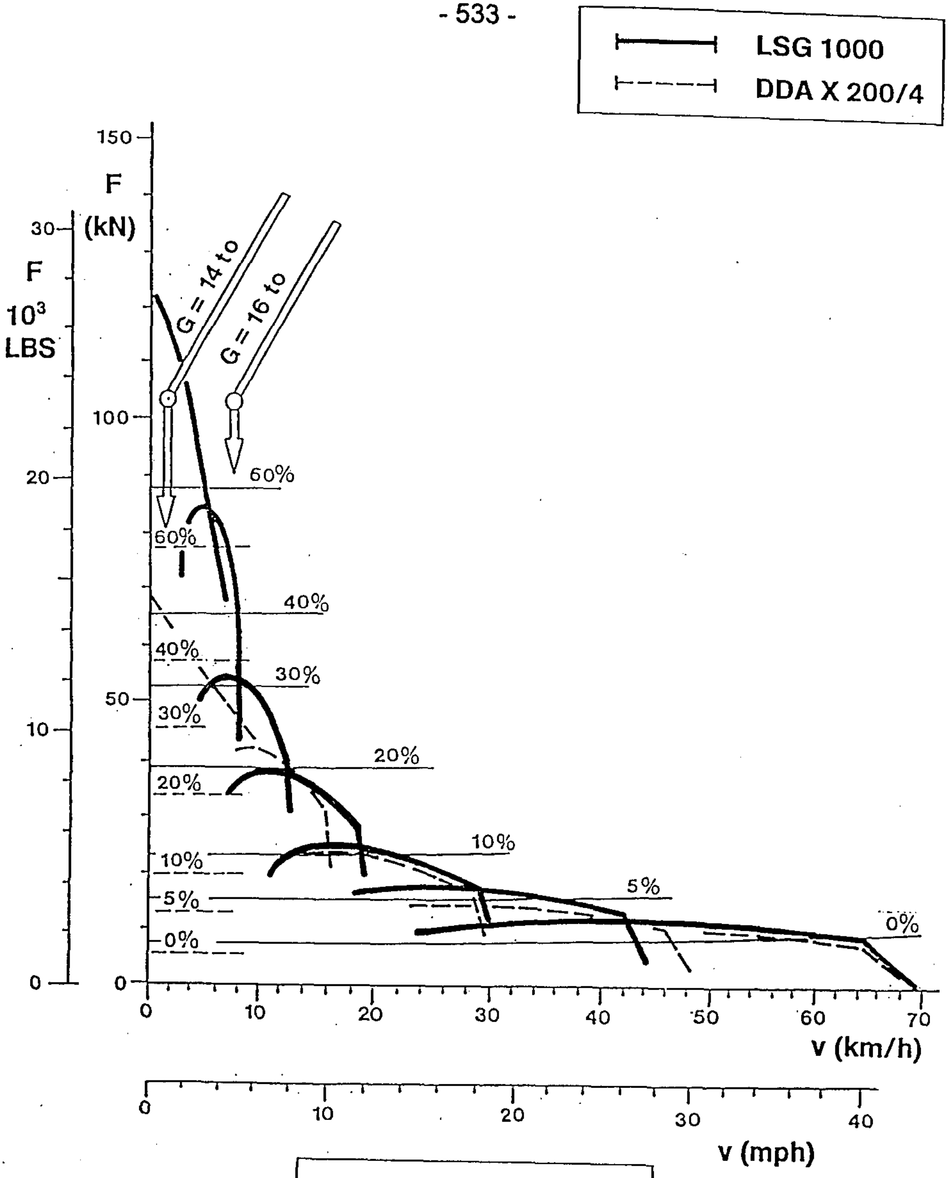

Vehicle: m = 14/16 to

Engine: N = 221 kW
n = 2100 rpm

Tractive force comparison

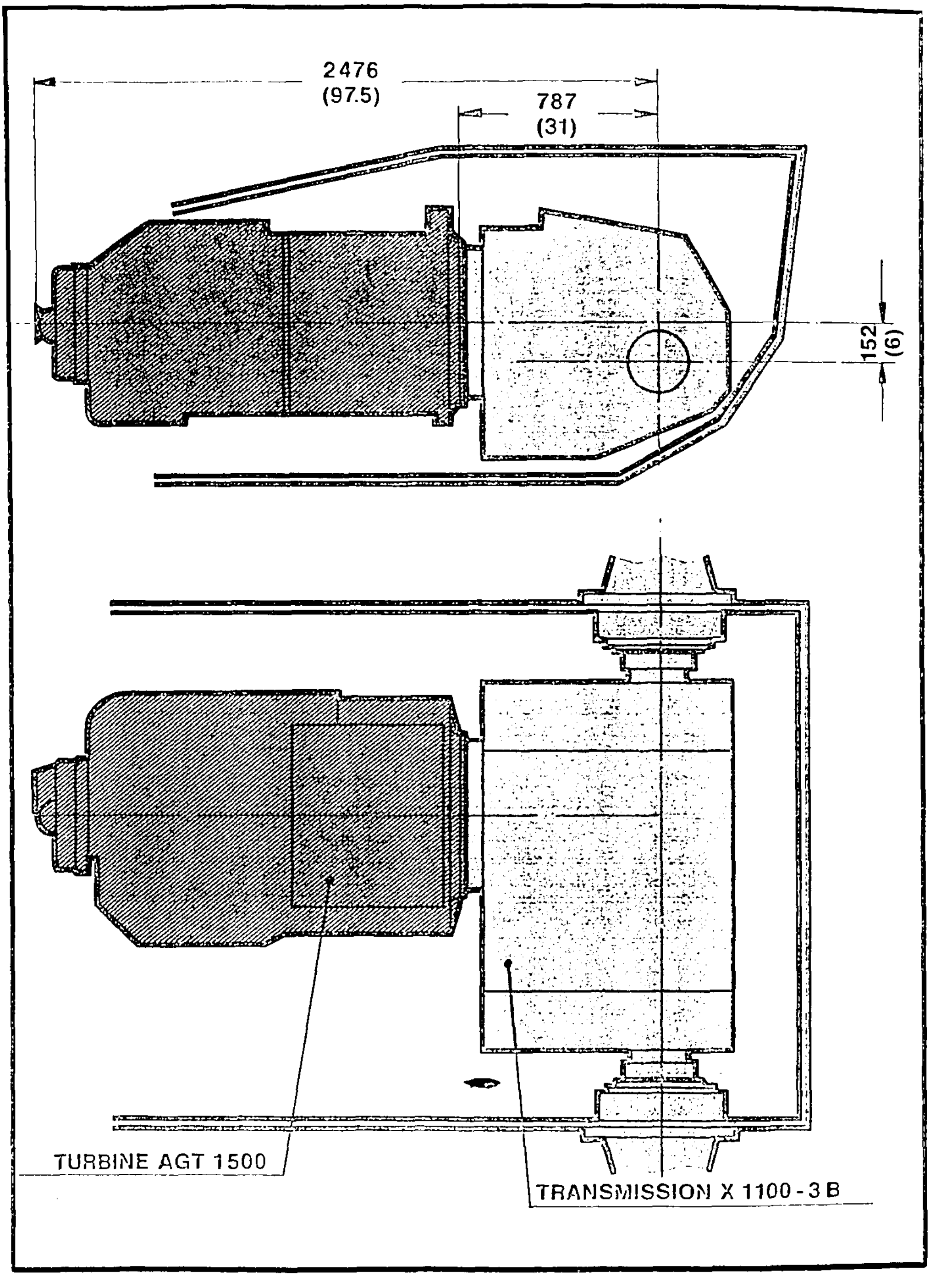
2476
(97.5)
787
(31)
152
(6)
TURBINE AGT 1500
TRANSMISSION X 1100 - 3 B

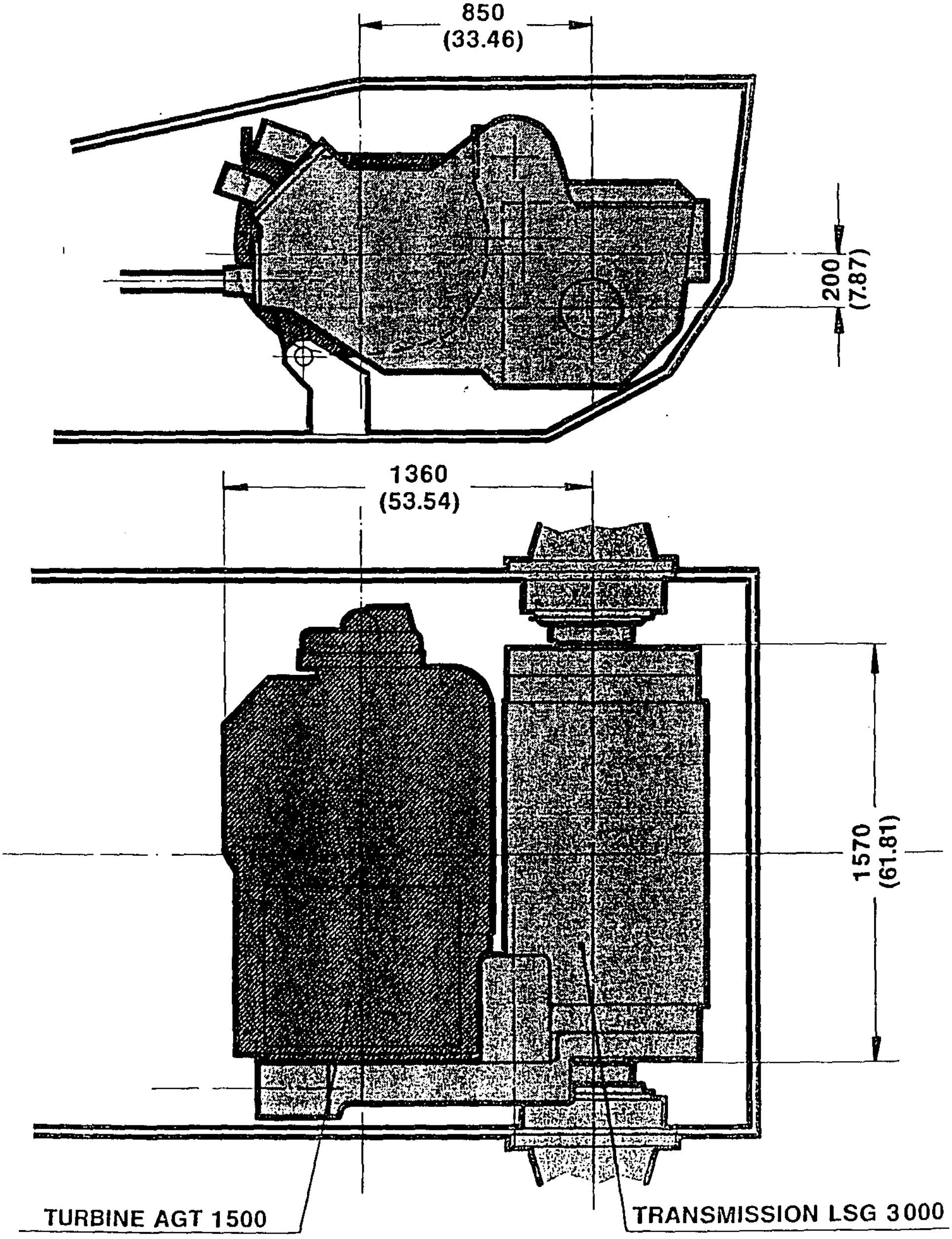
850
(33.46)
200
(7.87)
1360
(53.54)
1570
(61.81)
TURBINE AGT 1500
TRANSMISSION LSG 3000

MODULAR SYSTEM

Due to the different requirements for transmission systems in tracked vehicles and based on the always degreasing number of identical production units, the industry has reacted and started with the so called modular design.

The different functions of transmissions were splitted in modules which can be changed or assembled without major problems.

The picture no. 7

shows the modularity of the LSG 3000. The input group no. 11 is able to work with different engine speeds between 2100 and 3000 rpm, and the input shaft is variable in the height from + 90 to - 90 mm. This is to adapt the different crank shaft heights of engines. The planetary shifting group no. 8 runs under nearly all circumstances with similar speeds. This also assures that the lubrication system has not to be changed case by case.

The steering module no. 6 on top of the transmission is engine driven and different steering philosophies can be adapted in the same space of transmission.

The next picture (no. 8) shows the flexibility starting with 4 or 5 speed shifting groups which can be substituted in the same space by a CVT transmission. Different fan drives can be mounted on top of the transmission and the steering group is available in mechanical 3 radii system, or electro mechanical CVT steering as well as a hydrostatic mechanical version. The central housing is built to receive all the modules and allow the different power pack configurations, L-version, T-version or side-by-side arrangement.

The torque converter is an individual module and can be adapted to the different engine characteristics.

For a combined braking system the secondary retarder can be fitted directly on the planetary shifting group.

The following examples show some typical examples of modularity. Installation of 4 speed or 5 speed module (picture no. 9) or CVT steer unit and 3 radio and mechanical steering.

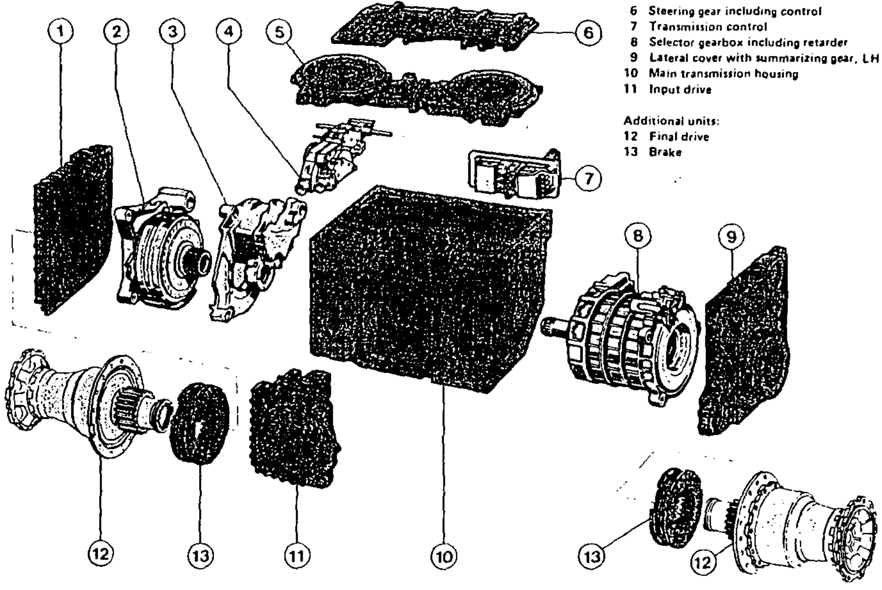

1 Lateral cover with summarizing gear, RH
2 Torque converter with housing insert, RH
3 Housing insert, center unit
4 Pumps
5 Fan drive unit
6 Steering gear including control
7 Transmission control
8 Selector gearbox including retarder
9 Lateral cover with summarizing gear, LH
10 Main transmission housing
11 Input drive

Additional units:
12 Final drive
13 Brake

LSG 3000 SYSTEM
EASY MAINTENANCE

504
171

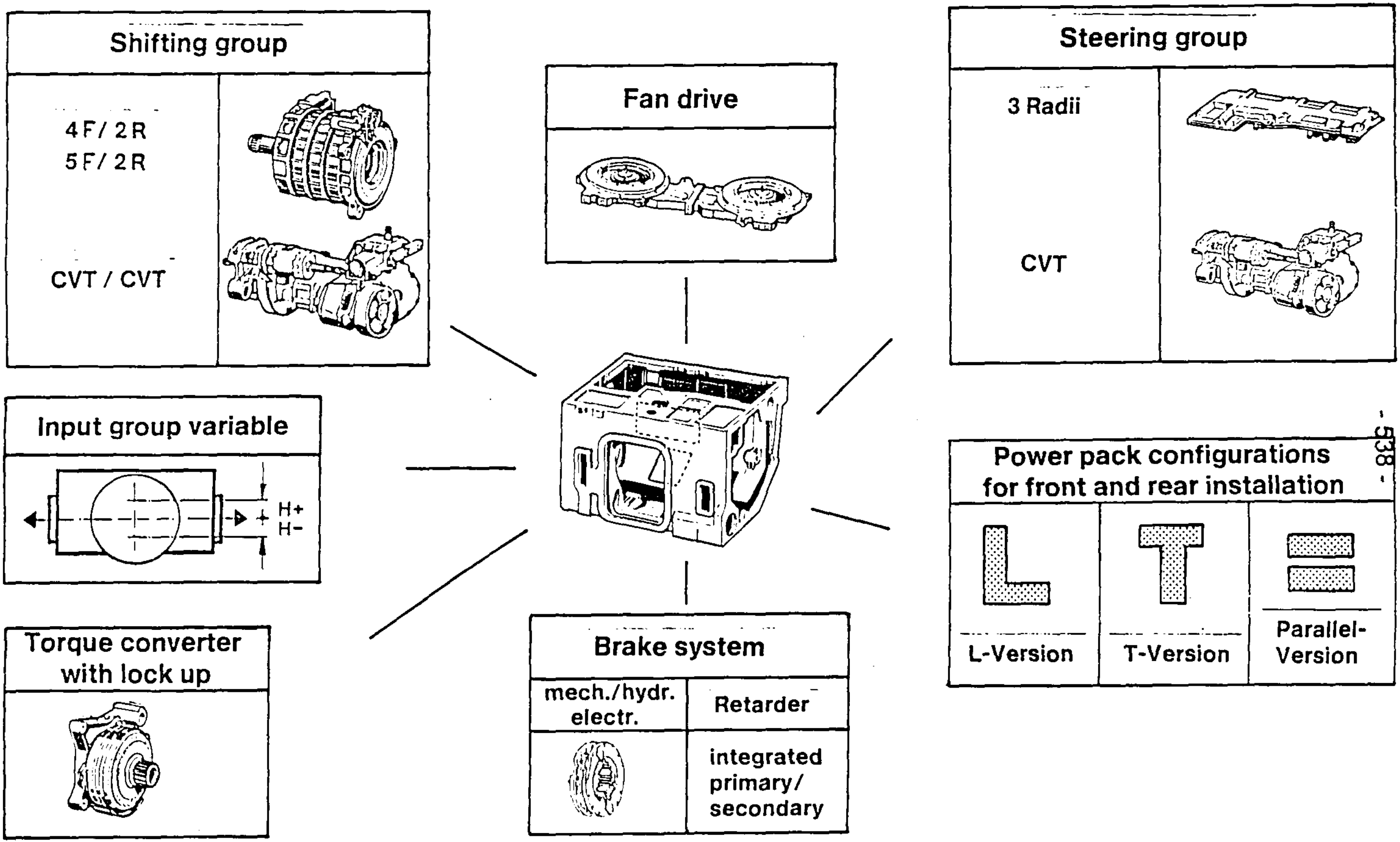

Shifting group

- 4 F / 2 R
- 5 F / 2 R
- CVT / CVT

Fan drive

Steering group

- 3 Radii
- CVT

Input group variable

Power pack configurations for front and rear installation

L-Version	T-Version	Parallel-Version

Torque converter with lock up

Brake system

mech./hydr. electr.	Retarder
	integrated primary/ secondary

LSG Flexibility

ZAHNRADFABRIK
FRIEDRICHSHAFEN AG
Geschäftsbereich
Friedrichshafen

SF

4 SPEED MODUL

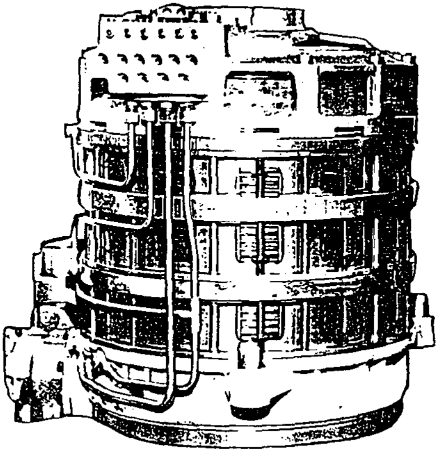

5 SPEED MODUL

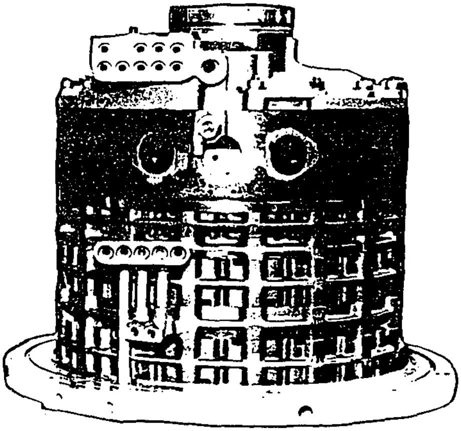

LSG 3000
PLANETARY SHIFTING MODUL

504
464

CVT - STEERING UNIT

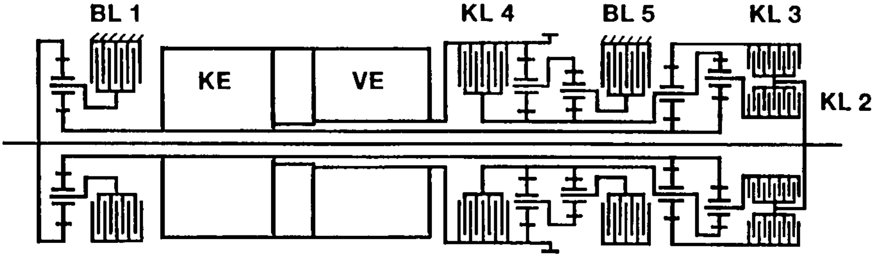
BL 1
KL 4
BL 5
KL 3
KE
VE
KL 2

3 – RADII MECHANICAL STEERING

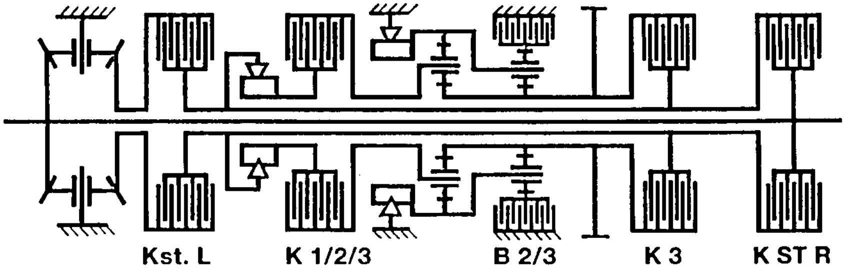
Kst. L
K 1/2/3
B 2/3
K 3
K ST R

LSG 3000

COMPARISON STEERING SYSTEMS

504
465

The shifting transmissions are in general systems between 4 and 9 speeds, electro hydraulically shifted and depending on power and space requirements either in counter shaft or planetary system.

Picture No. 11

In the LSG 1000 the counter shaft principle was used because the power leading parts of the shifting groups were used out of mass production transmission to find an economic repowering solution. Hydrostatic mass production pumps and motors are used for the steering unit to reduce the production and life cycle costs to a minimum. Picture 11 shows the gear schematic of a counter shaft principle transmission.

Picture No. 12

The following picture shows a typical example of a transmission system for tracked vehicles in the planetary system.

Here the torque converter is not mounted between engine and transmission but coaxial to the planetary shifting set. This reduces the installation space between fly wheel of engine to output to final drives down to approximately 300 mm.

On top of the transmission there is a 3 radii mechanical steering system which is input driven and in the side covers the summation gears are summing up the steering speed to the output speed.

Picture 13

The most important modul for the mobility of tracked vehicles is the steering unit. Depending on the different systems the available power on the sprocket differs in a very wide scale.

All examples show overlapped regenerative steering systems. The mechanical 3 radii steering system works with an overall efficiency of approx. 92 %. This system allows in most of the driving cases the CVT range and only at narrower curves the mechanical radii are used. This high efficiency is based on the mechanical components where only the losses of gear mashing and bearings must be taken in consideration.

The hydrostatic mechanical steering is a combination where the comfort of the hydrostatic is combined with the good efficiency of the mechanical system.

The next steering system shows an example of a complete CVT steering, this can be achieved by different means, either by a fully hydrostatic steering unit or a combination of hydrostatic drive plus fluid couplings, which in function of the filling grade add additional torque to the hydrostatic driving unit.

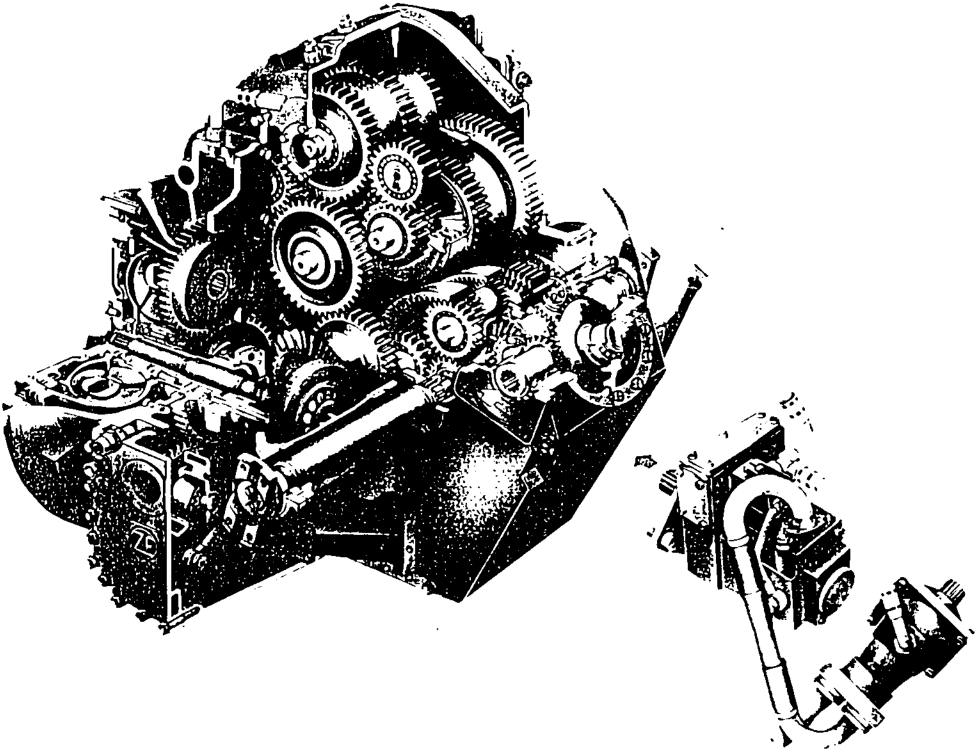

LSG 1000

504
335

Transmission diagram (example)

Gear		Clutches engaged						
		KV	KR	K1	K2	K3	K4	
	Pvt			●	●			+Steering gear on
Reverse	1st		●	●				Emerg. gear change
	2nd		●		●			
	3rd		●			●		
	N					●		
Forward	1st	●		●				
	2nd			●			●	Emerg. gear change
	3rd	●			●			
	4th				●		●	
	5th	●				●		
	6th					●	●	

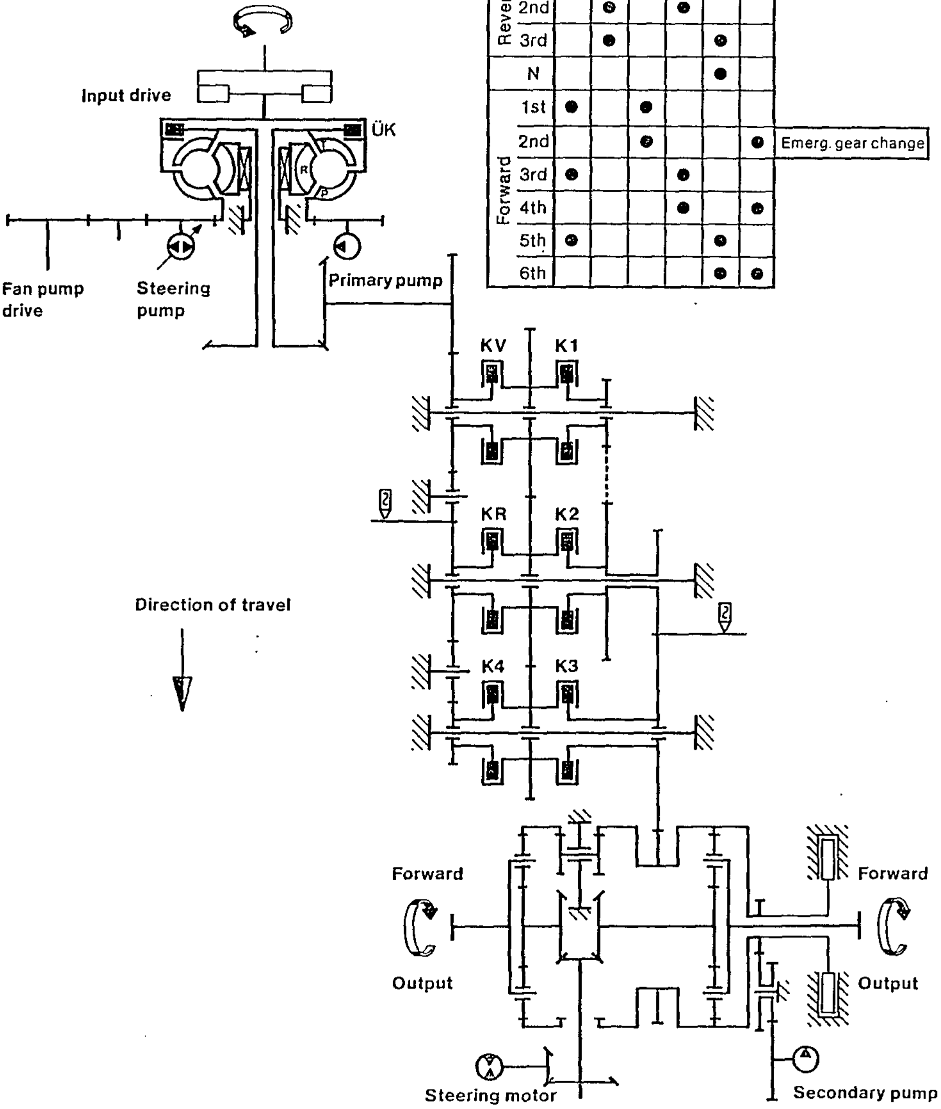
Input drive
ÜK
R
P
T
Fan pump drive
Steering pump
Primary pump
KV
K1
KR
K2
K4
K3
Direction of travel
Forward
Output
Forward
Output
Steering motor
Secondary pump

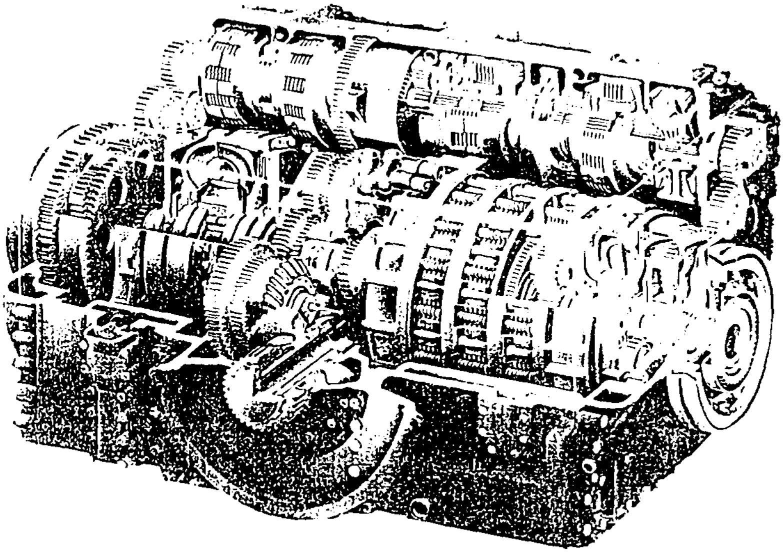

LSG 3000

504
148

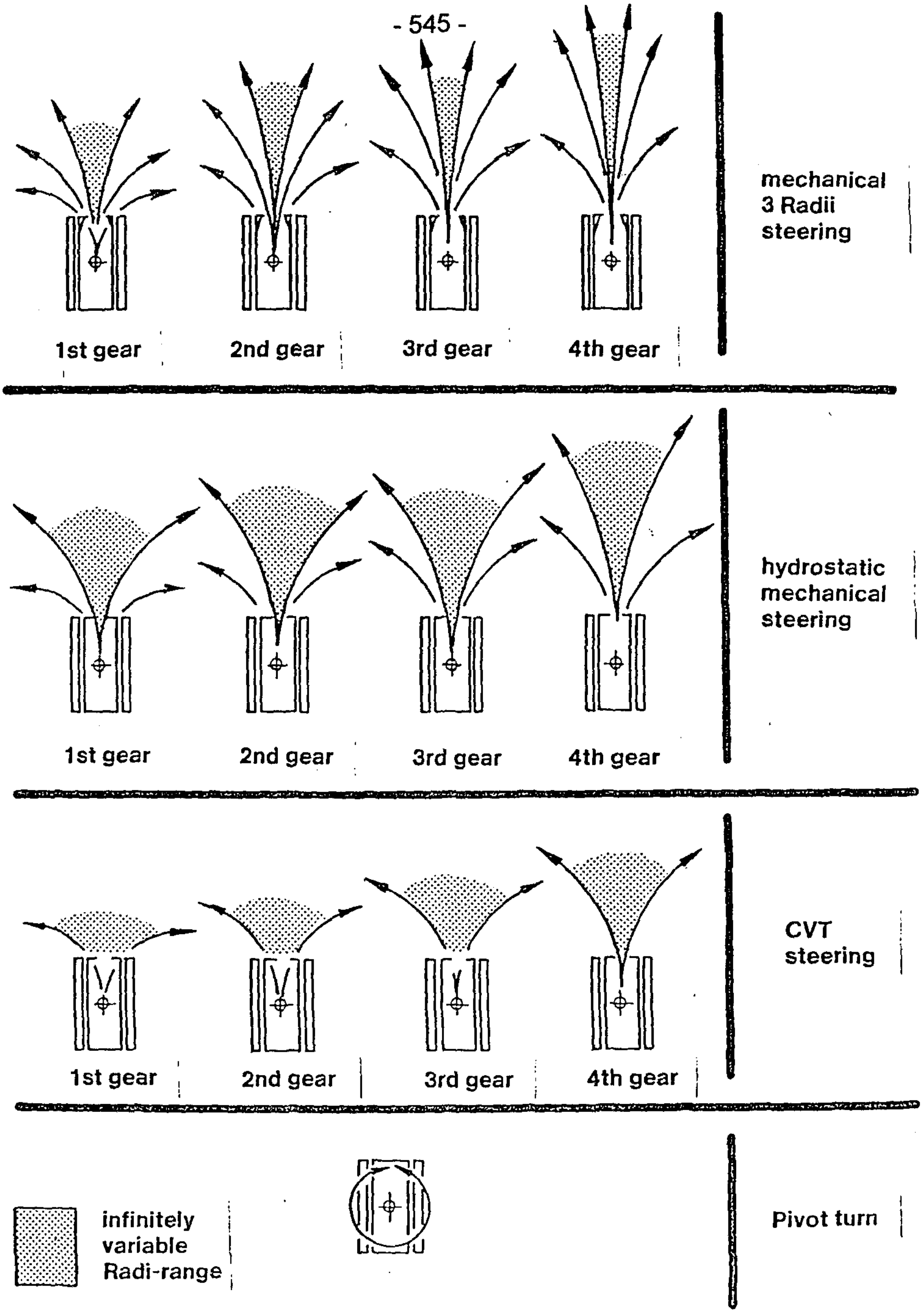
1st gear
2nd gear
3rd gear
4th gear
mechanical
3 Radii
steering
1st gear
2nd gear
3rd gear
4th gear
hydrostatic
mechanical
steering
1st gear
2nd gear
3rd gear
4th gear
CVT
steering
infinitely
variable
Radi-range
Pivot turn

ZAHNRADFABRIK
FRIEDRICHSHAFEN AG
Geschäftsbereich
Friedrichshafen

Steering Philosophy

SF

Picture No. 14

This diagram shows the power consumption as well as all the different efficiencies of this combined steering system.

The efficiency curve of the hydrostatic gear drive as shown on curve No. 2 and the overall efficiency of hydrostatic plus hydrodynamic system is curve No. 5. This shows that in narrow curves the steering efficiency can achieve values of only 50 %.

Considering a steering power of up to nearly 900 kW the overall cooling system has to cool down 450 kW plus the additional heat rejections of driving unit plus heat rejection of engine.

Picture No. 15

Still today tracked vehicles are equipped with the steering differentials which are working with a very low efficiency.

The white area shows the general transmission losses of approx. 20 %. Below the horizontal curve the blue area represents the steering losses which are system depending and cannot be influenced by the transmission maker. The yellow area shows the steering power available on the output and the red area the remaining drive power.

Assuming a steering ratio IL of approx. 10 the yellow part shows the needed steering power and below that the remaining drive power.

Picture No. 16

shows the efficiency curves of a regenerative steering system. The transmission losses on the white area are same as on picture 15. The blue area of the steering losses is remarkable small and considering the same steering power for the steering ratio IL of 10 the remaining drive power is more than 60 % of the installed engine power.

Picture No. 17

One significant difference between the European and the American steering philosophy is the power flow. In the US transmissions the steering moduls are driven after torque converter and in the European version steering power is directly driven by engine revolutions.

The main difference can be noticed when vehicle is operated in an off-road condition and lock-up clutch of torque converter is opened. Under these circumstances the output speed of torque converter is degreasing in function of the rolling resistance of vehicle.

Due to this fact the input speed of steering modul is degreasing and the driving curve is enlarging. The consequence is, the higher the rolling resistance, the more inefficient the steering system works.

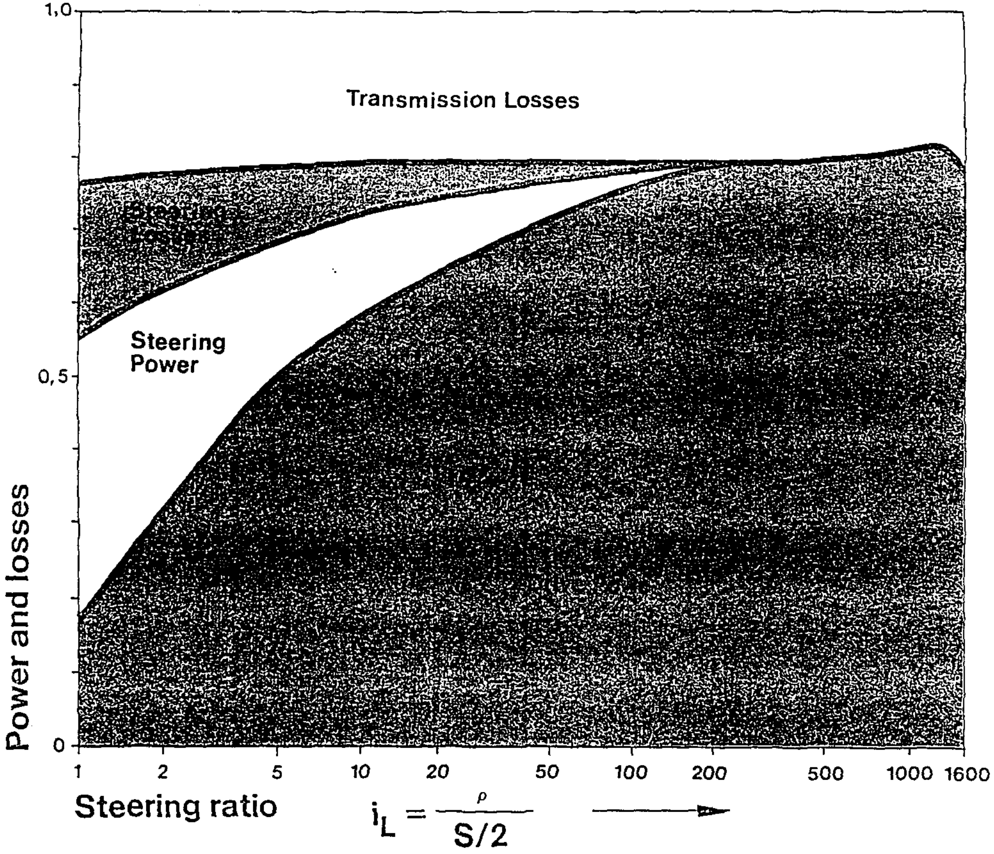

Transmission comparison
ZF-LSG

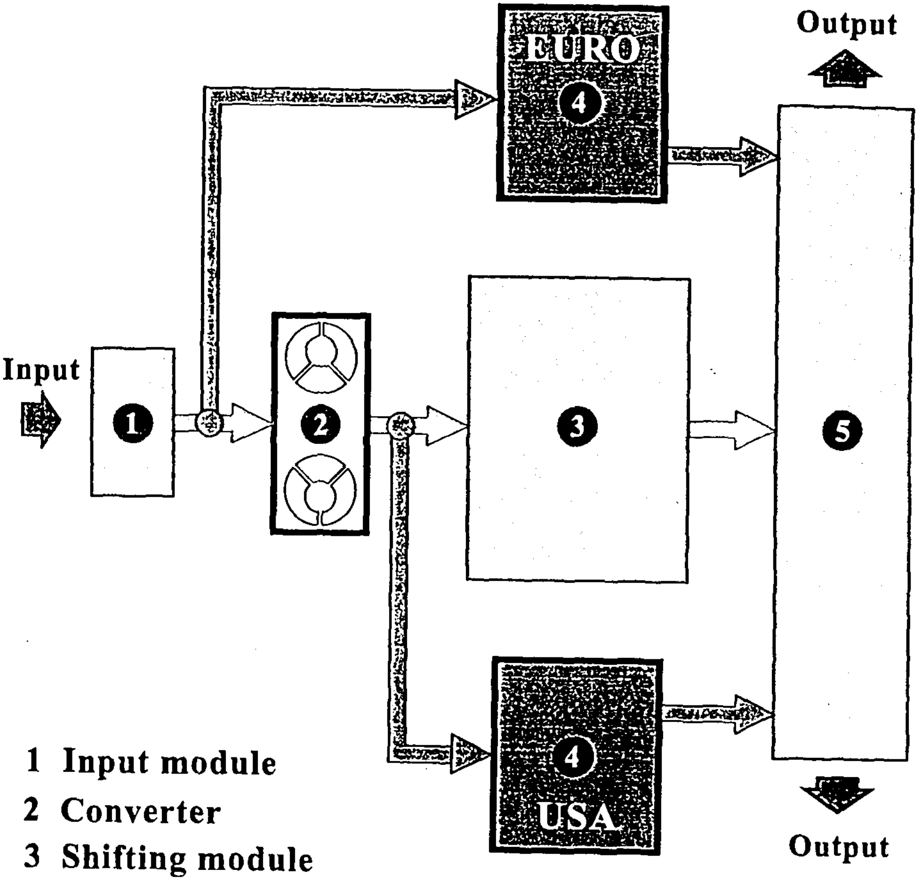
Output
EURO
4
Input
1
2
3
5
4
USA
Output

1 **Input module**
2 **Converter**
3 **Shifting module**
4 **Steering module**
5 **Summarizing module**

Powerflow
of steering systems

SF
07003e

This has been proven in a practical example during the test phase of the M1A1 vehicle in the Swiss Alpes where the pin curves could not be run in one turn.

In the European principle special provisions have to be taken not to stall the engine with the steering unit and also the true neutral function is an additional extra, if required.

BRAKE SYSTEMS

Picture 18

Combined brake system for heavy tracked vehicle are working with a secondary retarder in combination with a mechanical brake which can be either fitted on the output of the transmission or on the input of final drive.

The diagram shows the working principle of this combined system. In function of the vehicle speed, up to approx. half of maximum speed the whole retardation is done by the hydrodynamic retarder. As soon as the braking torque of retarder is not able to maintain the same deceleration, automatically the mechanical brake is coming to compensate this lack of braking torque.

Looking to the diagram approx. 80 % of the braking torque will be done wareless by the hydrodynamic retarder, and only approx. 20 % are done mechanically.

This will increase the lifetime of the brake pads, depending on the use of vehicle up to approx. 10 000 km.

Picture No. 19 an 20

show an integrated brake system, where retardation is done in front of steering system without influence to the driving radius during braking.

TRANSMISSION SYSTEM FOR TRACKED VEHICLES TOMORROW

Picture No. 21

Here the development faces can be seen to increase the power density.

Considering the powerpack of the LEO No. 1 with 100 % in 1965 the MBT 2000 in 1995 will be in the range of 215 %.

For a further increase of power density engines will be developed which are working with the 2 stage turbo-charger and will bring high engine torque at a very limited usable revolution range.

MECHANISCHE BREMSE + RETARDER

mechanical brake + hydrodynamic retarder

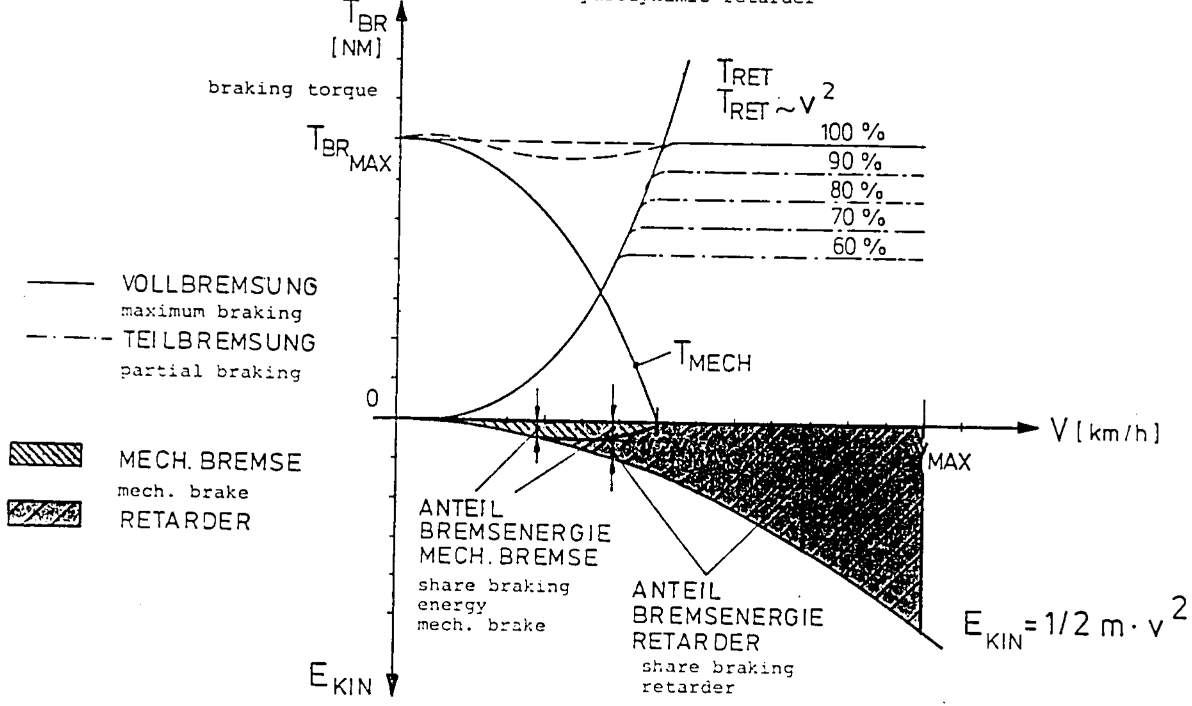

ZAHNRADFABRIK
FRIEDRICHSHAFEN AG
Geschäftsbereich
Friedrichshafen

KOMBINATIONS - BREMSSYSTEM
(DUAL-BRAKING SYSTEM)

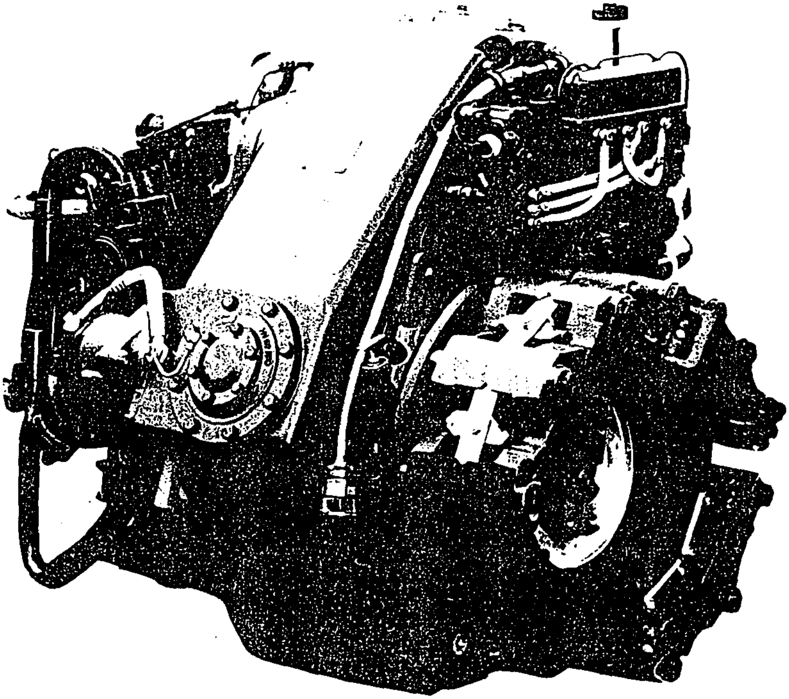

LSG 1000

504
347

① CONVERTER
② POWER TAKE OFF GROUP
③ ADAPTER GEAR TRAIN
④ SHIFTING GROUP
⑤ SUMMARIZING UNIT
⑥ STEERING GROUP
⑦ BRAKE

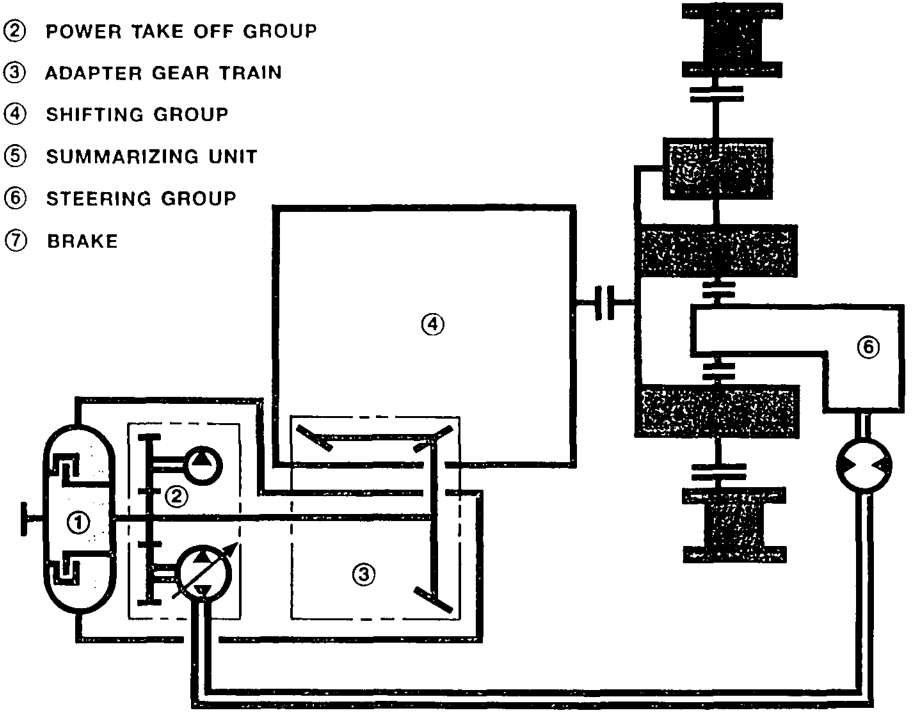

LSG 1000

MODULAR CONCEPT

504
437

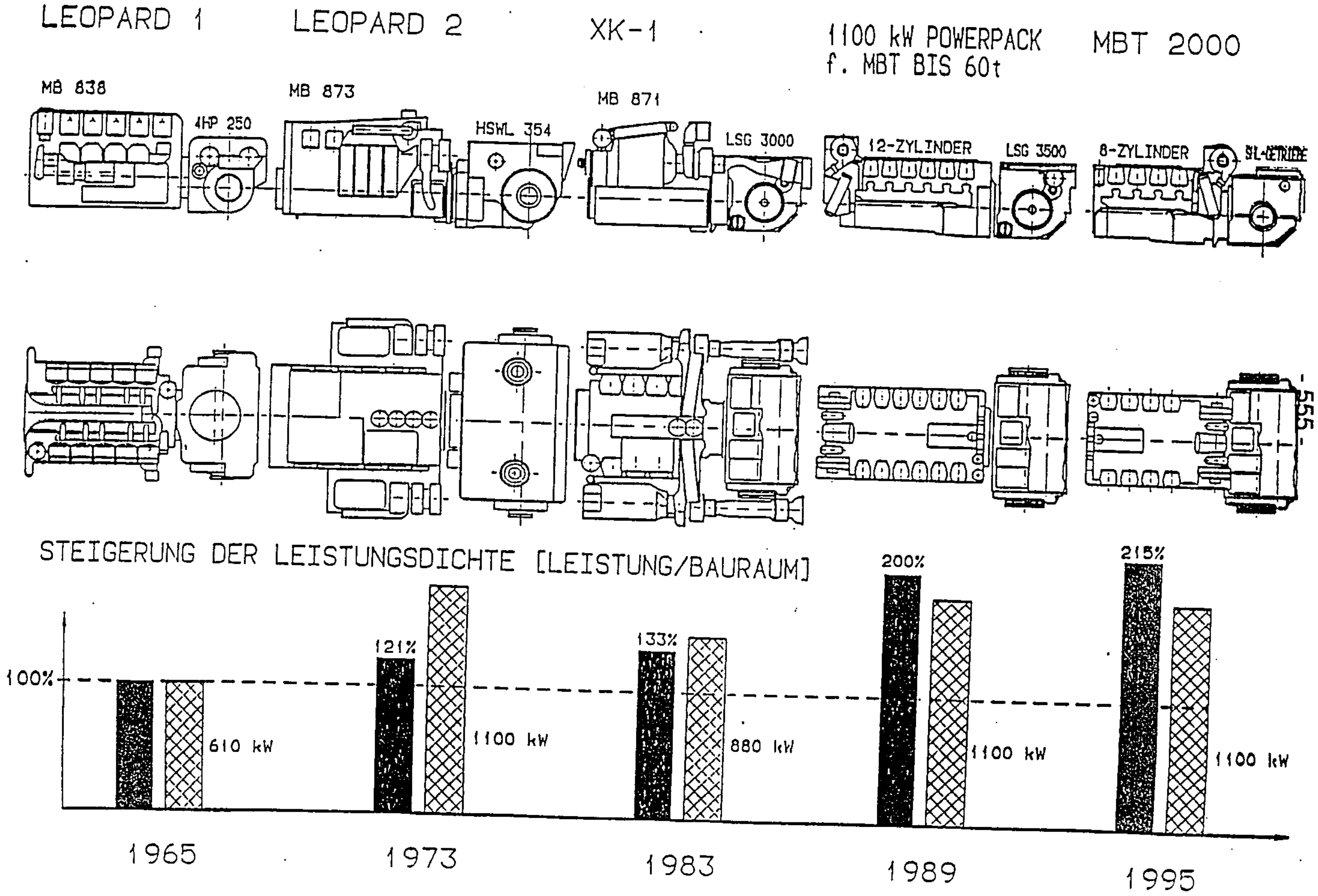
LEOPARD 1
LEOPARD 2
XK-1
1100 kW POWERPACK
f. MBT BIS 60t
MBT 2000
MB 838
4HP 250
MB 873
HSWL 354
MB 871
LSG 3000
12-ZYLINDER
LSG 3500
8-ZYLINDER
SL-GETRIEBE
STEIGERUNG DER LEISTUNGSDICHTE [LEISTUNG/BAURAUM]
100%
121%
133%
200%
215%
610 kW
1100 kW
880 kW
1100 kW
1100 kW
1965
1973
1983
1989
1995

Picture No. 22

This typical example shows the possibility of an engine power of 1100 kW with an 8 cylinder instead of 12 cylinder engine. Due to this characteristic, only CVT driving transmissions are possible to be matched with this engine.

Picture No. 23

shows a hydrostatic mechanical power-divided system for the steering and driving mode. It consists of a mechanical planetary set combined with hydrostatic units.

Picture No. 24

One further step will be the diesel-electrical drive, where either the whole engine power is converted into electrical power or a combination of electrical and mechanical power split is used.

Development efforts are actually done in Europe and the United States. Test vehicles with engine powers up to 500 kW have been successfully tested in Europe. But the influence of the magnetic radiation to the human nature is still unknown.

In resume new transmission systems will be developed with different technology standards to increase the power to weight ratio, to increase the reliability, to reduce the life cycle and maintenance costs, to degrease the down-time and to facilitate the ease of driving.

4

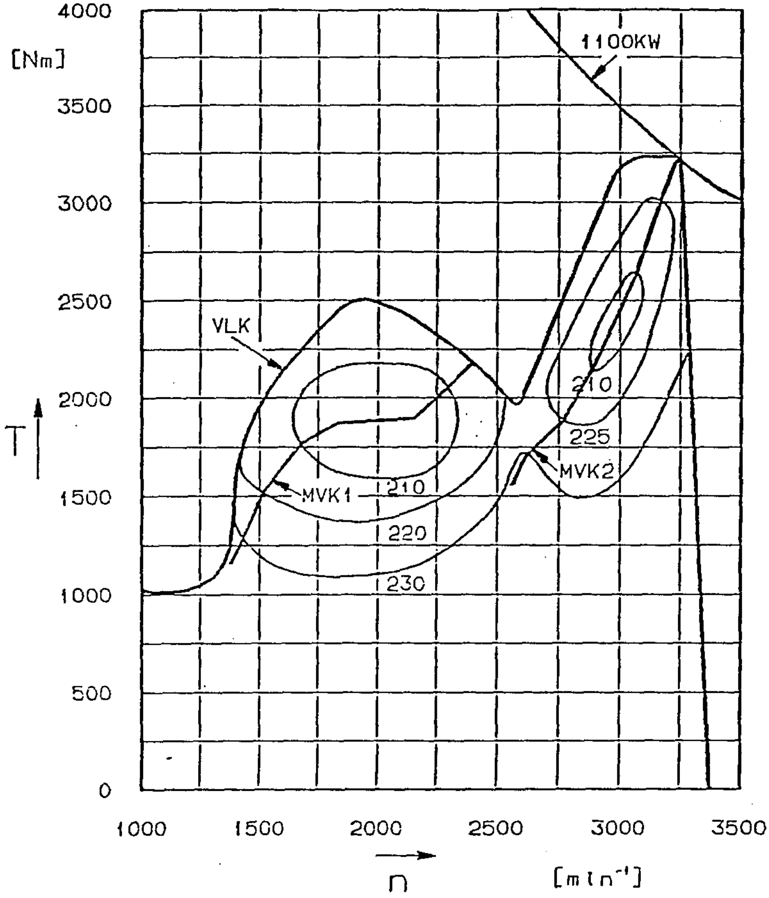

Stationäres Kennfeld eines 8 Zyl. Motors
mit zweistufigem Abgas-Turbo-Lader

$P = 1100$ kW

VLK ≙ Vollastkennlinie
MVK1 ≙ Vorzugskennlinie 1. Laderstufe
MVK2 ≙ Vorzugskennlinie 2. Laderstufe

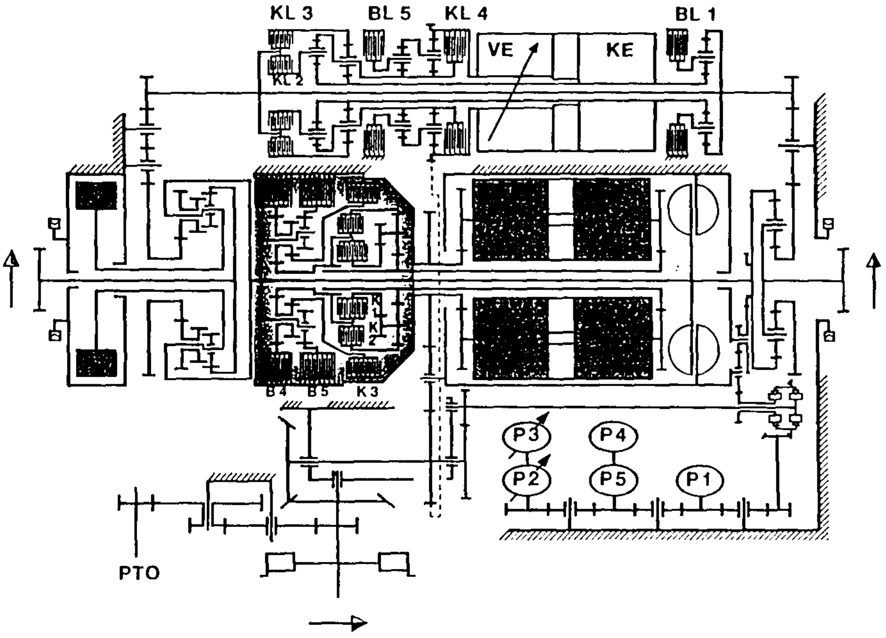
KL 3
BL 5
KL 4
BL 1
VE
KE
KL 2
K 1
K 2
B 4
B 5
K 3
P 3
P 4
P 2
P 5
P 1
PTO

LSG 3000 SHL (CVT)

504
468

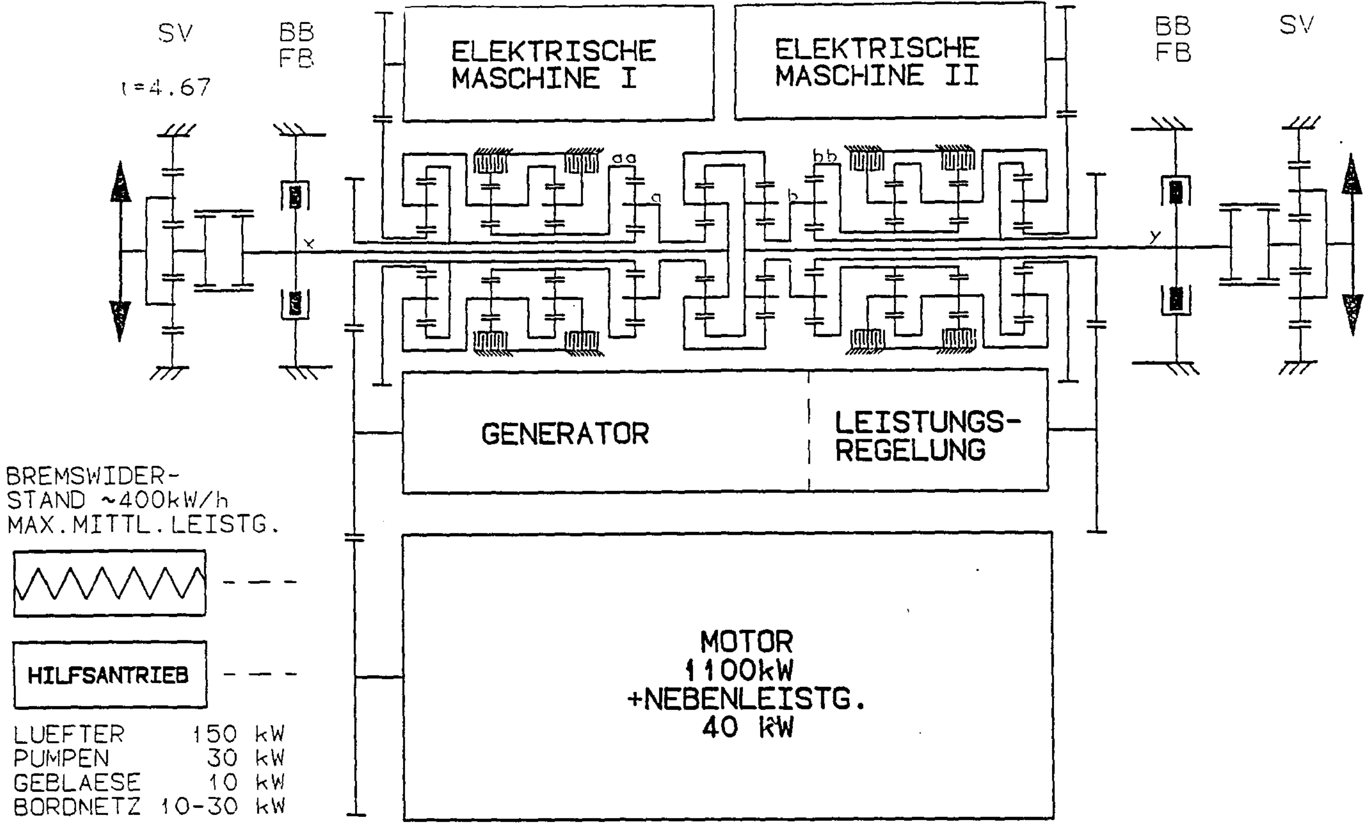
SV
BB
FB
i=4.67
ELEKTRISCHE MASCHINE I
ELEKTRISCHE MASCHINE II
aa
a
b
bb
x
y
BB
FB
SV
GENERATOR
LEISTUNGS-REGELUNG
BREMSWIDERSTAND ~400kW/h
MAX.MITTL.LEISTG.
HILFSANTRIEB
LUEFTER 150 kW
PUMPEN 30 kW
GEBLAESE 10 kW
BORDNETZ 10-30 kW
MOTOR
1100kW
+NEBENLEISTG.
40 kW

DIESEL-ELEKTRISCH-MECHANISCHER
KETTENFAHRZEUGANTRIEB VARIANTE ZF8

SF-S
9108052

ON CONSTITUTIVE EQUATIONS USED AT ANALYSIS OF STEERING OF TRACKED VEHICLES

Mart MÄGI

Machine and Vehicle Design
Chalmers University of Technology
S-412 96 GÖTEBORG, Sweden

ABSTRACT

Attention is called to the fact that two almost parallel streams seem to exist in the world literature regarding constitutive equations used when analyzing the mechanics of steering of tracked vehicles.

One of them, which has emerged from straight ahead traction analysis, treats the frictional characteristics along and across the track quite independently of each other, thereby allowing for advanced constitutive relationships along the track. The other assumes ground and track to be completely rigid, which easily allows a consistent treatment of the 2D picture of forces and motion in the ground plane. A brief overview will be given, demonstrating the characteristics, pros and cons of each method.

Finally is discussed the possibility to develop methods that in the future will combine the best of both the presently practiced procedures when analyzing the steering mechanics of tracked vehicles.

INTRODUCTION

The present author was introduced to one of the two parallel methods used to analyze steering of tracked vehicles already in the late 50-ies by his that time teacher, professor Bengt Jakobsson. He had a decade earlier carried out a very detailed analysis of the process of steering of tracked vehicles, which was supported by the Volvo Corp. and Swedish Defence Authorities. The results were made public in a report that was written in Swedish as theses for earning the swedish academic degree of Doctor of Engineering Sciences in 1947 [1].

This work had its conceptual basis in ideas, which were published already before the Second World War by H. E. Merritt in 1939 [2], implying the assumption of completely rigid ground and track links, as well as Coulomb type dry friction at all sliding contacts between track links and ground. Similar ideas were published even earlier in German by G. Lindenau in 1938 [3], but he was not quoted by neither Merritt, nor Jakobsson, probably due to pre-war communication difficulties.

These ideas were later on elaborated by two of professor Jakobsson's former students, G. Gerbert and K.-O. Olsson, who - with some extensions - transformed the procedures given by Jakobsson to computer format and applied them to the analysis of transient steering [4]. Similar ideas inspired also the present author to the work, which was summarized in 1974 as a dissertation [5]. There the power transfer through rolling and spinning Hertzian contacts in mechanical variators was studied. The contacting surfaces were assumed to be completely rigid in the tangential direction and dry friction conditions were assumed to exist locally over the entire Hertzian contact area. Also, there was made systematic use of the concept of force and spin/speed/motion poles and their offsets from some theoretical point of reference, which for a track of a vehicle was so elegantly introduced by Merritt (but was not thoroughly utilized by Jakobsson).

This first mentioned approach based on dry friction and rigid matter will hereafter be referred to as the Merritt-Jakobsson approach.

An alternative approach became familiar to the present author via an excellent textbook, Theory of Ground Vehicles, written by J. Y. Wong [6]. There ideas and concepts, which seem to be originally published by M. G. Bekker in 1956 [7], were extensively elaborated and promoted. The same ideas have also been supported, e. g., by I. Hayashi in 1975 [8].

The alternative approach has its roots in the study of the tractive effort and track slip at straight ahead motion. Such studies require as a minimum the modeling of friction beyond the Coulomb dry friction concept and the consideration of shear effects in the uppermost layers at the surface of the ground.

The mechanics of steering is then a kind of an add-on feature to the straight ahead motion. This approach seems to be successfully applied by the off-road vehicle industry, and seems also to be embedded in MultiBody System analysis program package applications, such as ADAMS and DADS.

The second of the described approaches, where tractive and steering efforts are dealt with quite independently, will hereafter be referred to as the Bekker-Wong approach.

SOME GENERAL REMARKS

In the study of mechanical systems in general, three categories of equations are significant:

- ***equilibrium***, interrelating forces or loads in a generalized sense,
- ***compatibility*** or ***continuity***, interrelating geometry and/or motion, and
- ***constitutive relationships***, relating forces/loads to geometry/motion.

As far as the classical mechanics according to Newton will apply, equilibrium relationships are axiomatic: proposed equations are either correct or in error.

Also, as far as classical geometry according to Euclid will apply, compatibility or continuity relationships are axiomatic: proposed equations are either correct or in error.

However, constitutive relationships are always hypothetical, they are more or less correct, and hypotheses adopted could only be evaluated by a comparison of theoretical predictions and experimental evidence.

The steering action of vehicles is achieved by creating transverse forces (perpendicular to the heading direction of the vehicle) at the ground contacting and weight transferring devices, e. g., wheels and/or tracks. For ground vehicles (even on rails) these forces are basically some kind of frictional/shear forces between the ground and the weight transferring devices. These forces are further related to the relative motion between the ground and the wheels/tracks by some set of constitutive relationships, which are hypothetical by nature.

Thus constitutive equations, and hence the related frictional forces, are not correct or in error, but more or less realistic, and the same applies to the total results of the analysis of the steering action. This hypothetical nature is commonly accepted when dealing with wheeled vehicles, whereby it exists a number of quite well established alternative models for tires, embedding more or less transparently a variety of constitutive relationships, as is reported in the overview prepared by the U. S. Department of Transportation [9].

THE FORMAT OF CONSTITUTIVE EQUATIONS

Constitutive equations may be formulated in macroscale for contacts between entire components of mechanical systems and in microscale for local (small) subcontacts within the entire (large) contact.

In the case of wheels or tracks traveling on a flat ground surface, a typical 2D situation prevails. The significant geometrical overall or macroscale parameter is then the relative motion between the wheel/track and the ground, described by some combination of three mutually independent components. Correspondingly, there are also three mutually independent force/moment components that describe in macroscale the transferred load in the (horizontal) ground plane.

These three components may be defined in various ways. For wheels, both composite pneumatic and homogeneous steel (e. g., at railroad applications, cf. J. J. Kalker [10]), a well defined theoretical point of contact exists. At that very point a cartesian frame of coordinates will serve well for the definition of these three components. This frame has axes along the heading or longitudinal, transverse and surface normal directions of the wheel.

The relative motion at the point of reference may be partitioned into sliding in the heading/longitudinal and transverse directions, as well as spin about the normal axis. Furthermore, the sliding could be made non-dimensional with respect to the traveling (or rolling) speed in the heading direction, leading to the slip/skid coefficient and the drift or slip angle. The corresponding planar load as observed at the point of reference is partitioned into forces in the heading and transverse directions, as well as a moment about the normal axis.

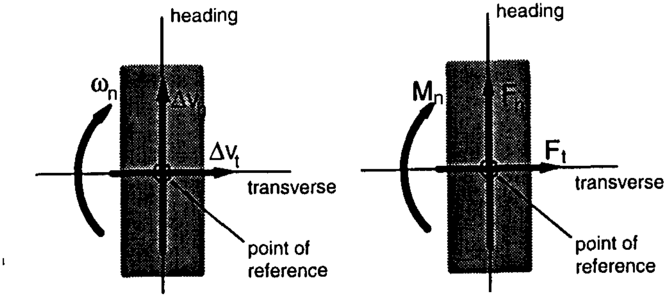
heading
ω_n
Δv_h
Δv_t
transverse
point of reference
heading
M_n
F_h
F_t
transverse
point of reference

Fig. 1: Macroscale motion and loads in cartesian representation

Alternatively, one could take full advantage of basic concepts used in planar mechanics. Any planar motion between two bodies is just pure rotation about an instantaneous center of rotation or a ***spin pole***. The three components of motion are then the (1) heading and (2) transverse ***components of offset*** of that pole from the point of reference and (3) the spin velocity, all three quantities with magnitude and sense.

The resulting action of any planar forces between two bodies is a single force, acting along a unique line. The three components of the force action are then (1) the magnitude of the force, (2) the orientation of the line of action (expressed, e. g., as some heading angle) and (3) the shortest distance of that line from the point of reference. A complete definition of senses of these quantities needs some additional elaboration. However, the interpretation of positive senses will become almost obvious, if one specific point on the line of force action, which is located closest to the point of reference, by definition will be the ***force pole***. Then, analogously to the motion description, the three force characterization components are the (1) heading and (2) transverse ***components of offset*** of that pole from the point of reference and (3) the total planar force (which is directed perpendicularly to the force pole offset), all three quantities with magnitude and sense, whereby force in positive sense will produce moment in the positive sense about the normal axis.

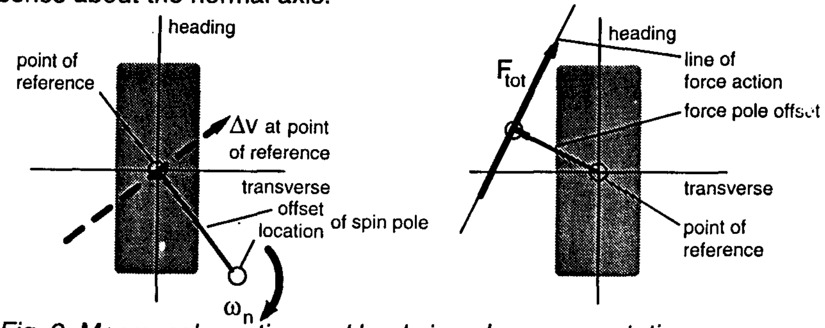
heading
point of reference
ΔV at point of reference
transverse
offset
location
of spin pole
ω_n
F_{tot}
heading
line of force action
force pole offset
transverse
point of reference

Fig. 2: Macroscale motion and loads in polar representation

In any case, if the three geometrical components are denoted g_1, g_2 and g_3, respectively, and their three equivalent planar load components are denoted l_1, l_2 and l_3, respectively, then the constitutive equations for a wheel or a track as a whole read in general

$$l_1 = R_1(g_1, g_2, g_3)$$

$$l_2 = R_2(g_1, g_2, g_3) \qquad \text{Eq. (1)}$$

$$l_3 = R_3(g_1, g_2, g_3)$$

where R_i indicate three ***non-linear*** relationships. These relationships could either be determined experimentally, or analytically by departing from a study in microscale and arriving by integration at the end result in macroscale.

The format, either cartesian or polar, is a matter of personal preference and will not influence the inherent characteristics of the constitutive equations.

THE MERRITT-JAKOBSSON APPROACH

In the Merritt-Jakobsson approach it is assumed that both the ground and the mutually backlashfreely pivotable individual links of the track are completely rigid. The constitutive relationships for the track and ground interface are assumed at each local point to follow the Coulomb or dry friction hypothesis, quantified by a coefficient of friction, μ. The assumption of rigid ground and track makes further hypotheses for constitutive relationships within these parts of the system to be excessive.

Merritt [2] treats a very idealized case. The width of the track is assumed to be negligible compared to the length of the track. The fraction of the total vehicle weight that is carried by the track considered, is assumed to be distributed evenly along the length of the track. Then it is easy to find an analytical solution for a special case, at which the track transmits no macroscale transverse frictional force.

Applying the pole concept, the spin pole is assumed to be located on a line perpendicular to the track and passing through its midpoint. The local microscale transverse load distribution is then skew-symmetric about that line, why the resulting transverse load will vanish and the total load is acting in the heading direction. It is further easy to prove that the force pole must be located on the opposite side of the track than the spin pole. The non-dimensional pole offsets are (with the notation used by Merritt, who has one half of the length of the track, L, as the characteristic length): α for the force pole and β for the speed or spin pole offsets. The utilized frictional force is a fraction K of the maximum frictional force, which per se is μ times the total weight carried by the track.

At analysis, β is the obvious independent variable, defining explicitly the two others according to Eq. (2):

$$K = 0.5\beta[\ln(\sqrt{1+\beta^2}+1) - \ln(\sqrt{1+\beta^2}-1)]$$

$$\alpha = 0.5(\sqrt{1+\beta^2}/K - \beta) \qquad \text{Eq. (2)}$$

Besides the details in Eq. (2) it is interesting to observe that any one of the three variables α, β and K defines uniquely the two others. As an example, such a dependence is visualized in Fig. 3 for K as the independent variable.

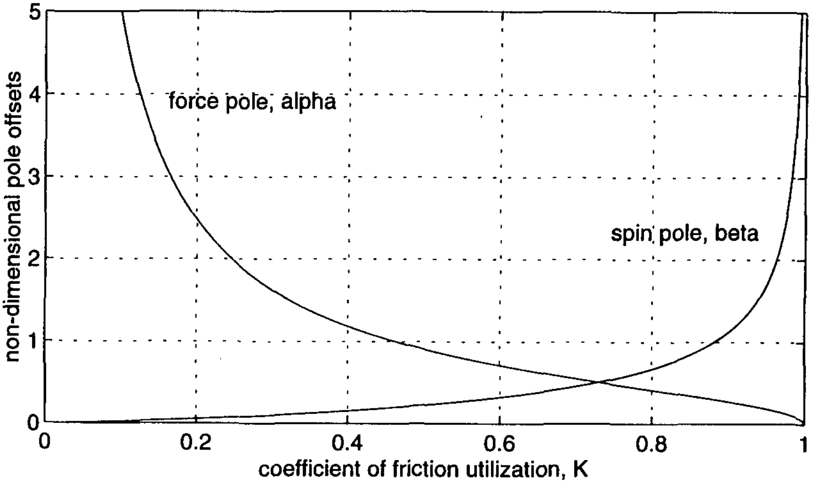

Fig. 3: Non-dimensional speed and force pole offsets vs. coefficient of utilization at special idealized Merritt conditions

THE BEKKER-WONG APPROACH

In the Bekker-Wong approach the deformability of the ground in the shearing mode ***along*** the track is highly significant, both (and initially) when traveling straight ahead, and (as a consequence) when making steering maneuvers.

When traveling straight ahead, the ***longitudinal*** force component (along the track) is uniquely and non-linearly related to the longitudinal slip of the track. The local shear deformation of the ground may be both recoverable (elastic) and non-recoverable (plastic and/or cohesive). The leading edge of the track is assumed to enter virgin ground. When the entire track then travels over any specific point on the ground, the local shear deformation (strain) and shear force (stress) will increase. Between the leading and trailing ends of the track the stress and strain will vary and be mutually related at each location according to some constitutive relationship.

As an example, such a relationship could read (for loose soils according to Wong, [6]):

$$\tau = (c + \sigma \tan \phi)(1 - e^{-j/K}) \qquad \text{Eq. (3)}$$

where τ is the local shear stress, c is the apparent cohesion, σ is the local normal stress, φ is the angle of internal shearing resistance, j is the local shear deformation and K the horizontal shear deformation modulus.

The longitudinal slip of a track is the velocity of track links in the heading direction of the track relative to some reference point in the ground well below the surface, made non-dimensional by the traveling speed of the track gear. It creates - according to compatibility - a linearly varying shear deformation, j, between track and ground. Constitutive relationships, such as Eq. 3, translate shear deformations to shear stresses, τ. Equilibrium fulfillment implies a summation or integration of local microscale shear forces to form a total macroscale force between track and ground in the direction of the track.

Changing direction of travel of a vehicle requests action of transverse forces. Also, when turning a track relative to the ground, transverse components of sliding and shear force appear. According to Bekker-Wong, this action is superimposed as an add-on feature to the action taking place purely in the heading or longitudinal direction, which was just described.

However, Eq. (3) (or similar) is then ***not*** used in the transverse direction! Instead, Coulomb type friction is assumed to relate the transverse sliding to local transverse shear forces in the same manner as if a spin pole according to Merritt virtually existed somewhere ***along*** the track. In macroscale this generally creates a couple that counteracts turning, as well as a transverse component of force.

A unique location of such a virtual spin pole or instantaneous center of rotation between track and ground - at the "center of gravity" of normal loads between track and ground - will cancel the resulting transverse force, which approximates the conditions when turning at low traveling speed.

THE ANISOTROPIC DRY FRICTION APPROACH

The original Merritt-Jakobsson approach has by many authors been developed further to include observed differences in dry friction along vs. across the track. In this context the anisotropic dry friction concept proposed by E. W. E. Micklethwait in 1944 [11] seems to be a cornerstone.

When applying that concept, the local sliding vector of magnitude s_{tot} in some arbitrary direction is decomposed into orthogonal components along and across the track, of the magnitudes s_{long} and s_{trans}, respectively. Different coefficients of dry friction are prescribed in those directions: μ_{long} and μ_{trans}, respectively. The local constitutive equations then read using standard additional notation:

$$F_{long} = \mu_{long} N s_{long} / s_{tot}$$

Eq. (4)

$$F_{trans} = \mu_{trans} N s_{trans} / s_{tot}$$

Constitutive equations according to Eq. (4) generally predict non-parallel sliding and friction force vectors, which might be surprising, as dry friction normally counteracts sliding motion.

These equations are further easily implemented into the Merritt-Jakobsson approach. One of the first to do so was W. Steeds in 1950 [12]. He has had many followers, including G. Gerbert and K.-O. Olsson in 1982 [4].

This approach may be considered to constitute an extended Merritt-Jakobsson approach.

SOME COMMENTS TO THE DISCUSSED APPROACHES

Any frequently used approach to formulate constitutive relationships for tracked vehicle applications must have its merits. Probably they also have their draw-backs.

The extended Merritt-Jakobsson approach

- predicts steering action on hard grounds quite accurately
- predicts steering action on soft grounds less well
- cannot predict slip at variable tractive effort in a realistic way
- is capable to handle some anisotropy along and across the track
- is consistent from a theoretical point of view

The Bekker-Wong approach

- predicts slip at variable tractive effort quite well
- is well suited to deal with anisotropic track behavior
- predicts steering action on soft grounds reasonably well
- predicts steering action on hard grounds less well
- ***is in itself not fully consistent from a theoretical point of view***

The lack of full consistency in the Bekker-Wong approach is related to the superposition of transverse track forces upon separately evaluated longitudinal track forces. Superposition yields correct end results only if the dependent variables are linear combinations of the independent variables.

In the constitutive equations, as outlined in Eq. 1, loads l are the dependent variables and relative motion components g are the independent variables.

Neither at dry friction, nor at plastic/cohesive ground are these equations linear! Only very high dry friction combined with elastically soft ground would yield approximately linear constitutive equations.

The consequences of the lack of full consistency in the Bekker-Wong approach are hitherto not clarified to the knowledge of the present author.

POSSIBLE DEVELOPMENTS IN THE FUTURE

Regarding future possible development of constitutive equations for track-ground interaction applications, at least two separate paths may be presently imagined:

(a) Extension of 1D constitutive equations similar to Eq. 3 to true 2D functionality. This may cause problems with treating properly the pre-history of each individual spot of the ground that is passed by some portion of the track. If versatile equations are found, the present lack of consistency in the Bekker-Wong approach could be eliminated.

(b) Introduction of additional relevant flexibility into the track-ground structural system and refinement of related added constitutive equations. As an example, however not too close, may serve the experience of the present author. At the power transfer through rolling and spinning Hertzian contacts, the contacting surfaces were initially assumed to be tangentially rigid [5], which is relevant for mechanical variators. Alternatively, J. J. Kalker [10] allowed the surfaces to be tangentially elastic, which is relevant at railroad applications. Regular dry friction was assumed to act in both the cases.

SUMMARY

Two almost in parallel used approaches to handle longitudinal and transverse forces between a single track and the ground have been

- identified,
- given some historical background,
- briefly described and
- summarily evaluated.

Although such approaches are by nature hypothetical, and thus never fully correct or completely in error, some lack of consistency is pointed out in one of the approaches. The consequences of that lack of consistency are so far not known.

Future research is expected to (a) clarify the consequences and (b) eliminate the lack of consistency by finding or developing new truly 2D and still versatile constitutive equations for the rigid track & soft ground contact. Eventually such new knowledge may unify both the approaches that exist presently in parallel!

REFERENCES

1. ***Jakobsson, B.:*** Styrning av bandfordon (Steering of tracked vehicles), Dissertation, Chalmers University of Technology, Göteborg, 1947.
2. ***Merritt, H.E.:*** Some considerations influencing the design of High-speed track-vehicles, J. Inst. Automobile Engrs, 1939.
3. ***Lindenau, G.:*** Beitrag zur Mechanik der Kurvenbewegungen von Baggern und Abraumförderbrücken, Dissertation, TH Berlin, 1938.
4. ***Gerbert, G. & Olsson, K.-O.:*** On track vehicles running through curves, Joint report, Div:s of Machine Elements, Chalmers University of Technology, Göteborg & Lund Technical University, 1982.
5. ***Mägi, M.:*** On Efficiencies of Coplanar Shaft Power Transmissions, Dissertation, Chalmers University of Technology, Göteborg, 1974.
6. ***Wong, J.Y.:*** Theory of Ground Vehicles (1st Ed.), John Wiley & Sons, 1978.
7. ***Bekker, M. G.:*** Theory of Land Locomotion, University of Michigan Press, Ann Arbor, 1956.
8. ***Hayashi, I.:*** Practical Analysis of Tracked Vehicle Steering Depending on Longitudinal Track Slippage, Proc. 5th ISTVS Conf., 1975.
9. ***Clark, S. K. (Editor):*** Mechanics of Pneumatic Tires (2nd Ed.), U.S. Department of Transportation, Washington, D. C., 1981.
10. ***Kalker, J. J.:*** On the Rolling Contact of two Elastic Bodies in the Presence of Dry Friction, Dissertation, TH Delft, 1967.
11. ***Michlethwait, E. W. E.:*** Soil mechanics in relation to fighting vehicles, Military College of Science, Chertesy, 1944.
12. ***Steeds, W.:*** Tracked Vehicles, Automobile Engineer, Apr., May & June, 1950.

ISSN 1022 - 0313

ISTVS thanks the European Research Office of the U.S. Army for the financial support to the conference.